

PARTICULATE MECHANICS OF GRANULAR SOILS

A thesis submitted to the
University of London

by

Yogendra Kumar Sharma, B.E. (Civil), M.E. (Soils), D.I.C.

for the degree of
Doctor of Philosophy in the Faculty of Engineering

Imperial College of Science and Technology

LONDON, S.W.7.

June, 1976

To my wife

ABSTRACT

Granular soils are not continua. Their macroscopic behaviour depends upon the nature of the interparticle contacts and the deformation of these contacts. The deformation mechanism is likely to depend upon the physical properties of the constituent particles and the arrangement of particles in the fabric of the granular mass. Interparticle friction is one of the physical properties on which most of the existing particulate stress-strain theories depend. An inquiry was made into the mechanism of friction. The values of the coefficient of interparticle friction of the test materials were determined under the same environmental conditions as those that exist in plane strain tests where these materials were to be used.

In this work X-ray photogrammetry was applied, probably for the first time in Particulate Mechanics, to locate representative particles in space by fixing their position and angular orientation. This technique was found to be very satisfactory.

Using the observed data, it has been possible to establish the peculiarities of the granular samples and to verify the existing postulate of interparticle slip as the mechanism of deformation of granular mass under shear. The most probable major deformational behaviour is suggested.

One of the basic assumptions of most of the current stress-strain models, namely, co-axiality of the principal stress axes and the principal strain increment axes, is examined.

Finally, the observed data were used to examine the existing stress-strain models of cohesionless soils. It is recommended that in the absence of any better particulate theories, the stress-dilatancy theory can be used under restricted deformation conditions.

ACKNOWLEDGEMENTS

The work described in this thesis was carried out in the Department of Civil Engineering of the Imperial College of Science and Technology, in the Soil Mechanics Section headed by Professor A.W.Bishop. The research was supervised by Dr. A.E.Skinner.

The study was made possible by a Commonwealth Scholarship and by support from the Leche Trust and the Lady Edwina Mountbatten Trust. The work was done while the writer was on leave of absence from the Government Engineering College, Jabalpur, India. The writer would like to express his gratitude to his employer, the Government of Madhya Pradesh, Department of Education who has generously sponsored him and granted him the necessary leave of absence.

The writer is indebted to Professor A.W.Bishop, who suggested the topic, and for the encouragement, help and interest shown by him during this study.

The writer is very grateful to Dr. A.E.Skinner for inculcating deep interest in this field of research, critical discussions and useful suggestions.

Thanks are also due to Mrs. Janet Skinner for the help and inspiration.

The writer would like to express his thanks to the following:

1. Dr. J.R.F.Arthur of University College and Mr. R.Gould of A.Q.D.Laboratories for the useful discussions which helped in the development of the X-ray technique used in this work.
2. Mr. B.Chiat and Mr. S.K.Sharma of the Surveying Section in the Civil Engineering Department for frequent discussions and for constructive suggestions on Photogrammetric aspect of X-ray Photogrammetry. Further thanks are due to them for reading the manuscript of Chapter 5 and for making useful comments.

Appreciation of the co-operation and help received from his many research-fellows, particularly from Drs. Jane Walbanke, M. Maguire, L. Wesley and from Messers M. Hamza and J. Apted, is also acknowledged.

The work would not have progressed or be presented in the present form without the use of the facilities extended by the following:

1. Radiology section of the A.Q.D. Laboratories, Harefield, Middlesex, where the work connected with X-rays was carried out.
2. Department of Photogrammetry, University College, where the preliminary work on photogrammetric data observation was carried out.
3. Surveying and Terrestrial Photogrammetry Section of the Department of Civil Engineering, City University, where most of the stereo-radiographic observations were carried out. The facilities were extended by Mr. N. Lindsey and observations were done by Mr. A. Kenny.
4. London University Computer Centre, University College Computer Centre and Imperial College Computer Centre where the computation involved in reduction of the data were carried out.

and without the services rendered by the following:

1. The Soil Mechanics technical staff, under D. Evans, for their help and encouragement. Thanks are due to Mr. L. Spall for his excellent machine work which was essential for this study and for helping the writer in setting-up the experimental set-up at the A.Q.D. Laboratories, Harefield.
2. Miss J. Gurr for the photographic reproduction.

The support, encouragement and patience of his wife, Shyama were vital in sustaining the effort required throughout this research, for which he cannot thank her enough. The writer wishes to acknowledge the forbearance of his children Gowrie, Dhiraj and Niraj, who have patiently accepted the writer's pre-occupation with the mechanics of particulate soils.

And last but by no means least, the writer would like to record with deep gratitude the blessings of his parents.

CONTENTS

	Page No.
ABSTRACT	i
ACKNOWLEDGEMENTS	ii
CHAPTER 1	
REVIEW OF PREVIOUS WORK AND OUTLINE	
OF PRESENT RESEARCH	1.1-1.5
1.1	Introduction 1.1
1.2	Scope and Outline of Present Work 1.4
CHAPTER 2	
TEST MATERIAL, APPARATUS AND EXPERIMENTAL	
TECHNIQUE	2.1-2.24
2.1	Introduction 2.1
2.1	Test Material 2.1
2.2.1	Selection of test materials 2.2
2.2.2	Selection of shape and size of particles of test materials 2.2
2.2.3	Material origin and properties 2.4
2.3	Selection of Type of Shear Test 2.4
2.4	Plane Strain Apparatus 2.5
2.4.1	Preliminary considerations and basis of design 2.5
2.4.2	Specimen size 2.6
2.4.3	Loading platens 2.9
2.4.3.1	Axial platens 2.9
2.4.3.2	End platens 2.10
2.4.4	Frictionless ends 2.11
2.4.5	Loading, sensing and monitoring systems 2.13

	Page No.	
2.4.5.1	Lateral loading and sensing system	2.13
2.4.5.2	Axial loading and sensing system	2.13
2.4.5.3	Electronic monitoring system	2.14
2.5	Material Preparation	2.14
2.5.1	Surface topography	2.15
2.5.2	Surface cleanliness	2.15
2.5.3	Drying of particles	2.15
2.6	Marker Particles	2.17
2.7	X-Ray Set-Up	2.18
2.8	Latex Rubber Membrane	2.18
2.9	Test Specimen Preparation	2.19
2.10	Test Programme	2.20
2.11	Instruments Used for Data Reduction	2.21
2.12	Interparticle Friction Apparatus	2.21
	(8 plates, 3 figures and 2 tables)	
 CHAPTER 3	 INTERPARTICLE FRICTION	 3.1-3.41
3.1	Introduction	3.1
3.2	Friction and Its Laws	3.3
3.3	Friction Theories	3.4
3.4	Friction Theories for Brittle Materials	3.7
3.4.1	Adhesion-ploughing theory	3.7
3.4.1.1	Skinner's extension to the adhesion theory	3.10
3.4.2	Friction theories based on elastic contacts	3.13
3.4.3	Friction theory based on brittle fracture of asparties	3.16
3.4.4	Coulomb type approach or power law of friction	3.19

		Page No.
3.5	Polymers and Friction	3.21
3.6	An Experimental Inquiry of Friction of the Test Materials Used in this Study	3.24
3.6.1	Need for experimental investigation	3.24
3.6.2	Friction tests	3.25
3.6.3	Test programme	3.27
3.6.4	Method of calculations	3.29
3.7	Friction Test Results	3.31
3.8	Discussion of Test Results	3.32
3.8.1	Test apparatus and method	3.32
3.8.2	Experimental results	3.33
3.8.2.1	Glass balls	3.33
3.8.2.2	Ceramic balls	3.38
3.8.2.3	Polymeric materials	3.38
3.8.3	Friction model	3.39
3.8.3.1	Brittle materials	3.39
3.8.3.2	Polymeric materials	3.40
3.9	Is the Coefficient of Friction Constant? (7 figures and 3 tables)	3.40
CHAPTER 4	X-RAY PHOTOGRAMMETRY - DATA ACQUISITION SYSTEM	4.1-4.43
4.1	Introduction	4.1
4.2	A Suitable Technique - Survey and Selection	4.3
4.2.1	General	4.3
4.2.2	Thin section technique	4.3
4.2.3	Two dimensional models	4.5
4.2.4	Photographic methods	4.5
4.2.5	Radiographic technique	4.6

	Page No.	
4.3	Radiography and Photogrammetry	4.8
4.4	Some Basic Definition and Terminology	4.10
4.4.1	Radiological terminology	4.10
4.4.2	Photogrammetric terms	4.14
4.4.3	Soil mechanics terms	4.14
4.5	Selection of Source of Radiation	4.14
4.6	X-Ray Photogrammetry	4.15
4.6.1	General	4.15
4.6.2	Major problems of X-ray photogrammetry	4.16
4.7	Basic Requirements of X-ray Data Acquisition System	4.17
4.8	Quality of X-ray Image	4.18
4.9	Factors Affecting Radiographic Sensitivity	4.19
4.9.1	Introduction	4.19
4.9.2	Factors affecting contrast	4.19
4.9.2.1	Quality of radiation	4.19
4.9.2.2	Filters	4.20
4.9.2.3	Scattered radiation	4.20
4.9.2.4	Films	4.21
4.9.2.5	Intensifying screens	4.21
4.9.2.6	Processing of exposed X-ray film	4.23
4.9.2.7	Density	4.23
4.9.2.8	The object being radiographed	4.24
4.9.3	Factors affecting definition	4.25
4.9.3.1	Introduction	4.25
4.9.3.2	Geometric factors	4.26
4.9.3.3	Inherent unsharpness	4.29
4.9.3.4	Film resolution	4.29

		Page No.
4.10	X-ray Set-Up	4.30
4.10.1	X-ray apparatus	4.30
4.10.2	Scattered radiation	4.33
4.10.3	Selection of film	4.35
4.10.4	Film developing technique	4.36
4.10.5	Film to focus distance and film to object distance	4.37
4.11	Stereo Model and Photogrammetric Considerations	4.39
4.12	Radiographic Results and Discussion (5 figures, 10 plates)	4.41
CHAPTER 5	X-RAY PHOTOGRAMMETRY-DATA REDUCTION	5.1-5.37
5.1	Introduction	5.1
5.2	Basic Terminology and Definition of Terms	5.2
5.3	Data Reduction System	5.2
5.3.1	General classification	5.2
5.3.2	Analogue approach	5.2
5.3.3	Automatic stereo-compilation	5.3
5.3.4	Analytical approach	5.4
5.4	Selection of Data Reduction System	5.5
5.5	Analytical X-ray Photogrammetry	5.8
5.6	Co-ordinate System	5.9
5.6.1	Image co-ordinate system	5.10
5.6.2	Object space co-ordinate system	5.11
5.6.3	Sign Convention of co-ordinate system	5.11
5.7	Radiograph Orientation	5.11

	Page No.	
5.7.1	Orientation parameters	5.11
5.7.2	Interior orientation parameters	5.12
5.7.3	Exterior orientation parameters	5.12
5.8	Space Resection - A Basic Concept	5.15
5.9	Mathematical Formulation	5.16
5.9.1	Basic assumptions	5.16
5.9.2	Condition equations	5.16
5.9.3	Collinearity condition equations	5.17
5.9.4	Mathematical formulation	5.18
5.10	Systematic Approach for Calibration	5.22
5.10.1	Various approaches	5.22
5.10.2	On-the-job calibration and control points	5.23
5.10.3	Spatial co-ordinate measurement of control points	5.24
5.10.4	Linearization of observation equations	5.26
5.10.5	Method of least squares	5.28
5.10.6	Initial approximation	5.30
5.11	Space Intersection	5.31
5.12	Instrumentation for Analytical Data Reduction	5.32
5.13	Scheme of Computation	5.33
5.13.1	Major Steps	5.33
5.13.2	Image coordinate computation	5.34
5.13.3	Computation for orientation parameters	5.34
5.13.4	Statistical parameters	5.35
5.13.5	Object coordinates	5.36
5.13.6	Inter-active computer graphic programme	5.36

(1 plate and 29 figures)

		Page No.
CHAPTER 6	PLANE STRAIN TEST RESULTS	6.1-6.11
6.1	Introduction	6.1
6.2	Load-Deformation Relationship	6.1
6.3	Corrected Area and Volume Change	6.3
6.3.1	Corrected Area	6.3
6.3.2	Volume change	6.4
6.4	Plane Strain Compression Test Results	6.8
6.5	Stress-Instability	6.8
6.6	Discussion	6.11
	(13 figures)	
CHAPTER 7	MECHANICS OF DEFORMATION OF PARTICULATE MATERIALS	7.1-7.42
7.1	Introduction	7.3
7.3	Basic Test Data	7.4
7.4	Components of Deformation and their Relevance to the Deformation Mechanism	7.4
7.4.1	Deformation on microscopic level	7.4
7.4.1.1	Deformation of grains	7.5
7.4.1.2	Deformation of fabric	7.5
7.4.2	Macroscopic deformation	7.9
7.5	Reference State	7.9
7.6	Zones of Deformation in a Test Sample	7.10
7.7	Rotation of Particles	7.11
7.8	Data Processing and Presentation	7.12
7.8.1	Flow diagrams	7.13

	Page No.
7.8.2	Trace of tip of markers on a stereo-net 7.13
7.8.3	Displacement-rotation vector plots 7.13
7.8.4	Histograms and statistical parameters 7.14
7.8.5	Phi-rotation-dilatancy plots 7.14
7.9	Deformation Response of Granular Samples Under Plane Strain Compression Test 7.14
	Conditions
7.10	Strain Distribution Inside the Test Samples 7.19
7.11	Rotation of Particle - A Peculiarity of Granular Materials 7.21
7.12	Phi-Rotation-Dilatancy Rate Relationship 7.23
7.13	The Existence of Roller Particles - A Distinct Possibility 7.24
7.14	Formation of Zones of Deformation 7.28
7.15	Behavioural Trend of Deformation of Granular Samples 7.30
7.16	The Relevance of Particle Shape and Surface Friction on Deformation Behaviour of Granular 7.33
	Samples
7.17	Deformation Mechanism of Particulate Materials 7.36
	Including Cohesionless Soils
7.17.1	Deformation mechanism and observed stress- instability 7.42

(194 figures and 12 tables)

CHAPTER 8

	THE SIGNIFICANCE OF OBSERVED BEHAVIOUR WITH RESPECT TO CURRENT STRESS-STRAIN MODELS 8.1-8.12
8.1	Introduction 8.1
8.2	Relevance of Stress and Strain Concepts in Particulate Mechanics 8.2

		Page No.
8.3	Non-Co-axiality of Principal Stress and Principal Strain Increment Directions	8.6
8.4	Evaluation of Current Stress-Strain Models with Particular Reference to the Stress- Dilatancy Theory (14 figures)	8.10
CHAPTER 9	CONCLUSIONS AND RECOMMENDATIONS FOR FURTHER WORK	9.1-9.6
9.1	Summary and Conclusions	9.1
9.2	Recommendations for Further Research	9.5
APPENDIX A	ERROR ANALYSIS	A.1-A.11
A.1	General	A.1
A.2	Friction Tests	A.2
A.3	Error Propagation in Plane Strain Tests and in X-ray Photogrammetric Observations (2 tables)	A.3
APPENDIX B	COMPUTATION OF STRAIN AND DILATANCY (3 figures and 2 tables)	B.1-B.6
REFERENCES		15 pages R.1-R.15

CHAPTER 1

REVIEW OF PREVIOUS WORK AND OUTLINE OF PRESENT RESEARCH1.1 INTRODUCTION

Particulate material is consisting of a network or skeleton of solid particles, enclosing voids of varying size. The voids may be filled with a liquid and/or gas. Due to the presence of bonds (generally of any type) acting between the solid particles, the solid phase has a clearly definable fabric. Soils are the most widespread type of particulate materials. There are a number of familiar difficulties associated with the treatment of particulate materials in general and granular soils in particular. One of the major sources of difficulties is that they are not continua, and therefore, their macroscopic behaviour depends upon the nature of the inter-particle contacts and the movements and deformations of constituent particles at these contacts.

A soil engineer is often called upon to predict stress and strain behaviour of a granular mass. He is obviously expected to know the strength and deformation characteristics of such a material. Theories leading to an understanding of the actual process of deformation are, therefore, necessary to predict the soil behaviour.

The stress-deformation behaviour of particulate soils is not well understood. The lack of understanding arises primarily from the complexity of the physical properties of the granular soils. The strength-deformation behaviour of granular soils can be studied by using either of the two approaches: a) continuum approach, or b) particulate approach.

Although it was long recognized that the correct approach for the study of granular soils must be based on particulate mechanics, surprisingly very

little effort has so far been made in this direction. It is the object of this investigation to make a contribution in understanding the mechanical behaviour of particulate materials.

In order to describe the mechanics of granular soils and other similar materials various discrete models have been proposed. In these models, the constituent particles are generally assumed to be in direct, elastic contact with one another. The force-deformational characteristics of these contacts are then considered and ultimately this leads to the macroscopic stress-strain relations of the granular material. Most of these models and stress-deformation theories has already been reviewed in an earlier review by the writer (Sharma, 1972), here is a brief summary with attention being given particularly to work not mentioned in the earlier review.

Rowe (1962, 1963) proposed a "stress-dilatancy" theory. By analyzing the behaviour of regular packing of spheres and cylinders, he derived an energy ratio criterion for the critical angle of sliding between particles. Later he generalized it to apply to a random assembly of rotund and rigid particles. From his studies, Rowe postulated that the ratio of rate of dissipation of energy in the internal friction to rate of energy supply in the direction of major principal effective stress shall be a minimum. Horne (1965) employed a different approach to the mechanics of a random packing of rotund, rigid particles but his analysis gave results relating stress ratios and strain rate that are similar to Rowe's original analysis. However, Rowe's theory was criticized by Gibson & Morgenstern (1963), Roscoe and Schofield, Scott (1964), who questioned the mechanism of deformation used in his analysis.

In the last few years, some contributions have been made for the understanding of particulate mechanics of granular medium, notably by Oda and his co-workers (Oda, 1972a, b, c; 1974, 1975; Oda et al, 1972; Oda and Konishi, 1974a, b), Murayama and Matsuoka (1973), Murayama and Yagi (1965). Although Oda (1972, b) has observed from his own experiment that the rolling of particles is likely to be one of the mechanism of deformation, he and all the researchers mentioned above have ignored this observation and have assumed the same basic assumption as made by Rowe (1962) i.e. the deformation mechanism is primarily of interparticle sliding only, and the effect of rolling of particles, if any is negligible.

Some theoretical studies have been made by Mogami (1965, 1969) from the viewpoint of classical statistical mechanics. He and his collaborators (Mogami, 1966, a & b, 1967, 1968, 1969 a, b; Mogami and Imai, 1967, 1969; Mogami & Yoshikoshi, 1968, 1971) have obtained a relationship between the void ratio and the coefficient of internal friction. Mogami's method can be criticised on the basis of the arbitrary nature of the possible sub-volume porosities and the consequent application of statistical mechanics, Jowitt and Munro (1975).

Skinner (1969, 1975) showed that the mechanism of deformation is not only of sliding as was assumed by Rowe (1962), but it may accompany rolling as well depending upon the coefficient of surface friction. He concluded that "... when particle fracture is not a feature of the shear process, the shear strength of a mass of spherical particles is not a unique function of the interparticle friction." This conclusion is in variance with Rowe's observations.

1.2 SCOPE AND OUTLINE OF PRESENT WORK

Detailed literature survey and from this brief discussion it becomes apparent that very little amount of work has been done in this important field which has a wider scope of application not only in geotechnical engineering but also in other branches of engineering where granular materials are used for engineering purposes.

One of the main objectives of this research programme is to verify and to point out the inadequacies of the existing postulates of the deformation mechanism. Further it is intended to propose the most probable mechanism of deformation based on the experimental observations. There are various factors which affect the shear response of a granular sample, Taylor (1948). It is not possible to investigate the effect of all the variables on the deformation mechanism of the test samples. In this investigation our scope will be limited to study the effect of surface friction, surface hardness, degree of saturation and to a lesser degree of particle shape on the deformation mechanism of cohesionless material and keeping other variables practically constant. Attention herein will be confined to the response of granular test samples to external forces of deformation.

Since it is our interest to obtain the deformation mechanism of granular sample, it requires the study of movement of particles at various stages of deformation. In fact we have to use a suitable method "to see" the particles at microscopic level and without disturbing the test sample under shear. This will obviously require the need of new apparatus which are generally uncommon in the conventional soil mechanics laboratory. The selection of material, apparatus and testing technique is the subject matter for the Chapter 2.

It is generally believed that surface friction is one of the major physical properties of the constituent particles of the granular mass which plays the dominant role in the deformation response of the deforming medium. Chapter 3 deals with this important topic.

Chapter 4 and Chapter 5 describe the development and application of X-ray photogrammetry which is developed for the present investigation so as to trace the movement of particles, both linear and rotational, without disturbing the test sample.

The stress-strain behaviour (macroscopic) of all the test samples is presented in Chapter 6.

The data obtained from the experimental investigation of this study is re-processed for finding the possible deformation mechanism and also for the evaluation of existing mechanisms of deformation. Detailed discussions in support of the proposed mechanism of deformation along with the relevant observed data are given in Chapter 7.

The current stress-strain models are examined in Chapter 8. Summary, main conclusions and recommendations for further work are presented in Chapter 9.

Appendices A and B are also included. Appendix A gives the error analysis whereas Appendix B outlines the scheme of computation for the components of strain and dilatancy rate.

CHAPTER 2

TEST MATERIAL, APPARATUS
AND EXPERIMENTAL TECHNIQUE2.1 INTRODUCTION

In contrast to the continuum approach applied to the strength-deformation analysis of soil media, the experimental study of a granular medium based on particulate mechanics requires either a special equipment or testing technique of both which are usually uncommon in Soil Mechanics Laboratories. The materials selected and the new technique applied to study the deformation behaviour of granular masses at microscopic level are discussed in this chapter. Elaboration of the reasons for the selection of this particular technique is reserved for the chapter to follow. The reasons for selecting five test materials are discussed in brief in this chapter. An account of X-ray apparatus, X-ray layout and of the stereocomparator is also included. Finally the interparticle friction apparatus and testing procedures are described.

2.2 TEST MATERIALS2.2.1 Selection of Test Materials

The strength of granular materials may be said to consist of two major parts, the first part is due to interparticle frictional resistance, which is a combination of rolling and sliding friction, and a second part for which most common name is 'interlocking' (Taylor, 1948). For the study of deformational behaviour of granular masses, it is important to test real granular particles as well as model granular particles. In fact the success of the whole research programme depends on a judicious selection of test

materials. Whilst selecting the test materials, the following major considerations must be kept in mind, so as to widen the scope of this study as far as possible. The range of materials should be selected in such a way as:-

- i) to cover a wide range of friction (between 0.04 to 0.9) and surface hardness (between 2 to 7 on 'Mohs' scale),
- ii) to select such a material whose surface frictional properties could be changed easily by changing only the environmental conditions. The other mechanical properties of the material remain practically unchanged,
- iii) to include materials with different mechanism inducing friction behaviour or variation under varying conditions of normal load,
- iv) to have at least one natural material constructing a granular soil, and
- v) to have materials with different bulk characteristics e.g. brittle-fracture and visco-elastic materials under moderate pressure.

Every effort was made to select materials which could satisfy the above requirements, the following materials being the ones selected:

- 1) Gravel
- 2) Glass
- 3) Ceramic
- 4) PTFE
- 5) Polypropylene

2.2.2 Selection of Shape and Size of Particles of Test Materials.

The selection of shape and size of particles of test materials is as important as the selection of test materials themselves. The whole object of the experimental work is to trace the movement of at least a few particles of the test material, (these will be called marker particles or

simply markers in this study) forming the specimen at various stages of deformation during its stress-deformation study. The sizes of particles forming the test specimen must be large enough so that the spatial movement of marker particles can easily be traced. The marker particles are randomly selected from the particles of each test material. Another requirement, additional to the above, is the grain shape and size required by the interparticle friction tests. The particles must be large enough so that these could be held in the friction apparatus, described in section 2.12.

In addition to these two requirements imposed by the testing technique used here, other requirements are imposed by the various factors affecting the strength-deformation behaviour of a granular mass. The factors which are relevant to this section are geometric and packing characteristics of the samples which depend mainly on the particles' shape and size and their distribution. There are obviously numerous combinations of particle shape and size distribution which are possible. To investigate all of these combinations will be a formidable task. Hence efforts are made to reduce the number of variables as far as possible. It was therefore decided to use particles of single size, rotund in shape approaching spherical geometry and approximately fixed initial packing density of the test specimen. From these considerations particles of 5 to 7 mm in size (nominal) were selected. Real granular soil particles were rotund in shape. Out of the four model materials used in this study, particles of two test materials, namely glass and ceramic, were spherical in shape, the particles of the third material, namely polypropylene, were spheres whilst the geometric configuration of the fourth test material i.e. of PTFE was cuboid. The last shape was chosen to find out the possible effect of particle shape on the deformation mechanism of test sample.

Along with the shape and size of particles used, the initial packing of the test sample was also fixed. It was therefore possible to maintain approximately same level of interlocking in all tests except in the case of PTFE where the shape of particles was cuboidal. Plate 2.1 shows a photograph of the actual materials used in this study.

2.2.3 Material origin and properties

The origin and relevant properties of the five materials used in this investigation are given in Table 2.1.

2.3 SELECTION OF TYPE OF SHEAR TEST:

Various laboratory methods are available for obtaining the stress-deformation behaviour of granular materials including sands and gravels. Reference could be made to any standard text book on Soil Mechanics e.g. Taylor (1948), Bishop and Henkel (1962). In this work the plane strain test was selected for various reasons including the following:-

- i) Simplicity
- ii) Inexpensive
- iii) Simple for radiography
- iv) Ease to trace the movement of marker particles on radiographs since all the particles, theoretically speaking, move during deformation of the test specimen in a plane at right angles to the σ_2 -direction.
- v) According to stress-dilatancy theory the angle of internal friction ϕ_f lies between limits ϕ_{μ} and ϕ_{cv} depending on the type of test and initial porosity. Rowe (1964) has shown that ϕ_f approaches ϕ_{cv} for dense granular soils. Consequently the plane

- strain test removes another variable as it could be said that $\phi_f = \phi_{cv}$.
- 6) In many field loading conditions the shear deformations which may eventually lead to failure of a granular material occur mainly in plane strain test conditions e.g. failure of soil beneath a strip footing, failure of long retaining wall etc. The test condition chosen therefore approximates many practical situations.

2.4 PLANE STRAIN APPARATUS

2.4.1 Preliminary Considerations and Basis of Design

While discussing the requirements of a general soil testing apparatus Hambly & Roscoe (1969) listed simplicity of operation, interchangeability of the principal stress directions and suitable range of available strain as the basis for the design; ease in radiography of the test specimen during the test and minimal effects of platen interference on radiography may be added to this list. However, the writer is of the opinion that it is, at least for the present, neither feasible to construct a single apparatus satisfying all the requirements nor absolutely essential for the present work to have such a machine. It is, therefore, better to have a machine, which is custom made, suitable for a rather narrow set of boundary-loading and -deformation conditions, of course, constructed at the expense of versatility. Consequently an apparatus was designed and constructed to test cuboidal samples of coarse granular materials under only plane strain conditions.

The plane strain test apparatus conceived and designed was relatively simple. The sample, prismatic in shape, was tested under plane strain conditions through two pairs of rigid platens and one pair of flexible platens. The displacements and hence the strains across the axial top and bottom platen were measured both from direct measurements of displacements of the

bottom relative to the top fixed platen by means of a displacement transducer and also from the stereo-radiographic measurements. In order to eliminate the effect of membrane penetration on volumetric strain calculations, a radiographic method was used to obtain lateral strains and thus the volumetric strains on the assumption that no overall linear strain occurred in the σ_2 direction i.e. the lateral σ_2 -platens were absolutely rigid and did not deform or displace laterally during the test. The vertical deviatoric stress was calculated by dividing the total axial load, measured across the top and bottom platen by a load cell fixed on the top platen, by the X-sectional area calculated from the stereo-radiographic measurements. The stress across the flexible platens was always equal to the suction pressure acting inside the test specimen which was measured by means of a pressure transducer. No attempt was made either to measure the stress acting on the lateral rigid platens or to measure the stress distribution across both pairs of rigid platens; instead the assumption was made that each platen imposed a uniform normal stress on the sample and that this was always a principal stress. The validity of this assumption will be discussed in Chapter 8. As a consequence of the assumption that no shear stresses occurred at the rigid platen - soil interfaces, the principal stress directions coincide with the orthogonal axes of the test sample.

2.4.2. Specimen Size

Having selected the size of the particle and grain size distribution of the granular mass to be tested in the plane strain test, the next stage is the selection of sample size. Ideally speaking the sample must be of the largest dimensions, but practical considerations restricts such a choice. While selecting the size of the test specimen, the effect of the

following major variables must be taken into consideration a) particle size
b) sample-platen interference and c) radiographic considerations.

a) Ratio of Specimen Size to Particle Size:

The ratio of specimen size to particle size (d_s/d_{max}) affects the stress-deformation behaviour of the test specimen. This factor influences the stress-strain behaviour of granular material in different ways depending upon whether the granular material is a mixture of different size particles or uniform. In the first case the strength characteristics will increase with the reduction in d_s/d_{max} ratio which is caused by the interference between the larger particles.

In the latter case the strength characteristic of the test sample is expected to decrease. The main reason being the non-uniform distribution of voids in the whole specimen. This disturbance of non-uniformity in voids extends about 2 to 3x grain diameters from the boundaries inward, see Verman & Banerjee (1946). The non-uniformity in voids ratio pulls down the strength up to certain d_s/d_{max} ratio and then with increase in this ratio does not significantly affect the strength characteristics of the test sample. El-Ruwayih (1975) suggests, based on the findings of various investigations, that the d_s/d_{max} for uniform materials should be approximately 16 and 4-5 for well graded soils. The difference between the values of d_s/d_{max} for the two extreme limits of gradation of granular materials is worth noting.

The minimum dimension of the test specimen used in this series was 97.5 mm which gave the value of d_s/d_{max} for all the test materials in the range of 15 to 17.

b) Specimen - Platen Interference

In any shear apparatus which involves the loading of small samples across their boundaries the interference between the loading platens and the specimen and between the adjoining platens, must have a considerable influence on the observed behaviour. The influence of this factor can be minimised either by providing frictionless platens (Green, 1969; Reades, 1972; Rowe and Barden, 1964), or by selecting a suitable sample size such that the effects of rough platens are small or by placing load sensing devices into the platen face that are capable of measuring both normal and shear stresses (Roscoe, 1970).

Evidently the solution to this problem of inter-platen interference hinges on the proper design of apparatus to prevent collision between adjacent platens during deformation and without having to provide large gaps. In the case of plane strain tests, which were performed in this investigation, the situation is simplified since one pair of platens must remain at a fixed spacing and the other pair of axial platens can be arranged to move inside the fixed pair. Even so some gap must inevitably be provided. However, this small gap does not present any serious problem as the test particles were large, about 6-7 mm in diameter, in comparison to the gap of 1.0 mm provided.

c) Radiographic Consideration

In addition to the two variables mentioned above, a third factor which is equally important is the radiographic consideration. The thickness of test specimen which could be used is governed by the penetrating power of X-radiation and the maximum time of exposure per radiograph acceptable under given constraints, which are discussed in Chapter 4.

In an effort to satisfy the above requirements, a cuboidal test specimen

of nominal size of 100 mm cube was used in the present series, with lubricated 'frictionless' end platens. The use of a cubical sample has other advantages too. First, in addition to obtaining a more homogeneous sample, it almost eliminates the possibility of buckling and tilting. However, it imposes a stringent requirement on the design of test apparatus namely the friction between the interacting sample faces and loading platens must be as small as possible, though its total elimination is ideal. Secondly if this investigation is extended at a later date to include the effect of the various stress-paths and boundary stresses or deformation conditions, (most of the so-called "Independent stress controlled" triaxial apparatus use cubical test samples, Green (1969), Arthur and Menzies (1972) Ko and Scott (1967)), the results obtained and presented here could be used and even the apparatus could be readily modified.

2.4.3.1 Axial Platens

A pair of enlarged polished perspex platens, shown in Plate 2.3 (c) were built. These platens were made about 12 mm longer in σ_3 -direction on either side of the sample so as to conform to the recommendations made by Bishop and Green (1965) and also by Rowe and Barden (1964) for obtaining "frictionless end platens". Porous discs of coarse Carborundum porous stone, 19 mm in diameter were used in both axial platens to permit drainage and, measurement and regulation of σ_3 . Also to allow water to be circulated should any air bubbles be trapped either in the leads or in the test sample after the sample preparation in fully saturated plane strain tests. These porous stones each placed 1.5 mm proud of the polished surface of the platen to facilitate placing of lubricating rubber sheets of the frictionless ends and to avoid partial covering of the porous stones during the deformation stages by these rubber membranes.

An I.C. load cell of high sensitivity was securely connected to the

top platen by means of a stud to ensure that the latter could not tilt and that essentially uniform overall axial deformation was applied to the specimen during the compression test. The bottom platen was seated on the aluminium plinth which was bolted to the moving ram of the loading frame. The orientation of this platen was fixed with the help of four locating pins provided in the plinth plate and corresponding matching holes in the bottom platen.

In addition to the porous stones on the faces of the loading platens in contact with the sample faces, each face of the top and bottom plates carried tungsten markers embedded in them in two lines at right angles to each other and parallel to σ_2 - and σ_3 - planes respectively, as shown in Plate 2.3 (c). The images of these marker wires on the radiographs were used in the X-ray photogrammetric calculations, see Chapter 5.

2.4.3.2 End Platens

In order to attain plane strain conditions the sample must be confined between two parallel plane sheet walls of material which fulfil the requirement of a) rigidity, b) low coefficient of friction with the test sample, and c) transparency to X-rays. These requirements were satisfied within practical limits by using a pair of polished perspex end platens of adequate rigidity. The use of perspex end platens fulfilled the last two requirements, but not the first, theoretically speaking. However, every possible step was taken so as to make these platens rigid and at the same time keep them transparent to X-rays. Marachi et al (1969) have shown that the strength of an imperfect plane strain sample in which a small amount of strain (less than about 0.85% for a test sample with initial void ratio of 0.65) is allowed does not differ materially from the strength of a perfect plane strain specimen, see Fig. 2.1. The effect of the very small bulging of the plane strain test sample was small and hence will not be

considered in further discussions, particularly for two reasons; firstly the strains in the σ_2 -directions by bulging of each platens were very small due to very low confining pressure of less than 70 kPa used in the present series and secondly, all the tests reported here were conducted under roughly the same confining pressures so the effect of bulging of the end plates will be of same order of magnitude in all the tests. The bulging of end platens was minimised by using stiffening plates in addition to the four stainless steel tie bars, see Plate 2.2 and Plate 5.1(a).

These end platens were linked with each other by the four tie bars mentioned above. Four spacers in conjunction with the tie bars were used to keep the two platens parallel to each other and at the same time at the required fixed distance apart. The base of the σ_2 -platens was connected to the plinth platen by a lever arrangement so that the mid point of the σ_2 -platen and of corresponding sample face was nearly coincident at all stages of a test.

2.4.4 'Frictionless' Ends

Various methods for reducing the effects of friction between soil specimen and rigid platens in contact are available. These include the provision of platens with deformation properties similar to the material being tested, a choice of sample dimensions such that the interference effects have a negligible effect on the properties being measured or the provision of a frictionless interface between the two interacting bodies i.e. between soil grains of the sample and the rigid platens. For the reasons mentioned earlier, cubical samples were used in this study. For simplicity and for minimal interference in radiography, the second method was preferred, namely interposing a "frictionless" interface.

In case of sands the "frictionless" interface is generally obtained by interposing a single sheet or more than one sheet of thin rubber membranes with some kind of lubricating agent applied on the surfaces of these membranes except that which is in direct contact with the soil or granular material forming the test specimen (Green, 1969; Reades, 1972). For relatively short term tests on sands, most of the researchers, including Green (1969), Reades (1972), Rowe and Barden (1964) prefer to use a very thin smear of silicone grease. In the plane strain tests, whose results are presented here, high vacuum silicone grease manufactured by Midland Silicone Ltd., U.K. was used.

Since the size of particles used in the test specimens is much larger than that of sands, even two layers of this rubber sheets with silicone grease as the lubricating agent did not give satisfactory frictionless ends as the particles embedded themselves and squeezed the lubricating agent out and thus reduced its efficiency. In order to obtain frictionless ends, either an increase in the number and thickness of rubber sheets which, in turn, will show large bedding strains; or the use of a rubber sheet which is modified so as to distribute the contact loads over a larger area are two alternative approaches. The second alternative was used for obvious reasons. The rubber membrane was reinforced by sticking 6 mm wide and 1.0 mm thick strips of plastic across the width of the rubber membrane. In other words the length of the plastic strip was parallel to σ_2 -direction when it was placed on the axial platens and therefore was perpendicular to the direction of major movement of the granular particles. This gave freedom in the direction of movement as well as the required rigidity and thickness for load dispersion onto a larger area. Further by using these plastic stripped rubber sheets over a thin rubber membrane with a very thin smear of a lubricating agent, we were able to obtain very satisfactory results

and we minimised the bedding error. This rubber membrane is shown in the inset of Fig. 2.2 and in Plate 2.3 (b).

2.4.5 Loading, Sensing and Monitoring Systems

2.4.5.1 Lateral Loading and Sensing System

Lateral pressure was applied to the test sample by suction acting from inside the rubber membrane confining the sample. The fluid suction, giving a confining pressure, was generated by connecting the sample to a vacuum pump. However, a suction controller made by Edwards Vacuum Components Ltd., Crawley, Sussex, was interposed between the sample and the vacuum pump at a suitable point so as to maintain constant vacuum and thus the σ_3 -stress. The σ_3 -stress was measured by an electrical resistance pressure transducer made by Bell and Howell (designated type 4-306-0131-03MO). For the test on saturated samples, zero was set on the transducer read-out system when the water in the cell was at the mid-height of the sample. Since the lateral stress was applied through a flexible platen and was maintained constant throughout the test, corrections for any reason were not made.

2.4.5.2 Axial Loading and Sensing System

Here the test sample was compressed in the axial direction and its response was measured in the axial direction in the form of deviatoric force. The axial deformation was generated by pushing the lower platen against the

deforming sample but keeping the top axial platen and the load cell attached to it in a fixed position, the displacement of the bottom platen was sensed electronically by a displacement transducer. The deviator force in the axial direction was sensed by means of I.C. Load Cell fixed with the upper axial platen.

2.4.5.3. Electronic Monitoring System

The signals from the three sensing elements namely load cell, pressure transducer and displacement transducer were fed to transducer meters for necessary processing. The output from these transducer meters were either read directly or fed to a x-y recorder for recording them. Out of the three signals mentioned above, the signals from load cell and from the displacement transducer were continuously recorded by a x-y recorder, made by Leeds and Northrup, U.K. and the pressure transducer readings were noted directly.

2.5 Material Preparation

The frictional behaviour of contacting solid bodies depends on various factors; the major factor being the surface conditions of the contacting surfaces. The surface condition of a body can broadly be treated under two main headings: a) surface topography and b) surface cleanliness. The reproducibility of surface friction test results, in particular, and success of proper evaluation of the experimental study rests on this major variable. It can, therefore, be said that the primary requirement for this study is to have the same surface conditions for all particles used either in the plane strain test specimen or in surface friction test.

2.5.1 Surface Topography

Surface topography or surface roughness affects the friction coefficient of brittle materials, Byerlee (1970), but does not affect significantly the frictional characteristics of polymeric material providing the roughness is not excessive. It is, therefore, essential that the constituent particles forming the test specimen must be as far as possible, identical. Evidently careful preparation of surface finish of the particle cannot be over-emphasized. However, no additional treatment for three out of five test materials used in this study, namely a) natural rotund gravel, b) polypropylene sphere and c) PTFE cuboids, was considered necessary. In these cases either the material was taken from the natural environment i.e. beach gravel, or particles were made under identical conditions. In the latter case the possibility of their surface topography getting altered since their manufacture to the time they were actually tested in the laboratory, was remote.

The surface treatment was, therefore, applied to remaining two brittle materials namely glass balls and ceramic balls. It must be emphasized that the surface treatment was not given to make them absolutely smooth but to bring the roughness on all the particles to the same level.

The glass balls were first roughly grounded by rolling the particles with Carborundum powder of 240 grit size for 12 hours. Then thoroughly washing them and finally polishing them by rolling them at slow speed with rouge powder for 24 hours. The same procedure was repeated for ceramic balls.

2.5.2. Surface Cleanliness

In addition to surface roughness, surface cleanliness or presence of surface contamination does affect the surface friction of a particle. Further the variation in the degree of surface cleanliness from particle

to particle will affect the reproducibility of friction test results and finally in their evaluation. Accordingly surface cleaning of the particles was carried out meticulously and every effort was made to keep the same degree of cleanliness throughout the test programme.

The method of surface cleaning was standardized and was applied to every material whether its particles were subject to surface treatment or not. The whole operation of surface cleaning was carried out in the following steps:-

1. Particles were first washed with ordinary detergent and thoroughly rinsed under running tap water.
2. Particles were then soaked for 24 hours in 10% solution of Decon 90 concentrate in distilled water.
3. Washing them thoroughly with distilled water.
4. Repeating step 2 and 3 again.
5. After the final thorough rinse of particles with distilled water, the particles were stored in deaired distilled water and were always kept under water unless required for dry tests.

During the whole cleaning operation and thereafter the particles were never touched by bare fingers or allowed to come into contact with any greasy surface. The cleaned particles were handled with utmost care either by using degreased hand gloves or forceps.

2.5.3 Drying of Particles

The particles for the tests with zero degree of saturation were prepared by first oven drying the cleaned particles for 12 hours. Then the particles were allowed to equilibrate in laboratory atmospheric conditions. However, effort was made to avoid the particles getting contaminated from the floating dust particles and other floating impurities in the air by covering the particles by two layers of tissue papers.

2.6 MARKER PARTICLES

There is another important factor which contributes towards the success of this study. It is the preparation and proper placement of representative particles, called here marker particles or simply markers, in the test specimen and then following their movement throughout the history of specimen deformation. The marker particles must satisfy the following conditions:-

- a) The marker particles must be of same shape, size, material and identical surface smoothness
- b) The X-ray images of these particles must be recognizable, and
- c) Some form of axis must be present so that their rotation in space could be determined.

The condition (a) was fulfilled by random selection of particles from the test materials. These randomly selected particles were made recognizable on radiographs by inserting cylindrical tungsten wire 5 to 6 mm long and 0.5 mm in diameter in glass, gravel and ceramic particles and of 1 mm diameter in PTFE chunks and polypropylene spheres. The embedded tungsten wire served two main purposes:-

(a) to identify these particles on radiographs, and (b) to indicate the local orientation of the particle. (Every care was taken to place the tungsten wire centrally so that the centres of gravity of tungsten wire and particle coincide.)

It was found practically impossible to keep the surface of markers undamaged. Part of the surface of markers had to be destroyed by drilling the hole which was needed for the insertion of the tungsten wire. However, care was exercised to keep the diameter of the hole to the minimum size and not drilling a through hole and thus minimising

surface area damaged by drilling and by filling the hole after the tungsten wire was placed in it. Typical area ratio of the damaged surface to the surface area of the particle was of the order of $1/400$.

2.7 X-RAY SET-UP

The first part of the experimental X-ray photogrammetry was carried out at A.Q.D. Laboratories, Harefield, Middlesex. The X-ray set-up used in the present study along with that used for the plane-strain tests is schematically shown in Fig. 2.2 and general layout is shown in Plate 2.2.

The X-ray equipment used was an Industrial type made by Pantak Dunlee 150 kV constant potential, continuously rated at 5 mA when operated at 150 kV. The X-ray head had a dual focus but fine focus of 0.5 mm with beam angle of 20° was used. The H.T. generator of the X-ray unit was Greinacher type which emitted a very low percentage of soft radiation.

Industrex 'M' film made by Kodak Ltd., U.K. was found to give the best results and was used for all radiographic work carried out and reported here. The exposure time, KV and current were adjusted for every test. The most suitable combination of these parameters was obtained by running trial runs on the test specimen under actual conditions.

The processing of the exposed film was standardized for all tests and irrespective of the type of material used. In fact all exposed films were processed in an automatic film processing unit, PAKOROL XU, supplied by Agfa-Gevaert Ltd., U.K. The temperature and developing process was automatically controlled. The processing time, including developing, fixing, rinsing and drying was about 8-10 minutes.

2.8 LATEX RUBBER MEMBRANE

For the plane strain test, a special rubber membrane was required to fit the shape of the pedestals and specimen, this was done so as to

minimise the unknown confining effect of the rubber membrane had a conventional cylindrical membrane been used. Plate 2.4 shows the actual mould used for making the latex rubber membrane. It may be noted that the mould was made about 10% larger in every dimension than was needed for the finished and properly cured latex membrane. The membranes were formed by adopting the cold casting technique of latex rubber. By this process membranes of thickness of about 0.40 to 0.50 mm (.015" - .020") were made. The rubber membrane was properly cured before it was actually used.

2.9 TEST SPECIMEN PREPARATION

The method of test specimen preparation adopted here was used in a rather standardized way in all the tests carried out in this study. The specially prepared latex rubber membrane was first placed on the lower axial platen and secured to it. In order to minimise sample disturbance at the time of dismantling the sample former after the sample was formed, a special former was designed and made in perspex, see Plate 2.5. This former can be disassembled without disturbing the sample. This sample former was used in forming the sample of required size. Once the former was placed in its proper position and properly secured to the plinth plate on the ram of the test frame, the rubber membrane was folded over it. The particles were deposited in the sample former in three layers of approximately equal height and each layer was tamped 25 times by a tamper. Finally the top finished face of the sample was carefully made parallel to the base by removing excess particles. All the samples obtained by this technique gave almost same overall porosity.

Method of Placing Marker Particles:

Two very thin steel plates were used to guide the marker particles in a near vertical mid plane parallel to the σ_2 -platen. These two steel plates were placed in centre and parallel to σ_2 -platens with a cavity of width slightly greater than the size of particles. In this cavity the marker particles were placed nearly to the same height as that of the adjoining layers on either side of the cavity. So as to eliminate the possibility of formation of non-uniformity caused by deposition of markers between the two plates, the parallel plates were pulled up after the markers were deposited and then the layer formed by markers of ordinary particles were tamped as outlined above. This process was repeated for the three layers. A typical sample, as prepared by the method outlined above is shown in Plate 2.6 (a) before the test and in Plate 2.6 (b) after the test.

2.10 TEST PROGRAMME

The testing programme envisaged to achieve the main objectives outlined in Chapter 1 consisting of two test series on all the five materials selected for the investigation. In the first test series, all the materials were tested under laboratory air-dry conditions and under two confining pressures of about 35 kPa and 70 kPa. In the second series of tests, tests under similar conditions, but with fully saturated test specimens, were carried out. In every test between 7 to 8 pairs of stereo-radiographs were taken for X-ray photogrammetric analysis. Although all the four sets of the two test series were completed, only one set each of the two test series were analysed because the stereo comparator was available only for a limited time. However, this reduction in number of experiments included here should not in any way affect the findings of

this investigation. The data for these experiments was analysed and is presented here. Table 2.2 gives the important details and nomenclature of these tests. The identification of tests, as mentioned in this table, will be used throughout this thesis.

2.11 INSTRUMENTS USED FOR DATA REDUCTION

One of the major equipment used for the data reduction stage of the X-ray photogrammetry was a precision stereocomparator. This instrument and its ancillary apparatus are available at the Surveying and Terrestrial Photogrammetry section of the City University and was used for reading the stereo-radiographs. This stereocomparator is made by VEB Carl Zeiss Jena of G.D.R. and marketed under the trade name of "Stecometer". Plate 2.7 shows the stecometer and its peripheral equipment. The reading accuracy of the stecometer was 0.001 mm and mean square coordinate error of $\pm 1.0 \mu\text{m}$. The output from the stecometer, that is the image coordinates and their corresponding parallaxes, were obtained in the form of punched paper tapes and typewritten output as well. These punched paper tapes were used as input to the other equipment used in the data reduction namely high speed electronic digital computer. The computer facilities available at Imperial College Computer Centre as well as University of London Computer Centre (ULCC) were extensively used for data reduction and for other numerical operations.

2.12 INTERPARTICLE FRICTION APPARATUS

This apparatus is comprised of three main units:-

1. Mechanical System,
2. Loading system, and
3. Electronic Monitoring System.

The basic instrument was designed by Skinner (1975). Its mechanical system was modified by the writer to suit the particle size tested. Further the electronic monitoring system was improved, firstly by using high speed chart recorder and secondly continuously recording the output signals of the load cell and that of the vertical displacement transducer. The basic apparatus is shown in Plate 2.8 and its layout in Fig. 2.3.

Mechanical System:-

This system consisted of a special device for holding the particles in a given geometric configuration, an electric motor and other arrangement for reducing its speed as well as for converting the rotational motion of the low speed shaft of the reduction gear to translatory motion of the lower carriage. This lower carriage was used to hold either the two particles forming the valley in which the upper particle slides or for holding the plane surfaces. A pair of stiff springs was used for quick return back movement of the carriage particularly when the direction of rotation of the electric motor was reversed. In order to minimise the friction as well as any possibility of the seizure of the lower carriage, the needle bearings were interposed between the base of the carriage and the steel travel race. The carriage carrying the lower particles or plane surface was pushed or pulled at a constant linear speed of 0.028 mm/sec.

The lower carriage, see Fig. 2.3, incorporates a special vice which was used to hold a block of flat surface or a pair of particles secured with the body of the lower carriage so that the line joining the centre of particles were at right angles to the direction of movement. Further, in this new mechanical device it was possible to raise or lower the lower plane surface or the pair of lower balls fixed in this vice. The upper

particle or ball was clamped in a chuck attached to the tangential force measuring system i.e. load cell, see Plate 2.8 and Fig. 2.3.

Loading System:-

The load cell was used to serve two purposes. Firstly to carry out its primary work for which it was used namely to measure the friction between the two sliding surfaces. Secondly, it was used to provide the required normal force at the contact surfaces of the particles. A very simple arrangement, see Plate 2.8, was used to apply the vertical force to the grain configuration.

The friction apparatus was completely isolated from the electric motor, which was the main source of vibrations, by placing the main friction apparatus, electric motor & reduction gears on separate tables with rubber dampers interposed between their bases and table tops. The torques from the motor and from the reduction gears were transmitted through universal joints with rubber dampers so as to absorb as much vibrations as practicable.

The basic friction apparatus was covered during the test so as to minimise the contamination and thus maintain controlled condition as far as possible.

Electronic Measuring and Monitoring System:-

The frictional resistance was measured by an inductive displacement transducer manufactured by Boulton Paul Aircraft Ltd., which was mounted in the load cell and was energised from a carrier source generated in a transducer meter type C61 made by the same firm. The response from the transducer was fed back to the C61 transducer meter, and then the remaining

unbalanced voltage was fed to one of the channels of the multipen 'Leeds and Northrup' Speedomax chart recorder. This recorder had a full scale deflection for input signals of, in steps of, 2 mV, 10 mV, 20 mV, 50 mV and 100 mV.

The vertical movement of the top ball or particle was monitored by another induction type of transducer and connected to the chart recorder in a similar way as described above.

By employing the electronic sensing and monitoring system, higher accuracy in measuring the friction resistance and in finding the topmost point of the friction track or in tracing the movement of the ball on the flat surface, was attained.



Gravel Particles

Glass Balls

Ceramic Balls

PTFE Chunks

Polypropylene Spheres

Plate 2.1 TEST MATERIALS

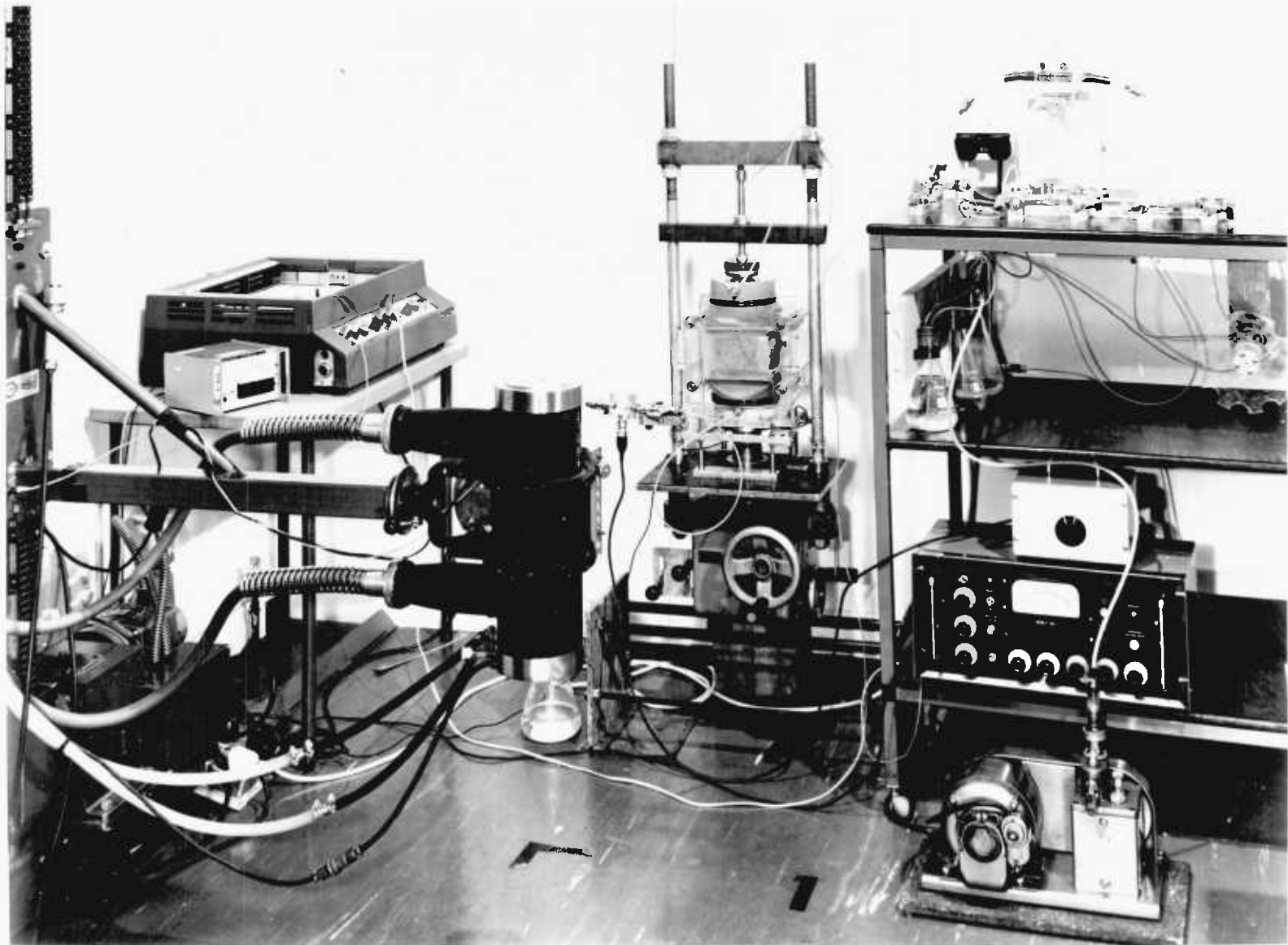
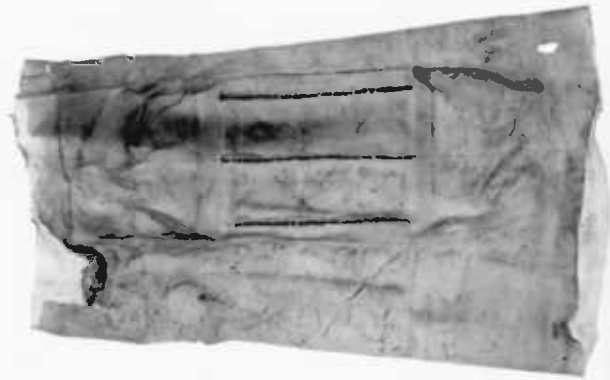
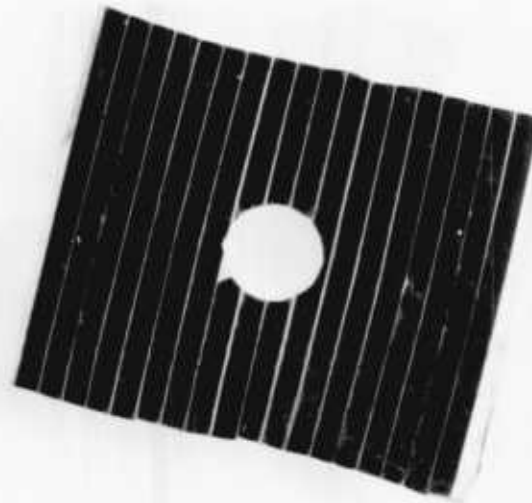


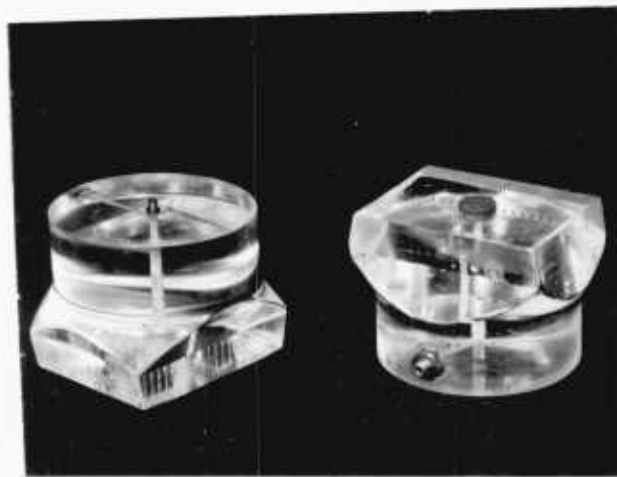
Plate 2.2 GENERAL LAYOUT OF PLATE STRAIN TEST APPARATUS AND X-RAY DATA ACQUISITION SYSTEM



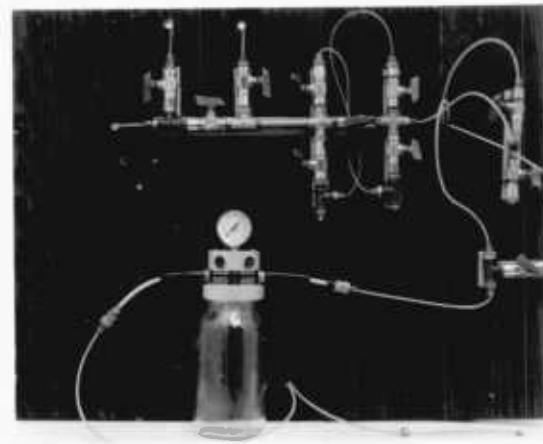
a



b



c



d

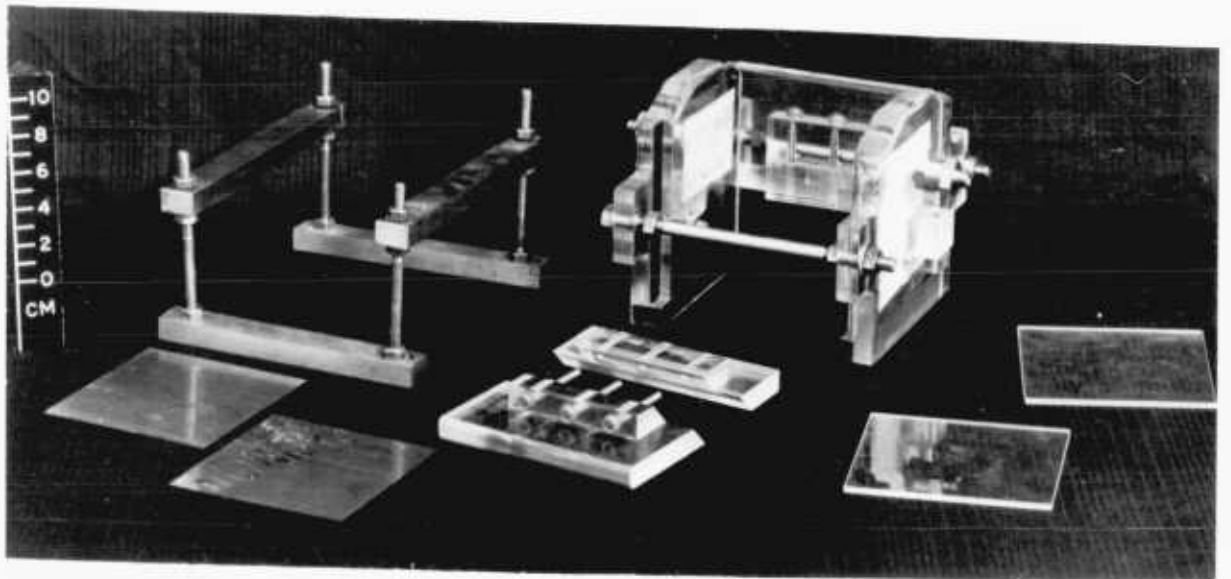
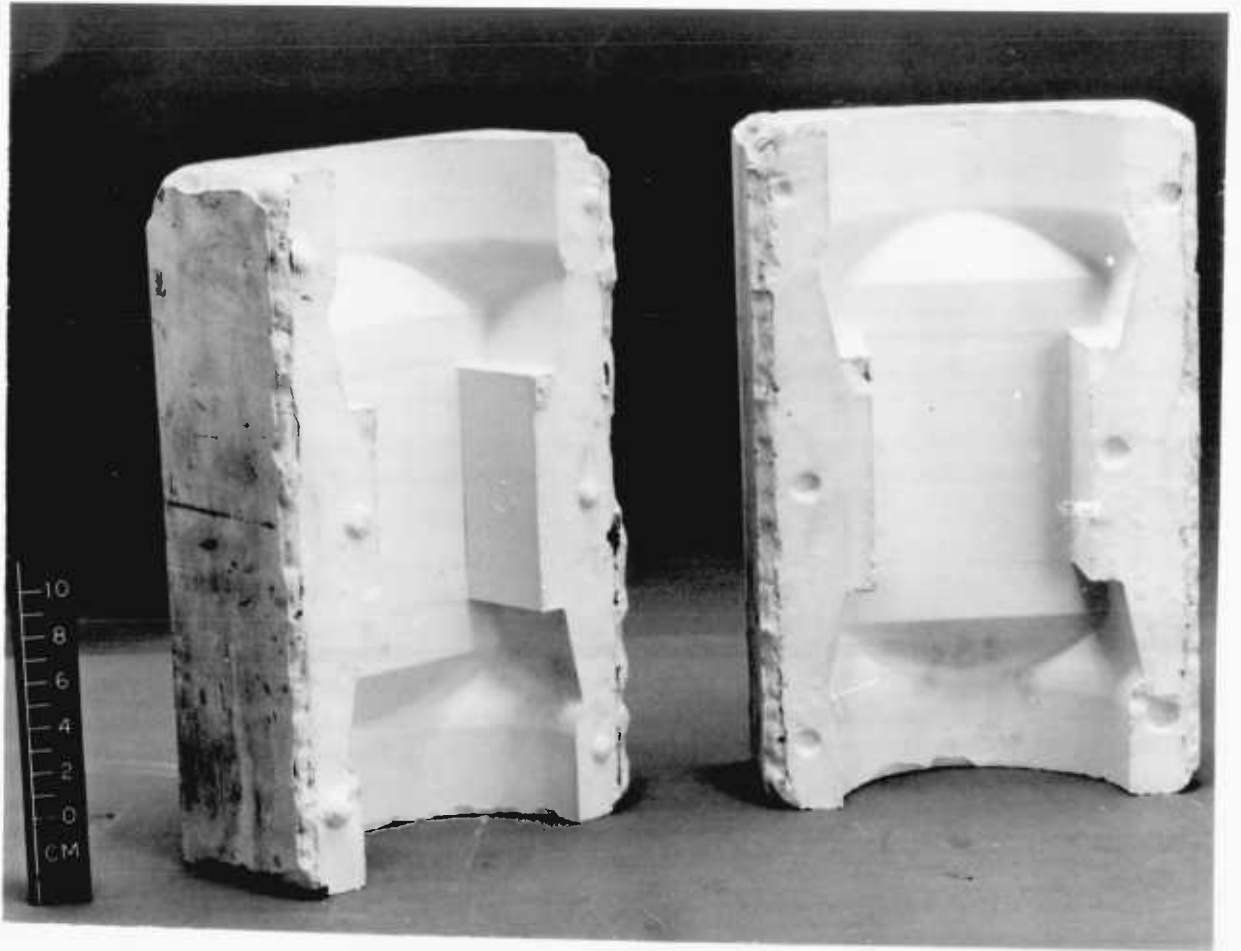


Plate 2.4 RUBBER MEMBRANE MOULD (TOP)

Plate 2.5 SAMPLE FORMER (BOTTOM)



a. Before test



b. After test

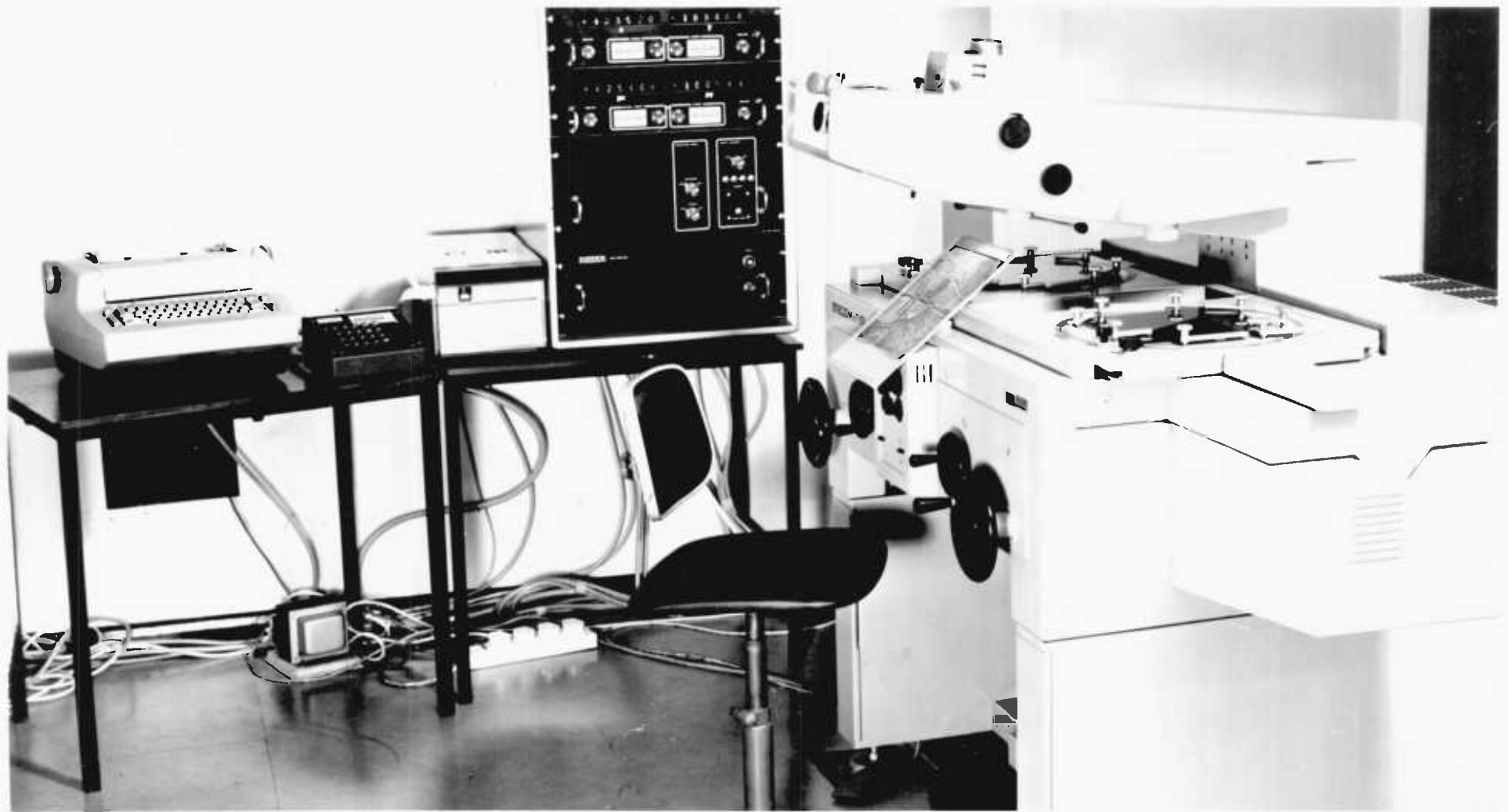


Plate 2.7 STECOMETER AND ITS PERIPHERAL EQUIPMENT

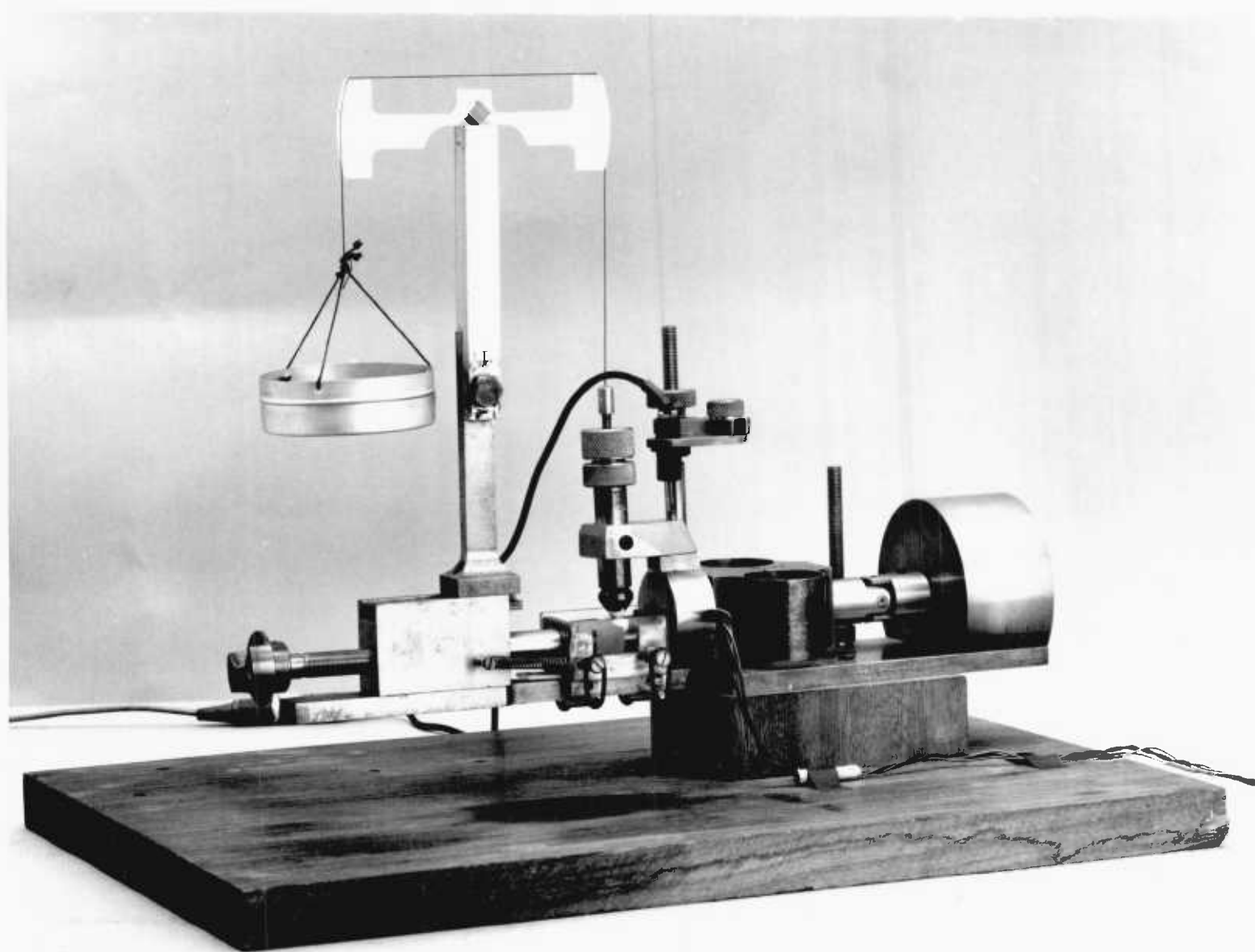
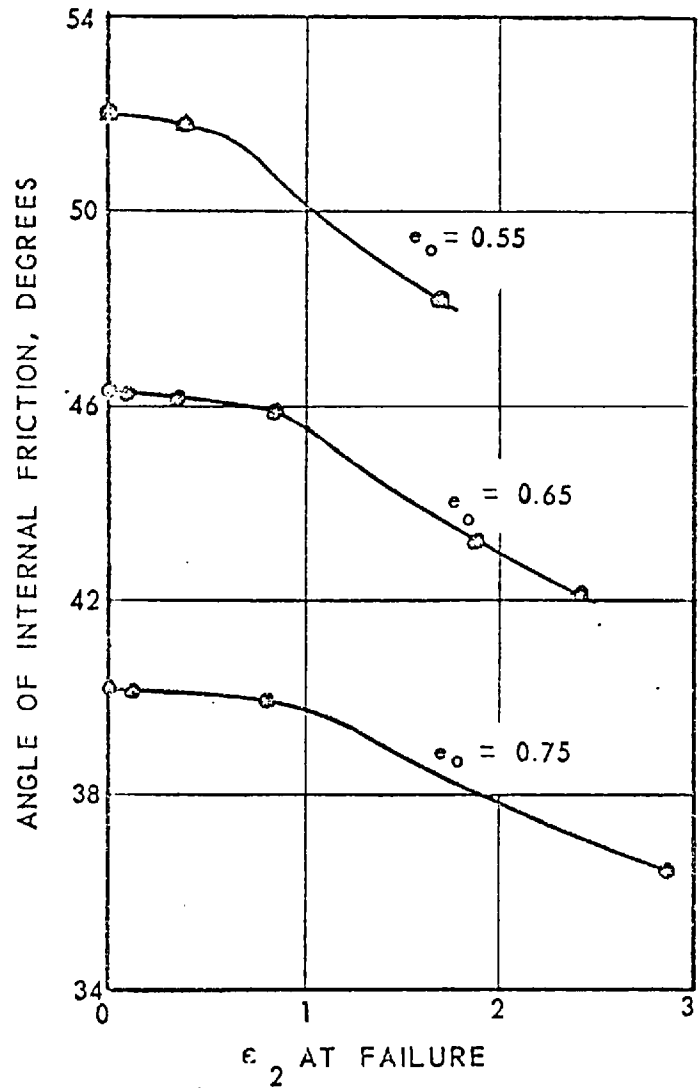
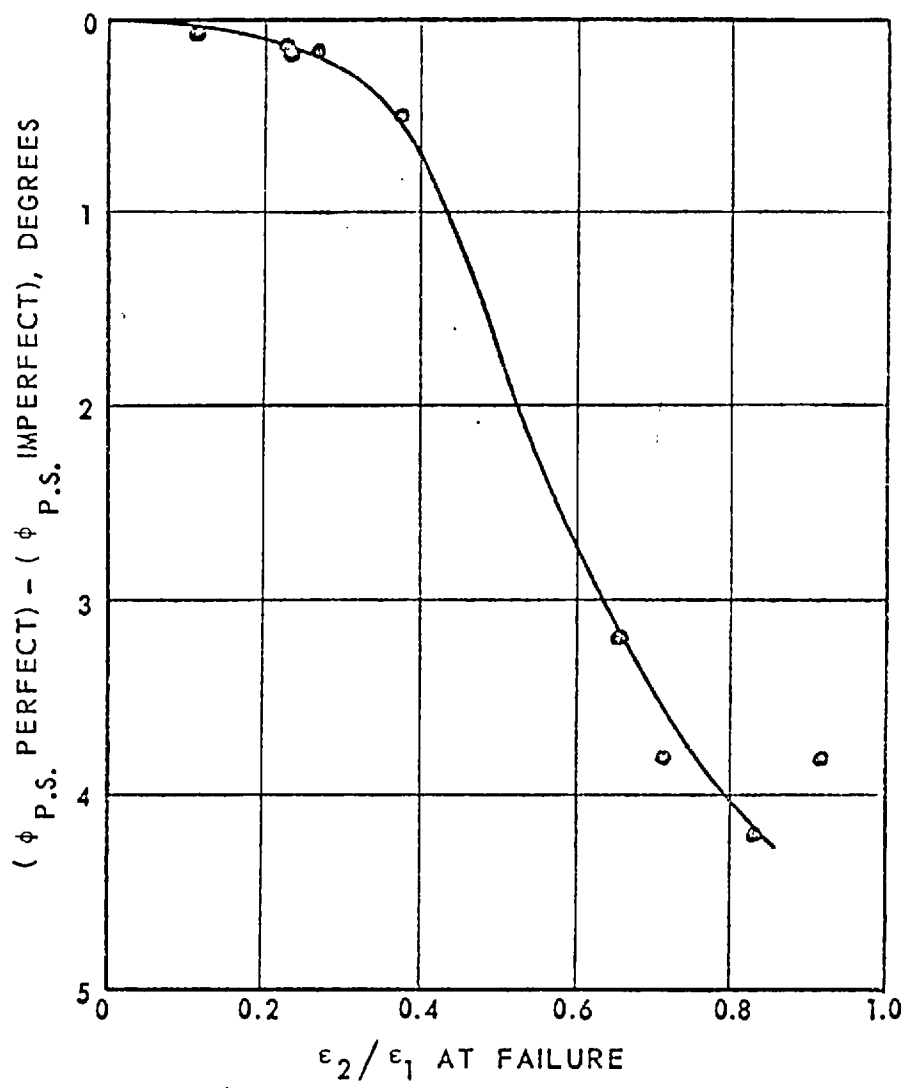


Plate 2.8 INTERPARTICLE FRICTION APPARATUS



a) VARIATIONS OF ϕ WITH ϵ_{2f}
 FOR MONTEREY #20 SAND, $\sigma_3 = 10$ PSI



b) SIGNIFICANCE OF STRAIN CONDITION
 AT FAILURE

FIG. 2.1

After Marachi et al , 1969.

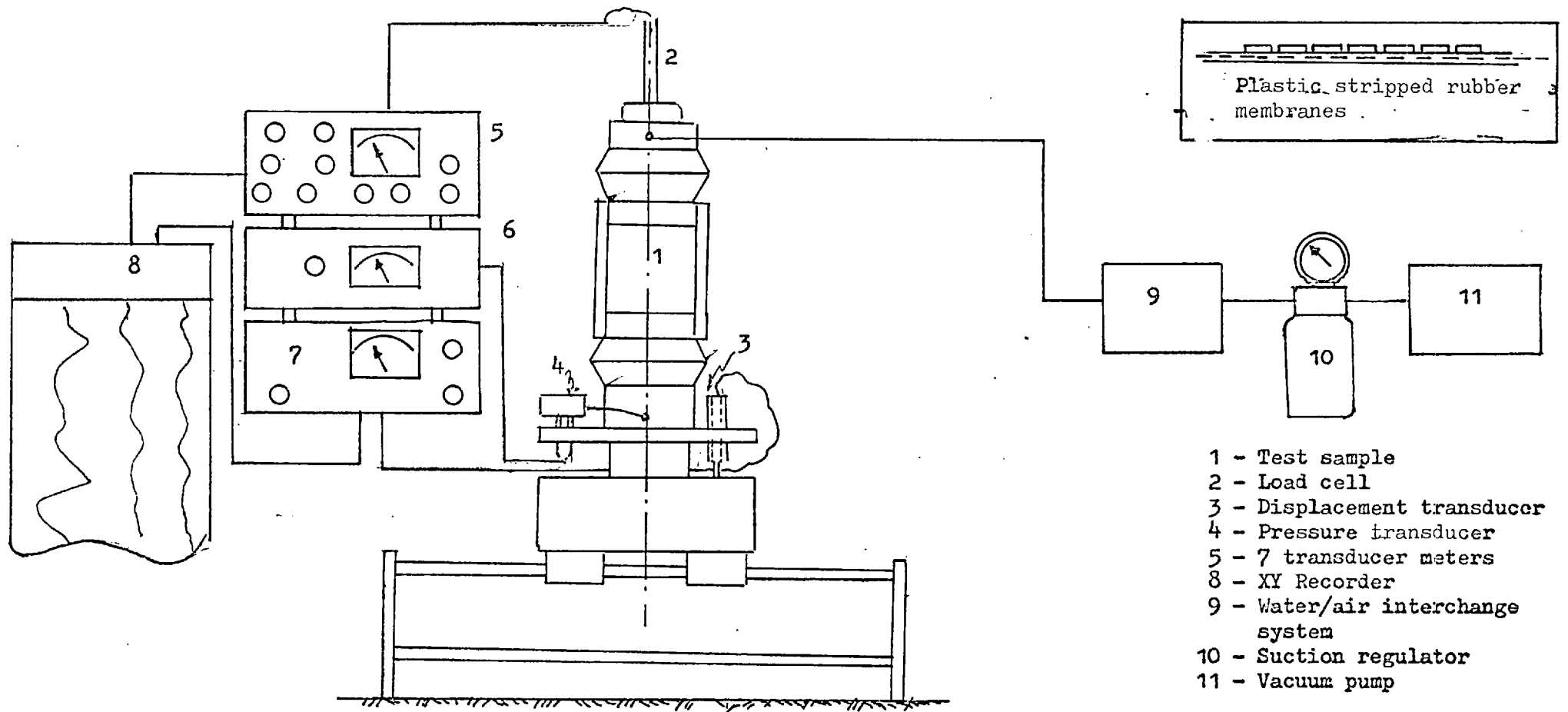
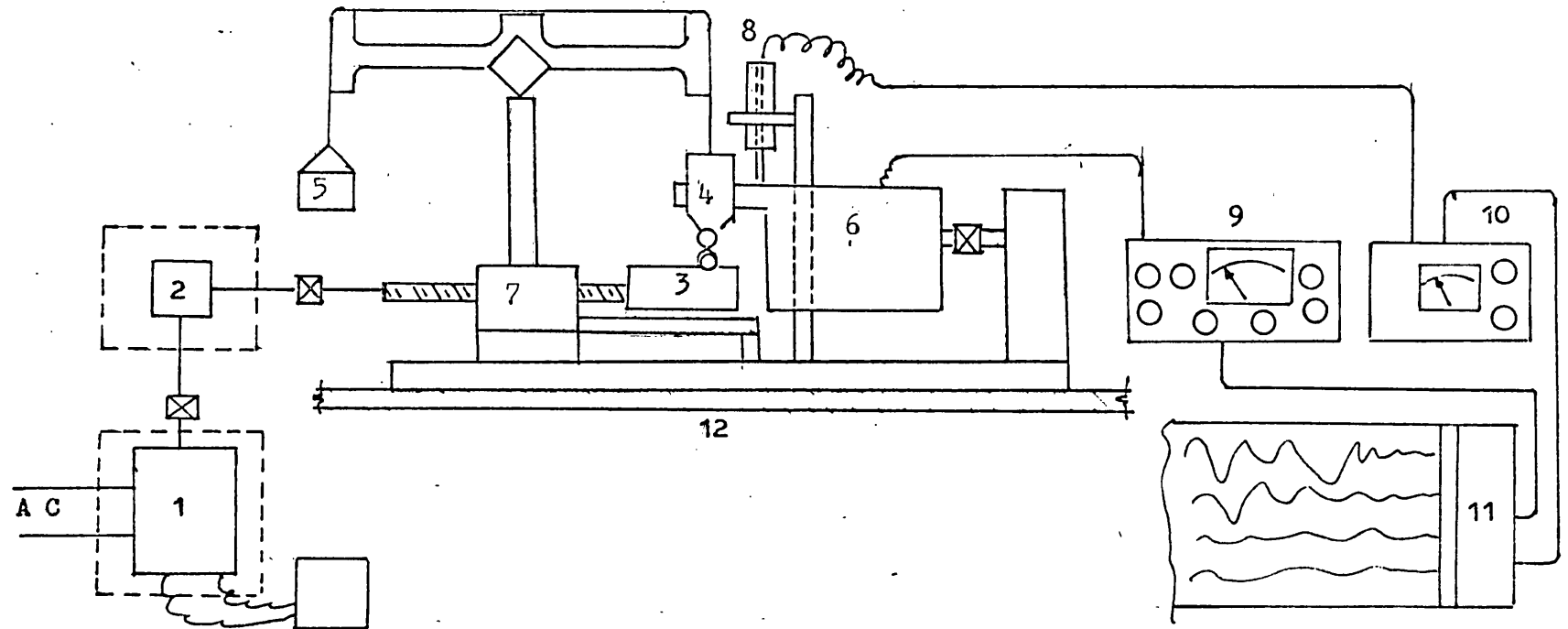


FIG. 2.2 SCHEMATIC LAYOUT OF PLANE STRAIN TEST APPARATUS



- | | |
|------------------------------|----------------------------------|
| 1 - Induction motor | 7 - Motion converter |
| 2 - Reduction gear | 8 - Vertical Displacement sensor |
| 3 - Lower carriage and anvil | 9 - Transducer meter, type C61 |
| 4 - Quill ball vice | 10 - Transducer meter, type c62 |
| 5 - Vertical loading system | 11 - Multichannel recorder |
| 6 - Load cell | 12 - Rubber damping pads |

FIG. 2.3 SCHEMATIC DIAGRAM OF THE FRICTION TEST APPRATUS

Table 2.1

Test Materials Used

S. No.	Material	Structure & Bulk Behaviour	Symbol Used	Petrological or Material Type	Surface Friction μ	Sp. Gr.	Description of Particles			Source of Supply
							Size in mm	Shape	Texture	
1	Gravel (Beach)	Crypto-Crystalline Brittle	B	Flint	0.4 to 0.6	2.61	4.5-6.5	Rotund	Very Smooth	Chesil Beach Bridport, Dorset supplied by TRRL
2	Glass	Amorphus Brittle	G	Glass	.04 to 0.8	2.69	6.0-6.5	Very Rounded Balls	Very Smooth	Smith Glassware & China (London) Ltd., London
3	Ceramic	Poly-Crystalline Brittle	C	Steatite	0.5 to 0.6	2.75	6.25-6.75	Very Rounded Balls	Smooth	Kera Soestenberg Holland
4	PTFE	Poly-Crystalline Visco-Elastic	T	Polymer	.05 to 0.07	2.0	5.5-7.0	Cuboidal	Very Smooth	PolyPenco London
5	Poly-Propylene	Poly-Crystalline Visco-Elastic	P	Polymer	.2 to .3	0.9	6.25	Spheres	Very Smooth	Insley Precision Ball Co., England

Table 2.2

S.No.	Test number		Test Material	Degree of Saturation	Confining pressure		Initial porosity
	Alpha-numeric	Numeric			Nominal in of Hg	Actual kPa	
1	B20D	1200	Gravel (Beach)	Dry	20	64.5	0.396
2	B20S	1201		Sat.	20	59.1	0.384
3	G20D	2200	Glass Balls	Dry	20	65.8	0.387
4	G20S	2201		Sat.	20	67.4	0.398
5	C20D	3200	Ceramic Balls	Dry	20	70.7	0.391
6	C20S	3201		Sat.	20	66.8	0.396
7	T20D	4200	PTFE Cuboids	Dry	20	65.9	0.361
8	T20D	4201		Sat.	20	27.7	0.360
9	P15D	5150	Polypro- pylene Spheres	Dry	15	48.8	0.436
10	P20S	5201		Sat.	20	60.9	0.429

C H A P T E R 3

INTERPARTICLE FRICTION3.1 INTRODUCTION

The strength-deformation theories of Particulate Mechanics are generally developed around the concept of interparticle friction e.g. Rowe (1962 , 1971), Horne (1965, 1969), Murayama and Matsuoka (1973), Frydman (1972). Also in the past attempts have been made notably by Caquot (1934), Bishop (1954), Dantu (1957), Haythornthwaite (1964), Parkin (1965), Thurston and Deresiewicz (1959) and Scott (1963) to correlate the angle of interparticle friction ϕ_{μ} with the angle of internal friction at constant volume ϕ_{cv} . Any experimental verification of such theories or of new postulates, for that matter, will obviously require an understanding of interparticle frictional behaviour of the constituent particles of the medium.

Surface friction and its associated theories are profound physical, experimental and theoretical studies in their own right. Accordingly, detailed discussions and many subtleties are beyond the scope of this study. Nonetheless, since physical friction plays a dominant role in existing strength-deformation theories based on Particulate Mechanics, it is natural to dig into the literature on geotechnical engineering and its allied fields for a recognised theory and then for a bank of information giving the numerical values of coefficient of friction of the desired materials tested under identical conditions. A thorough search of the literature revealed that there is a lack of an acceptable theory of friction which could be used to explain the frictional

behaviour of non-metallic solids, in general, and brittle materials in particular especially for small interparticle loads. In his eleventh Rankine Lecture, Jaeger (1971) emphasized the paucity of systematic study and remarked: "Many different types of measurement on the sliding of rock surfaces have been made under different conditions and for different purposes. There is a lack of any systematic study and so these tend to be lumped together and figures quoted without real appreciation of the complexity of the situation". His remarks are on friction of rock surfaces but are very relevant to soil-forming minerals. Moreover, in Soils, the situation is even more complex. Having emphasized the non-availability of a friction theory, no attempt will be made to postulate or to develop a new friction model for two main reasons. First, it is outside the scope of the present study and secondly, by itself it is a research topic for a separate investigation. Nevertheless, a brief search is made to find a suitable theory which could be used but under certain constraints.

In this chapter, main theories of friction which are generally used and are relevant to the 5 test materials employed in this study, will be outlined and finally with the help of this discussion, a friction model will be selected. Later, it will be shown that under most circumstances, published data on the same material, based on the same frictional concept and theory, cannot be used. This will obviously justify the need to experimentally determine the coefficient of friction of the material used in this study. The actual test method followed will then be described and the results presented and discussed. Finally, a few comments will be made on the suitability and the selection of a model.

3.2 FRICTION AND ITS LAWS

Intergranular friction or sliding friction or simply friction, as the term generally used, is the resistance offered to sliding of one solid body over another, regardless of how that resistance is generated or of what relation it may have to other forces or condition involved. It is a phenomenological concept covering several unspecified mechanisms which are either poorly understood or not understood at all, and which may differ from one situation to another. In one situation, sliding of one solid upon another may need only that the molecular attraction across the contacting surfaces be overcome, in other conditions, the two contiguous solids may have to be forced apart in order to allow the small irregularities on each sliding surfaces to pass by each other. Still there may be other situations where the asperities on the surface of the solid bodies in contact may be flattened or sheared off or junctions may be formed and subsequently broken off under the application of tangential traction. None of the friction mechanisms or relations between them are known quantitatively either for Soils or Rocks. The classical laws of friction are empirical. Leonardo da Vinci (1452-1519) discovered the first two laws of friction but they remained unnoticed for more than 250 years. It was Amontons (1699) who rediscovered them, presumably without having the knowledge of Leonardo da Vinci's work. These two laws, generally known as Amontons' laws of friction, are 1) that frictional resistance is directly proportional to the force normal to the sliding surfaces, 2) that it is independent of the area of the surfaces. Symbolically these laws can be written as:

$$F = \mu N \quad (3.1)$$

Where F is the frictional resistance
 μ is the coefficient of friction
 N is the normal load.

Alternatively, e.g. (3.1) can be written:

$$\mu = \tan \phi_{\mu} = F/N \quad (3.2)$$

Where ϕ_{μ} is the angle of interparticle friction.

3.3 FRICTION THEORIES

Most of the friction theories are based on the fact that the real contacts are rough on the microscopic level and so the contact of the contiguous surfaces is limited to discrete spots on these surfaces. Friction between sliding surfaces, therefore, arises from local adhesion at the regions where asperities come into real or molecular contact. In addition to this accepted fact, major theories of friction are developed on the postulates that the solids do not seriously deform due to the sliding process and that the surface asperities retain their identity though they may be quite severely deformed. These friction theories differ in their assumptions as to how the coefficient of friction should depend on the flow pressure, the real area of contact and on the strength of bulk material.

Most friction theories, which are developed essentially for non-brittle materials notably by Terzaghi (1920a,1925) Bowden and Tabor (1954,1964) and their collaborators, Archard (1957), Rubenstein (1956) and others, are based on one common assumption namely the frictional

force between the sliding surfaces is equal to the real area of contact times the shear stress necessary to break the adhesive bonds between two solids in contact. However, these theories differ in the evaluation of the area of true contact. Bowden and Tabor (1954, 1964) asserted that the real area of contact is formed by plastic deformation of asperities in contact and the adhesion arises from cold welding or adhesion at these plastically deformed asperities. They have shown experimental evidence in support of their assertion. The friction theories based on this concept are called "Adhesion Theories" or "Coldwelding theories". On the other hand, Archard (1957) postulates that under certain situations, the real area of contact is formed primarily by elastic deformation of contacting asperities on the two surfaces. Rubenstein (1956) on his part assumes that the deformation of asperities in contact can be considered as a function of some power of stress σ^x which produces it. This postulate inherently includes both aspects of elastic and plastic deformation of asperities in the contacting zone between the two sliding solids. It is clear from these discussions that from three different basic assumptions of deformation, three different expressions for frictional forces as a function of shear strength of the adhesive bond, flow pressure and the normal force between two solids in contact can be derived.

Byerlee (1967) is probably the first to present a friction theory for brittle solids. He supposed that the asperities in contact fail in a brittle manner and not by plastic shear under the combined traction (normal and tangential) acting at their tips. Although appreciating the efforts made by Byerlee in developing a friction

theory based on brittle fracture, Jaeger (1971) found it simpler to assume that the mechanism of friction as one of shear failure so that criteria similar to those used for the strength properties of the bulk of the material, in his case, rocks would apply.

Skinner (1975) extended the adhesion theory of friction to model the frictional behaviour of brittle material with particular application to quartz which exhibits an increase in strength with increase in effective stress, in this case, with increase in hydrostatic confining pressure. He blended together with considerable success, the concept of adhesion or cold welding due to Bowden and Tabor (1954,1964) and the intrinsic shear strength concept of Skempton (1960).

In the present investigations, the materials used to form particulate test specimens can be classified under two main groups a) brittle materials e.g. gravel, glass and ceramic, and b) polymers e.g. polypropylene, polytetra Fluoro Ethylene generally known as PTFE and commercially available under trade names Fulon (ICI) or Teflon (Dupont).

In the absence of a suitable mathematical model or a friction theory for the materials used, either theories developed in other branches of engineering or science can be borrowed and used with or without modifying them or propounding new ideas and theories suitable to explain the behaviour of material under investigation. For the reasons outlined earlier, effort will be directed to choose a

suitable model from amongst the available theories. To assist in such a selection, the available friction theories will be divided for convenience of discussions, into the following two major groups with their sub-groups:

A. Theory of friction for Brittle Materials based on -

- i) Plastic deformation of asperities
- ii) Elastic deformation of asperities
- iii) Brittle fracture of asperities
- iv) Coulomb type relationship or Power Law

B. Theory of Friction for Polymers

In these discussions, it is intended to bring out salient features of the theories, their limitations and possibility of being used for the materials studied in the present work.

3.4 FRICTION THEORIES FOR BRITTLE MATERIALS

3.4.1 Adhesion - Ploughing Theory

Terzaghi (1920a) presented his first preliminary concept of friction partly based on the work of other researchers. However, he improved and modified his original concept and offered a meaningful explanation of the laws of friction. His theory is now known as the adhesive theory of friction (Terzaghi, 1925). Terzaghi observed that the proportionality between load and frictional resistance actually exists for smooth as well as rough sliding surfaces and both with or without lubricated

sliding surfaces. Based on the observed phenomena, he came to the conclusion that the frictional resistance is caused by physical-chemical interaction between the bodies in contact. He elaborated his concept by stating that there is formed, so to say, a firm or semi-firm bridge between the surfaces and the frictional resistance is the shear strength of the bridge. He made an assumption of plastic shear resistance offered by the asperities in contact so as to explain the proportionality between normal load and frictional force.

Bowden, Moore & Tabor (1943) propounded, independently and presumably without any knowledge of Terzaghi's work, a theory of friction based on similar concept due to Terzaghi (1925). In Tribology which is the science and engineering solely devoted to the study of friction, this theory is now well established and is, therefore, widely used for a variety of materials satisfying the basic assumptions made in the development of the theory, refer Bowden and Tabor (1954,1964). Initially, the adhesion theory was developed for ductile, non-work hardening materials. Bowden and Tabor (1954,1964) and their collaborators have shown that the adhesion theory could be applied to non-metallic substances including certain brittle materials and plastics. Bowden, Brookes and Hanwell (1964) and Bowden and Brookes (1966) carried out detailed study of the behaviour of solids which, although inherently brittle compared with metals, are capable of a varying degree of plastic deformation during the process of sliding. They found experimental evidence that the frictional anisotropy of all these crystals is due mainly to their anisotropic modes of bulk deformation. It was observed that the shape of the slider and the crystallographic direction influence both nature and extent of deformation.

The studies of Bowden and Brookes (1966) on magnesium oxide crystals revealed that the frictional behaviour of a hard conical slider on crystal faces can best be considered in two regimes. In the first regime, with light loads on blunt sliders, the load is carried largely by elastic stresses and plastic flow contribution towards friction made by ploughing or cracking is small. The friction, therefore, appears to be primarily due to adhesion. It can be said that the main contribution to the friction arises from interfacial adhesion provided the load is not sufficient to cause deep penetration of the surface. The second regime occurs when the load exceeds a critical value which depends on the apical angle of the cone. The sharper cones have smaller critical load. In this regime, penetration of the crystal occurs and the friction rises to a higher value and shows a marked anisotropy. If the cones are sharper the crystal will undergo a certain amount of plastic flow, but brittle fracture will lead to varying degrees of penetration and will exhibit frictional anisotropy. Whereas with a very blunt and rounded slider (semi-apical angle greater than 85°), the transition from one regime to the other does not occur; no penetration of slider takes place; the friction remains low and isotropic; the bulk deformation is essentially elastic although the asperities will behave plastically. It can be concluded that the frictional anisotropy is associated primarily with the forces necessary to plough out a track in the crystal and to produce plastic deformation and cracking of the crystal underneath the surface. Figure 3.1 shows a very interesting and important relationship between coefficient of friction and Knoop indentation hardness. The anisotropy in the 'Knoop hardness' of the

magnesium oxide surface confirms that low 'hardness' corresponds to high friction and vice versa.

Another significant contribution is made by Bowden and Henwell (1966) in the understanding of clean crystal surfaces. One of their conclusions of immediate importance is that their crystals behaved in a very similar manner to magnesium oxide.

3.4.1.1 Skinner's Extension to the Adhesion Theory

Skinner (1975) extended the adhesion theory due to Bowden and Tabor (1954, 1964) to include those materials whose stress/strain (strength) characteristics are significantly influenced by hydrostatic component of stress. This is the class of materials under which most of the soil-forming minerals and very many brittle materials such as glass, ceramic, etc. can be classified. Most of these materials behave in an elastic/brittle mode at low pressure, changing to an elastic/plastic mode at higher pressures. In the elastic range, the stress/strain behaviour is generally only slightly influenced by confining pressure. Skinner has shown that it is so.

Skinner based his theory of friction on the following assumptions-

1. The normal and shear stresses, produced by the applied loading, are interdependent as per the following expression (McFarlane and Tabor, 1950):

$$\sigma_n^2 + \alpha^2 \tau^2 = P_o^2 \tag{3.3}$$

Where σ_n is the normal stress at the surface of sliding

τ is the shear stress
 P_0 is the yield pressure
 α is a constant

2. The mean contact stress produced by the applied load, under conditions of no shear loading with zero ambient pressure, will be taken to be equivalent to the Vicker's hardness, H_V , measured with the same load. Further, it will be assumed that the mean pressure in a hardness test at a pressure other than atmospheric is increased by the ambient pressure σ_3 in such a way that the mean confining pressure in the indentation is equal to the sum of the ambient pressure and the self-induced hydrostatic pressure for zero ambient pressure.
3. The mean confining pressure $\bar{\sigma}_3$ at the junctions between contacting asperities is equal to the sum of the ambient and self-induced hydrostatic pressures.
4. No work hardening takes place during shear.
5. The shear strength of the contact region material increases linearly with the mean normal pressure, (Skempton, 1960)

$$\tau_i = k + \sigma_n \tan \psi \quad (3.4)$$

Where τ_i is the intrinsic shear strength of the material
 k is the intrinsic cohesion
 ψ is the angle of intrinsic friction

6. When gross slip is about to occur, the yield stress is given by

$$Y = 2\tau_s / \cos\psi \quad (3.5)$$

where τ_s is the shear stress at the junction at slip, refer Fig. 3.2, and that the junction would have behaved in the same way if this 'flow stress' had been operative throughout the yielding process.

The friction model postulated by Skinner, based on the above assumptions and that the coefficient of friction is a function of the intrinsic strength parameters, indentation hardness and to a lesser degree on the ambient confining hydrostatic pressure, shows for the confining stress range, in which Soil Engineers are generally interested, coefficient of friction, for all practical purposes is independent of confining stress and the relationship derived in its simplified form is:

$$\mu = \tan \psi + k / (\sin\psi \cdot H_v) \quad (3.6)$$

Like many materials of Mohs hardness 5 or more, the major soil forming mineral namely quartz shows a marked dependence of hardness on the load applied to the indenter (Brace, 1963). Skinner's experimental observations are in good agreement with his model and also confirm the observation made by Bowden & Brookes (1966), mentioned earlier, that as hardness decreases friction increases. However, the variation in hardness with load is a problem in correctly using the friction equation (3.6). In this equation, the appropriate value of H_v is that relevant to the loading condition. As H_v varies considerably especially at very low load, it becomes essential to use profilometric method, for example Talysurf profilometer, shadow graph etc. to estimate the number of asperities which

may deform in a plastic manner under the given load. Although it inserts a subjective factor in the calculation, the friction model proves its worth.

Skinner has also suggested that the effect of contaminant or soft interfacial layer on the coefficient of friction could be taken into account. He supposed, following Bowden and Tabor (1964, p. 74), that the contaminant layer is weaker than the bulk material and its strength is equal to $\beta \tau_s$, where β is a coefficient between 0 and 1.

Equation 3.6 for this situation can be modified and is finally written as

$$\mu_c = \beta \tan \psi + \frac{\beta k}{\sqrt{1 - \beta^2 \cos^2 \psi} \cdot H_V} \quad (3.7)$$

Since it is rather difficult to know the numerical value of β for various surface conditions and surface contaminant layer, its use for the present is limited. The equation clearly indicates that the coefficient of friction decreases with decrease in the strength of the surface contaminant layer.

3.4.2 Friction Theories Based on Elastic Contacts

The friction theories under this heading are based on the following basic assumptions:-

- i) the asperities in contact deform elastically under normal loads, and
- ii) once these asperities are deformed under normal load, their area remains unchanged under tangential traction.

In an effort to find a plausible explanation of Amontons' laws of friction, various types of models have been proposed. Archard (1957)

proposed a model with micro-asperities over asperities. On the other hand Greenwood (1967) and his coworkers, e.g. Greenwood and Tripp (1967) have postulated that the surface asperities heights are randomly distributed and assumed that tips of such asperities have constant radius of curvature. It is worth mentioning that both of the above approaches come to the same final conclusion when the two contacting surfaces are under normal loads only. Their final conclusions are that under low loads and on rough surfaces the area of contact is proportional to the normal force, whereas at high load the area-load relationship approaches a Hertzian relationship i.e. the area is proportional to $W^{2/3}$. Since in the friction theories based on the elastic contacts it is implicitly assumed that the junction or asperity contacts do not grow with tangential traction, it could be said that the Amontons' laws are obeyed for rough surfaces in elastic contact at low loads. In other words the frictional resistance is proportional to normal force N . At high loads or for smooth contacts, the frictional forces are proportional to W^n where n varies from 0.67 to 1.0 depending upon the topography of the surfaces and loading conditions.

In all contact surfaces under normal load and tangential traction, some of the contacting asperities will inevitably be deformed plastically. It is very difficult, if not impossible, to find out the exact proportion of elastic and plastic contacts of a real contact area. This information could then be used to say what mechanism could be used for the interaction of surfaces. Greenwood (1967), with the help of statistics, came up with a criterion by which he was able to distinguish between the predominantly elastic contacts and plastic contacts. For this he proposed the following relationship and coined a new term, "Plasticity Index", at least in Tribology and this term is totally different with that used in Soil

Mechanics

$$\psi^* = \frac{E'}{H} \sqrt{(\sigma/\beta)} \quad (3.8)$$

where ψ^* = Plasticity index

E' = Plane stress elastic modulus,

H = Hardness

σ = R M S Roughness

β = Radius of curvature of asperity.

He suggested that if ψ^* is less than 0.7 the contact will be elastic and if the value is more than 1.0, then the contacts will predominantly be plastic. Greenwood and Williamson (1966) have very emphatically asserted that the wide spread idea that in general contact is elastic at low loads and becomes plastic as the load increases is wrong. Their assertion is correct for those surfaces with large asperity densities. Further they regarded ψ^* as a generalized surface texture parameter combining both material and topographic properties. They concluded that the contact between solid surfaces is controlled by two material properties; plane stress modulus and hardness, and three topographic properties; surface density of the asperities, standard deviation of their height distribution and their mean radius.

Greenwood (1967) commented that generally man-made surfaces will be rough and most of them will lie in the plastic range under load. Bowden (1967) has also shown by a simple calculation that the conical asperities will deform plastically particularly when E'/H ratio is $1/10$ or less.

It is, therefore, clear that in most of the massive soil-forming minerals, asperities will deform plastically and hence the theories based on it will be near to reality. But one can find materials and situations

where the elastic deformation at contacts are possible and there we have to use elastic contact theories. Bowden and Tabor (1964) have tried to explain the frictional behaviour of materials which were thought to have elastic contacts, by means of their plastic deformation theories.

3.4.3. Friction Theory based on Brittle Fracture of Asperities.

Byerlee (1967) is probably the first to come up with a theory of friction based on brittle fracture of the asperities. His model of the friction mechanism is based on the following assumptions:-

1. The surface of the material is made up of asperities.
 2. The resistance to sliding is determined by the strength of these asperities.
 3. The asperities are brittle and they fail in a brittle manner rather than by plastic shear as is assumed by Terzaghi (1925), Bowden and Tabor (1954, 1964).
 4. The stress to cause brittle fracture in tension is much less than the stress to produce plastic shear.
 5. No interlocking of the asperities is assumed.
- 6(a) As a first approximation asperities are assumed to have the form of a wedge. Further it is also assumed that all angles of asperities - half wedge angles lie between 0 and $\pi/2$ are equally probable and on average the load is shared equally by all angles of asperities. If this assumption is accepted the coefficient of friction may be found by averaging over all angles of asperities in contact.
- (b) As a second approximation, the asperities are assumed to have the form of a cone. The average value of coefficient of surface friction is obtained by averaging over asperity angles of 0 to 81° . Since if the angle of asperity in contact is greater than 81° , this asperity

experiences tensile forces even under normal contact force alone. The angle of asperity will be reduced by fracture of such an asperity.

Bowden and Tabor (1964, page 117) have questioned the validity of the friction theories based on the brittle fracture on the following grounds. Brittle solids, by definition and unlike metals, are not considered to be ductile and these solids crack and fragment at very small tensile strains. In such solids, what determines the true contact area? Does the contact surface first deform elastically prior to fracture? If this is true, the area of contact would be indeterminate and irreproducible. Obviously there would be a corresponding irreproducibility in the surface friction. They further raise the question whether adhesion or cold welding, as observed in metallic surfaces in contact, is possible? There is experimental evidence which shows quite convincingly that in fact the friction of many brittle materials is highly reproducible and is generally of the same order of magnitude as observed for metals. Further Amontons' laws are approximately obeyed by such materials.

In addition to the above arguments, the following are the main objections against the brittle fracture theory of Byerlee (1967), at least, in its present formulation:-

1. In case of smooth surfaces, there is a possibility of having asperities with semi-apical angles greater than 81° . In the formulation derived by Byerlee (1967), such asperities are either non-existent or if they existed, will be crushed down or fail under compressive forces only. This obviously leads to the conclusion that a large number of flat asperities even at low normal loads, are crushed when smooth surface are slid together which apparently would give rise to irreproducibility of friction results. This conclusion is not confirmed experimentally. On the contrary, the results are very reproducible and consistent for smooth brittle sur-

faces in contact.

2. Byerlee's theory fails to explain the increase in coefficient of friction when the material is submerged in water. The experimental results published by various researchers, for instance by Horn and Deere (1962), Skinner (1969, 1975), and the friction test results of the present study, show conclusively that the coefficient of friction of certain brittle materials, such as quartz and glass, does increase considerably when the surfaces are submerged under water. In fact, if the brittle theory is valid, the coefficient of friction should decrease on submergence of the sliding surface in water as the strength of brittle materials slightly decreases when wet, Colback and Wiid (1965). However, Byerlee tried to explain the increase in the coefficient of friction due to the presence of van der Waal forces. This explanation does not seem to be plausible. The numerical values of the existing normal forces will not increase significantly, due to the cause mentioned by Byerlee, for two main reasons. Firstly, the interacting sliding surfaces possess roughness in the form of asperities. These asperities, depending on their heights, will not allow the sliding surfaces to come closer and so any contribution made by the forces of attraction between the two bodies, will be exceedingly small in comparison to the applied normal force. Secondly, in the case of convex surfaces in contact, such as between gravels, glass balls etc., the separation between the two contacting surfaces rapidly increases and thus will obviously reduce the Van der Waal forces. However, the Van der Waal forces are predominant in minerals having layer-lattice structures, with surface roughness of a few atoms thickness, for example mica. For such materials the brittle fracture theory of friction breaks down and hence Byerlee's theory is not applicable.

The writer is of the view that this theory in its present form could not usefully be used.

3.4.4 Coulomb Type Approach & Power Law of Friction

Jaeger (1959) regards the mechanism of friction as the process of shear failure of asperities under normal load and used the criteria similar to those adopted for the mechanical properties of rock elements. Using Coulomb's equation:-

$$\tau = c + \sigma_n \tan \psi \quad (3.9)$$

in terms of intrinsic parameters, we can write the variable coefficient of surface friction as:-

$$\mu^* = \mu_0 + \frac{c}{\sigma_n} \quad (3.10)$$

where μ^* is the variable coefficient of friction

μ_0 is the constant part of the coefficient of friction and $\frac{c}{\sigma_n}$ is the slope of τ - σ_n relation.

The other method of presenting the friction-normal stress relationship, which is mostly favoured in Rock Mechanics, is by using a power relationship, such as suggested by Archard (1957).

$$\mu^* = k \cdot \sigma_n^{m-1} \quad (3.11)$$

where $2/3 < m < 1$

Its use has been advocated by Murrell (1965), Hobbs (1970), and others.

Patton (1966) presented the experimental evidence which suggests that the frictional behaviour of surfaces, particularly rock surfaces, can be divided into two separate domains, depending on the applied normal stress. At low normal stress, the effect might be one of sliding up asperities with zero cohesion, but that at higher normal stresses there might be shearing of asperities which would give an effect similar to cohesion. The simplest representation of this is the bi-linear law.

$$\text{For } \sigma_n < \frac{c}{\mu_0 - \mu_1} \quad (3.11)$$

$$\mu_1^* = \tau/\sigma_n = \mu_0 \quad (3.12)$$

$$\text{and for } \sigma_n > c/(\mu_0 - \mu_1) \quad (3.13)$$

$$\mu_2^* = \tau/\sigma_n = \mu_1 + c/\sigma_n$$

where μ_0 is the slope of the τ - σ_n relation in the low normal stress σ_n range.

μ_1 is the slope of τ - σ_n relation in the high normal stress range.

μ_1^* and μ_2^* are the variable coefficients respectively of friction in low and high pressure ranges.

c is the intercept of τ - σ_n line in the high normal stress range.

The reason for the dependence of friction coefficient on the normal stresses and thus the breakdown of Amontons' laws of friction is associated with the interlocking of the asperities on the interacting surfaces. This interlocking depends on the intimacy of the contact of the asperities, which

in turn, depends on the magnitude of the normal stress σ_n . Although a number of theoretical models of this interlocking behaviour of rock surfaces have been considered by Murrell (1966), Patton (1966) and by others, the problem has not been adequately solved and a considerable amount of theoretical work is still necessary.

None of these proposals has real theoretical or experimental status so that any attempt to fit experimental points to one of them may lead to misleading results. Jeager (1971), in fact, has cautioned that the law and the frictional values should be used with certain reservations.

3.5 POLYMERS AND FRICTION

Polymeric materials are thermoplastics with visco-elastic properties and all consisting of very long molecular chains. Due to practical importance and scientific interest, a considerable amount of work has gone into the understanding of frictional behaviour of polymeric materials, with emphasis on certain polymers for instance Polytetra-Fluoro-Ethylene (PTFE). The frictional characteristics of these materials, in general, can be explained in terms of the Bowden-Tabor's Adhesion theory discussed in section 3.4.1 of this chapter. However, there are three fundamental differences. First, the area of contact depends on the geometry of the surfaces as well as on the load and there is a corresponding dependence of the friction coefficient. Secondly, in certain situation the ploughing or grooving term may form an appreciable part of friction but with these materials this takes the form of elastic hysteresis instead of the more usual plastic deformation in metallic surfaces. Thirdly, the friction depends on speed and temperature which reflects the visco-elastic characteristics of the polymers.

Shooter and Tabor (1952) reported the results of their experimental study of certain polymers whose surfaces were rubbed against each other at a constant speed of 0.1 mm/sec. They found that the friction of clean metals sliding on plastics is about the same as the friction of plastics sliding on themselves. Their results confirmed the hypothesis that shearing during sliding occurs within the bulk of the plastic. Bowden and Tabor (1967) have shown that over a restricted load range, rubbing speed and temperature the true area of contact A is proportional to the load and the friction may again be written $F = As$, where s is the shear strength of the interface. Comparison with shear strength experiments on the plastics shows that s is roughly equal to the bulk shear strength of the plastic itself. Consequently, under the above restricted test conditions, the mechanism of friction can be said to be essentially the same as for metals and the coefficient of friction may be taken as being approximately equal to s/p , where p is the normal contact stress.

As pointed out earlier, one major difference between the frictional behaviour of these materials and metals is the effect of load. With metals the deformation at the regions of contact is truly plastic and for this reason the real area of contact is directly proportional to the load. With long chain polymers this is not so. The materials are visco-elastic and their deformation depends on the geometry of the surface, the load w , temperature and time of loading. In general, the area of contact A follows a relation of the type $A = f(\text{geom}, W, t, T)$, where geom is the geometry of the contacting surfaces, W is the normal load, t is the time of loading and T is the temperature. For a fixed geometry and with fixed time of loading and temperature, the said relationship can be written as $A \propto w^n$ where exponent n is less than 1.0. Accordingly the coefficient of friction increases as the normal load is reduced.

The increase of coefficient of friction at light loads has been found by various researchers including Shooter and Tabor (1952), and found by Archard (1957). It will be shown that the experimental evidence of this study substantiates the above findings. Shooter and Tabor offered the following three possible hypotheses for this, viz.

- 1) effect of static electricity,
- 2) the presence of surface films and
- 3) the nature of the deformation process.

Based on the arguments in favour of each of the above hypotheses presented by them, the writer is inclined to accept the third explanation. It is the nature of the deformation process which controls the frictional behaviour of polymers. It has been shown by them that at heavy loads the deformation of the plastic is apparently plastic, the area of contact being proportional to the load. At very light loads, however, the area of contact will be determined by elastic deformation. Under idealized elastic conditions and provided the shear strength of interface is constant, $A = kW^{2/3}$ so that $\mu = \text{const. } W^{-1/3}$. The coefficient of friction should increase rapidly as the load is reduced while other conditions kept constant, but the observed friction coefficient increases less rapidly than that predicted by the above relationship. Ostensibly the change from plastic to elastic deformation is not abrupt. In other words there is a gradual change from $A \propto W$ to $\propto W^{2/3}$. It can easily be inferred from this that surface asperities play an important part in determining the nature of the deformation.

PTFE exhibits exceptional frictional behaviour. It is generally attributed to its molecular arrangement and the cylindrical streamlined structure of molecular units. This results in the reduction of inter-

action between molecules and so the specific adhesion at the interface is remarkably small. Its low friction has generally been ascribed to the poor adhesion which exists between it and most other solids. Bowden & Tabor (1967) postulate that in the case of PTFE the low friction must, in some way, be connected with intrinsic structure and its intercrystalline slip properties.

It must be emphasized that whilst the exact mechanisms involved are still not fully understood (Bowden and Tabor, 1966) recent investigations have shown that the coefficient of friction is dependent upon various factors including the load (or pressure), the rubbing speed, the temperature, the mating surface, the orientation of plastic molecules, the environment and the time of running. Obviously the above discussion is centered around certain simplifying assumptions and conditions. The results obtained from such theories must be used with caution and due attention must be given to the various factors affecting the coefficient of friction.

3.6 AN EXPERIMENTAL INQUIRY OF FRICTION OF THE TEST MATERIALS USED IN THIS STUDY

3.6.1 Need for Experimental Investigation

From the discussion presented so far it would appear that for certain materials, such as soil-forming minerals, not a single friction theory is available which could be used without any reservations. In addition to different theoretical formulation, many different types of friction measurements on various types of soil-forming minerals and rock surfaces have been made under different conditions and for different purposes.

Although inter-particle friction has long been recognized as important in geotechnical engineering which is concerned with particulate mechanics, there is a lack of any systematic study of it, and thus, for obvious reasons, there is a tendency to lump together the results of friction tests obtained under different environments and purposes and to quote numerical values without a real appreciation of the complexity of the situation. Nevertheless from the point of view of particulate mechanics and for the present work it is desirable to have quantitative measures or numbers which describe the frictional behaviour of contiguous grains of a soil sample or of a model material used here.

3.6.2 Friction Tests

Unfortunately there is no standard method for determining the coefficient of friction in geotechnical engineering and not even in Tribology. Consequently various methods have been developed and used for specific purposes by various researchers. However, the most widely used method of studying friction is to slide a small slider on a larger surface of like or different material than that of the slider. This method has been preferred and used by various investigators including Horn and Deere (1962), Hafiz (1950), Byerlee (1970), Bowden and Tabor (1954, 1964) and Archard (1957). This method, generally known as the classical method, suffers from a major drawback namely the difficulty in the reproduction of identical sliding surfaces to those which actually exist in the real bodies in contact particularly the plane surface on which the slider has to move.

This limitation, however, can be overcome by carrying out a friction test on actual particles provided the particles are approximately spherical in shape and are large enough so that they can be held in some sort of

of mechanical device and then slid against each other while measuring the forces which would ultimately give the value of coefficient of friction. Hafiz (1950) and Skinner (1975) have used this method in which a particle of the actual material is forced to move in the valley formed by two fixed particles placed side by side and mounted in a clamp. Barton (1972) used this technique but slid one particle over another instead. In this technique it is rather difficult to guide the movement of one particle relative to the other precisely. Further the measuring system used by him appears to be too soft. However, these difficulties do not arise in the technique used by Skinner (1975) and are used in obtaining the coefficient of friction in the present work. This technique is itself not free from another limitation. In addition to minimum size of particles requirement, the grains should be approximately spherical or elliptical in shape. In this investigation due consideration was given for suitability of particle size and shape for the friction tests. For the whole series of tests particles were of sizes 5 mm to 7 mm and approximately spherical in shape, with the exception of gravel particles and PTFE chunks. Since the gravel particles were not available at the time when the friction tests were conducted, the friction result reported by Tombs (1969) is used but with due caution. In the case of PTFE chunks, the friction tests were conducted on the spherical shaped particles made from the PTFE bars which were used in making the 6.5 mm size chunks.

The actual testing apparatus, accessory electronic monitoring system and testing procedure employed are described in Chapter 2. Also in the same chapter the surface preparation technique and rigorous surface cleaning technique are described. It must be emphasized once again that surface cleanliness and particle surface topography play major roles in correct evaluation and on the reproducibility of the test results. Further in order

to have the replica of environment of the particles in the friction tests and those used in the plane strain tests, every precaution was taken to keep these particles at the same level of surface conditions, for details see Chapter 2.

3.6.3 Test Programme

Two series of tests were conducted in this investigation. In the first test series the classical method of measuring coefficient of friction was used. However, in the second series of tests, actual particles were used to find the coefficient of interparticle friction. Moreover each of the two test series was subdivided into two sub-sets depending on the moisture content of the contacting surfaces of the particles. In one sub-set the particles were oven dried and then equilibrated to the laboratory atmospheric condition but keeping the particles properly covered so as to avoid any gross contamination of the surfaces taking place. In the second sub-set the particles in the friction test apparatus were submerged in de-aired distilled water. The same water was used in the saturated plane strain compression tests on specimens formed from the same particles.

Although the test results of the first series are not directly relevant for the present study, those results of this series which have relevance either in explaining the frictional behaviour of a test material or have helped in designing the experiments for the second series of tests are included. The tests reported here were conducted on particle to particle contact and with normal force varied in the range 0.15 N to 4.0 N. Based on the test results of the first series it is assumed that a) the difference between the coefficient of static friction and coefficient of kinetic friction of the materials

tested is not significant; b) the coefficient of friction is assumed to be unaffected by the strain-hardening of the asperities; and c) the coefficient of friction is unaffected by slight variation in the speed of sliding.

The preliminary test results showed that it made practically no difference to the measured coefficient of friction at a given normal load, particularly at loads less than 4.0 N, whether a new friction track was used for every traverse or the same track was used in multiple traverses provided other test conditions were maintained constant. Further it was observed that the coefficient of friction under a given load calculated from the first traverse was within the range of test results obtained from at least 50 traverses on the same track and under the same normal load but after the friction track was traversed by the slider particle number of times, at least 50 times.

Some researchers (e.g. Jaeger, 1959) raise the normal force on the sliding surface (that is they use positive increment) whilst others such as Ruiz et al (1968) lower it (i.e. give negative increment to the normal force). These procedures are not the same since the nature of the sliding surfaces at any instant depends on the normal stresses to which it has been subjected. However, such phenomenon with the material tested here, if at all present, was not discernible in the normal force range used. It is, therefore, justified to assume that for a given normal force and under kinetic and static conditions as well as under the given normal force approached to this pre-specified value either using positive or negative loading increment, the coefficient of friction remains unchanged for all practical purposes.

In order to check the reproducibility of the test results, at least two identical tests were performed for every material and for both saturation conditions, but by using new sets of particles. The results which are reported here are the averages of these two sets of experiments.

3.6.4 Method of Calculations:

In the friction tests described here two traces were produced by the X-Y recorder, one for the load cell output and the other for the vertical position of the slider on the friction track. A typical trace is given in Fig. 3.3 which was produced by advancing the slider in forward direction till it passed the highest point of the friction track and then by reversing the direction of the motion of the slider particle. The highest point of the friction track and in fact the vertical position of the slider particle at any given instant was indicated by the second trace produced by the output signal from a displacement transducer located at the free end of the load cell and very near to the slider particle, see Fig. 2.3 and Plate 2.8. The tangential force required to move the slider particle in either direction is taken to be one half of the force needed to move the trace of the load cell transducer output from right to left or vice versa for the same fixed position of the slider on the friction track. In this way it was possible to eliminate the effect of dilatation, or in other words of moving up and down the asperities, by finding the difference between the forward trace and backward trace of the load cell output for a given position of the slider on the friction track and then dividing it by two so as to get the tangential traction in either direction. In particular the point chosen as the fixed point is the apogee of the friction track which could easily be located by finding the highest point of crest of the trace generated by the displacement transducer. The vertical movement of the slider particle

could be discriminated to the order of 5 microns. Consequently, from the geometry of the arrangement of particles, and friction track, Fig. 3.4, we can find a relationship between coefficient of surface friction μ , measured change in surface traction due to forward and backward traverse of the top particle at the apogee F , the vertical force transmitted by the slider particle W and the angle θ between the vertical and the normal to the plane of contact at the contact point.

At the apogee of the friction track

$$N_c = \frac{W}{2 \cos \theta} \quad (3.14)$$

where N_c is the normal force at either of the contacts

θ is the angle between the vertical line and the normal to the contact, and

W is the vertical force applied to the top particle.

Since spherical particles of very nearly equal diameters were used and they were so arranged that the top ball was always touching the lower anvil balls. The angle θ can, therefore, be taken as 30° . So the tangential traction at each of the two contacts is

$$F_c = \frac{F'}{2} \quad (3.15)$$

where F' is half of the change in the surface traction F in one cycle of forward and backward motion,

$$\text{or } F' = \frac{F}{2}$$

$$\text{thus } F_c = \frac{F}{4}$$

Finally, by definition, the coefficient of friction is the ratio of tangential traction to normal force at a point of contact, we can write

$$\mu = \frac{F_c}{N_c} = F \cos \theta / (2W) \quad (3.16)$$

when $\theta = 30^\circ$, equation (3.16) can be simplified as follows

$$\mu = \tan \phi_\mu = 0.433 \frac{F}{W} \quad (3.17)$$

The various sources of error which affect the value of coefficient of friction are discussed in Appendix A and their combined effect on the numerical values of μ are also given there.

3.7 FRICTION TEST RESULTS

The average values of coefficient of friction obtained for various materials tested in the present investigation under air-dry and fully submerged conditions are given in Table (3.1) and Table (3.2). Figures 3.5 and 3.6 show the variation of friction with the vertical force and they also show the spread in the values of friction. From these tables and figures a general trend can easily be observed. The coefficient of friction of brittle materials tested, namely glass and ceramic, increases with normal load at least for the range of normal force used here. On the other hand the results for polymeric materials, PTFE and polypropylene, clearly show a decrease in the coefficient of friction with increase in normal load.

In order to investigate the effect of long exposure to laboratory atmospheric conditions on the value of μ , one test each on the four test materials was

conducted. The test particles were first properly cleaned as usual, oven dried at 105°C for 12 hours and then kept in the laboratory, where the humidity was not controlled, properly covered with tissue papers, for 72 hours. The test results of this series of tests are presented in Fig.3.7. No other material except glass showed an appreciable change in its coefficient of friction. The coefficient of friction of glass increased from about 0.1 to 0.4 that is a four-fold increase. However, it did not reach the friction values attained when fully submerged in distilled water.

3.8 DISCUSSION OF TEST RESULTS

The test results will be discussed here under three main headings namely (a) test apparatus and method, (b) test materials and (c) the mechanism of friction and extrapolation of test results.

3.8.1 Test Apparatus and Method

The friction apparatus and the electronic monitoring system responded very well for the normal and tangential loads for which it was primarily designed. The continuous monitoring and recording system, as used here, was found to be better than the measurement of responses of load cells and displacement transducers at arbitrarily selected discrete time intervals. However, the present friction set-up suffers from a major limitation. It can not be used either for very low loads i.e. less than 0.15N or when the tangential traction generated is more than 220N. This limitation is imposed by the load sensing system. Nevertheless it does not, in any way, affect the results for vertical loads generating the tangential forces within the range mentioned above. As far as the apparatus is concerned additional attention is needed in keeping the universal joint, which connects

the load cell with the body of the apparatus, frictionless and that no dust particle gets inside it and is always kept well lubricated with silicone oil.

The results obtained on various materials shown in the Tables (3.1) and (3.2) clearly show that the apparatus is capable of measuring friction over a very wide range i.e. between 0.03 to 0.9. It can therefore be concluded that the frictional properties measured are the actual material behaviour rather than apparatus characteristics.

3.8.2 Experimental Results

3.8.2.1 Glass Balls

Glass ballotini and balls are the most common model material used by researchers involved in particulate mechanics, perhaps because of their five to ten fold change in friction between glass surfaces by merely changing its surface conditions. However, it is a most complex material particularly with regard to its capricious surface chemistry. Probably this has not been properly appreciated by researchers. This may be one of the reasons why there is a lot of controversy about its frictional behaviour. In the published research works there are various explanations and sometimes wild speculations are made to explain the cause of high or low value of friction coefficient obtained by an investigator. Inter-particle friction test results on glass presented in Table 3.1 for oven dried laboratory equilibrated specimens and in Table 3.2 for submerged test conditions, very clearly show that the coefficient of friction of glass increases by 7 to 9 fold by simply submerging the glass balls under water and then testing them. Another complex behaviour of glass is shown in Fig. 3.7 where the effect of change of atmospheric humidity, in which the glass particles were placed, on friction characteristics is depicted,

In this test no effort was made either to measure the laboratory atmospheric humidity or 'degree of dryness' of the surface of the glass particles. Nevertheless this experiment on glass showed very clearly that the coefficient of friction particularly in 'dry' condition changes considerably under uncontrolled atmospheric condition. It is rather difficult to say with certainty or even estimate the true coefficient of surface friction of glass under differing environmental conditions which are generally grouped under 'laboratory dry conditions'.

Skinner (1975) has carried out friction tests under well controlled test conditions on various metallic and non-metallic materials including glass ballotini. He performed his tests under similar test conditions including degree of saturation and normal load. Except that the composition of glass of these two ballotini samples was different and one ballotini was 1 mm in diameter and the other was 3 mm diameter. The values of coefficient of friction μ obtained for these two ballotini were respectively 0.775 and 0.88. Skinner (1976) suggested that this difference in coefficient of friction may be due to the composition and hardness of the glass and not due to the particle size of the test ballotini.

From this experimental observation it becomes obvious that the values of friction of a material cannot be lumped together and quoted under a broad heading of a material in this case glass. In fact these frictional values must be properly given along with the test conditions including surface cleanliness and moisture condition.

The values of μ for glass balls obtained, both under air-dry and submerged condition in this investigation, are of the same order of magnitude as obtained by Skinner (1975) for 3 mm glass ballotini. Is it a

mere coincidence or a real frictional behaviour of the glass? In the past doubts and even slight hesitation to accept these values have been expressed for example by Rowe (1971), Barton (1972), and Proctor and Barton (1974). In order to explain the above behaviour, one can make the following speculations and it is very necessary to find which one can give a plausible explanation:-

1. Whether it was by chance that certain glass balls were selected for the test which gave these values, or
2. Whether the values of coefficient of friction particularly under full submergence condition were obtained due to the apparatus used since in Skinner's work as well as in this study the same friction apparatus with certain modification was used, or
3. Whether these high friction coefficients are due primarily to surface conditions particularly surface cleanliness and roughness.

In order to remove those factors which might be attributed to mere chance, two series of tests as mentioned in section 3.6.3 were carried out on all the materials including glass. Further, every test of both series of tests was repeated at least once and always with randomly selected balls or flat surfaces. The typical test results of these series are given in Table 3.3. From these results it is evident that both series gave results of the same order of magnitude of coefficient of friction. The results of the two series are not equal, the main reason being the difference between the surface roughness of artificially produced flat surfaces and the surface roughness of balls. Nevertheless these results prove conclusively that the occurrence of high coefficient of friction is not by chance.

As regards to the possibility of rejection of the second speculation is concerned, advantage may be taken of the test results obtained from the same equipment under similar test set-up and testing conditions except using different materials. In the present investigations materials with high coefficient of friction i.e. glass and materials with very low coefficient of friction were used. It has been established by researchers in the field of Tribology that the coefficient of friction of PTFE is not very much affected by the surface contamination or the degree of saturation. The reference to Tables 3.1 & 3.2 clearly shows that the experimental results obtained in this study are in close agreement with the published results (Shooter and Tabor, 1952). It can therefore be concluded that the friction apparatus and its electronic monitoring system are capable of measuring friction between a wide range of friction values ranging from 0.03 to 0.9. These facts, therefore, prove that the second speculation is totally unfounded.

Let us now examine the third hypothesis namely the surface conditions of the contiguous particles. Hardy and Hardy (1929), Holland (1964) have reported that the coefficient of friction for chemically clean glass surfaces is about 1.0. The values of coefficient of friction obtained in the present investigation and those by Skinner (1975) are in the range of 0.8 - 0.9. It can be inferred that the surface cleanliness obtained by the technique used and explained in Chapter 2 are fairly clean surfaces although not completely chemically clean. Further the variation of the observed coefficient of friction at various normal forces gives further evidence of the degree of surface cleanliness attained. It is found that the coefficient of friction increases with increase in the normal load. This observation fits very well with Bowden and Tabor's (1964) explanation of interaction of

interposed layer of contaminants and also with the brittle fracture - plastic deformation approach due to Skinner (1975). Bowden and Tabor (1964, 1967) have convincingly demonstrated that the coefficient of friction decreases with normal load if a soft layer of contaminant is present on relatively smooth surfaces of the contacting bodies. Further they assert that in the case of smooth surfaces, in our highly polished surface of glass balls or ballotini, only a few molecules thick layer is sufficient to reduce the friction. Putner (1959) (reported by Holland, 1964) observed that merely rubbing a velvet cloth over a glass surface was sufficient to reduce the coefficient of friction from about 0.8 to 0.07. The results of Rowe (1971), Tong (1970), and Proctor and Barton (1974) show two distinctive features: (a) the coefficient of friction is low and is never reported by them as high as 0.8 for the cleaning technique used by them, and (b) their results show a possible trend of reduction of coefficient of friction with increase in normal load. In the light of the above discussion, these observations clearly support the possibility of existence of surface contaminants on the surface of glass ballotini tested by Rowe (1971) and his co-workers. Another important observation is made by Duffy and Mindlin (1957) which in fact support the said postulate. They reckon that the principal source of error in their tests on energy dissipation in a granular bar is the degree of cleanliness of the balls used in the tests. Cleaning the surface with only acetone for instance, instead of cleaning them in successive baths of carbon tetra chloride, toluol and acetone affected their results tremendously. Incidentally Rowe and his co-workers, e.g. Tong (1970), Barton (1972) have used acetone as one of their cleaning agents.

3.8.2.2 Ceramic balls

The test results on ceramic balls, Table 3.1 and 3.2, show that the coefficient of friction does not vary very much between the two extreme limits of surface moisture condition namely air dry and fully submerged in de-aired distilled water. In the absence of the profilometric measurement of surface asperities, it is difficult to make firm comments. However, the experimental results do point towards the possibility of the surface of the ceramic balls being rough in comparison to the smooth glass surface. The water does not act as an antilubricant or otherwise. These results clearly indicate the role played by asperities and are in full agreement with Horn and Deere's (1962) remarks on roughness and efficacy of water as anti-lubricant.

3.8.2.3 Polymeric materials

As mentioned in Chapter 2, in this study two visco-elastic thermo-plastic polymers have been used, namely PTFE and polypropylene. Out of these two plastics, PTFE is the most widely studied material due to its practical use as a low friction material. There is a much less published work on the frictional behaviour of polypropylene and that too is restricted to normal loads greater than about 20 N, which is outside the range of normal loads used here. Our discussions, of obvious necessity, will be directed towards the PTFE and the results obtained from this investigation will be discussed in the light of published data on it. The friction test results on polymeric materials used in this study, see Tables 3.1-3.2 show that the coefficient of friction increases with decrease in normal force under the given test conditions. A similar trend of behaviour has been reported by Shooter and Tabor (1952). The friction behaviour of PTFE as well as of

polypropylene can easily be explained either by using Bowden and Tabor's (1954, 1964) adhesion theory or by Archard's (1957) elastic contact theory. Both of these approaches predict similar types of behaviour at low normal loads.

It must be noted that in these tests no effort was made to investigate the effect of all the factors mentioned in section 3.5, which are characteristics of the visco-elastic materials. Instead the tests were carried out under restricted test conditions namely at a fixed constant speed of 0.028 mm/sec. and with a fixed geometrical arrangement. Further in these tests the vertical load on the top sliding particle was varied from 0.02 N to 4.0 N.

3.8.3 Friction Model

As pointed out earlier it is not possible to carry out friction tests for all possible expected forces which are likely to occur at the points of contact of grains in the particulate medium. It is, therefore, essential to have a model, whose selection is based on limited experimental results, which could explain qualitatively and predict quantitatively, if possible, the frictional behaviour of the material under study. As we have seen earlier in this chapter, there are various models or theories based on certain specific simplifying assumptions.

3.8.3.1 Brittle materials

The test results of the brittle materials namely of glass and of ceramic, fit very well with the extended Terzaghi - Bowden and Tabor model proposed by Skinner (1975). It must be noted that Skinner's (1975) model is based on the

assumption that the contacting surfaces are clean and smooth. However, this theoretical equation could be applied to moderately rough surfaces under moderate or low normal loads, providing that the necessary correction is made for the dilatation effect caused by the interlocking of the interacting asperities. Skinner (1975) extended his model further so as to include the effect of contaminant or of soft interfacial layer on the coefficient of friction. The value of the β factor, which accounts for the degree of surface cleanliness, in equation (3.7) is difficult to measure experimentally and no method has been suggested by Skinner for its numerical evaluation. Nevertheless the modified model could be used in qualitative explanation of friction behaviour of brittle materials.

3.8.3.2 Polymeric materials

The friction test results of polymeric materials, namely PTFE and polypropylene fit very well with the existing frictional models especially those proposed and developed by Bowden and Tabor (1964, 1967) and by Archard (1957). Either of these models will be used in this study. However, these models must be used with certain reservations if the effect of other visco-elastic parameters, e.g. stress level, time, temperature etc., has to be taken into consideration.

3.9 IS THE COEFFICIENT OF FRICTION CONSTANT?

The results of the present investigations have clearly shown that the coefficient of friction is not a constant quantity, see Tables (3.1) and (3.2), and Fig. (3.3) and (3.4), but varies with load. Whether the coefficient of friction of a given material increases or decreases with load is arguable and needs further deliberations and research. However,

Rowe (1971) has recognized that coefficient of friction changes with load although his relationship for brittle materials under full submergence in water is contrary to the experimental results of this study as well as of Skinner (1975). Nonetheless the writer agrees with Prof. Rowe for the necessity to record the average applied pressure and particle size, he will even go further and suggest that either a model or a graphical relationship between load and coefficient of friction would be better.

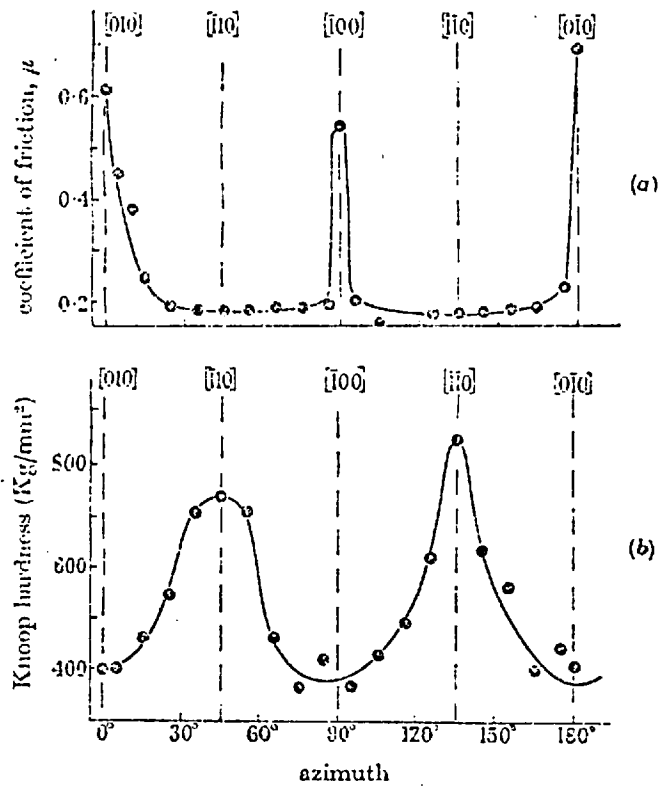


Fig. 3.1 (a) Frictional anisotropy between a 120° diamond cone and the (001) surface of magnesium oxide.
 (b) The anisotropy in the hardness of the (001) magnesium oxide surface confirms that low 'hardness' corresponds to high friction and conversely.
 (After Bowden & Brookes, 1966)

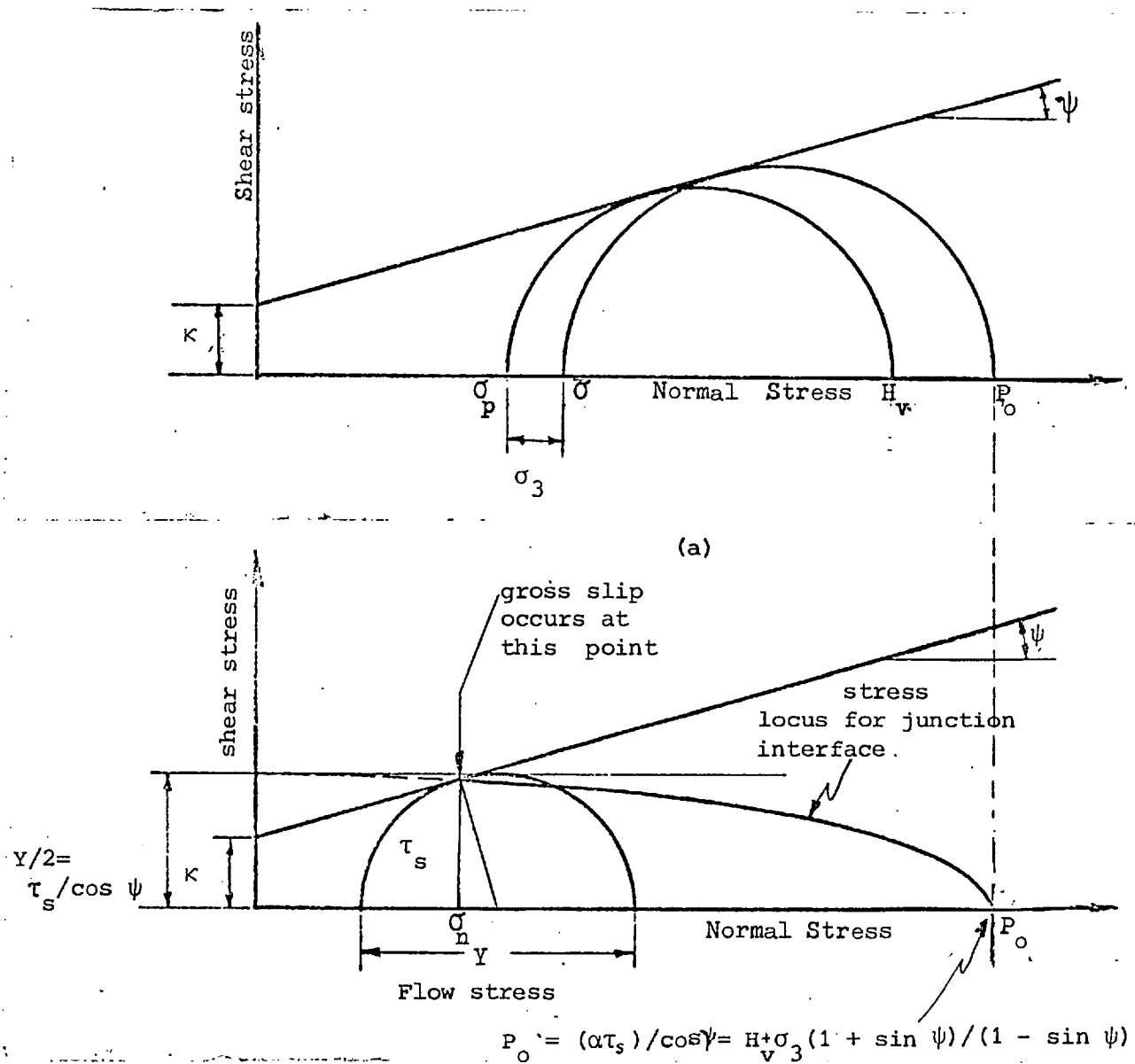


FIG. 3.2 (a) Initial stress condition with no shear traction
 (b) Stress locus for junction interface material.
 (After Skinner, 1975)

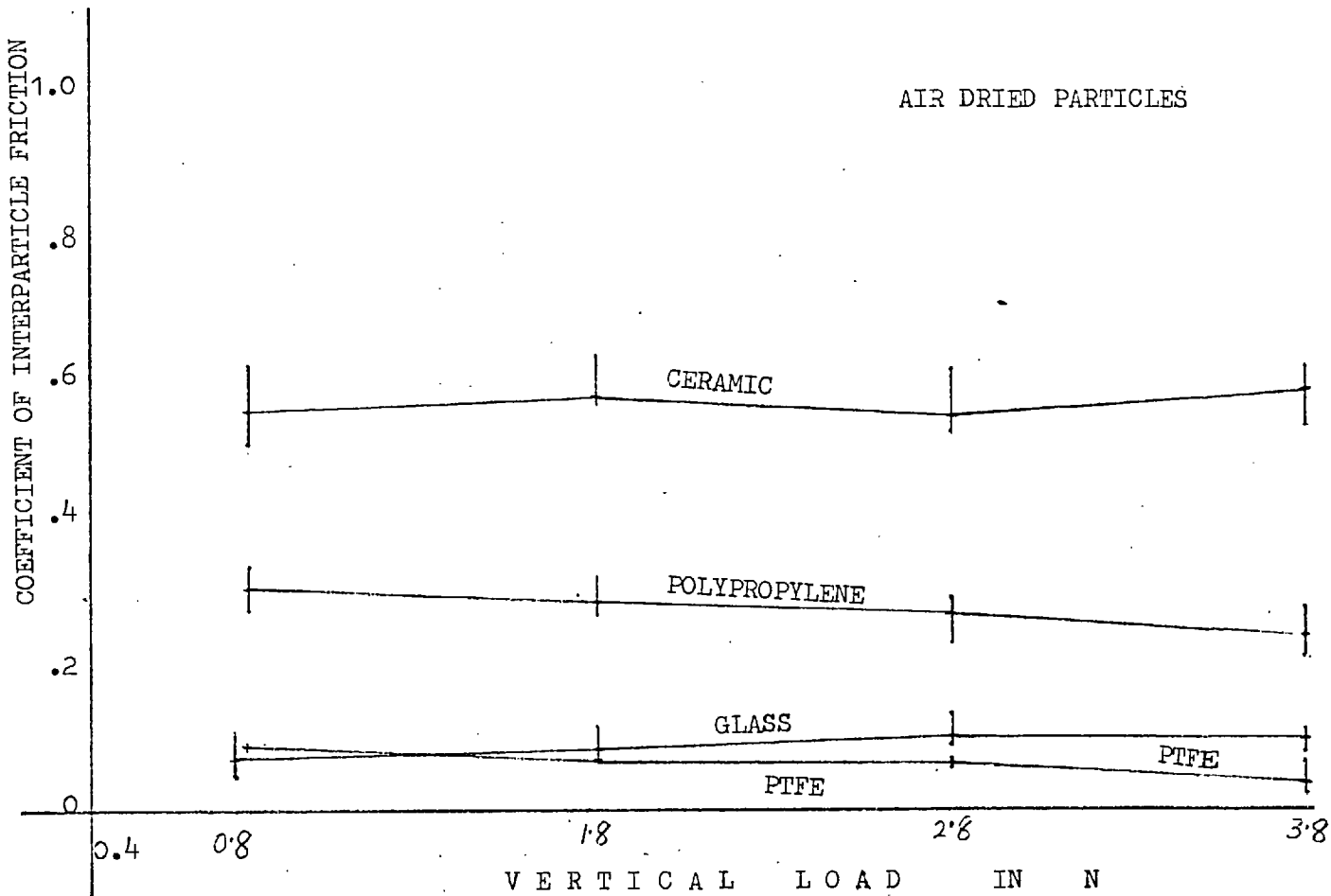


FIG. 3.5 INTERPARTICLE FRICTION TEST ON AIR-DRIED PARTICLES

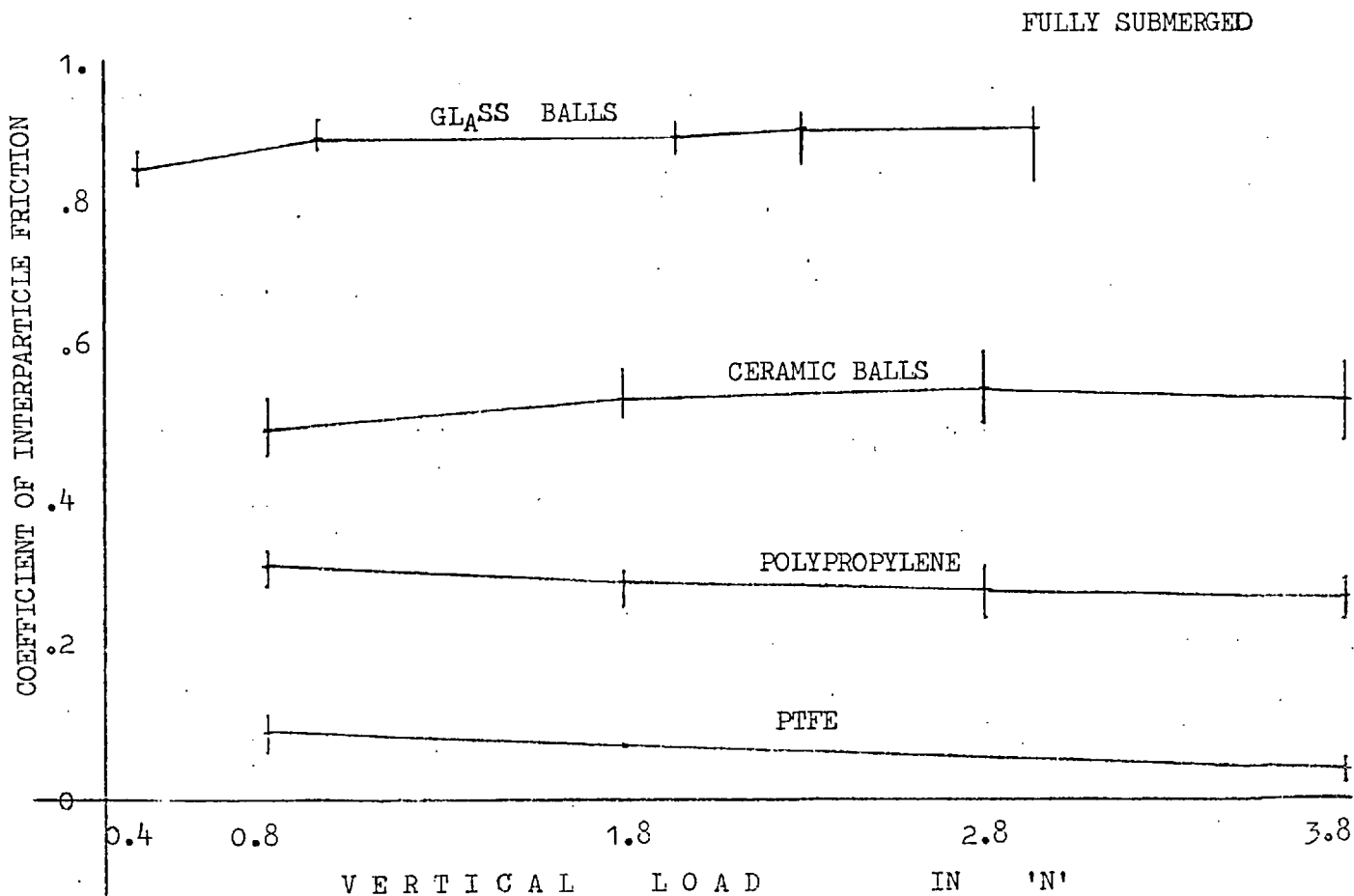


FIG. 3.6 INTERPARTICLE FRICTION TEST ON FULLY SUBMERGED PARTICLES

Vertical displacement - time trace
of the top ball

Tangential force-time trace

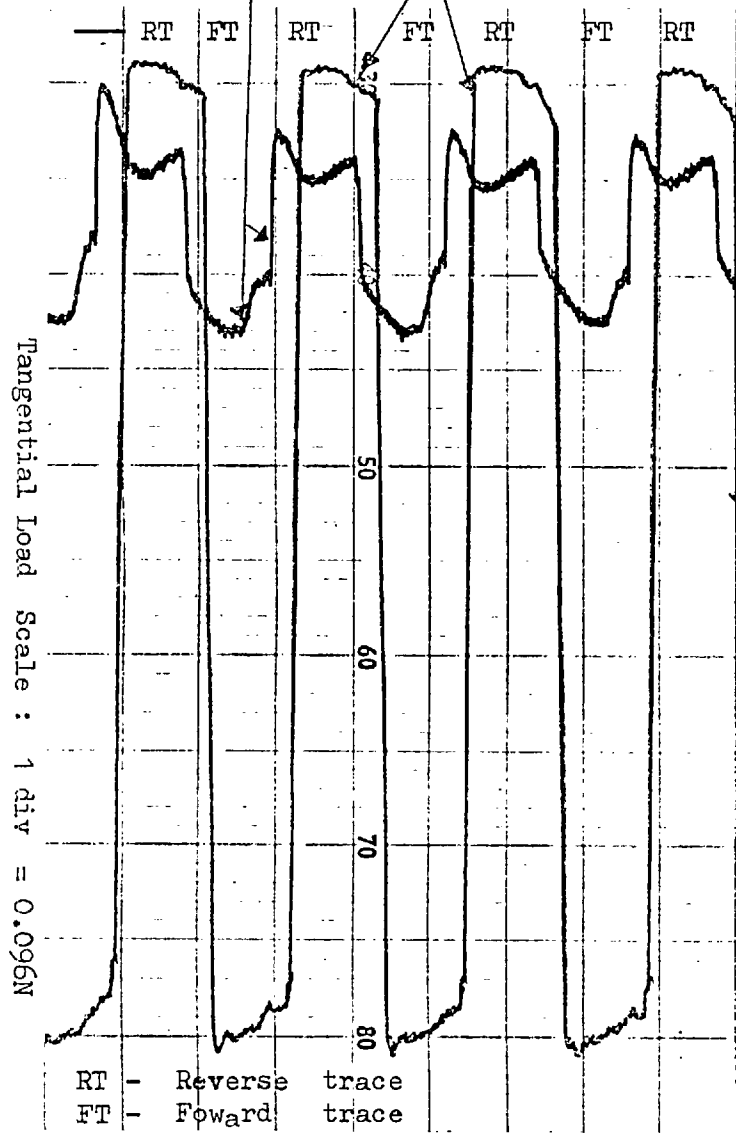
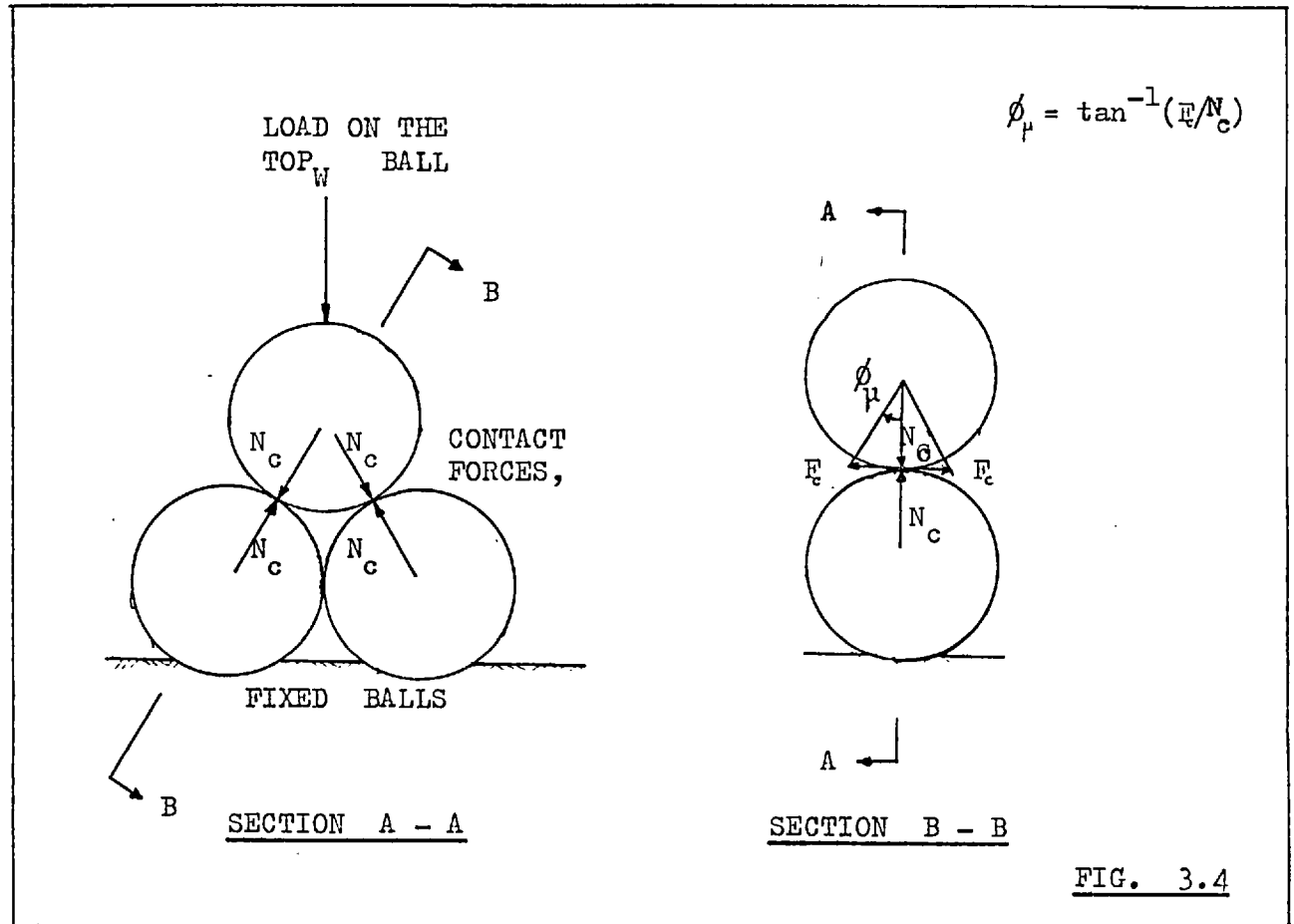


FIG. 3.3 A typical recorder trace of test on Glass ball on Glass ball, fully submerged under water & $W = 2.3N$



COEFFICIENT OF IN PARTICLE FRICTION

1.0

0.5

INTERPARTICLE FRICTION TESTS UNDER VARYING HUMIDITY

CERAMIC BALLS

GLASS BALLS

POLYPROPYLENE

PTFE

0

3

4

5

6

7

8

T I M E I N D A Y S

FIG. 3.7

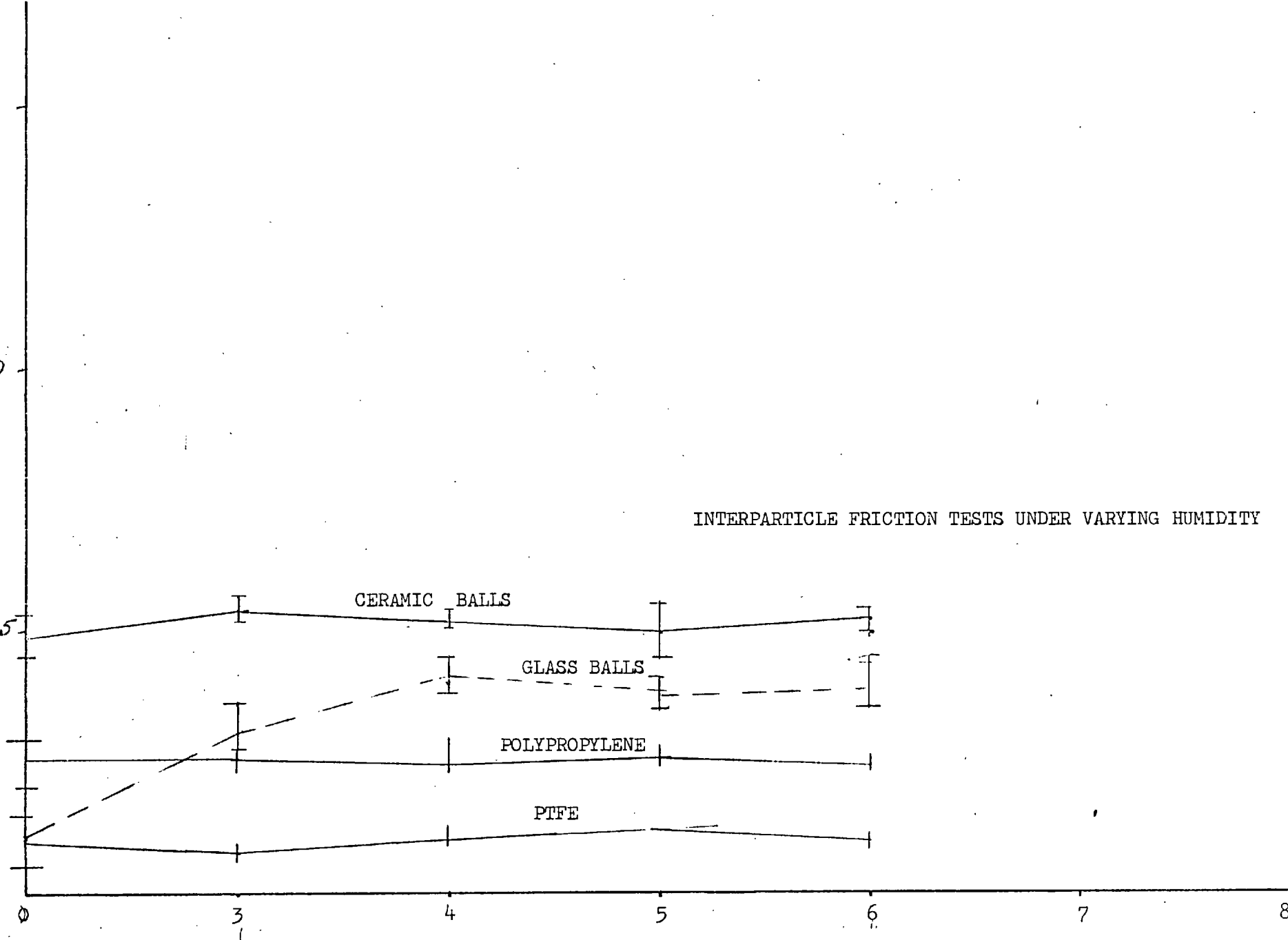


TABLE 3.1 COEFFICIENT OF INTERPARTICLE FRICTION OF AIR DRIED TEST MATERIALS

MATERIAL	VERTICAL LOAD W (N)	AVERAGE COEFF. OF FRICTION μ	ANGLE OF FRICTION ϕ (Deg)	STAND. DEV. σ_{μ}
1. Glass balls	0.8	0.074	4.23	0.012
	1.81	0.089	5.09	0.008
	2.80	0.102	5.84	0.006
	3.78	0.101	5.77	0.007
2. Ceramic balls	0.84	0.569	29.65	0.019
	1.81	0.577	29.98	0.011
	2.80	0.548	28.74	0.015
	3.78	0.587	30.34	0.012
3. PTFE	0.84	0.093	5.31	0.002
	1.81	0.0745	4.26	0.002
	2.80	0.067	3.83	0.002
	3.78	0.040	2.30	0.009
4. Polypropylene	0.84	0.31	17.22	0.011
	1.81	0.29	16.17	0.010
	2.80	0.272	14.84	0.012
	3.78	0.248	13.93	0.012

TABLE 3.2 COEFFICIENT OF INTERPARTICLE FRICTION OF FRICTION OF FULLY SUBMERGED BALLS

MATERIAL	VERTICAL LOAD W (N)	AVERAGE COEFF. OF FRICTION μ	ANGLE OF FRICTION ϕ (Deg)	STAND. DEV. σ_{μ}
1. Glass	0.98	0.891	41.71	0.016
	1.96	0.896	41.86	0.018
	2.30	0.907	42.22	0.019
	2.94	0.903	42.08	0.017
2. Ceramic	0.84	0.50	26.6	0.008
	1.81	0.54	28.5	0.010
	2.80	0.55	28.98	0.015
	3.78	0.54	28.34	0.013
4. PTFE	0.84	0.093	5.33	0.008
	1.81	0.075	4.27	0.005
	3.78	0.038	2.18	0.006
5. Polypropylene	0.84	0.315	17.48	0.007
	1.81	0.295	16.43	0.006
	2.80	0.283	15.80	0.010
	3.18	0.271	15.16	0.009

TABLE 3.3 TYPICAL FRICTION TEST RESULTS

MATERIAL	TEST CONDITION	VERTICAL LOAD W (N)	AVERAGE COEFF. OF FRICTION μ	ANGLE OF FRICTION ϕ (deg)	STAND. DEV. σ μ	
1. Glass	Sub.	Ball on flat	2.80	0.891	41.7	0.016
		Ball on ball	2.94	0.903	42.08	0.017
	Dry	Ball on flat	3.78	0.070	4.00	0.010
		Ball on ball	3.78	0.100	5.75	0.007
2. Ceramic	Sub.	Ball on flat	3.78	0.481	25.6	0.009
		Ball on ball	3.78	0.539	28.34	0.013
3. PTFE	Sub.	Ball on flat	1.81	0.071	4.06	0.009
		Ball on ball	1.81	0.075	4.27	0.005

CHAPTER 4

X-RAY PHOTOGRAMMETRY - DATA ACQUISITION SYSTEM4.1 INTRODUCTION

In order to understand the deformation behaviour of a granular medium, it is essential to explore its behaviour at microscopic level under given deformation conditions. Evidently, this requires the use of methods or techniques unfamiliar in conventional geotechnical engineering which is mainly based on continuum approach. If such methods are developed and are used so as to supplement the existing methods, it can offer an added advantage of analysing the granular mass under study both from continuum approach, in which we, the geotechnical engineers, are generally trained, and from particulate approach, which is the correct approach to apply (Terzaghi, 1925; Rowe, 1971; Skinner, 1975). One such experimental method is developed and used in this study. As it involves two totally different stages, first stage of this method is described in this chapter and the second is outlined in the following chapter. In this chapter, it will be shown how one can "look inside" a "representative" granular mass of limited size and can acquire the necessary information for further analysis without disturbing the deforming mass. The mechanical behaviour of particulate media is very complex and intricate. It is, therefore, necessary to probe the medium in various ways and observe its response both at the macroscopic level and microscopic level. As already mentioned in Chapter 1, one of the main objectives is to investigate the deformation mechanism under the given conditions outlined earlier. This will require the determination of rotation

and translation in three dimensional space of all the constituent particles. This ideal and theoretically desirable requirement is rather difficult if not impossible, at least for the present.

However, certain compromises can be made. For instance, in this work only a limited number of particles placed in suitable positions were observed. The whole exercise of finding translation and rotation of particles quantitatively may be accomplished in two distinctively different stages; namely

a) Data Acquisition Stage

This stage consists of finding or developing a method or technique most suitable under the given constraints, for example available equipment, granular material and deformation conditions, time and money, etc. After having selected a method, it is then employed to record the movement of pre-selected particles placed anywhere in the granular mass and at any stage of deformation. One of the basic requirements of this stage - as for any other method - is that the data obtained from any test must be in appropriate form and must be open for further analysis, if needed, was fulfilled by obtaining stereo-radiographs of test specimen at various stages of deformation. These radiographs were, in fact, input data to the second stage of the method namely Data Reduction Stage.

b) Data Reduction Stage

Once the information of particle displacements is available in a suitable form such as photographs, radiographs, etc., the next logical and obvious step is to reduce this data into a suitable format preferably in digital form for further analysis and interpretation.

The first stage of operation is the subject matter for this chapter. The later stage will be discussed in the next chapter.

4.2 A SUITABLE TECHNIQUE - SURVEY AND SELECTION

4.2.1 General

In the past various non-conventional techniques have been employed in an effort to study the granular test specimen or its model at the microscopic level. It is the burden of this section to show inadequacies of the available methods and thus bring out the need for a technique which has never been used in Particulate Mechanics, to the best of the writer's knowledge.

Most of the available methods can be classified under the following headings:

- i) Thin section technique,
- ii) Methods based on idealised 2-D models,
- iii) Photographic methods, and
- iv) Radiographic techniques.

A brief discussion is presented here but for detailed information reference should be made to the original papers mentioned in the relevant sub-sections.

4.2.2. Thin Section Technique

This technique has been used successfully for the study of microstructure and soil fabrics usually in fine grained soil e.g. by

Morgenstern and Tchalenko (1967); Lafeber (1966). It has also been used by Oda et. al. (1972) for studying the void ratio distribution in a triaxial compression test and by Oda (1972a) and Borowicka (1973) for studying the statistical distribution of particle contacts in a coarse grained medium.

Thin section technique, when applied to study the response of fabric under various boundary conditions, essentially consists of running identical tests on a number of "statistically similar" test specimens. Each test is stopped once it has reached the predetermined deformation condition. At this stage, the fabric is frozen by employing a suitable impregnating technique. The thin sections are then prepared from selected areas of these "fabric frozen" specimens. These thin sections are studied under an optical or electron microscope. The information gathered from the study of these sections of specimens, each of which has been deformed up to a predetermined deformation or stress level, is used to construct the deformation history of a "statistically" similar test specimen.

Although thin section technique is useful for microstructure studies of soils, it is not very suitable for studying the deformation mechanism of coarse grained particulate media. Firstly, this technique cannot give quantitative information of translation and rotation experienced by a particle or by a group of particles in a specimen under study at various stages of deformation. Secondly, the method relies on the implicit assumption that all the specimens which supply the information to form the complete history, have statistically

identical initial fabric and behave identically under the given deformation conditions. It is a formidable task to prepare and test the specimens so as to obtain identical results. The success of the method thus depends both on the preparation of the test specimen and testing method. Thirdly, the technique is destructive in nature. It is therefore evident that thin section technique is not an ideal one and a further search of a suitable technique is necessary, particularly for the study of coarse grained particulate mass.

4.2.3 Two Dimensional Models

In the past, two dimensional (2-D) models have been used to explore the behaviour of a granular mass. A single layer of particles, which are of regular geometrical shapes, has been extensively used, for instance, discs by Marsal (1973); Oda and Konishi (1974a); Drescher and de Josselin de Jong (1972); cylinders by Murayama and Matsuoka, (1973); Logani (1973). Some of the researchers including Oda and Konishi (1974a), Drescher and de Josselin de Jong (1972) have advocated the use of 2-D models made from photo-elastic materials. It has an added advantage over the other 2-D models because measurements of the contact forces as well as of the displacements of the constituent particles of the granular model under study can be done. Despite these advantages, it is rather difficult to say with certainty that 2-D models correctly model the real situation in the granular mass. It looks as if 2-D models oversimplify the reality.

4.2.4 Photographic Methods

Photographic methods can be used for the study of particulate

media. The potential of this method can be further enhanced if the photogrammetric technique is properly blended in. Close range photogrammetry is a fast developing off-shoot of the parent field, namely photogrammetry. Butterfield et. al. (1970), Andrawes and Butterfield (1973), have utilized the stereo-photogrammetric technique for determining the planar displacements and velocity fields. Moreover, they have used very simple photography as well as viewing equipments (Butterfield and Andrawes, 1971). Due to the limitations imposed by the photography, their work is restricted to measurement and plotting of planar fields or other parameters which could be measured or calculated from the movement of particles located on the surface of granular mass photographed. Since the constituent particles of granular mass are not transparent, conventional photography cannot bring out the inside details and trace the movements of particles inside the medium.

4.2.5 Radiographic Technique

The radiographic technique as its name suggests, is the technique based on the application of Radiology - the science and application of ionizing radiation such as X-rays and gamma-rays. This technique is a non-destructive method of testing, and at the same time, by adopting this method one can see either on a radiograph or on a fluorescent screen the images of lead shot or specially prepared particles, called here markers or marker particles, placed inside the specimen radiographed. One can also observe the density variation by measuring the density variation of the radiograph, Arthur and Dunstan (1969). This enables us, in a way, to look "inside" the particulate medium.

G ber (1929) used the radiographic technique to determine the overall displacements of a medium when it was made to fail under certain loading conditions. Davis and Woodward (1949) refined the technique in an attempt to measure relatively small incremental displacements. They used the information as obtained to distinguish between pre- and post-peak conditions.

Arthur (1962) improved the radiographic technique and applied the method, perhaps for the first time, to find the internal strain distribution in a backfill of a model retaining wall under the plane strain condition of observing the displacements of lead shot which were placed at the nodes of a co-planar regular net-work within the soil mass.

Roscoe, Arthur and James (1963) and other researchers at Cambridge University made substantial contribution in radiological soil studies. They even designed and constructed a very sophisticated computer controlled automatic film measuring machine (FMM), James (1973). This machine is capable of locating images of lead shot embedded in the test specimen within an accuracy of ± 6 microns. The FMM is specifically designed to determine the location of small circular images of about 2.5 mm in diameter on a radiographic film up to 50 8 mm x 50 8 mm in size. The radiographic technique developed at Cambridge is suitable only for the study of a continuum deforming under plane strain or axi-symmetric deformation conditions. It is,

therefore, difficult to apply this technique to the study of a particulate medium. Nevertheless, the radiographic technique has got a wide field of application in Soil Mechanics and in other branches of engineering.

Arthur (1971) and his co-workers have made yet another major contribution by introducing and adapting Tomography as a non-destructive testing tool for the study of particle packing in a test specimen. Although Tomography is a very powerful technique, it poses insurmountable difficulties, at least in its present form, to trace the rotational and translatory movements of spherical or very nearly spherical particles inside the test specimens. Therefore, it cannot be used in this study.

4.3 RADIOGRAPHY AND PHOTOGRAMMETRY

Radiographic techniques, as apparent from the above discussions, are very useful in observing the behaviour of a granular medium by monitoring the internal deformations. It is possible to use the radiographic technique so as to observe the behaviour of granular mass at microscopic level. One of the possible ways to achieve this, particularly in a coarse grained particulate medium is suggested here and has been used in the present investigation. In this method, a few particles of granular mass are made to absorb more radiation than that absorbed by the rest of the constituent particles. If the zone of high radiation absorption in the marker particles is fixed in volume and in dimensions, and is of suitable geometrical shape,

their images on a radiograph can easily be identified when these markers are placed in the specimen of granular material under study. Further, these radiographic images should be of simple geometrical shape with well defined long axis so that from its measurement the determination of both translation and rotation should be possible. Also the shape, size and physical properties of these marker particles must be similar to the other particles in the medium. The radiographic opacity of particles, fulfilling the above requirements, was achieved in this study by inserting tungsten wire in the particles and the method is described in Chapter 2.

Once the radiographs of relatively high quality containing the images of marker particles and control points are obtained and the images on such radiographs identified, and individually and uniquely numbered, it remains to find a method or a technique by which the spatial co-ordinates of the marker particles can be accurately determined. The method should be general in nature and must not put any constraint on the initial placement and subsequent movement of marker particles at various stages of deformation. In order to achieve this goal, the use of photogrammetry is made in addition to radiography.

Photogrammetry is defined as the science or art of obtaining reliable measurements by means of photography. Therefore, the basic principles of photogrammetry can be applied to radiography if the principles of shadow (or image) formation are the same both in

photography and radiography. Fortunately, both radiation and light rays travel in straight lines with the velocity of light, and so the geometric law of shadow formation may be applied to both types of rays. Also, when a photographic film, having a coating of a thin layer of gelatine containing silver halide colloids in suspension, is exposed to light or ionizing radiation, e.g. X-rays, similar invisible reaction with the silver halide takes place and a latent image is formed. Hence the principles of photogrammetry can be applied to radiography.

4.4 SOME BASIC DEFINITIONS AND TERMINOLOGY

For a better understanding of the mechanism of deformation of a particulate medium, we need an intelligent combination of three different branches of science and engineering. They are Radiology, Photogrammetry and Soil Mechanics. Adequate knowledge of three types of terminology is therefore essential. The definition of the basic terms which are relevant to this work are included in the following sub-sections. Nevertheless, for a more comprehensive coverage of Radiological terminology, reference is made to the British Standard 2597:1955 "Glossary of Terms used in Radiology"; and for the photogrammetric terms, the basic reference is the Manual of Photogrammetry edited by Thompson, (1966).

4.4.1 Radiological Terminology

Backscatter: That part of scattered radiation which has a scattering angle of more than 90° .

Cassette: A light tight aluminium container for holding radiographic

film under uniform pressure during exposure.

Contrast: The relative brightness of two adjoining areas in a radiograph.

Definition: The sharpness of demarcation of image detail in a radiograph.

Density: The logarithm of ratio of the light intensity incident upon the film to the luminous flux transmitted by the film.

Filter: Sheet of material interposed in the path of radiation so as to reduce selectively the intensity of radiation of certain wave length or energy.

Focal Spot or Focus: The area of the target on which the stream of electrons strike and from which X-radiations are emitted.

Focus-to-film distance (f.f.d.): The perpendicular distance from the focus of an X-ray tube to the X-ray film set up for radiographic exposure.

Intensifying Screen: A layer of suitable material such as lead or calcium tungstate which when placed in close contact with an X-ray film enhances the photographic effect of the incident radiation.

Latent Image: An invisible image produced in a layer of photographic emulsion by exposure to radiation, visible light or UV rays, and capable of being changed into a visible image by development, i.e. by treatment of the emulsion with a suitable chemical solution known as developer and this process is known as development.

Mask: A device made of a substance, e.g. sheet lead, employed to restrict the area irradiated.

Metal Screen: An intensifying screen of metal foil, generally lead foil which emits secondary radiation under the action of ionizing radiation.

Objective definition: It is determined by the width of the separation between the adjacent fields of different but uniform densities. The narrower the width, the better is the objective definition.

Objective Contrast: The quantitative density difference between two areas measured with the help of a densitometer.

Optical Focus: The projection of the focal spot on a plane perpendicular to the axis of the beam of X-rays emitted from the X-ray tube. It is also known as 'focus'.

Primary Radiation: Radiation which is incident on the absorber and which continues without change in photon energy and in direction after passing through the absorber such as filter or intensifying screen.

Processing: A series of operations, namely developing, fixing and washing, connected with the conversion of a latent image into a stable visible image.

Quality or Hardness of radiation: It is a relative term used to describe the penetrating power of the radiation.

Radiograph: A photographic image produced by some form of ionizing radiation, e.g. X-rays or gamma rays which has passed through the object.

Radiography: Production of radiographs.

Radiology: The science and application of ionizing radiation such as X-rays, gamma-rays.

Scattering: The deflection of radiation with or without change in wave length and quantum energy.

Secondary Radiation: Radiation, other than primary radiation, emerging from the absorber.

Sensitivity: The extent to which a radiograph is able to show clearly details of a given object.

Subjective Contrast: It is the contrast perceived by the human eye.

Subjective Definition: It is the definition or sharpness of an image as seen by the eye.

Target: The surface of the anode of an X-ray tube on which the stream of electrons strike and from where the main beam of X-rays is emitted.

Tube diaphragm: A device, such as slit or opening in a thick sheet of lead, normally fixed to an X-ray head to limit the divergence of the X-ray beam.

Tube-shift Radiography: The method of determining the position and dimensions of details within an object by measurement made on radiographs taken from two different directions or locations.

Unsharpness: A quantitative measure of lack of definition. It is generally expressed as the width of separation between a sudden change in the intensity of radiation incident on the film.

X-Rays: Electromagnetic radiation generated due to the loss of energy of charged particles (e.g. electrons) and having shorter wave length than the ultra-violet radiation spectrum.

4.4.2 Photogrammetric terms:

Base: The line joining two exposure stations, or the length of this line.

Base Height Ratio: The ratio between the base and height of a stereoscopic pair of radiographs.

Perspective Centre: The point of origin or termination of bundles of perspective rays.

Resolution: The minimum distance between two adjacent features or the minimum size of a feature, which can be detected by a photographic system.

4.4.3 Soil Mechanics Terms:

Most of the Soil Mechanics terms used here are standard terms and all are well known to Soil Engineers. However, reference can be made to any standard text book or glossary, e.g. Taylor (1948) for a complete coverage of definition of terms.

Those terms, which are not usually very common, are defined wherever they first appear in the text.

4.5 SELECTION OF SOURCE OF RADIATION

X-rays and gamma-rays are electromagnetic radiation. X-rays

are generated by means of an X-ray tube with their energy and intensity generally adjustable, whereas the gamma-rays arise from the disintegration of certain natural elements, such as radium, or are emitted from the artificially produced unstable radio-isotopes, such as Cobalt 60, Iridium 192, Caesium 137.

The energy and intensity of X-radiation can easily be controlled by suitable control of current and voltage across the anode and the cathode of the X-ray tube. The energy of gamma-radiation cannot be controlled as it depends solely upon the radioactive source. Also, its intensity is uncontrollable since it is not possible to change the rate of disintegration of a radioactive substance. Further, they emit radiation generally of higher penetration power than that from an X-ray tube and therefore the radiographs are of low contrast. Due to the inherent low contrast of radiographs obtained from gamma-radiation, the accuracy of measurement on the radiographs is much lower than those on radiographs obtained by X-radiation.

For the reasons mentioned, X-radiation is a better source of radiation and hence it is the obvious choice for the higher quality radiographic work carried out for the X-ray photogrammetric investigation of the present study.

4.6 X-RAY PHOTOGRAMMETRY

4.6.1 General

If X-radiation, also known as Roentgen, is used for photography

and such photographs, usually called radiographs, fulfil the basic requirements of conventional photogrammetry, then the basic principles of photogrammetry can be applied for calculating the spatial co-ordinates of marker particles from the measurements made on radiographs. The science or art of obtaining such measurement may be termed as X-ray photogrammetry or "Roentgenogrammetry".

4.6.2 Major Problems of X-Ray Photogrammetry

The major difficulties which are common to photogrammetry and hence to X-ray photogrammetry, arise chiefly from the following two general sources:

- a) Data acquisition system is rarely perfect, fulfilling all the requirements. In other words, the conditions for obtaining the radiographs are never ideal.
- b) Data reduction from the information recorded on the radiographs can rarely be accomplished with complete accuracy.

An attempt was made to understand difficulties arising from source (a) and how some of these difficulties were overcome under given constraints of available equipment, films and the present state of knowledge of X-ray Photogrammetry. The second source of difficulties will be dealt with in Chapter 5. It may be of some interest to note that X-ray photogrammetry is a very recent addition to the field of applications of Close Range Photogrammetry and suffers from various limitations. However, the limitations and

shortcomings of the technique do not in any way hinder the use of the technique provided its limitations are fully appreciated and unduly high accuracy is not demanded until the present technique is developed further.

In the present investigation, it is intended to use X-ray photogrammetry as a tool for obtaining the measurements with maximum possible accuracy. Although fundamental research in X-ray photogrammetry is needed as will be clear from the discussion to follow, the scope of this study did not permit the writer to undertake any development in this interesting field of research. Nevertheless, where the basic information was lacking and could not be extracted directly from photogrammetry or from radiology, it was obtained either by modifying the existing formulation to suit the present application of close range photogrammetry or by making plausible simplifying assumptions. Care was taken to ensure that such modifications or assumptions did not excessively impair the accuracy of the final result.

4.7 BASIC REQUIREMENTS OF X-RAY DATA ACQUISITION SYSTEM

In X-ray photogrammetry, the data acquisition system consists of an X-radiation source (X-ray tube), X-ray film placed in a predetermined position and the object interposed between the X-ray source and film. The source of radiation in X-ray photogrammetry is assumed to be the focal spot of the X-ray tube. Although the focal spot is not a mathematical point, it is assumed to be a point and its corresponding point in conventional photogrammetry is the optical centre of the camera.

The essential requirements of any photogrammetric system as well as for X-ray photogrammetry are:

a) the radiographs which are to be interpreted must be of high quality. In other words, the radiographic sensitivity must be as high as possible, and

b) the radiographs of the sample, containing the marker particles should be taken in such a way so as to form a stereo-model in an optical measuring machine e.g. stereocomparator, stereoplotter, etc.

The first condition is concerned with the selection of apparatus and film, exposure control and processing for the given material and test sample configuration. The latter requirement is involved with the arrangement of X-ray source, object and film.

4.8 QUALITY OF X-RAY IMAGE

The success of a photogrammetric exercise depends primarily on the quality of the radiographs and on the consistency in their standard of image quality. The quality of X-ray image is affected by a number of factors; all must be accurately determined and controlled if consistently high radiographic quality is to be maintained. Conversely, in order to achieve radiographs of high sensitivity, proper X-ray source, film, developing process have to be selected and their production has to be standardized. It is felt that a short discussion on the factors affecting the sensitivity will be helpful in highlighting how the data acquisition system was selected and how some of the conflicting requirements were judiciously

balanced. Moreover, it is expected to bring out the need for further fundamental research in the field of X-ray photogrammetry.

4.9 FACTORS AFFECTING RADIOGRAPHIC SENSITIVITY

4.9.1 Introduction

The higher the objective contrast of the radiographic technique in use, the greater will be the difference in densities corresponding to the varying degree of radiation impinging on the film. Thus, it will be easier to recognize the markers and to carry out the necessary measurements. The human eye is unable to distinguish the differences in brightness i.e. density differences in the radiograph under examination below a certain limit known as "threshold limit". This threshold limit is affected appreciably by the definition of image, in other words, by the sharpness of transition from one density field to another. On the other hand, the eye can discriminate correctly even slight differences in density if there is a sudden transition from one density area to another. In the case of gradual transition of densities, quite high differences in densities may pass unnoticed by the human eye. Therefore, the contrast and definition of the radiograph are the two characteristics which determine the sensitivity of a radiograph. The radiographic sensitivity is affected by many factors which are summarised in Figure 4.1. The most important factors are briefly discussed in the following sub-sections.

4.9.2 Factors Affecting Contrast

4.9.2.1 Quality of Radiation

a) Kilovoltage of X-ray Source

The higher the energy of X-radiation i.e. its kilovoltage, the

higher will be its penetration power but the lower contrast. For optimum contrast and hence sensitivity, the lowest kilovoltage should be used, but it should be consistent with reasonable exposure time and minimal scattered radiation.

b) Generator Circuit

The percentage of soft rays present in the X-rays limited at a given voltage depends, among other things, on the kind of generator circuit used. For higher contrast, it is essential to choose that X-ray generator circuit which emits a low percentage of soft radiation, an example is the Greinacher circuit.

4.9.2.2 Filters

The filters, thin sheet of metals such as copper or lead interposed between the source and film, are generally used to reduce the proportion of soft radiation in the X-ray beam. They, therefore, act to some degree, in the same way as an increase in the energy of source of radiation in that they produce a radiograph of lower contrast. However, under certain conditions, a filter may be useful in reducing the scattered radiation.

The necessity for filters and their form is determined by trial and error.

4.9.2.3 Scattered Radiation

Scattered radiation, whether emerging from the specimen itself or from other neighbouring objects, produces an overall fogging and

reduces the contrast of the radiograph.

The sources of scattered radiation are:

- a) scatter from within the specimen
- b) scatter within the cassette
- c) "reflected" scatter, and
- d) back-scattered radiation

Figure 4.2 schematically shows the various types of scattered radiation.

It is impossible to eliminate completely scattered radiation; there are many methods, such as use of diaphragms, masks, localisers, screens, whereby its effects can be reduced. For achieving higher contrast in the radiographs, it is worthwhile to cut down effectively the scattered radiation by adopting some suitable method.

4.9.2.4 Films

Industrial X-ray films covering wide range of speed, definition and contrast are available. The films can be grouped under two main categories; direct type film for use with or without lead intensifying screen and screen-type for use with salt intensifying screen. Kodak and Agfa-Gevaert make a wide range of X-ray films to meet all requirements of industrial radiography. The salient information for only three films made by Kodak Ltd. is given in Table 4.1, as these were actually used in the trial runs for film selection.

TABLE 4.1 *				
Type of Film	Relative Speed	Contrast	Grain Size	Radiographic Quality
Industrex 'M'	1	Very High	Very Fine	↑ Improving Radiographic Quality
Industrex 'C'	4	High	Fine	
Industrex 'D'	8	High	Medium	

* After Kodak Ltd. (1965)

It may be worth noting, unlike films and plates specifically designed for aerial photography, no film or glass plate, as far as the writer is aware, is yet available which is specially designed and developed for X-ray 'photogrammetric' use. In such circumstances, one is left with no choice but to select film from the available Industrial-type films and to sacrifice some accuracy of measurement.

From Table 4.1, it is apparent that the natural choice will be of Industrial 'M' type film. But there are many factors affecting the choice of a film which must be taken into consideration before a final choice is made. The best method of choosing a film is by trials.

4.9.2.5 Intensifying Screens

Two types of intensifying screens, salt screens and lead screens, are generally used in Industrial radiography. Salt intensifying screen technique can produce radiographs of higher contrast but at

the cost of definition. Although it satisfies the requirement of high contrast, its resolution is very poor from the photogrammetric point of view. Hence, salt screens are not suitable for getting high quality radiographs. Lead screens are generally used as they cut the soft, scattered radiations and add to the intensification of hard, primary radiation and so produce a radiograph of slightly higher definition than if no screen were used. The subjective definition is often enhanced by the use of lead screens.

4.9.2.6 Processing of Exposed X-Ray Film

The amount of metallic silver which is formed by development and the contrast of the radiograph, is dependent not only on exposure but also upon the time of development and the temperature of the developer. Any increase in developer temperature, development time or amount of agitation will increase contrast and density of a radiograph. It must be remembered that any uncontrolled change in developing condition will change the contrast and density of the radiograph and create an inconsistency in the series of radiographs. It is, therefore, necessary to standardize the developing process and if possible use automatic processing machines which will save time, energy and, at the same time, standardize the procedure.

4.9.2.7 Density

The contrast of the radiographs increases with density up to very high densities. Therefore, for getting higher density with direct type films, the radiograph should be made with the highest

density that can be viewed with comfort. The density or amount of blackening on a radiograph depends upon the following:

- a) Quality and quantity of radiation
- b) Time of exposure
- c) The distance between source and film
- d) The X-ray film used
- e) The intensifying screen
- f) Processing conditions
- g) Filtration
- h) X-ray apparatus in use and the circuit employed
- i) The object being radiographed

The best way of finding the suitable technique to get high density is by trial and error.

4.9.2.8 The Object Being Radiographed

The X-ray absorption of an object depends upon its thickness, its density and upon the atomic numbers of the elements present. Of two specimens of the same material, the thicker will obviously absorb more X-ray energy. Same is also true with density. The denser specimen of same thickness as the other will show more absorption. The atomic weights of various elements in a specimen generally exert a far greater effect upon X-ray absorption than either its thickness or density. The contrast of a radiograph is therefore affected by : (a) the differences in the thickness of the specimen, (b) the differences in densities and (c) the differences in radio-opacity of the defects and specimen in conventional industrial radiography or of the specimen and the material of the marker wire in

the present study. In the case of specimens of granular materials the magnitude of scatter generated from within the specimen is considerably higher since every grain particle of the specimen acts as a source of scatter radiation. It is rather difficult to control the scatter radiation from this source. Arthur and Dunstan (1969) have designed a special filter which they used in their particle packing studies. These specially designed filters cannot be used, as images of scatter absorbing members of the filter might cover the images of some of the markers whose displacement history have to be traced. The need for design and development of filters for X-ray photogrammetric use in granular soils or finding some technique for reducing the scatter radiation is very essential if the quality of the radiograph is to be proved.

4.9.3 Factors Affecting Definition

4.9.3.1 Introduction

As mentioned earlier, the definition of a radiograph is as important as its contrast. Reference to Figure 4.1 will reveal that there are various factors which decide the definition of a radiograph. There are certain factors which affect both characteristics of sensitivity, for example quality of radiation, screens and film. These factors have already been discussed in the preceding sub-sections, no further comments will be made on them except on the film. In addition to remarks made in sub-section 4.9.2.4, a brief comment will be made on the film resolution. Another important factor, namely vibration of the specimen during exposure, adversely affects the definition of the radiograph obtained. Every precaution must be

taken to avoid vibration of the specimen during the exposure interval.

4.9.3.2 Geometric Factors

The X-ray source or any gamma-ray source is not a point source from which radiation rays are emitting, therefore the geometrical unsharpness also known as penumbral unsharpness can never be eliminated. However, for optimum definition, the penumbra should be as small as possible. The following conditions should be fulfilled in order to achieve optimum sharpness of images:

1. Focal spot or source size should be as small as possible.
2. The film to focus distance should be as large as practicable.
3. The film to object distance should be as small as possible.

Geometric Principles

Ionizing radiation rays and light rays travel in straight lines. Although the analogy between light and X-rays is not perfect, the geometric laws of shadow formation may be applied to both types of rays.

In Figure 4.3, the source from where the rays are emitting is assumed to be a circular surface with a diameter - 'a'. An object p, located at the distance z from the source, is assumed to be of circular shape of diameter 'b'. This assumption is made just for the sake of simplicity. In Figure 4.3 (a) and 4.3 (b), two sets of three types of images can be distinguished depending on the location

of film namely at f_1 , f_2 , and f_3 . In one set the focal spot is smaller than the object and in another the focal spot is larger than the object.

a) Focal spot is bigger than object:

In Figure 4.3 (a), the image at f_1 consists of a dense shadow and a penumbra, the image at f_2 consists of penumbra only and the third image at f_3 consists of a ring of penumbra around an unexposed centre spot.

b) Focal spot is smaller than object:

Reference to Figure 4.3 (b) will show that for all the three positions of the film i.e. at f_1 , f_2 and f_3 both dense shadow of the object and the penumbra are formed. The size of dense shadow as well as the penumbra increases with the increase in the film to object distance. Further it will be seen from this figure that an unexposed centre spot, as formed in the previous case, is never formed. It is therefore better to keep the film to object distance as small as possible.

From the knowledge of elementary geometry we can find the following expressions for the diameter of the shadow and the penumbra, see Figure 4.3 -

$$\text{Diameter of the total shadow: } d' = b(f/z) + a\{(f/z)-1\} \quad (4.1)$$

$$\text{Diameter of the dense shadow: } d' = b(f/z) - a\{(f/z)-1\} \quad (4.2)$$

$$\text{The penumbra: } d - d' = 2a\left\{\frac{f}{z} - 1\right\} = 2(ah/z) \quad (4.3)$$

where $f = h + z$

From the above geometrical relationship, we find that the geometrical unsharpness depends on:

1. Focal spot size - Penumbra \propto focal spot size 'a'
2. Film object distance - Penumbra \propto film-object distance 'h'
3. Object - source distance - Penumbra \propto 1/ object source distance 'z'.

In order to minimise geometrical unsharpness and increase the definition, the focal spot size should be as small as possible, and the film should be placed as close to the object as physically possible and the source should be kept far away from the object but consistent with the exposure time available to produce acceptable contrast of the radiograph.

These geometrical requirements impose some conflicting requirements with other factors which affect the sensitivity of a radiograph such as scatter, contrast and the exposure time.

For the given X-ray source and focal spot size and the object to be radiographed, the best practically possible geometrical layout of the source, object and the film can only be obtained by carrying out trial runs with various geometrical configurations and exposure conditions. Finally, the layout and exposure conditions which gave

the best results should be selected.

4.9.3.3 Inherent Unsharpness

When ionizing radiation penetrates a photographic emulsion, electrons are dislodged. These electrons fly off in all directions and the silver halide grains with which they come into contact then become developable in addition to the latent image of the object formed by radiation absorption by the object. The result is that when the film is exposed to radiation, grains of silver form not only in the portions of latent image of the object but also to a lesser degree over an area surrounding the exposed portions. This area represents the "inherent unsharpness", see Figure 4.4, and its width is governed by the distance travelled by the electron through the emulsion, and thus it depends upon the energy radiation.

4.9.3.4 Film Resolution

The film resolution is governed by the thickness of the emulsion layer and the size of grains and their concentration per unit volume. All films exhibit graininess to a greater or lesser degree. Usually the slower very fine grained film will show less graininess. The graininess of radiographs increases with increase in the penetrating power of radiation. This effect is less marked on the fine grained slower film. Further the graininess of the exposed film is also affected both by the development process and by the time of its development. If the time of developing an exposed X-ray film is increased so as to increase the speed of film, the graininess of the

resulting radiograph also increases as a direct consequence of increase in developing time. On the other hand, if a development technique is used in an effort to reduce the graininess effect in the finally developed radiograph, the speed of the film is reduced accordingly. From these reasons, it is obvious that here again engineering judgement, of course based on trial tests, is needed for selecting a suitable type of film and the developing technique for processing the exposed X-ray films.

Thickness of emulsion layer: The smaller the thickness of emulsion layer, the better is the resolution of the film. Most of the radiographic films, which are suitable for radiation source of 100 KV and above, are double emulsion layered i.e. having emulsion coating on both sides of the base. The double emulsion layer increases the contrast as well as the speed of the film but at the cost of reduction in definition. Unfortunately, ultra fine grained one side emulsion coated X-ray films which are fast enough so as to keep the exposure within practical limits and complying with the requirements of photogrammetry are not yet available. In the absence of such film, one is left with no alternative but to use Industrial X-ray film of ultra fine grains and of relatively slower speed.

4.10 X-RAY SET-UP

4.10.1 X-Ray Apparatus

From the above discussion, it is obvious that the solution to the problems of selection of X-ray apparatus, film and its developing technique, and geometric layout of the set-up is not straightforward.

Further the variables affecting the quality of a radiograph are inter-related and so the manipulation of one variable affects the other which makes the task of proper selection of set-up really difficult. The practical method of solving the problem and of satisfying the conflicting requirements of radiography is to run trial tests and obtain the X-ray set-up which gives the best results and fulfilling as many conditions of photogrammetry under given constraints as possible. In order to achieve this goal, a laboratory equipped with a wide variety of radiation sources and its peripheral equipment is desirable. Fortunately, such a laboratory was available and its full use was made in the experimental radiography required for the present investigation.

The experimental X-ray photogrammetric work of this study was performed at the A.Q.D. Laboratories, Harefield, Middlesex. The Radiology Section of this establishment is fully equipped with all sorts of ionizing radiation equipment and sources covering a wide range of industrial radiology from micro-radiology to radiation energy of a few million volts. In addition to equipment and films, other facilities including photographic facilities, technical advice on various aspects of industrial radiology are available. These facilities were generously made available to the writer throughout the testing programme.

In addition to the excellent facilities at Harefield, the X-ray machine with rotating anode and other facilities at the Royal Armament Research and Development Establishment (R.A.R.D.E.) at Fort Halstead were used for conducting experiments on improving

the contrast and definition of radiographs.

Availability of wide range of X-ray equipments gave flexibility in the selection of the right machine. Out of all the available machines, the choice was narrowed down to three X-ray machines keeping in view the paramount importance attached to the quality of X-ray radiographs. These three machines covered the possible useful range of voltage, 70 kV to 300 kV and with smallest focal spot size of 0.5 mm to largest of 4.0 mm. With the help of trial exposures made on actual test specimen, final selection of the X-ray apparatus was made. A 150 kV, X-ray machine with 0.5 mm focal spot size was selected. The salient details of this machine are given in Chapter 2.

Once the X-ray apparatus was selected, extensive trial tests were undertaken for finding the correct radiographic exposure, film and its developing technique, and finally in determining the most suitable geometric layout of the X-ray set-up. In this rather important exercise, two objectives were kept in view:

- 1) Reasonable exposure time consistent with high quality of radiography needed: the time of exposure should not be unduly too long for the two main reasons. Firstly, long exposures are not suitable as the additional advantage of achieving high contrast and definition is lost by the increase in scatter radiation, particularly from inside the granular test specimen, reaching the film. Secondly, the definition of radiographic images of markers is considerably reduced, due to the increase in their movements caused either by creep or by stress-relaxation of the test specimen (depending on

the loading system used) during the exposure of specimen when deformation of the specimen is stopped.

2) Consistency in quality of both radiographs of a stereo pair: the two radiographs forming a stereo pair and taken at a given stage of deformation of a test specimen must be of nearly the same quality. Difference in quality of these radiographs seriously affects the correct formation of stereo model and thus it ultimately affects the final accuracy of measurement attained in the X-ray photogrammetric exercise.

4.10.2 Scattered Radiation

Before any selection of film and of other parameters of X-ray set up is made, concerted efforts must be made to minimise the scattered radiation reaching the film and affecting its quality. Accordingly, right from the trial run until the end of the test programme, the following steps were taken in order to reduce the scatter radiation and its detrimental effects:

1) Diaphragm: A very thick sheet of lead with an adjustable opening was mounted on the window of the X-ray head in order to restrict the area to be irradiated.

2) Mask: The parts of the test apparatus most likely to have acted as a source of scattered radiation were covered with thick lead sheets. Further to arrest the back scatter, the test apparatus was surrounded by wooden boards having layer of very thick lead sheet.

3) Lead Intensifying Screen: The film was placed between two

lead foils. The lead foil placed on the X-ray head side of the film was 0.010 mm thick and the other placed on the side of the film remote to the X-ray head was 0.015 mm thick. These lead foils when placed in close contact with the film, helped in two ways, a) by absorbing the scattered radiation reaching the film and b) by intensifying the primary rays of radiation.

4) Cassette: The film and cassette dimensions were chosen so that the film was just large enough to accommodate the image of the whole specimen. This, in fact, minimised the scatter radiation from inside and outside of the cassette.

5) Filter: In an effort to further reduce the scattered radiation which might have been generated by the presence of softer radiation rays in the X-ray spectrum, experiments were conducted by interposing lead or copper filters of varying thicknesses between the X-ray head and the sample. It was found that the filters were not effective, and so were not used. One of the possible reasons for this may be that the percentage of soft rays present in the beam of X-rays was very low. As mentioned in sub-section 4.9.2.1 (b) the percentage of soft radiation present in the X-ray beam emitted at a given voltage depends, among other factors, on the type of generator circuit used in the X-ray apparatus. The generator circuit of the X-ray machine used was the Greinacher circuit which obviously produced an X-ray beam with a very low percentage of soft radiation. Hence, the quality of radiation was not improved by using a filter. In addition, the contrast of the radiograph was slightly reduced, may be by slight absorption of the energy of the primary rays by the filter.

4.10.3 Selection of Film

The X-ray film cannot be selected in isolation and without taking into account the effect of other variables, for example, permissible maximum exposure time, object to be radiographed, etc., on the final quality of radiograph. As mentioned earlier, the choice of film depends primarily on the relative emphasis placed on subjective definition and contrast, exposure time and available kilovoltage of the source of X-radiation.

In the absence of an X-ray film with resolution comparable with that of aerial films, trial experiments were conducted on various types of industrial X-ray films and on a line film.

The line film selected for the trial test was Ilford N40E film made by Ilford, U.K. This film is generally used in Graphic Arts because of its extremely high definition. Further, instead of using conventional industrial X-ray apparatus, Mullard rotating anode type of X-ray head, which was available at R.A.R.D.E., Fort Halstead, was used as a source of X-radiation. The X-ray machine was operated at 80-90 Kv and 4 ma current in order to obtain better contrast and definition. This experiment did not prove to be successful as the time of exposure needed was excessively long and was unacceptable, at least for the present series of experiments reported in this thesis.

The efforts were then directed towards the selection of film from the available industrial films. Amongst these films, the

obvious choice is to select very fine grained direct type of film; accordingly the top two best films available, namely Industrex 'C' and 'M' films made by Kodak Ltd., U.K., were chosen for trial exposures. Table 4.1 (on Page 4.22) gives the comparative details of these two films. The sensitivity of both of these films after exposure was checked according to DIN 54 110 (1954), see Kodak Ltd. (1965). On visual inspection, both films gave similar results and the radiographs could be classified as category - 1 with high sensitivity according to the said DIN standard. But when these radiographs were viewed on the stereocomparator under 18x magnification, radiograph on the Industrex 'C' film showed more graininess than that exhibited by the radiograph on the Industrex 'M' film. It may be noted that both these films were processed under identical conditions. Even though the Industrex 'M' film is about four times slower than the Industrex 'C' film, see Table 4.1, Industrex 'M' films were selected and used to take advantage of their ultra-fine grains and high contrast results.

4.10.4 Film Developing Technique

Since so many variables exist in the production of radiographs, the need to standardize as many factors as possible cannot be over-emphasized. One of the critical variables which affects the exposure conditions most is the proper selection of film processing technique. In fact, the consistency in processing forms the basis for the standardization of exposure conditions. It may be noted that it is a necessary requirement from a photogrammetric point of

view that the quality of both radiographs of a stereo pair must be approximately the same. Fortunately, an automatic film processing unit was available at the A.Q.D. Laboratories and full advantage was taken in developing all exposed X-ray films with it. The automation of the film processing did not only cut the total processing time considerably; it also standardized the processing, and consequently the exposure technique as well. The complete cycle of processing and drying took about 8 minutes only. The details of the processing unit are given in Chapter 2.

4.10.5 Film to Focus Distance and Film to Object Distance

The X-ray source is never a mathematical point and it will, therefore, always create a geometrical unsharpness in the radiographic imagery. From sub-section 4.9, it is obvious that the geometrical unsharpness can be minimized by using the X-ray source with minimum focal spot size, by having a long film to focus distance and by putting the film as close to the object as possible. It is rather difficult to fulfil these conditions, particularly the second namely long film to focus distance. This requirement is in direct contradiction to the requirement of minimum time of exposure. For instance, for a given kV and amperage of operation, the time of exposure increases as the square of the distance. It is, therefore, essential to choose judiciously the X-ray set-up so as to get the best, possible results under given conditions.

As mentioned in Section 4.10.1, the X-ray source of 0.5 mm

focal spot size was selected for the present study. Having selected the X-ray apparatus, film and its processing method, the next logical step is to fix the lay-out of the X-ray set-up and to determine exposure time for each test material. Once again, trial tests were carried out, this time to find the layout of the X-ray set-up which would give acceptable geometrical unsharpness of the images and would also keep the exposure time in the reasonable limit. In order to minimise the unsharpness of images caused by the movement of particles due to creep or stress relaxation during the time of exposure when the overall deformation of the test specimen was stopped, it was thought that the exposure time of each radiograph should not exceed 6 minutes. In other words, the two radiographs of a stereo pair should be exposed within 10-12 minutes and during this interval minimum movement of particle should occur. It was observed that just on stoppage of the overall deformation of test specimen, the load dropped instantaneously almost to its equilibrium position. The release of load during the period of exposure of both the radiographs was observed to be very small and could easily be assumed to be negligible. If load release may be assumed to be the effect of particle rearrangement, it can be concluded that the readjustment of particles takes place in the first few seconds just after the stoppage of the test and then practically no movement occurs. Further in order to allow for major particle readjustment to complete, at least two minutes were allowed to elapse before the first exposure was made.

After a number of trials, the geometrical layout of X-ray data

acquisition system was obtained, see Figure 4.5 and found to give very good results. It is rather difficult to find the actual contributions made by a) inherent geometrical unsharpness, refer Section 4.9.3.3, b) geometrical unsharpness due to particle movement discussed above and c) geometrical unsharpness created by focal spot. However, if we assume that the focal spot is of finite shape and size, the contribution made by this source can easily be calculated by using Eqn. (4.3). For the typical layout of the X-ray system shown in Figure 4.5, the width of penumbra around the images of particles which are placed approximately in the mid plane about 75 mm away from the film plane is 0.026 mm. In addition to these three factors, there are other factors which also contribute towards the reduction of definition. It is neither practically possible nor desirable to know separately the unsharpness created by various sources. However, their collective effect on the measurement of image co-ordinates and finally on the object space co-ordinates of the markers is discussed in Appendix A.

4.11 STEREO MODEL AND PHOTOGRAMMETRIC CONSIDERATIONS

The main object of using X-ray photogrammetry is to determine the displacement and rotation of particles particularly of marker particles, at various stages of deformation with reasonably high accuracy. It is therefore required to determine spatial co-ordinates of the ends of tungsten wires embedded in the particles by making measurements on two radiographs forming a stereo pair taken at a given deformation. A stereo pair can be obtained either by placing the X-ray tube at two known positions and keeping the object in the

fixed position. This method is generally known as tube-shift method. Alternatively, a pair of radiographs may be obtained from a fixed X-ray tube position but placing the object at two different predetermined locations. The latter technique of obtaining stereo pairs was found to be most suitable and was used in this study.

In order to perceive a stereo model, the two radiographs of an object forming a stereo pair must fulfil the following requirements. The steps taken to fulfil them are also mentioned after every requirement below:

i) The axis of beam of X-rays of both radiographs should approximately lie in one plane as the human eye can accommodate only a limited degree of non-coplanarity. During the radiography the object was invariably positioned on the predetermined fixed locations and hence the X-ray beam axes of the left and right radiographs were kept in the same plane.

ii) The scale of the two radiographs should be nearly the same. Difference of up to 15% in the scales of the radiographs may, however, be successfully fused. The two exposure positions were selected in such a way so that they were nearly equidistant from the X-ray head. Further the X-ray film during every exposure was always placed in predetermined location and at a fixed distance from the rear σ_2 -platen. This ensured that the scales of the left and right radiographs of a stereo pair were approximately equal.

iii) The density of the two radiographs of a stereo pair should be similar. The radiographs at various stages of deformation were taken under certain fixed exposure conditions. In addition to this, the film and its processing was also standardized. This, in turn, ensured radiographs of very nearly equal density.

iv) The B/H ratio, also known in photogrammetry as base to height ratio, where base B is the distance between the two exposure locations of the specimen and H is the perpendicular distance between the focal spot and the line joining the two exposure positions of the specimen, must have an appropriate value. If this ratio is too small, say smaller than 0.03, depth perception of the stereo model would be difficult. The ideal value of B/H ratio is not known but it may not be very different from 0.25. In the set-up used in this work B/H ratio was kept between 0.25 and 0.30. The arrangement of data acquisition system as used here is shown schematically in Figure 4.5 and its general layout in Plate 2.2.

4.12 RADIOGRAPHIC RESULTS AND DISCUSSION

A pair of stereo-radiographs is randomly selected from each set of radiographs of those tests whose results are reported in this thesis. These typical pairs of radiographs are presented in Plates 4.1 to 4.10. Since each of these stereopairs has been randomly selected, every pair reflects the quality of other radiographs of the same set to which it belongs. These prints are obtained by re-photographing the positive contact prints of the original stereo-radiographs and are smaller in size than that of the actual radiographs. Obviously, the quality of these prints presented in Plates 4.1-4.10 is not as good as that of

the original X-ray radiographs. However, the degree of reduction in the quality of these prints is expected to be the same because of the same photographic process used. These prints of radiographs are therefore used for the comparative study of the quality of the original radiographs of various materials tested under different environments i.e. under dry or saturated conditions.

Plates 4.1-4.10 provide clear evidence in support of what has been said in section 4.9.2.8 i.e. the absorption of X-radiation energy depends on the atomic number of the elements present in the test material used, on the density of the test particles, and on the thickness, porosity and the degree of saturation of the test sample. Since the tests were performed under approximately similar conditions, the difference in energy absorption, scattered radiation generated and thus the difference in the quality of radiographs can be attributed to the materials of the test particles used. The degree of X-radiation absorption can be qualitatively evaluated by comparing that average density of radiographs of different materials exposed under similar conditions. The examination of the radiographs presented in Plates 4.1-4.10, shows that the absorption capacity increases in the following order according to the material used:-

Polypropylene → PTFE → Ceramic → Gravel → Glass.

By comparing Plate 4.1 with Plate 4.2, it becomes evident that the X-radiation energy absorption by the dry test sample was less than that by saturated test sample of the same material.

The main aim of using X-rays was to obtain images of marker wires with acceptable definition. The definition of an X-ray image depends on various factors including the difference in the level of energy absorption by the marker wire and by the remaining volume of the test sample bounded by the same bundle of X-rays forming the boundaries of the image of the marker wire. As pointed out above, the general level of energy absorption increases according to the said order of the material used. It is, therefore, apparent that the definition of the image of a marker wire of a given material will decrease as the general energy absorption level of the test sample increases. In order to keep this level of difference as large as possible, two steps were taken. Firstly, the material with very high radiation absorption capacity, namely tungsten, was used; secondly, other sources of general X-radiation energy absorption were minimised, particularly by using perspex for the platens and by replacing the conventional water confining system for the application of σ_3 by a vacuum system, see Chapter 2.

Although it is difficult to achieve ideal conditions for obtaining the perfect image of a marker wire, the technique used here gave acceptable results, see Appendix A.

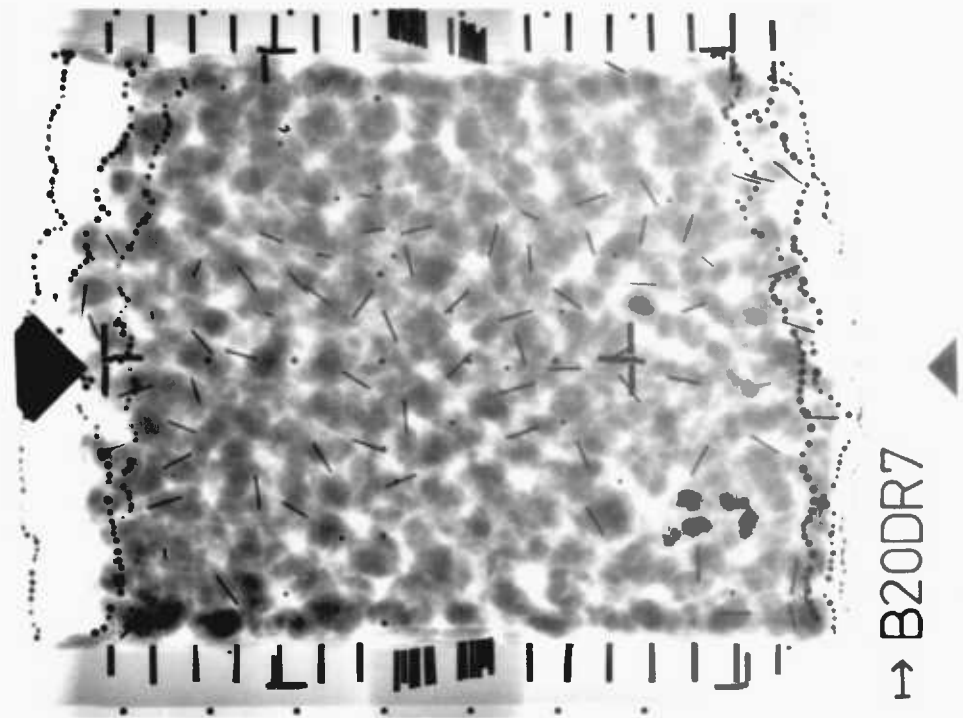
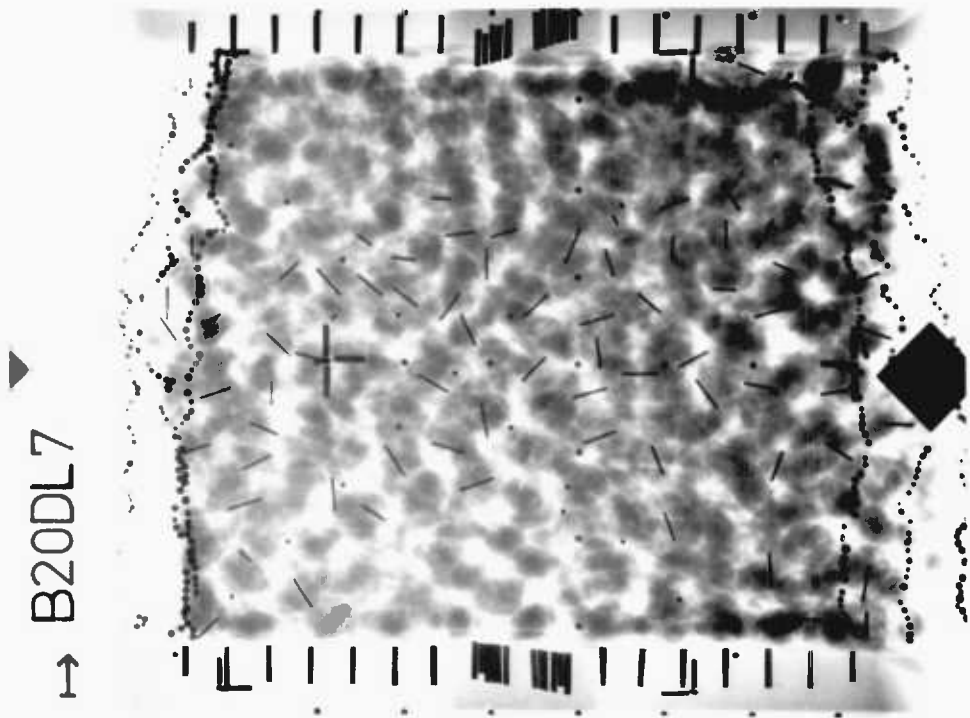
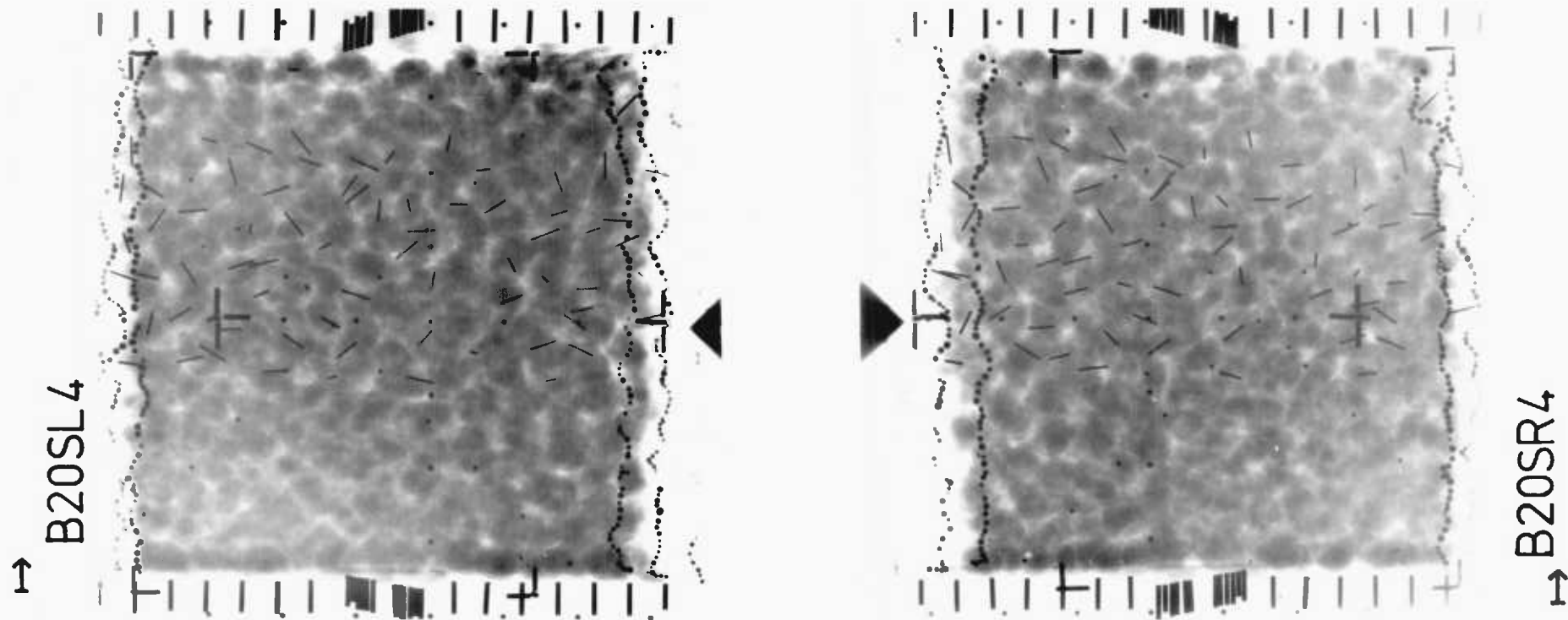
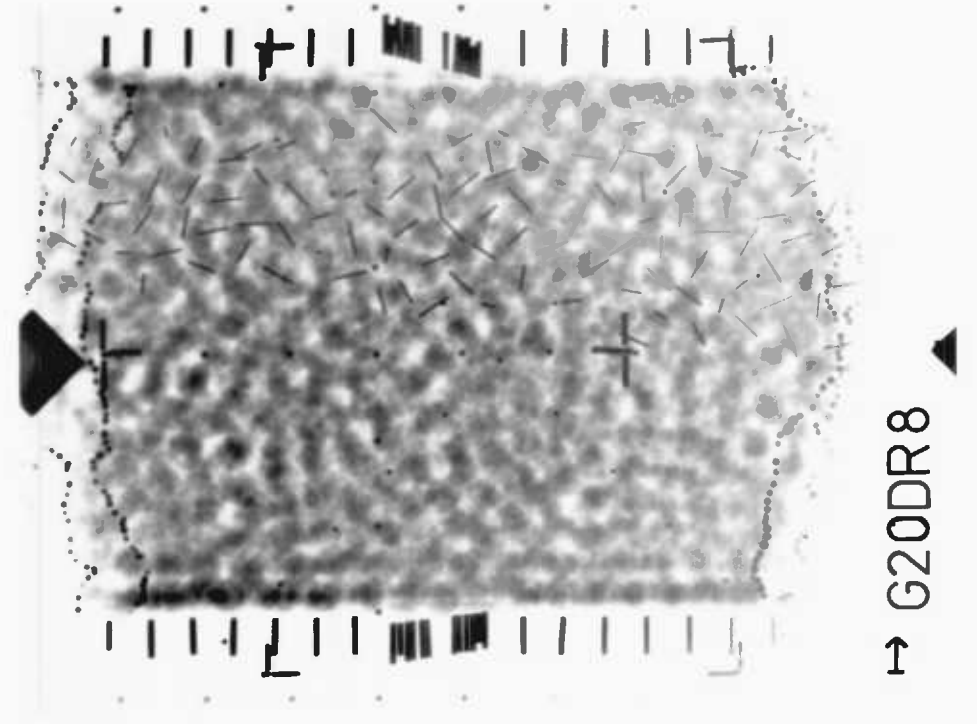
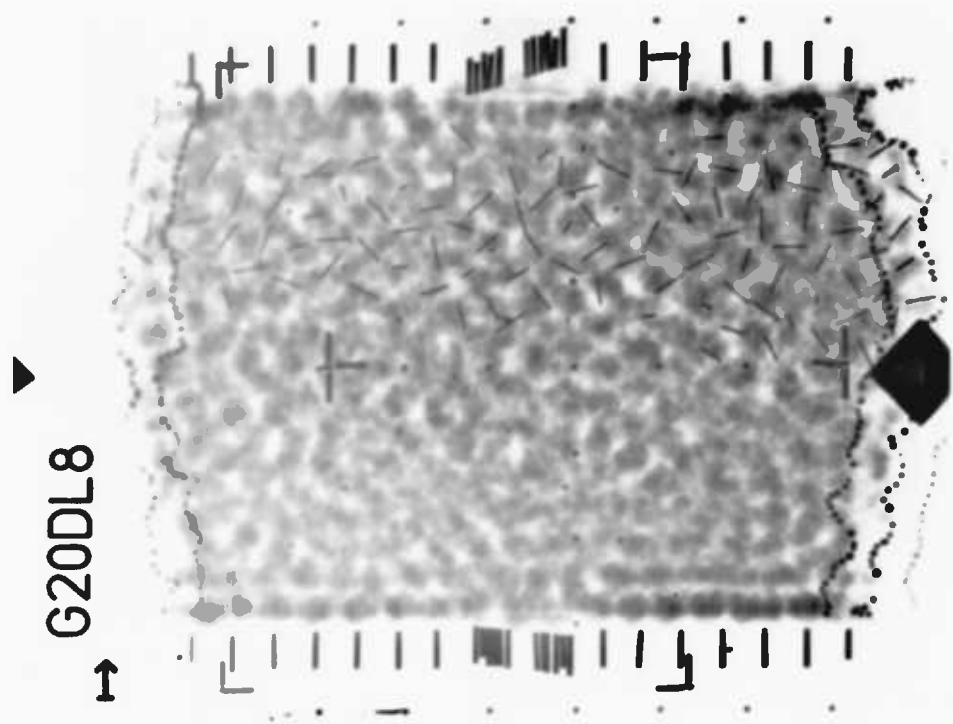


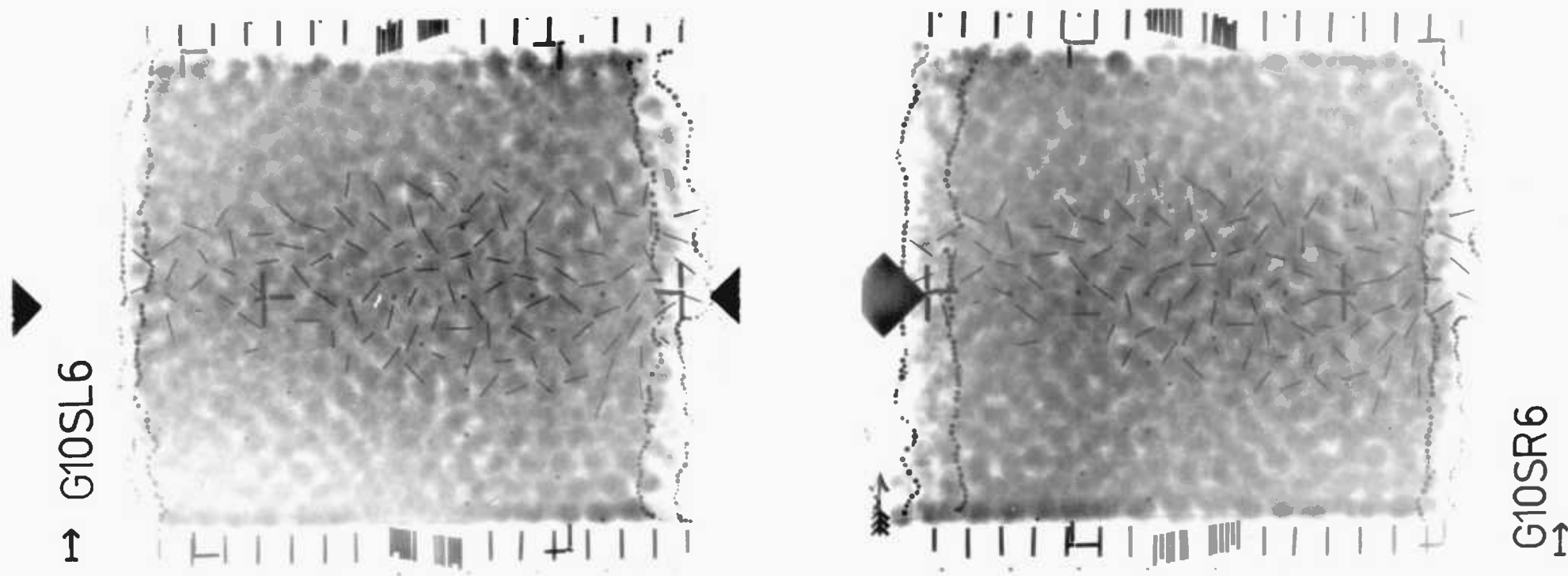
Plate 4.1

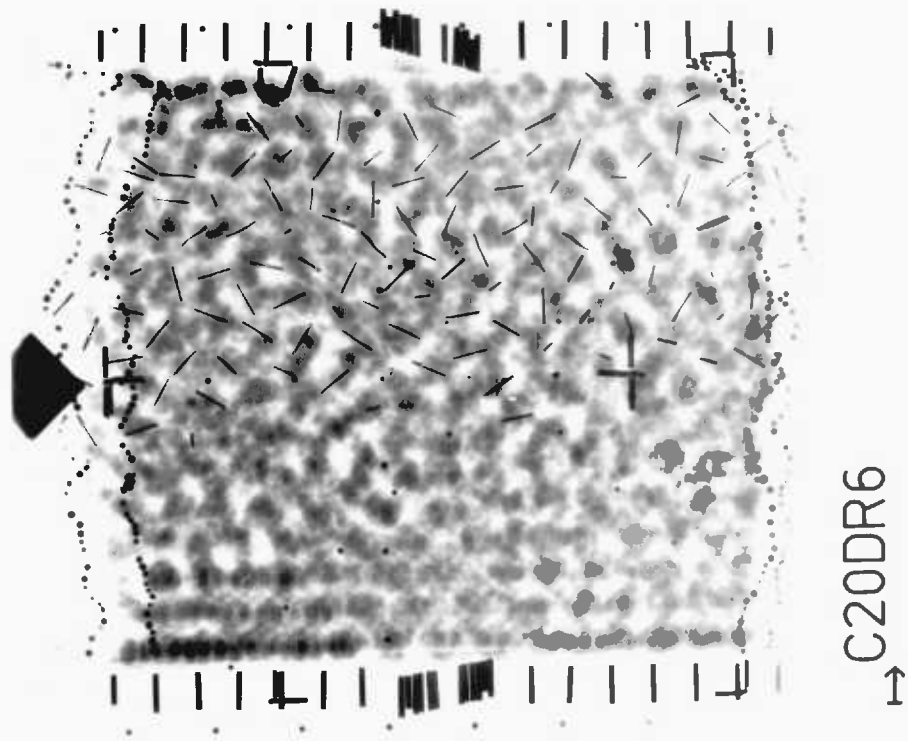
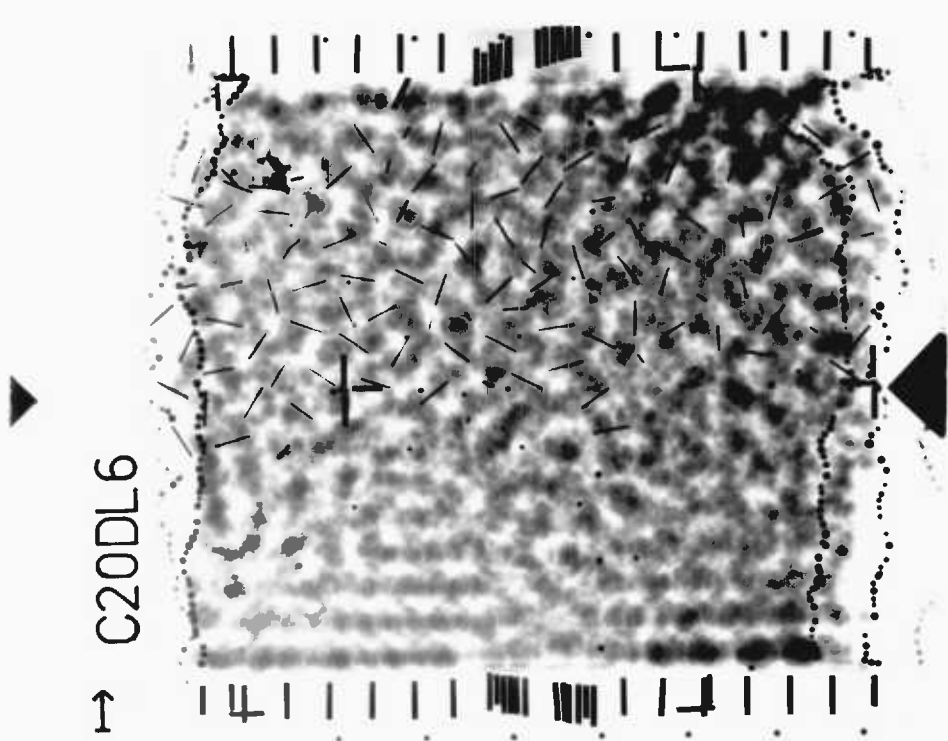
TYPICAL STEREO-PAIR OF RADIOGRAPHS OF GRAVEL TEST SAMPLE (DRY)

TEST NO: 1200/7









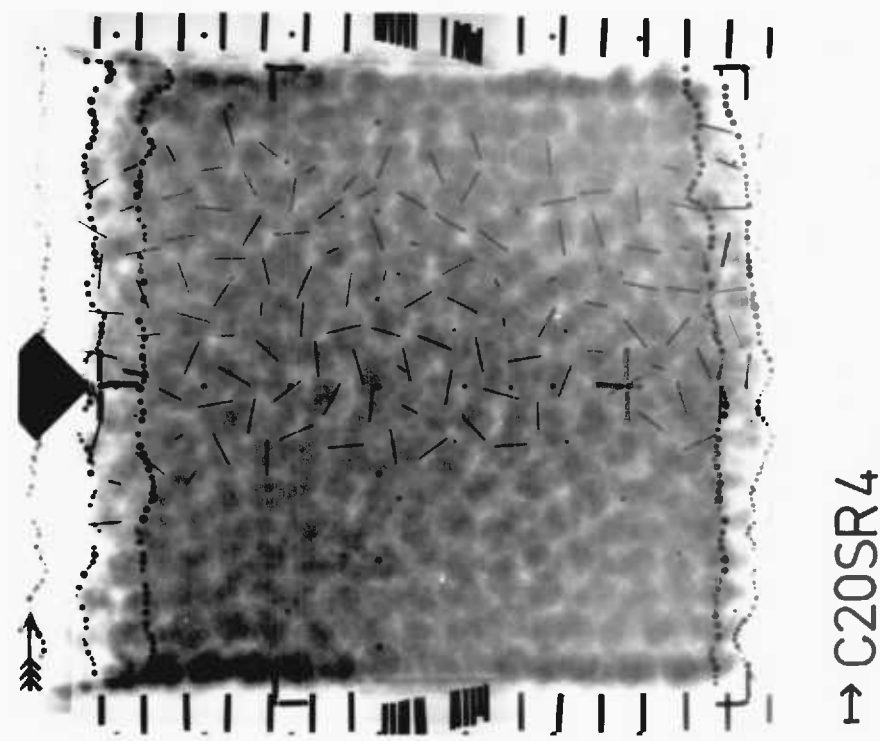
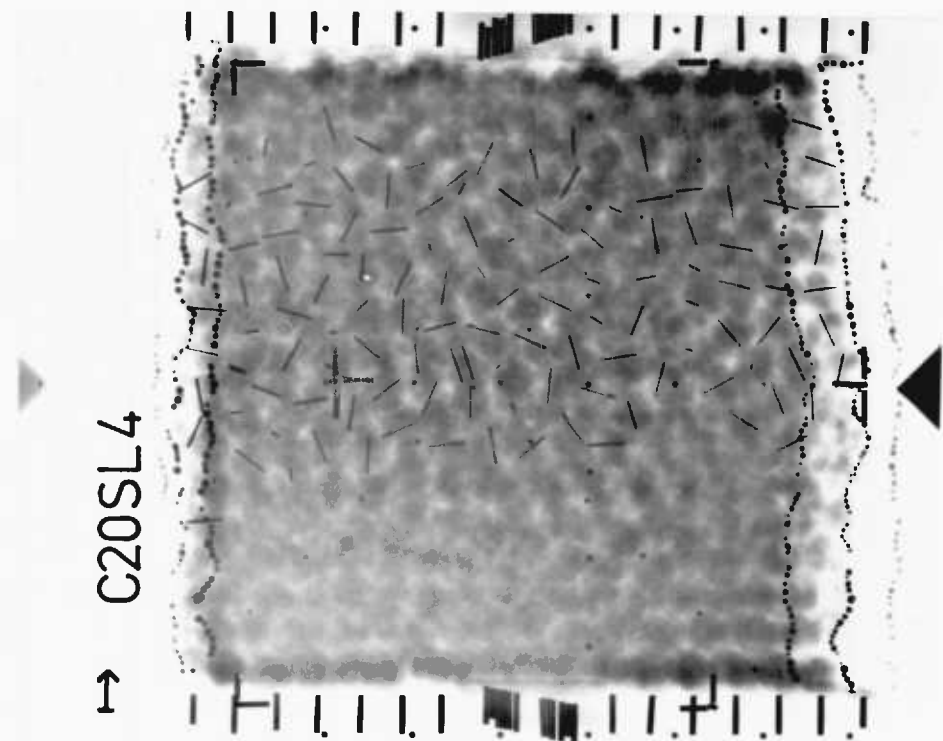
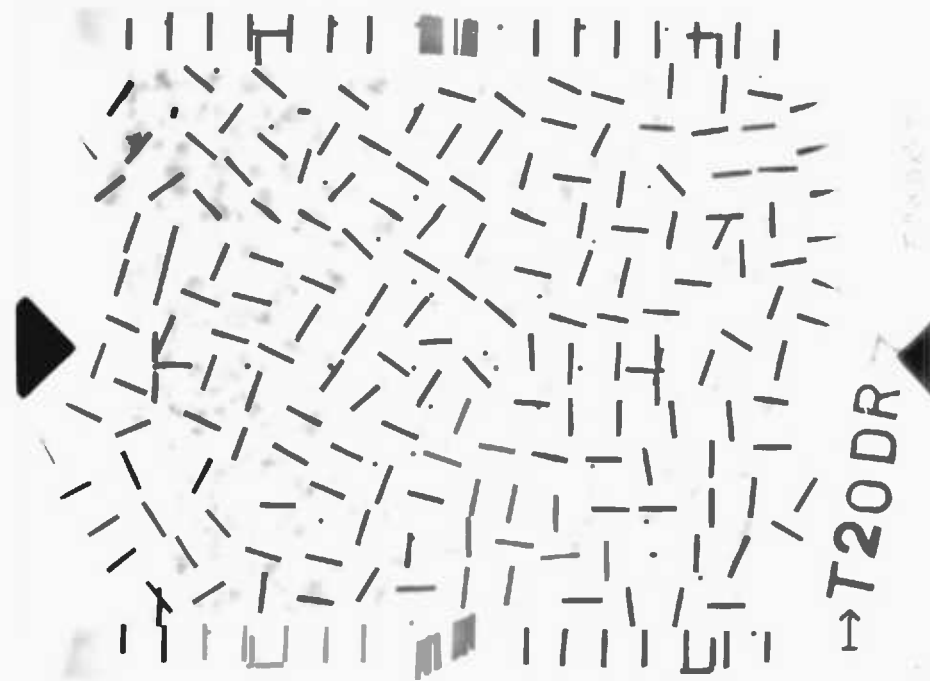
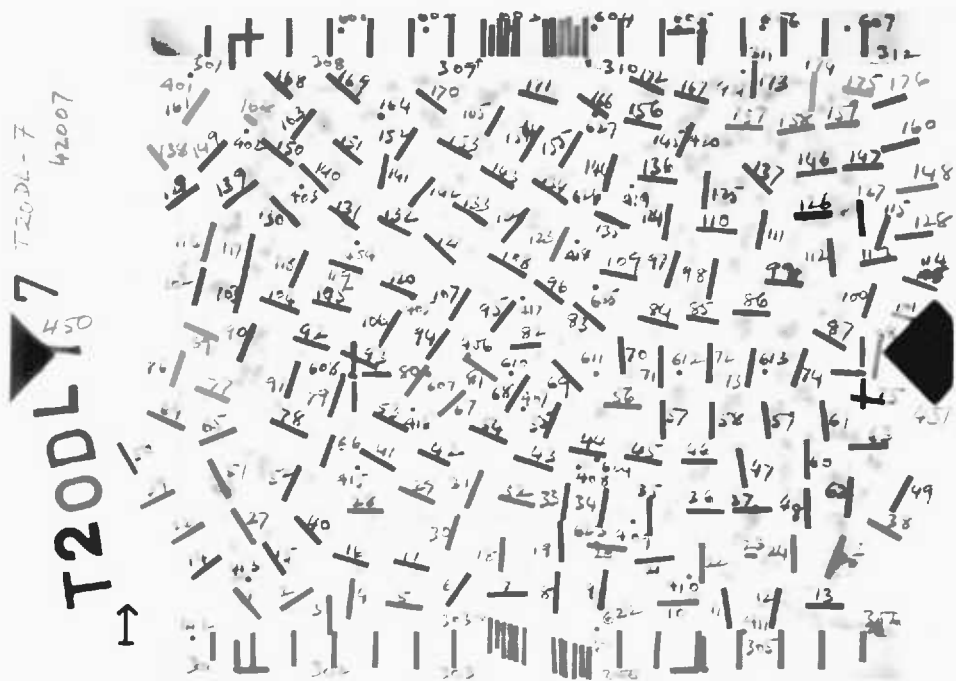
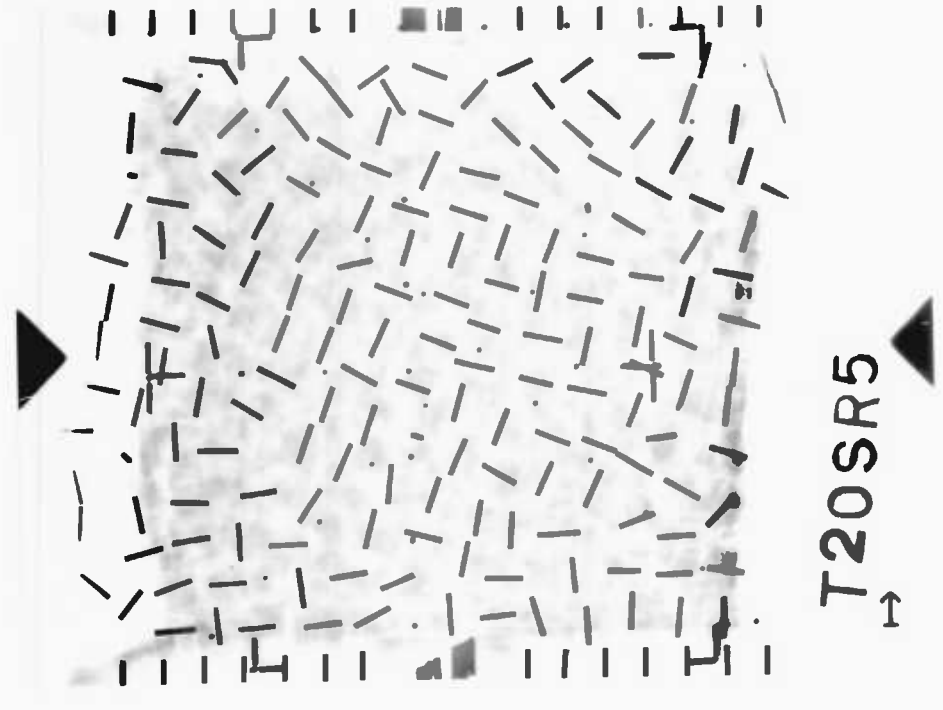
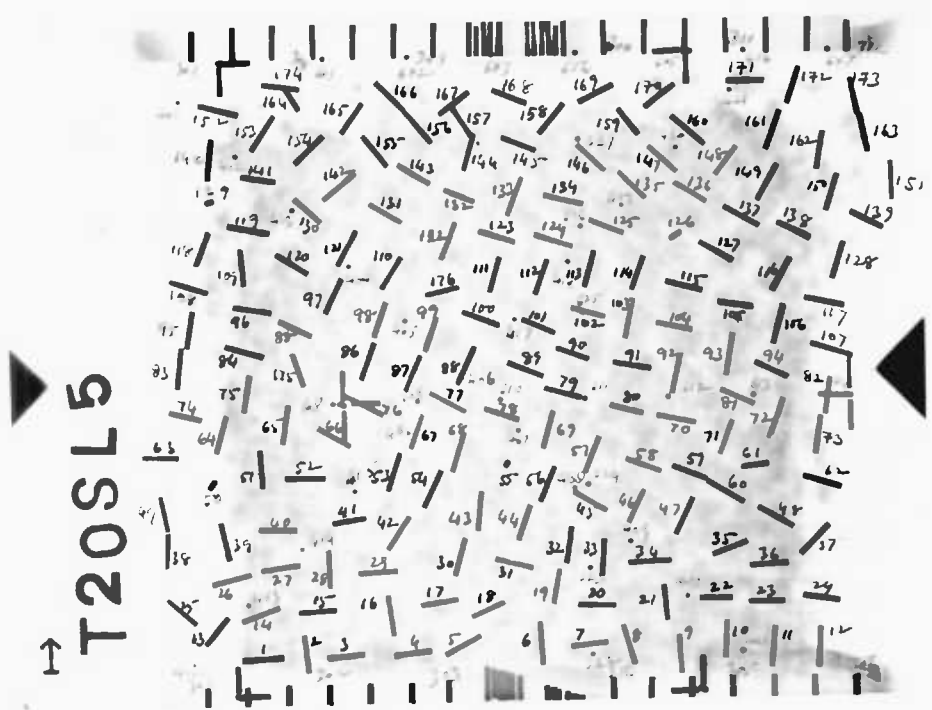
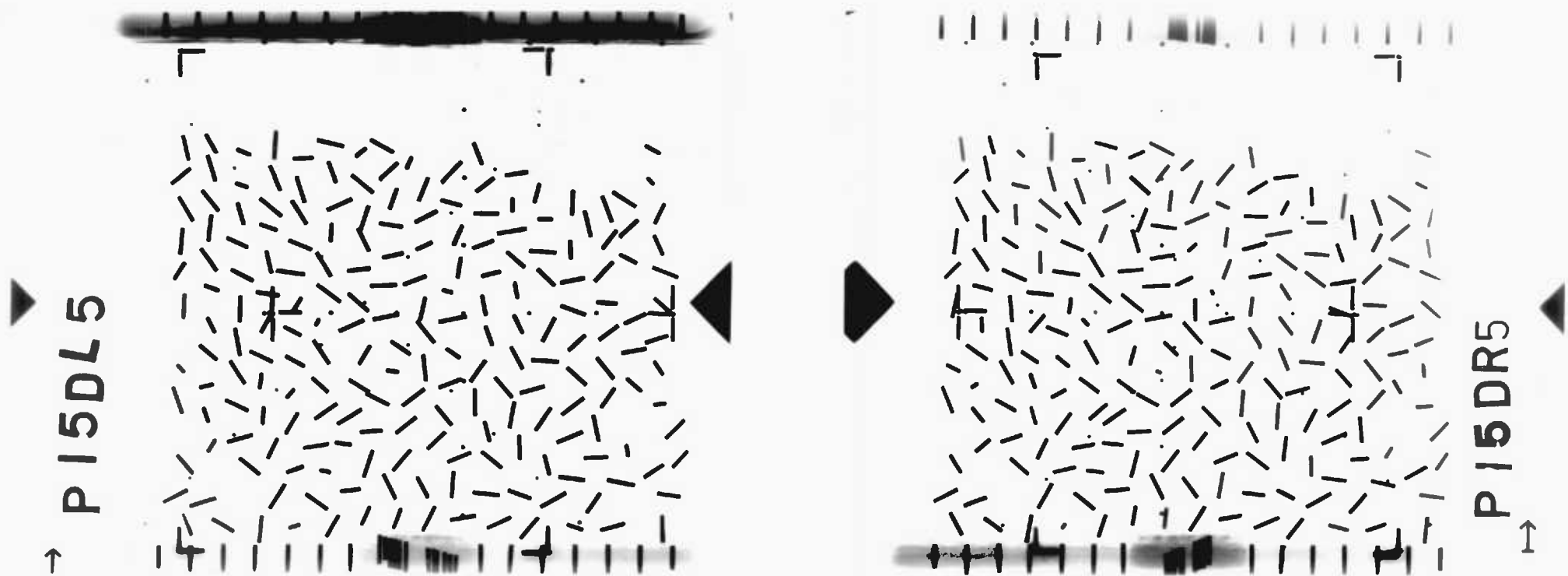
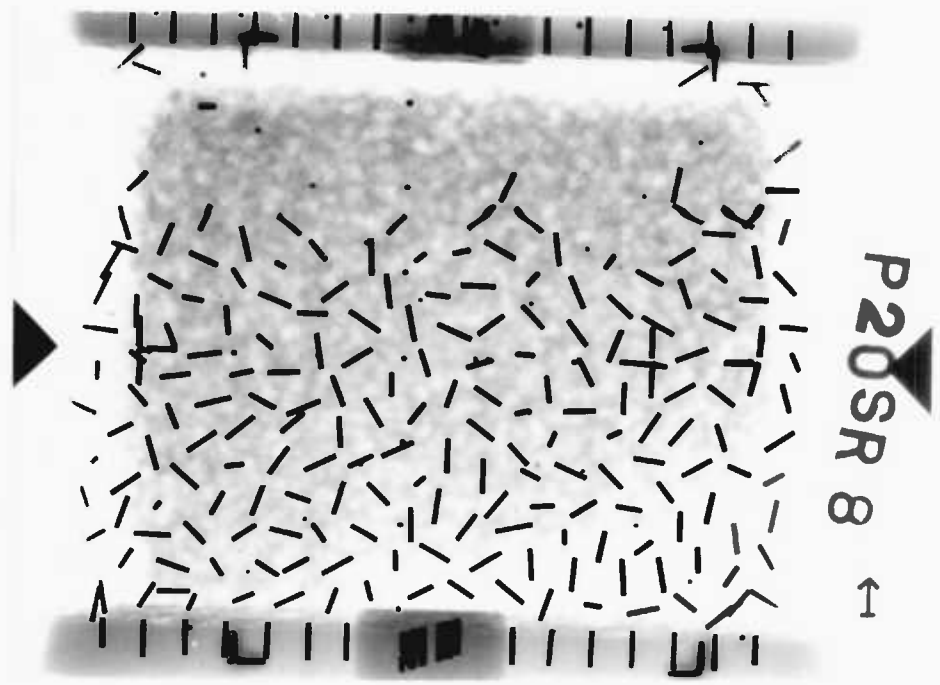
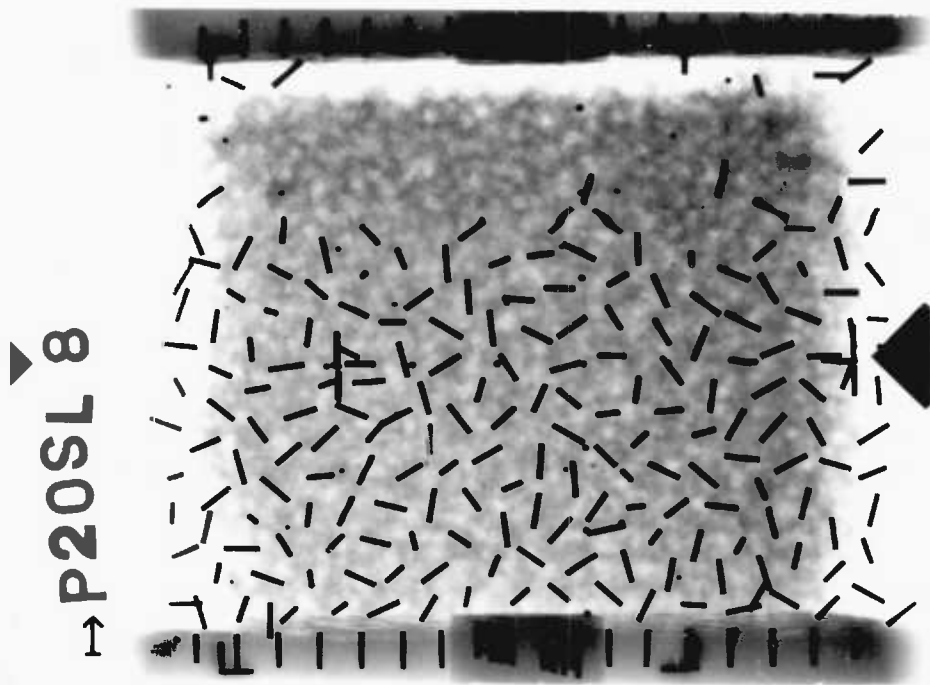


Plate 4.6 TYPICAL STEREO-PAIR OF RADIOGRAPHS OF CERAMIC TEST SAMPLE (SATURATED) TEST NO: 3201/4









P20SL 8

P20SR 8

Plate 4.10 TYPICAL STEREO-PAIR OF RADIOGRAPHS OF POLYPROPYLENE TEST SAMPLE (SATURATED)

TEST NO: 5201/8

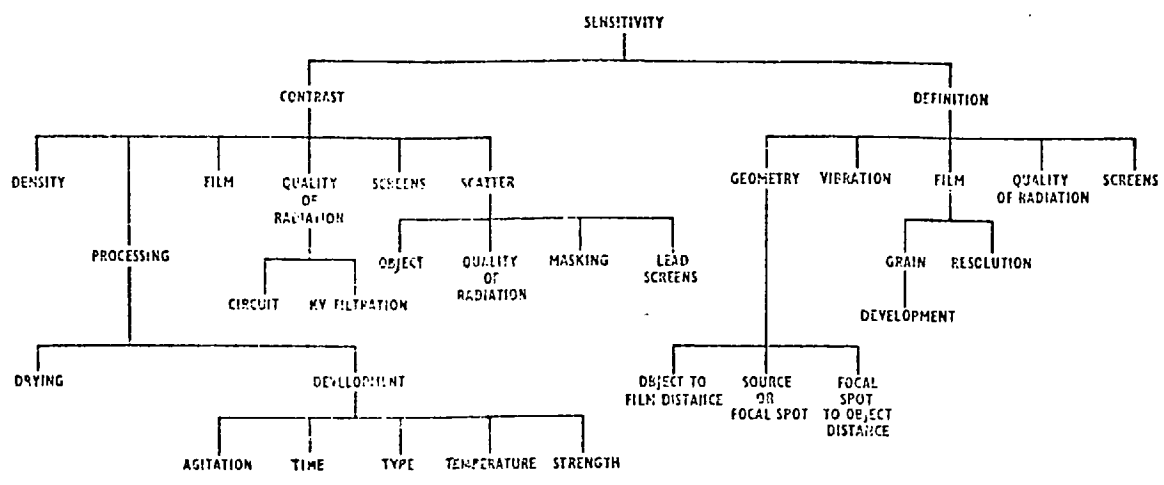


Fig. 4.1 Factors affecting the quality of a radiograph

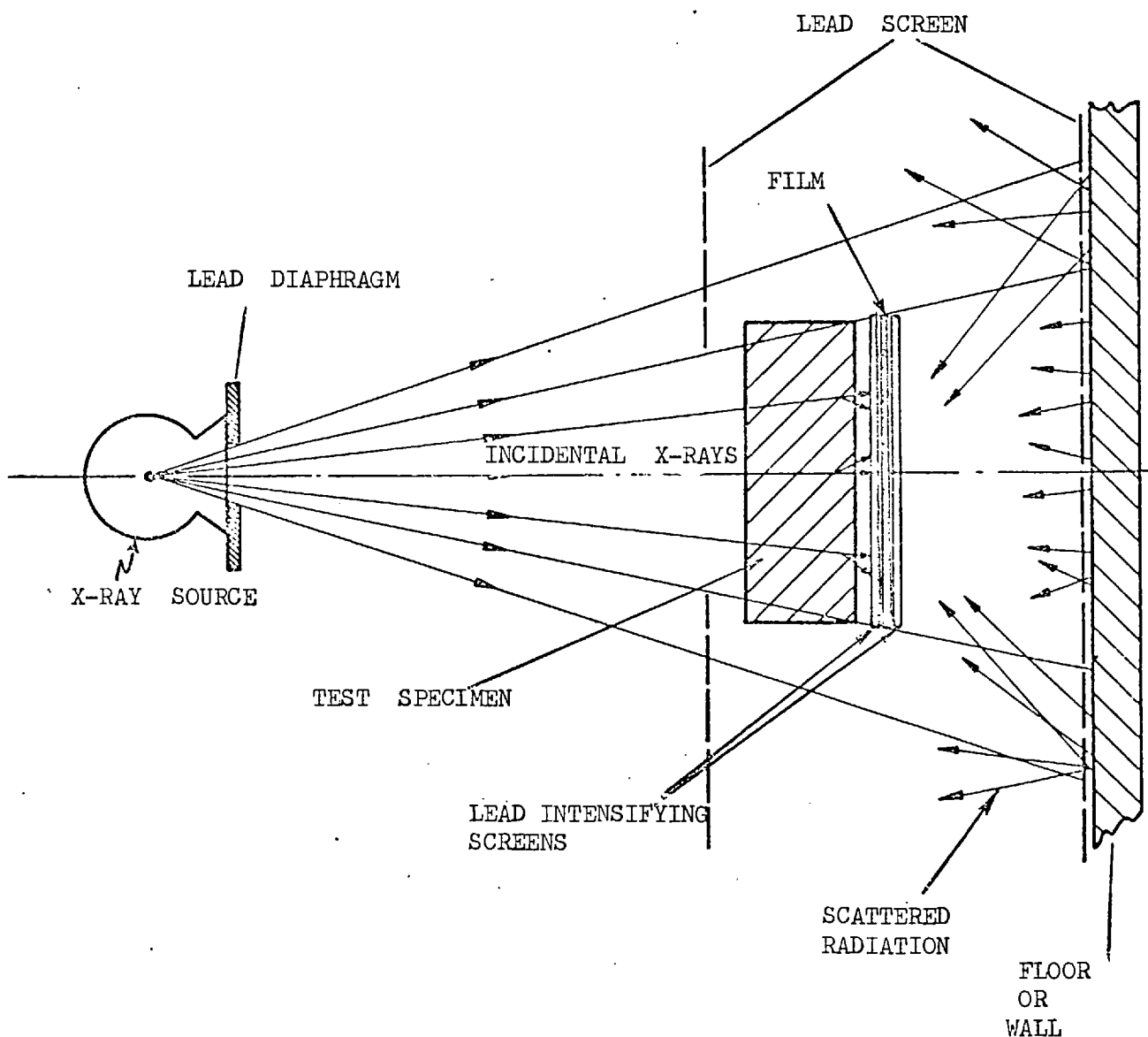


Fig. 4.2 Scattered radiation

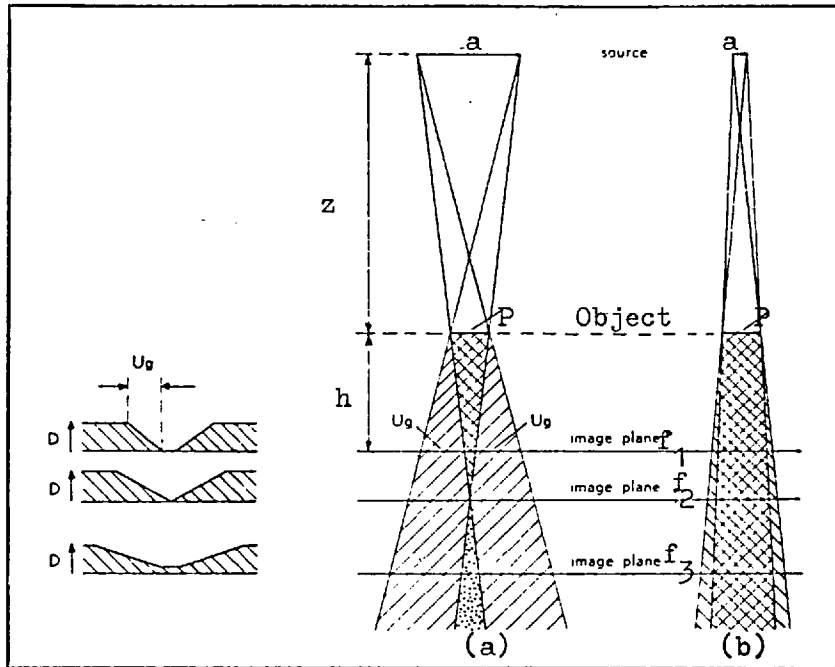


Fig. 4.3 Penumbral effect

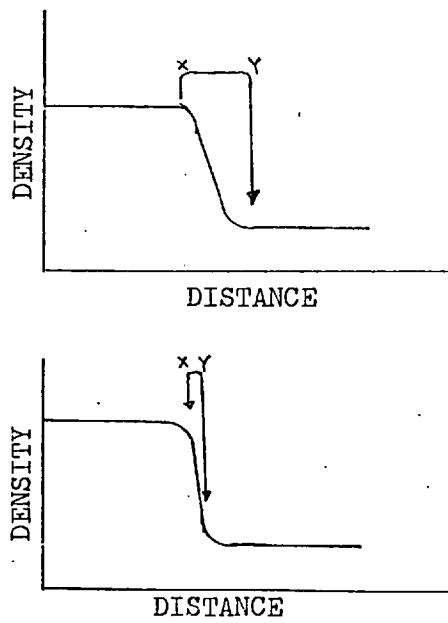
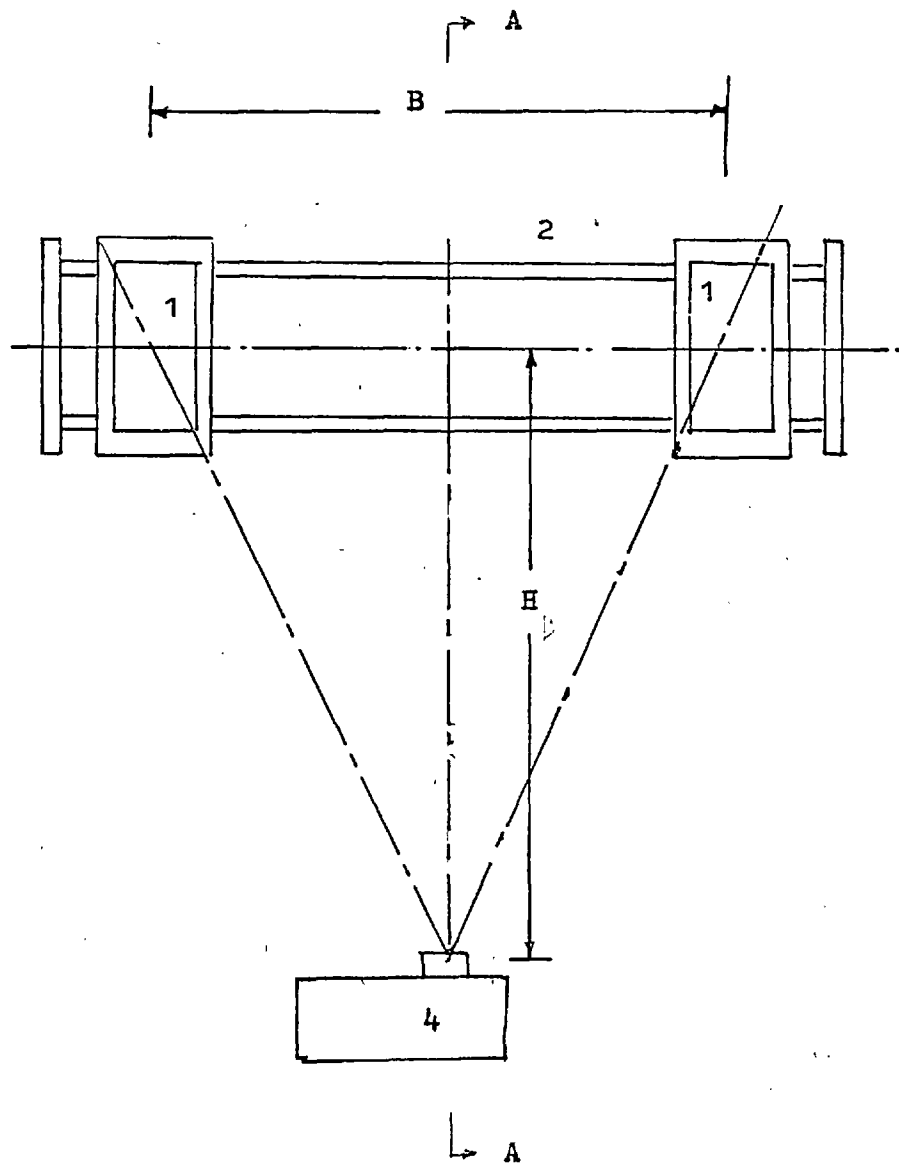
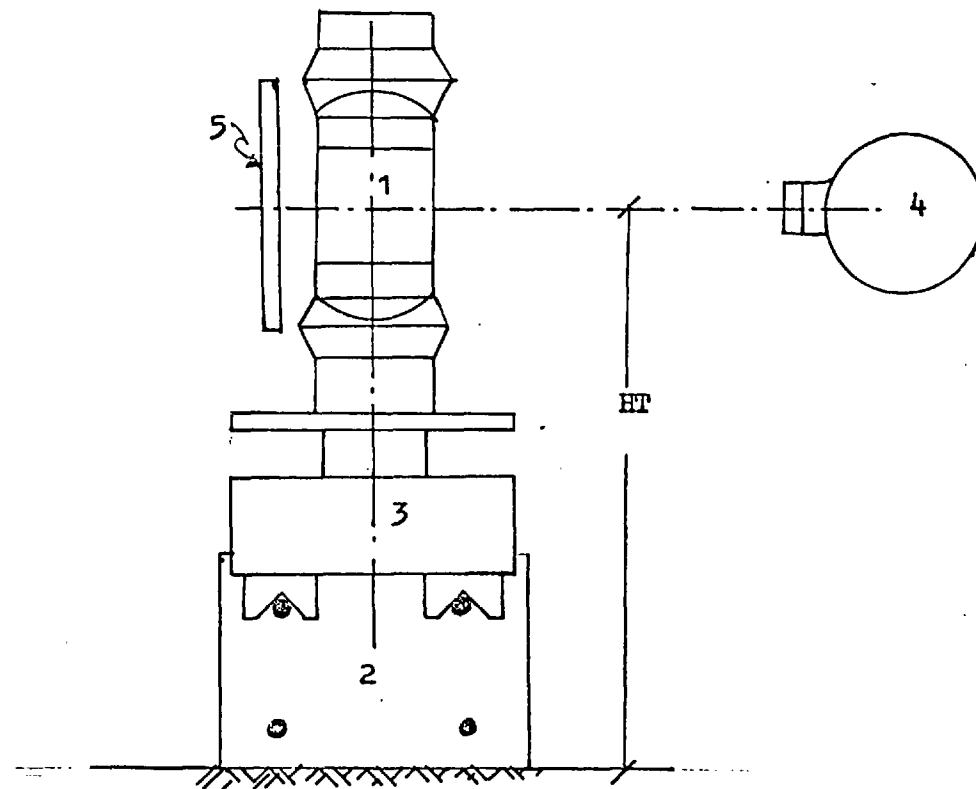


FIG. 4.4



Plan



Section A-A

- 1 - Test sample
- 2 - Rails
- 3 - Part of the reaction frame
- 4 - X-ray head
- 5 - X-ray film and cassette

FIG. 4.5 SCHEMATIC LAYOUT OF X-RAY DATA ACQUISITION SYSTEM.

CHAPTER 5

X-RAY PHOTOGRAMMETRY - DATA REDUCTION5.1 INTRODUCTION

The second and equally important phase of X-ray photogrammetry is the data reduction. This is concerned with retrieving the recorded information, which are in fact radiographic images, and then carrying out necessary computations and finally in obtaining the output of the required data in the desired format. As will be seen in the following sections, the selection of a suitable, efficient and accurate method of data reduction depends, in addition to other factors, on the system of data acquisition used in radiography and form of the output needed.

Although the scope of the present work precludes a general survey of various data reduction methods of photogrammetry for which reference is made to the Manual of Photogrammetry published by the American Society of Photogrammetry, a very brief discussion is included in this chapter, primarily to bring out the constraints imposed by the available data acquisition system. It is worth mentioning that, at present, no data reduction system is available, to the writer's knowledge, which is specifically designed and developed for X-ray photogrammetry and could be used for the X-ray photogrammetric set-up used in the experimental work presented here. Further with the help of these discussions, it is expected to emphasize the need for further research in the very versatile field of X-ray photogrammetry and thus increase the effectiveness and potentials of its application in Particulate Mechanics.

5.2 BASIC TERMINOLOGY AND DEFINITION OF TERMS

The photogrammetric terms and symbols used in this chapter, if not defined where they first appear in the text, are according to the accepted usage of the American Society of Photogrammetry. (Refer Chapter 24 of the Manual of Photogrammetry, 1966; vol. 2 pp 1125 - 1160)

5.3 DATA REDUCTION SYSTEMS

5.3.1. General Classification

The various approaches available for data reduction in the general field of photogrammetry can be broadly grouped under the following main headings:

- a) Analogue Approach
- b) Automatic Stereo Compilation Approach
- c) Analytical Approach

5.3.2 Analogue Approach

In this approach, some kind of instrumental method is used which is based on the measurements of a stereoscopic model which is perfected or solved through the use of an analogue device. The stereoscopic model can be formed in the instrument either with a correct reconstruction of the perspective bundles or with deformed perspective bundles.

A plotting instrument, also known as "restitution instrument",

is a device which is employed to transform the photographic information into a line map by continuously and automatically solving the mathematical relationships between the co-ordinates of the image of a point in the photograph, to those of the corresponding point in the object and on the map. Therefore, the restitution instrument, in a wider sense, is an analogue computer.

Karara (1971) was of the view that stereo-plotters could be used for data reduction of metric imageries taken with a very stable and properly calibrated data acquisition system, such as by Aerial photogrammetric camera. He did not recommend its use for the evaluation of non-metric photography due to their rather large and irregular distortions. It is worth noting that X-ray data acquisition configuration used in the present work falls in this category, namely "non-metric" photography.

5.3.3 Automatic Stereo-Compilation

In contrast to the analogue approach, no stereo model in a strict sense is reconstructed but is based on realising the relation between the co-ordinate systems automatically by means of computations or correction devices. In order to achieve high speed of compilation, sometimes an on-line computer is used in conjunction with the other instruments needed for compilation.

Many of the instruments used for auto-stereo compilations, known as analytic stereo plotters or automated stereo systems, are equipped with several types of correction devices, e.g. for lens distortion compensation, for refraction correction, etc. Once again these sophisticated devices are designed for reduction of metric

imageries. Unlike stereo plotters, they do not impose any restriction regarding the principal distance or the direction of photography. Further, this approach of data reduction has other advantages including high speed of compilation and precision.

These automated systems suffer from serious limitations. The observations taken over various kinds of terrain by an analytic stereo plotter show lack of reliability. Since the plotter is devoid of memory, it occasionally gets lost when it can not find identical images on the two photographs of a stereo pair. The automated stereo instruments use an electric or optical technique to measure the positions of two nearly identical images and they do not possess any automatic recognition capability like that of human eyes. The system, is therefore not capable of recognising identical objects which differ in scale or aspect. These drawbacks make this approach highly unsuitable for stereo radiography as used here.

5.3.4 Analytical Approach

In the analytical approach, a mathematical model is constructed to represent the relationship between the images, on the photograph, the perspective centre and the corresponding points in the object space. The numerical evaluation of this mathematical model results in the solution of various photogrammetric problems such as precise calibration of data acquisition system, orientation problems and space intersection for the determination of spatial co-ordinates of object points.

The analytical method is a very versatile and accurate method with built-in flexibility. It offers many advantages accruing from automation, digital accuracy, least squares adjustment and freedom from mechanical discrepancies contributed by the restitution instruments.

5.4 SELECTION OF DATA REDUCTION SYSTEM

The selection of a suitable data reduction system depends on various factors including the data acquisition system used in radiography or photography, desired accuracy, format of final output and the type of instruments available for measurements. The data acquisition system used in this work is rather unconventional, peculiar and highly unstable in the photogrammetric sense. In order to obtain the final results of fairly high accuracy compatible with the data acquisition configuration, certain conditions must be fulfilled by the data reduction system:

1. It must be able to accommodate long taking principal distance, e.g. 1200 mm or more.
2. The system should be flexible enough to accommodate principal distances between 1000 mm to 1500 mm or more.
3. It should be possible to centre the radiograph on a plotting machine, in case the principal point lies outside the radiograph.
4. It should give the highest possible accuracy, of course, depending upon the quality of the radiographic images.

5. The system should be capable of solving directly or indirectly for orientation parameters - interior and exterior as well as for perturbation parameters to account for the systematic errors, if included in the solution and finally in achieving the main objective of the whole exercise, namely the determination of spatial co-ordinates of the object points, in our case, corners of the marker wires, in every stereo pair.

6. The final output should be in the form of spatial co-ordinates of pre-selected discrete points rather than continuous lines.

7. It should possess flexibility in procedure and should have room for further improvement and sophistication as the problem may demand.

The analogue approach is most suitable for reduction of metric imageries with known interior orientation. (Karara 1971, Hallest 1970). However, its use cannot be recommended to non-metric imageries in view of their rather large and irregular distortions (Karara, 1971). Further, it is worthwhile to note that the standard first order plotting instruments do not have sufficient principal distance range to evaluate radiography taken with principal distances ranging between 1000 to 1500 mm. Eden (1962) investigated the whole question of modification of the standard stereo plotters if they were to be used in such circumstances where the principal distances set in the plotters are grossly different than that used in the photography. He concluded that although it may be possible to make the necessary modifications, they would be very complicated and

economically unviable. He recommended that one should have a separate plotter specifically designed for such use.

No such restitution instrument was available which could project radiographs taken with principal distances ranging between 1000 to 1500 ^{mm} and with principal point located outside the radiograph.

The automated stereo plotters, also known as analytical stereo plotters, are also not suitable for the present work due to various reasons including lack of reliability, incapability of recognising identical objects which differ in scale or in aspect, lack of memory. (Esten et. al. 1966)

The analytical approach is highly suitable to those applications in which a simple central projection concept is not adequate to describe the physical characteristics of the imageries. The class of problems demanding relatively high accuracy requires the elimination or minimisation of the effect of various perturbation factors arising from tangential and radial distortions, lack of perpendicularity or straightness of the comparator rays and errors arising from penumbral effects, etc. Such perturbations which are rather difficult, if not impossible, to include in the analogue approach can easily be incorporated by suitable mathematical models in the analytical approach. Further, the analytical approach does not in any way impose any restriction either on the magnitude of the principal distance or on the location of the principal point. An added advantage is derived from its very nature of measurement at discrete points in obtaining

the needed information in digital form which could be used for further analysis and plotting by computer.

From the above discussions, it is evident that the analytical approach is the best technique available today for non-metric photogrammetry, as used in the present work, in particular.

5.5 ANALYTICAL X-RAY PHOTOGRAMMETRY

Significant advances have been made recently in the development and perfecting of the analytical approach and in utilizing this highly powerful and versatile technique for the solution of photogrammetric data reduction problems. For such applications, sophisticated mathematical models and their computer algorithms are developed and are available for interested researchers. Concerted efforts are being made at various universities and research establishments involved in photogrammetry to develop a general computer programme which could be used in solving most of the photogrammetric problems. One such computer programme was developed at New Brunswick University under the direction of Professor Faig and was made available to the writer (Faig, 1974). It was expected that this 'general' programme in its original form or after making slight modifications could be used in solving the present X-ray photogrammetric problem. Although the basic principles underlying conventional photogrammetry and X-ray photogrammetry are the same, the available mathematical models and standard computer programmes including that supplied by Faig (1974), cannot be used in the data reduction of X-ray photogrammetry in its present application for the following reasons:

a. The principal point is not located near the centre of gravity of images in a radiograph; in fact, the principal point is well outside the format of the radiograph.

b. No fiducial marks are used in the radiography and hence the image of one of the control points has to be used as a reference origin. Unlike the fiducial marks in the metric cameras which lie in the film plane, this control point is not in the plane of the film and also the principal distance of the left and right radiographs are not exactly the same; there is a distinct shift between the origins of the two radiographs of a stereo pair.

c. A suitable mathematical model which could be used for the correction of the effects of various perturbation parameters were not available.

Hence, the attempt is made here to develop a single mathematical model and its computer programme to suit our purpose and at the same time to be capable of giving the accuracy compatible with the radiography obtained by using the data acquisition set-up described in Chapter 4. The analytical approach used here for data reduction involves space resection and intersection formulation.

5.6 COORDINATE SYSTEM

In analytical photogrammetry, the two fundamental coordinate systems used relate to the image plane and to the object space. The right-handed co-ordinate system is generally used in photogrammetry and is also employed here.

5.6.1 Image Co-ordinate System

In contrast to standard photogrammetry, the radiographs obtained do not contain any fiducial marks and also the principal point is located well outside the format of the radiograph. However, with the help of a set of fixed discrete points on each radiograph, the rectangular axes are defined for the measurement of xy co-ordinates of the image point. Further complying with the convention used in photogrammetry, the positive x-axis is taken as the one which coincides very nearly with the line joining the two 'equivalent' exposure stations (see Figure 5.1). Two such systems, the first called the comparator co-ordinate system having its origin at the image of point 301 and x-axis defined by the line joining the points 301 and 306 and the second with origin at the principal point and with x and y co-ordinate axes parallel to the corresponding axes in the first system, are used.

The two systems are related by the following relationship:

$$\begin{bmatrix} p \end{bmatrix} = \begin{bmatrix} x_p \\ y_p \end{bmatrix} = \begin{bmatrix} x_o + x \\ y_o + y \end{bmatrix} \quad (5.1)$$

Where x_p, y_p are the image co-ordinates of p with reference to the principal point,
 x_o, y_o are the co-ordinates of comparator origin with reference to the principal point, and
 x, y are the image co-ordinates of the point p in the comparator co-ordinate system.

5.6.2 Object Space Co-ordinate System

The right-handed plane co-ordinate system, as illustrated in Figure 5.2 is adopted for the object space co-ordinate system with its X- and Y- axes nearly parallel to the image x- and y- axes and thus the Z-axis is predetermined. It may be mentioned that Y-axis is taken to be in the vertical direction. In other words, the XY-plane lies in the vertical plane of the object space.

5.6.3 Sign Convention of Co-ordinate System

For the linear co-ordinate systems, the right-handed co-ordinate system is adopted with positive X-axis to the right and parallel to the line joining the "equivalent" exposure stations, the Z-axis at right angles to the XY plane and its positive direction pointing towards the exposure station; hence, the positive direction of Y-axis is predetermined.

A rotation is defined to be positive when it is clockwise about the positive direction of an axis as viewed from the origin. (Refer Figure 5.5(a)).

5.7 RADIOGRAPH ORIENTATION

5.7.1 Orientation Parameters

One of the major tasks in photogrammetry is the reconstruction of the bundle of rays by which the object was projected on to the film. This basic problem can be solved, in principle, if certain parameters of projective geometry are known at the time of exposure.

As in conventional photogrammetry, these parameters are termed orientation parameters. For the orientation of a radiograph, these are composed of two sets:

1. Interior orientation parameters, and
2. Exterior orientation parameters.

5.7.2 Interior Orientation Parameters

The interior orientation of a radiograph is defined by three parameters - co-ordinates of the principal point (x_0, y_0) in the image plane and the principal distance f - which in fact defines the spatial co-ordinates of the perspective centre in the image co-ordinate system. The geometry of these parameters is shown in Figure 5.3.

5.7.3 Exterior Orientation Parameters

These are concerned with the position of the mathematical focus of the X-ray source at the time of exposure expressed in the object space co-ordinate system and with the angular orientation of the radiograph axes with respect to the object space co-ordinate axes. These parameters can be represented in a very concise form with the help of matrix notation

a) Location of Exposure Station

$$\bar{C} = \begin{bmatrix} X_c \\ Y_c \\ Z_c \end{bmatrix} \quad (5.2)$$

Where X_c , Y_c , and Z_c are co-ordinates of \bar{C} in the object space co-ordinate system with origin at 0, as shown in Figure 5.4.

b) Angular Rotation Parameters

The angular relationship between the image axis system and the object space co-ordinate system is given by the following (3x3) orthogonal matrix and is made up of 9 direction cosines:

$$\begin{bmatrix} R \end{bmatrix} = \begin{bmatrix} a_{11} & a_{12} & a_{13} \\ a_{21} & a_{22} & a_{23} \\ a_{31} & a_{32} & a_{33} \end{bmatrix} \quad (5.3)$$

It can be shown that the direction cosines are not independent quantities (Schut 1958-59). Instead of using direction cosines in this study just as in photogrammetry, three sequential independent rotational angles ω , ϕ , κ which are defined in Figure 5.5 (b) are selected. This leads to three sets of transformation formulae; in each one of which, one of the co-ordinates is invariant and the final rotation matrix is given by the product of these three transformation matrices:

$$\begin{bmatrix} R \end{bmatrix} = \begin{bmatrix} R_{\omega} \end{bmatrix} \begin{bmatrix} R_{\phi} \end{bmatrix} \begin{bmatrix} R_{\kappa} \end{bmatrix} \quad (5.4)$$

Thompson (1959) has shown that any 3x3 orthogonal matrix can in its simplest form be represented in the Rodrigue's matrix. For computational purposes, the Rodrigue's matrix with small angular rotations ω , ϕ , κ , is best expressed in the form (Thompson, 1958-59; Miles, 1968)

$$[R] = \frac{1}{\Delta} \begin{bmatrix} \Delta' & \kappa & -\phi \\ -\kappa & \Delta' & \omega \\ \phi & -\omega & \Delta' \end{bmatrix} + \frac{1}{2\Delta} \begin{bmatrix} \phi \\ \omega \\ \kappa \end{bmatrix} \begin{bmatrix} \phi & \omega & \kappa \end{bmatrix} \quad (5.5)$$

Where

$$\Delta = 1 + \frac{1}{4} (\phi^2 + \omega^2 + \kappa^2)$$

$$\Delta' = 1 - \frac{1}{4} (\phi^2 + \omega^2 + \kappa^2)$$

In the present study, near normal radiography is attempted, therefore, the second and higher order terms can be ignored.

The expression for $[R]$, Eqn. 5.5, becomes linear and reduces to

$$[R] = \begin{bmatrix} 1 & \kappa & -\phi \\ -\kappa & 1 & \omega \\ \phi & -\omega & 1 \end{bmatrix} \quad (5.6)$$

If the co-ordinates of a point in the object space co-ordinate system are (X, Y, Z) and the corresponding co-ordinates in the co-ordinate system parallel to the image co-ordinate system X', Y', Z' , and if the rotation of one system with respect to the other is presented by an orthogonal matrix $[R]$, we have

$$\begin{bmatrix} X' \\ Y' \\ Z' \end{bmatrix} = [R] \begin{bmatrix} X \\ Y \\ Z \end{bmatrix} \quad (5.7)$$

5.8 SPACE RESECTION - A BASIC CONCEPT

The photogrammetric problem dealt with in this investigation can be expressed by the following functional relationship:

$$P = f(O, p) \quad (5.8)$$

where P - Spatial co-ordinates of the object point in the object point in the object space co-ordinate system,

p - Image co-ordinates of the corresponding point on the radiograph,

O - Orientation parameters of the data acquisition system at the time of exposure. These include interior and exterior orientation parameters and also perturbation parameters, if any.

In order to arrive at a numerical solution of equation (5.8) we must know (a) the mathematical relationship between the three sets of the parameters i.e. between P, p and O, and (b) the values of two sets of variables out of three so as to calculate the values of the third. It may be emphasized here that the set of parameters 'O' has fixed values for a radiograph and generally the 'p' co-ordinates are known from measurements made on radiographs. Knowing the values of the 'O' parameters and the image co-ordinates of the photopoints, the object space co-ordinates of the corresponding object points, in our case, corners of the marker wires, can be calculated.

Space resection in photogrammetry is generally employed as the basis for data reduction, calibration and determination of the

orientation parameters of individual radiographs. The basic theory of the space resection problem consists of the collinearity principle of central projective geometry in which each image, its corresponding object, and the perspective centre lie on a common straight line (Schmid, 1953).

5.9 MATHEMATICAL FORMULATION

5.9.1 Basic Assumptions

In order to form a simple mathematical model which relates the three sets of variables, Eqn 5.8, the following assumptions have to be made:

1. Both image and object co-ordinate systems are right-handed.
2. The sequence of angular rotations is ω , ϕ and κ , where ω is the first rotation and is about the X-axis, & etc.
3. The image co-ordinates x , y and f refer to a radiograph.
4. The radiography is normal or near normal, in terms of conventional photogrammetry.
5. The plate co-ordinates are assumed to be free from systematic errors arising from all sources, such as film distortion, penumbral effects, etc. and are affected by random errors only. In other words, in the mathematical formulation perturbation parameters are assumed to be non-existent.
6. The focus of the X-ray source is assumed to be a point. The validity of the above assumption is discussed in Appendix A.

5.9.2 Condition Equations

In order to arrive at a solution of the photogrammetric problem

discussed in the earlier section of this chapter, a set of condition equations relating the observed quantities and other known and unknown parameters must be established. In photogrammetry, there are three usual forms of condition equations (Tewinkel et al., 1966)

1. Collinearity condition equations
2. Coplanarity condition equations
3. Scale-restraint condition equations

The collinearity condition equations are concerned with individual radiographs. Further, these equations contain all the elements of the problem in which we are interested namely interior and exterior orientation parameters, measured image co-ordinates and object space co-ordinates of homologous points. Thus their equations are self-sufficient for the solution of any analytical photogrammetric problem, whereas the other condition equations - coplanarity and scale-restraint - do not include the co-ordinate of object points expressed in the object space co-ordinate system. For the complete solution of the photogrammetric problem, these constraint equations would have to be supplemented by some kind of collinearity equations. It is, therefore more expedient to use collinearity condition equations. Incidentally, these equations form the basis of Space Resection.

5.9.3 Collinearity Condition Equations

The collinearity condition equations state mathematically the simple basic fact of projective geometry, that the object point P (X_p, Y_p, Z_p), the image point p (x, y), and the perspective centre i.e. the exposure station C , all lie on the same straight line.

Each image point gives two condition equations, one each for the two co-ordinates (x,y) in the image plane. The condition equations of collinearity can be obtained directly from the projective equations and may be written as follows:

$$x_p = x + x_o = -f \left(\frac{a_{11} (X_p - X_c) + a_{12} (Y_p - Y_c) + a_{13} (Z_p - Z_c)}{a_{31} (X_p - X_c) + a_{32} (Y_p - Y_c) + a_{33} (Z_p - Z_c)} \right) \quad (5.9)$$

$$y_p = y + y_o = -f \left(\frac{a_{21} (X_p - X_c) + a_{22} (Y_p - Y_c) + a_{23} (Z_p - Z_c)}{a_{31} (X_p - X_c) + a_{32} (Y_p - Y_c) + a_{33} (Z_p - Z_c)} \right)$$

where (x_p, y_p) , (x,y) and (x_o, y_o) are defined by Eq. 5.1

(X_p, Y_p, Z_p) are the spatial co-ordinates of point P in the object co-ordinate system

(X_c, Y_c, Z_c) are the co-ordinates of the perspective centre in the object co-ordinate system, refer Eq 5.2

f principal distance

$a_{11} \dots a_{33}$ elements of the rotation matrix, Eq. 5.3 $a_{11} \dots a_{13}$

5.9.4 Mathematical Formulation

For the reasons outlined in section 5.5, a simplified mathematical model is used. It is important to note that the basic geometric projective principles used here are the same as those used in conventional photogrammetry. Various co-ordinate systems used here are shown in Figure 5.6. The transformation of co-ordinates from one

system to another can be accomplished by using the following relations:

a) From comparator co-ordinate to image co-ordinate system

$$\begin{bmatrix} p \end{bmatrix} = \begin{bmatrix} x_p \\ y_p \end{bmatrix} = \begin{bmatrix} x + x_o \\ y + y_o \end{bmatrix} \quad (5.1)$$

where (x_p, y_p) are the image co-ordinates
 (x, y) are the measured comparator co-ordinates
 (x_o, y_o) are the co-ordinates of the origin of the comparator co-ordinate system expressed in the image co-ordinate system

b) From the object co-ordinate system to a co-ordinate system parallel to the image co-ordinate system but with its origin at the focus (perspective centre).

$$\begin{bmatrix} P \end{bmatrix} = \begin{bmatrix} X_p \\ Y_p \\ -H_p \end{bmatrix} = \begin{bmatrix} X_o \\ Y_o \\ Z_o \end{bmatrix} + \begin{bmatrix} R \end{bmatrix} \begin{bmatrix} X \\ Y \\ H \end{bmatrix} \quad (5.10)$$

where $(X_p, Y_p, -H_p)$ are the spatial co-ordinates of P in the perspective centre system.

(X_o, Y_o, Z_o) are the co-ordinates of the origin of the object space co-ordinate system in the perspective centre system.

- $[R]$ is the rotation matrix defined by Eq. 5.5
- (X, Y, H) are the co-ordinates of the point P in the object space co-ordinate system
- Z_0 is $(-f + H_0)$
- H_0 is the perpendicular distance between the object space co-ordinate origin and of the image plane.

If the angular rotations ω , ϕ and κ are small, the equation 5.10 can be simply written as

$$\begin{bmatrix} X_P \\ Y_P \\ -H_P \end{bmatrix} = \begin{bmatrix} X_0 \\ Y_0 \\ -f + H_0 \end{bmatrix} + \begin{bmatrix} 1 & \kappa & -\phi \\ -\kappa & 1 & \omega \\ \phi & -\omega & 1 \end{bmatrix} \begin{bmatrix} X \\ Y \\ H \end{bmatrix} \quad (5.11)$$

From equation 5.10, we get -

$$H_P = f - H_0 - H - (\phi \cdot X - \omega \cdot Y) \quad (5.12)$$

In Figure 5.6, if O is the principal point, C is the perspective centre, P is the object point, P_0 is the foot of the perpendicular from P on the image plane and p is the image of the object point P; we know from projective geometry that the vectors $\overline{C_P}$ and $\overline{C_p}$ are collinear and also the points O, C, P, p and P_0 are coplanar. With the help of these geometrical relations and from Figure 5.6, we can write in matrix form:

$$\begin{bmatrix} c_p \end{bmatrix} = \frac{o_c}{o_c} \begin{bmatrix} C_p \end{bmatrix} \quad (5.13)$$

$$\text{or} \quad \begin{bmatrix} x_p \\ y_p \\ -f \end{bmatrix} = \frac{f}{H_p} \begin{bmatrix} X_p \\ Y_p \\ -H_p \end{bmatrix} \quad (5.14)$$

On substitution of the values of (x_p, y_p) from equation (5.1) and the values of $(X_p, Y_p, -H_p)$ from equation (5.11), in which ω, ϕ and κ are assumed to be small, in the above equation we get -

$$\begin{bmatrix} x + x_o \\ y + y_o \\ -f \end{bmatrix} = \frac{f}{f - H - H_o - (\phi X - \omega Y)} \begin{bmatrix} X_o \\ Y_o \\ -f + H_o \end{bmatrix} + \begin{bmatrix} 1 & \kappa & -\phi \\ -\kappa & 1 & \omega \\ \phi & -\omega & 1 \end{bmatrix} \begin{bmatrix} X \\ Y \\ H \end{bmatrix} \quad (5.15)$$

It can easily be shown that of these three equations, the first two are independent and the last one is an identity; the two independent equations can be written as -

$$\begin{bmatrix} x + x_o \\ y + y_o \end{bmatrix} = \frac{f}{f - H - H_o - (\phi X - \omega Y)} \begin{bmatrix} X_o \\ Y_o \end{bmatrix} + \begin{bmatrix} X + \kappa Y - \phi H \\ -\kappa X + Y + \omega H \end{bmatrix} \quad (5.16)$$

Since ω, ϕ and κ are small angles for near normal radiography, we can rewrite Eq. (5.16) as

$$\begin{bmatrix} x + x_o \\ y + y_o \end{bmatrix} = \frac{f}{f-H-H_o} \left(1 + \frac{\phi X - \omega Y}{f-H-H_o} \right) \left\{ \begin{bmatrix} X_o \\ Y_o \end{bmatrix} + \begin{bmatrix} X + \kappa Y - \phi H \\ -\kappa X + Y + \omega H \end{bmatrix} \right\} \quad (5.17)$$

The above equations are non-linear and are derived on the assumption that the angular rotations are small in addition to those given in Section (5.9.1). Equations (5.17) are a mathematical version of the functional relationship given in Equation (5.7). Here x, y are the comparator co-ordinates, (x, y, H) are the object co-ordinates, (x_o, y_o, f) are the interior orientation parameters and (X_o, Y_o, H_o) , $(\omega, \phi$ and $\kappa)$ are the exterior orientation parameters. For every individual radiograph, the orientation parameters must be known. These are generally obtained by calibration of the data acquisition set-up.

5.10 SYSTEMATIC APPROACH FOR CALIBRATION

5.10.1 Various Approaches

The interaction between actual object radiography and calibration of the system depends mainly on the stability of the acquisition system and on the repeatability of the orientation parameters. The data acquisition configuration adopted in this work, which is analogous to the non-metric cameras of close-range photogrammetry, is rather difficult to call stable. In Figure 5.7, various calibration approaches are summarised. From this chart, it is obvious that the on-the-job calibration approach 'D' is the most suitable if fairly accurate final results are to be expected and hence this approach is followed for calibration and subsequent data reduction.

5.10.2 On-the-job Calibration and Control Points

The stability of the X-ray data acquisition set-up is highly questionable which makes the on-the-job calibration a must and for every individual radiograph complete calibration is essential. This obviously requires adequate control points well distributed around the object. As we have seen in the earlier sections of this chapter, in order to determine the orientation parameters, 9 in number, an adequate number of properly distributed object points, called control points, whose spatial co-ordinates must be known. From Eqn.5.17, it is clear that for every object point we get two independent equations, known as observation equations, in terms of 9 unknown orientation parameters. To solve for these 9 unknowns, we require, at least 9 equations and therefore at least 5 control points whose co-ordinates both in object space and in image plane, are known. If just the minimum required number of control points are selected, in such a case the control points should be so dispersed in the object space that no more than 3 control points lie on a line or on a plane $X = \text{constant}$. Since the observations are in no way perfect and are assumed to be burdened with random errors only, the systematic errors, if any, are either compensated or assumed to be negligible. It is a normal practice in photogrammetry to have redundant observations. Then the method of least squares is used for determination of the most probable values of the unknowns. The significance of a least squares adjustment increases with the number of redundant observations available for the determination of the unknowns (Schmid, 1971; Ackermann, 1964). In all 50 control points, arranged in two planes as shown in

Figure 5.8 (a) and (b), are used in the calibration set-up. Lead shot of approximately 0.5 mm in diameter is embedded in the σ_2 -platens. In order to identify the images of the control points on a radiograph, the control points are arranged on the front and the rear σ_2 - platens in two distinctive and unambiguous patterns and are shown in Figure 5.8 (a) and Figure 5.8 (b). After the patterns of the points are recognised on the radiographs, every control point is uniquely numbered according to the scheme shown in Figures 5.8 (a) and 5.8 (b). This system of identification is used as a standard practice on the whole series of tests reported here. It may be mentioned here that the layout of control points and even the calibration method used here may not be the best from a photogrammetric point of view. In X-ray photogrammetry which at present is in its infancy, there are so many questions to be answered and uncertainties to be resolved before one can come up with the best method of calibration. This obviously needs concerted efforts both by the photogrammetrist and the engineer who want to use it as an engineering tool. In order to avoid further indulgence in the realm of X-rays, radiography and photogrammetry, a compromise has to be made based on the present state of knowledge.

5.10.3 Spatial Co-ordinate Measurement of Control Points

Since the scale of radiography is very nearly unity, the measurements of the spatial co-ordinates posed a very difficult problem. In aerial photogrammetry where the accuracy requirement for ground surveys is never as stringent as that of image co-ordinate measurements mainly due to comparatively small scale of photography, whereas in

X-ray photogrammetry, in the present context, the accuracy of measurements of the spatial co-ordinates of the control points must be of the same order, if not better than that of the image co-ordinate measurements. This in turn imposes another requirement on the calibration device on which the control points are located. This requirement can be fulfilled either by making the calibration device dimensionally stable under the test conditions or by using a suitable mathematical model which adequately describes the systematic changes in the control co-ordinates due to various agencies including pressure, temperature, etc. prevailing at the time of radiography. The X-ray acquisition system suffers from other inherent sources of errors such as film distortions, geometrical unsharpness, etc. and in comparison to these errors the error caused by the dimensional instability of the device will be small provided every effort is made to use the calibration device with maximum attainable stiffness.

The solution of the difficult problem of measurement of the co-ordinates of control points is sought under certain given constraints, namely availability of measuring equipment, time, money and limited scope of the present study which has precluded the depth of desirable research in the very useful field of X-ray photogrammetry. Nevertheless the following method has proved to give measurements with an acceptable degree of accuracy. The measurements of the spatial co-ordinates of the control points were accomplished in two stages and by using different measuring machines in every stage. In the first stage, both σ_2 - platens which are the parts of the calibration device and

contain the control points were separated from the device by dismantling it. The X and Y co-ordinates of the control points on both the σ_2^- platens were read by the stereo-comparator. In the second stage, the calibration device was properly assembled and correctly mounted on the Gambin F27^S Universal Milling Machine which has a resolution of 12.7 μm . The spatial co-ordinates including Z co-ordinates of all the points were then measured. The variation in the measurements of X,Y co-ordinates made by the stereo comparator and by the milling m/c are found to be within $\pm 12.7 \mu\text{m}$, which is the resolution of the later machine. The standard error of Z measurement was found to be $\pm 15.6 \mu\text{m}$. Further measurements for (x,y,z) co-ordinates were carried out so as to find out with what accuracy the calibration device can be assembled every time. The standard error remained nearly the same and as mentioned above. Thus the method of stiffening and assembling used was satisfactory. The unassembled and assembled forms of calibration device are shown in Plate 5.1 (a) and 5.1 (b) respectively.

5.10.4 Linearization of Observation Equations

The mathematical relations between the object co-ordinates, its image co-ordinates and the orientation parameters based on certain assumptions have been developed in Section 5.9.4. The theoretical solution for the unknown orientation parameters is not practical for two reasons: the equations 5.17, as noted earlier, are non-linear and secondly, the number of image points observed are more than needed for the explicit solution. However, a practical solution is obtained by linearizing the equations 5.17 with the

help of Taylor series and then using the method of least squares to account for the redundant observations.

So far, it was implicitly assumed that the observations were error free and were of fixed value. However, in practice this assumption is far from reality. Now it will be assumed that the measured co-ordinates of a control point (X, Y, H) are fixed and error free; but the comparator co-ordinates (x, y) of homologous point are burdened with observational errors of v_x and v_y in its x and y co-ordinates respectively. Let $dx_0, dy_0, dX_0, dY_0, df, dH_0, d\omega, d\phi$ and $d\kappa$ be the unknown corrections to the estimated values of $x_0, y_0, X_0, Y_0, f, H_0, \omega, \phi$ & κ respectively. The corrections to the estimated values are obtained by the method of variation of co-ordinates (Ashkenazi, 1970). From Eq. (5.17), the observation equations can be written down as -

$$\frac{f+df}{f-H_0-H+df-dH_0} \left(1 + \frac{x(\phi+d\phi) - Y(\omega+d\omega)}{f-H_0-H+df-dH_0} \right) \left\{ \begin{array}{l} \left[\begin{array}{l} X_0+dX_0 \\ Y_0+dY_0 \end{array} \right] + \left[\begin{array}{l} X+Y(\kappa+d\kappa) - H(\phi+d\phi) \\ -X(\kappa+d\kappa) + Y + H(\omega+d\omega) \end{array} \right] \end{array} \right\} = \left[\begin{array}{l} x+v_x \\ y+v_y \end{array} \right] \quad (5.18)$$

The simplification is made to the Eq. (5.18) on the assumption that since the radiography obtained is near normal, the initial value of each of ω, ϕ and κ is assumed to be zero and the most probable value is given by the correction $d\omega, d\phi$ and $d\kappa$. As the corrections $d\omega, d\phi$ and $d\kappa$ are small, they are not added to their

estimated values after the end of every iteration. Equation (5.18)

can be written as follows:

$$\begin{bmatrix} -1 & 0 & \frac{f}{(f-H'')} & 0 & -\frac{H(X+X_0)}{(f-H'')^2} & \frac{f(X+X_0)}{(f-H'')} & \frac{fY}{(f-H'')} & -\frac{fY(X+X_0)}{(f-H'')^2} & \frac{fX(X+X_0)}{(f-H'')^2} & -\frac{fH''}{(f-H'')} \\ 0 & -1 & 0 & 0 & \frac{-H(Y+Y_0)}{(f-H'')^2} & \frac{f(Y+Y_0)}{(f-H'')} & \frac{-fX}{(f-H'')} & \frac{-fY(Y+Y_0)}{(f-H'')^2} + \frac{fH''}{(f-H'')} & \frac{fX(Y+Y_0)}{(f-H'')^2} \end{bmatrix}$$

$$\begin{bmatrix} dx_0 \\ dy_0 \\ dx_0 \\ dY_0 \\ df \\ dH_0 \\ dk \\ dw \\ d\phi \end{bmatrix} = \begin{bmatrix} x+x_0 - \frac{f(X+X_0)}{(f-H'')} \\ y+y_0 - \frac{f(Y+Y_0)}{(f-H'')} \end{bmatrix} + \begin{bmatrix} v_x \\ v_y \end{bmatrix} \quad (5.19)$$

where $H'' = H + H_0$

5.10.5 Method of Least Squares

The method of least squares is the "best estimator" for the unknowns provided the observations are independent and normally distributed. Thompson (1962) commented on the method of least squares: "It is true, that if observations are independent and

normally distributed, then (in a certain sense) the method of least squares is the "best" estimator for the unknowns. But since we have no means in any particular case of finding out whether the observations are so distributed and there are usually reasons to suppose that they are not, the method of least squares can in practice be no more than a thoroughly systematic and unobjectionable way of making good use of redundant observations to be used only when no equally systematic but simpler ways are available".

It is assumed that the unknowns are independent and that they are related to the observations by the observation equation (5.19). Equation (5.19) can be written in the following concise form by using matrix notation, assuming that all observations are of equal weight:

$$[B] \cdot [\Delta] = [l] + [v] \quad (5.20)$$

where

$[B]$ represents the first matrix on the L.H.S. of Eq. (5.18)

$[\Delta]$ represents the second matrix of unknown corrections on the L.H.S. of Eq. 5.18

$[l]$ represents the first matrix of observations on the R.H.S. of Eq. (5.18)

$[v]$ represents the second matrix of observational error on the R.H.S. of Eq. (5.18)

From the above observation equations, the following normal equations are formed -

$$[B]^T [B] [\Delta] = [B]^T [l] \quad (5.21)$$

The correction Δ^S are computed. Mathematically we can say -

$$[\Delta] = \left([B]^T [B] \right)^{-1} [B]^T [l] \quad (5.22)$$

These corrections are then accepted and the estimated values for all the unknown parameters, excepting those for angular parameters updated by adding the computed Δ^S to their initial approximate value. This iterative process, which can be shown to be based on Newton's method of iteration, is continued until the values of the elements of $\left[\Delta \right]$ are very small and are less than a prefixed amount.

5.10.6 Initial Approximation

It is obvious that the success of using the linearized equations and principle of least squares depends on having a good initial estimate for the 9 unknowns. In other words, these equations 5.19 can only be used if the increments $\Delta x_o, \Delta y_o, \dots, \Delta k$ are small. In the present work, the initial values of linear quantities are obtained by direct measurements of the data acquisition

set-up. The angular rotation angles are assumed to be zero which is the logical and acceptable assumption for the near normal radiography of this study.

5.11 SPACE INTERSECTION

Once the orientation parameters are known and the observations for corresponding image points appearing on the radiographs of a stereo-pair are available, then the spatial co-ordinates of homologous object points can be calculated by space intersection.

The equations (5.15) can be rewritten as

$$\frac{(f-H_o)}{f} \begin{bmatrix} x+x_o \\ y+y_o \\ -f \end{bmatrix} - \frac{1}{f} \begin{bmatrix} x+x_o \\ y+y_o \\ -f \end{bmatrix} \begin{bmatrix} \phi & -\omega & 1 \end{bmatrix} \begin{bmatrix} X \\ Y \\ H \end{bmatrix} - \begin{bmatrix} X_o \\ Y_o \\ -f+H_o \end{bmatrix} = \begin{bmatrix} 1 & \kappa & -\phi \\ -\kappa & 1 & \omega \\ \phi & -\omega & 1 \end{bmatrix} \begin{bmatrix} X \\ Y \\ H \end{bmatrix} \quad (5.23)$$

and equation (5.16) can be rewritten as

$$\begin{bmatrix} 1 + \frac{\phi(x+x_o)}{f} & \kappa - \frac{\omega(x+x_o)}{f} \\ -x + \frac{\phi(y+y_o)}{f} & 1 - \frac{\omega(y+y_o)}{f} \end{bmatrix} \begin{bmatrix} X \\ Y \\ H \end{bmatrix} = \frac{(f-H_o)}{f} \begin{bmatrix} x+x_o \\ y+y_o \end{bmatrix} - \begin{bmatrix} X_o \\ Y_o \end{bmatrix} \quad (5.24)$$

From equation (5.24) it is obvious that every image point yields two equations involving three unknowns, namely, its object space co-ordinates. Using the co-ordinates of images of the same object point on the two radiographs of the same stereo pair and their respective orientation parameters, we can get four equations in 3 unknowns (X,Y,H). Since X, Y, H are over determined, the least squares principle is applied to obtain the most probable value of X, Y, H. It is worth emphasising that in space intersection photogrammetry, it is assumed that the orientation parameters are independent and precise. This assumption, though not correct, is made to avoid inevitable complications, (Thompson, 1958).

5.12 INSTRUMENTATION FOR ANALYTICAL DATA REDUCTION

In data reduction, proper instrumentation is required for the measurements of the co-ordinates of the image co-ordinates. In addition to a measuring machine, other peripheral instrumentation such as digital readout, printer, paper tape punch, etc. are required. Two major alternatives are available for the problem of obtaining image co-ordinates -

1. Monocular measurements and the instrument used for such measurements is called a monocomparator.
2. Stereoscopic measurements. A stereo-comparator is needed for measurements of co-ordinates.

Tewinkel (1975) suggested that monocular observations and hence the monocomparator is very well suited to those applications where

all objects are suitably premarked before photography. However, a stereocomparator is considered to be more economical than a monocomparator as it allows simultaneous identification and measurements of points in two radiographs at a time. The economy afforded by the simultaneous identification of points on both radiographs of a stereo-pair and the availability of a machine with digitising equipment tilted the balance towards the selection of a stereocomparator for this study.

The stereocomparator at the City University was used. The said stereocomparator is made by Zeiss-Jena and is called a steconometer. The salient features of the machine are given in Chapter 2 and its set-up is shown in Plate 2.7.

5.13 SCHEME OF COMPUTATION

5.13.1 Major Steps

The computations connected with the study were carried out in four stages:

1. Conversion and editing the measurement data obtained from the stereocomparator.
2. Computations for the determination of the most probable values of unknown parameters.
3. Statistical parameters.
4. Computation of object co-ordinates.

For each of the above stages, separate computer programme was developed by the writer and written in Fortran IV language compatible with CDC 6400 at Imperial College Computer Centre (ICCC) and CDC 6600 at the University of London Computer Centre, London (ULCC).

5.13.2 Image Co-ordinate Computation

The stereoscopic measurements of co-ordinates were made on the steconometer. The output from the steconometer was in the form of punched paper tape which gave, in addition to test number, point number, corner number of the marker wire, the co-ordinates x , y and their parallaxes. A separate programme was written to edit the data and convert the x , y and the parallaxes to two sets of co-ordinates, one each for the left and right radiographs of a stereo pair.

The measurements for all the stereo-pairs were collected, checked for possible blunders and tabulated so as to minimise the size of the data file and for ease of inputting the data for the next stage of computation. This was accomplished by having another programme which tabulated the data and stored them on the magnetic tapes.

5.13.3 Computation for orientation parameters

The input data for this stage of computation are as follows:

1. Measured space co-ordinates of all control points.
2. Measured image co-ordinates of all control points.
3. Initial estimates of the 6 orientation parameters

$$x_0, y_0, f, X_0, Y_0, H_0$$

The scheme of computation is shown by means of a flow chart in Figure 5.9.

The steps in the solution can be summarized as:

1. Formation of observation equations.
2. Formation of normal equations from the observation equations. All observations were assumed to be of equal weight.
3. Simultaneous solution of the normal equations by Cholesky's method for obtaining the corrections to the estimated values of the unknown orientation parameters. Sharma (1973) has developed a computer routine for this method and has been used here.
4. Updating the last estimated values of the orientation parameters by adding the corrections obtained in Step 3.
5. Steps 1 through 4 are repeated until sufficient convergence is obtained as indicated by the small values of the corrections to the parameters and comparing them with the prefixed minimum value.

5.13.4 Statistical Parameters

In this stage of computation, the residuals for the image co-ordinates and for the control points are calculated and then RMSE's for the co-ordinates of the control points. The significance of these parameters is discussed in Appendix A.

5.13.5 Object Co-ordinates

The spatial co-ordinates of the corners of all the marker wires in the test specimen at a given stage of deformation were calculated by the method of least squares. From the co-ordinates of the four corners of a marker wire, the co-ordinates for the centre of its tips and hence the centre of the marker particle as well as the angles made by its projections in XY, YZ and ZX plane with X, Y and Z axes respectively were calculated and stored.

In this way, the calculations were performed for all the marker wires in a test specimen at a given stage of deformation. This procedure of computation was followed for all stages of deformation and for all the plane strain tests for which the image co-ordinates of the markers were read with the help of the steconometer.

5.13.6 Inter-Active Computer Graphic Programme

A general inter-active programme was written for plotting and studying the data. With the help of this programme, the digital information can be converted into graphic display or can be plotted on off-line plotting machines e.g. Calcomp plotters or King-matic plotting machine or using a microfilm software.

Just to illustrate the use of this powerful and versatile tool namely computer graphic, plots showing the projection of particles only on the XY plane at the start and at the end of every test reported are presented in Figure 5.10 to Figure 5.29. These plots were drawn by using the microfilm software and other plotting facilities available

at Imperial College Computer Centre and at the University of London Computer Centre (ULCC), London. The plotting programme was developed by the writer during the present study.

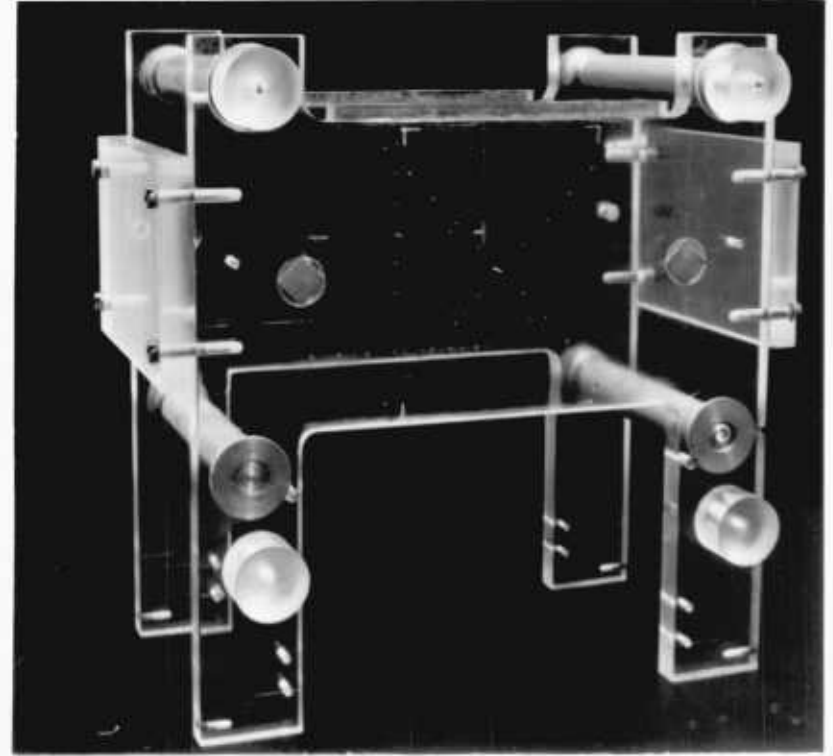
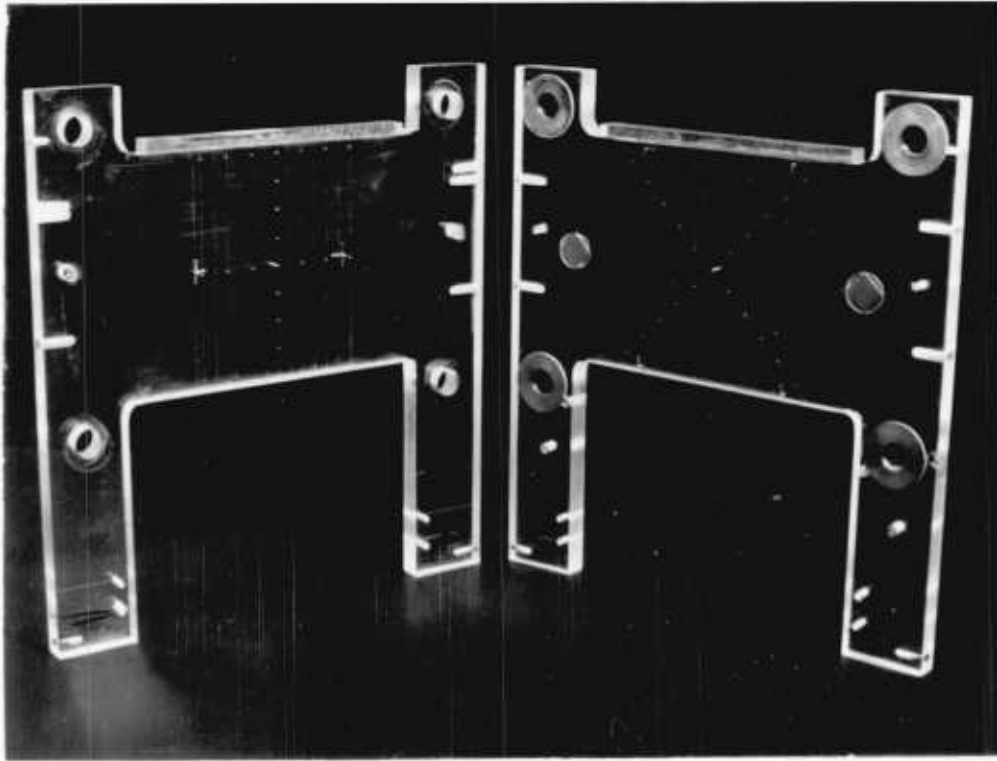


Plate 5.1 CALIBRATION DEVICE (σ_2 PLATENS)

a. Unassembled

b. Assembled

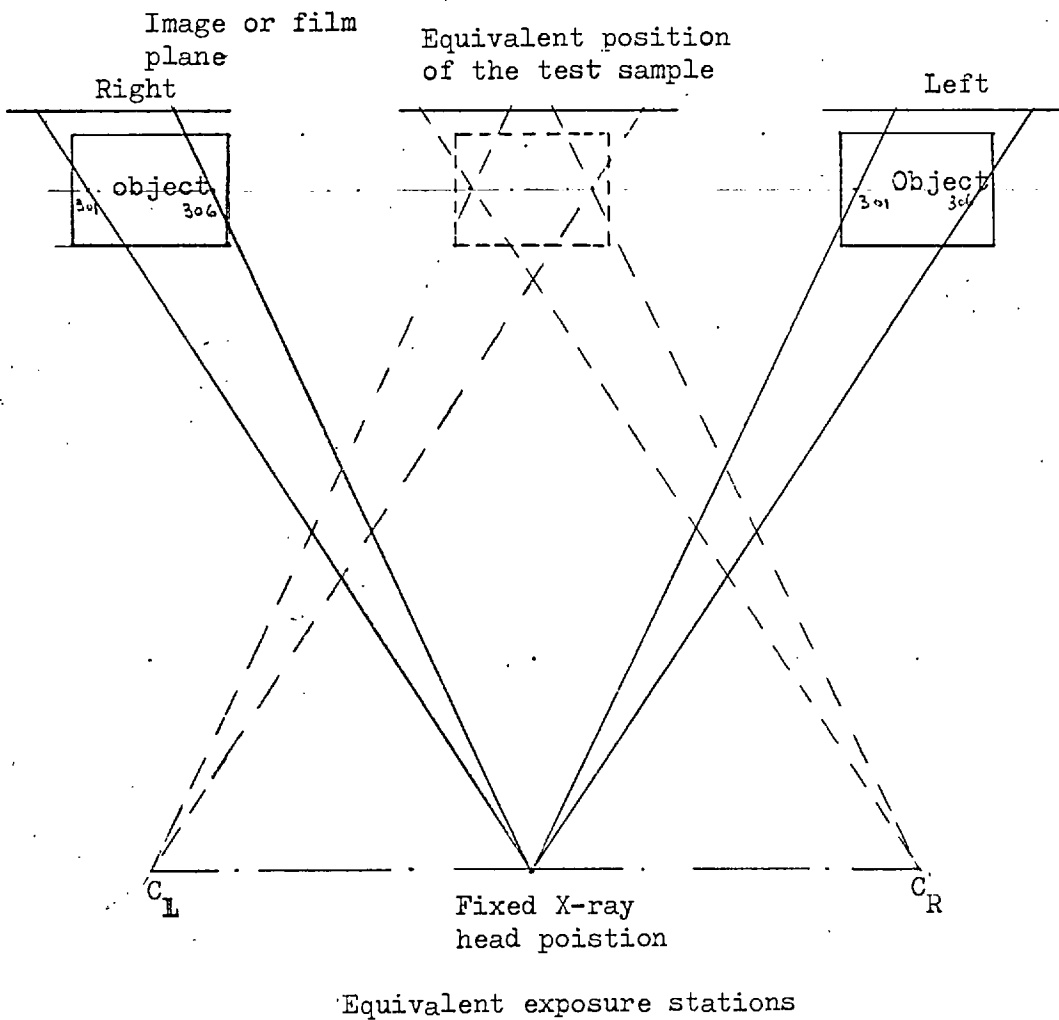


FIG. 5.1 Equivalent exposure stations

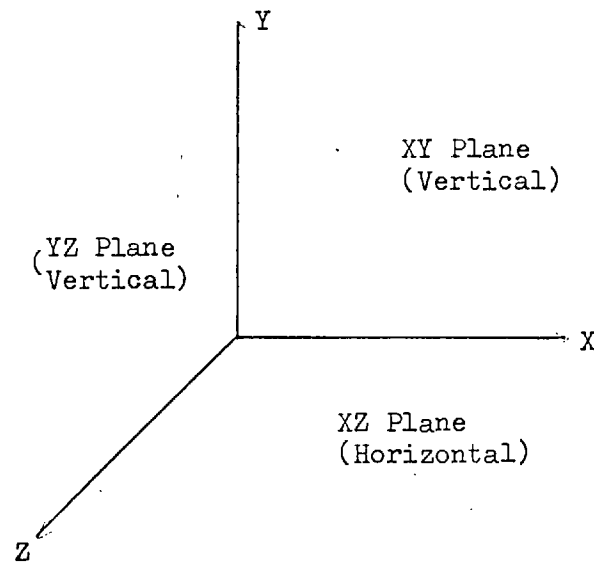


FIG. 5.2 Right handed Co-ordinate System

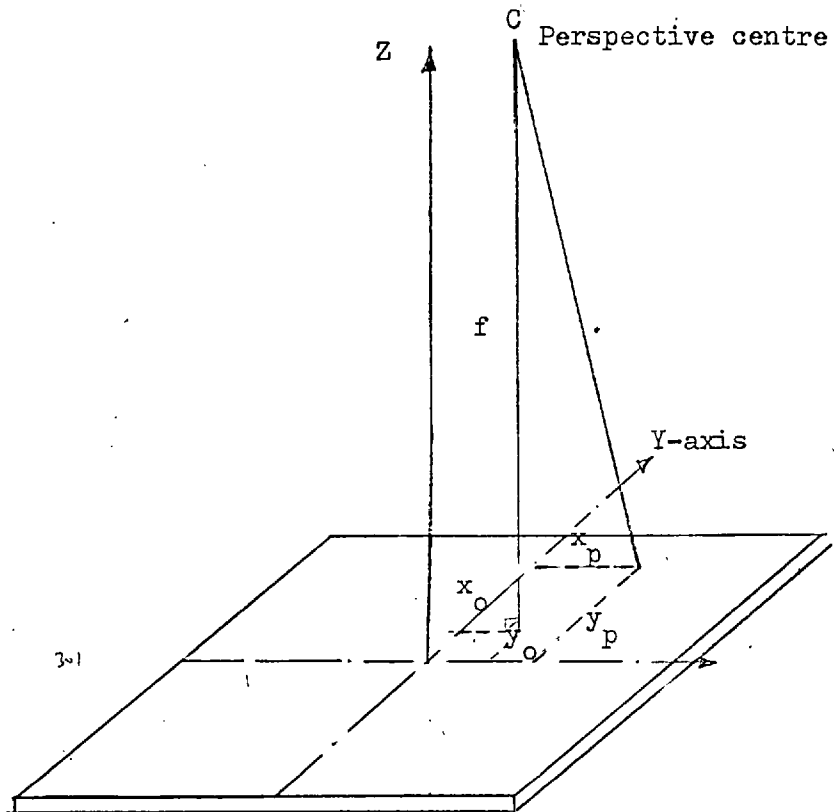


FIG. 5.3 Image co-ordinate system and Interior orientation

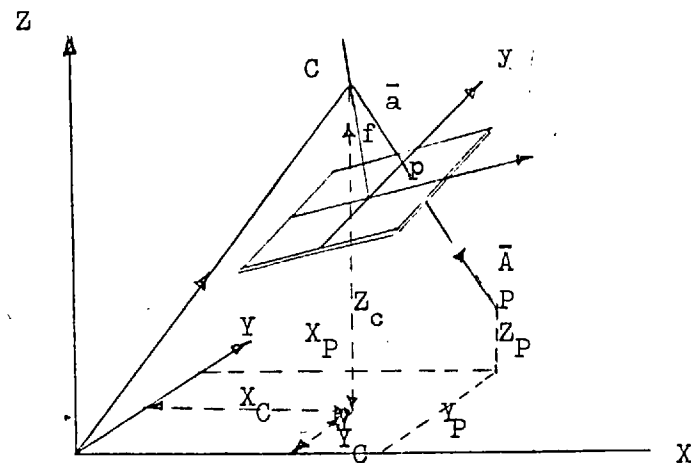


FIG. 5.4 Exterior Orientation

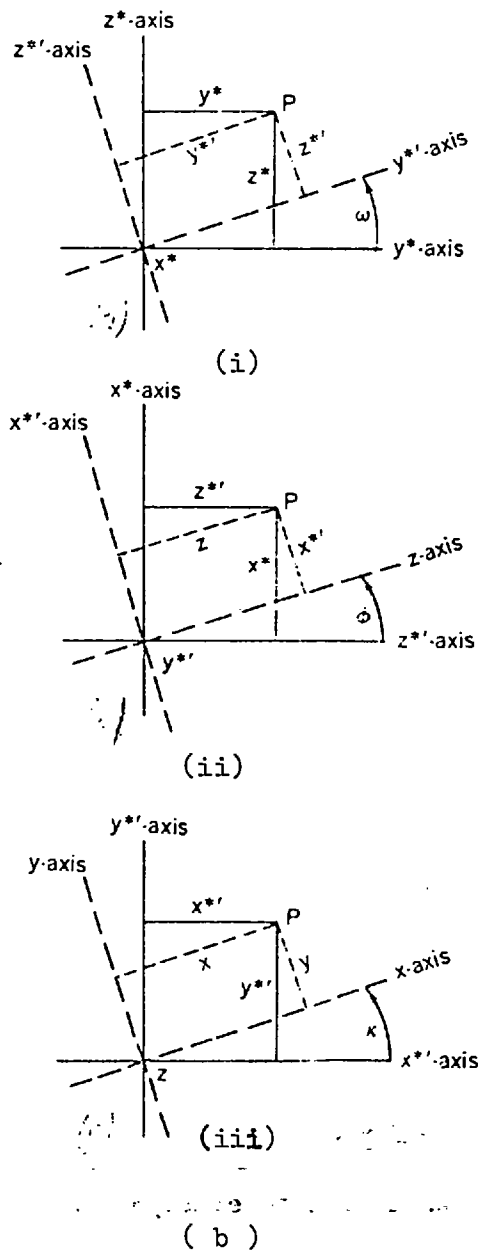
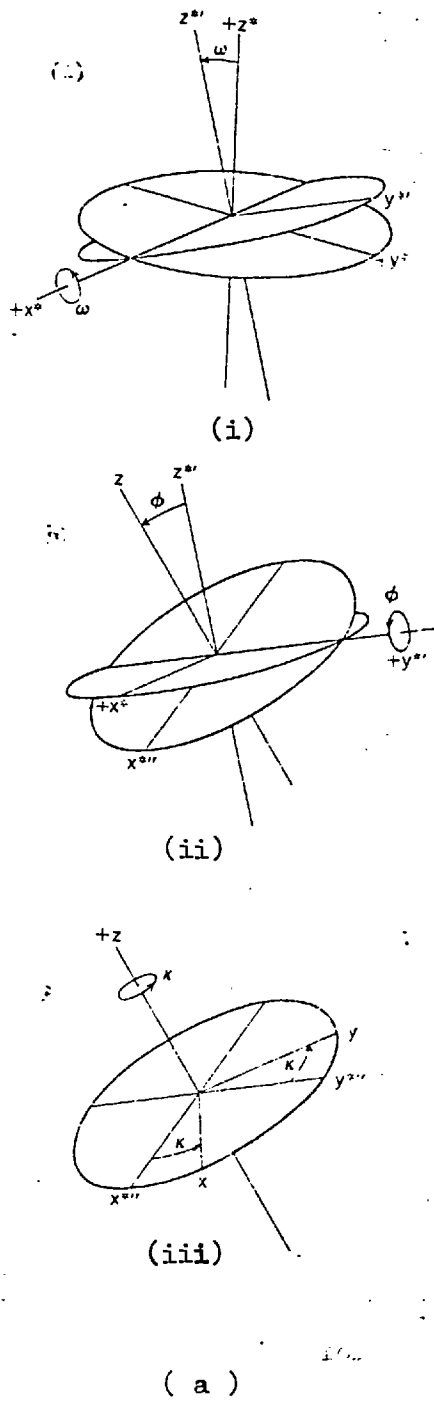


FIG. 5.5 a) Sign convention for rotations
 b) The sequence of rotations

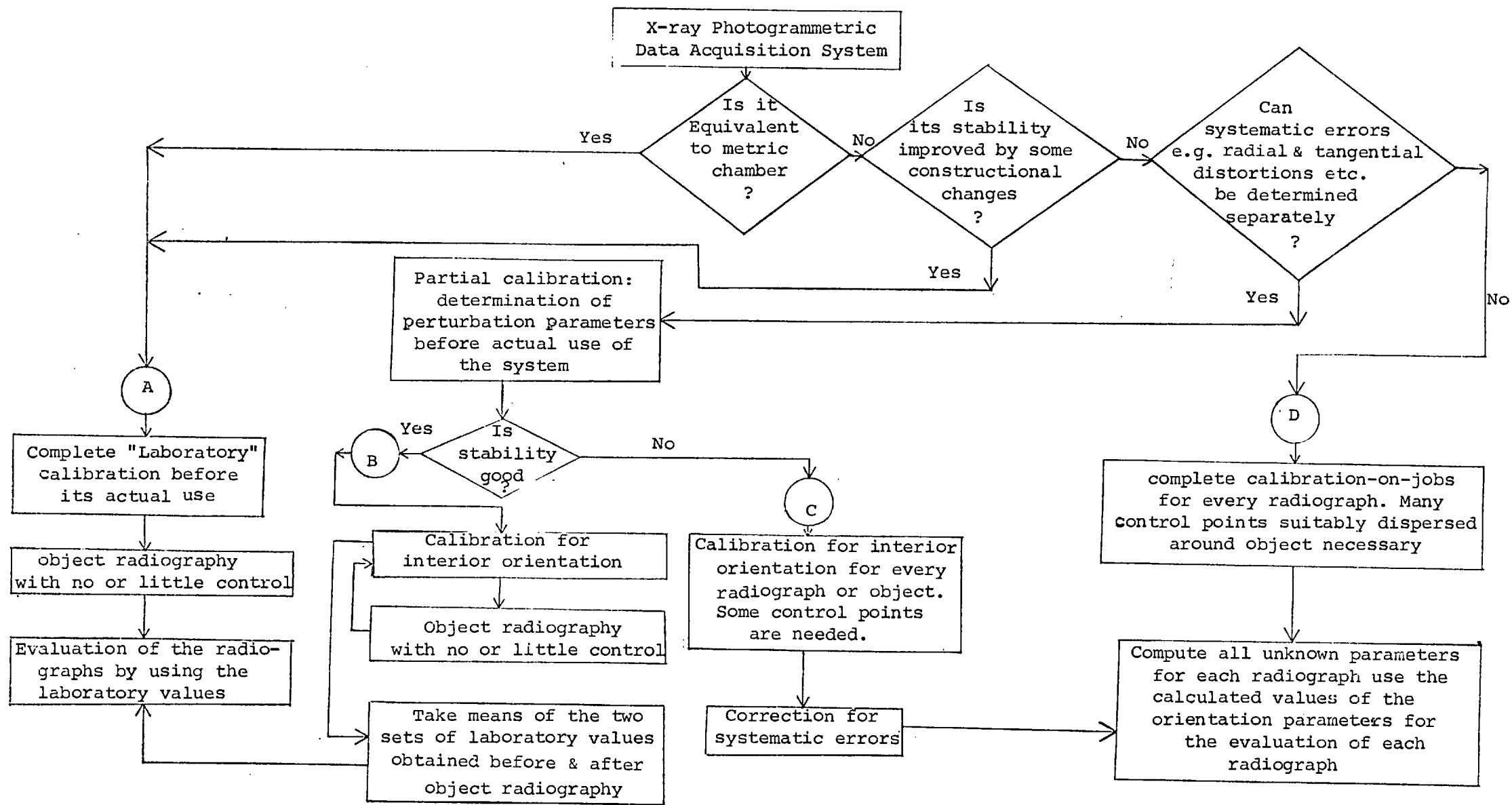
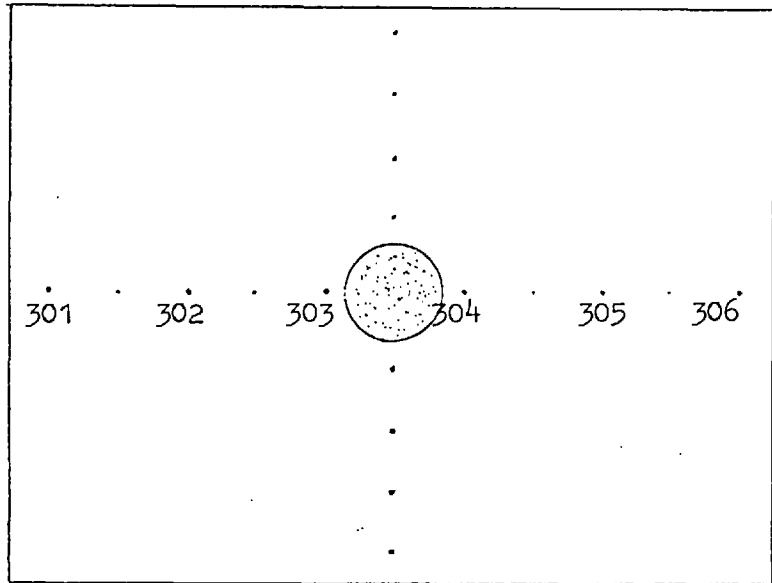
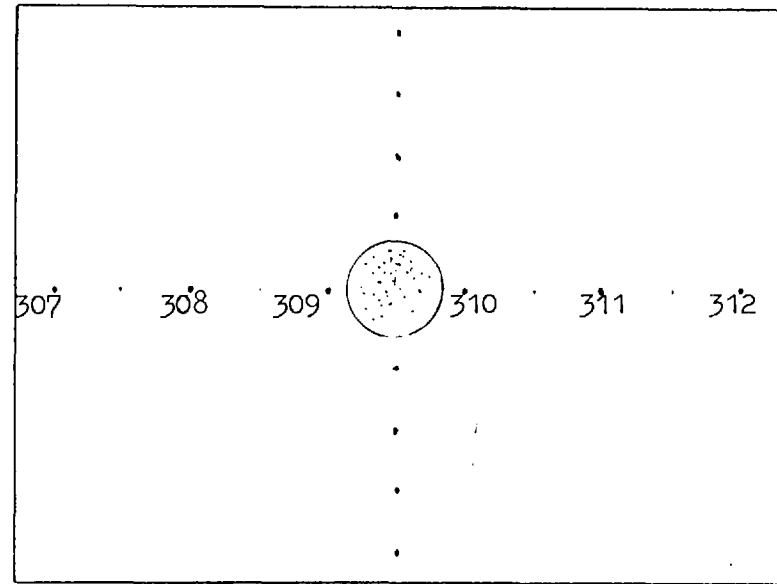


Fig. 5.7 Calibration Approaches - Laboratory Against On-The-Job Calibration.

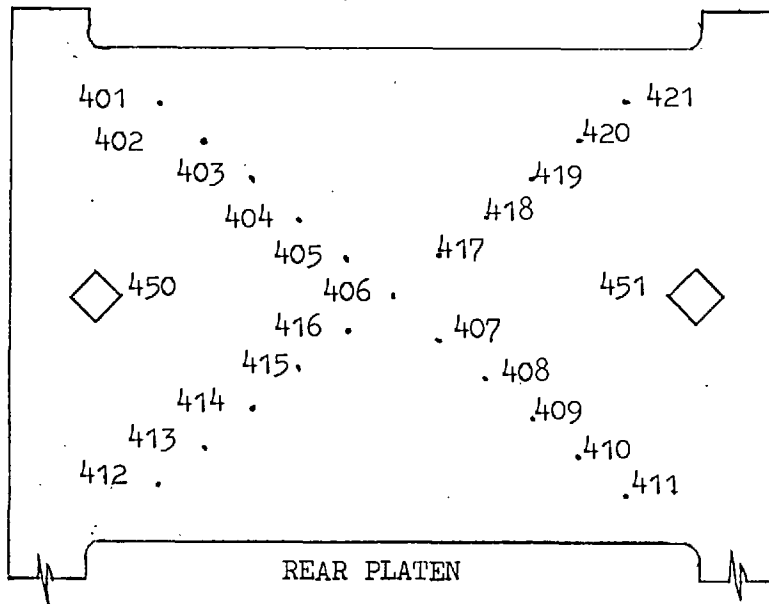


BOTTOM AXIAL PLATEN



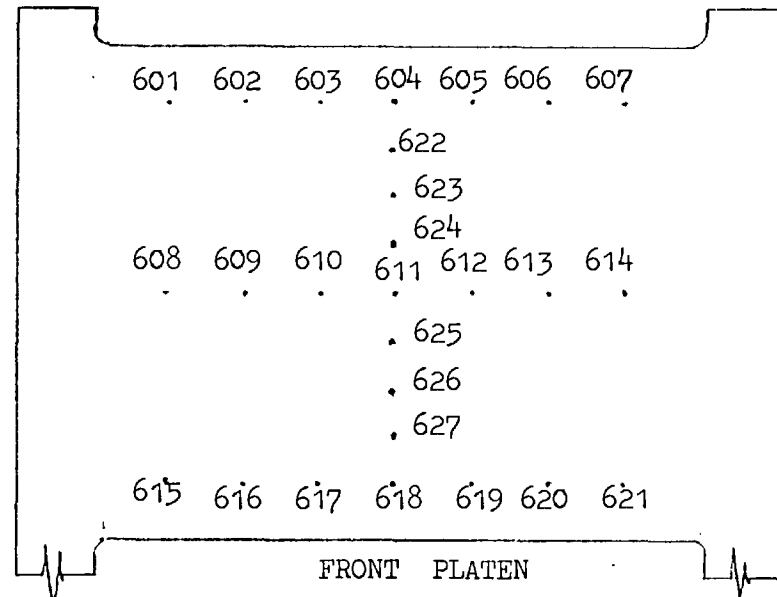
TOP AXIAL PLATEN

a) Axial Platens



REAR PLATEN

b) O₂- Platens



FRONT PLATEN

FIG. 5.8 General layout of control points

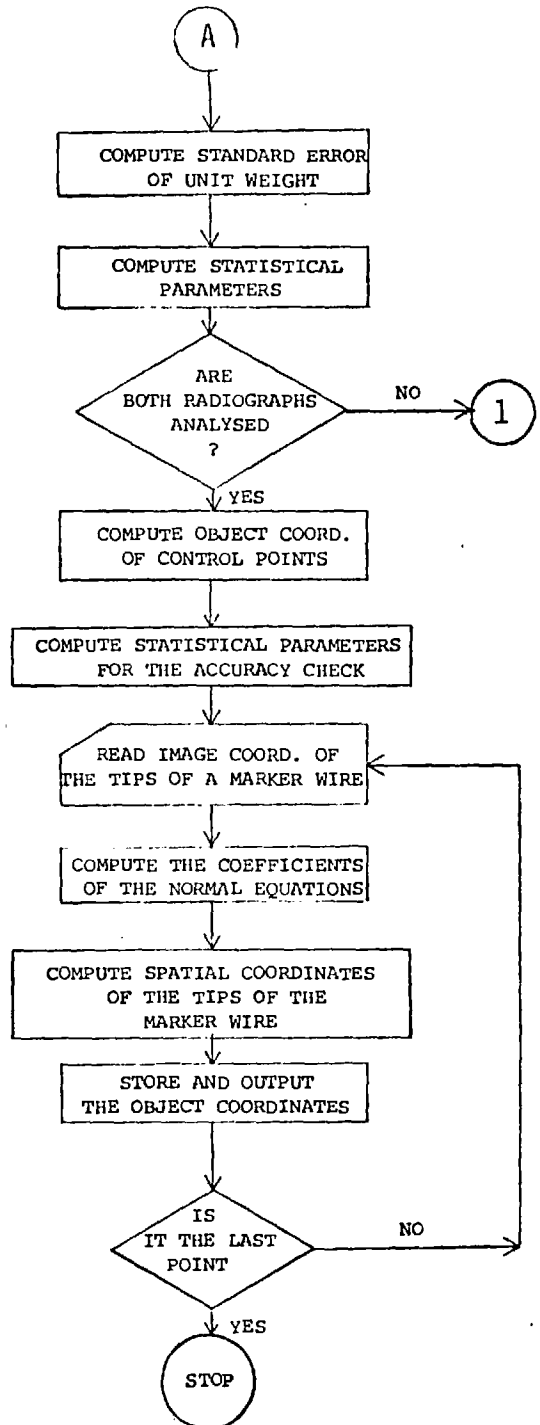
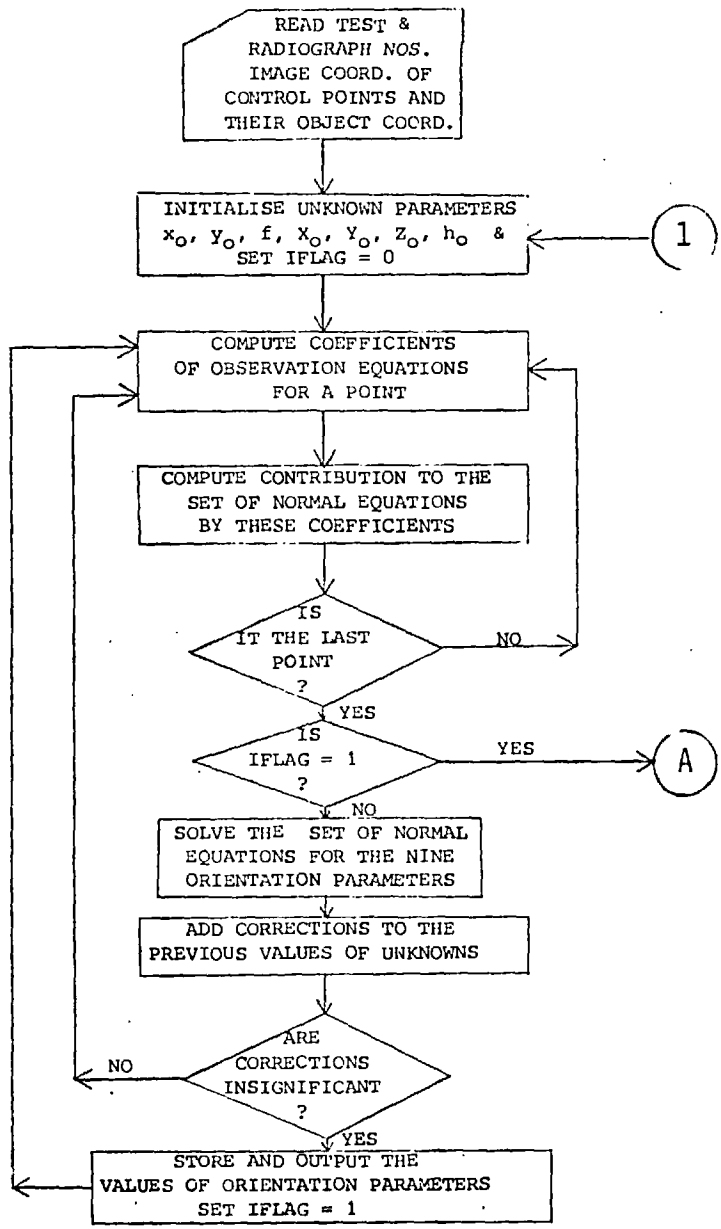
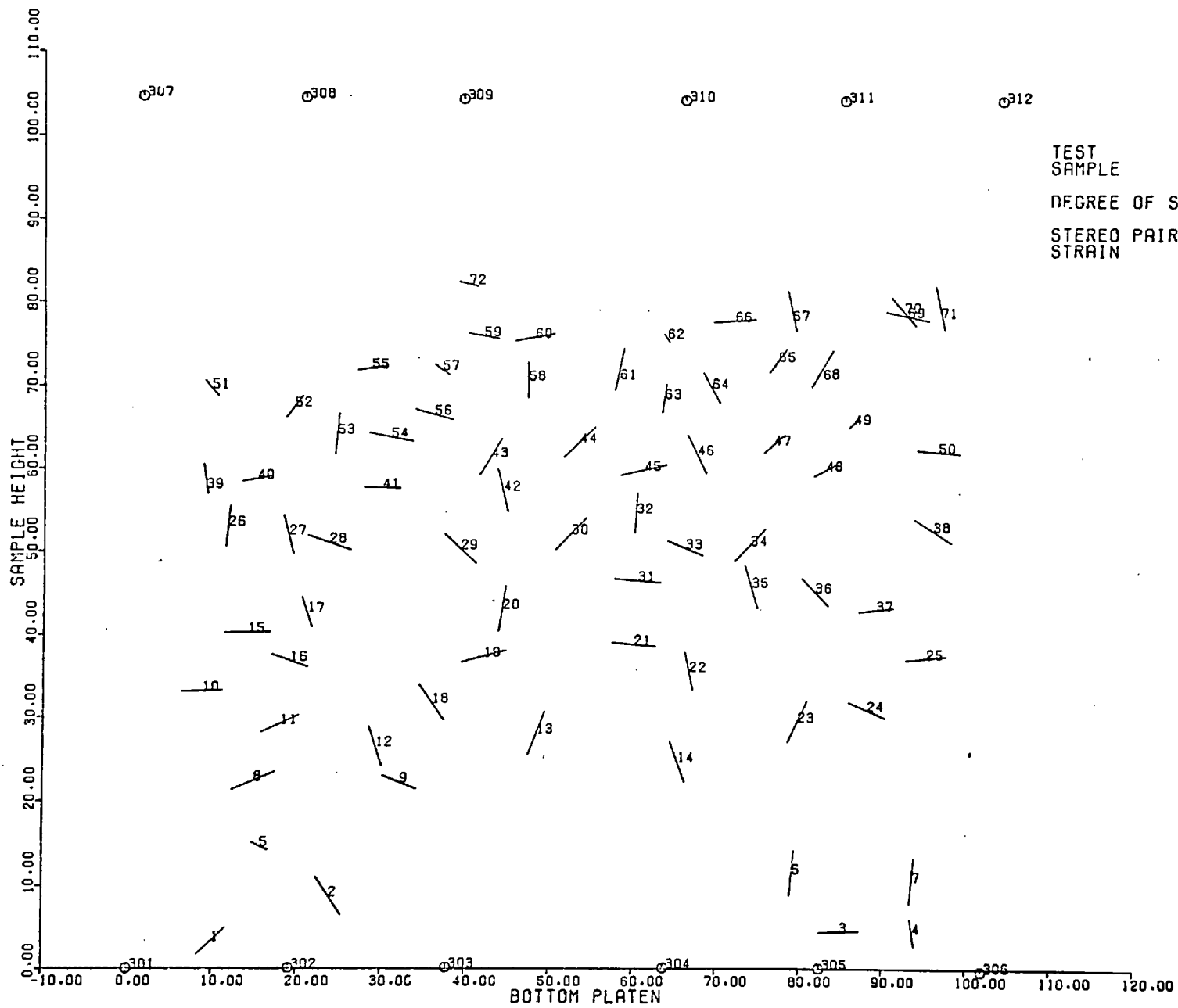


FIG. 5.9 Flow diagram

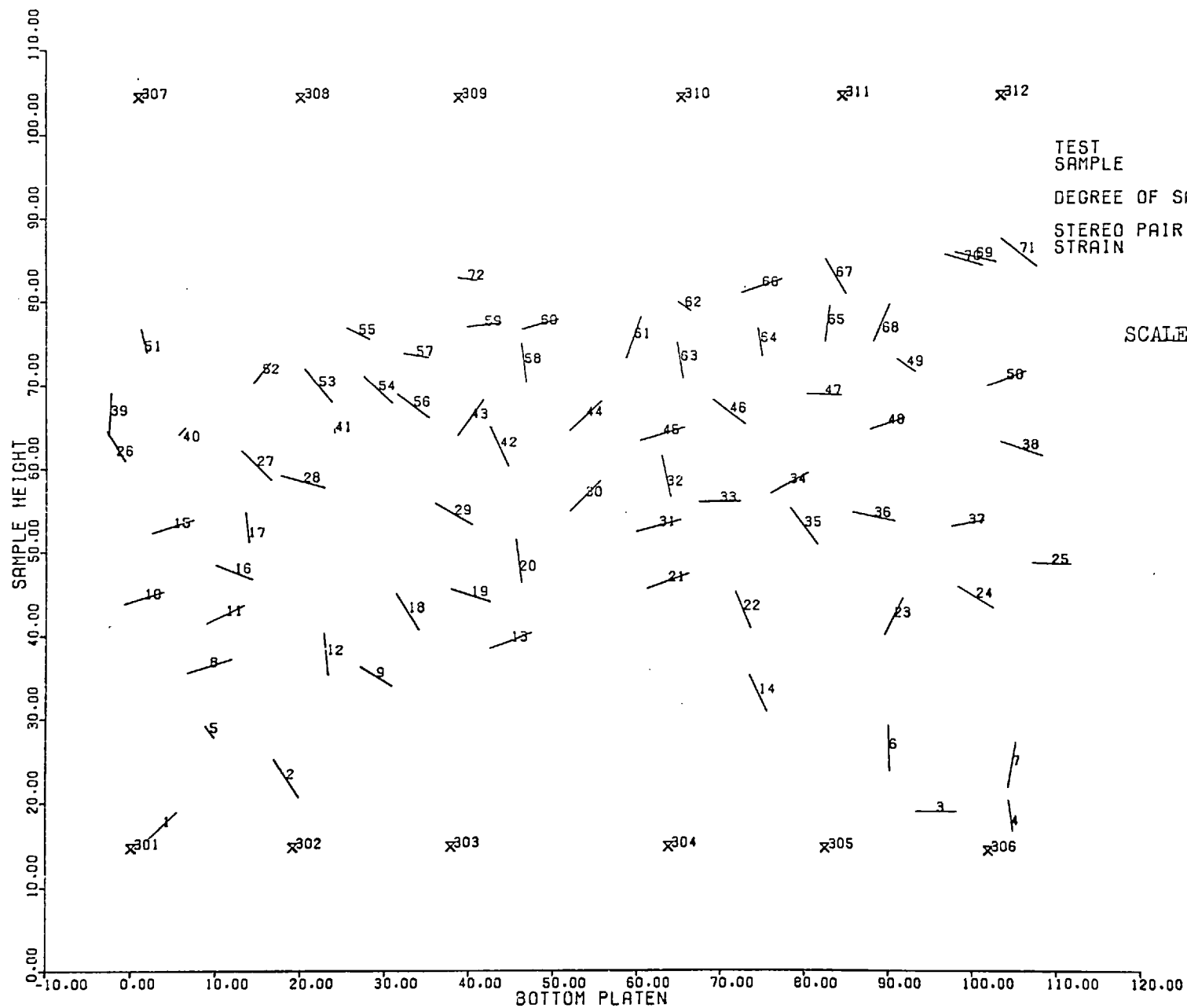


TEST SAMPLE
 DEGREE OF SAT. DRY
 STEREO PAIR NO. 1
 STRAIN 0.000

PLANE STRAIN (DRAINED)
 GRAVEL (ROTUND)
 DRY
 1
 0.000

SCALE 10 mm

FIG 5.10 MARKER PARTICLES - THEIR PROJECTION ON XY PLANE



TEST
SAMPLE
DEGREE OF SAT.
STEREO PAIR NO.
STRAIN

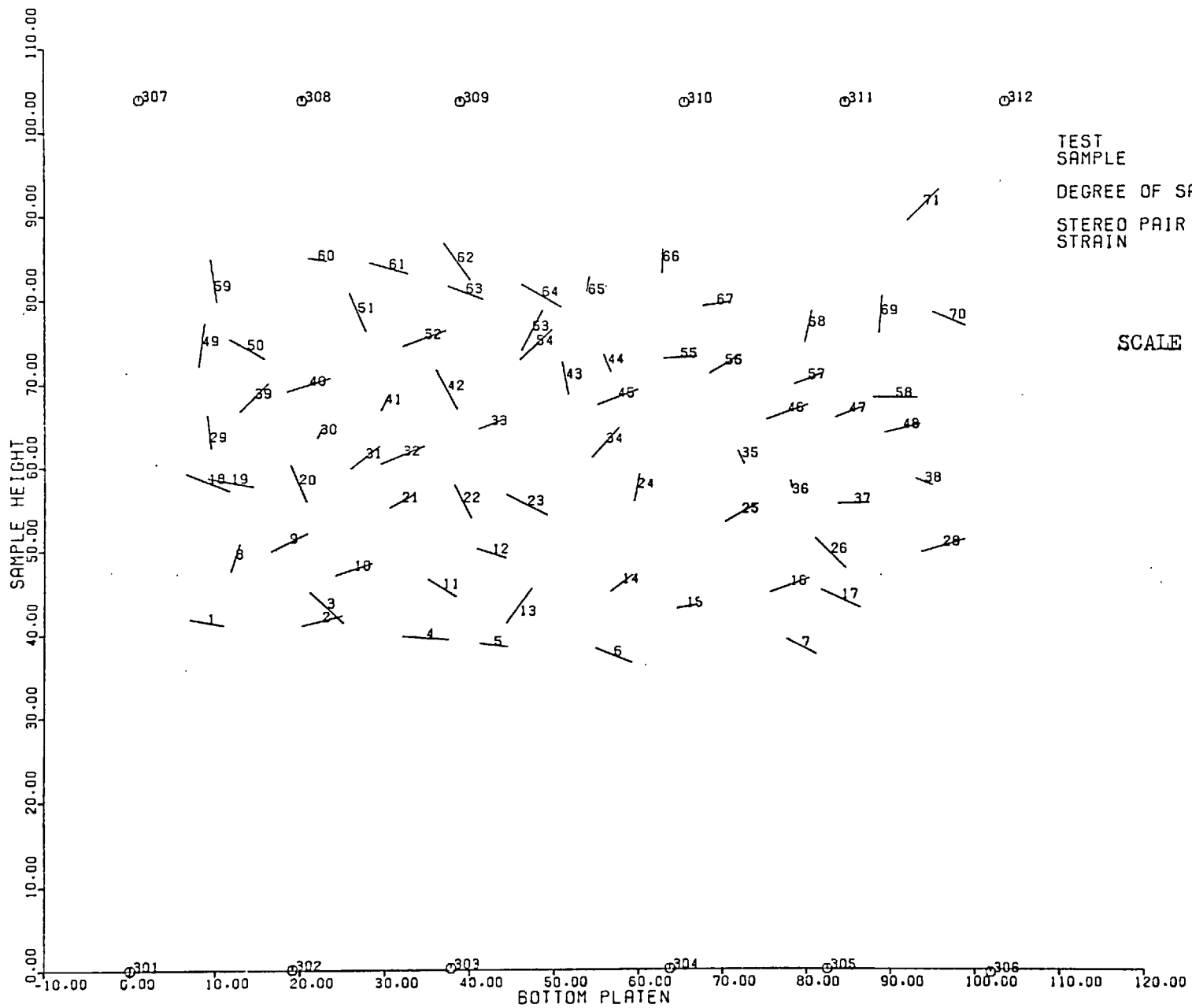
PLANE STRAIN (DRAINED)
GRAVEL (ROTUND)
DRY
7
14-814

SCALE

10mm

FIG 5.11

MARKER PARTICLES - THEIR PROJECTION ON XY PLANE



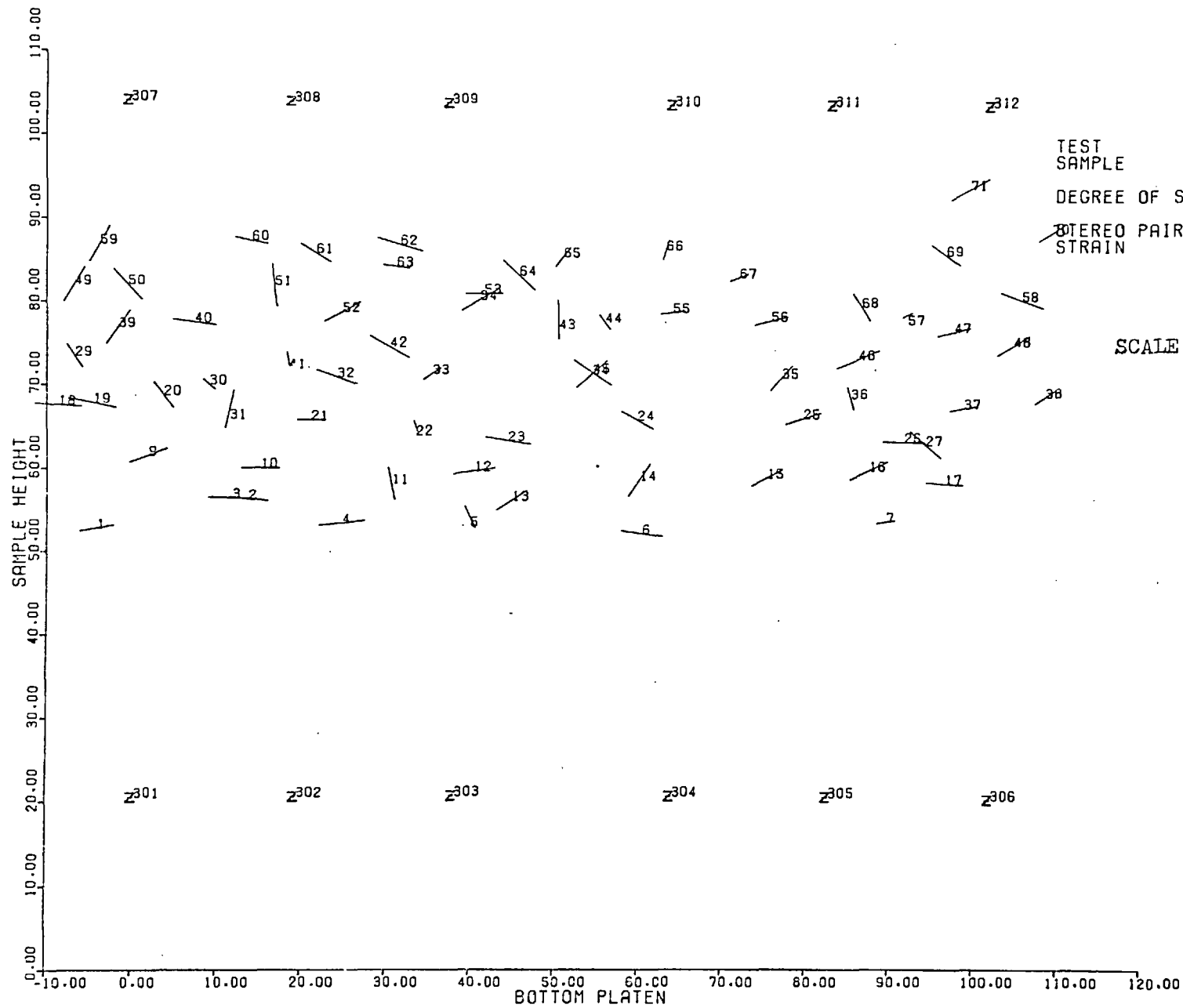
TEST SAMPLE
 DEGREE OF SAT.
 STEREO PAIR NO.
 STRAIN

PLANE STRAIN (DRAINED)
 GRAVEL (ROTUND)
 FULLY SAT.
 1
 0.000

SCALE 10mm

FIG 5.12

MARKER PARTICLES - THEIR PROJECTION ON XY PLANE



TEST
SAMPLE
DEGREE OF SAT.
STEREO PAIR NO.
STRAIN

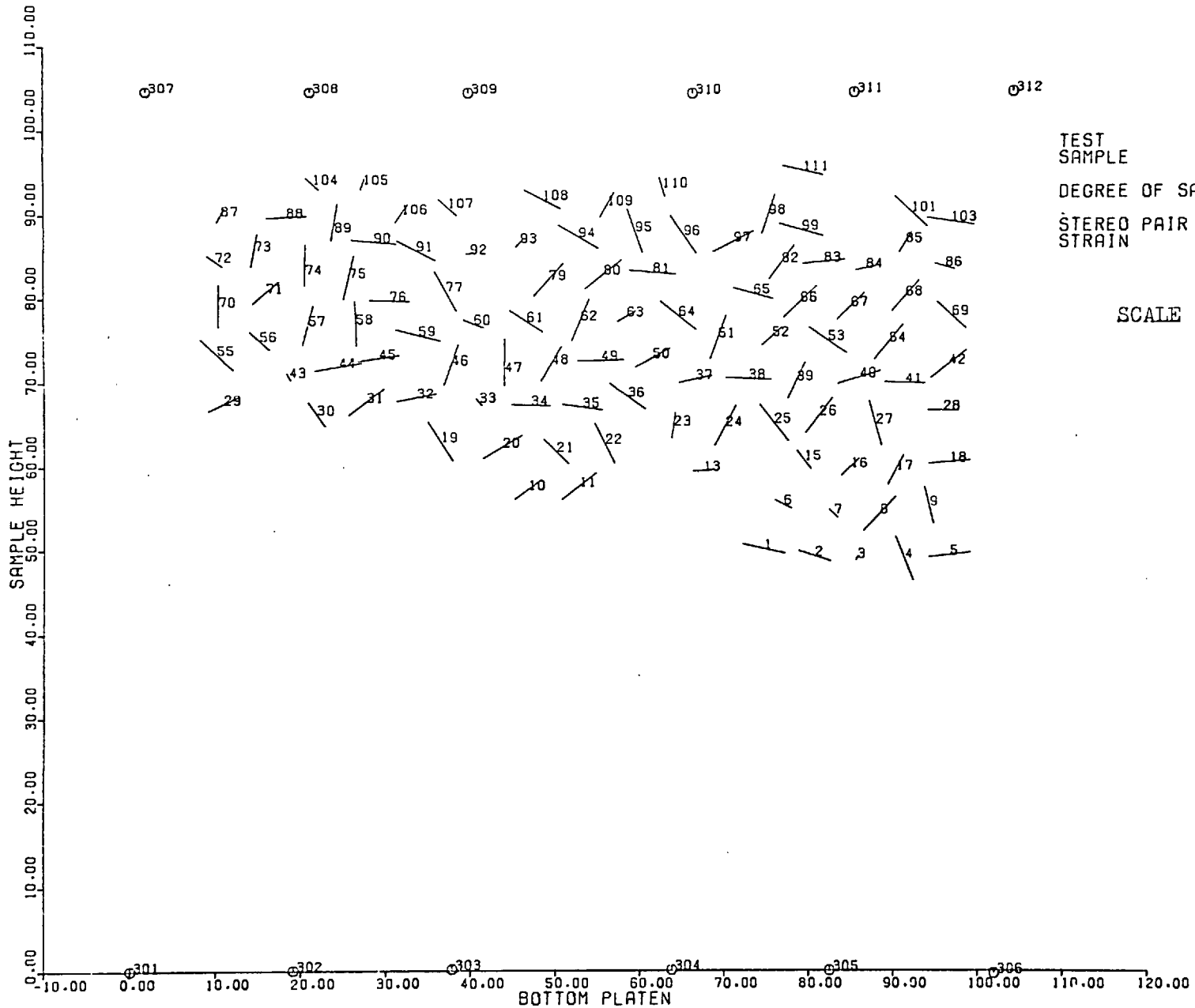
PLANE STRAIN (DRAINED)
GRAVEL (ROTUND)
FULLY SAT.
8
19.359

SCALE

10mm

FIG 5.13

MARKER PARTICLES - THEIR PROJECTION ON XY PLANE



TEST
SAMPLE

DEGREE OF SAT.

STEREO PAIR NO.
STRAIN

PLANE STRAIN (DRAINED)
GLASS BALLS

DRY

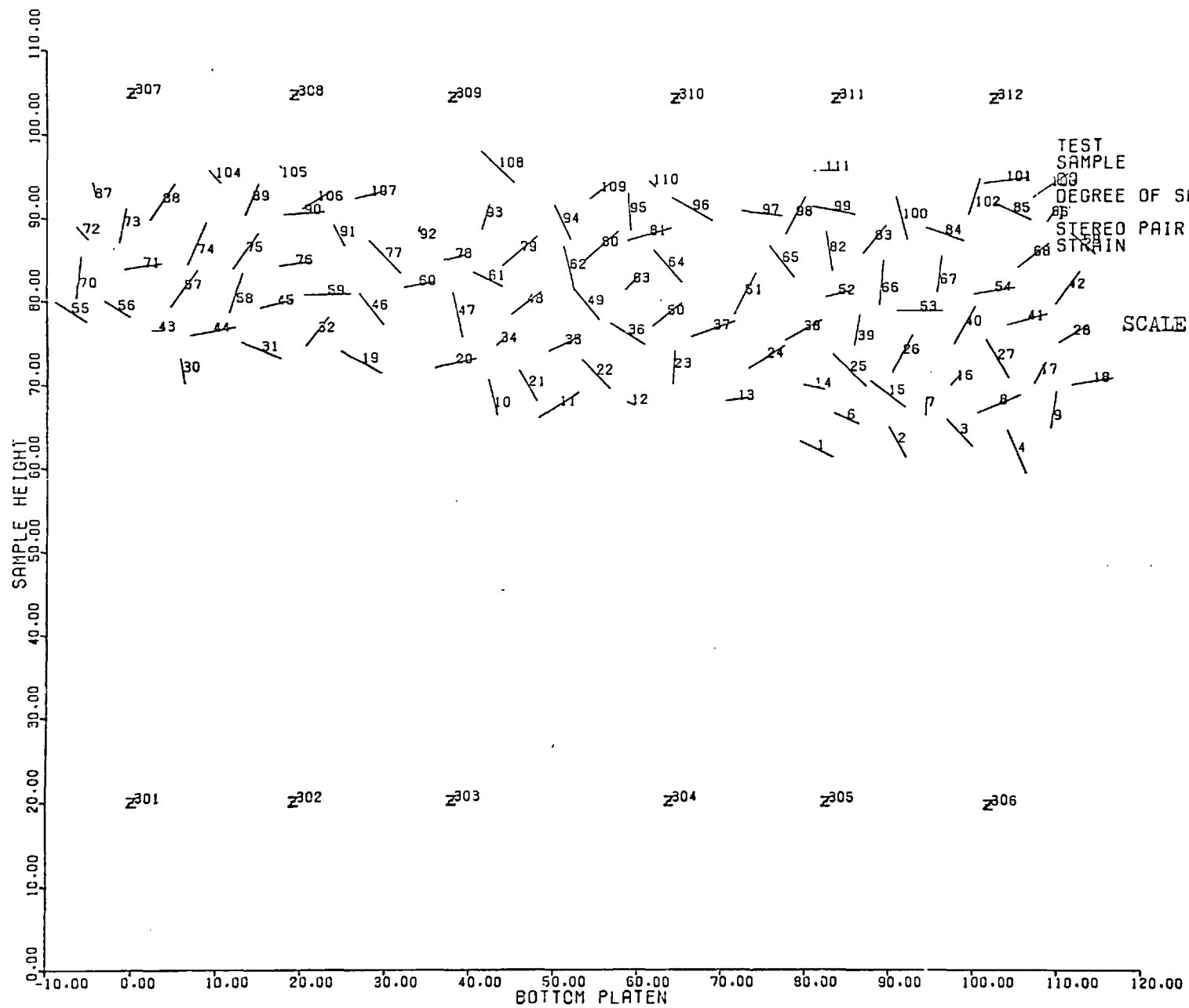
1
0.000

SCALE

10mm

FIG 5.14

MARKER PARTICLES - THEIR PROJECTION ON XY PLANE



TEST
SAMPLE
DEGREE OF SAT.
STEREO PAIR NO.
STRAIN

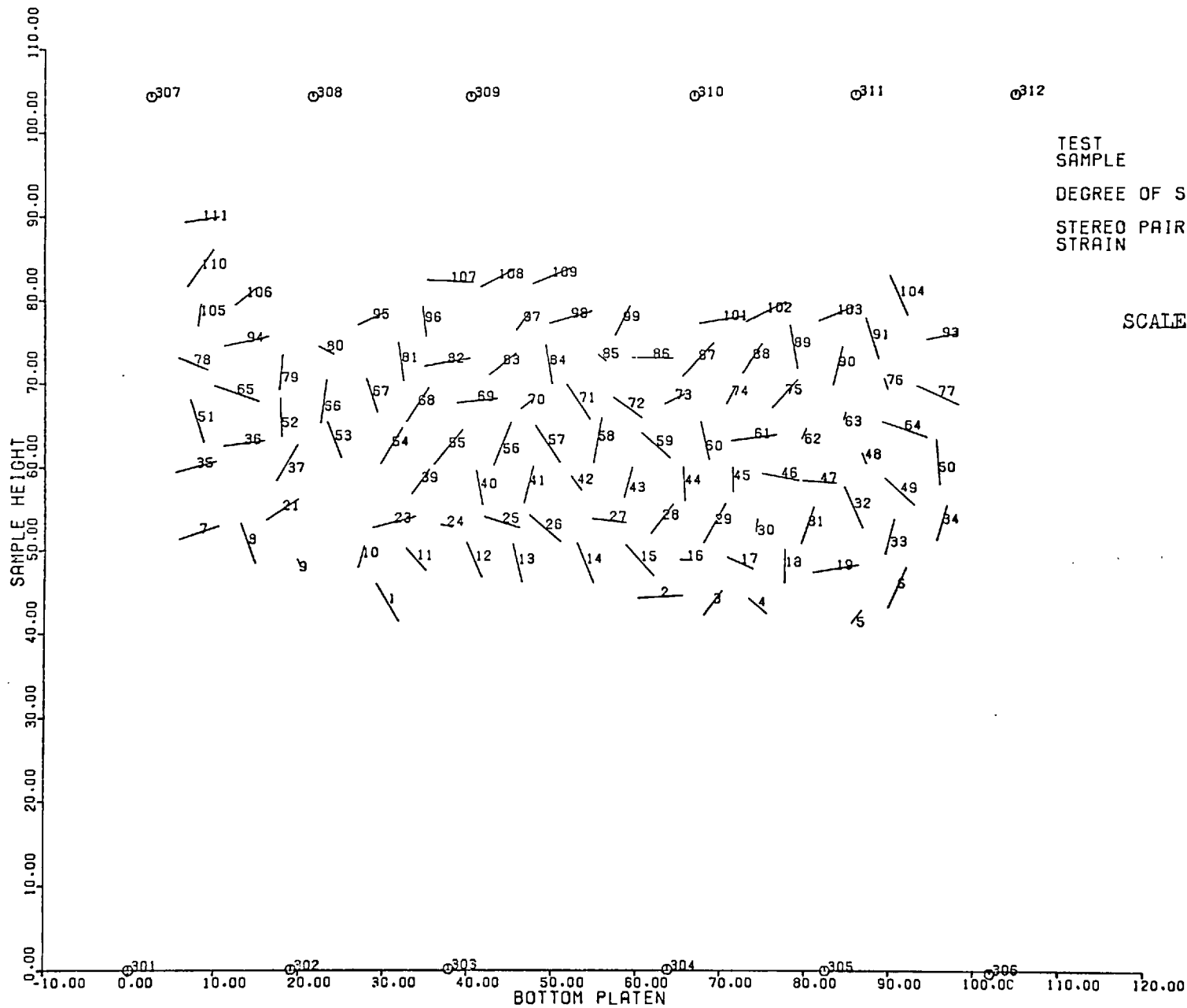
PLANE STRAIN (DRAINED)
GLASS BALLS
DRY
8
19.414

SCALE

10mm

FIG 5.15

MARKER PARTICLES - THEIR PROJECTION ON XY PLANE



TEST
SAMPLE
DEGREE OF SAT.
STEREO PAIR NO.
STRAIN

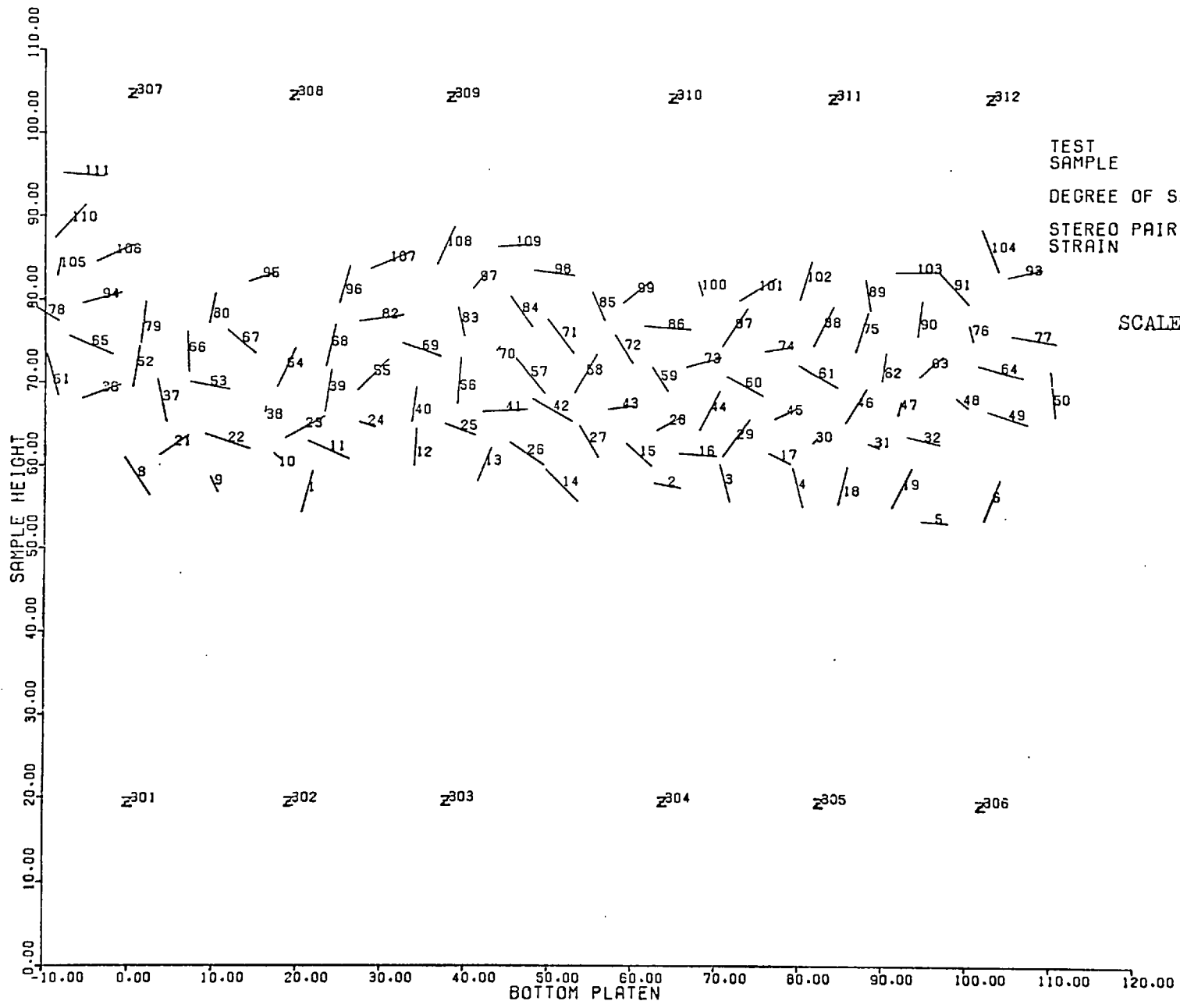
PLANE STRAIN (DRAINED)
GLASS BALLS
FULLY SAT.
1
0.000

SCALE

10mm

FIG 5.16

MARKER PARTICLES - THEIR PROJECTION ON XY PLANE

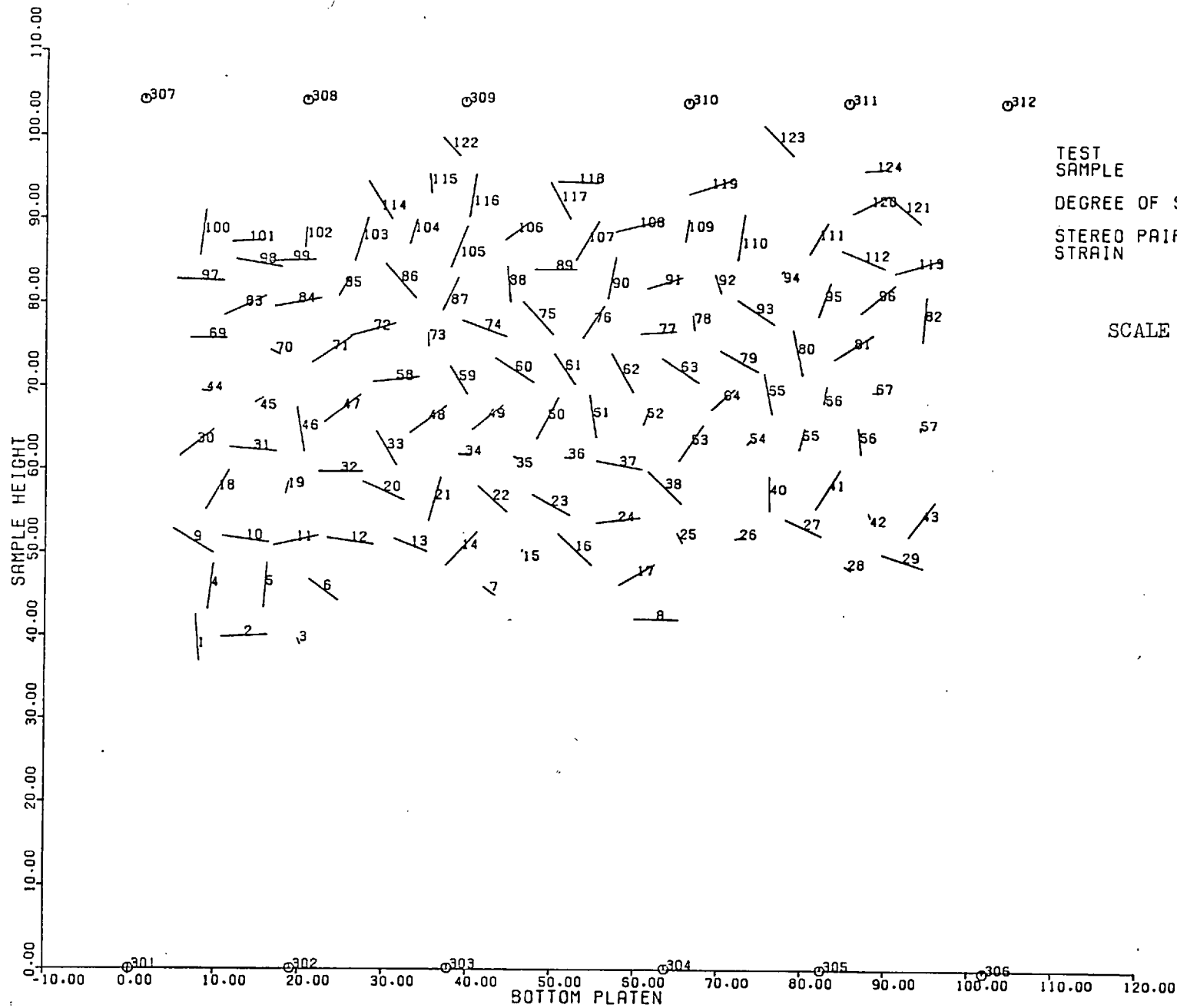


TEST
SAMPLE
DEGREE OF SAT.
STEREO PAIR NO.
STRAIN

PLANE STRAIN (DRAINED)
GLASS BALLS
FULLY SAT.
8
18.833

SCALE 10mm

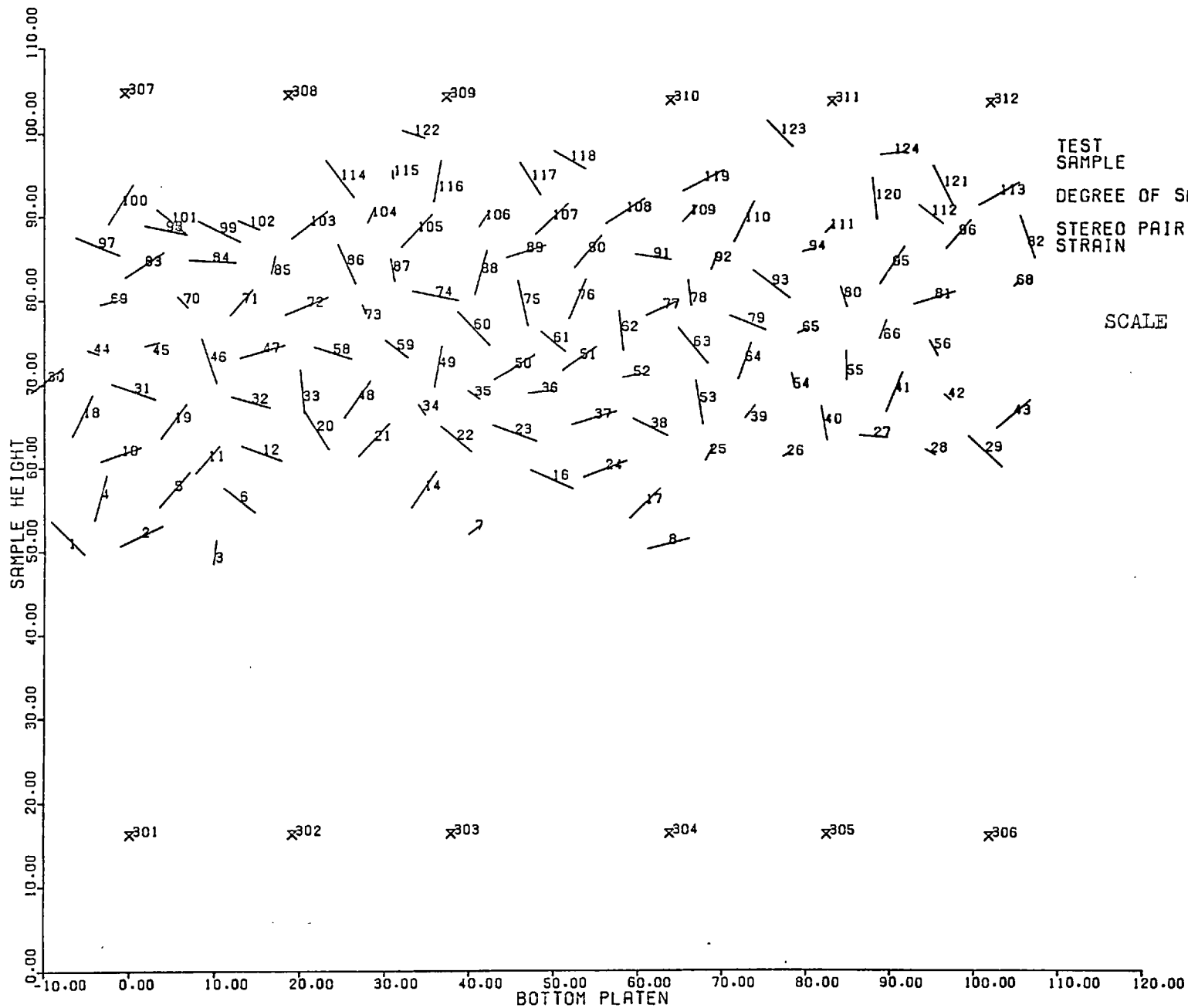
FIG 5.17 MARKER PARTICLES - THEIR PROJECTION ON XY PLANE



TEST SAMPLE PLANE STRAIN (DRAINED)
 CERAMIC BALLS
 DEGREE OF SAT. DRY
 STEREO PAIR NO. 1
 STRAIN 0.000

SCALE 10mm

FIG 5.18 MARKER PARTICLES - THEIR PROJECTION ON XY PLANE



TEST
SAMPLE
DEGREE OF SAT.
STEREO PAIR NO.
STRAIN

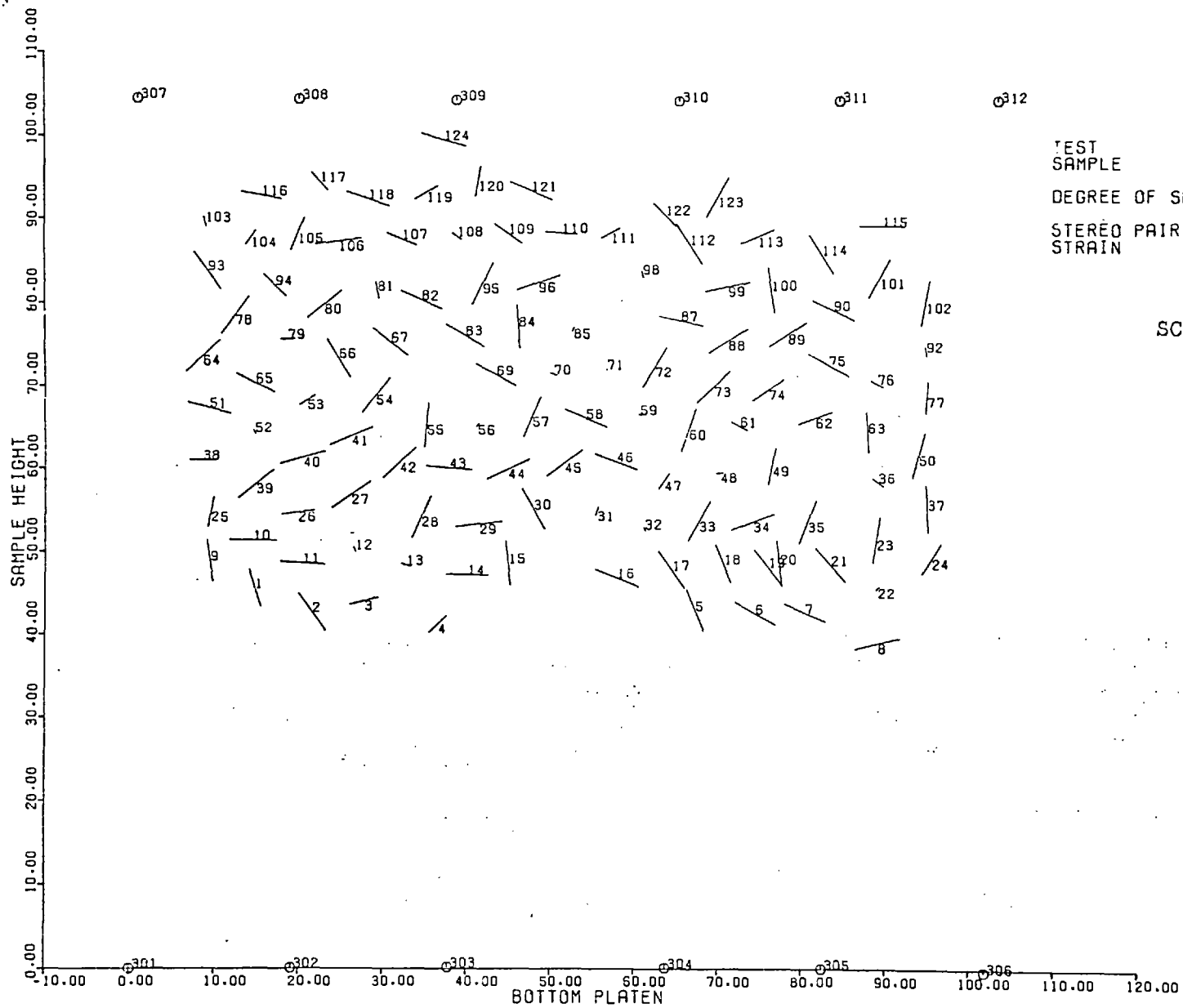
PLANE STRAIN (DRAINED)
CERAMIC BALLS
DRY
7
15.704

SCALE

10mm

FIG 5.19

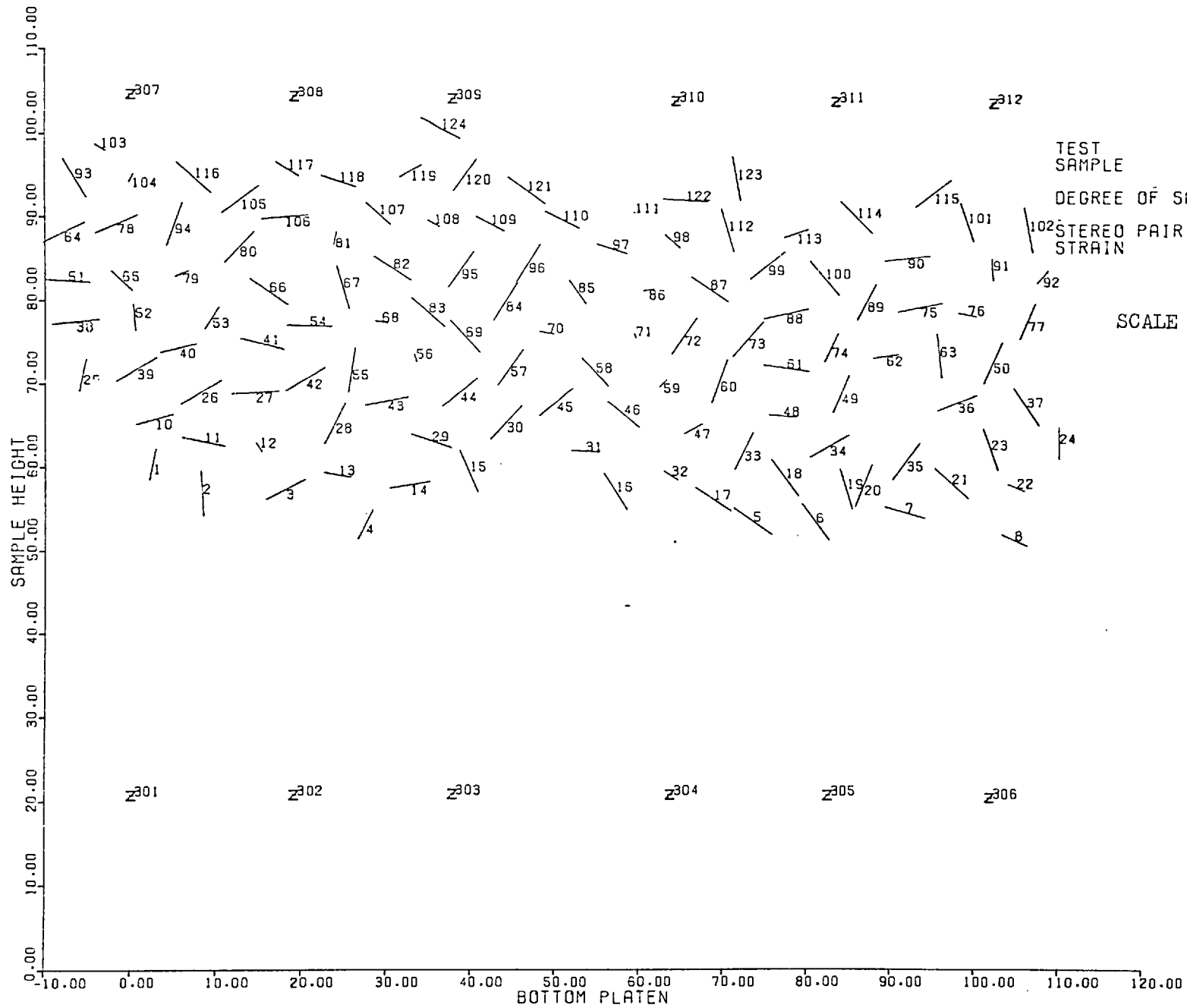
MARKER PARTICLES - THEIR PROJECTION ON XY PLANE



TEST SAMPLE
 DEGREE OF SAT. FULLY SAT.
 STEREO PAIR NO. 1
 STRAIN 0.000

SCALE 10mm

FIG 5.20 MARKER PARTICLES - THEIR PROJECTION ON XY PLANE



TEST
SAMPLE
DEGREE OF SAT.
STEREO PAIR NO.
STRAIN

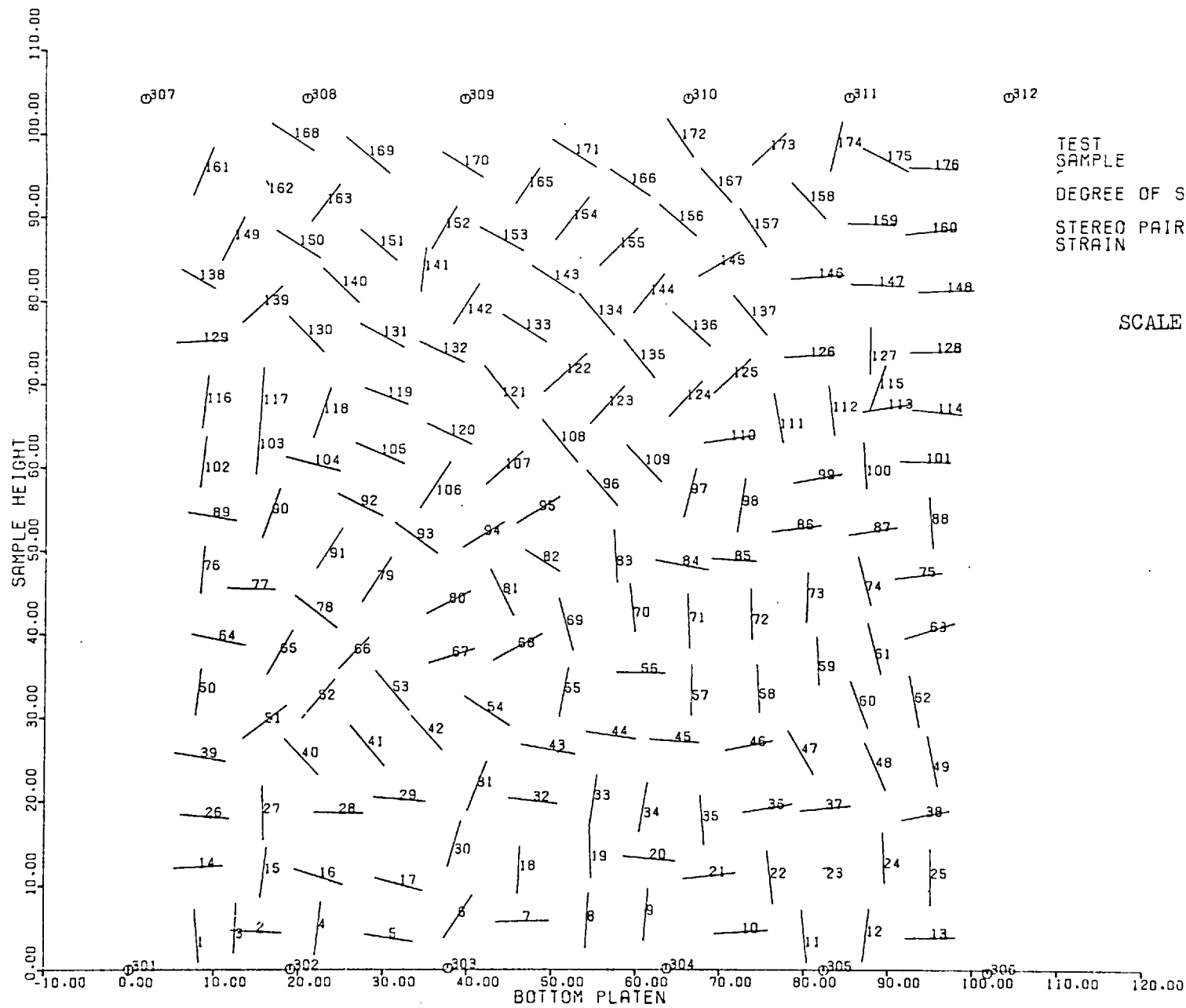
PLANE STRAIN (DRAINED)
CERAMIC BALLS
FULLY SAT.
8
20.193

SCALE

10mm

FIG 5.21

MARKER PARTICLES - THEIR PROJECTION ON XY PLANE



TEST
SAMPLE

DEGREE OF SAT.

STEREO PAIR NO.
STRAIN

PLANE STRAIN (DRAINED)
PTFE CHUNKS

DRY

1
0.000

SCALE

10mm

FIG 5.22 . MARKER PARTICLES - THEIR PROJECTION ON XY PLANE

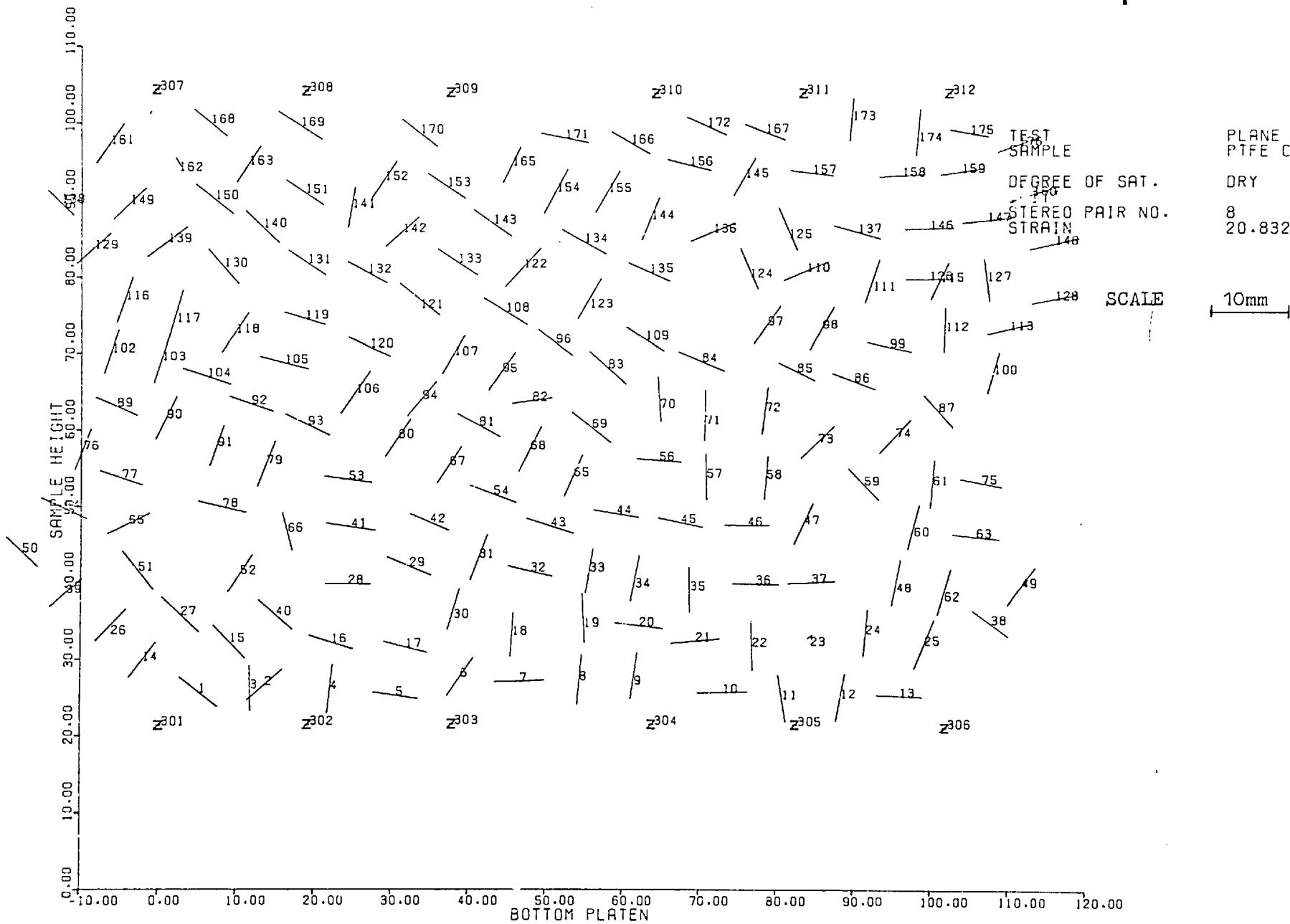
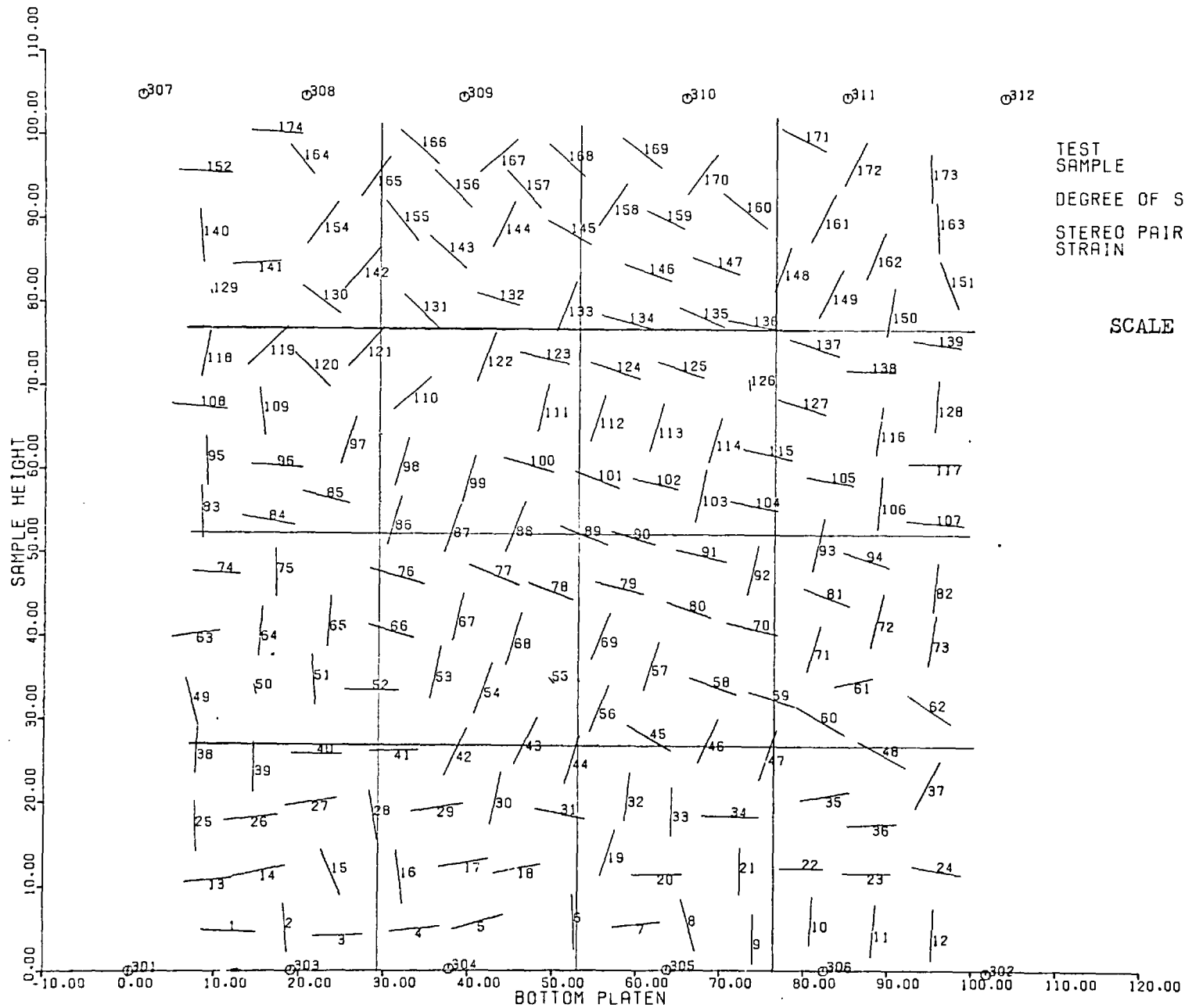


FIG 5.23 MARKER PARTICLES - THEIR PROJECTION ON XY PLANE



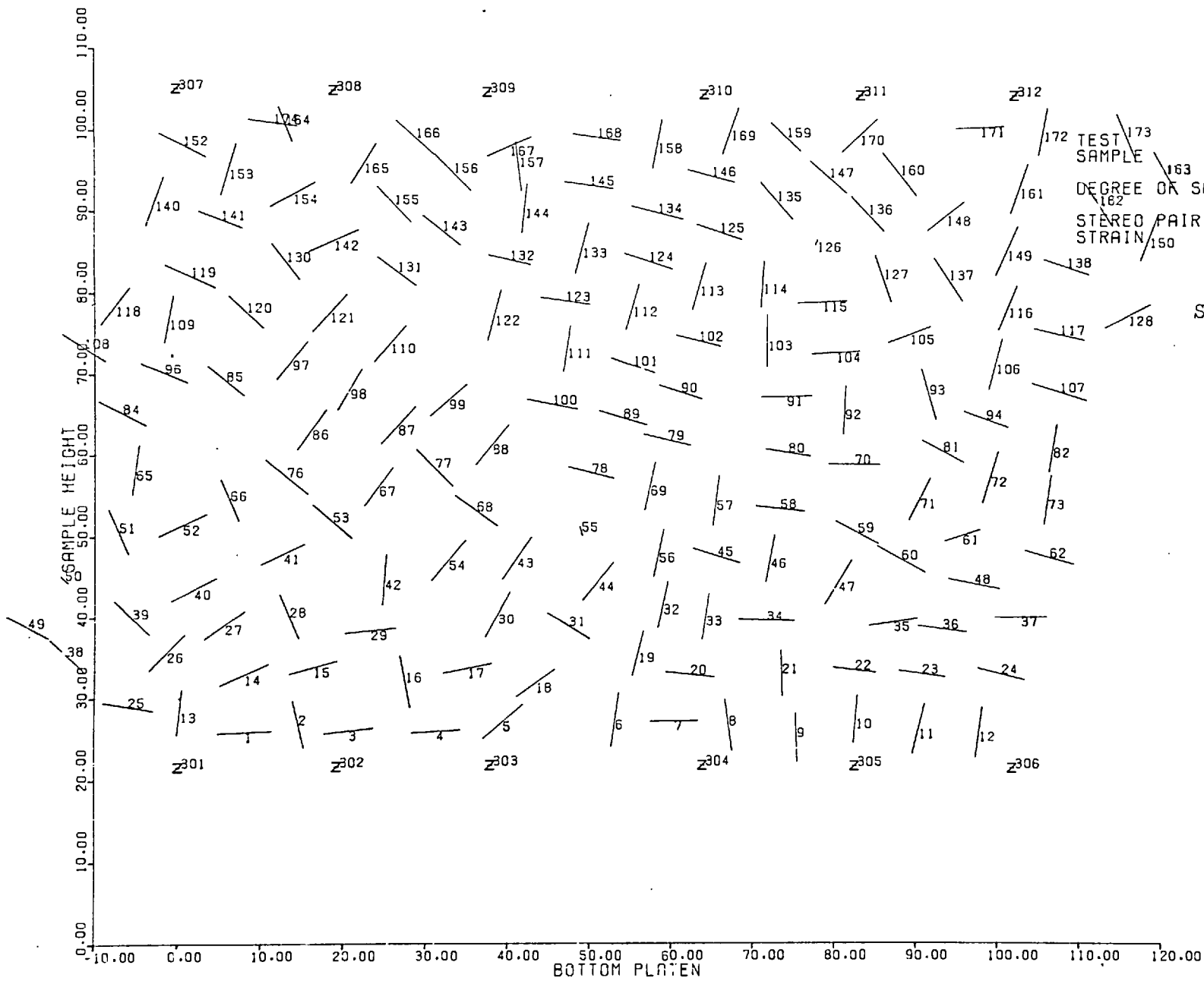
TEST SAMPLE
 DEGREE OF SAT.
 STEREO PAIR NO.
 STRAIN

PLANE STRAIN (DRAINED)
 PTFE CHUNKS
 FULLY SAT.
 1
 0.000

SCALE 10mm

FIG 5.24

MARKER PARTICLES - THEIR PROJECTION ON XY PLANE

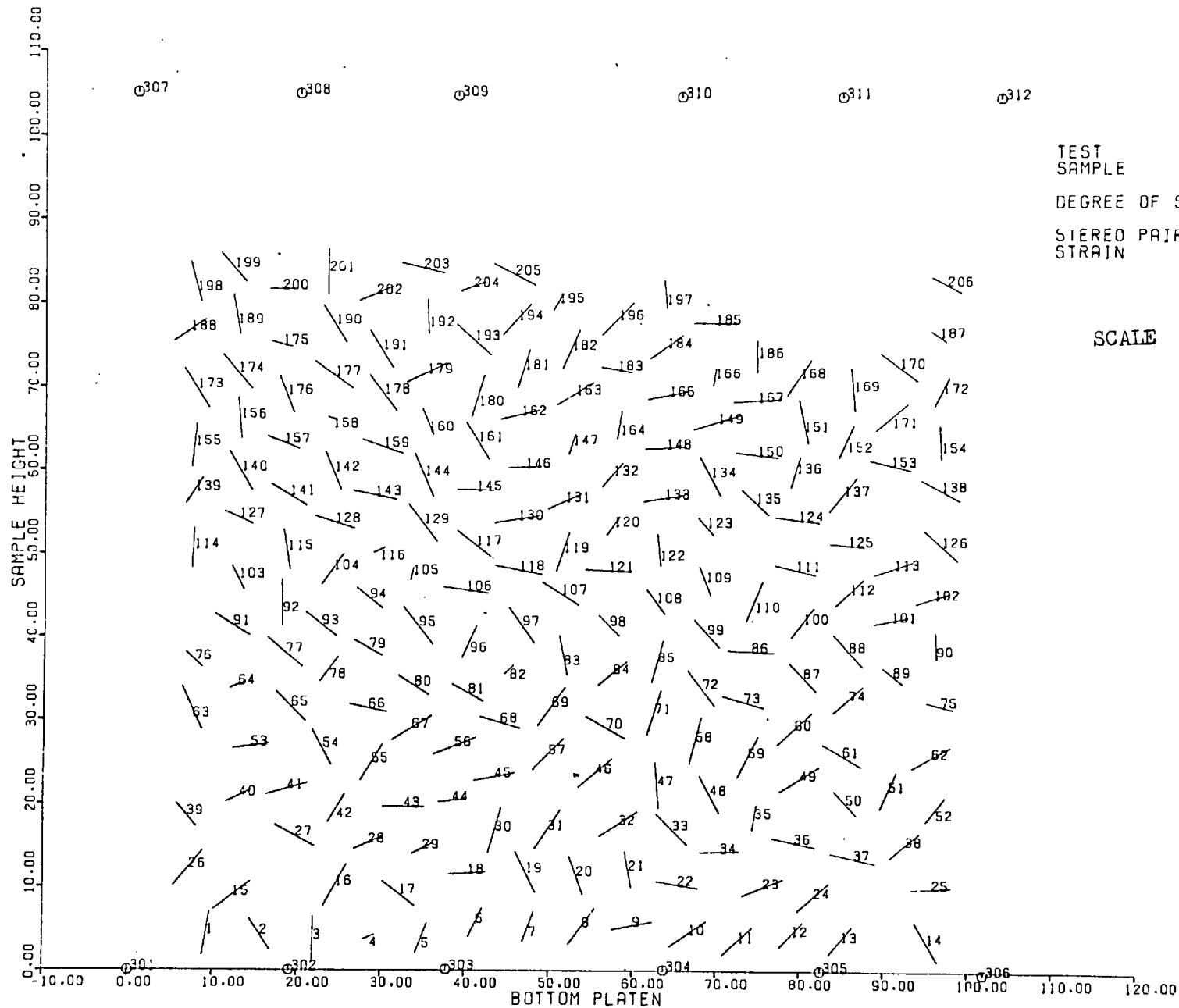


TEST SAMPLE
 DEGREE OR SAT. 162
 STEREO PAIR NO. 150

PLANE STRAIN (DRAINED)
 PTFE CHUNKS
 FULLY SAT.
 8
 20.964

SCALE 10mm

FIG 5.25 . MARKER PARTICLES - THEIR PROJECTION ON XY PLANE



TEST SAMPLE PLANE STRAIN (DRAINED)
 POLYPROPYLENE BALLS
 DEGREE OF SAT. DRY
 STIERED PAIR NO. 1
 STRAIN 0.000

SCALE 10mm

FIG 5.26 MARKER PARTICLES - THEIR PROJECTION ON XY PLANE

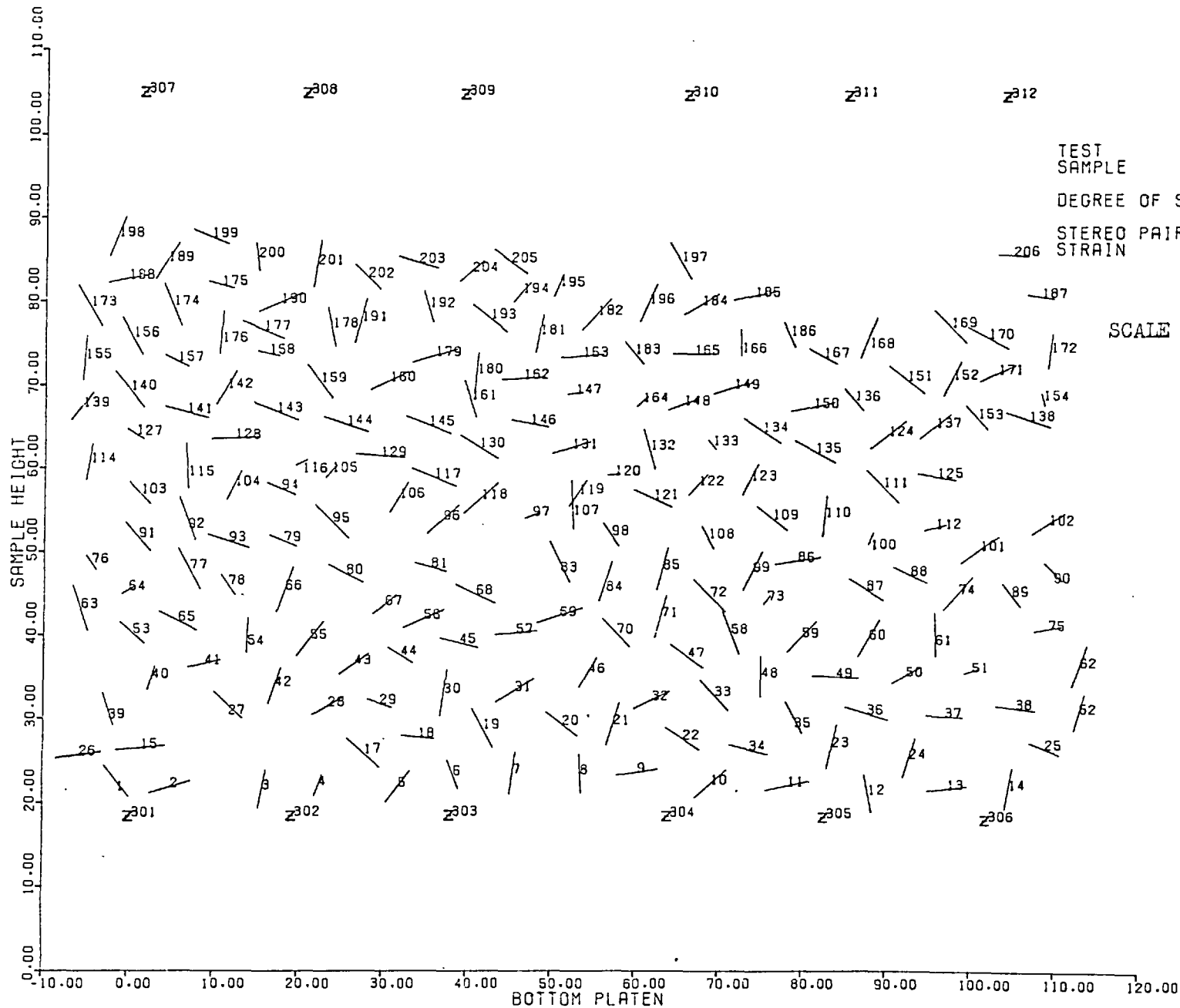
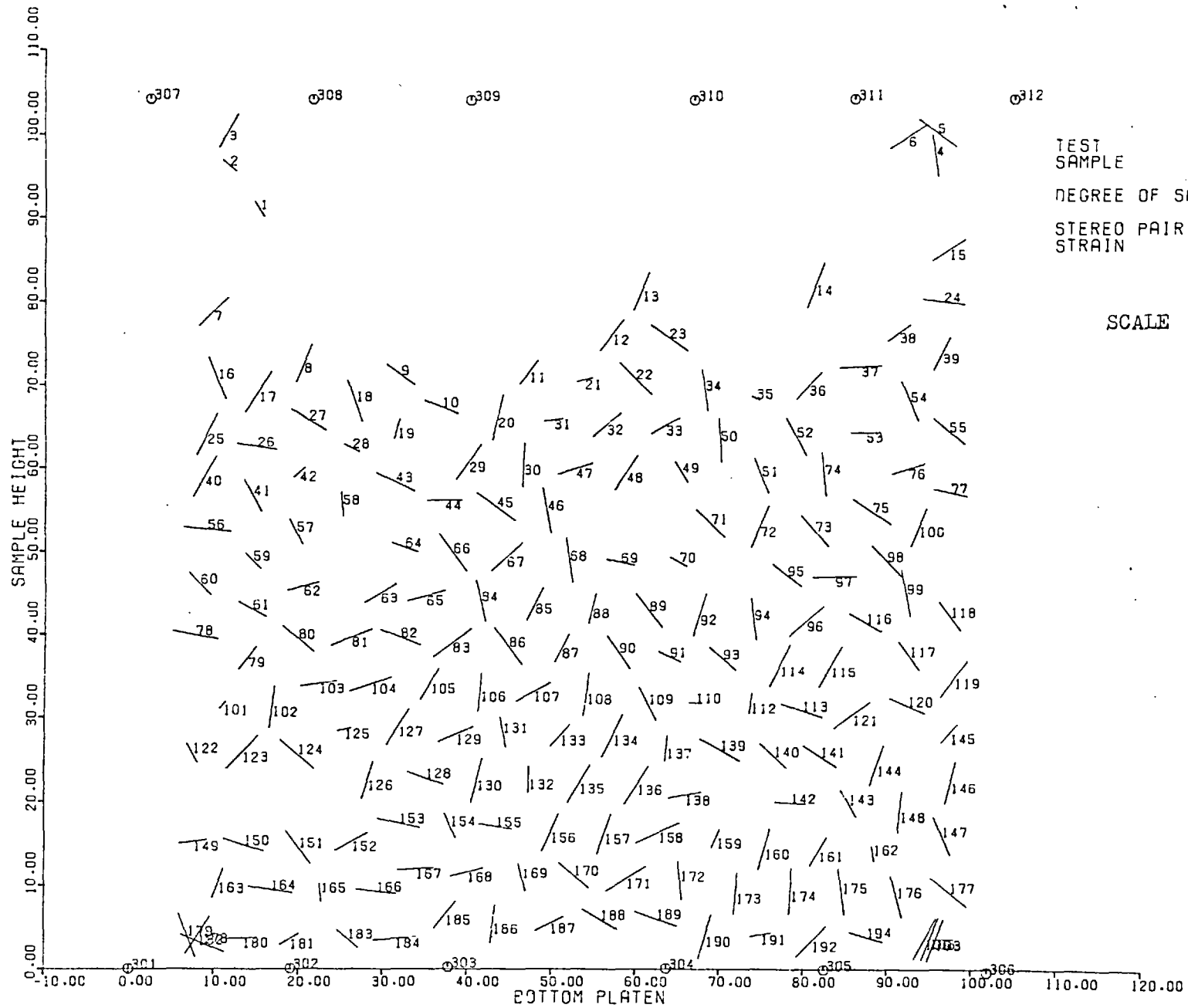


FIG 5.27 MARKER PARTICLES - THEIR PROJECTION ON XY PLANE



TEST
SAMPLE

PLANE STRAIN (DRAINED)
POLYPROPYLENE BALLS

DEGREE OF SAT.

FULLY SAT.

STEREO PAIR NO.
STRAIN

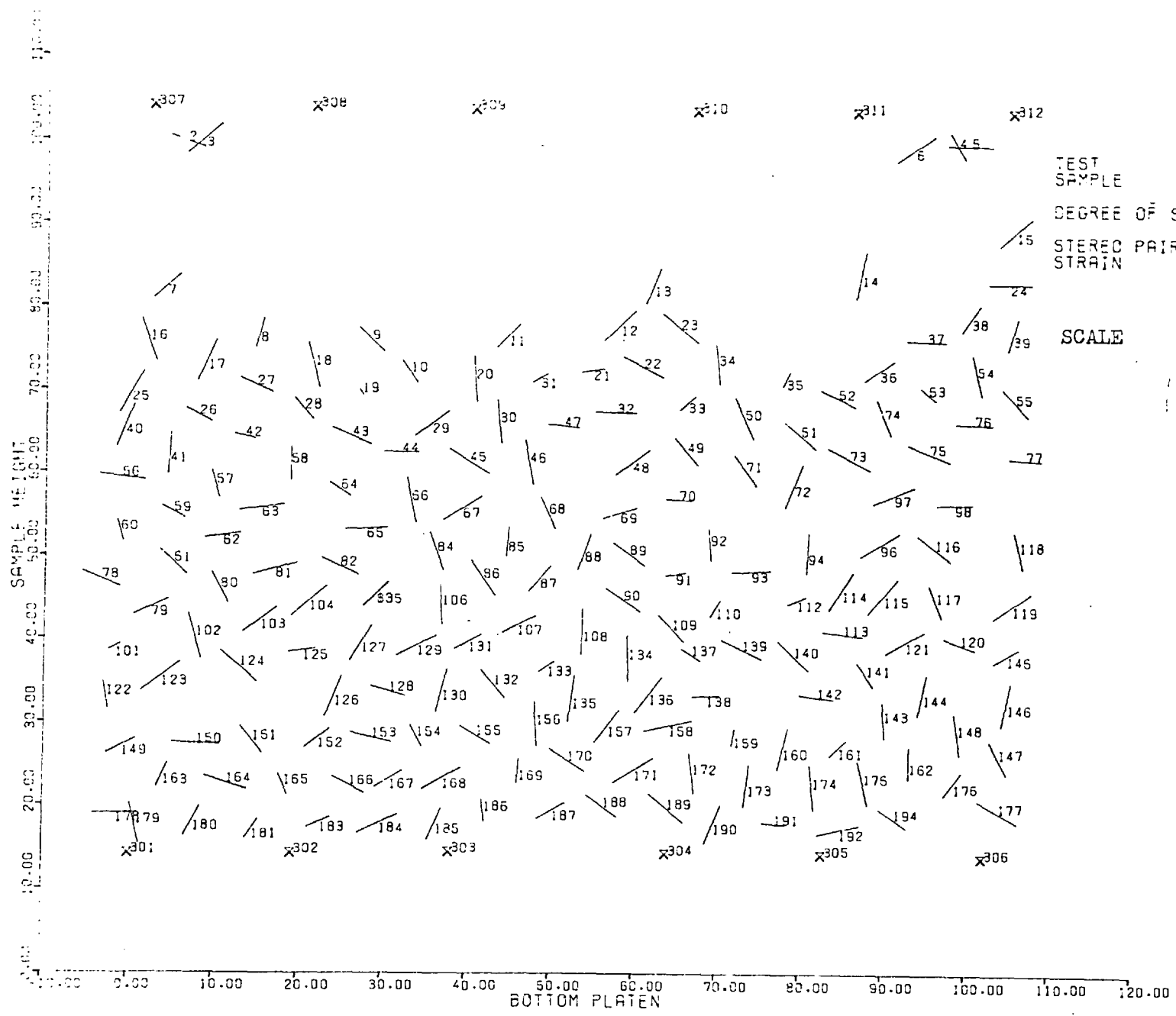
1
0.000

SCALE

10mm

FIG 5.28

MARKER PARTICLES - THEIR PROJECTION ON XY PLANE



TEST SAMPLE
 DEGREE OF SAT. FULLY SAT.
 STEREO PAIR NO. 7
 STRAIN 13.800

SCALE 10mm

FIG 5.29 MARKER PARTICLES - THEIR PROJECTION ON XY PLANE

CHAPTER 6

PLANE STRAIN TEST RESULTS6.1 INTRODUCTION

For the macroscopic investigation of a granular mass based on continuum mechanics, the normal testing methods, definitions and nomenclature in vogue in Soil Mechanics are used. However, in the experimental work presented here special equipment has been designed and used so as to evaluate the response of granular materials at both microscopic and macroscopic levels. In this chapter, the test results observed at the macroscopic level and their analysis based on continuum mechanics are presented. The interpretation of these results from the microscopic view point is reserved for Chapter 8. The important details of the test equipment materials and testing procedure adopted here are described in Chapter 2.

6.2 LOAD-DEFORMATION RELATIONSHIP

As mentioned earlier, every plane strain compression test was carried out in arbitrary stages of deformation. Once the test specimen had reached a predetermined overall deformation, the test was stopped so as to take stereo-radiographs which were needed for microscopic investigation of the deforming specimen. Due to the relatively high stiffness of the loading system in comparison to that of the test specimen, stress relaxation occurred during the stoppage of overall deformation. It was observed that the major

part of stress relaxation occurred almost instantaneously on the stoppage of deformation. The radiographs which were taken in the interval mentioned above did not show any measurable movement of marker particles. In other words, if there were any particle movements, they were submerged in data acquisition and data reduction accuracies. Typical deviatoric force - axial deformation plots actually obtained on the continuously recording electronic system are shown in Figures 6.1 - 6.3. From these figures, the following observations can be made:

- a) the magnitude of deviatoric force (or stress) relaxation increases with σ_1 / σ_3
- b) the load-deformation curve is not adversely modified due to the interruption of the test for stereo radiography. On resumption of deformation after stoppage, the recovery back to the original stress level prior to stoppage is very rapid in the pre-peak stages of deformation and is fairly quick in the later stages of deformation particularly at large post-peak stages of shear.
- c) after the load prior to the stoppage is reached, further deformation of the test specimen results in a deviatoric force-displacement curve which could easily be taken as the continuation of previous curve. Thus, it would appear as if the deformation of the sample was not interrupted but was rather continuous.

For the calculation of deviatoric stress, the deviatoric force just before the stoppage was taken. The stress was obtained by dividing this force by the cross-sectional area of the test specimen at the end of deformation. The methods of obtaining the correct

cross-sectional area are discussed briefly in the following section.

6.3 CORRECTED AREA AND VOLUME CHANGE

6.3.1 Corrected Area

The correct calculation of deviatoric stress and thus of shear strength parameters depend on how correctly the relevant cross-sectional area is obtained. The deviatoric stress and then the angle of internal friction may be evaluated in three ways:

- i) on the basis of the average cross-sectional area over the full height,
- ii) on the basis of the cross-sectional area at mid-height of test sample, and
- iii) on the basis of the average cross-sectional area of the middle half or middle third of the sample.

In the case of uniform deformation of the sample, all the three methods will give the same results. However, despite using "frictionless end platens" the sample in general does not deform uniformly over its full range of deformation. One has to make certain plausible assumptions with regard to the calculation of area. In this work, the use of the third method has been favoured. Instead of measuring the cross-sectional area or the relevant dimensions externally, the cross-sectional area was calculated by internal measurement of the position of marker particles placed next to the flexible boundaries. It may be recalled that the marker particles were, very

nearly, placed in a plane normal to the σ_2 - direction and midway between the two plane strain boundaries. Also the spatial co-ordinates of their centres are already known, see Section 5.13.5. The average x-co-ordinates of the particles at either boundary lying in the mid-half of the height of the sample were calculated. The difference between these two co-ordinates gives the current length of the sample in σ_2 - direction. Since the length in the direction is known which is the distance between the opposite platens less $2 \times$ (thickness of membrane + thickness of rubber sheets, if used for obtaining "frictionless" σ_2 - platens), we can easily calculate the cross-sectional area on which the deviator force was acting. Here it is implicitly assumed that the thickness of rubber membranes, etc. and the distance between the σ_2 - platens do not change throughout the test. Although this assumption is not totally valid, the error caused is not expected to be significant particularly for the very low stress levels used in this study. The method described above gives better results in the earlier stages of deformation where the bulging of the specimen is minimal particularly in the horizontal plane. When the sample bulged in both planes, like a barrel, this method does not give very good results. The use of the method described in the following section is recommended. It was in fact used in this study whenever the samples bulged in the form of a barrel.

6.3.2 Volume Change

The volume change in a specimen can be measured by adopting any of the two methods namely (a) direct method and (b) indirect method.

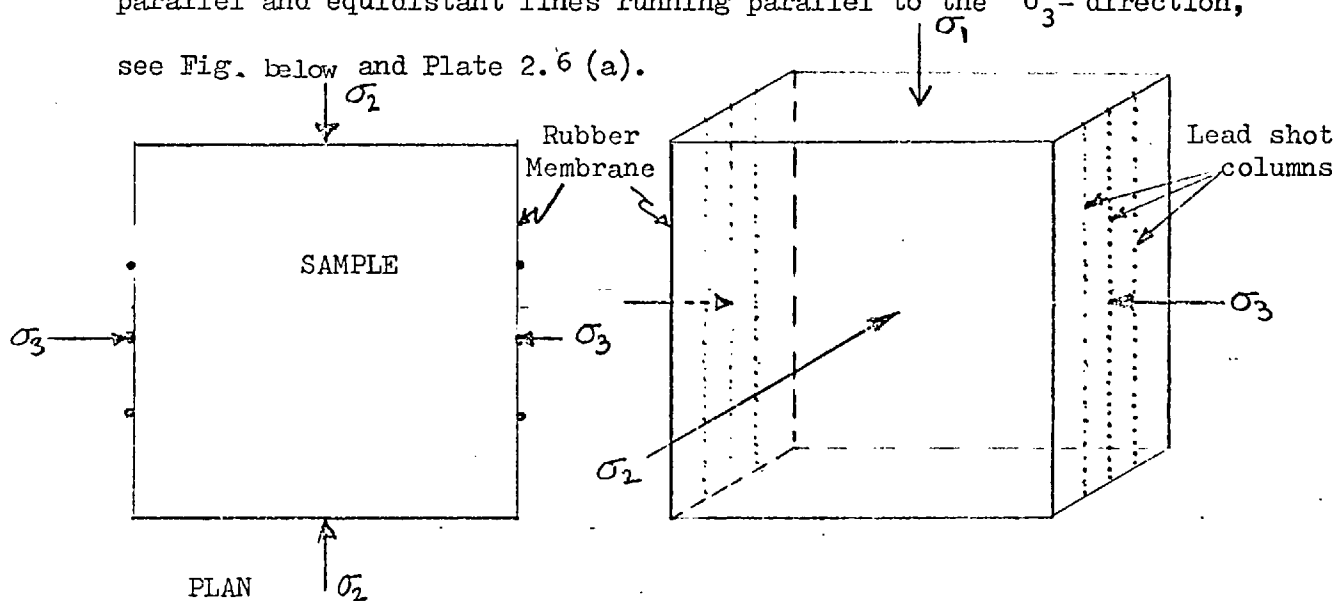
In the direct method, the volume change is measured by interposing an apparatus in the test set-up e.g. Bishop's Volume Change Gauge (Bishop and Henkel, 1962). This method suffers from one major source of error, namely membrane penetration. The membrane penetration becomes more pronounced when the constituent particles of specimen are large. Although numerous efforts notably by Roscoe et. al. (1963) and by many other researchers have been made to separate out the volume change caused by membrane penetration, a satisfactory method is yet to be found by which one can estimate fairly accurately the volume change contribution made due to this source.

On the other hand, in the indirect method of volume change calculation, the knowledge of linear strains in three mutually perpendicular directions is necessary. Recognizing the significant source of error caused by membrane penetration, El-Ruwayih (1975), Marachi et.al. (1969) and Holubec (1966) have attempted to measure lateral deformation of samples at pre-determined points. From these observations, they were able to calculate correct cross-sectional areas as well as the volumetric strains. The success of this method depends on the uniformity of strain and the number of gauges used to measure the deformation or lateral dimensions at any stage of the test.

The Cambridge group (James, 1973) use internal markers i.e. lead shot to find both linear strains and volumetric strains.

In the present experimental programme, advantage was taken of those markers which were lying on the boundaries of the test specimen.

From the known spatial co-ordinates of such particles at various stages of deformation, the average dimensions of the test specimen can easily be calculated. Since in the present study, most of the marker particles were placed very nearly in one plane which was midway between the σ_2 - platen and parallel to them as well. To minimize the error caused by relying on the information obtained from one plane, particularly when the sample also bulges in the horizontal plane, fine lead shot were glued on the two exterior faces of the rubber membrane which actually formed the σ_3 boundaries. These lead shot were arranged in three approximately parallel and equidistant lines running parallel to the σ_3 - direction, see Fig. below and Plate 2.6 (a).



The main reason for selecting lead shot was their X-ray opacity and therefore their images can easily be identified. Further, the lead shot were arranged in close contact in single files so that their images gave an impression of a nearly continuous line. The configuration of three lead shot lines on either side of the flexible boundary gave a good idea of the shape of the deformed specimen. In order to find out the average length of the specimen in the σ_3

direction at the end of a given stage of deformation, the radiographic images of the lead shot were used. Since the stereo comparator was available for a limited time, it was used for the most essential and important measurements without which no further work would have been possible, for instance, taking measurements of control points which were needed in the calibration of the X-ray data acquisition set-up, measurement of image co-ordinates of object points. For the measurement of configuration of lead shot, a slightly less accurate method was used. The Dmac X-Y Reader of the Earthquake Engineering Section was used. Its resolution is 10 microns. With the help of this reader, the x,y co-ordinates of the crests (convex outwards) of the wavy lead shot curve images on one of the radiographs of a given stereo pair were read. The average co-ordinates for every lead shot line were then calculated. For these six (x,y) co-ordinates the photogrammetric calculations were carried out to find the X co-ordinate for every line, since all the necessary orientation parameters for the radiograph in question were known from calibrations, see Chapter 5. . The six X values so obtained were divided into two sets of 3 each according to which flexible boundary the line belonged. The data was further reduced to 2 by taking the average of the X values in each of the two sets. It gave two average horizontal co-ordinates in the X direction of the object space, one for the left hand side boundary and the other for the right hand side boundary i.e. \bar{X}_L and \bar{X}_R respectively. The difference between the two gives the length of the specimen in the σ_3 direction $L_3 = \bar{X}_R - \bar{X}_L$. If the dimensions of the other two sides of the cuboid are known, then its volume and cross-sectional area in any plane can easily be calculated. The current

axial length L_1 can be obtained by subtracting algebraically the total axial deformation from its initial length or incremental axial deformation from its previous length. On the other hand, the length in the σ_2 - direction L_2 is fixed at least theoretically for a plane strain test. However, in the present test a slight change in the L_2 was observed due to the bending of σ_2 - platens. The incremental effect on the volume changes and the cross-sectional area would however be insignificant. The lateral strain and volumetric strain were calculated by first calculating the change in dimensions due to any given incremental deformation and then calculating the linear strains and volumetric strains.

6.4 PLANE STRAIN COMPRESSION TEST RESULTS

The stress - strain and volumetric strain results for the various materials tested under air-dried and fully saturated conditions in a plane strain test apparatus are presented in Figure 6.4 to Figure 6.13. The test specimens showing stress-instability i.e. fluctuation of deviatoric force with deformation, the deviatoric stress and other parameters were calculated for the deviatoric force value located mid-way between the extreme upper and lower limits of variations.

6.5 STRESS-INSTABILITY

The deviatoric force and axial deformation of test specimens were continuously recorded by an electronic sensing and recording apparatus. The continuous plots of axial deformation vs. deviatoric force showed an increasingly unsteady stress state as the deformation was increased. The amplitude of this instability was observed to

increase with surface friction. Typical plots for high and low friction materials namely Glass (Sat), Teflon (Dry) and Glass (Dry) are given in Figures 6.1 - 6.3 respectively.

There is an inherent instability, generally known as base noise level, in the electronic data sensing and monitoring system. It is rather difficult to eliminate this system noise. However, it is essential and is possible to minimize them by proper design and selection of sensing elements and monitoring system so that the noise generated by them is small enough relative to the signals to be recorded. The calibration test of the electronic sensing and monitoring system revealed that the noise level of the system was very low in comparison to the signals to be measured and can therefore be neglected. It can safely be said that the measured instability in a test is due to the instability of the specimen and not due to the electronic measuring system used. The stress-instability becomes measurable and more pronounced when the deviatoric force reaches its peak and in the post-peak region. Tassois and Sotiropoulos (1973), and Skinner (1975) have suggested that this phenomenon may be due to a sample size effect. Tassois and Sotiropoulos (1973) carried out tests on gravel of maximum grain diameter of 10 mm and uniformity coefficient of 1.5 and found the following:

- i) the instability level becomes negligible when sample size to maximum particle size is greater than 20, and
- ii) the instability increases with increase in confining pressure.

From the test results obtained in this study, see typical results in Figures (6.1) - (6.3), and those presented by Skinner (1975) and Tassios and Sotiropoulos (1973), it can be concluded that the stress instability is influenced by various factors including the following dominant factors:

- i) sample diameter to maximum grain diameter ratio,
- ii) uniformity or gradation of test material,
- iii) coefficient of inter-particle friction,
- iv) hardness of the material, and
- v) confining pressure.

This can be written in mathematical functional form:

$$\text{Stress instability} = f(d_s/d_{\max}, U, \mu, n_o, \sigma_3)$$

where	d_s	=	diameter or dimension of the test sample
	d_{\max}	=	maximum grain diameter
	U	=	uniformity coefficient
	μ	=	coefficient of interparticle friction
	n_o	=	initial porosity
	σ_3	=	confining pressure.

Here the grains are considered to be unbreakable.

The possible mechanisms causing stress instability will be discussed in Chapter 7 from the microscopic point of view.

6.6 DISCUSSION

The tests, whose results are presented here, were carried out under low confining pressure less than 70kPa. It was, therefore, required to minimise confining effect of the membrane. This was accomplished in two ways. Firstly, special rubber membranes were made to fit the exact configuration of the sample and platens instead of using rubber membranes meant for cylindrical specimens as used by Green (1969) and Reades (1972) for their prismatic samples. Secondly the sample width was kept about 10% smaller than that of the rubber membrane so as to provide room for the specimen if it was to dilate in the lateral direction with minimum constraint. It was expected that with these two precautions, it was possible to minimise the confining effect of the rubber membrane and therefore no correction for this confining effect was deemed necessary. And in any case, the same constraint, if any, was applied to each specimen, therefore, difference in behaviour would be valid expressions of the material used and not because of apparatus effects.

During the shear tests on glass, ceramic and gravel and particularly when tested under saturated condition, a squeaking sound was heard. However, no sound was audible in the case of polymer materials tested, namely PTFE and polypropylene.

G205

Oct 30, 1973

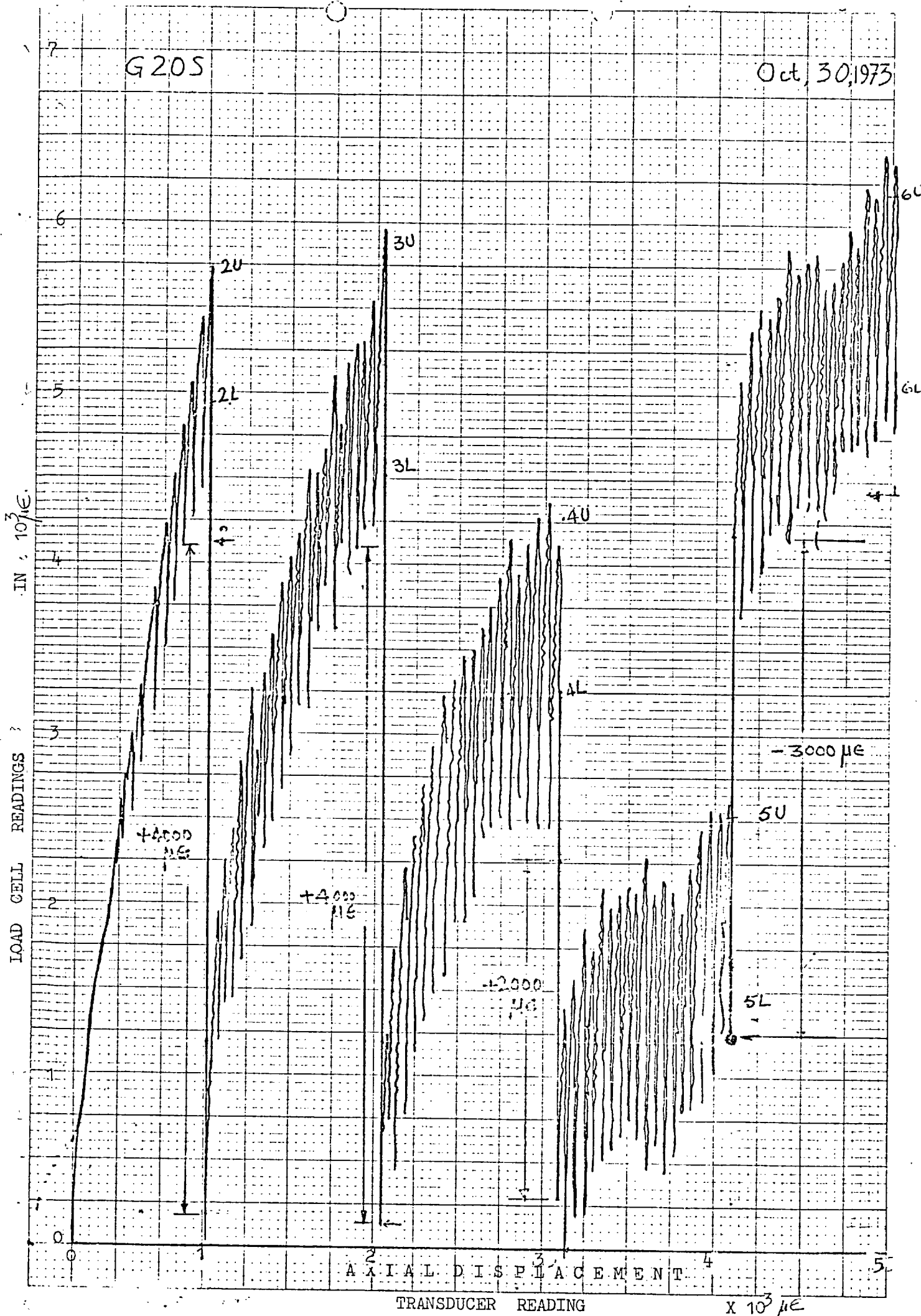


FIG. 6.1

Aug. 14, 1973

T 20D

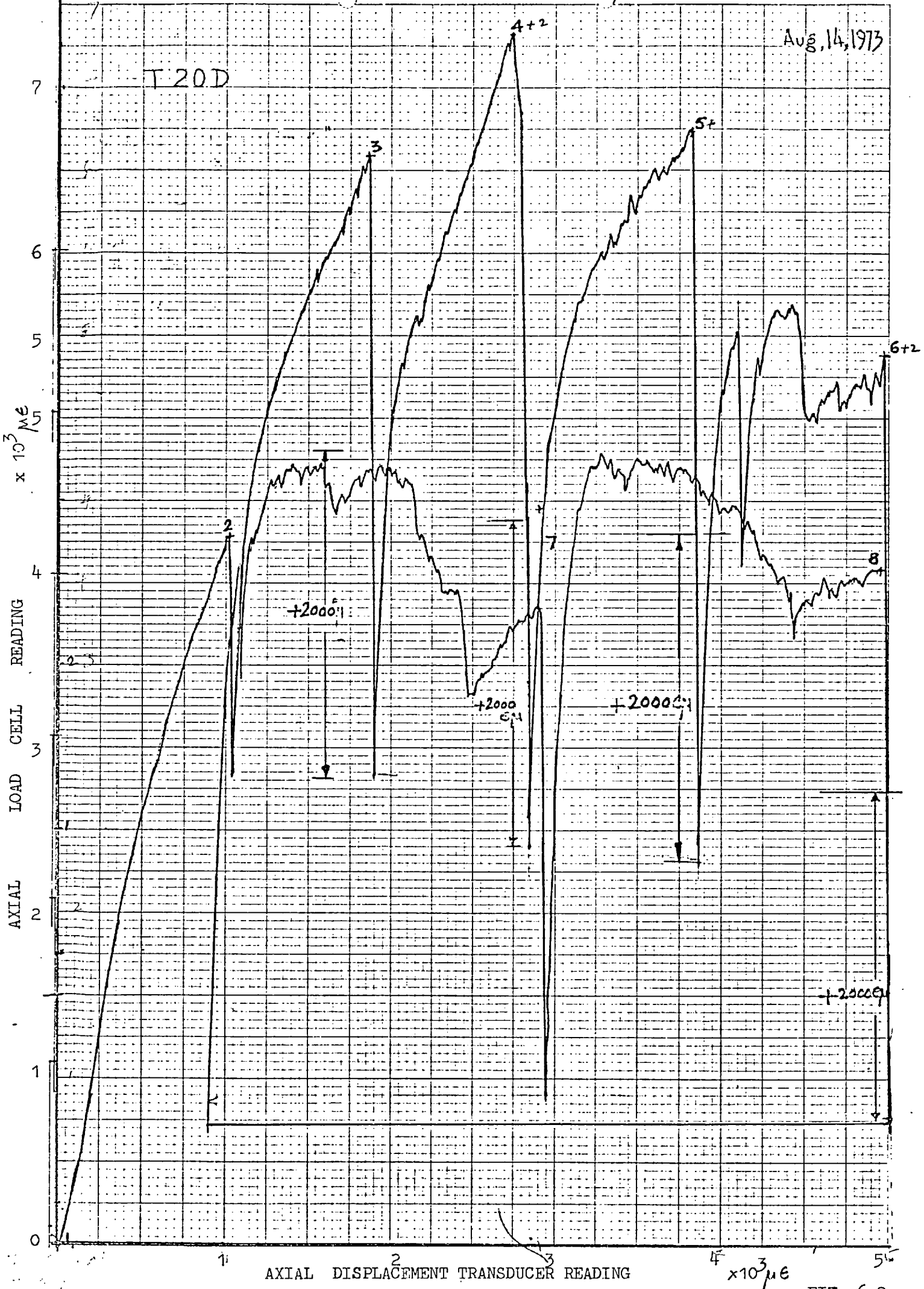


FIG. 6.2

Oct, 23, 1973

G 20D

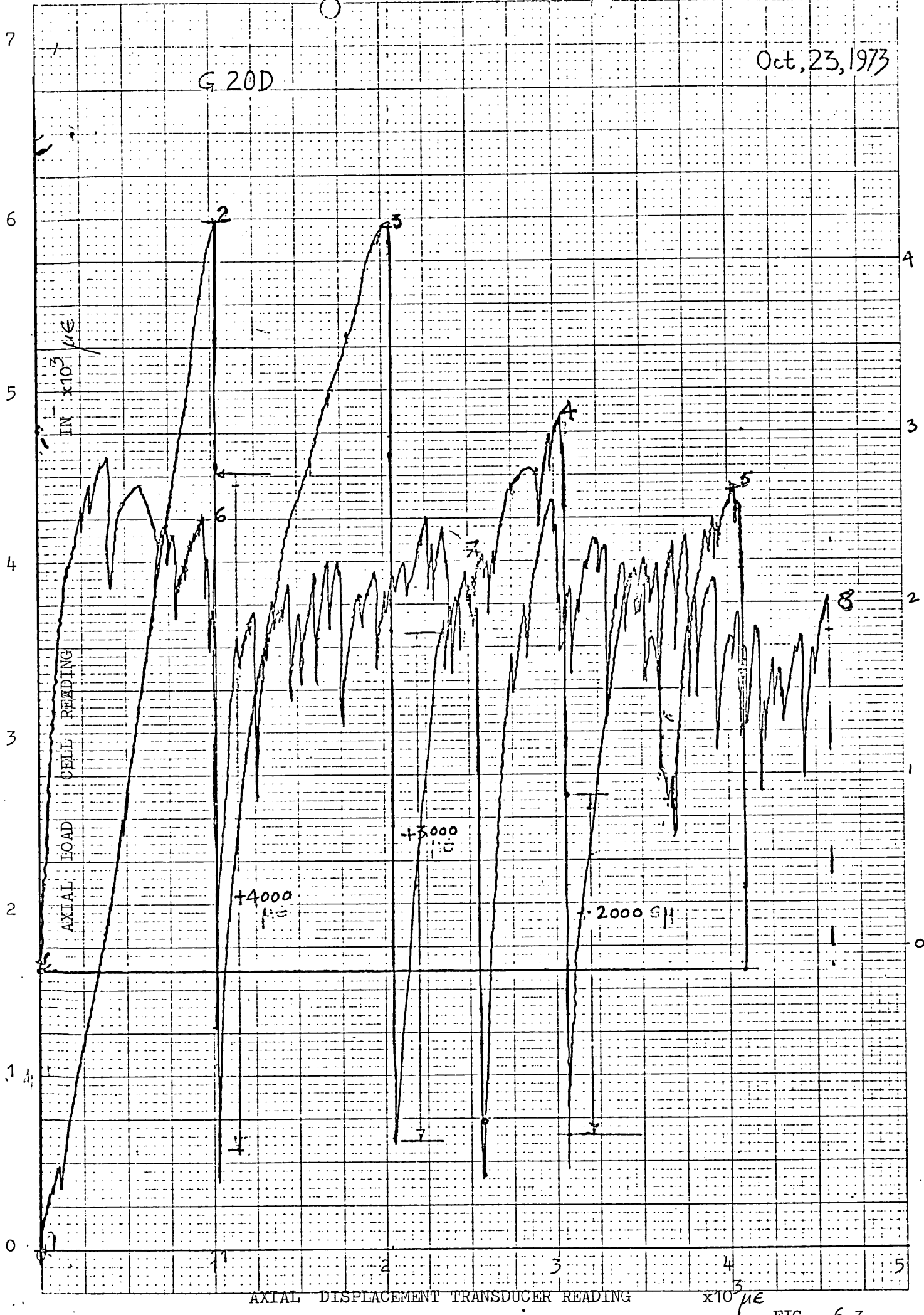


FIG. 6.3

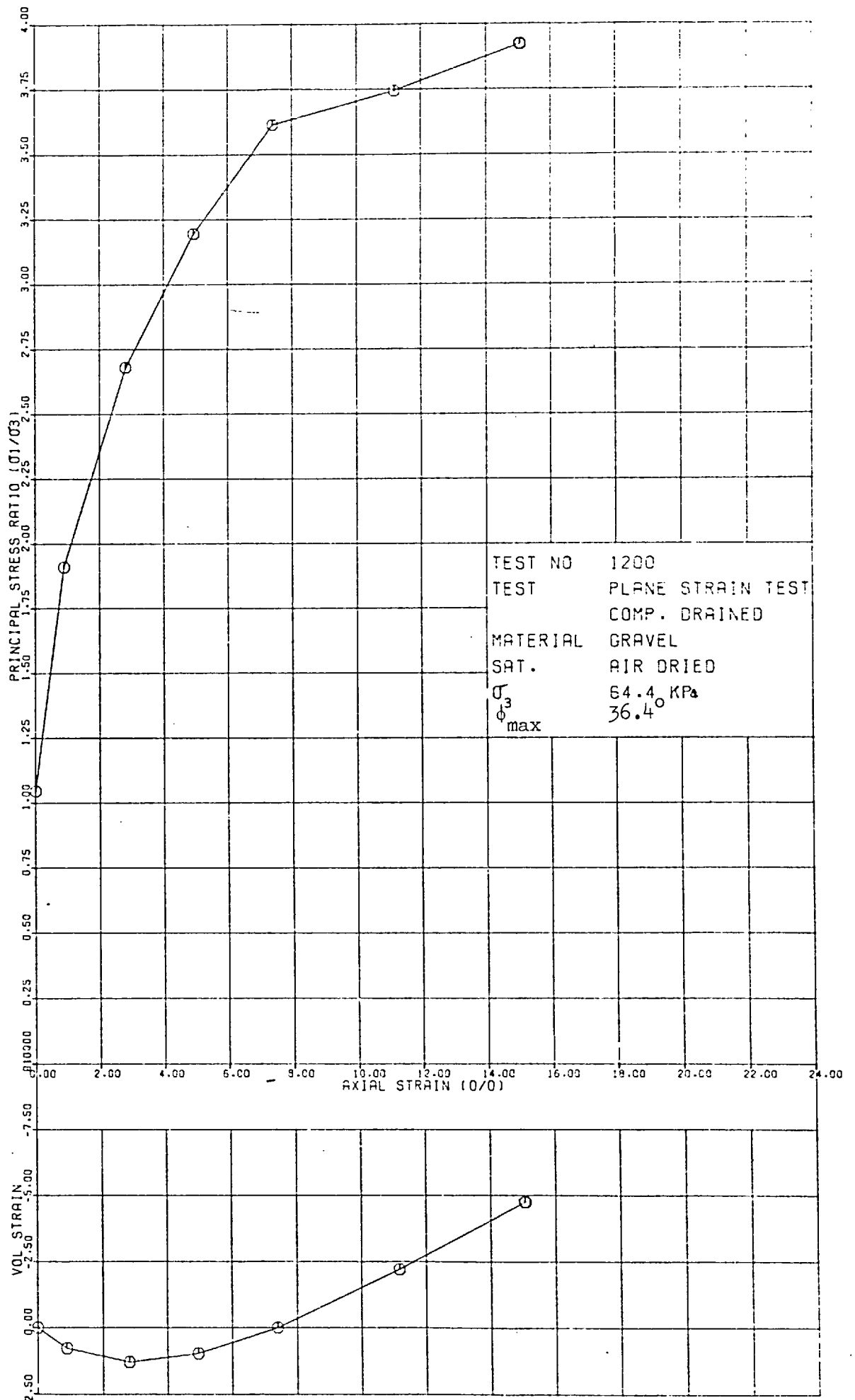


FIG 6.4 STRESS-STRAIN AND VOL STRAIN CURVES

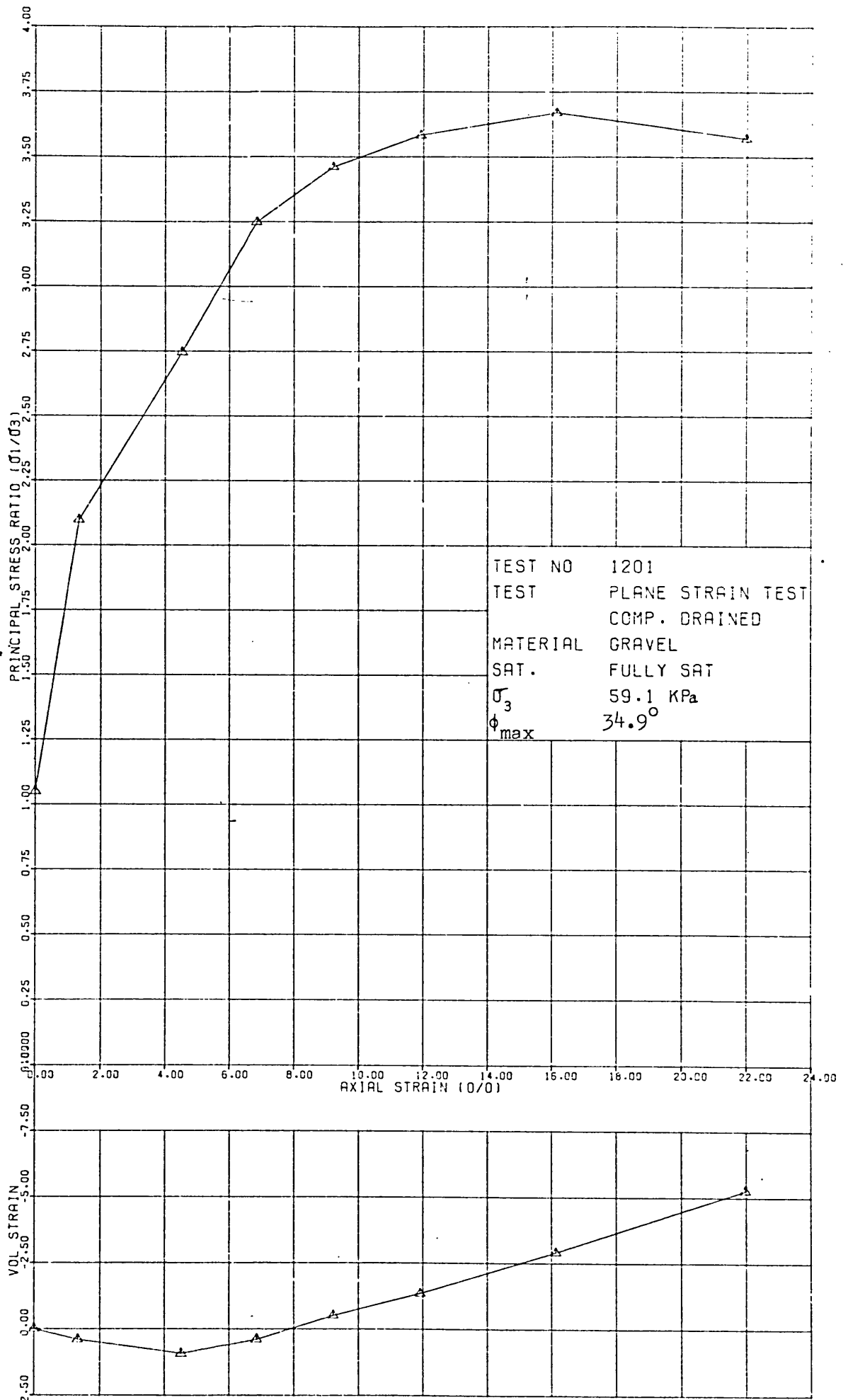


FIG 6.5 STRESS-STRAIN AND VOL STRAIN CURVES

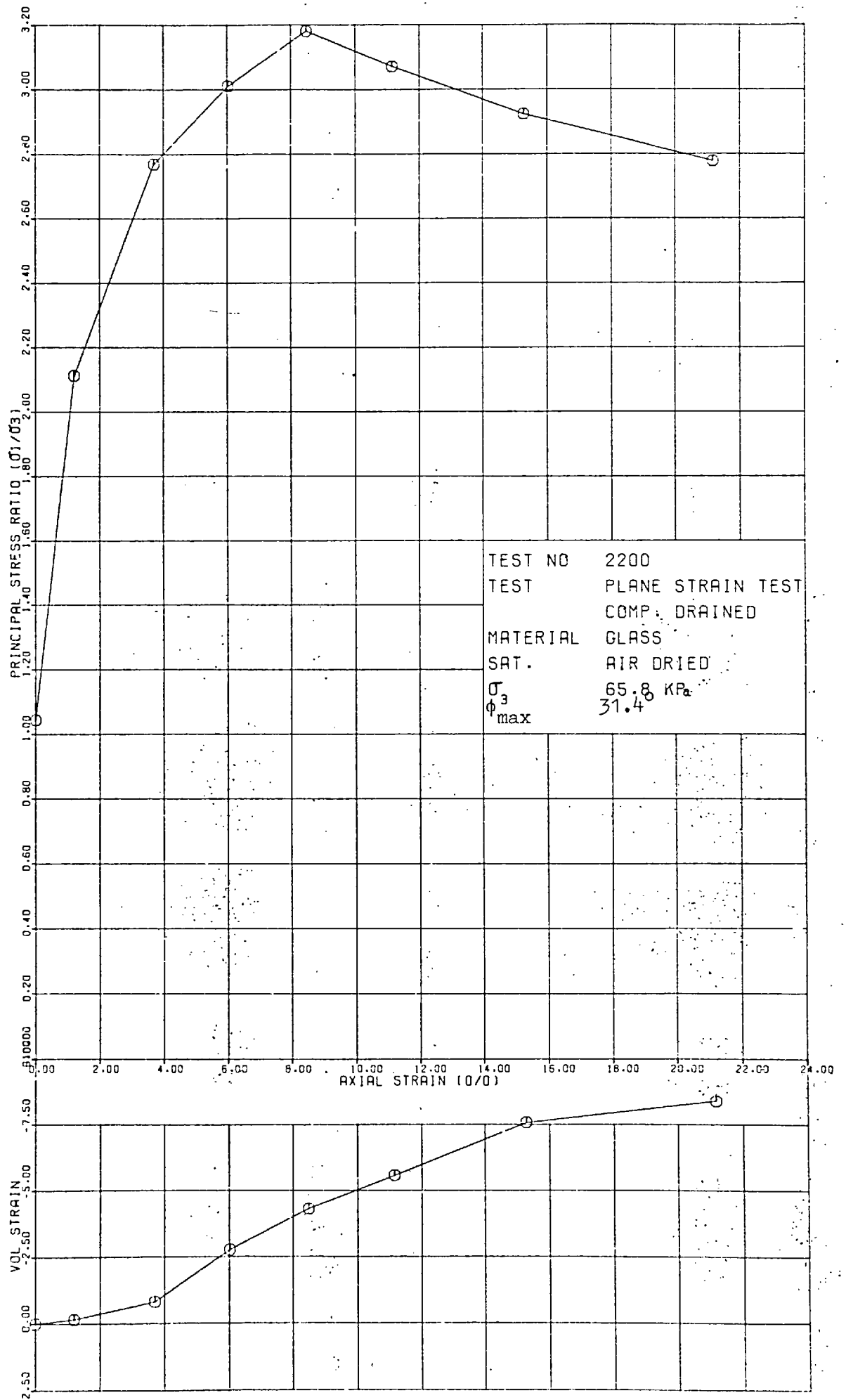


FIG 6.6 STRESS-STRAIN AND VOL STRAIN CURVES

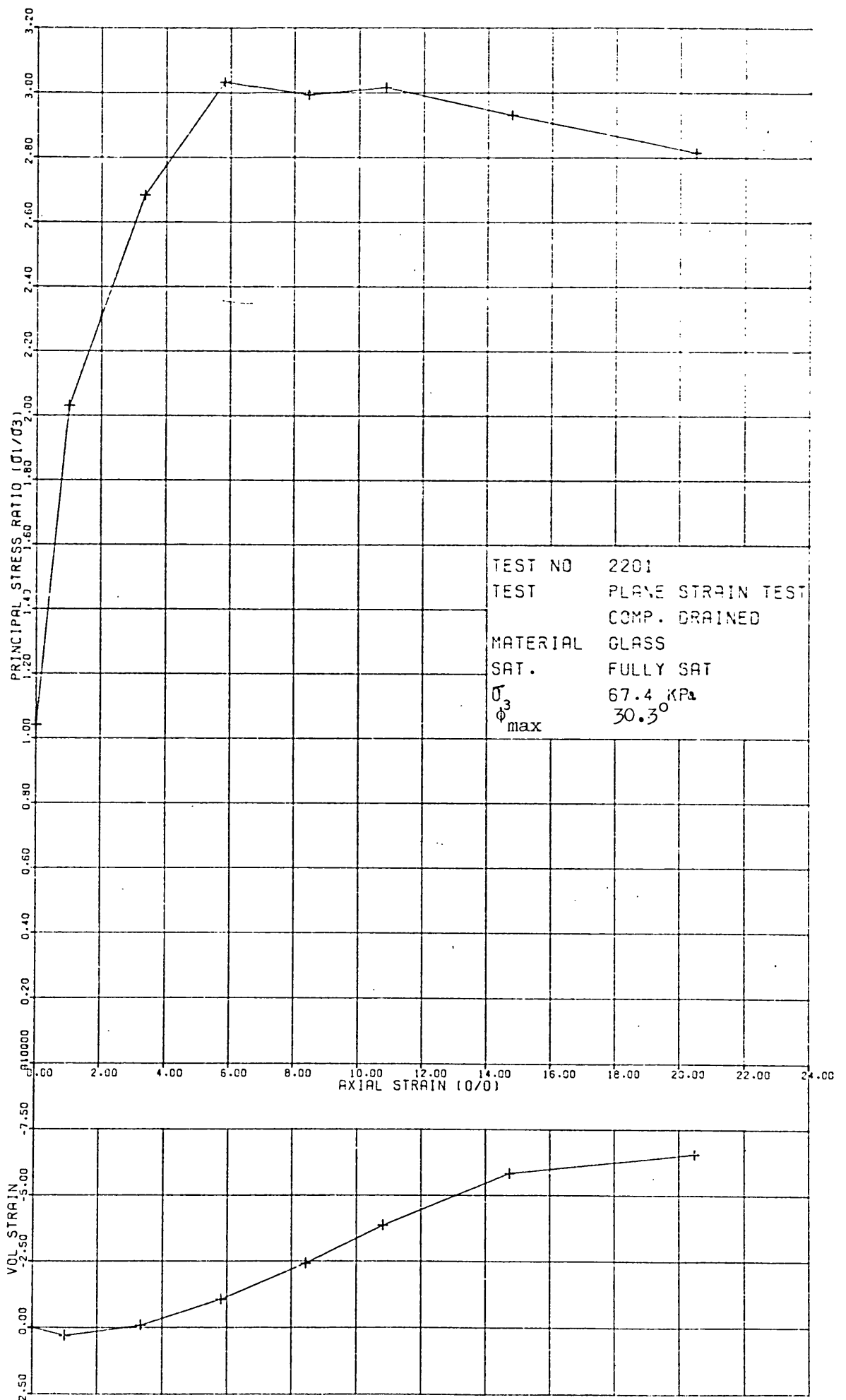


FIG 6.7 STRESS-STRAIN AND VOL STRAIN CURVES

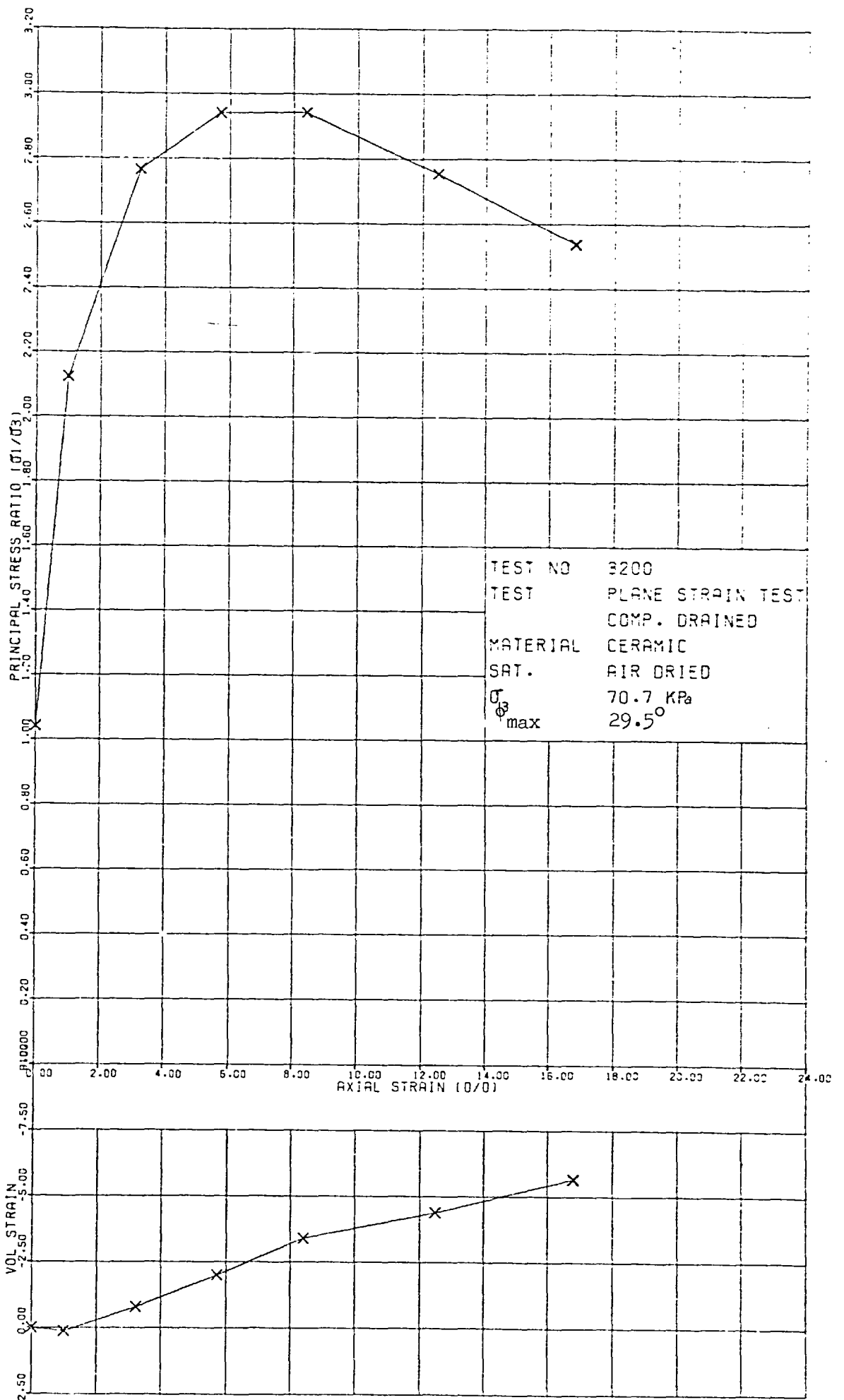


FIG 6.8 STRESS-STRAIN AND VOL STRAIN CURVES

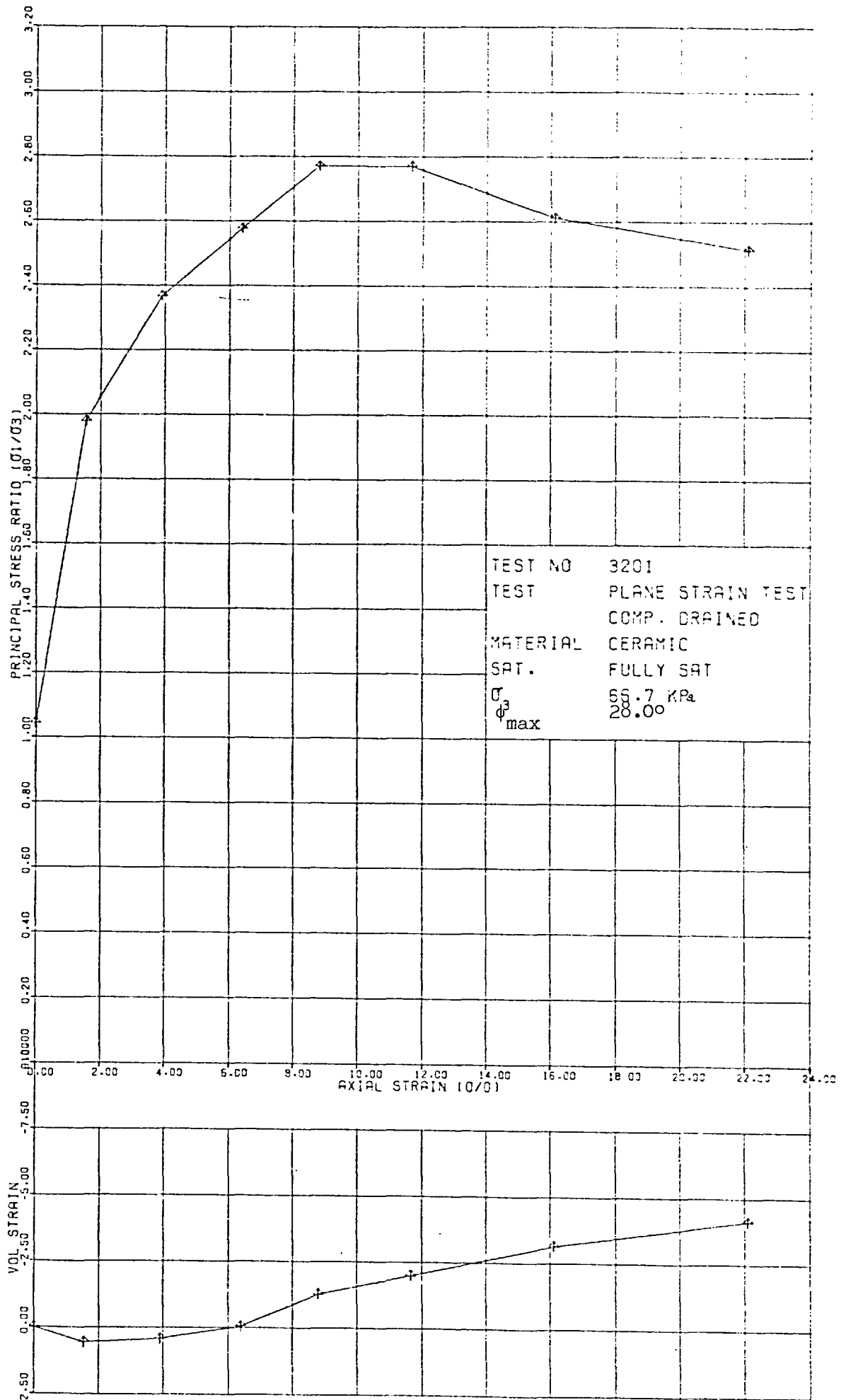


FIG 6.9 STRESS-STRAIN AND VOL STRAIN CURVES

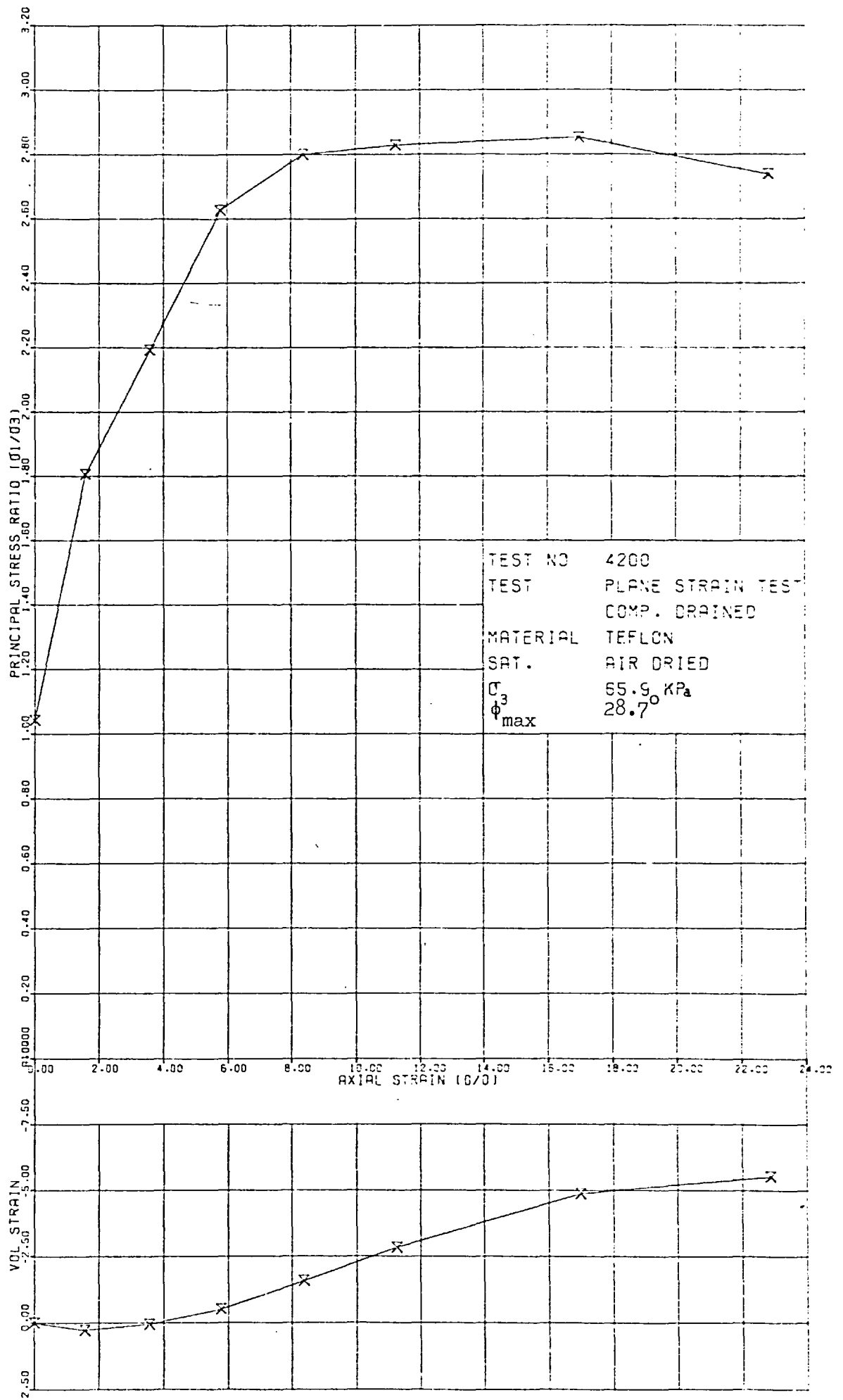


FIG 6.10 STRESS-STRAIN AND VOL STRAIN CURVES

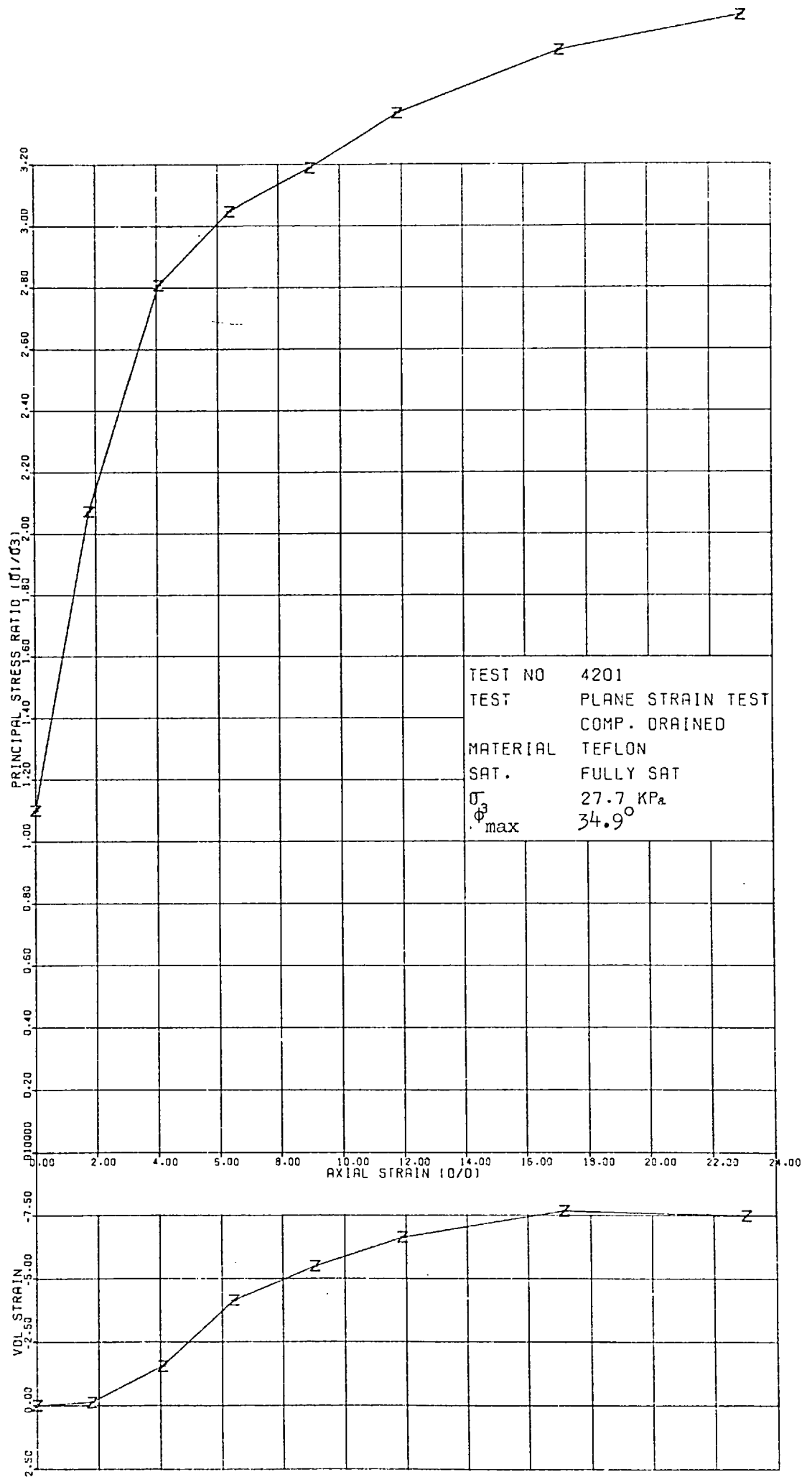


FIG 6.11 STRESS-STRAIN AND VOL STRAIN CURVES -

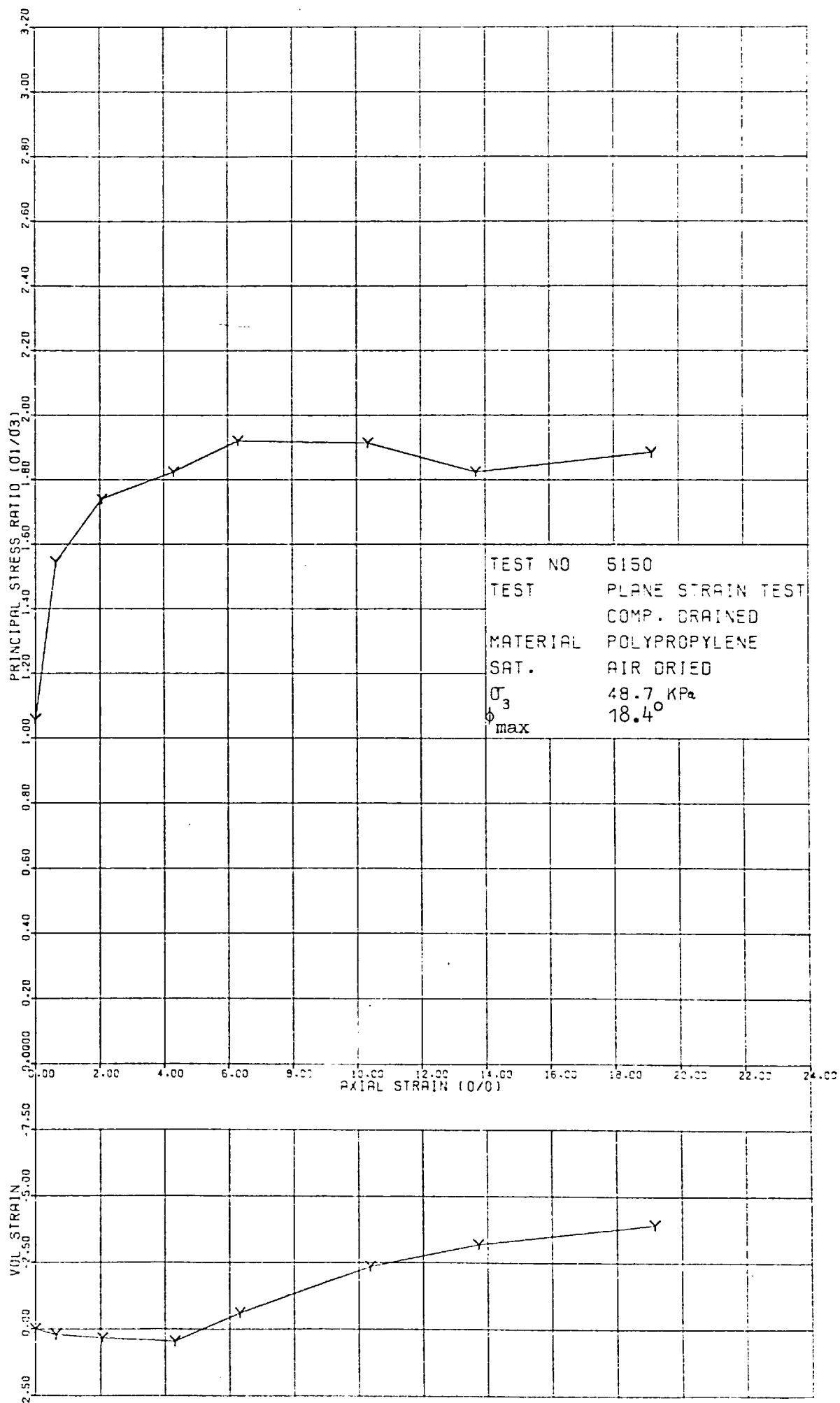


FIG 6.12 STRESS-STRAIN AND VOL STRAIN CURVES

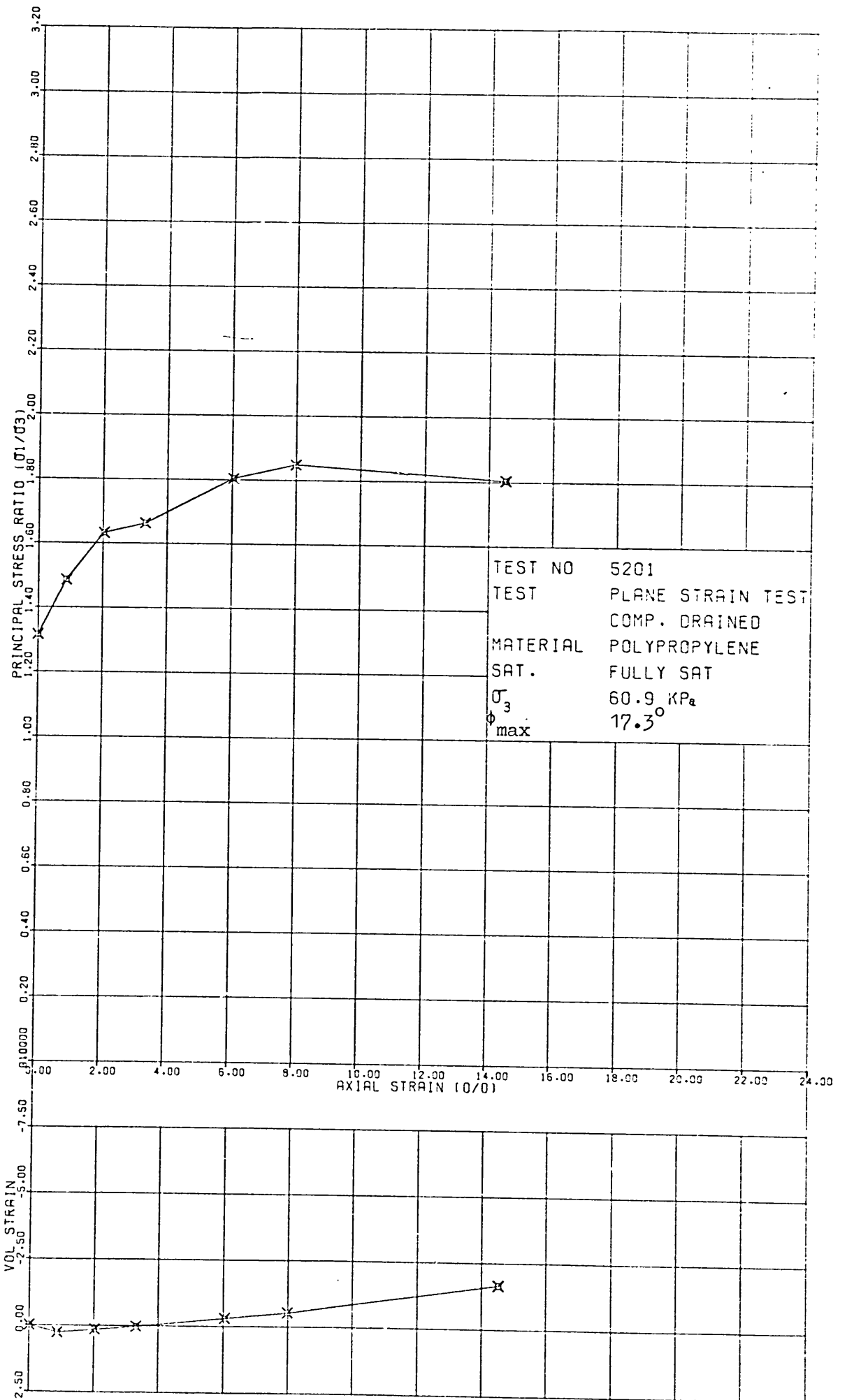


FIG 6.13 STRESS-STRAIN AND VOL STRAIN CURVES

CHAPTER 7

MECHANICS OF DEFORMATION OF PARTICULATE MATERIALS7.1 INTRODUCTION

The basic problem in the study of stress-deformation behaviour of a particulate medium is to understand its deformation. Unfortunately, the general mechanics of deformations is not as well understood as one might desire. Basically, deformation can occur either continuously or discontinuously. Continuous deformation is generally defined as the condition where neighbouring points in a deforming medium always remain neighbouring points and this deformation can be represented by a continuous function. On the other hand in discontinuous deformation this is not the case. Many branches of Continuum Mechanics, which deal with the continuous deformation of a medium have been very intensively developed and very highly refined, for example theory of elasticity and theory of plasticity.

These theories, which have been developed for continuous bodies, have been applied to Soils and other granular materials which are in fact discontinuous and made of discrete particles. Obviously it cannot be expected that the application of such theories to particulate materials will lead to entirely satisfactory results.

Terzaghi (1920, b) emphasized the discrete behaviour of granular soils and pointed out the fundamental fallacy of Soil Mechanics theories based on continuum mechanics. His following comments are worth noting:-

The fundamental assumptions of the traditional earth pressure theories cannot, in fact, stand even superficial examination. The fundamental error was introduced by Coulomb, who purposely ignored the fact that sand consists of individual grains, and who dealt with the sand as if it were a homogeneous mass with certain mechanical properties. Coulomb's idea proved very useful as a working hypothesis for the solution of one special problem of the earth pressure theory, but it developed into an obstacle against further progress as soon as its hypothetical character came to be forgotten by Coulomb's successors.

The way out of the difficulty lies in dropping the old fundamental principles and starting again from the elementary fact that sand consists of individual grains. This method of dealing with the problem was first tried by Couplet, in 1727, forty-seven years before Coulomb published his theory, but Couplet failed. In 1916 and 1917 Professor Skibinsky of Limberg published a series of articles on the pressure exerted by a mass of spheres. Investigations concerning the arrangement of the spheres, and the investigations result therefore in rather complicated formulae of limited value. In 1917 the author, who had no knowledge of Professor Skibinsky's publications, started to investigate along the same lines. But in the attempt to check theoretical results by observations he became convinced that earth pressure is an experimental rather than an analytical problem, and that we ought first of all to learn the physical facts of earth behaviour.

Terzaghi (1920b) Cowin (1974), Hashin (1965) and other researchers in the field of geotechnical engineering have clearly pointed out the complex nature of such a medium and the lack of suitable theoretical tools for the

analytical study of granular materials. It is therefore, undesirable at this stage to attempt a general theory for describing mathematically the mechanics of deformation. Instead the experimental evidence obtained in this study and presented in the previous chapters will be used in explaining the possible deformation mechanisms.

7.2 FACTORS CONTROLLING MECHANICS OF DEFORMATION

Deformation behaviour of granular soils and other granular materials are affected by various factors. A comprehensive list of such factors has been given by Taylor (1948). It is rather difficult to investigate the effect of these factors on the mechanics of deformation in this present study. The results presented here and the discussions developed on them, of necessity, have to be restricted to the experimental data obtained and presented in preceding chapters. However, it is expected that the conclusions derived from these results will be valid for those real situations where the plane strain test conditions prevail.

A particulate medium is composed of discrete particles arranged in random fashion in most real situations or in regular packings in ideal conditions. In other words the individual particles of such a medium interact with their neighbours while they themselves are arranged in a fabric, globally speaking. It is therefore obvious that the following three factors must contribute towards the mechanism controlling the deformation of the said medium under given conditions:-

- a) the geometry and grain size distribution of constituent particles
- b) the physical properties of these particles and
- c) the fabric of medium.

The main object of this chapter is to find out which of the above mentioned factors control the mechanics of deformation.

7.3 BASIC TEST DATA

The essential information on the geometry of the particles of test materials and their grain size distribution is given in Chapter 2. The friction test results of these particles are presented in Chapter 3, whereas the typical data on the positions of the marker particles in a plane strain test specimens and at various stages of deformation have been given in Chapter 5. These test results along with those presented in Chapter 6 will be used here to find possible mechanisms of deformation.

7.4 COMPONENTS OF DEFORMATION AND THEIR RELEVANCE TO THE DEFORMATION MECHANISM

Deformation of a particulate mass can be presented in two different ways depending upon the analysis to be used. In the continuum approach, the information of deformation on macroscopic level is generally used, whereas particulate mechanics requires the details of deformation of the grain fabric as well as of the constituent grains forming the deforming granular mass.

7.4.1 Deformation on Microscopic Level

At microscopic level the deformation of the granular mass may be considered to be composed of two components:-

- i) deformation of constituent particles, and
- ii) displacement of the structural members of the grain fabric.

7.4.1.1 Deformation of grains

Contribution to the total deformation from this source essentially depends upon the applied contact forces on individual particles, mechanical properties of the grain such as, hardness, elastic parameters, strength and their brittleness. If the stress level to which the grains of the deforming medium are subjected, is low then the possibility of particle breakage, particularly through the bulk material, is remote. One of the reasons for using low confining pressures, less than 70 kPa, was to remove the chances of particle breakage. Not a single particle of all test samples was found to be broken in the test series reported in this thesis. The grains of a test sample can deform both elastically in the bulk of the grains and plastically at local points of contact where the contact stresses are large enough to cause plastic deformation. However, the major part of the grains will deform elastically and will store a certain amount of strain energy.

For the stress level used here, the elastic deformation and thus the strain energy stored by the constituent particles will be very small and need not be considered as a major contributing factor to the total deformation. Further the axial deformation of the test sample was increased monotonically, decoupling of this deformation is not necessary in the context of this study. However, it must be pointed out that whatever be the magnitude of the stored strain energy in the grains forming the fabric, it will cause some "snapping" displacement of certain particles located in an unfavourable position in the fabric.

7.4.1.2 Deformation of fabric

The fabric of a granular mass may deform due to micro-slip occurring at the particle contacts or due to relative movements of constituent particles

or to both sources.

a) Microslips

At particle contacts microslip occurs where either the particles are not rolling or the tangential force is less than the frictional resistance. Generally the magnitude of microslip at a contact is very small and may be of the order of a few tens of microns before gross slip can take place, see Fig. 7.2. If the number of non-slipping contacts are large, the contribution from this source is not insignificant. Their contribution to elastic strains becomes apparent upon unloading the test sample. The deformation generated from this source can be partly recovered depending on the direction and magnitude of normal and tangential traction, see Fig. 7.1. This deformation is termed here as "pseudo-elastic" deformation.

In actual granular masses with complex grain arrangement it seems impossible, at least with the present state of knowledge, to separate pseudo-elastic displacement and the elastic recoverable component of displacement. Nevertheless it is important to accept the existence of the micro-slips or pseudo-elastic deformation and this is probably the source of energy dissipation at particle contacts where gross slips do not occur. It might be argued that since the micro-slips are very small (of the order of tens of microns), their contribution to total energy dissipation will be insignificant. It must be pointed out that the level of significance of energy loss from this will depend on the number of such particle contacts, coefficient of surface friction of particles, the amplitude of the normal and tangential tractions at contact points.

b) Displacement of particles of the fabric

The components of gross displacements of particles in the ensemble of granular particles may be defined in at least two different ways. In

the first method, the displacement of a particle is measured from its own preceding position that is with respect to its position before the sample is subjected to given amount of deformation. In the other method the relative movement of a particle is reckoned with respect to its adjoining neighbours. For simplicity, the first method is used here for the calculation of displacement of particles.

The displacement of a particle may be divided into two components:-

- i) Linear translation,
- ii) Rotation.

i) Linear translation

Following the first method of calculation of displacement, the linear displacement of particles was calculated by taking the difference between the spatial coordinates of the C.G's of the marker particles after the deformation compared to the same particles before the test sample was subject to the deformation increment.

ii) Rotation

The calculation of rotation of a particle after a given deformation increment is very simple and straight forward. Here the rotations of the particle about its own axes were obtained. Since the orientation and the C.G. of the tungsten wire were known before and after the deformation increment, merely subtracting from its final orientation angles the initial orientation angles gave the rotation experienced by the given marker particles. Incidentally, the spherical coordinate system was used for representing the angular orientation of the particles and the cartesian co-ordinate system for the linear translation of the particles, see Fig. 7.4.

The total rotation of a particle can be considered as the combined effect of rigid body rotation of the group of particles of which it is a constituent member, rolling and sliding. Although it is desirable to separate the contribution made by these three factors, no suitable and acceptable solution to this rather complex problem was found. This was mainly due to the difficulty in finding the contribution made by the first factor. The question becomes more intractable with the possibility of the particle under study changing from one group to another during the given deformation increment. There is yet another insurmountable difficulty, that of finding the rotation of the particle due to rolling, particularly when the particle under study loses contact with its neighbouring particles. However, it is possible to isolate these contributions but it will require large numbers of marker particles placed in such a way that the displacement history of the particle under study and of all its neighbouring particles can be continuously traced. Further it will require very involved mathematics to separate the various components of rotation specially when the constituent particles are not spherical in shape. Despite these difficulties, the total rotation measured will give a clear indication whether a particle is acting as a roller between groups of neighbouring particles. This will be obvious when the rotation of a particle is much larger than the adjoining particles.

Although the difficulties in the separation of rotation into its various components does not affect the qualitative interpretation of possible deformation mechanisms, it is not possible to interpret the measurements in terms of an energy balance equation. Further effort is therefore needed in this direction.

7.4.2 Macroscopic deformation

In response to an applied stress system, the granular mass deforms internally at microscopic level and its cumulative effects appear on its external boundaries which are generally measurable. The other name given to these measurement of deformations is macroscopic deformation. Here again in soils and other granular materials, these deformations can be split into two types namely - elastic and plastic deformations. It must be borne in mind that the macroscopic deformations, elastic as well as plastic, are the consequence of the complex behaviour of the granular assembly at its microscopic level. Decoupling or splitting of the total deformation into its two components - elastic and plastic - is very difficult if not impossible. In the absence of a correct method, the technique, which is commonly used, is to unload the granular mass and then measure the recoverable deformation. The difference between the two deformations - total and elastic - will give the irrecoverable or plastic deformation. However, it is difficult to justify that the elastic deformation will be the same at the instant the sample was loaded, particularly when the granular structure of the deformed mass changes upon unloading. Barden (1969) also points out the difficulties and limitations of the present method of decoupling of the deformation components.

7.5 REFERENCE STATE

For the calculation of both macroscopic deformation and various components of microscopic deformation a reference state or a datum is needed. Mathematically speaking the true reference state, free from any strain or stress, is required. However, in a particulate mass no such state can really exist. It is, therefore, essential to choose arbitrarily a reference state. In this investigation the initial reference state of the test

specimen was defined as the one which was obtained just after consolidation of the test samples and before any shear deformation was applied to it. For the subsequent stages of deformation, the reference state was taken to be the one which existed just before the application of the deformation increment in question.

7.6 ZONES OF DEFORMATION IN A TEST SAMPLE

Before actually embarking on the discussion of the experimental data of the present study, a few general comments on the formation of different zones of deformation and on the rotation of particles in a test sample subjected to shear deformation are warranted. This is the most convenient place to include such comments. The first topic is dealt here, whereas the second is discussed in section 7.7.

In the field of geotechnical engineering, it has long been accepted that deformation of a granular medium under shear can be divided into three zones:-

1. Dead or rigid zone
2. Dilating zone
3. Shear zone.

Any or all of these zones can be present in the deforming medium depending upon the boundary conditions, applied stress or deformation condition.

Using the thin section technique Oda (1972, b) investigated the formation of these three zones at various stages of conventional triaxial compression of sand, see Figure 7.3. Oda et al (1972) observed that the distribution of voids ratio is not uniform within the test sample both in

the pre-peak and post-peak range of deformation. However, they recognized statistically homogeneous zones with regard to void ratio and their results confirm the existence of the various deformation zones mentioned earlier.

In the experimental data presented in this Chapter, every effort will be made to locate the presence of the above mentioned zones and to find how far the deformation zones are uniform, in the statistical terminology. Further the efficacy of the use of 'frictionless' platens will also be investigated.

7.7 ROTATION OF PARTICLES

The constituent particles of the granular skeleton do translate as well as rotate when such fabric is deformed under shear till these particles form a stable fabric again under the given stress or deformation conditions. Roscoe and Schofield (1964, p.148), while discussing the formation of anisotropy in the soil fabric under shear commented: "The writers have observed equal and opposite rotations of as much as 15° of neighbouring particles of dense sand which are against the glass walls of the plane strain earth pressure test apparatus. The axis of rotation is not necessarily perpendicular to the plane of strain." Although the stress-dilatancy theory propounded by Rowe (1962) does not allow for any contribution from the rotation of particles, Rowe (1962, 1973) accepts some rotation of particles. However he remarked while discussing Oda's (1972, b) paper: "Gradual rotations of particles do occur with structural rearrangement and these are in no way inconsistent with a model where stress ratios are dependent on frictional strength between sliding contacts as they reach the preferred orientations."

Oda (1972, b) made the following conclusion based on the experimental investigation which pertains to the rotation of particles in a test sample under shear: "... it is reasonable to conclude that "rolling" of particles must be an important factor to control the mechanism of fabric reconstruction". Further Skinner (1969, 1975) showed very clearly the possibility of particle rotation under the deformation conditions investigated by him. He suggested that a rolling mechanism accompanies sliding within the mass of particles, and that rolling increases as the values of the interparticle friction increases.

From this brief discussion it becomes obvious that there is a possibility of certain contribution made by rolling mechanism and that a sliding mechanism on its own is rather difficult to find in real situations.

7.8 DATA PROCESSING AND PRESENTATION

The basic test data described in section 7.3 can be used in various ways in obtaining the desired information in any format namely graphical plots or numerical values of certain parameters. Amongst the numerous combinations available for data processing and presentation, the following scheme has been favoured and used so as to present the information of a complex system in a simple way which at the same time is available to logical interpretation.

1. Flow diagrams,
2. Trace of the tips of marker particles on a stereonet,
3. Incremental displacement-rotation vector plots,
4. Histograms and relevant statistical parameters, and
5. Phi-rotation-dilatancy plots.

These plots have been arranged and presented here according to the test to which they belong.

7.8.1 Flow Diagrams

For every plane strain test included in this thesis two plots have been drawn and presented here. One showing the trace of the movement of the centre of the marker particles in the XY-plane and the other is the trace of these particles in the XZ-plane. These two plots give the complete history of the movement of particles in the test sample from the start of deformation to the end of every test.

7.8.2 Trace of Tips of Markers on a Stereo-Net

The flow diagrams mentioned above, by definition, are the cumulative plots and trace the history of the linear displacements without considering the angular rotations of particles, if any. Instead of using the conventional method of plotting separate plots for each angle as was done in the case of linear displacements, a stereographic projection technique is used for showing the trace of angular movements of the tips of marker wires at various stages of deformation. Two typical sets of stereonets for two different test materials are presented here.

In order to avoid overlapping of traces of the particle tips and to organize the information, the plane containing the marker particles has been divided into 16 approximately equal zones, for details see Appendix B. The rotation of marker particles contained in these zones are plotted on separate stereonets.

7.8.3 Displacement-Rotation Vector Plots:-

The incremental displacements dx and dy as well as their angular rotation increments of $d\phi$ and $d\theta$ of all the marker particles read from a given pair of stereo-radiographs have been plotted. Further such plots are

included for every stage of plane strain tests on all the materials tested.

7.8.4 Histograms and Statistical Parameters

For further study of rotation statistical techniques, in their simplest form, are employed. Histograms are, therefore, plotted for every deformation stage. And for every stage of deformation, separate histograms have been plotted for the two incremental rotations ϕ and θ .

7.8.5 Phi Rotation - Dilatancy Plots

In the phi-rotation - dilatancy plots, average incremental rotation angle ϕ of the particles enclosed in a given area, called the element here, at various stages of deformation are plotted against the corresponding dilatancy rate of this element. Two sets of such plots for two different materials have been included.

The zonalisation of the plane containing the marker particles is described in Appendix B, which also shows the method of calculation used to obtain the average rotation increments and dilatancy rates.

7.9 DEFORMATION RESPONSE OF GRANULAR SAMPLES UNDER PLANE STRAIN COMPRESSION TEST CONDITIONS

Under an applied deformation system, e.g. axial deformation applied to a test sample in a strain controlled test, or under an applied stress system, such as in a stress controlled test, every particulate body responds in the form of measurable boundary deformations and boundary forces. These boundary deformations and forces are, in fact, the consequence of

the deformational response and the resistance offered by its constituent particles respectively. As mentioned in Section 7.4 the deformation of a granular body can be divided into two main components namely linear translations and rotation of its individual particles.

One of the deformation characteristics of a cohesionless granular body, which distinguishes it from a solid body, is the rotation of its individual particles. Since the particulate body behaves differently than a solid body, it is essential to know the mechanism of deformation and to know which of the two approaches - continuum or particulate - can be applied to these bodies. The answer to these questions hinges on the possibility of representing these components of deformation by continuous analytic functions.

The observed data will now be examined in this context.

Reference to displacement-rotation plots presented here, for instance Figure 7.5, reveals that neither the displacements nor the rotations of the constituent particles are uniform and homogeneous under an application of a deformation increment to which the test sample was subjected. The lengths of the vectors* representing the components of rotation are not constant but vary from particle to particle. For the boundary deformation conditions applied to the test sample in this investigation and if the internal strains are assumed to be uniform and homogeneous, the X-components of the displacement of all the particles lying in a plane normal to σ_3 -direction must be equal and so must be the Y-components of displacement of all the particles lying in a plane normal to the σ_1 -direction (Fig. 7.4). As the particles were not arranged regularly in the test samples of the plane strain tests, it is highly improbable to obtain an arrangement of particles such that their centres of gravity lie on the above mentioned planes. The component of

*The term vector, as applied to incremental rotations, denotes the magnitude and the sense of incremental rotation and not the correct direction.

displacements were calculated by interpolation of the relevant displacement of particles lying on either side and close to the plane under study. Further in this study we are investigating the behaviour of those particles lying close to a representative plane, which is called here 'strain plane' and is approximately midway and parallel to the σ_2 -platens. The intersection of the above mentioned planes with this plane will result in a horizontal line AB and vertical line CD, see Fig. 7.4.

For a typical test and for a typical deformation increment, for instance test 5201 and for the fifth deformation increment, the X- and Y- components of displacements of the particles on the two arbitrarily chosen lines AB and CD, marked in Figure 7.181, are shown in Figure 7.183. This figure reveals that the displacements are not uniform. In order to prove the homogeneity or otherwise of the displacements, say for example of Y- component of displacements, another horizontal line EF, Figure 7.181, was arbitrarily chosen. And for the test and deformation stage mentioned above, the Y- displacements are plotted on this line, Figure 7.183. Comparison of the displacements of lines AB and EF, Figure 7.183, would show that the displacements are not uniform and also the distribution of Y- displacements is not similar to that for line AB. It is, therefore, reasonable to suggest that linear translations of particles are neither uniform nor homogeneous.

This can further be examined by investigating the behaviour of groups of particles instead of individual particles. The mean displacement components in the X, Y and Z directions for the particles enclosed in each of the 16 zones (Figure B.1) and for all the stages of deformation have been calculated. These displacements for a typical test, test no. 4200, are presented in Tables 7.5 - 7.7.

If the internal displacements imposed by the boundary displacements of the test sample are uniform and homogeneous, it is possible to calculate displacement distribution inside the sample. For the typical test under discussion, the Y-components of the displacements based on the assumption that the displacements are uniform, have been calculated and are given in Table 7.8. Table 7.9 gives the non-uniform component of the total Y-displacements, which are obtained by deducting the uniform component of Y-displacements of the group of particles from the corresponding average Y-displacements of the same group of particles displaced during the same deformation increment. Table 7.9 clearly shows the random nature of Y-displacements. An interesting observation can be made from the study of this table. Although the sample is monotonically compressed in its axial direction, the relative vertical displacement of the groups of particles in the adjoining zones is not always in the same direction as that of the externally applied deformation but instead it randomly changes its direction which is depicted by change in its sign. In other words, the distance between the centroids of the two adjoining groups is increased. We will come back to this point again in the next section.

For the analysis of rotational behaviour of particles, available techniques of statistical analysis can be employed. Histograms and other statistical parameters, namely mean and standard deviations, for both components of incremental rotation ϕ & θ are obtained and are presented here. Histograms for all the tests have been included here, for example see Figures 7.11-7.16 for a typical test. Other relevant statistical data of these tests is presented in Tables 7.1-7.4. Examination of these histograms and data presented in these tables show that the rotations are not constant but their magnitude is continuously changing. Histograms for the rotations

ϕ and θ are in general uni-modal for most part of the deformation history of a test sample, e.g. see Fig.7.11-7.13. But at very large strains, where the sample approaches the constant volume deformation condition, the histograms tend to become rectangular in shape, for example see Figure 7.64. This suggests that the rotation of particles with angles between the spread of the histogram for this stage of deformation are equally probable. The trace of linear displacement history of marker particles on the XY-plane and XZ-plane, such as Figures 7.65-7.66 as well as the trace of the rotational history of these particles, Figures 7.67-7.74, show the random nature of the movement of individual constituent particles of a test sample.

From the evidence presented so far, it is reasonable to suggest that the movement of constituent particles of a granular sample are continuous but random in nature, which differs basically from a continuous displacement field. Further with the help of the data presented, it can be said that every particle of a test sample suffers linear displacement and is most likely to rotate during the deformation history of the test sample. From the displacement data obtained from the static and stable positions of the particles which existed before and after the application of the deformation, it is rather difficult to prove or disprove the existence of the rigid or semi-rigid groups of particles which might have been formed and broken during the application of the deformation increment. However, the rotational similarity between group of particles at any stage of deformation might give an indication of movement of particles in groups. For instance particle nos. 50, 63, 76, 77 in Figure 7.94, show similar trend of deformation, particularly rotations and therefore, these particles might be members of a group.

7.10 STRAIN DISTRIBUTION INSIDE THE TEST SAMPLES

In most of the existing stress-strain theories, which are developed on the basic concepts of either continuum approach or particulate approach, uniformity of strains and stresses inside the deforming body as well as the coaxiality of axes of principal stress and principal strain rate are generally assumed. In these theories it is further assumed that the behaviour of an infinitesimal mass of the media is in no way different than that of the whole medium under similar deformation conditions. In other words local variation in the force-deformation behaviour of a medium is not recognized in these theories. For instance, the stress-dilatancy theory developed by Rowe (1962) is based on the assumption that the behaviour of a regular particle assembly can predict the behaviour of randomly arranged particles in actual granular soils and even of clays which generally have platy shaped and very small sized particles.

The experimental data obtained from the plane strain tests can advantageously be used to find the variations, if any, in the strain distributions inside the test samples and to check the validity of the basic assumptions mentioned above. Horizontal and vertical components of strain increments of a typical test, namely test no. 2201, are calculated according to the computation scheme outlined in Appendix B, and are presented in Tables 7.10 and 7.11 respectively. Reference to Table 7.11 shows that the vertical strain of element 2 at the end of first stage of deformations is a negative. In other words this element has undergone extension in the vertical direction, although the overall deformation of the test sample was compressive. The element under discussion is presumably unloaded during this stage of deformation. This behaviour suggests that inside the sample direction of principal stress axes or principal strain increment axes or both set of

axes are probably undergoing continuous rotation. It is also possible to find an element whose horizontal strain increment component is at variance, particularly its direction with its adjoining elements. If both horizontal and vertical strain increments are positive, such as in the element 7 at deformation stage 2, see Tables 7.10-7.11, the granular fabric of the group of particles of the elements would consolidate and might even collapse under the action of compressive forces. These sudden changes in the nature as well as in the magnitude of strain increment components affect the principal strain increment components and which, in turn, affects the values of dilatancy rate D . It was found that the values of dilatancy rate D of some of the elements, which was calculated from the internal strain increments, lie outside the accepted range of 0 and 2.

It is worth noting that no theoretical limits for the maximum or minimum value of D has yet been obtained for the plane strain test conditions (Barden, 1969).

From the study of Tables 7.10-7.11 one important observation can be made. The change in direction as well as in magnitude of various components of strain increments of an element occurs randomly. Further no discernable pattern of these changes emerges. Also from the data presented in Tables 7.10 - 7.11, it appears that the strains inside the test sample are not uniform and also lack in homogeneity.

Volumetric strain increment data for the typical test under study, namely test no. 2201, has been included in Table 7.12. The typical data presented in Table 7.12 confirms what has been said above regarding the non-uniformity of strain increment distribution and about the random character of individual elements at various stages of deformation.

From these results it can be suggested that during deformation the fabric is continuously, but randomly undergoing fabric reconstruction and possibly the particles are moving in quasi-rigid groups.

7.11 ROTATION OF PARTICLE - A PECUNIARITY OF GRANULAR MATERIALS

In section 7.9 the discrete nature of the rotation of the constituent particles was discussed. It must be recalled that these measured rotations are the incremental rotations and include the contribution made by rolling, sliding and rigid body rotation. It was also emphasized that for better understanding of the stress-deformation behaviour in general and in obtaining the energy balance relationship in particular it is very essential to resolve these rotations as well as the linear displacements into their basic components due to three main factors mentioned above namely rolling, sliding and rigid body rotation. The underlying difficulties which actually inhibited such desirable resolution has already been pointed out in section 7.9.

Despite these difficulties, which are the pointers for the need of further research to overcome these obstacles, incremental total rotations give clear indication of the behaviour of test samples at various stages of their deformation history. By careful study of their variations in the test sample during deformation, it may be possible to give some plausible explanation of the similarity of stress-strain curves of two different test samples which were tested under identical test conditions excepting the surface properties particularly surface hardness and surface friction.

Critical examination of the rotation vectors of constituent particles will give an indication of group formation amongst the particles, at least, for the rotation of particles. These group formation can be recog-

nized in all the tests reported here, for comparison, see figures 7.35-7.38. It is observed that the average rotation (absolute) of particles increases generally with the deformation but in certain tests a reduction in average incremental rotation was also noticed, see Tables 7.3 & 7.4. With increase in deformation, the rotation behaviour appears to change, see Figures 7.169-7.174 and marked change in the incremental rotation pattern at large strains is apparent, particularly when the test samples have well passed the peak, Figure 7.174. These large rotations, their magnitude as well as their direction of rotation appear to be largely affected by the surface friction, compliance of the material and the shape of the constituent particles. This behaviour becomes apparent from the comparison of a typical plot of displacement-rotation plots, Figure 7.51 with that of PTFE.

The following conclusions can be drawn from the study of the statistical parameters, presented in Tables 7.1 to 7.4, histograms for various tests, such as Figures 7.42-7.48, and from the relevant displacement-rotation plots:-

- 1) Under the application of a deformation increment, the constituent particles rotate. These rotations do not necessarily take place about the coordinate axes. In fact the axis of rotation changes from particles to particle. Although in a plane strain test major rotations are expected to take place in the strain plane (Fig. 7.4), large ' θ ' rotations are not uncommon, see Figure 7.93.
- 2) At low strains, large rotations in isolation are observed in all the tests except in the tests on PTFE samples.
- 3) At very large strains, well past the peak tendency of large rotation of individual particles in all the tests is noticed, see Figures 7.84, 7.98 or 7.174.

7.12 PHI-ROTATION-DILATANCY RATE RELATIONSHIP

In the discussion of the test data presented so far, the components of deformation namely linear translation and rotations have been considered separately and no attention was given to their possible interdependence. In this section these components of deformation will be analysed.

Under the plane strain deformation conditions as used in this study, the component of strain in the σ_2 -directions must be zero and therefore the volumetric strain accompanying any axial deformation increment must take place on an average in the σ_1 and σ_3 direction i.e. in the plane normal to the σ_2 -stress. Thus the volumetric strain increment is the sum of the components of strain increment in the horizontal and vertical directions. Since the strains which contribute to volumetric strains are planar strains, the component of rotation, which might have a relationship with the volumetric strain and other components of strain increment, is probably the ϕ incremental rotation. In order to find a possible relationship between ϕ rotations and volumetric strains, graphs between ϕ and the dilatancy rate D have been plotted. Dilatancy rate 'D' was chosen as a variable instead of volumetric strain increment for two main reasons. Firstly it normalizes the volumetric strain increments and secondly to take advantage of the stress-dilatancy theory which relates dilatancy rate D with the principal stress ratio, if a relationship between ϕ - D was found. Dilatancy - incremental ϕ rotation plots for two typical materials are included here in Figures 7.75-7.78 and 7.165-7.168. In these plots only those ordered pairs of ϕ - D values are plotted which lie within the range of the graphs presented. Those values which are not plotted are given in Table B.2.

It is worth mentioning that the largest value of D for the plots presented here was 187.3 which occurred in the element 7 in test 2201 during its first deformation stage and the lowest value was -9.8 in the element 5 in test 2201 during the fourth deformation stage.

From the examination of the ϕ - D plots, Figures 7.75-7.78 and 7.165-7.168, it appears that perhaps there is no direct relationship between ϕ and D . However, it is not justified at this stage to accept that ϕ and D are not related unless it is confirmed by further experimental evidence. One of the main reasons for the failure to find the relationship between ϕ - D is the use of total rotation increment, instead of its component which actually contributes to the volume change. As mentioned in section 7.9, rigid body rotation is one of the basic components of the incremental total rotation. This component of rotation does not contribute to volume change. It is therefore, essential to isolate the rigid body rotation component before any attempt is made for finding a relationship between particle rotation and volumetric strain increment. Even dilatancy rate ' D ' may not be the correct parameter for such a relationship since it is calculated from computed values of strain components which are based on continuum approach. We have already seen in section 7.9 that the movement of particles are discrete and in reality continuum concept cannot be applied to granular material. It is therefore suggested that additional efforts are needed in finding new parameters for correctly depicting the behaviour of granular materials.

7.13 THE EXISTENCE OF ROLLER PARTICLES - A DISTINCT POSSIBILITY

Difficulties associated in splitting the rotations and displacements into its basic components, which could be attributed to sliding, rolling

and rigid body rotation, have been highlighted in section 7.4.1.2. The arguments presented here in favour of the existence of roller particles in a test sample are, of necessity, tentative in nature and will obviously require further confirmation by rigorous mathematical analysis and by further experimentation.

Before the observed data can be presented in support of the arguments, it must be emphasized that the test samples were subjected to incremental axial deformations which were arbitrarily selected. A possibility must, therefore, be recognized that during the application of a given deformation increment, rather large steps were used, the particle might have acted as a roller for part of its displacement history for the given deformation. Hence the contribution made by it as a roller is partly obscured by the displacement when it was not acting as a roller. This obviously creates a situation in which the compatibility condition for displacement of particles around the roller particle is probably difficult to satisfy since the geometry of the particle skeleton just before a particle starts acting as a roller and also precisely at the end of its rolling movement must be known. There seems to be no reason to believe that only one particle is likely to act as a roller or all the potential roller particles will start rolling at the same instant and all will stop rolling at the same time. In real granular material this deformation condition can never occur. Even if it is assumed that such a hypothetical situation can occur, it is difficult to predict when such an event is going to start and end. The other alternative available is to take the radiographs at very close intervals of deformation. This will obviously require very high accuracy of observation and computation. With the present state of X-ray photogrammetry, it is difficult to attain. Concerted efforts in the develop-

ment of X-ray technique, X-ray films and formulation of correct mathematical expression for the systematic errors are essential before the X-ray photogrammetry could be used for giving quantitative positional description of granular skeleton of representative particles at very close interval of deformation. It is interesting to note that the RMS errors of observation and computation do not vary very much for a given X-ray photogrammetry data acquisition system and they are independent of the magnitude of deformation to which an object to be radiographed, in our case granular test sample, is subjected. In order to avoid results which are excessively loaded with these (random) errors which blur the actual behaviour, large increments of axial deformation must be used. This was one of the reasons of using large axial deformation increments in this investigation. The isolated large rotations observed cannot be attributed to random observational errors, since all these rotations are much larger than the maximum absolute error of measurements given in Appendix A. For example, the rotation of particle no. 16 in Figure 7.53 is 0.193 rad., which is much larger than the maximum absolute error of 0.011 rad. In fact, in this investigation a particle is said to have rotated from its previous orientation only and only when its angle of rotation (absolute, i.e. without considering its sense of rotation) was greater than 0.011 rad.

Another argument against such large rotations of a few particles may be put forward. Since these rotations were occurring in isolation and amongst very large numbers of observations, one might intend to think that these rotations might be due to the blunders committed either at the data acquisition stage or at the data reduction stage. This presumption is totally unjustified on the following grounds. Firstly every effort was made to check at every stage of data reduction for any blunders and rejecting those observations which might be attributed to arise possibly

from blunders. Secondly even if one makes this hypothetical assumption, despite filtering and checking at every stage of computation, it is statistically improbable that the blunders should occur in making the observations of the same particle in each of the stereo-pairs taken at three successive stages of deformation. The rotations as well as the linear displacements of a particle were calculated by deducting its spatial coordinates and angular orientation relative to the fixed global coordinate axes before the application of deformation from the corresponding coordinates and angular orientation after the deformation. If at any stage a blunder was made, it would obviously show approximately equal and opposite large rotation in the subsequent stage of deformation if the particle was not acting as a roller particle in these two stages. The data obtained and presented here does not corroborate the above possibility. Blunders or gross errors as the reason for observing large rotations observed can, therefore, be rejected. The above argument clearly suggest that large isolated rotations and for that matter, any rotation greater than 0.011 rad. cannot be attributed to error.

Reference to Figures 7.51-7.54 reveals that in the first few deformation increments, large rotation of particles in isolation can be observed. Further it can be seen from these figures, generally different particles of a test sample showed large rotations at different stages of the deformation history of the sample. However, it is probable that a particle of the test sample may continue to show large rotation in two or more successive stages of deformation. It is worth mentioning that the particles, which showed large rotations in isolation, were generally randomly disposed in the test sample. It may, therefore, be justified to say that any large rotation of a particle observed in isolation is a

clear indication of the particle acting as a roller particle. For instance, Figure 7.52 shows that particle nos. 24, 67, 74 etc. are showing large rotation and are most probably acting as rollers. Presence of roller particles is evident in other tests as well, for example see Figures 7.93-7.99 for test results of ceramic sample, test no. 3201.

7.14 FORMATION OF ZONES OF DEFORMATION

From the incremental displacement data, which is presented in separate plots for each stage of the deformation increments applied to a test sample, e.g. Figures 7.93-7.98, it is difficult to recognize a pattern, if any, of movements of particles when the sample is continuously deformed. Recognition of the pattern of movement of particles and identification of any peculiarity developed in the pattern will help in dividing the sample in various zones according to their deformational behaviour. Flow diagrams such as Figures 7.123-7.124, which are the plots showing the projection of the flow path of individual particles on the XY and XZ planes, can advantageously be used for recognizing the zones of deformation at microscopic level. From these diagrams alone it is generally not possible to obtain a numerical quantity or a parameter by which the behaviour of one zone can be compared with that of the other. In such situations the information obtained from microscopic study of the sample can be supplemented by the numerical values of components of strain increment of the 'element' or of the zone.

In conventional soil tests, slip zones, if formed, can only be identified when they appear on the boundary of the test sample. And it is generally not known when these zones of discontinuities had developed inside the test sample.

Flow diagrams of constituent particles may be used to locate the slip zones, if formed, during any stage of deformation. Further it may be possible to observe the enlargement of thin zone or their disappearance during the deformation of test sample.

In order to support the above statement, let us examine the flow diagrams of a typical test, say test 4200. Fig. 7.123, which is the trace of movement of markers in the XY-plane, shows that during the third stage of deformation, there is a change in direction of movement of the particles marked by broken line in Fig. 7.123. Further examination of this figure reveals that another shear zone appears but this time on the left side of the sample, which is marked by full line on the same diagram, Figure 7.123. The former shear zone appeared when the sample did not reach its peak strength, see Fig. 6.10. The latter zone appeared when the sample nearly reached its peak strength but still on its pre-peak part of the stress-strain curve Fig. 6.10. Although more experimental evidence is necessary before one can say with confidence as to when the shear zones are formed in the test samples, the results of the test presented above show that the shear zones are formed inside the sample before the sample has reached its peak strength (maximum principal stress ratio) and are not the consequence of the delayed action of failure as claimed by Rowe (1962).

Another important information on the formation of zones of deformation can be extracted from the trace of the path of movement of particles on the XZ plane. Again considering the above experiment i.e. test no. 4200. Reference to Figure 7.124 reveals that there is a zone in which the particles are showing minimum deformation activity, even though the sample was monotonically compressed. From the study of the data presented in this figure it is not possible to say whether this zone can be

termed as dead zone in the true sense of the term. The map of the incremental shear strain distribution, Fig. 7.184 shows that shear strains in this zone are very nearly zero. However, the study of displacements, see Tables 7.5-7.7, and the average incremental rotation of the group of the particles approximately enclosed in this zone of minimum activity show that a certain amount of deformation activity does take place in this zone. It is, therefore, ^{correct} to call this zone as zone of minimum activities rather than dead zone.

Study of other flow diagrams of the tests on test samples made from spherical particles, such as glass, ceramic and polypropylene balls, reveals that the shear zones did not appear to form at any stage of deformation. It suggests that constituent particles did not show any preferred direction of movement and acted randomly during their deformation history. Formation of shear zone may, therefore, be the characteristic of the granular materials whose particle shapes are other than spherical. It must, however, be noted that these comments are based on the limited number of test results obtained from the plane strain compression tests on single sized particles of various materials, which were randomly packed to a single density. Further efforts are, therefore, needed to investigate the effect of particle size distribution and packing density of granular samples on the formation of slip zones.

7.15 BEHAVIOURAL TREND OF DEFORMATION OF GRANULAR SAMPLES

If it is required to find the trend in the deformation behaviour of a granular sample in various stages of its deformation history, some form of averaging technique is needed by which one can compare the local deformation behaviour of various zones under the given deformation or compare

the deformation behaviour of the same zone but under various stages of deformation. The components of strain such as volumetric strain and maximum shear strain, may be used for this purpose particularly when other suitable parameters based on particulate concept are not available.

One test from each of the five materials used in this study will now be analyzed for the possible behavioural trend of deformation. Further the search for this trend will be limited to the middle third portion of the plane in which the marker particles were initially placed so as to exclude the possible influence of the platen friction. Volumetric strain increments and the maximum shear strain increments were calculated for elements number 7 to 12 (Fig. B.1) and are presented in Figures 7.185-7.189 and in Figures 7.190-7.194, respectively. The five test materials used here may be divided into two main groups according to the similarity in the trend of strain behaviour observed from these figures. Figure 7.185 and Figure 7.188 indicate the similarity in the trend of volumetric strain increment pattern. And the Figures 7.190 and 7.193 show the similarity in the shear strain rate behaviour. These figures happen to pertain to two samples, namely of Gravel and PTFE, whose constituent particles were not spherical in shape. The patterns of strain increment distribution for the remaining three materials, i.e. of glass, ceramic and polypropylene, appear to be similar. Further examination of these diagrams will show that the pattern of the volumetric strain increments and maximum shear strain increment of test materials of the same group show minor difference between themselves perhaps due to the difference in the hardness and compliance of their constituent particles. For instance, comparison between the plots for glass (wet) sample test no. 2201 Figure 7.191 and for a soft material, namely, polypropylene sample, test no. 5201, Figure 7.194,

shows that the overall pattern is similar specially during the initial stages of deformation where the maximum shear strain increments observed in both test samples were nearly uniform. At large strain rates, the behaviour is different, perhaps it is modified due to the difference in hardness, and compliance of these two materials.

In summary, it can be said that the trend of the variation of internal shear strain and volumetric strain rates depend on the compliance and surface hardness, as well as on the shape of particle and thus, in turn, on the fabric of the sample. From these figures one more observation can be made namely the shear strain and volumetric strain increments for an element show random variations under successive deformation increments. The magnitude as well as the sign of these strain increments of some elements were observed to change. For instance, element 8 in Figure 7.192 shows negative volumetric strain increment at the end of second stage of deformation, but the same element, Figure 7.192, shows positive volumetric strain increment in the next deformation stage. This random behaviour and shifting of maximum or minimum strain rates from one element to another suggests that the particles of the deforming test sample group themselves together into quasi-rigid groups. Making and breaking of these groups appears to be a continuous process during the interval in which the sample is deformed. With this postulate it is possible to explain the changing nature of the strain rates of the various elements at various stages of deformation. Further these quasi-rigid groups appear to arrange themselves in the form of column-like structures, which carry the major portion of the applied forces. The changing nature of these column-like structures is indicated by observed oscillatory shift of the maxima and minima of the volumetric strain increment curves, for example see Figure 7.186. These

oscillatory shifts are more pronounced in the test samples whose constituent particles are comparatively rigid, and spherical in shape e.g. glass, Fig. 7.186, ceramic, Figure 7.187. Similar behaviour, but not as pronounced as for the above test materials, is noticeable in the test results of PTFE Test samples whose constituent particles are relatively soft; cuboidal in shape and exhibit very low coefficient of friction, see Figure 7.188. The response of gravel to volumetric strain increments is not very different from that of PTFE.

From this discussion, it is possible to suggest that in the case of granular sample whose particles are spheres or very nearly spherical in shape, the behavioural trend of deformation seems to depend on compliance and surface hardness of the particles. On the other hand, deformation behaviour of test samples, whose constituent particles are of irregular shapes, appears to be dictated by the fabric. The compliance of the material, possibly does not influence the trend of deformation appreciably.

7.16 THE RELEVANCE OF PARTICLE SHAPE AND SURFACE FRICTION ON DEFORMATION BEHAVIOUR OF GRANULAR SAMPLES

In the current stress-strain theories of granular soils, particularly in the stress-dilatancy theory, surface friction of constituent particles is assumed to play a major role. It is, therefore, necessary to investigate the relevance of interparticle friction on the deformation behaviour of granular materials. Instead of discussing all the test results of this study in this context, the necessary and important point can be brought out by discussing the results of the tests of two materials which represent the extreme limits of surface friction of the test materials used and the particle shape used in this investigation. The discussion will therefore be limited to saturated

glass ball samples and dry PTFE chunk samples. The coefficient of interparticle friction of glass balls (submerged under water) and of PTFE was experimentally obtained, see Chapter 3 and was found to be in the range of 0.7-0.9 & 0.04-0.9 resp. The shape of glass balls is approximately spherical and that of PTFE is cuboidal. Glass balls were very hard and brittle, whereas PTFE chunks were soft and visco-elastic. Therefore glass represented one extreme limit of surface friction and hardness whereas PTFE chunks represented other end of these limits.

Both of these materials were tested under plane stress compression test conditions and their testing conditions were more or less similar. Their stress-strain test data is presented in chapter 6, see Figures 6.7 and 6.10 for glass and PTFE test samples respectively. Reference to these Figures shows that the stress-strain curves for these two tests are in general similar and the value of maximum angle of internal friction was found to be 31.0° for glass and 28.7° for PTFE. The difference between the values of ϕ_{\max} is not large despite more than 10 fold difference in their coefficients of surface friction. One is naturally surprised to find the similarity in the stress-deformation behaviour but not in their surface frictional properties. And specially when this behaviour of two materials is in conflict with the existing stress-dilatancy theory. In order to seek plausible reasons of such a behaviour, the deformation mechanism assumed in this theory needs re-evaluation. It is necessary to examine critically the displacement-rotational behaviour of these two samples under axial deformation which was monotonically increased. It can be seen from the plots, Figures 7.51-7.57, for the test on glass particles (wet) that isolated large rotation of particles occurs whereas in the case of PTFE, Figures 7.109-7.115, these did not appear during the early part of the deformation of the test sample. These isolated large rotations continue to occur in the glass test sample till the peak of the stress-strain curve was crossed. At very large strains, the particles of both the tests show large rotations.

Histograms for the $d\phi$ and $d\theta$ rotations for the test on saturated glass sample, test no. 2201, Figures 7.58-7.64, show the history of development and frequency distribution of rotation as the deformation of the sample was progressively increased. These Figures particularly Figures 7.58-7.61 indicate that the isolated rotations do occur and these rotations are not necessarily occurring in the same direction. Further with deformation the number of marker particles participating in rotational activity increases. At large strains, well past the peak, constituent particles develop large irregular rotations. The irregularity in rotation can easily be confirmed by looking at the shape of the relevant histogram, for example see Figure 7.57. From the study of the histograms of incremental rotations and of the displacement-rotation plots of the same stage of deformation of a test such as Figures 7.44-7.50 and Figures 7.51-7.57, we can infer that the mechanism of deformation is not of sliding only.

The rate of increase of PTFE particles, in test no. 4200, showing rotations more than $\pm .01$ radian did not increase at the same rate as that of the particles of the glass sample (saturated) in test no. 2201 under approximately similar test conditions, compare Figures 7.116-7.122 with Figures 7.51-7.57. In the case of PTFE samples, examination of rotational histograms, Figures 7.116-7.122, in conjunction with the corresponding displacement-rotation plots, Figures 7.109-7.115, suggests that majority of PTFE particles appear to slide and a small number of particles rotate, particularly in the pre-peak deformation stages; perhaps the shape and physical properties of the constituent particles, e.g. surface hardness and compliance, inhibit rotation of particles.

7.17 Deformation Mechanism of Particulate Materials Including Cohesionless Soils

It is generally observed that the angle of internal friction of two different particulate materials possessing different physical properties give very similar coefficient of internal friction when tested under similar test conditions including the shape, particle size distribution and particle packing. In this study, plane strain tests (drained) were carried out on a wide variety of materials ranging from high frictional, brittle material, i.e. glass (wet) to very low frictional, visco-elastic material, namely PTFE. Astonishingly similar values of coefficient of internal friction and stress-strain behaviour, in general, were obtained from most of the tests presented in this study. Leussink and Wittke (1963) reported the test results on balls of two different materials: glass and steel and both having different values of coefficient of surface friction. They arranged the particles of these two materials in regular arrays so as to obtain same fabric and degree of packing. In other words the level of interlocking in both the test was practically similar. Wittke (1963) summarised the results of the above tests as: "..... We found that the absolute value of the shearing strength of a regular packing of steel balls was almost the same as that for the corresponding arrangement piled out of glass balls, though glass has a higher angle of friction than steel." Although in the present series of tests reported here particles were randomly packed, still similar behaviour and results were obtained in most of the tests, which might suggest that surface friction does not appear to play a major role in the overall behaviour of granular samples.

At first sight these results surprise a few researchers, because it is generally believed that the transferrance of load takes place at the points

of contact and the relative movement of such contacts must involve physical friction between the contact surfaces. In other words, sliding between the constituent particles and interlocking are assumed to be the major factors which control the deformation behaviour of granular materials. With this as the assumed deformation mechanism and for a given degree of interlocking, it is natural to expect large angle of internal friction when the surface friction of constituent particles is large and low when it is low. Obviously this deformation mechanism cannot explain the above observed behaviour of granular materials. It is, therefore, essential to find some other plausible deformation mechanism which could explain the experimentally observed results of this study and that published by other researchers.

The deformation mechanism of granular mass, with particular reference to the test materials used and test conditions imposed in this investigation, can be explained by proper combination of two basic mechanisms originating from two different sources of a deforming particulate mass. The first source is in the geometric configuration of the packing of the constituent particles or fabric of the granular mass. This depends upon the particle size, shape and their size distribution, and also on the disposition or packing of these particles in the given medium forming a fabric. It is already shown in this chapter that if the initial fabric of different test samples, whose constituent particles possess different surface frictional properties is similar than their stress, deformation behaviour is not totally different from each other, see Chapter 6 and Leussink and Wittke (1963). If, however, some particles are used to form test samples but arranged in different fabric configurations and keeping the same overall porosity of the test samples, the stress deformation behaviour must be different and must reflect the effect of the initial fabric. Arthur and Menzies (1972) have confirmed this and have clearly shown the

importance of initial fabric on stress-deformation behaviour. The second mechanism, which supplements the above, arises from the physical properties forming the particles, particularly surface hardness and compliance of the constituent particles of the medium.

The deformation mechanism, which may be considered as the combination of these two mechanisms, can be explained with the help of an analogy between a structure having number of redundant members with some open joints and the granular skeleton of a particulate mass. The particles of granular fabric may, therefore, be thought as if these were the members of an analogous structure with complex arrangement of its members. The stability of this structure, which is of course, very complex, does not only depend on the disposition and the strength of its joints - the weakest points of the structure - created by the combination of normal force and frictional resistance at the contacts but also on the degree of redundancy. This depends on the geometric configuration of the members of the structure (fabric in case of granular sample) and on other physical properties of the structural members (constituent particles in case of the granular sample) which influence response to deformation. Given the same initial granular skeleton of two test materials, and that the particles of one material can deform more readily than that of the other, under similar test conditions the test sample composed of the softer material will exhibit larger values of coefficient of internal friction than that of the harder material. In some cases with low friction soft material, the angle of internal friction obtained is greater than its surface friction. This increase over the coefficient of friction may be due to the deformation of certain member particles under load which will remove any geometric imperfection initially present in the granular fabric. This will obviously increase the stability of the fabric, which will in turn, increase its strength

With the help of the two mechanisms mentioned above, it is possible to explain why the surprisingly high angle of internal friction of over 28.0° was obtained for PTFE samples which has a very low surface friction angle of about $\phi_\mu = 4^\circ-7^\circ$. Skinner (1975) reports the angle of internal friction of lead shot of 36° and its angle of surface friction varying between 4° to 6° . The plausible explanation of such high angles of internal friction can be given by the above mechanism.

On the other hand, when the physical properties of the particles are such that the contacts between particles do not deform appreciably under the given loading conditions, the overall deformation behaviour will be mainly governed by the fabric alone and friction will play a minor role. It may be due to this reason that the angle of internal friction of glass and steel balls, as reported by Leussink and Wittke (ibid), was similar since their packing and test conditions were identical.

In section 7.15, it was suggested that constituent particles of deforming medium move in groups under the application of shear deformation. Although it is not possible to identify physically the existence of particles in distinct groups and consequently their movement during deformation history of the test sample, the presence of potential roller particles, shown in section 7.13, phenomenologically proves the possibility of the existence of particle groups. Also the pattern of rotation of particles at any stage of deformation, for example see Figure 7.115, suggests that some of the particles might have moved in groups during the given deformation stage. Moreover, the test data, on the two dimensional tests on spheres, discs and cylinders presented by various researchers, show that the particles arrange themselves in quasi-rigid groups and they not

necessarily remain in the same group during the deformation history of the test samples. Oda and Konishi (1974, b), Drescher and de Josselin de Jong (1972), Mogami (1965, 1969) have presented photographic evidence which supports the above contention. Since these 2-dimensional tests represent plane strain deformation conditions, it is justified to suggest that in the 3-dimensional test samples, when deformed under plane strain test conditions, the constituent particles are likely to move in quasi-rigid groups. However, these groups of particles need not necessarily lie in a plane. During the deformation movement these groups may change their orientation either by losing old members of the group or by adding new members to themselves from the adjoining groups or modify their orientation by rotating and by internally adjusting the orientation of their members. By doing so these groups adjust themselves to the prevailing deformation condition.

As suggested in section 7.15, there is a possibility that the load transfer from one loading face to another might take place through a few randomly selected columnar structures. These column-like structure may be latticed three dimensional complex structures formed by the quasi-rigid group of particles mentioned above. Due to our inability to observe the existence of three-dimensional column structure, once again we can take the advantage of the published test result on 2-dimensional array, for example see Oda and Konishi (1974, a). Drescher and de Josselin de Jong (1972). Reference to series of photographs, which were taken at various stages of deformation to which photo-elastic cylinders were subjected, published by Oda and Konishi clearly show the presence of columnar structure at every stage of deformation. From the deformation behavioural trend, discussed in section 7.15, and from the data of 2-dimensional tests it can be concluded, at least tentatively, that the major portion of load

is transferred through a few relatively rigid column-like structure developed in the fabric due to the application of shear deformation.

The stability of these column-like structures, which are expected to fail mostly by buckling, will obviously depend upon the stability of constituent members and upon the arrangement of particles which are laterally supporting it. The stability of the group of particles, which are acting as the member of the structure, generally depends on the packing of its member particles and also on the interparticle friction.

In the deformation conditions used in this investigation, the test sample was exposed to loading for the first time and deformation was monotonically increased, groups of particles or the members of the complex column-like structure were probably continuously changing their orientation. This is reflected by the occurrence of rotation of constituent particles and also by rolling of a few particles.

As mentioned earlier, the measurement for deformation parameters were made at relatively large intervals of deformation, it was not possible to present visual evidence in support of presence of quasi-rigid groups and column-like structure. Additional experimental work is therefore warranted. Nevertheless the evidence presented in this chapter clearly shows the important and major role played by the fabric of the deforming medium rather than by interparticle friction which is generally accepted at the present.

7.17.1 Deformation mechanism and observed stress-instability

The deviatoric-stress-instability was observed in all the plane strain compressive tests reported in this study. The continuous load-displacement plots for three typical tests, see Figures 6.1-6.3, show that stress-instability occurs irrespective of the surface frictional characteristics of the constituent particles of test sample. From these figures it can be seen that the amplitude of the stress variation is more pronounced in brittle and harder materials, i.e. glass than in the softer material namely PTFE. If the existence of column-like structure is accepted, observed stress-instability can be considered as the result of continuous making and breaking of the columnar-structures. Further experimental investigation is necessary before one can pin point the reasons for the occurrence of this phenomena.

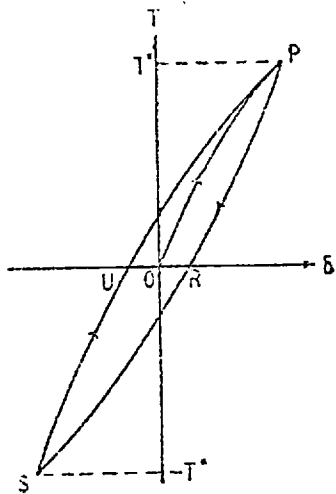
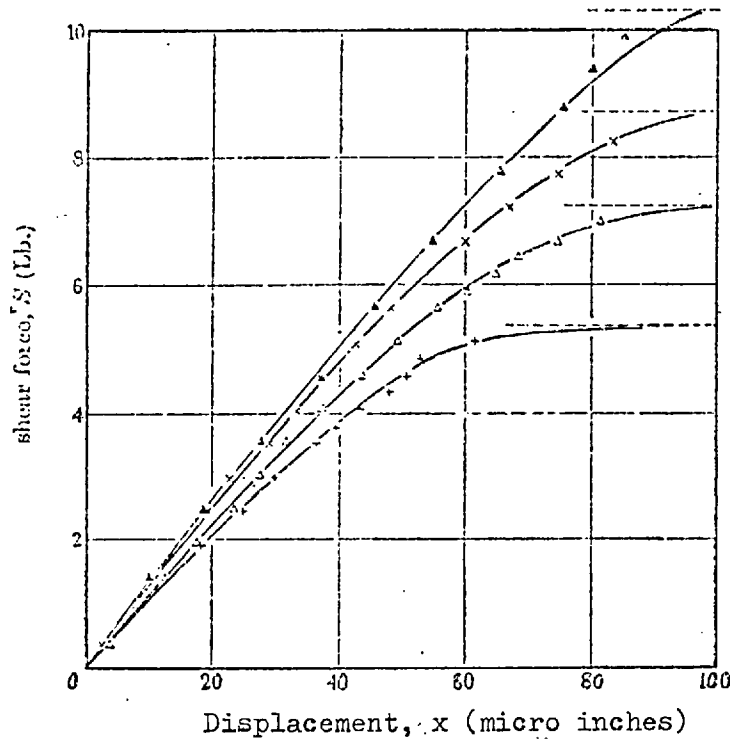
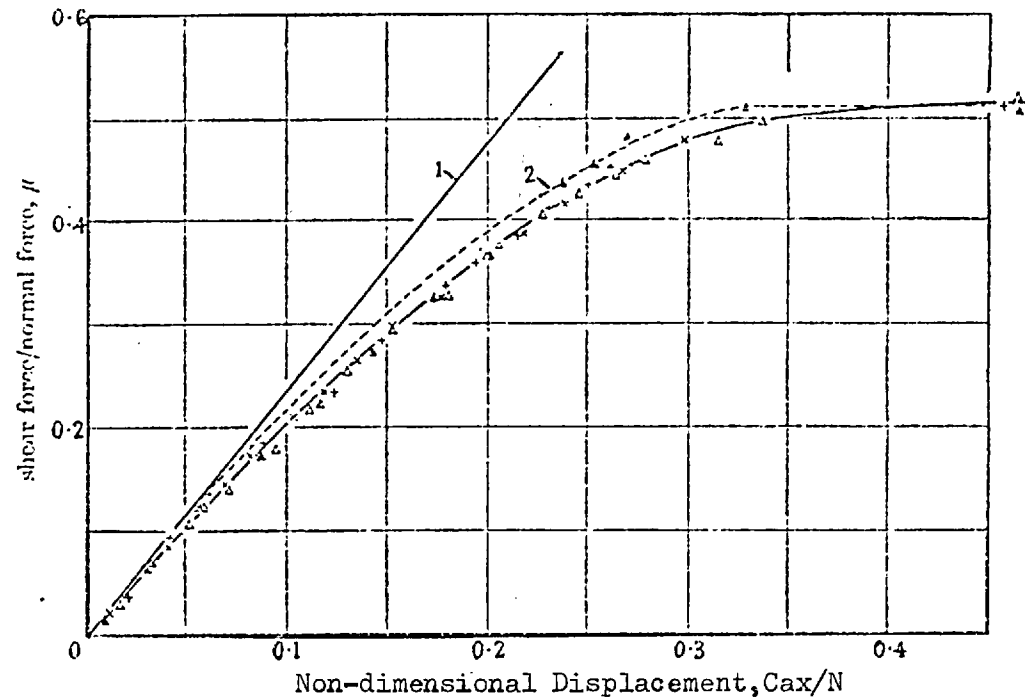


FIG. 7.1 Theoretical hysteresis loop due to oscillating tangential force.

(After, Mindlin & Deresiewicz, 1953)



(a)

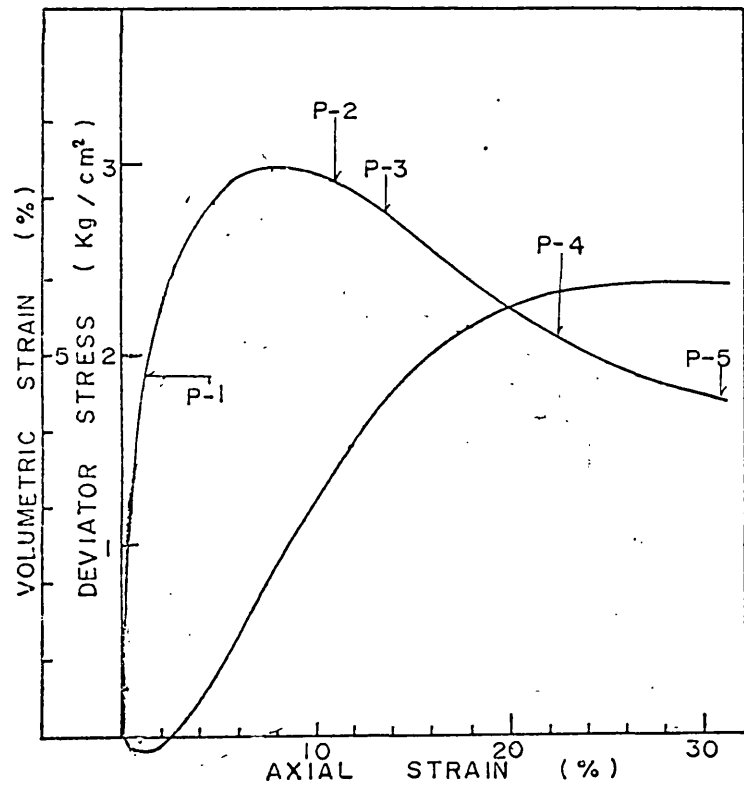


(b)

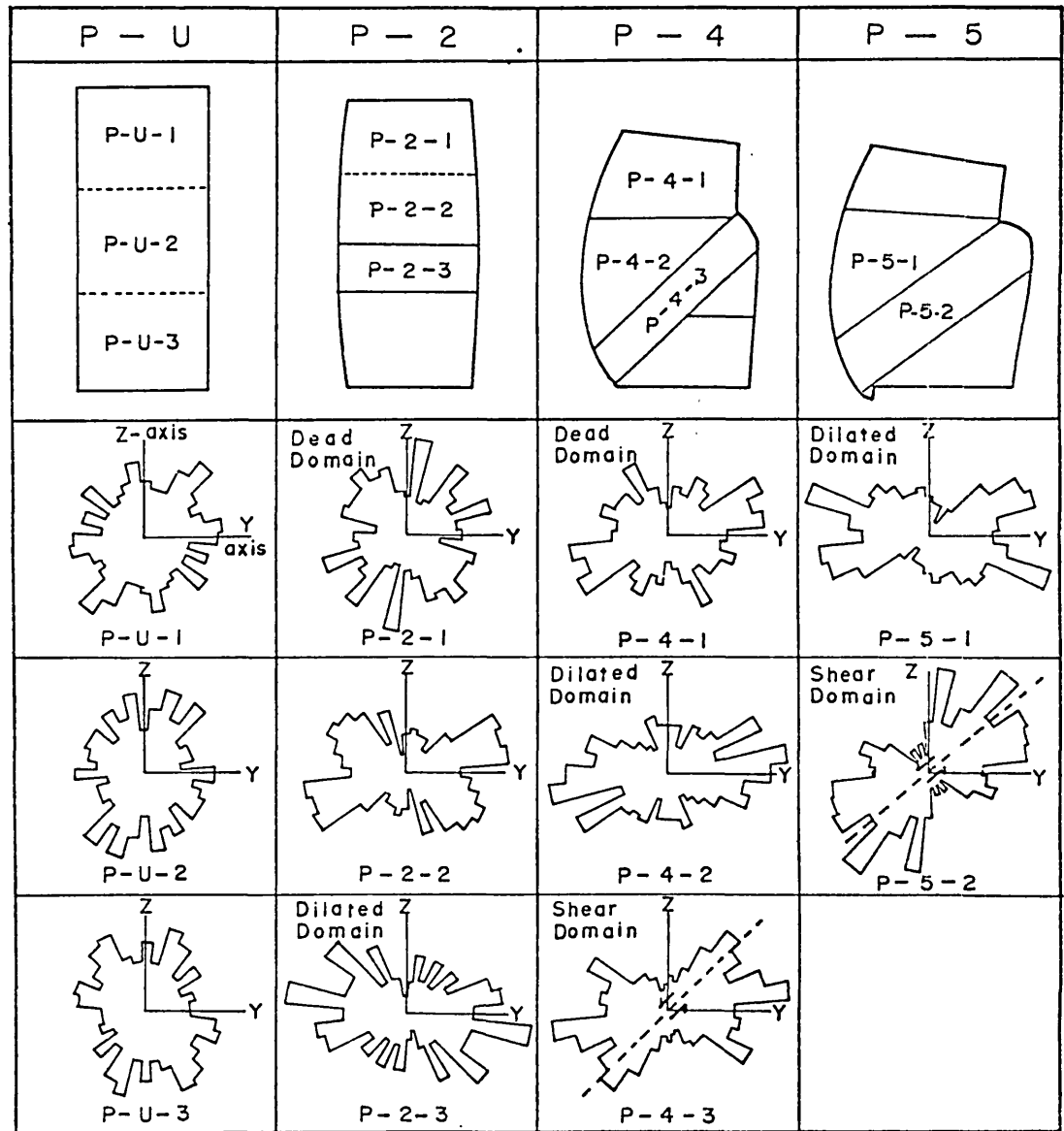
FIG 7.2 a) Static force-displacement tests. These experiments at varying normal loads were carried out without disturbing the points of contact. $D = 0.375\text{in}$; $N = 10.5(+)$, $13.9(-)$, $17.2(x)$ and $20.5(-)$ lb.

b) Non-dimensional correlation of results of figure (a). Broken curve shows Mindlin's theoretical relationship given by equation (2) for $\mu=0.51$. The elastic line is given by equation (1)

(After, Johnson, 1955)



a) STRESS-STRAIN-VOLUMETRIC STRAIN CURVE FOR A SERIES OF EXPERIMENTS OF A SAND



b) APPARENT DIMENSIONAL ORIENTATION OF GRAINS IN THE V-SECTION OF SPECIMENS COMPACTED BY THE PLUNGING METHOD

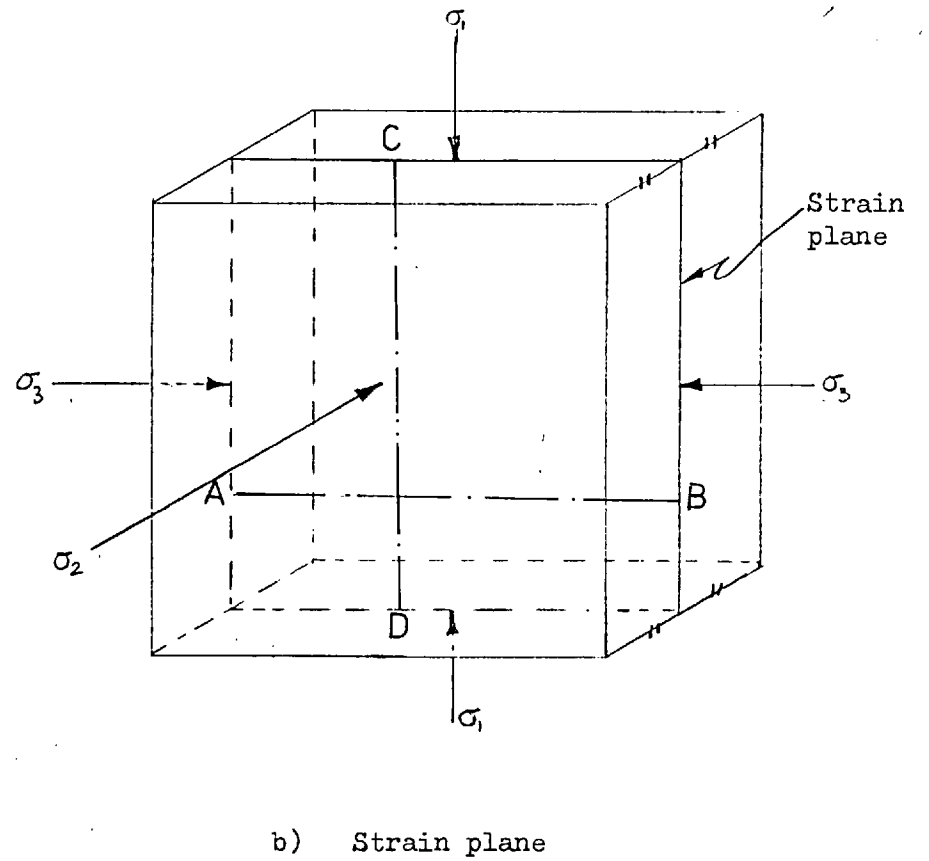
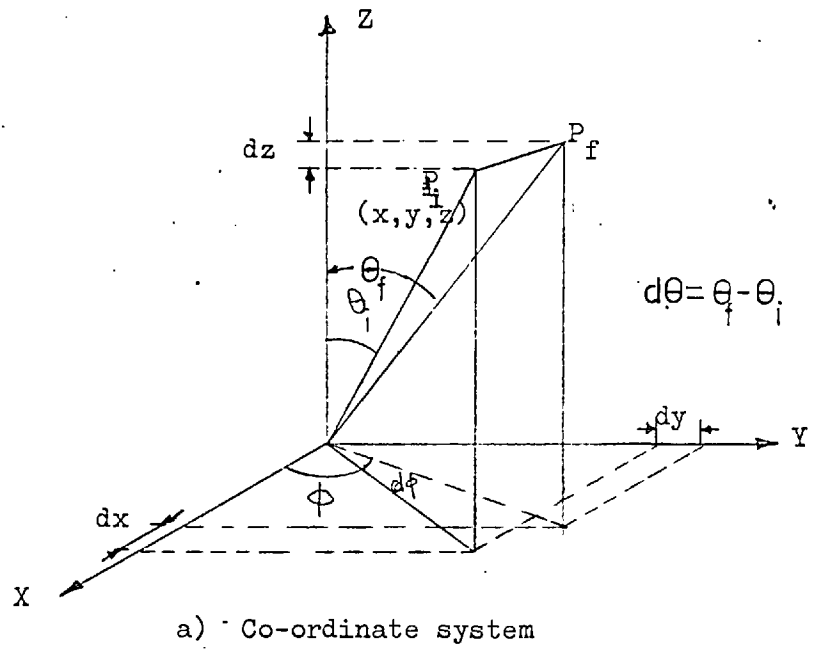
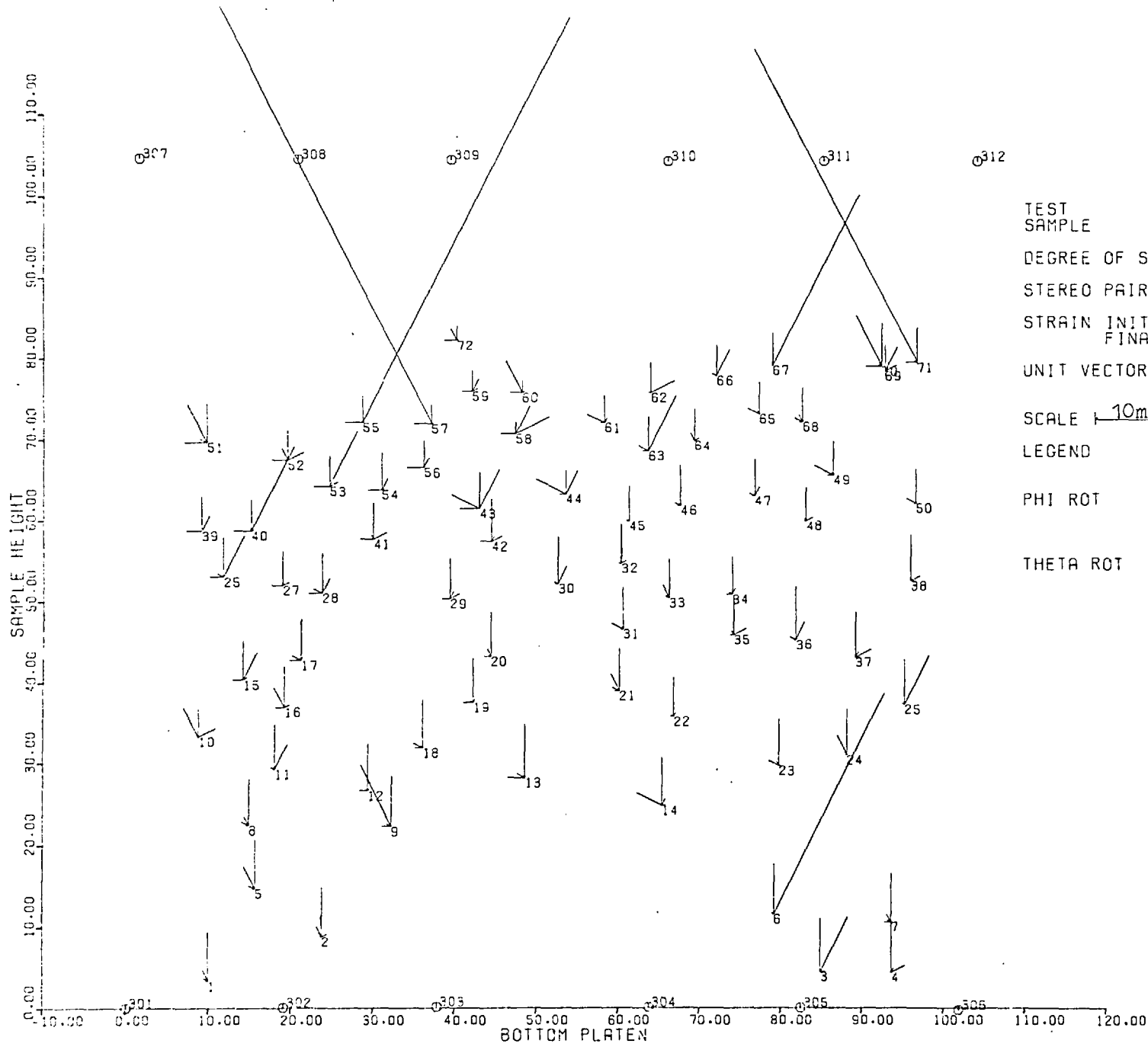


Fig. 7.4



TEST SAMPLE
 DEGREE OF SAT.
 STEREO PAIR NO.
 STRAIN INITIAL
 FINAL
 UNIT VECTOR DISP.
 SCALE 10mm
 LEGEND
 PHI ROT
 THETA ROT

1200/1
 PLANE STRAIN (DRAINED)
 GRAVEL (ROTUND)
 DRY
 FIRST 1
 FINAL 2
 0.0
 0.889
 HOR. X 1mm
 VER. Y 1rad

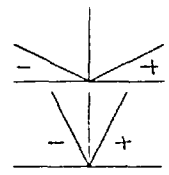
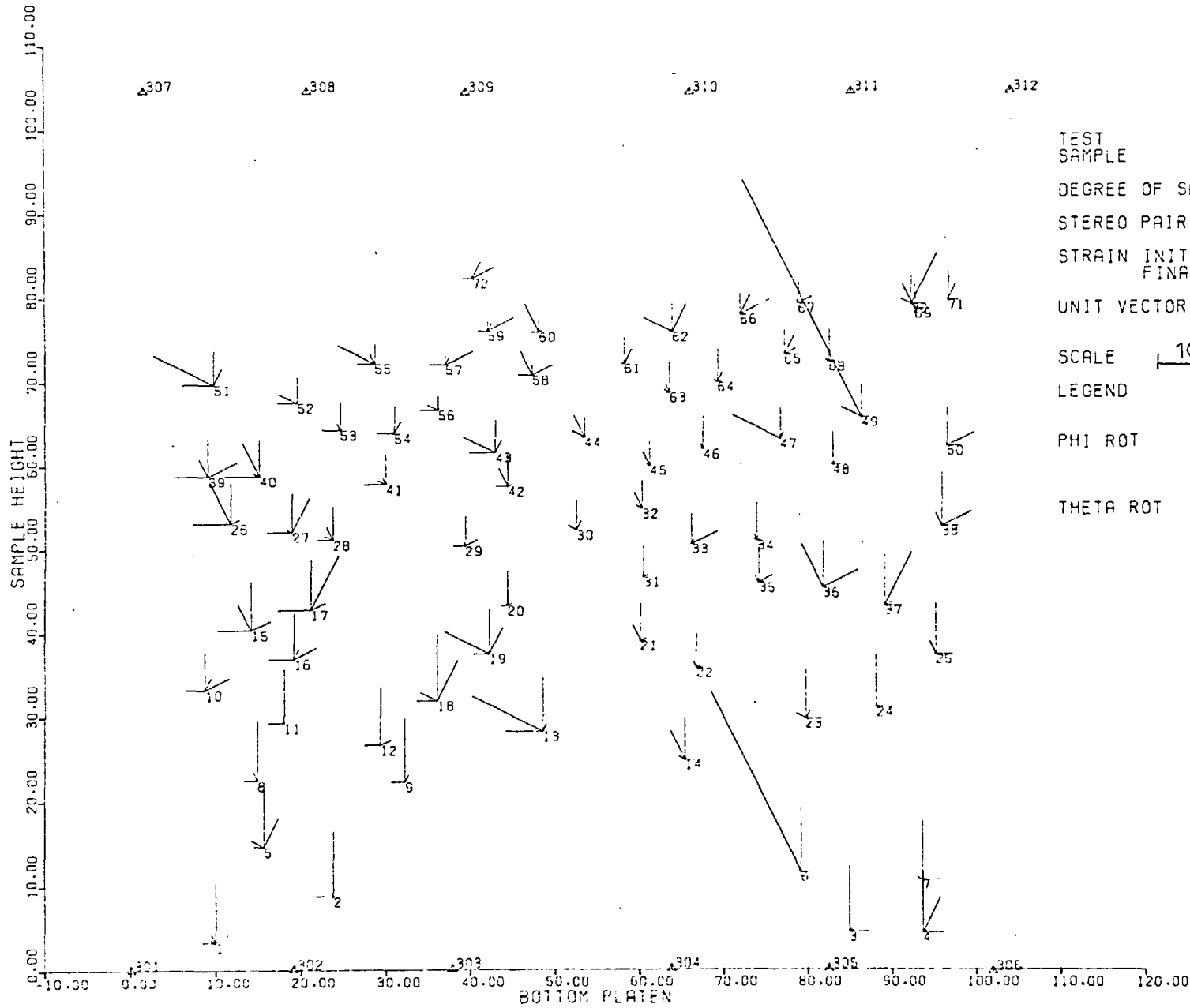


FIG. 7.5 DISPLACEMENT - ROTATION FIELD OF MARKERS IN XY PLANE



TEST SAMPLE 1200/2
 PLANE STRAIN (DRAINED)
 GRAVEL (ROTUND)

DEGREE OF SAT. DRY

STEREO PAIR NO. FIRST 2
 FINAL 3

STRAIN INITIAL 0.889
 FINAL 2.799

UNIT VECTOR DISP. HGR. X
 VER. Y

SCALE 10mm ROT. 2mm
 .2rad

LEGEND
 PHI ROT
 THETA ROT

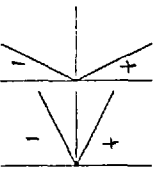
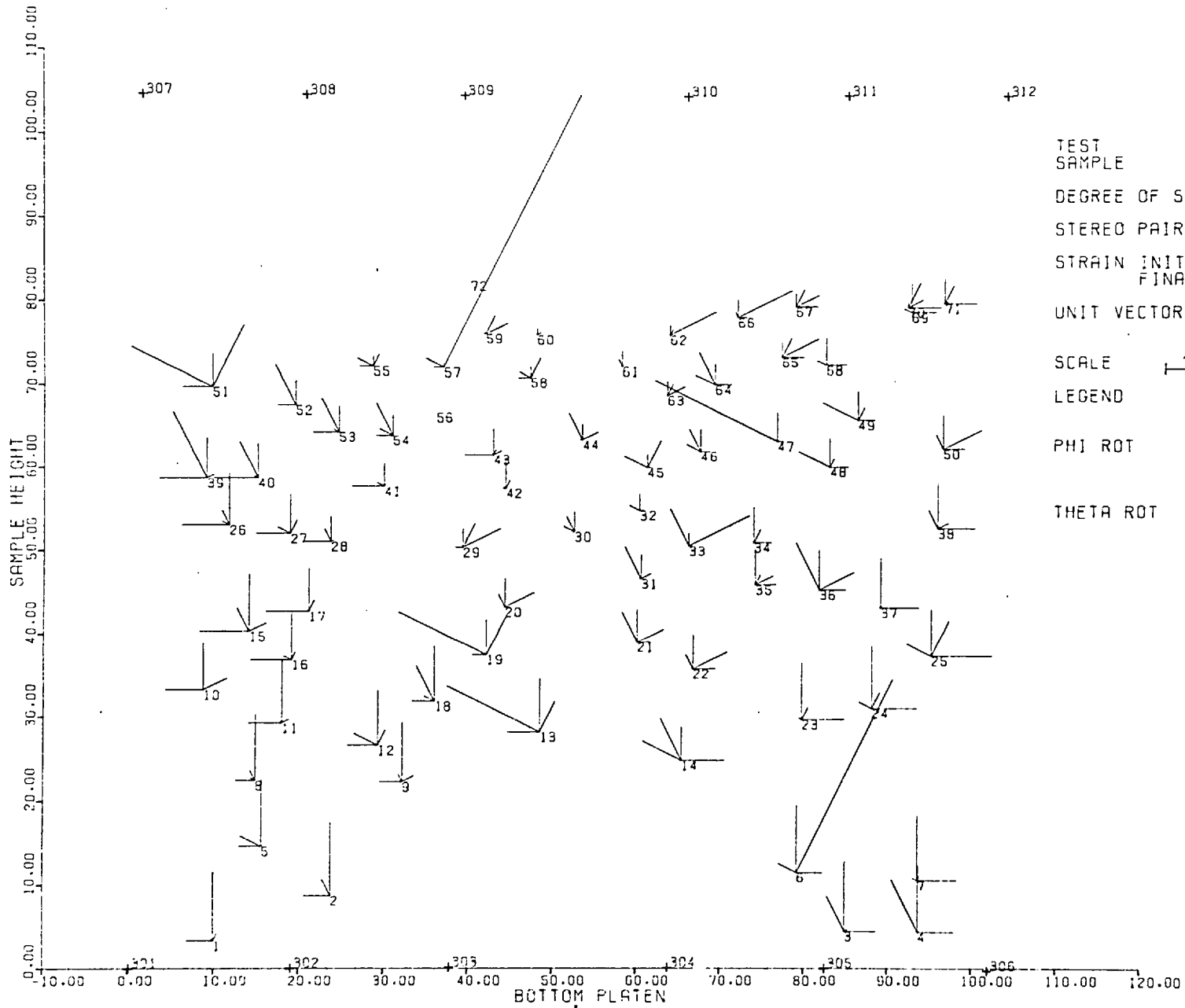
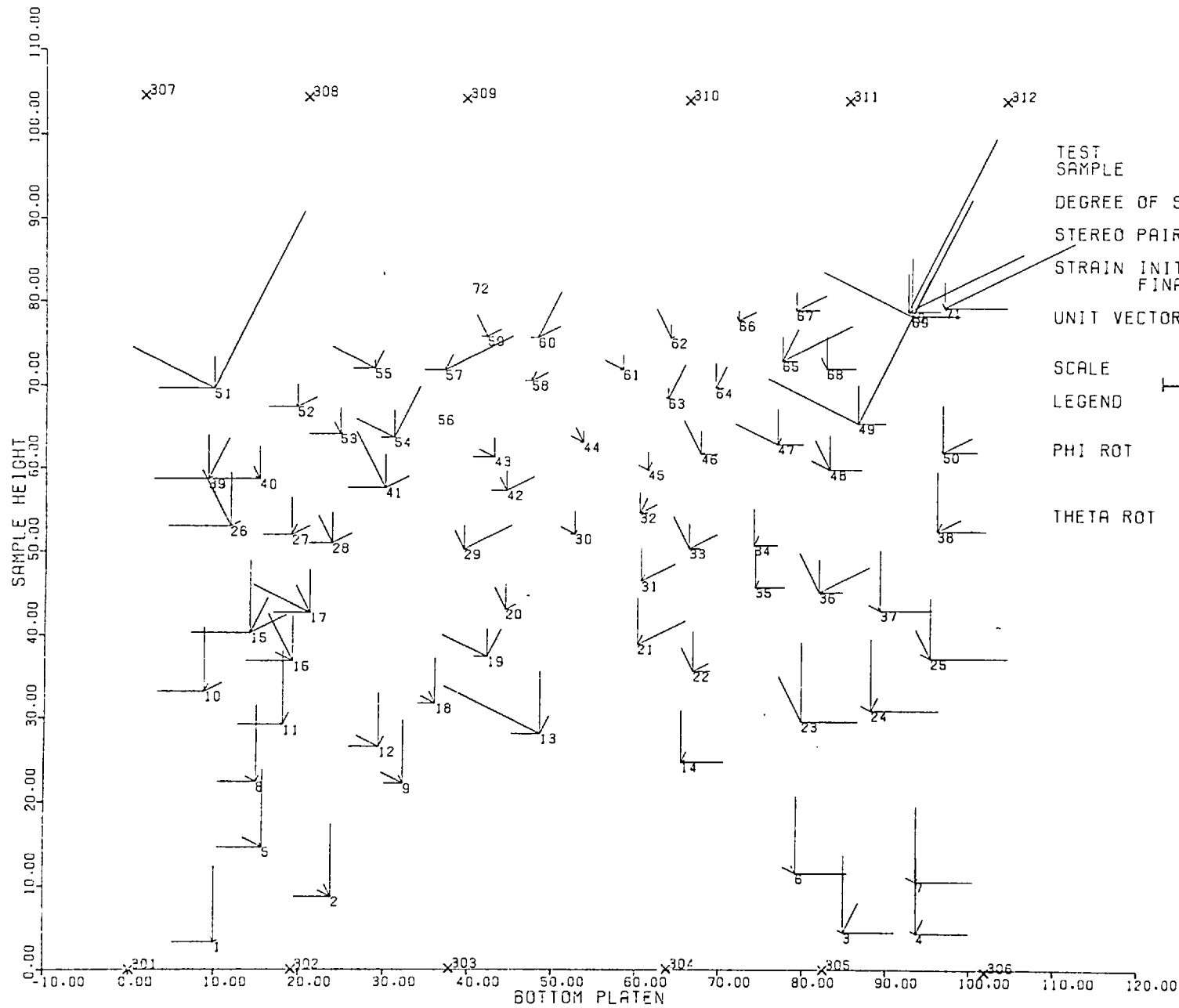


FIG 7.6 DISPLACEMENT - ROTATION FIELD OF MARKERS IN XY PLANE



TEST SAMPLE 1200/3
 PLANE STRAIN (DRAINED)
 GRAVEL (ROTUND)
 DEGREE OF SAT. DRY
 STEREO PAIR NO. FIRST 3
 FINAL 4
 STRAIN INITIAL 2.799
 FINAL 4.879
 UNIT VECTOR DISP. HOR. X 2mm
 VER. Y 2mm
 ROT. 0.2rad
 SCALE 10mm
 LEGEND
 PHI ROT
 THETA ROT

FIG 7.7 DISPLACEMENT - ROTATION FIELD OF MARKERS IN XY PLANE



1200/4
 PLANE STRAIN (DRAINED)
 GRAVEL (ROTUND)

TEST SAMPLE
 DEGREE OF SAT. DRY
 STEREO PAIR NO. FIRST 4
 FINAL 5
 STRAIN INITIAL 4.879
 FINAL 7.206

UNIT VECTOR DISP. ROT.
 SCALE 10mm
 LEGEND
 PHI ROT
 THETA ROT

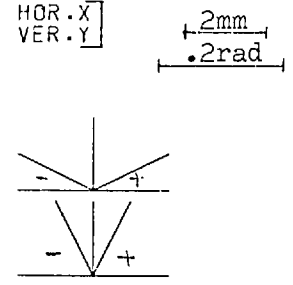
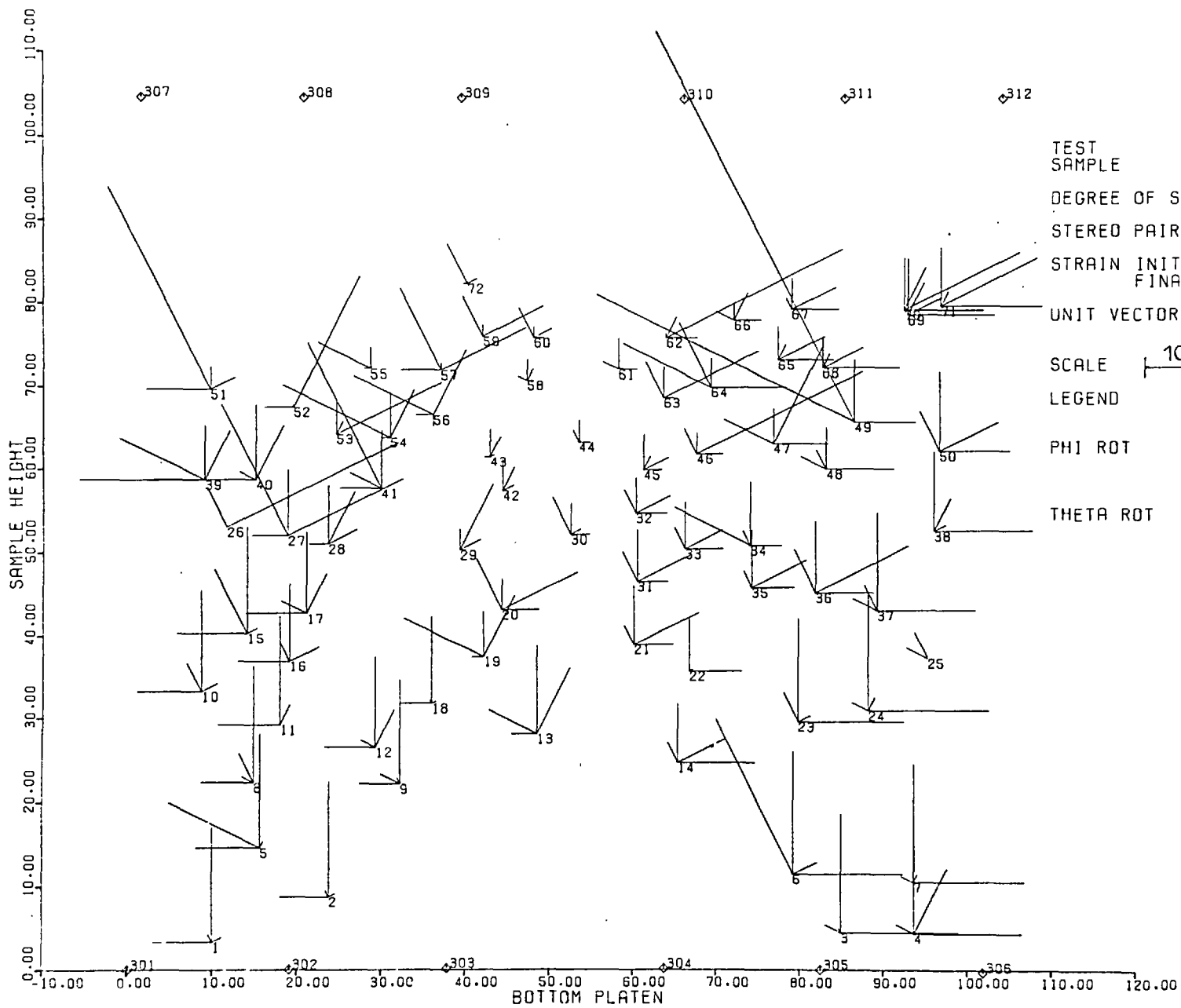


FIG 7.8 DISPLACEMENT - ROTATION FIELD OF MARKERS IN XY PLANE



TEST SAMPLE
 DEGREE OF SAT.
 STEREO PAIR NO.
 STRAIN INITIAL
 STRAIN FINAL
 UNIT VECTOR DISP.
 SCALE 10mm ROT.
 LEGEND
 PHI ROT
 THETA ROT

1200/5
 PLANE STRAIN (DRAINED,
 GRAVEL (ROTUND))

DRY

FIRST 5
 FINAL 6
 7.206
 10.715

HOR. X] 2mm
 VER. Y] .2rad

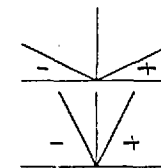
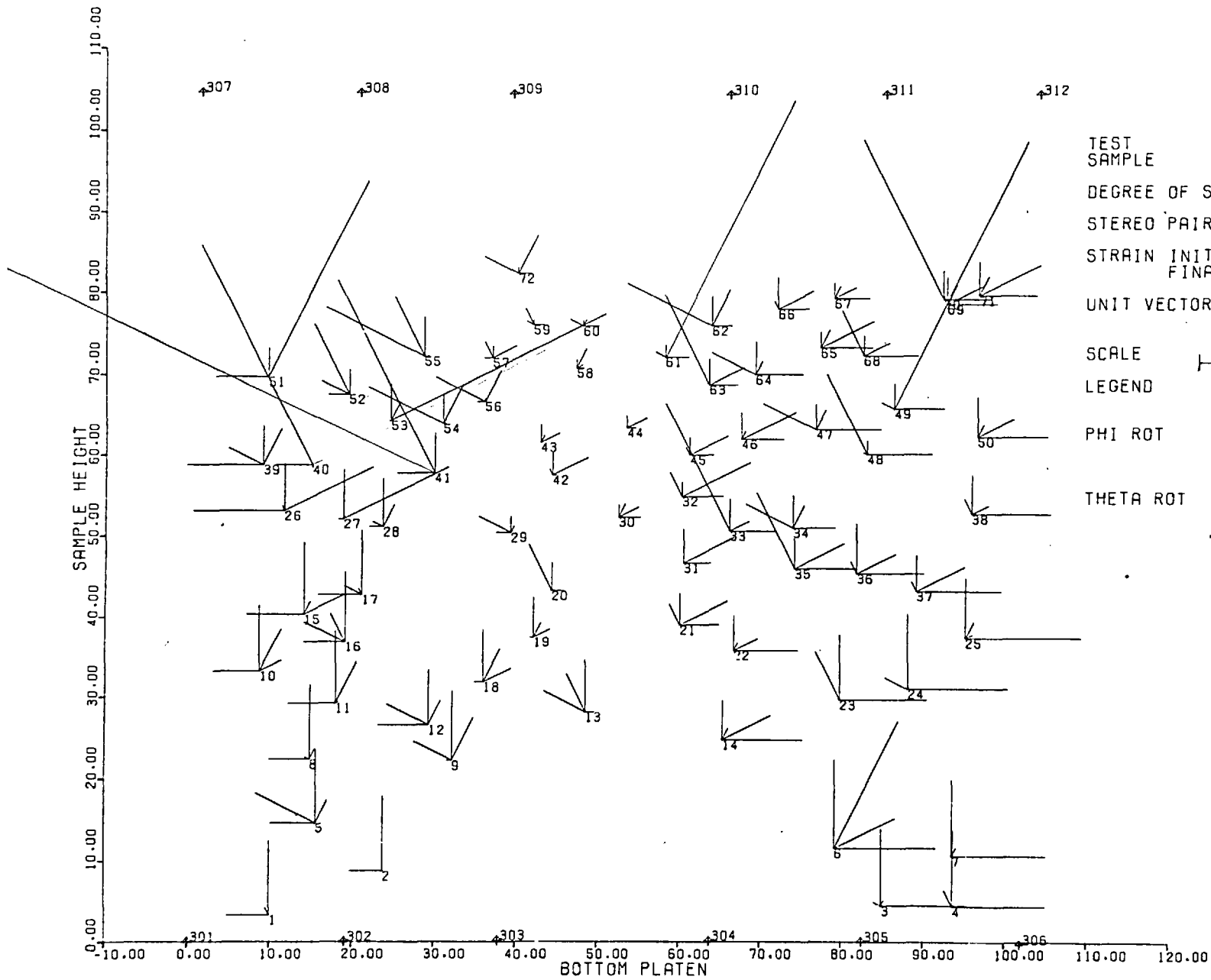


FIG 7.9

DISPLACEMENT - ROTATION FIELD OF MARKERS IN XY PLANE



TEST
SAMPLE

DEGREE OF SAT.

STEREO PAIR NO.

STRAIN INITIAL
FINAL

UNIT VECTOR DISP.

SCALE ROT.
10mm

LEGEND

PHI ROT

THETA ROT

1200/6
PLANE STRAIN (DRAINED)
GRAVEL (ROTUND)

DRY

FIRST 6

FINAL 7

10.715

14.814

HDR.X] 3mm
VER.Y] .2rad

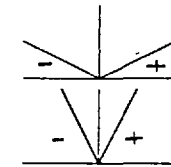


FIG 7.10 DISPLACEMENT - ROTATION FIELD OF MARKERS IN XY PLANE

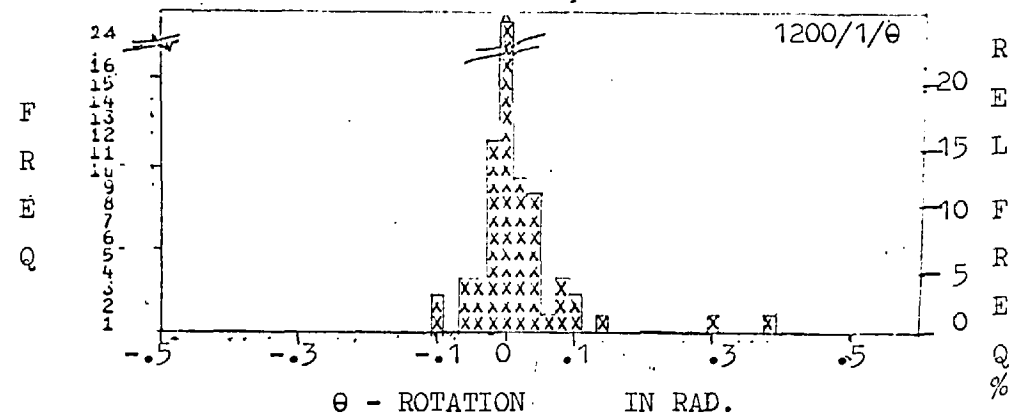
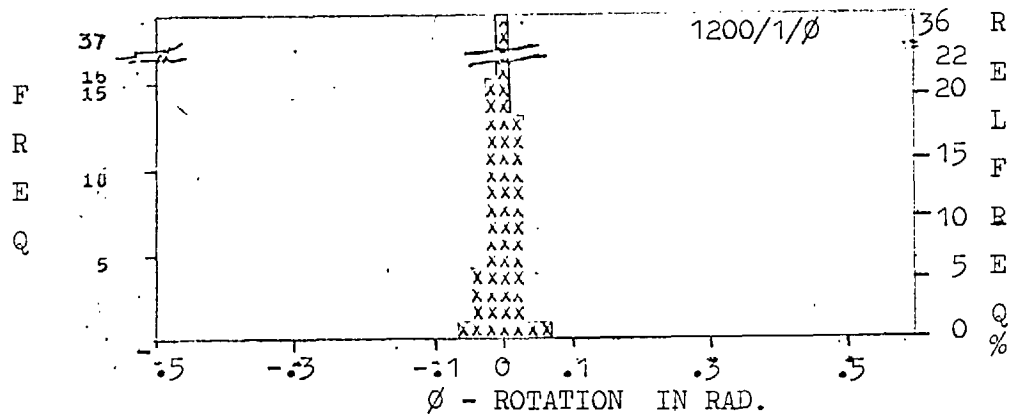


FIG. 7.11

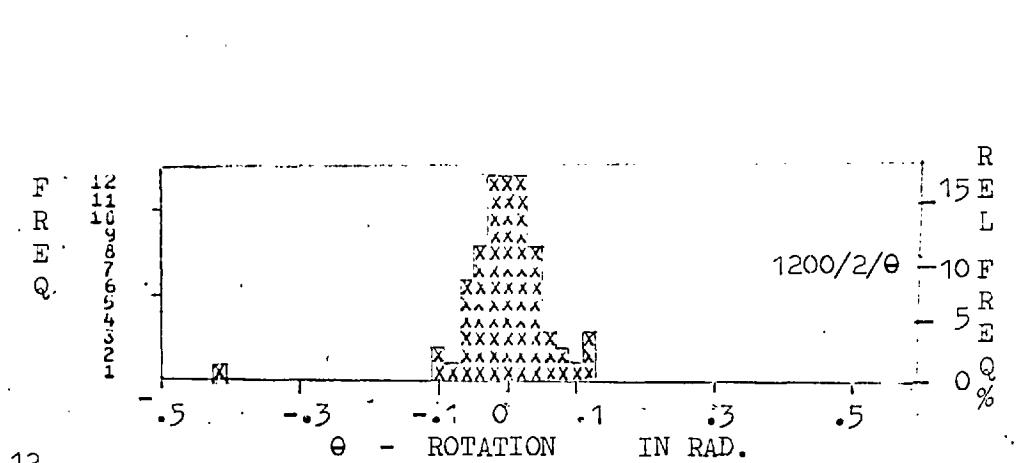
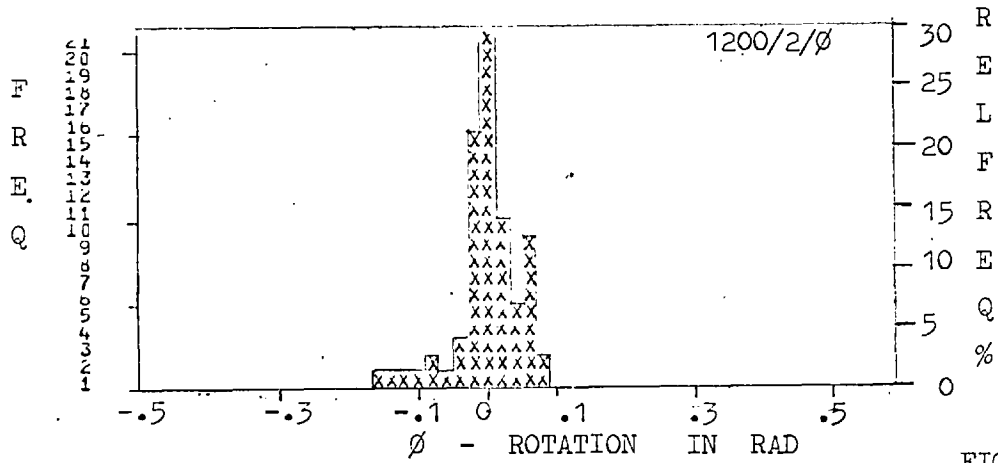


FIG. 7.12

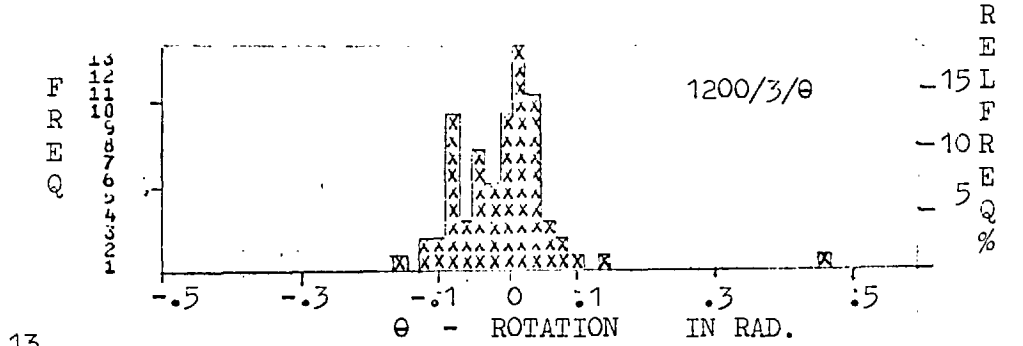
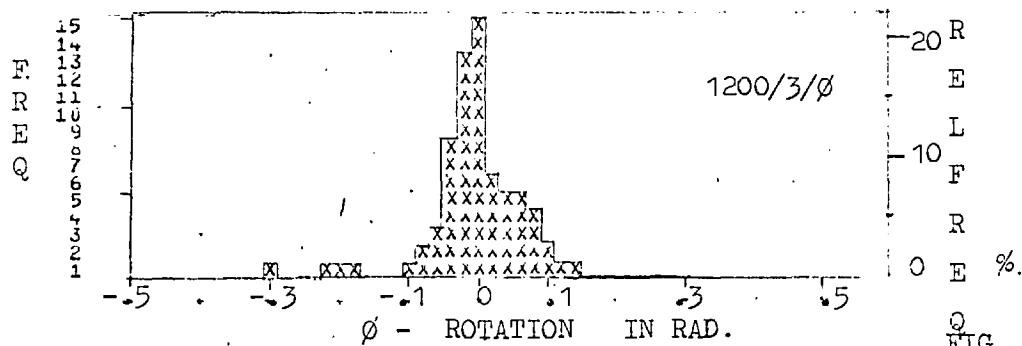


FIG. 7.13

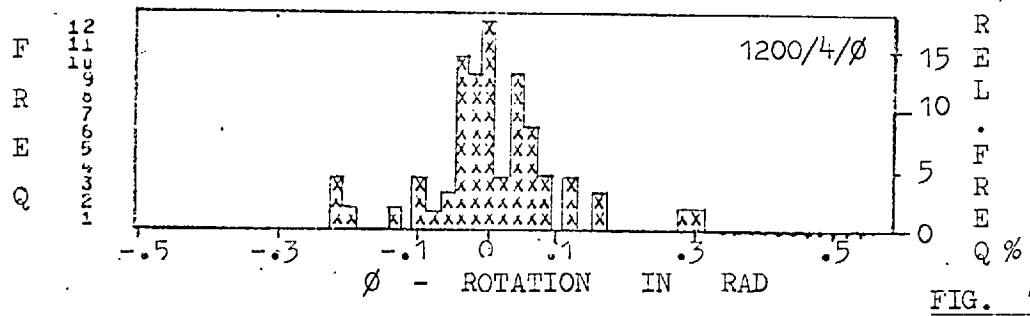


FIG. 7.14

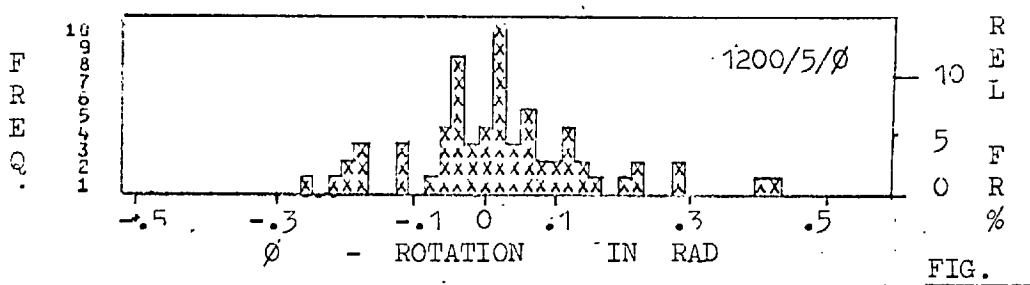
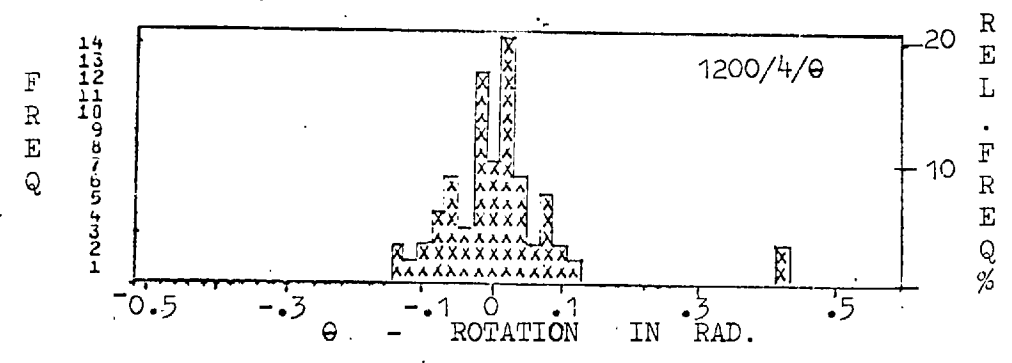


FIG. 7.15

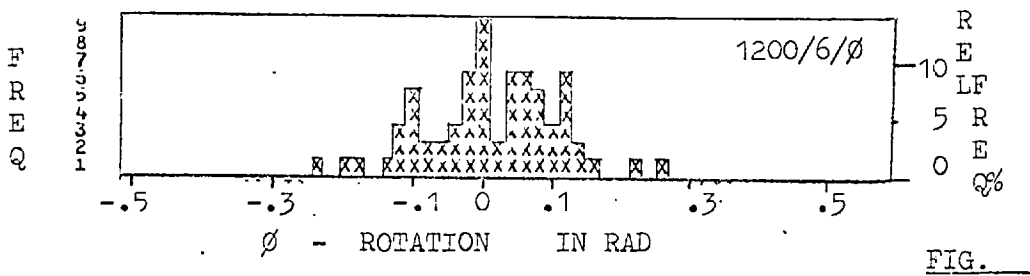
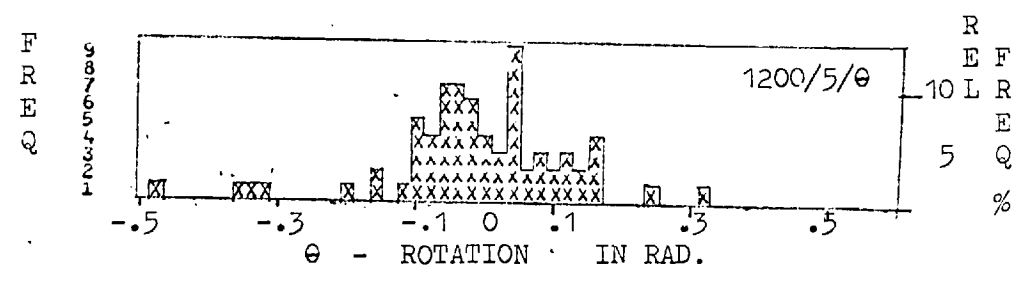
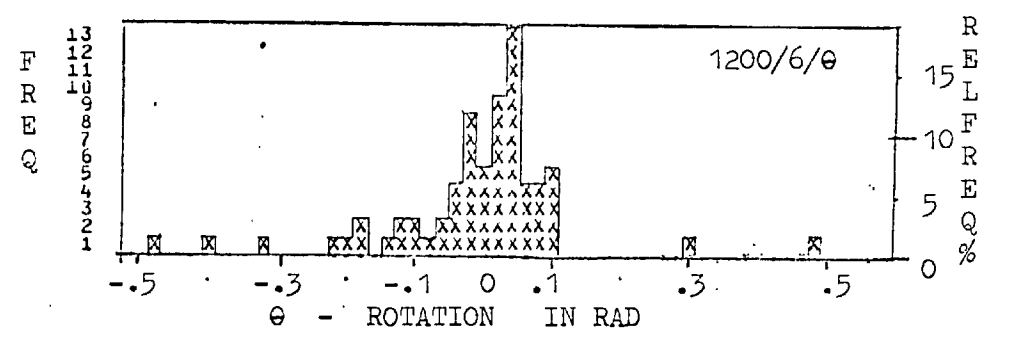
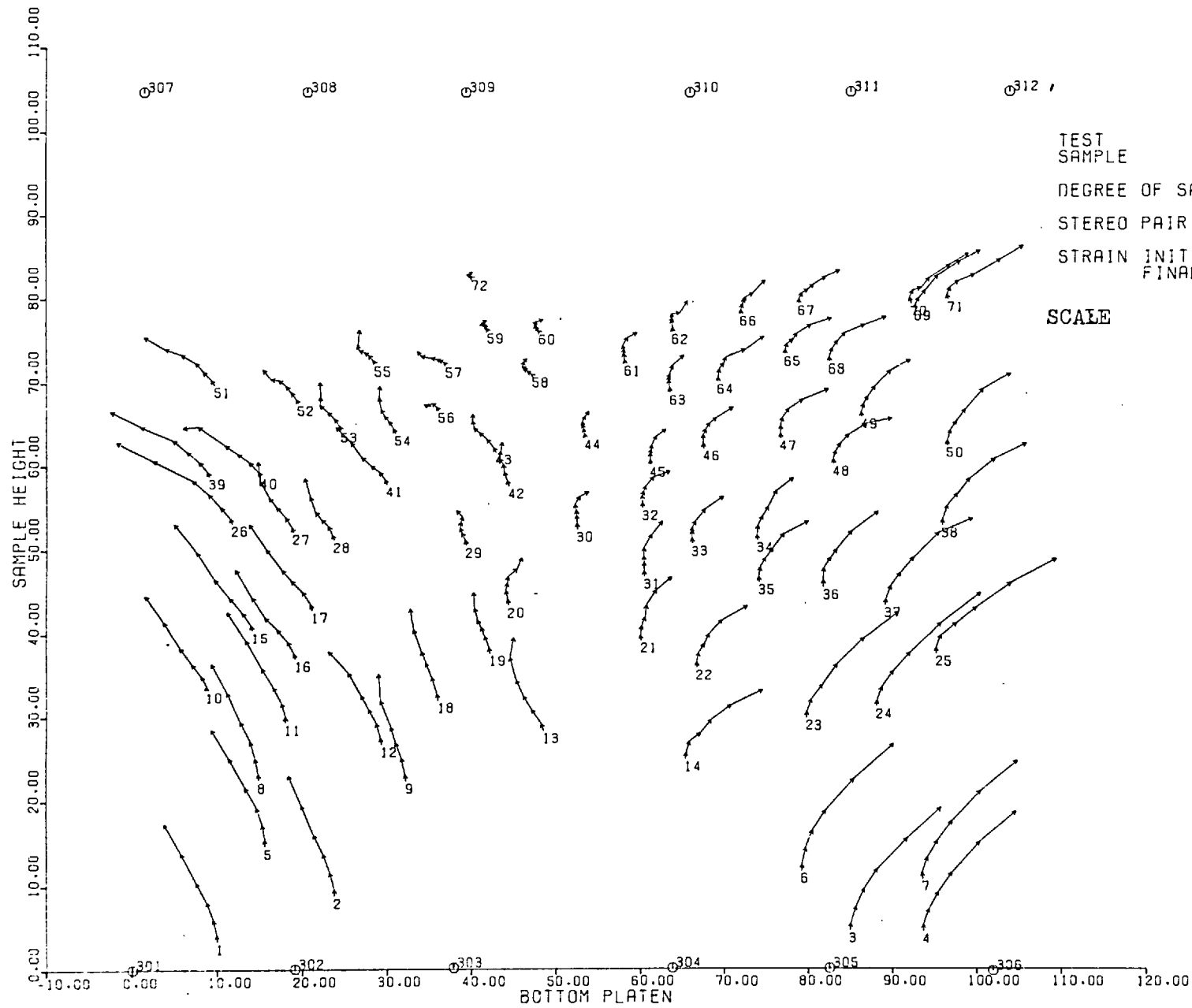


FIG. 7.16





307

308

309

310

311

312

TEST SAMPLE
 DEGREE OF SAT.
 STEREO PAIR NO.
 STRAIN INITIAL
 FINAL

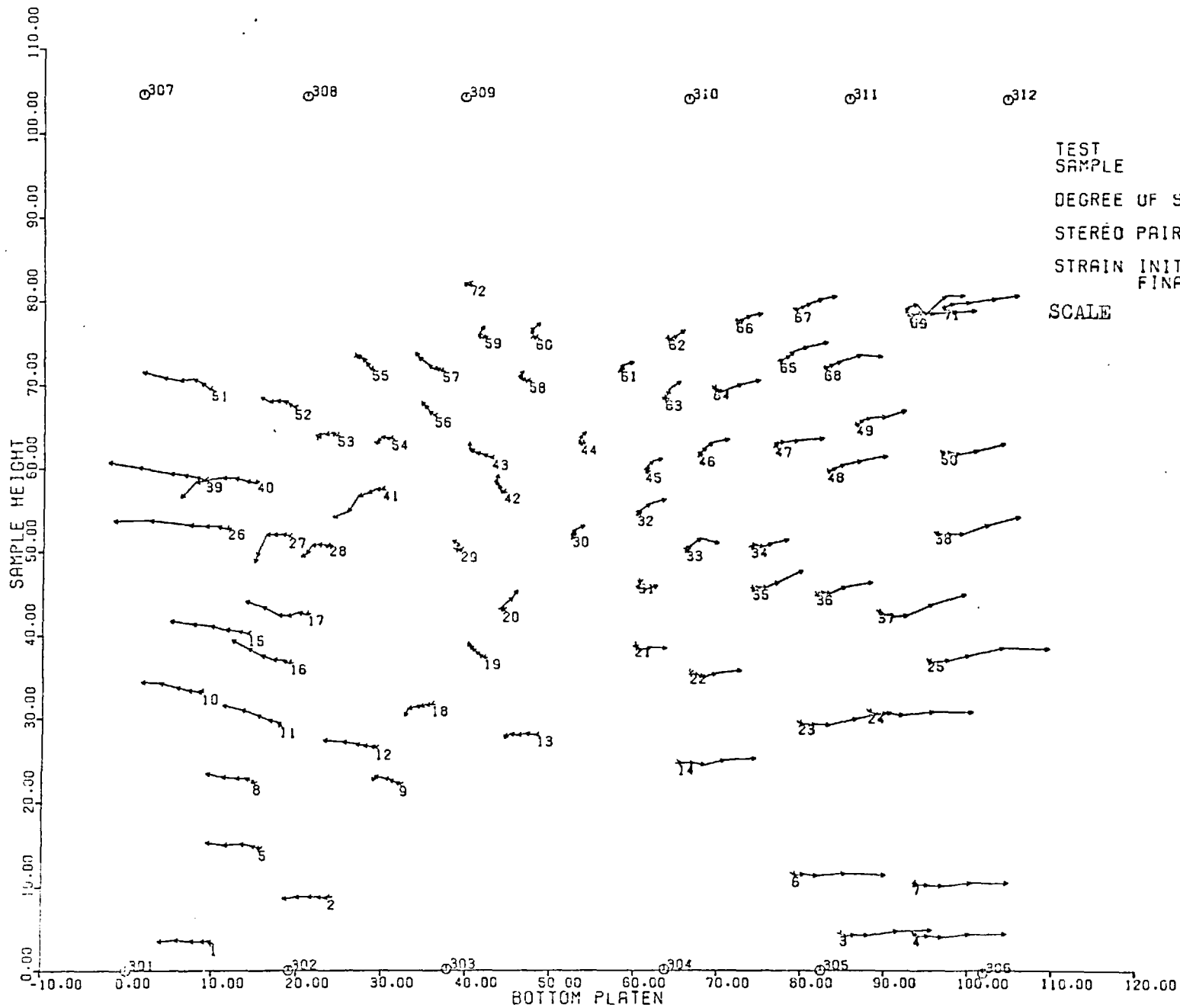
PLANE STRAIN (DRAINED)
 GRAVEL (ROTUND)
 DRY
 FIRST 1
 LAST 7
 O.C
 14.814

SCALE

10mm

FIG 7.17

TRACE OF DISPLACEMENTS OF MARKER CENTRES ON XY PLANE



307

308

309

310

311

312

TEST
SAMPLE

PLANE STRAIN (DRAINED)
GRAVEL (ROTUNDO)

DEGREE OF SAT.

DRY

STEREO PAIR NO.

FIRST 1
LAST 7

STRAIN INITIAL
FINAL

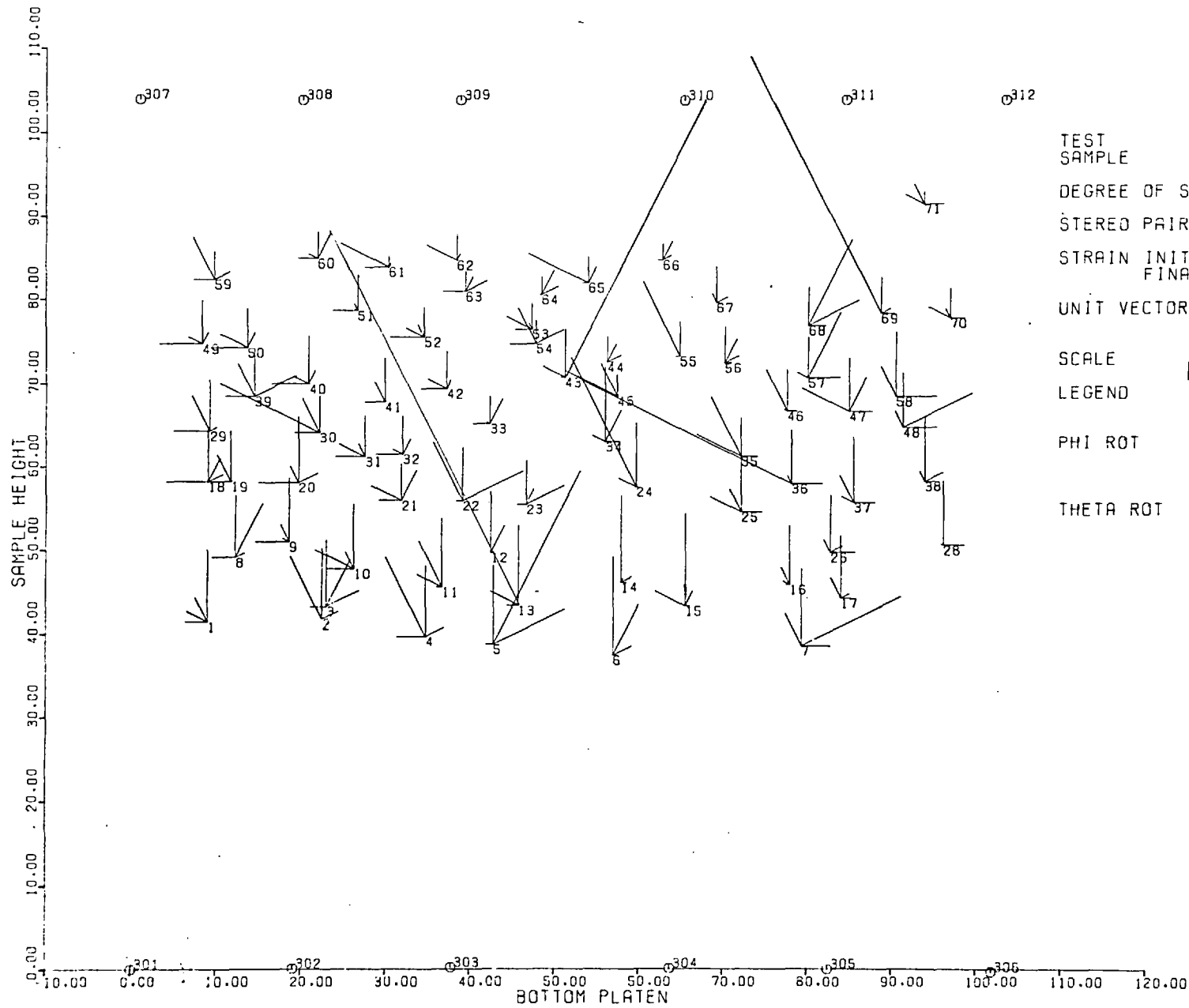
0.000
14.814

SCALE

10mm

FIG 7.18

TRACE OF DISPLACEMENTS OF MARKER CENTRES ON XZ PLANE



1201/1
 PLANE STRAIN (DRAINED)
 GRAVEL (ROUND)

DEGREE OF SAT. FULLY SAT.

STEREO PAIR NO. FIRST 1
 FINAL 2

STRAIN INITIAL 0.0
 FINAL 1.333

UNIT VECTOR DISP. ROT.] 1mm
 VER. Y] .1rad

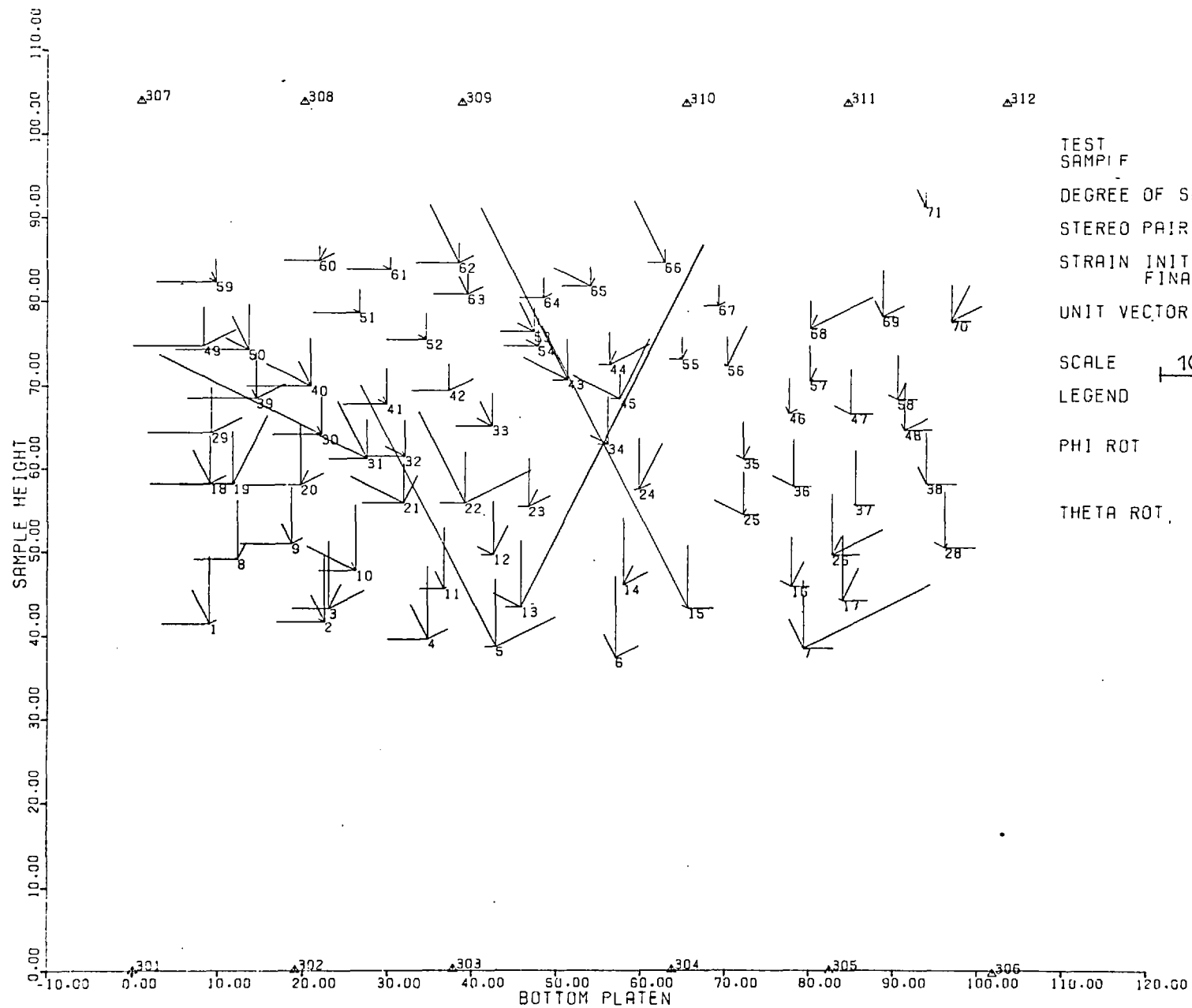
SCALE 10mm

LEGEND

PHI ROT

THETA ROT

FIG 7.19 DISPLACEMENT - ROTATION FIELD OF MARKERS IN XY PLANE



TEST
 SAMPL F
 DEGREE OF SAT. FULLY SAT.
 STEREO PAIR NO. FIRST 2
 FINAL 3
 STRAIN INITIAL 1.333
 FINAL 4.482
 UNIT VECTOR DISP. HOR. X
 VER. Y
 SCALE 10mm ROT
 LEGEND
 PHI ROT
 THETA ROT

1201/2
 PLANE STRAIN (DRAINED)
 GRAVEL (ROTUND)

2mm
 .2rad

FIG 7.20 DISPLACEMENT - ROTATION FIELD OF MARKERS IN XY PLANE

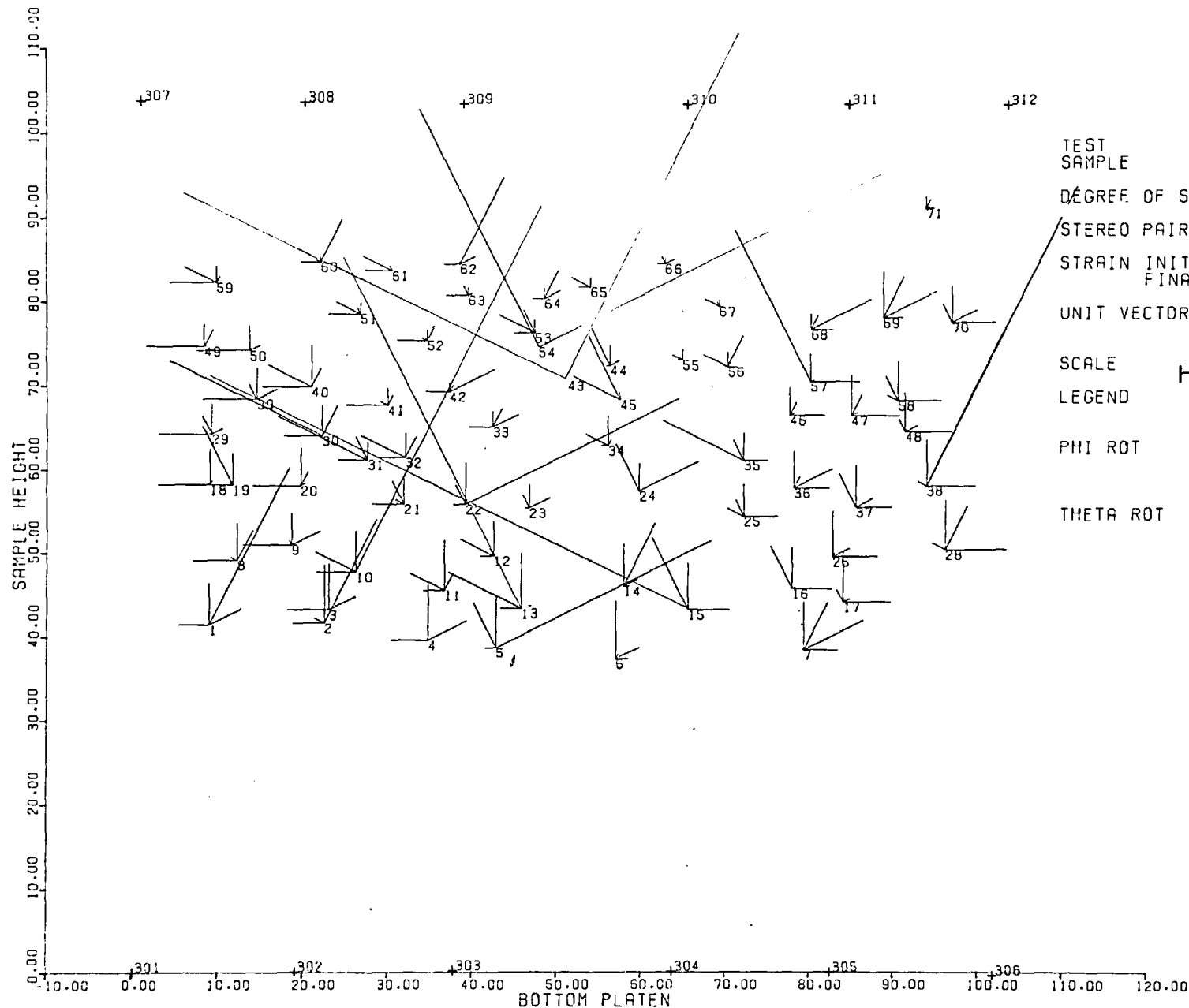
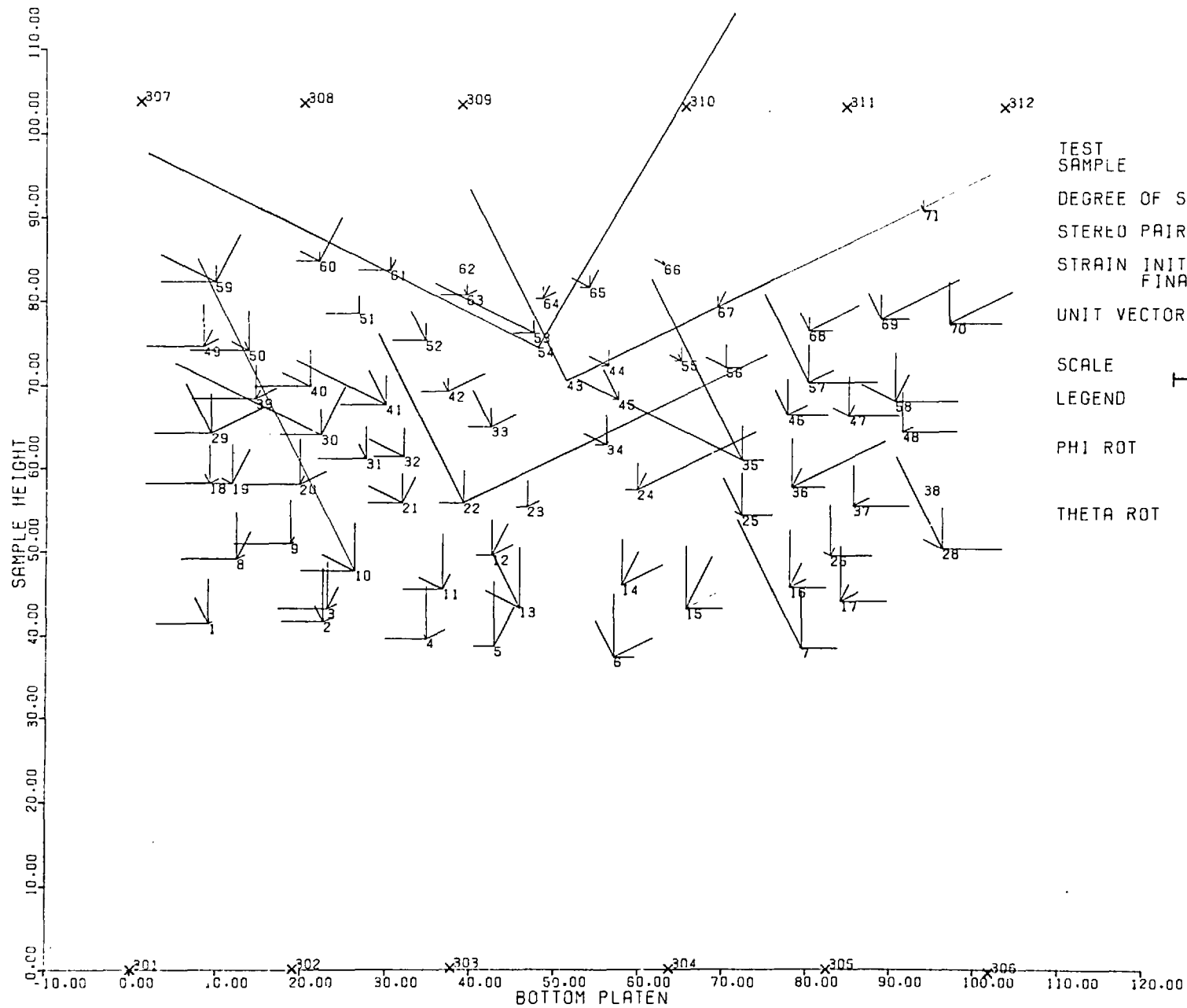
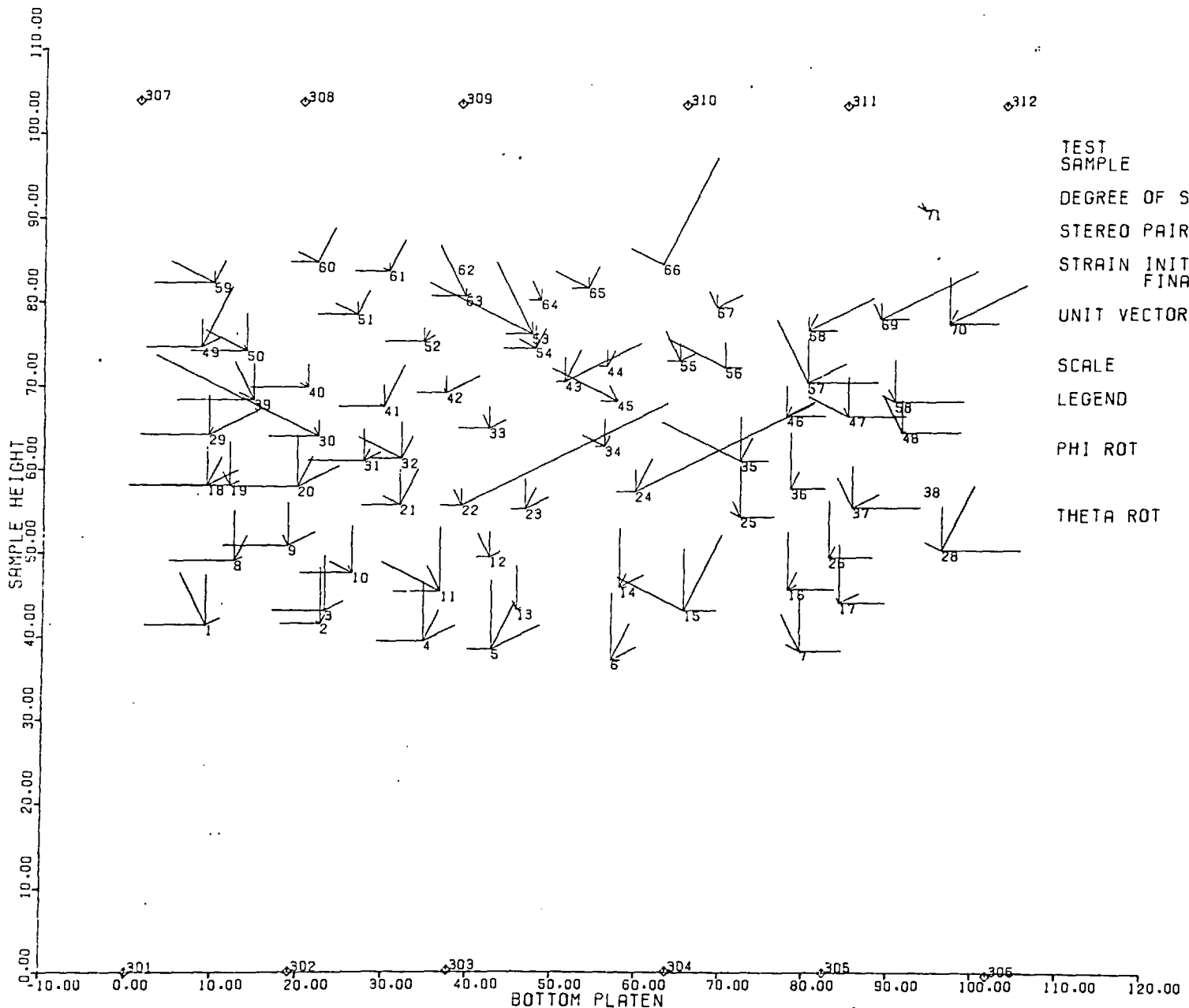


FIG 7.21 DISPLACEMENT - ROTATION FIELD OF MARKERS IN XY PLANE



TEST SAMPLE 1201/4
 PLANE STRAIN (DRAINED) GRAVEL (ROTUND)
 DEGREE OF SAT. FULLY SAT.
 STEREO PAIR NO. FIRST 4
 STRAIN INITIAL FINAL 6.706 8.917
 UNIT VECTOR DISP. HOR. X VER. Y
 SCALE ROT. 10mm 2mm
 LEGEND
 PHI ROT
 THETA ROT

FIG 7.22 DISPLACEMENT - ROTATION FIELD OF MARKERS IN XY PLANE



TEST SAMPLE 1201/5
 PLANE STRAIN (DRAINED) GRAVEL (ROTUND)
 DEGREE OF SAT. FULLY SAT.
 STEREO PAIR NO. FIRST 5
 FINAL 6
 STRAIN INITIAL 8.917
 FINAL 11.383
 UNIT VECTOR DISP. HOR. X] 2mm
 VER. Y] .2rad
 SCALE ROT. 10mm
 LEGEND
 PHI ROT
 THETA ROT

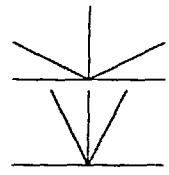
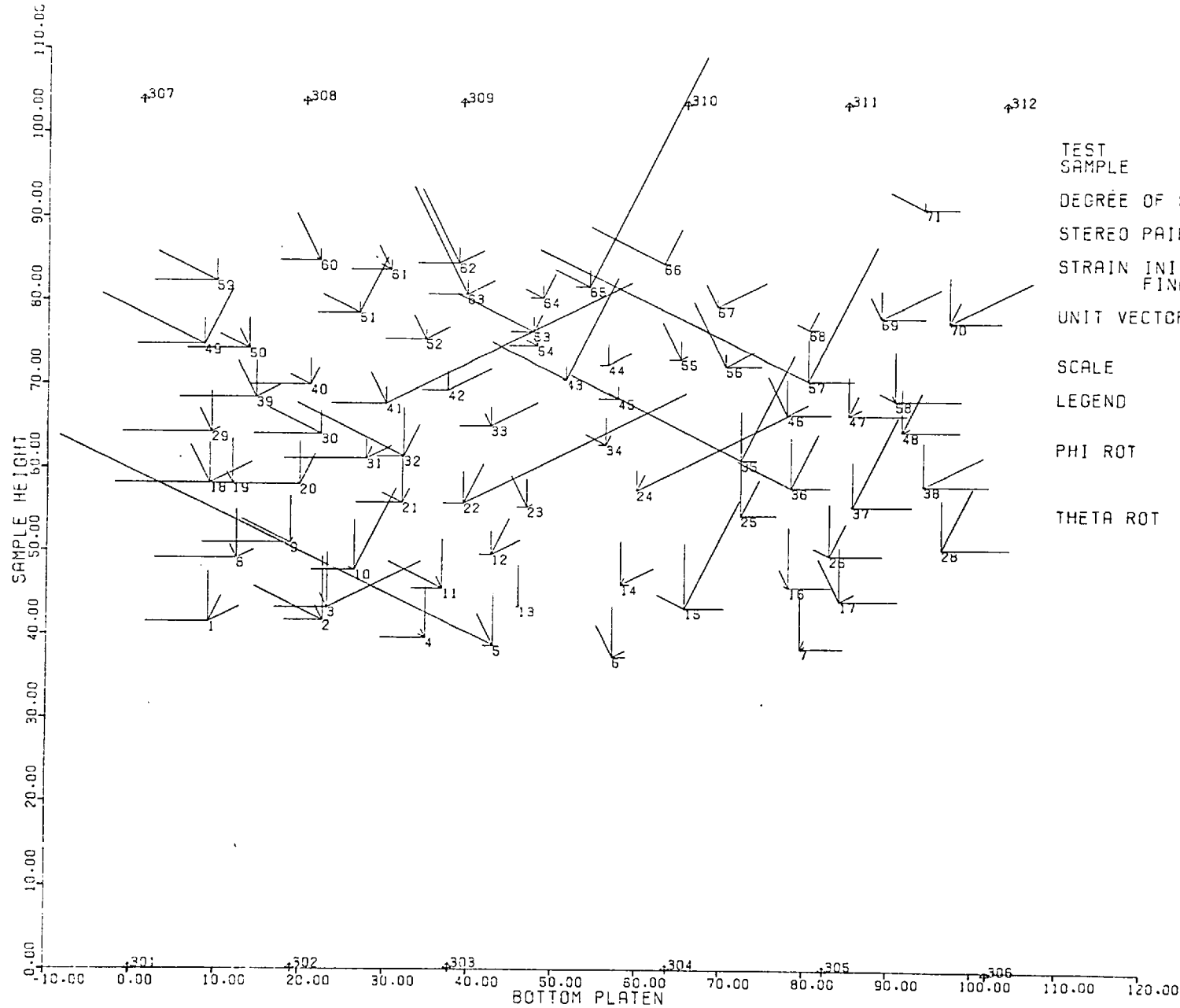


FIG 7.23 DISPLACEMENT - ROTATION FIELD OF MARKERS IN XY PLANE



TEST SAMPLE 1201/6
 PLANE STRAIN (DRAINED) GRAVEL (ROTUND)
 DEGREE OF SAT. FULLY SAT.
 STEREO PAIR NO. FIRST 6
 STRAIN INITIAL FINAL 11.383 7
 STRAIN FINAL 15.117
 UNIT VECTOR DISP. ROT. HOR. X VER. Y
 SCALE 10mm
 LEGEND
 PHI ROT
 THETA ROT

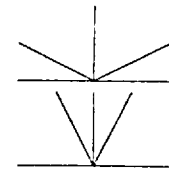
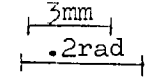
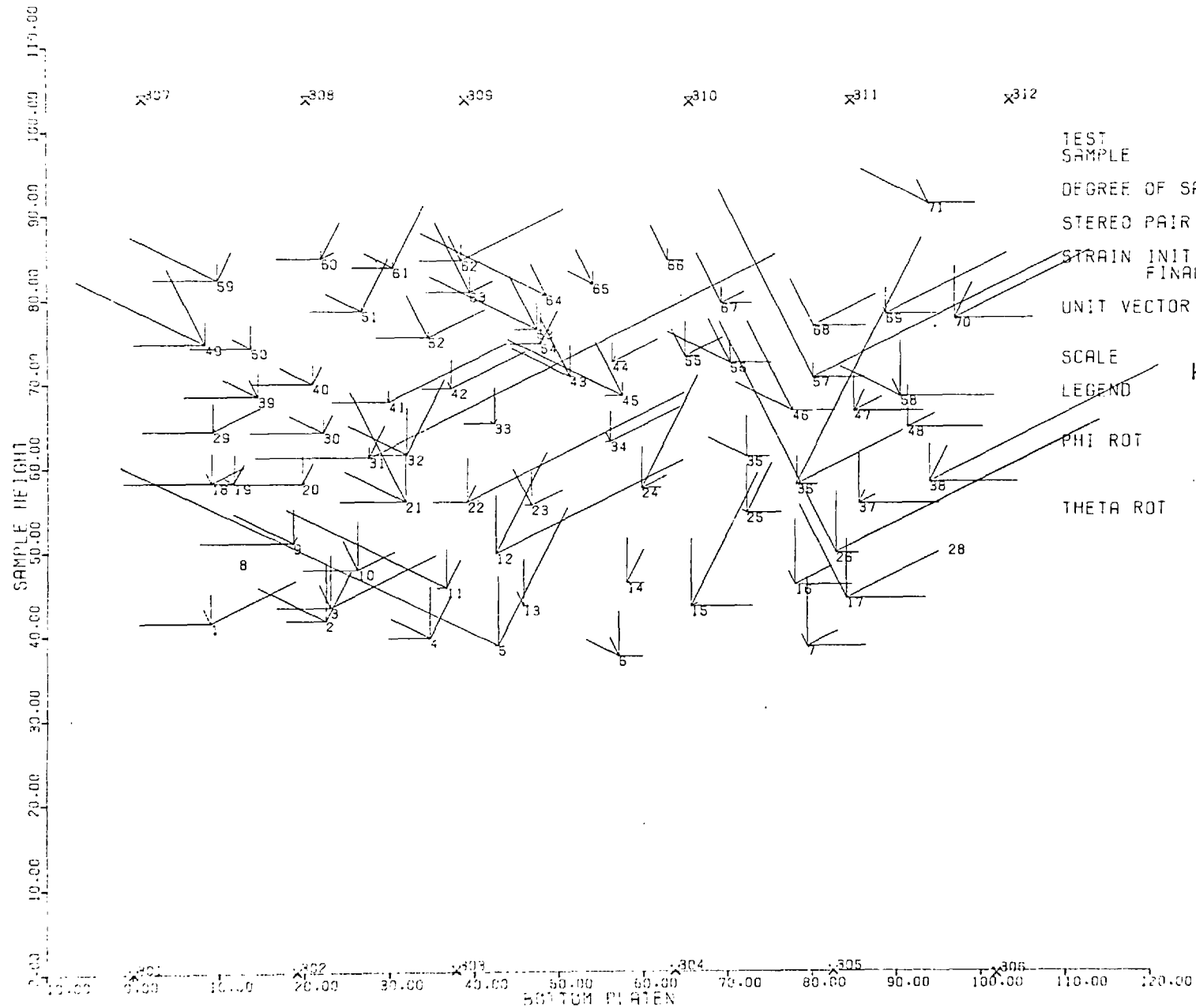


FIG 7.24 DISPLACEMENT - ROTATION FIELD OF MARKERS IN XY PLANE



TEST SAMPLE
 DEGREE OF SAT. FULLY SAT.
 STEREO PAIR NO. FIRST 7
 FINAL 8
 STRAIN INITIAL 15.117
 FINAL 19.359
 UNIT VECTOR DISP. ROT.
 SCALE 10mm
 LEGEND
 PHI ROT
 THETA ROT

1201/7
 PLANE STRAIN (DRAINED)
 GRAVEL (ROTUND)

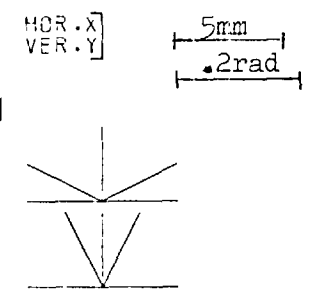


FIG 7.25 DISPLACEMENT - ROTATION FIELD OF MARKERS IN XY PLANE

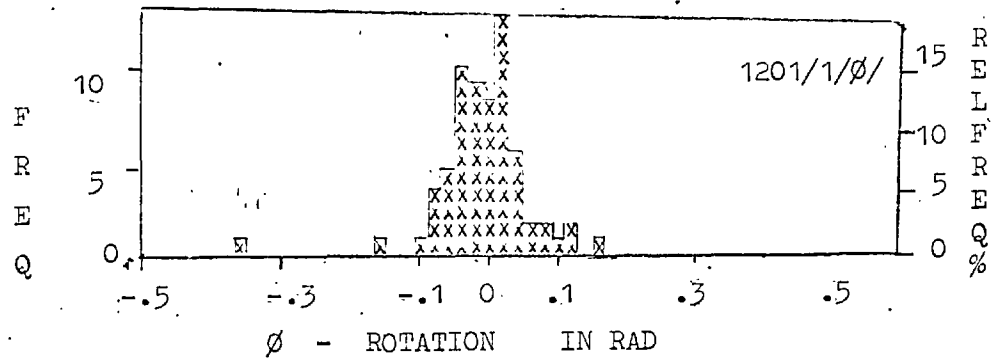


FIG. 7.26

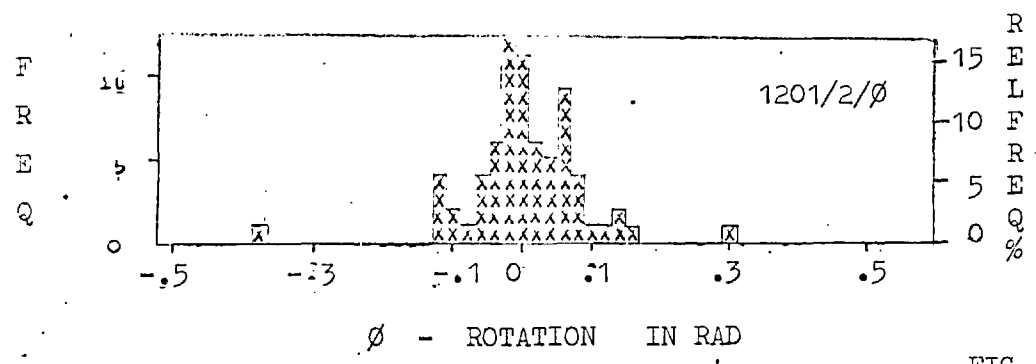
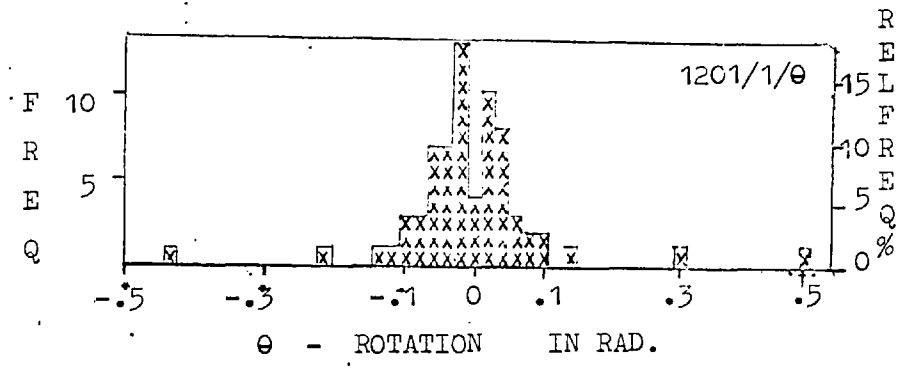


FIG 7.27

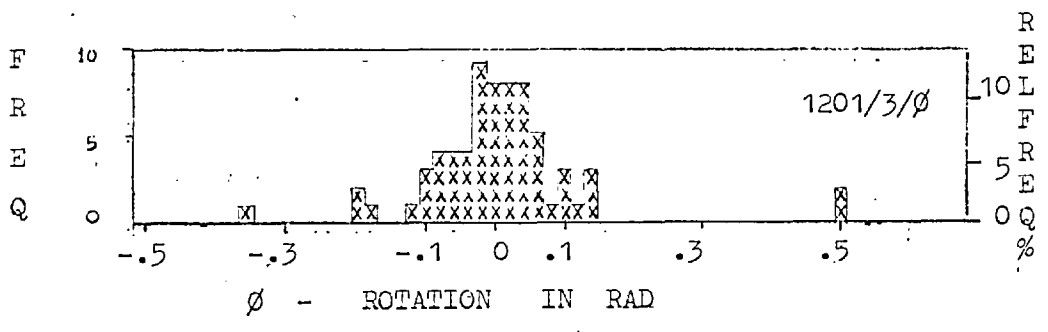
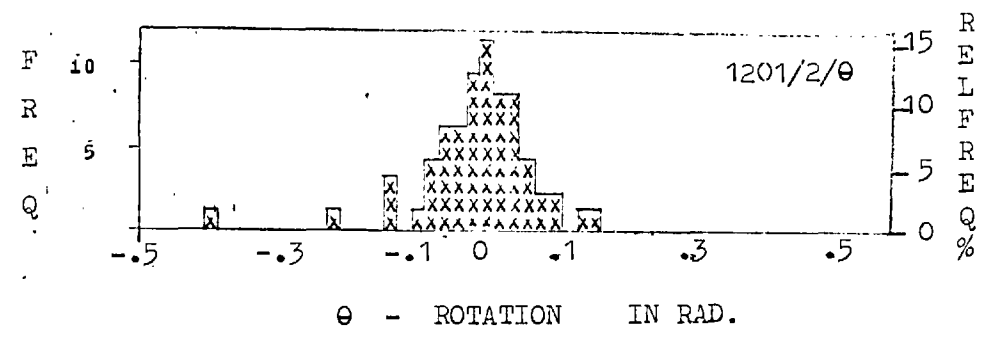
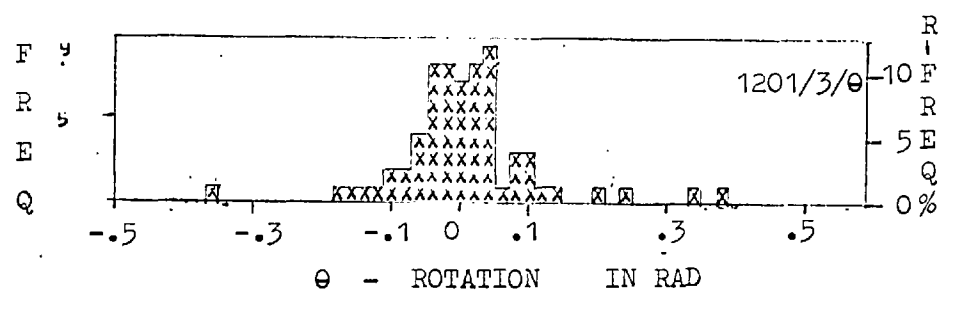


FIG 7.28



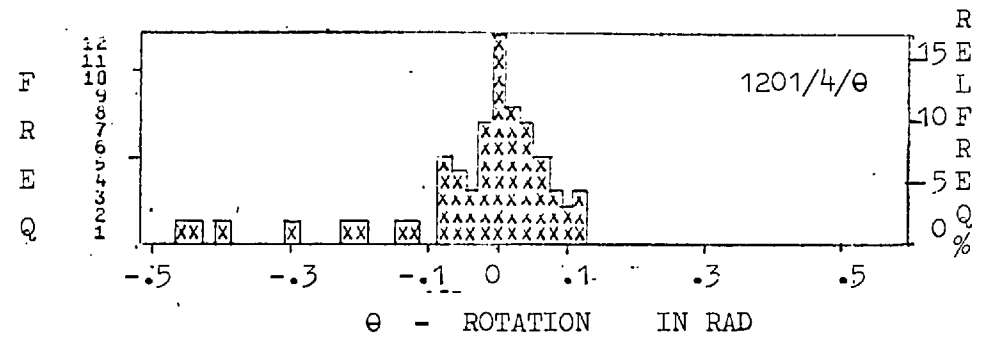
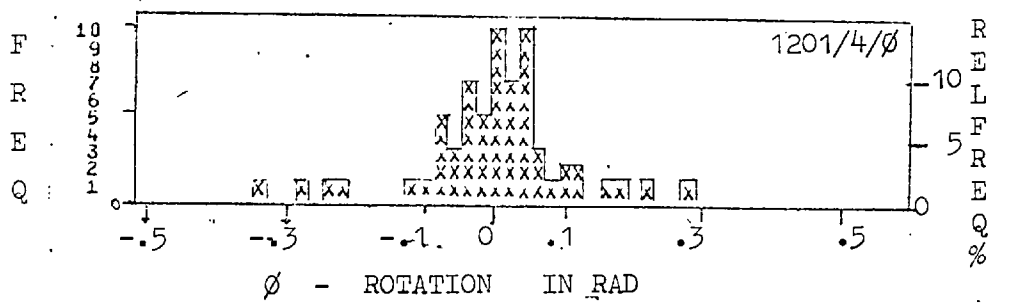


FIG. 7.29

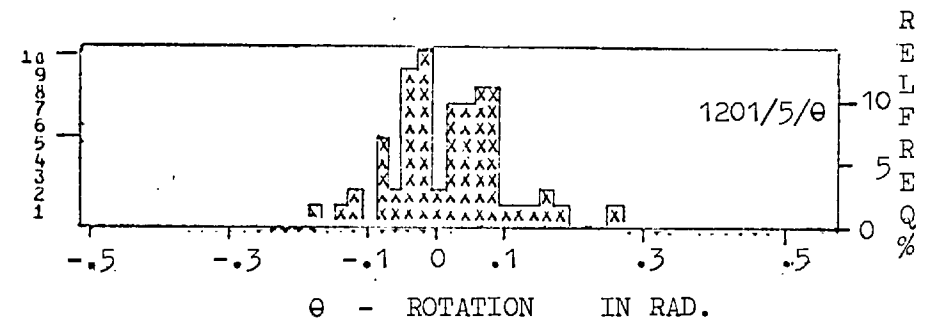
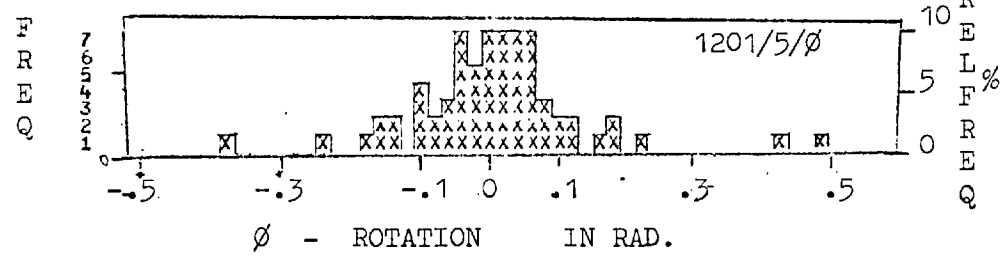


FIG. 7.30

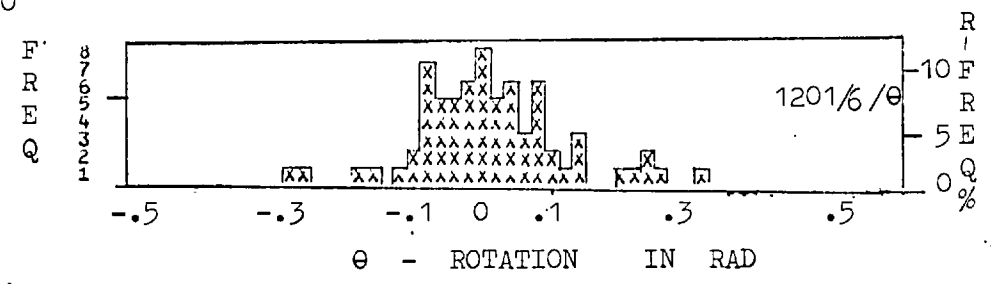
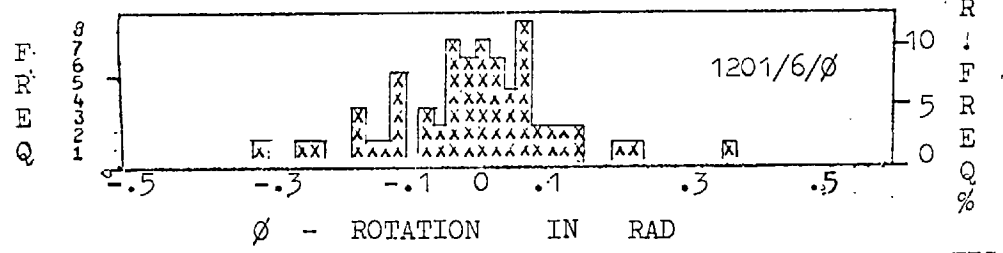


FIG. 7.31

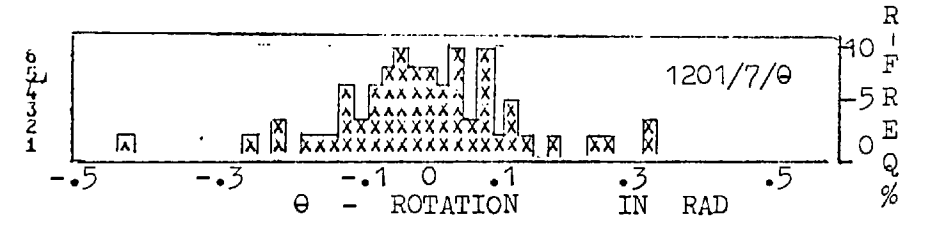
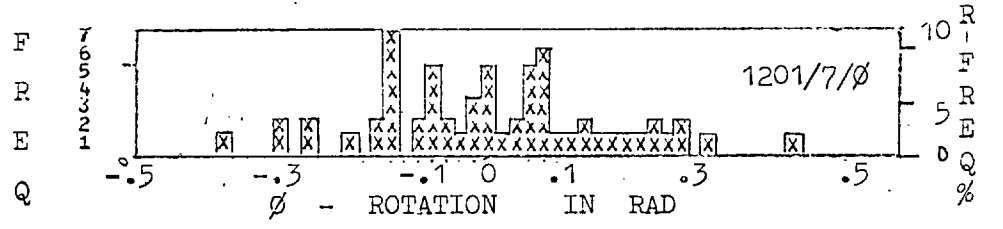
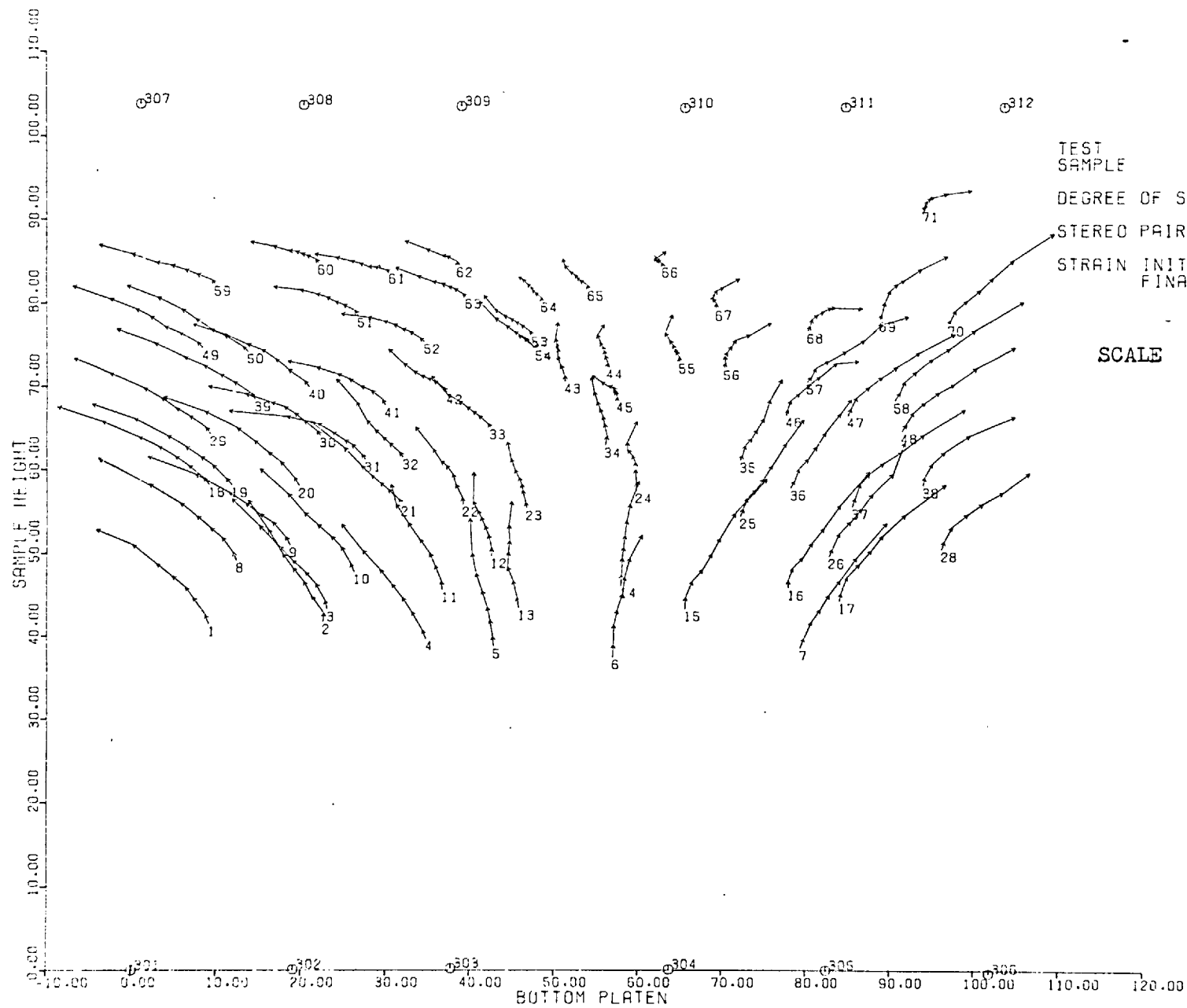


FIG. 7.32



TEST SAMPLE
 DEGREE OF SAT.
 STEREO PAIR NO.
 STRAIN INITIAL
 FINAL

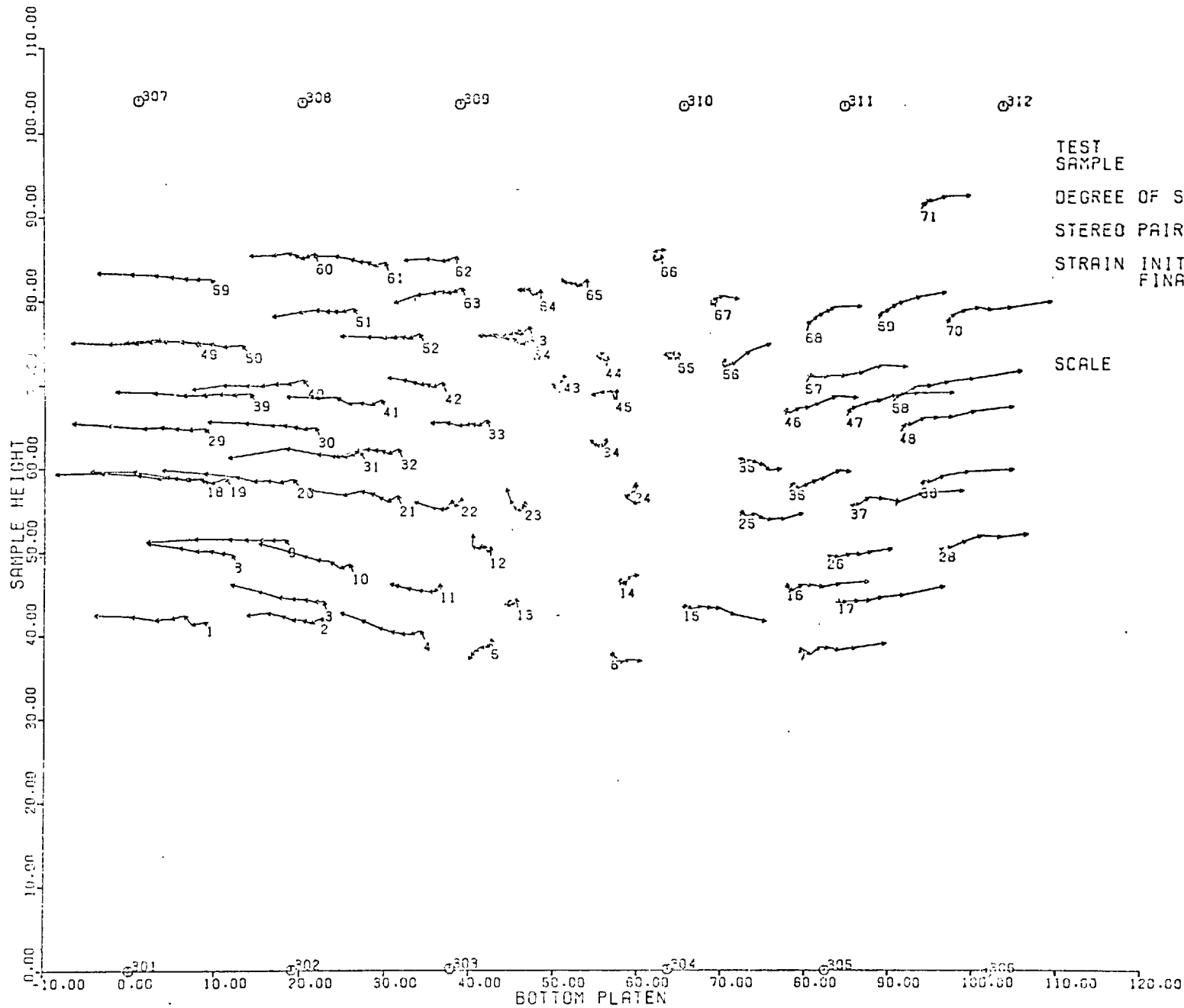
PLANE STRAIN (DRAINED)
 GRAVEL (ROTUND)
 FULLY SAT.
 FIRST :
 LAST 8
 0.000
 19.359

SCALE

10mm

FIG 7.33

TRACE OF DISPLACEMENTS OF MARKER CENTRES ON XY PLANE



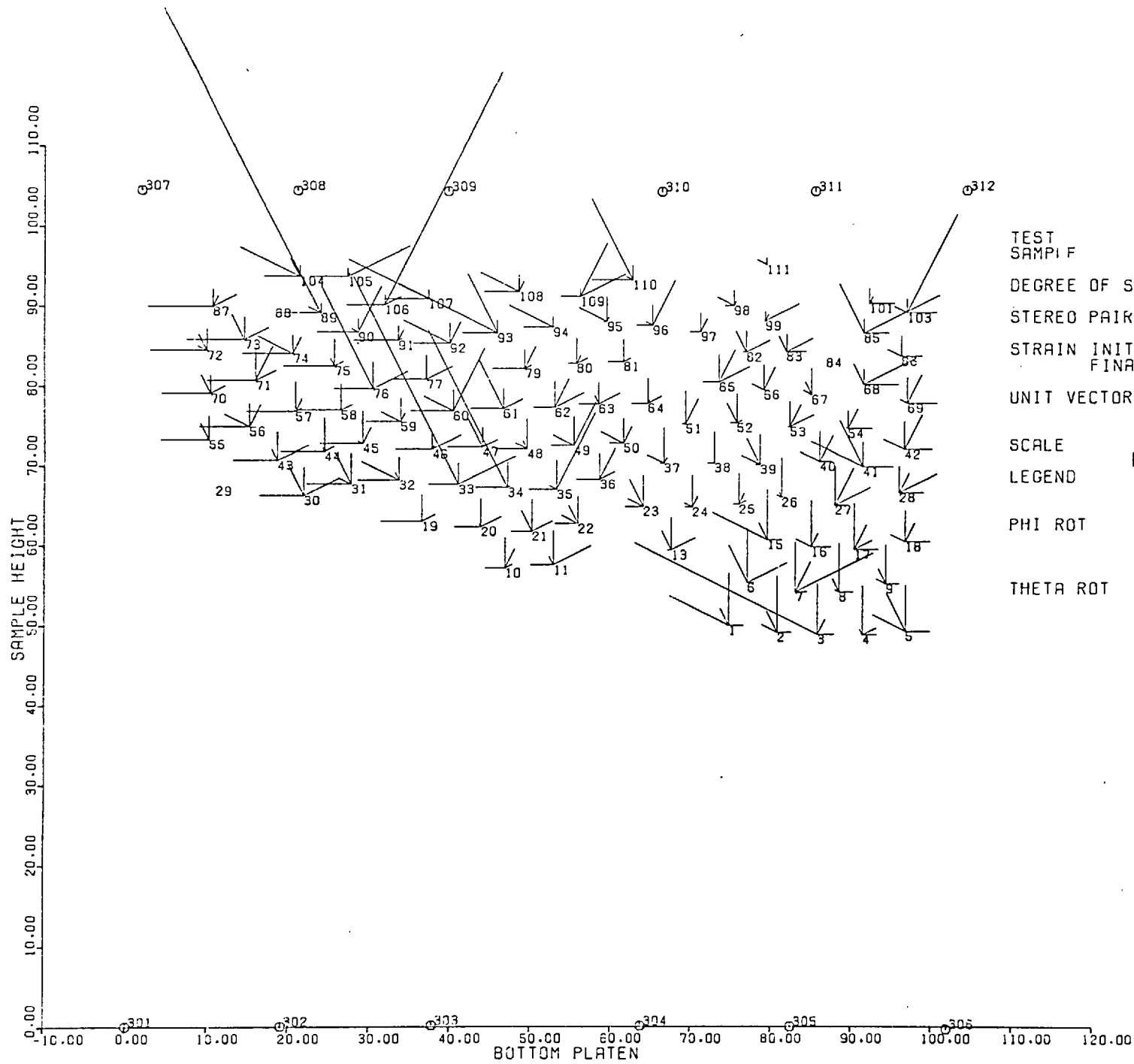
TEST SAMPLE	PLANE STRAIN (DRAINED)
DEGREE OF SAT.	GRAVEL (ROTUND)
STEREO PAIR NO.	FULLY SAT.
STRAIN INITIAL	FIRST 1
FINAL	LAST 8
	0.000
	19.359

SCALE

10mm

FIG 7.34

TRACE OF DISPLACEMENTS OF MARKER CENTRES ON XZ PLANE



TEST 2200/1
 SAMPLING PLANE STRAIN (DRAINED)
 GLASS BALLS
 DEGREE OF SAT. DRY
 STEREO PAIR NO. FIRST 1
 FINAL 2
 STRAIN INITIAL 0.000
 FINAL 1.201
 UNIT VECTOR DISP. HOR. X
 ROT. VER. Y
 SCALE 10mm
 LEGEND
 PHI ROT
 THETA ROT

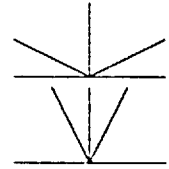
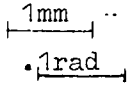


FIG 7.35 DISPLACEMENT - ROTATION FIELD OF MARKERS IN XY PLANE

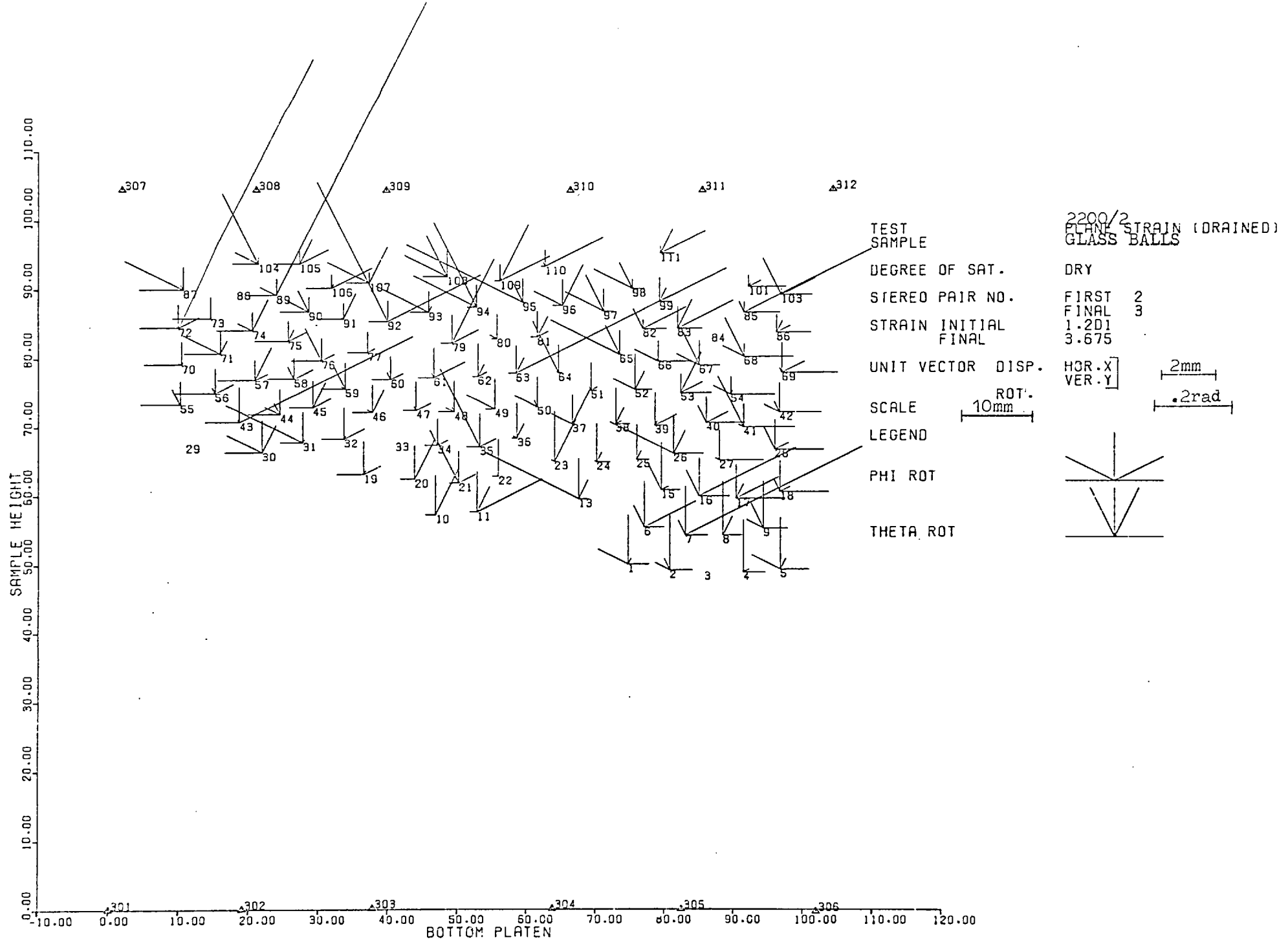
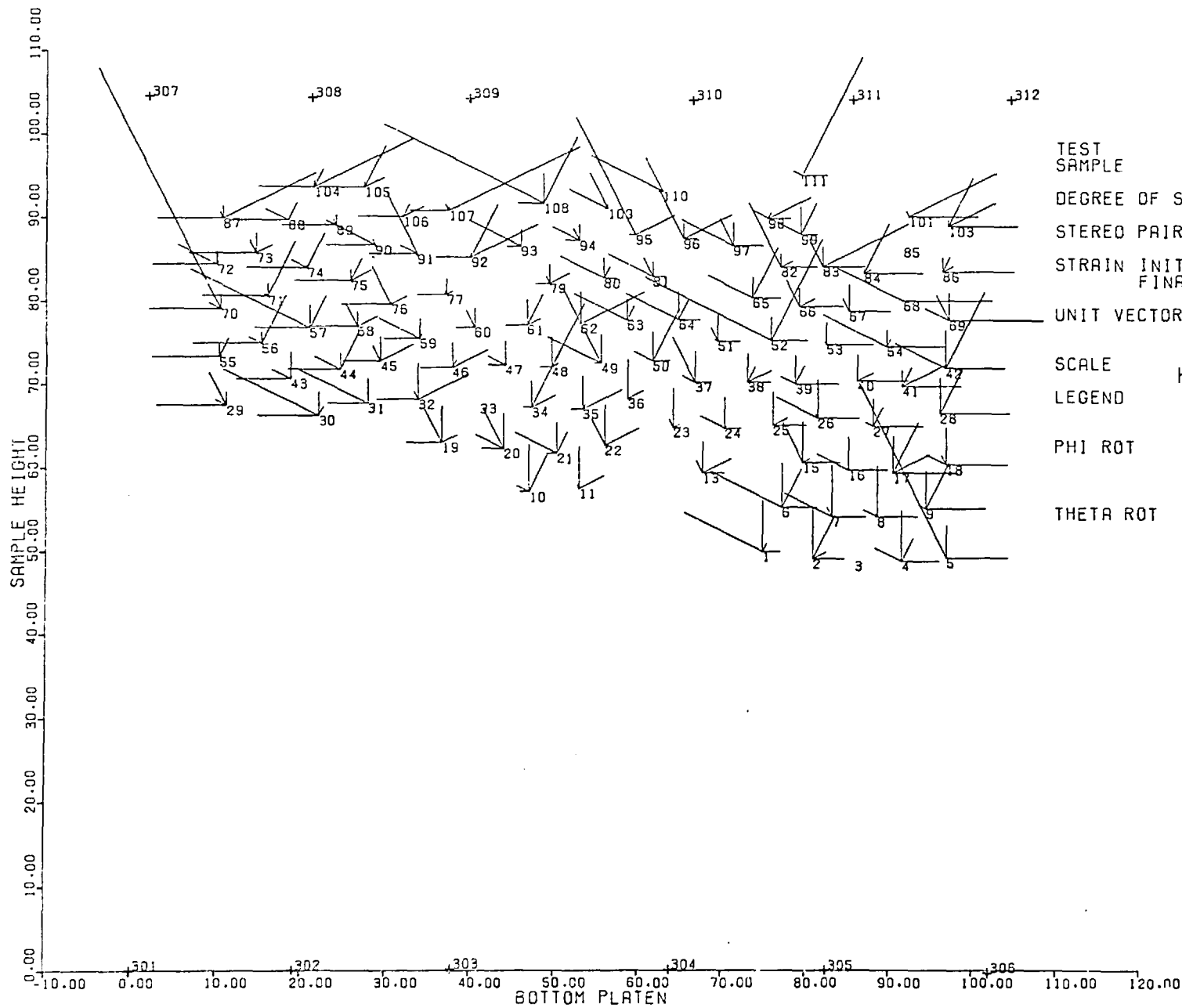


FIG 7.36 DISPLACEMENT - ROTATION FIELD OF MARKERS IN XY PLANE



TEST SAMPLE 2200/3
 PLANE STRAIN (DRAINED)
 GLASS BALLS
 DEGREE OF SAT. DRY
 STEREO PAIR NO. FIRST 3
 FINAL 4
 STRAIN INITIAL 3.675
 FINAL 5.913
 UNIT VECTOR DISP. HOR. X 2mm
 VER. Y 10mm
 SCALE ROT. 10mm
 LEGEND .2rad
 PHI ROT
 THETA ROT

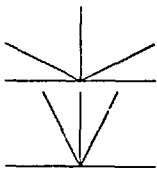


FIG 7.37 DISPLACEMENT - ROTATION FIELD OF MARKERS IN XY PLANE

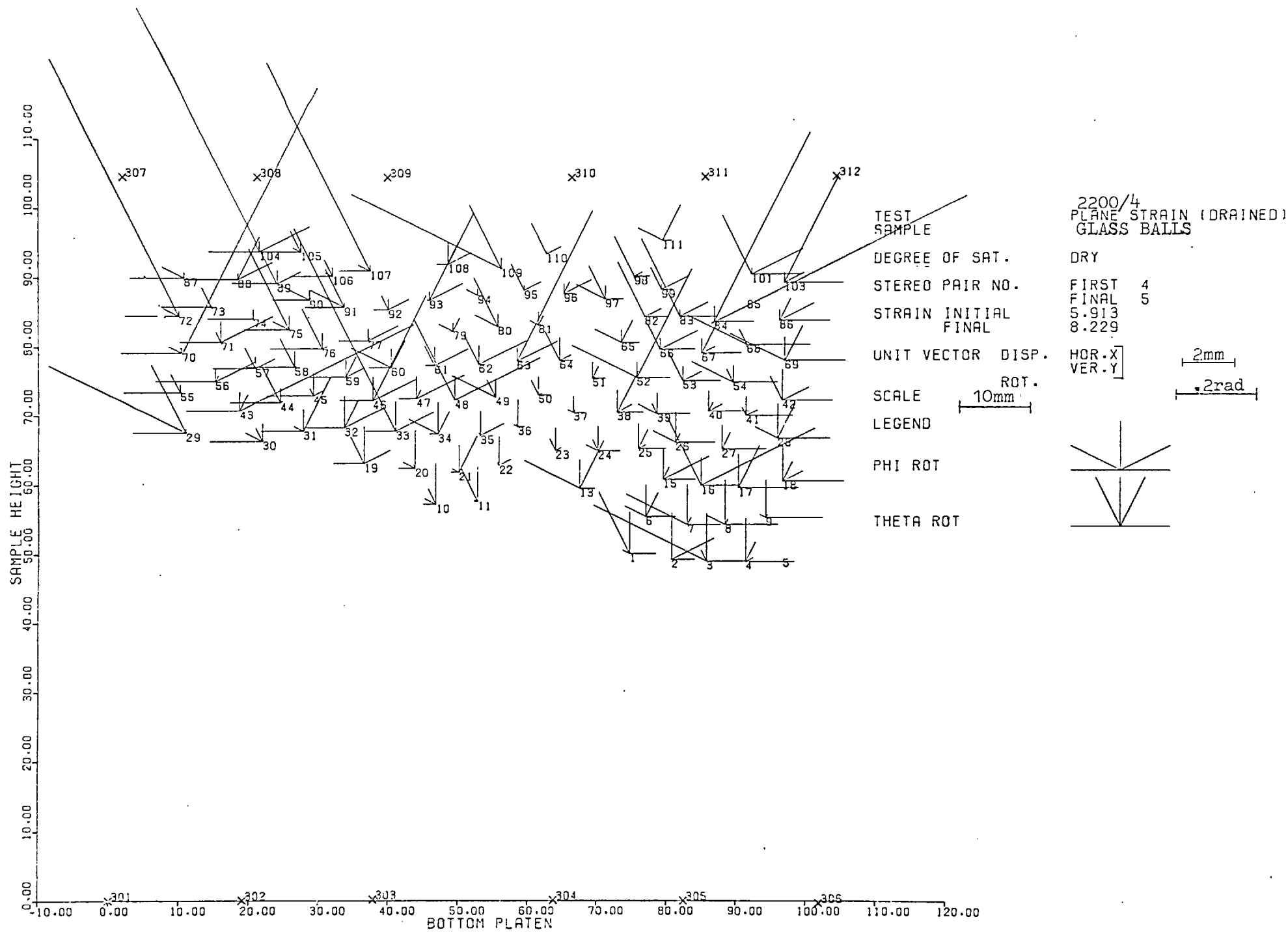


FIG 7.38 DISPLACEMENT - ROTATION FIELD OF MARKERS IN XY PLANE

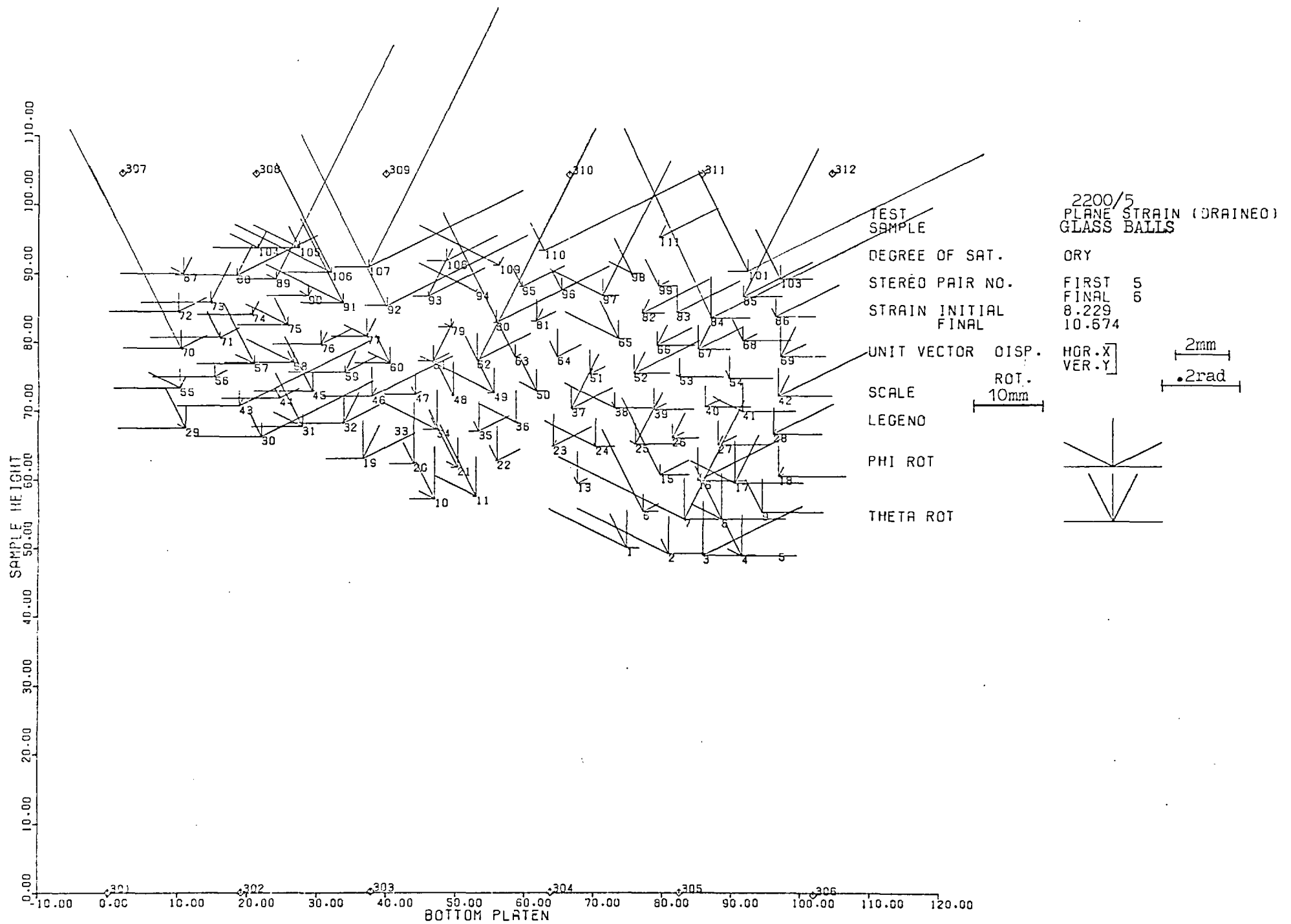
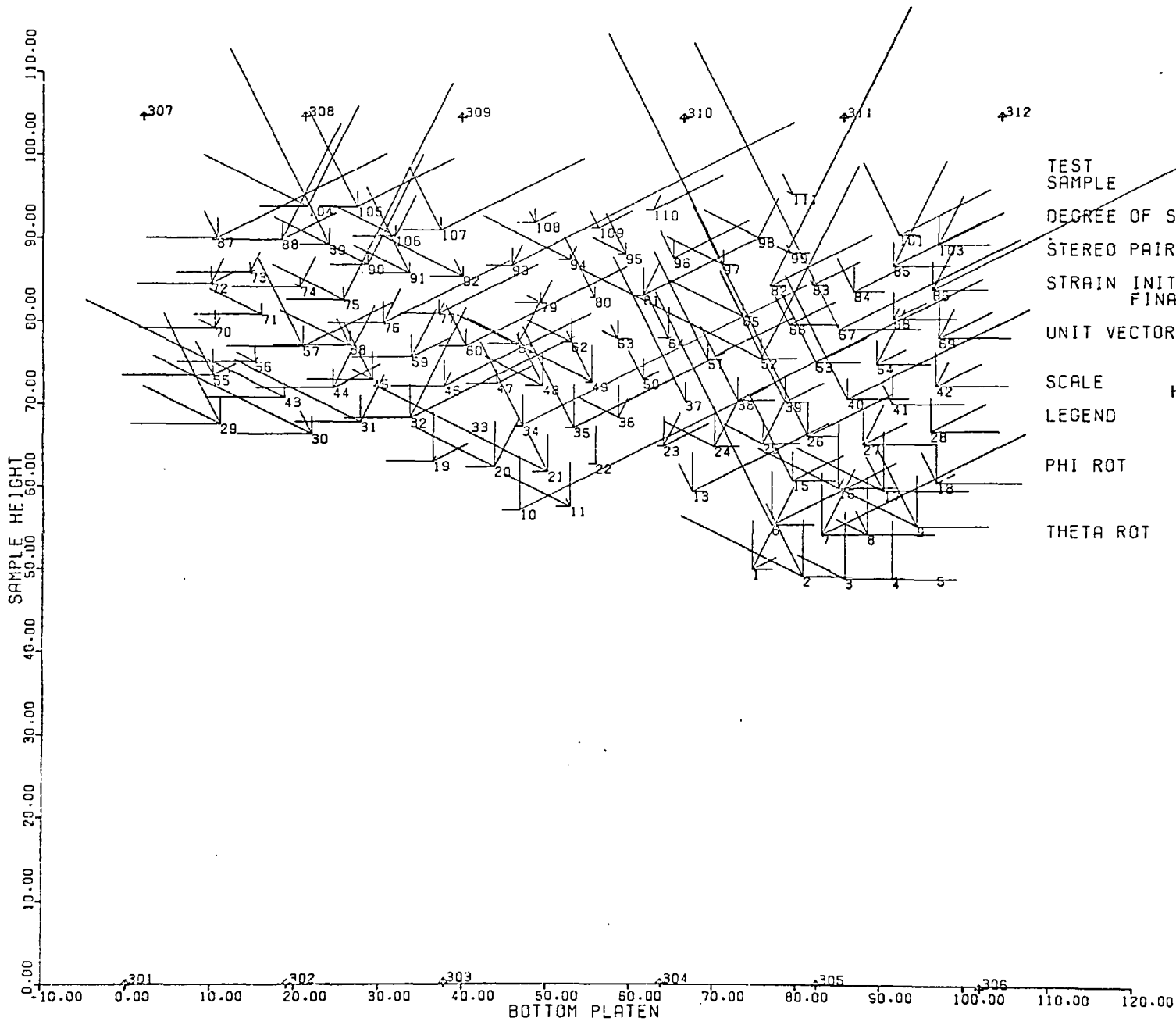


FIG.7.39 DISPLACEMENT - ROTATION FIELD OF MARKERS IN XY PLANE



TEST
SAMPLE

DEGREE OF SAT.

STEREO PAIR NO.

STRAIN INITIAL
FINAL

UNIT VECTOR DISP.

SCALE

LEGEND

PHI ROT

THETA ROT

2200/6
PLANE STRAIN (DRAINED)
GLASS BALLS

DRY

FIRST 6
FINAL 7

10.674
14.364

HOR. X
VER. Y

ROT.
10mm

3mm
.2rad

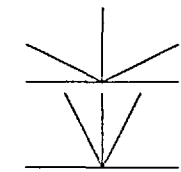


FIG 7.40 DISPLACEMENT - ROTATION FIELD OF MARKERS IN XY PLANE

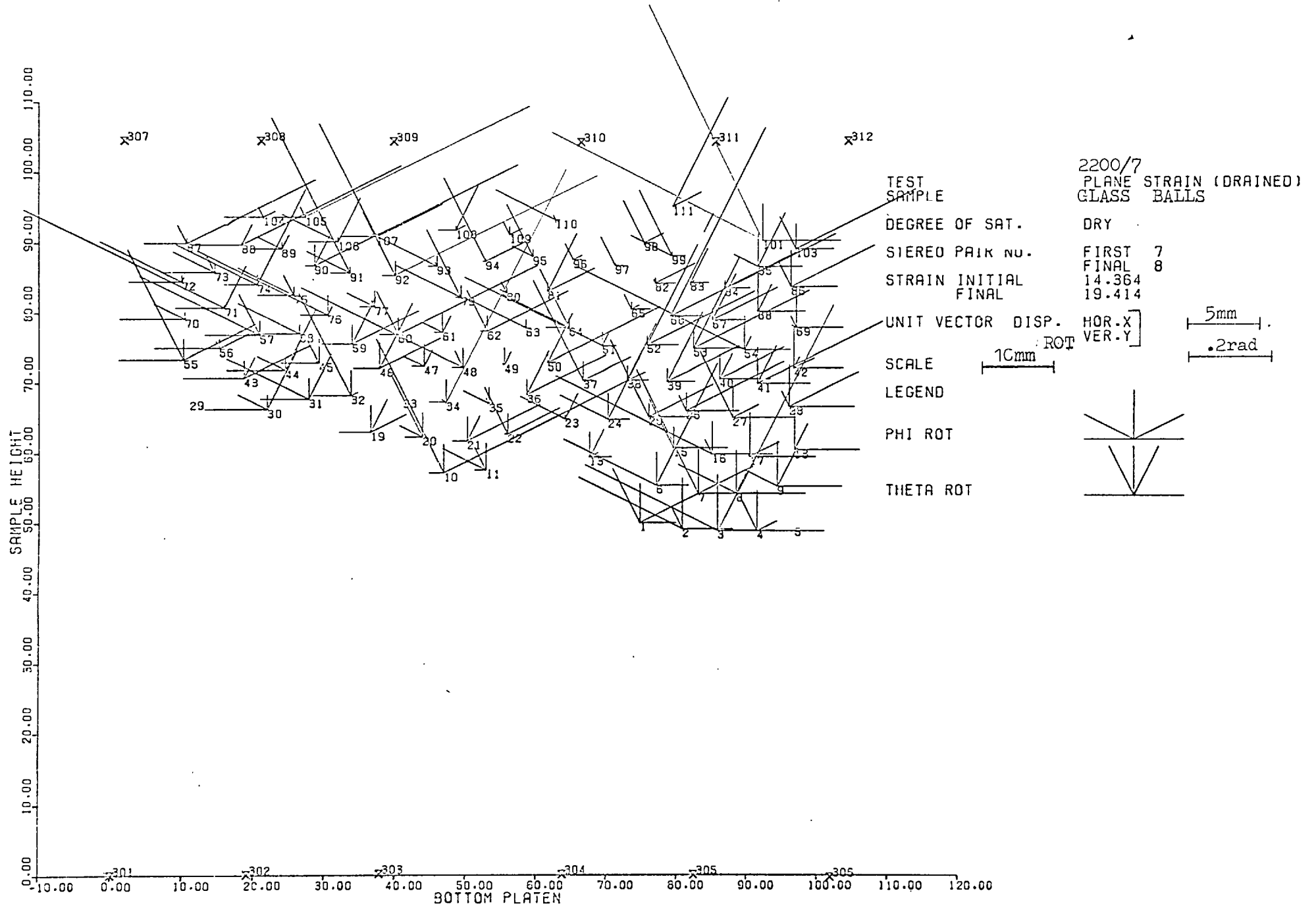


FIG 7.41 DISPLACEMENT - ROTATION FIELD OF MARKERS IN XY PLANE

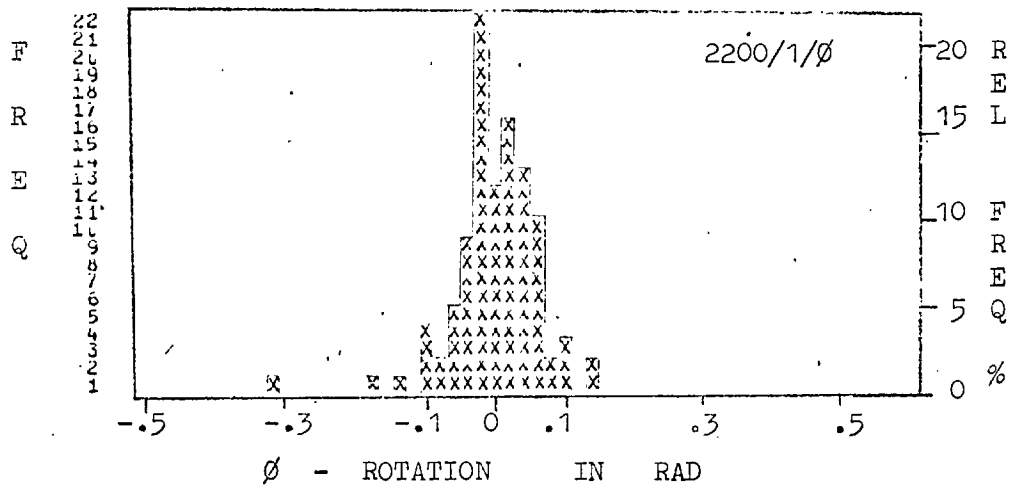


FIG. 7.42

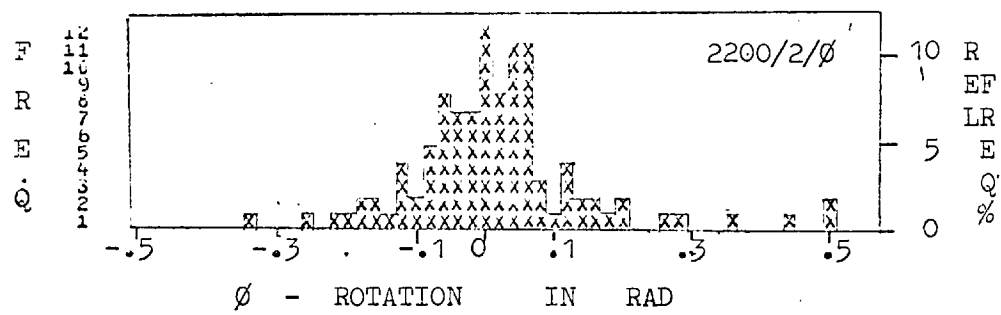
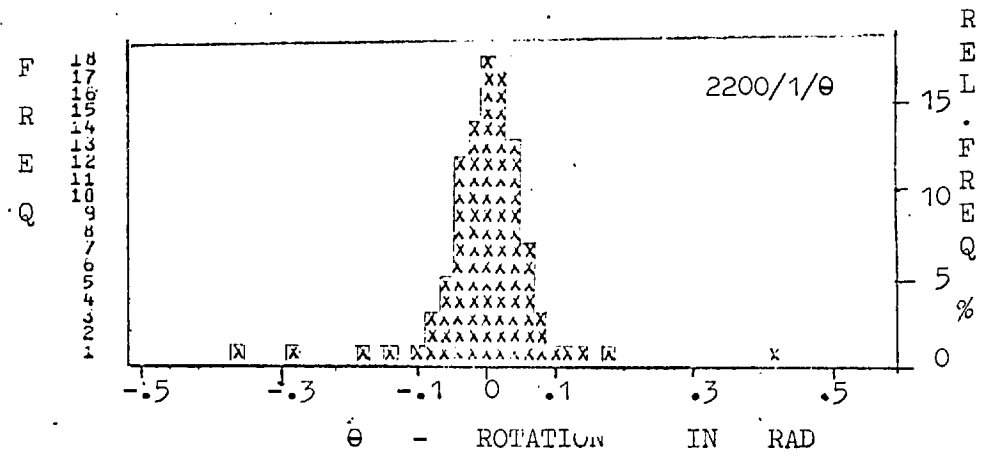


FIG. 7.43

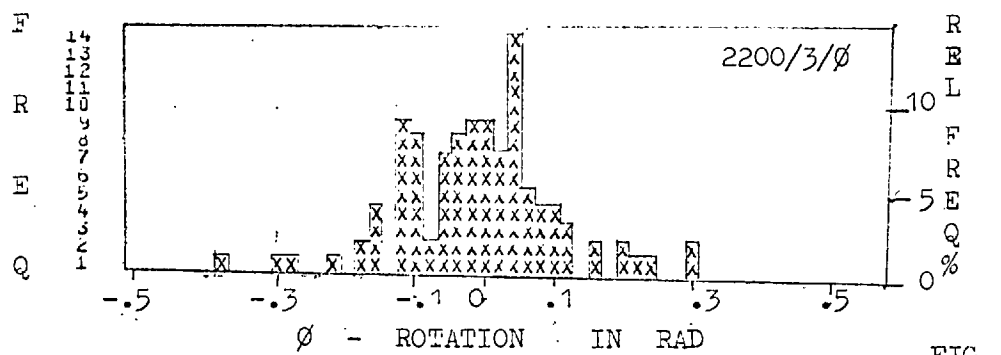
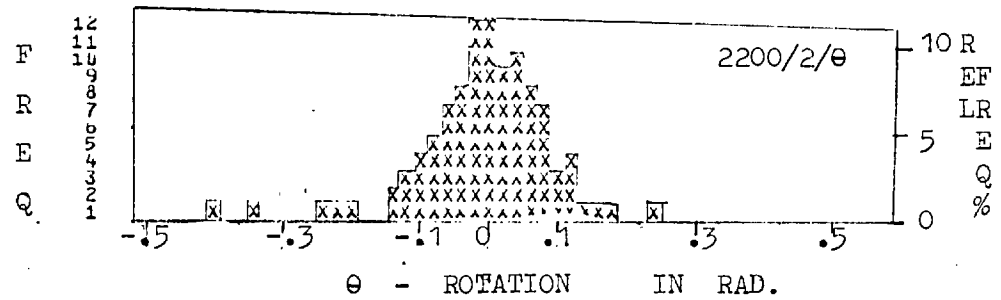
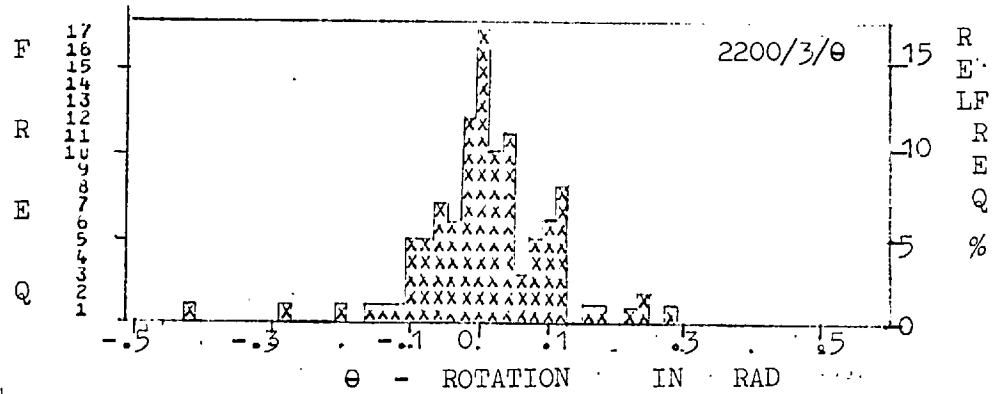
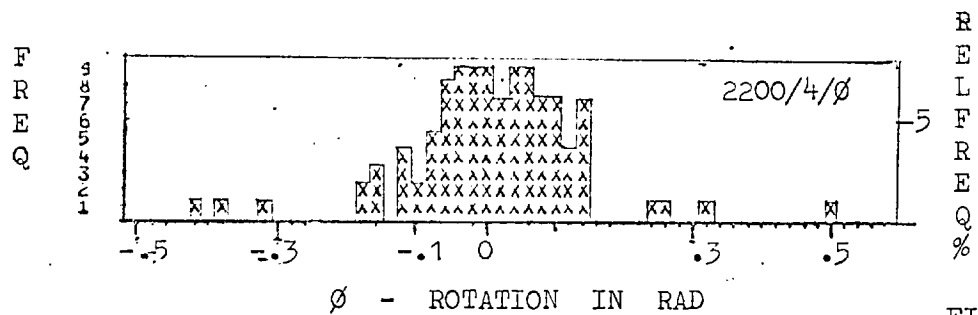


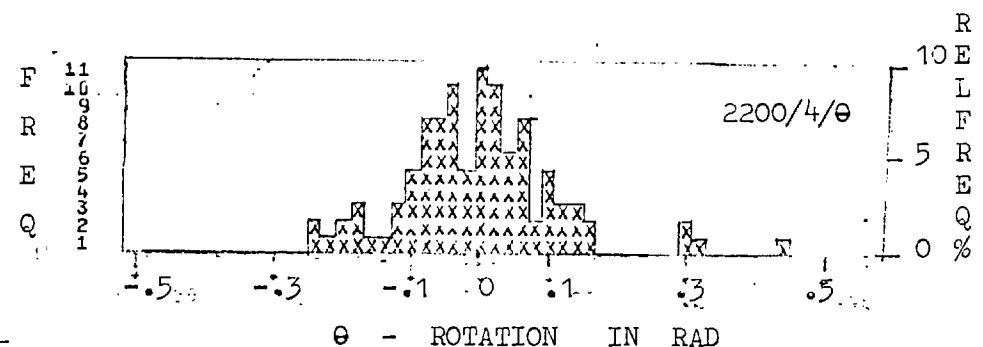
FIG. 7.44



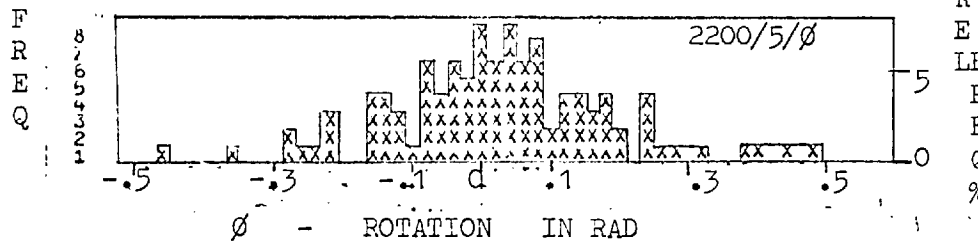


FREQUENCY %

FIG. 7.45

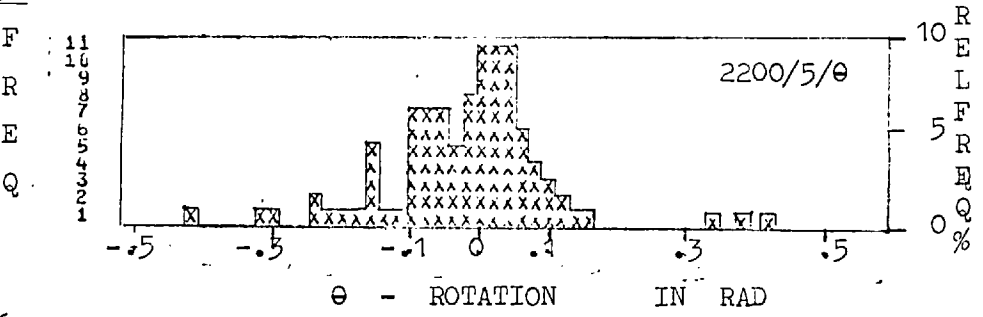


RELATIVE FREQUENCY %

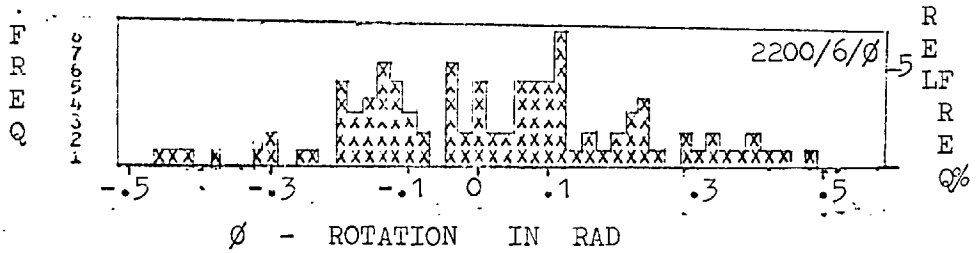


FREQUENCY %

FIG. 7.46

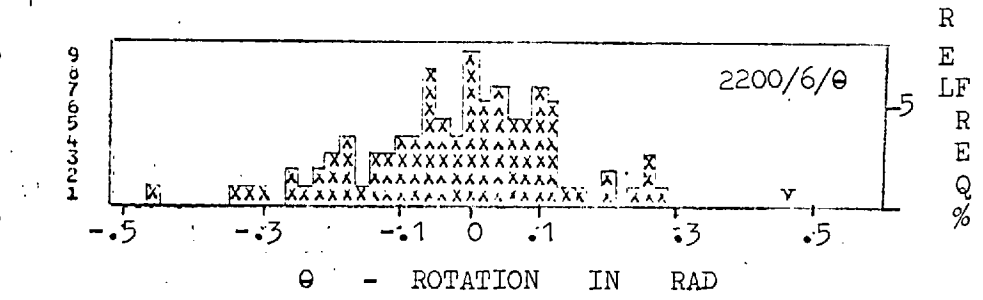


RELATIVE FREQUENCY %

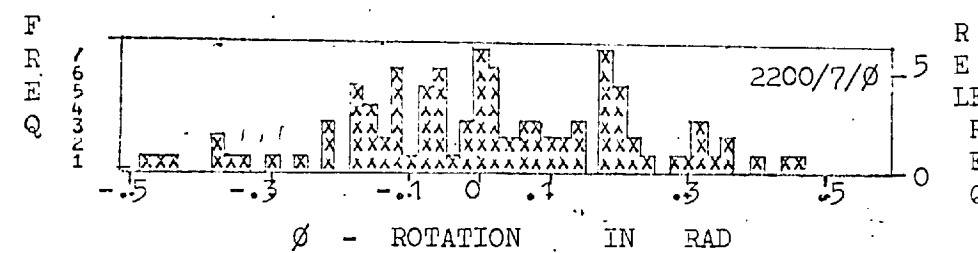


FREQUENCY %

FIG. 7.47

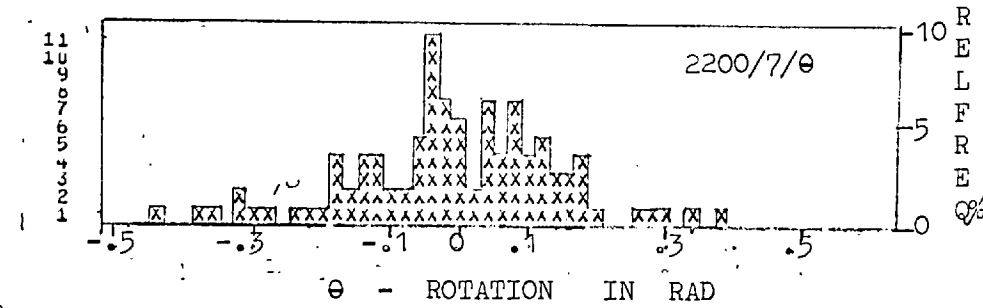


RELATIVE FREQUENCY %

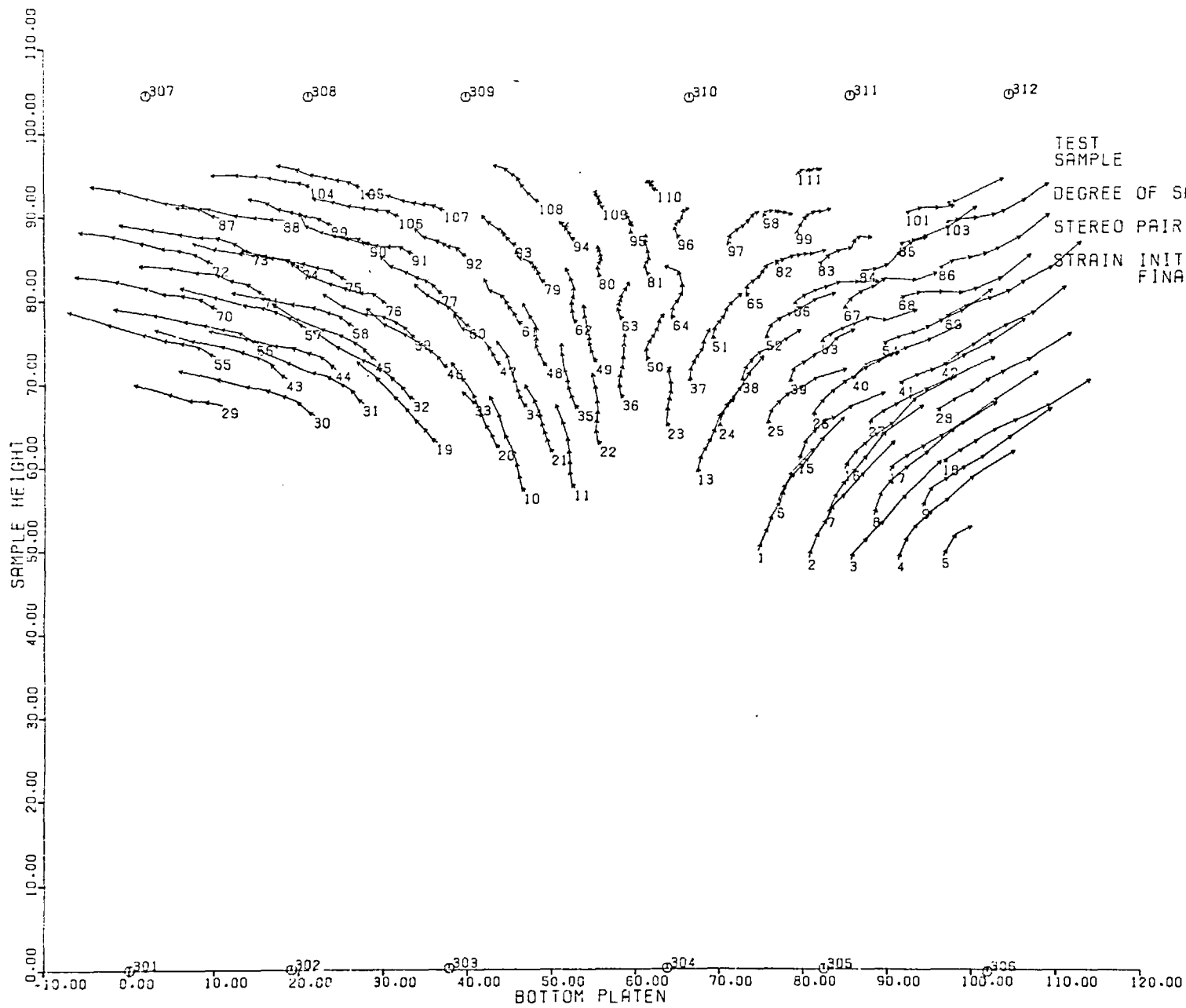


FREQUENCY %

FIG. 7.48



RELATIVE FREQUENCY %



TEST
SAMPLE

PLANE STRAIN (DRAINED)
GLASS BALLS

DEGREE OF SAT.

DRY

STEREO PAIR NO.

FIRST 1

STRAIN INITIAL

LAST 8

FINAL

0.0

19.414

SCALE

10mm

FIG 7.49

TRACE OF DISPLACEMENTS OF MARKER CENTRES ON XY PLANE

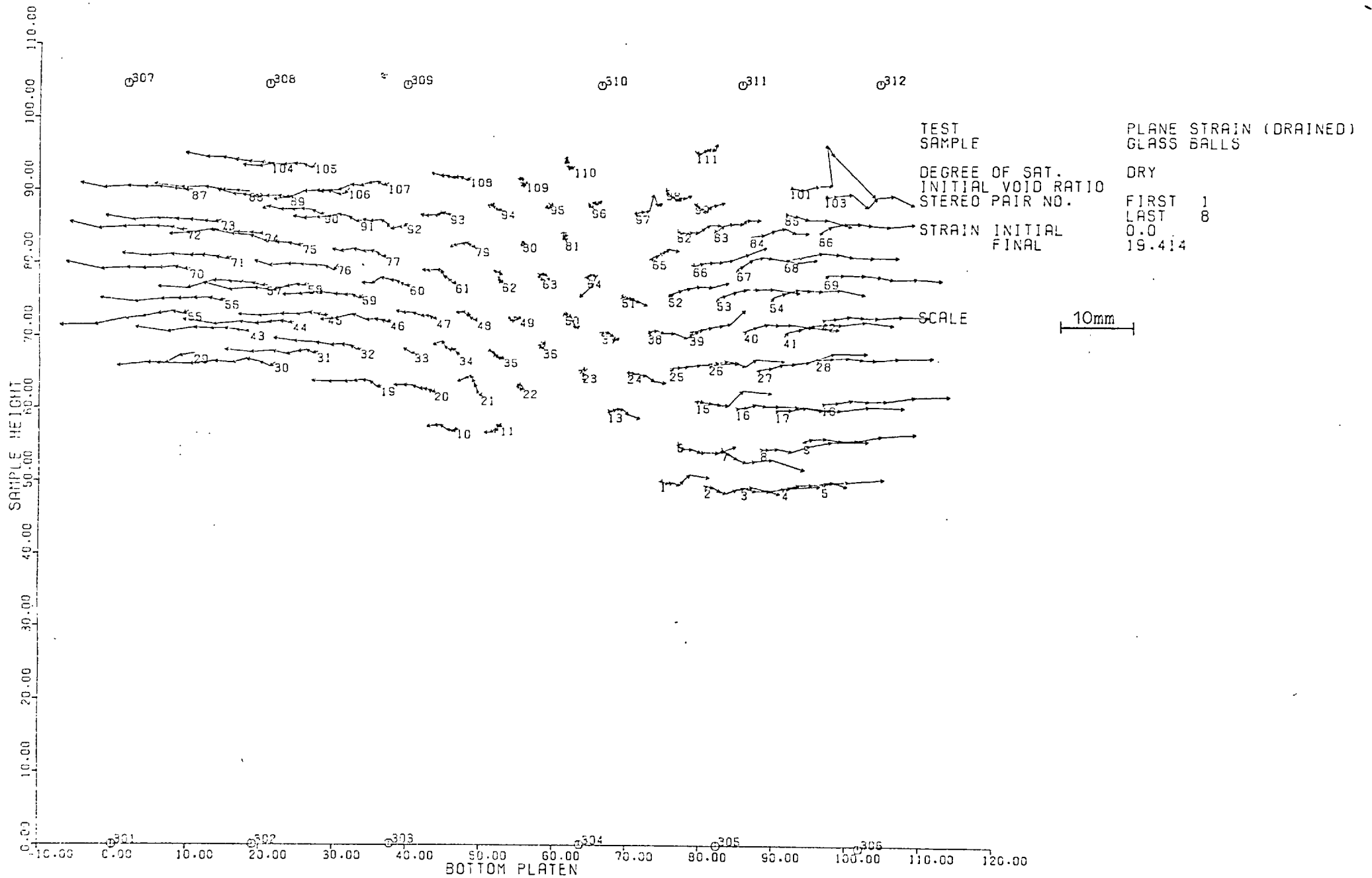
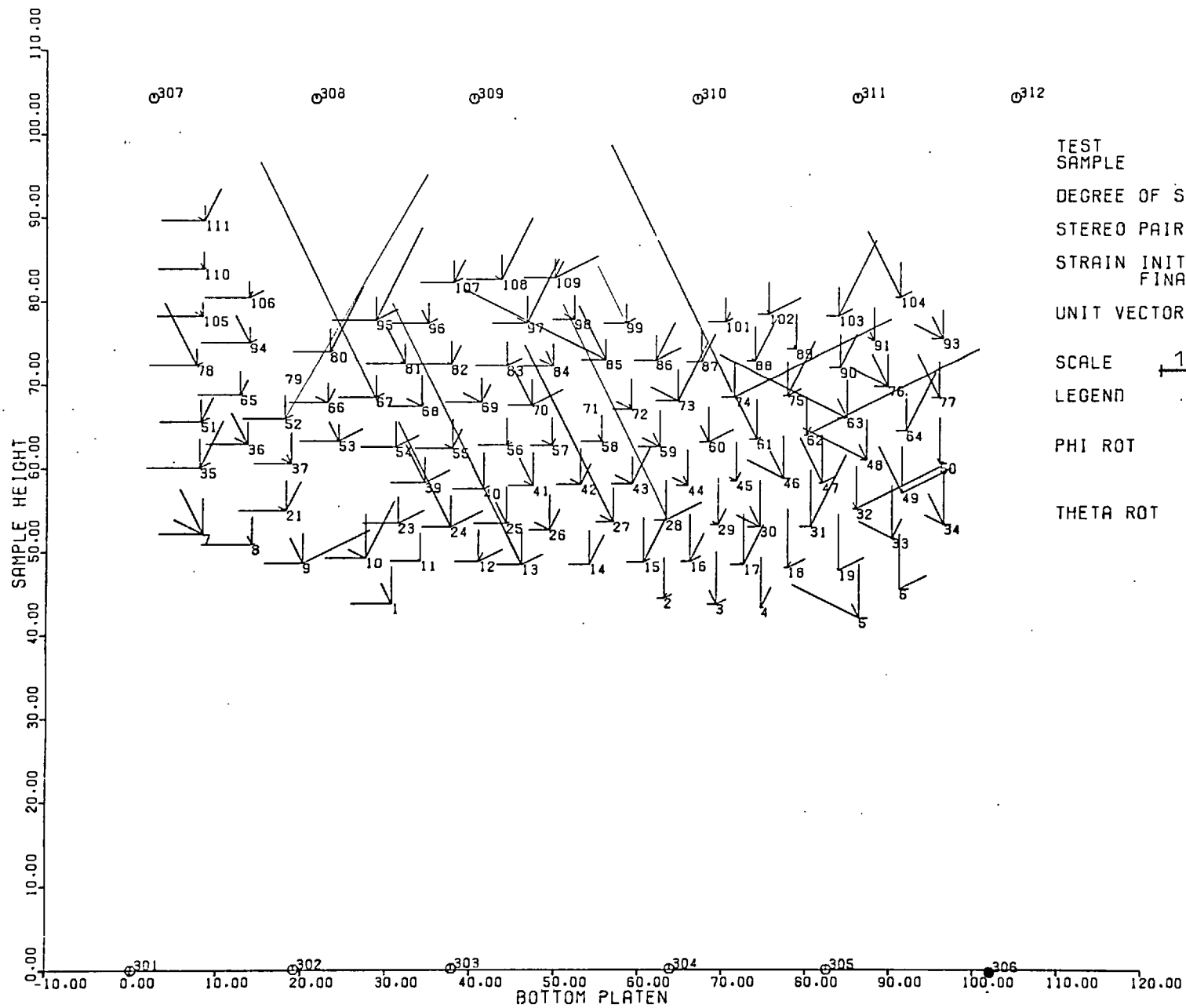


FIG 7.50

TRACE OF DISPLACEMENTS OF MARKER CENTRES ON XZ PLANE



TEST
SAMPLE

DEGREE OF SAT.

STEREO PAIR NO.

STRAIN INITIAL
FINAL

UNIT VECTOR DISP.

SCALE $\overline{10mm}$

LEGEND

PHI ROT

THETA ROT

2201/1
PLANE STRAIN (DRAINED)
GLASS BALLS

DEGREE OF SAT. FULLY SAT.

STEREO PAIR NO. FIRST 1
FINAL 2

STRAIN INITIAL 0.000
FINAL 1.007

UNIT VECTOR DISP. HOR. X $\overline{1mm}$
VER. Y $\overline{.1rad}$

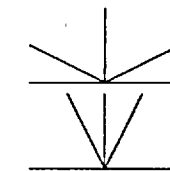
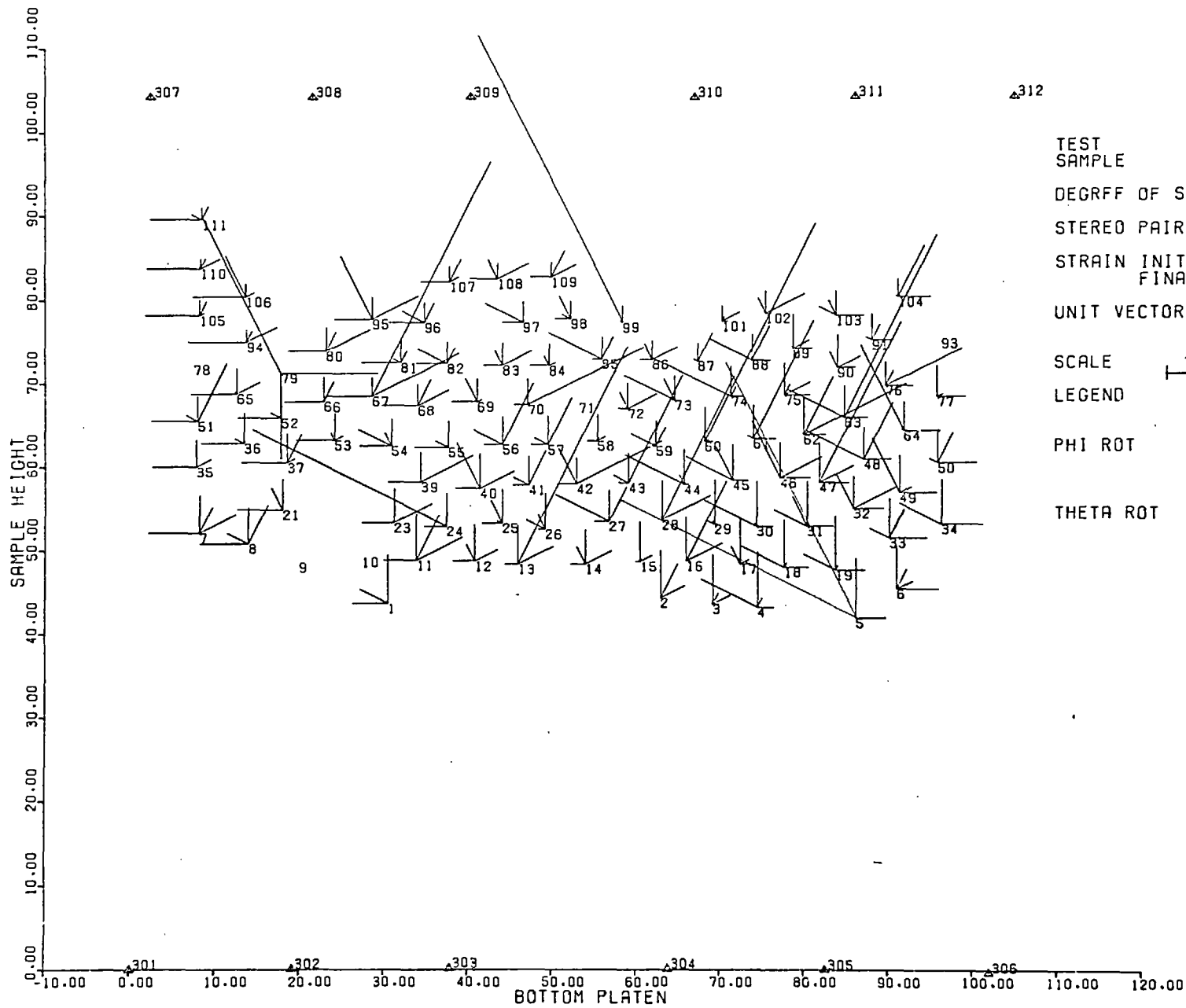


FIG 7.51 DISPLACEMENT - ROTATION FIELD OF MARKERS IN XY PLANE



TEST
SAMPLE

DEGRFF OF SAT.

STEREO PAIR NO.

STRAIN INITIAL
FINAL

UNIT VECTOR DISP.

SCALE

LEGEND

PHI ROT

THETA ROT

2201/2
PLANE STRAIN (DRAINED)
GLASS BALLS

FULLY SAT.

FIRST 2
FINAL 3
1.007
3.321

HOR.X] 2mm
VER.Y]
ROT. 10mm
2rad

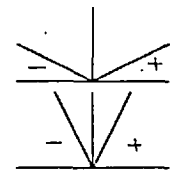
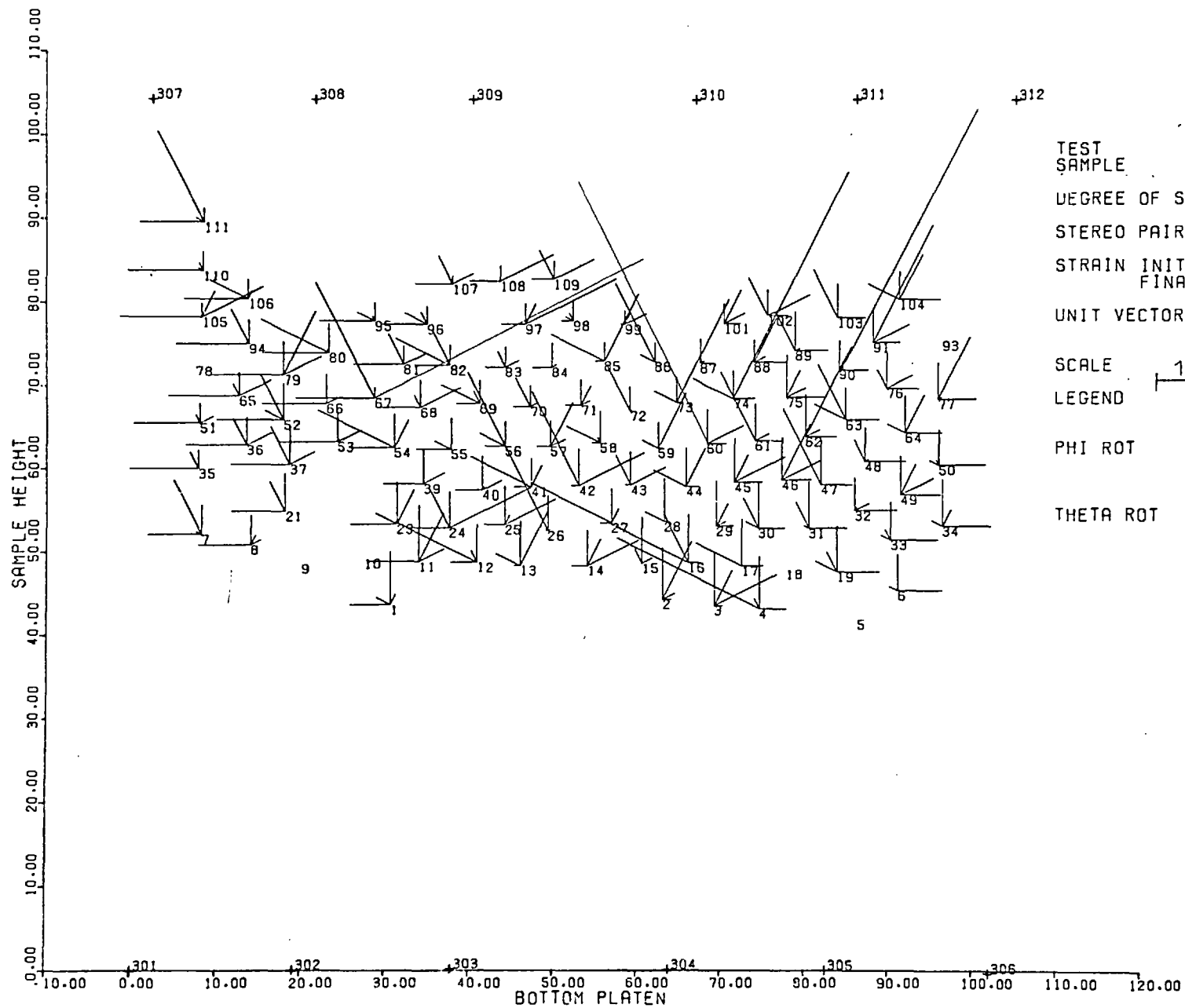


FIG 7.52 DISPLACEMENT - ROTATION FIELD OF MARKERS IN XY PLANE



TEST SAMPLE
 DEGREE OF SAT.
 STEREO PAIR NO.
 STRAIN INITIAL
 FINAL
 UNIT VECTOR DISP.
 ROT.
 SCALE 10mm
 LEGEND

2201/3
 PLANE STRAIN (DRAINED)
 GLASS BALLS
 FULLY SAT.
 FIRST 3
 FINAL 4
 3.321
 5.715

HOR. X
 VER. Y
 2mm
 .2rad

PHI ROT
 THETA ROT

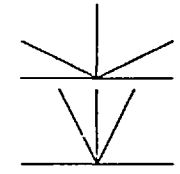
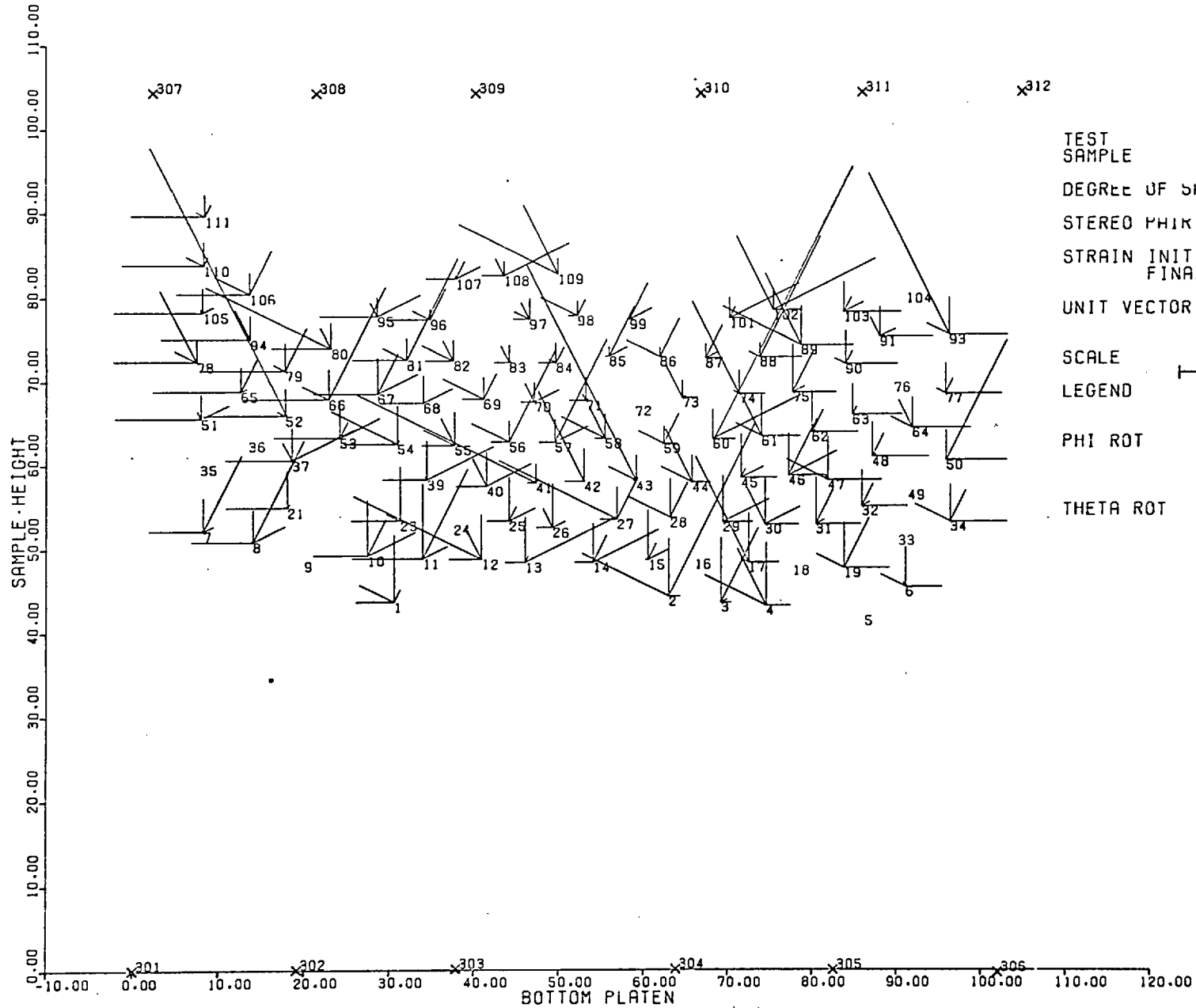


FIG 7.53 DISPLACEMENT - ROTATION FIELD OF MARKERS IN XY PLANE



TEST
SAMPLE

DEGREE OF SHI.

STEREO PAIR NO.

STRAIN INITIAL
FINAL

UNIT VECTOR DISP.

SCALE

LEGEND

PHI ROT

THETA ROT

2201/4
PLANE STRAIN (DRAINED)
GLASS BALLS

FULLY SAT.

FIRST 4
FINAL 5
5.715
8.197

HOR. X
VER. Y

2mm
.2rad

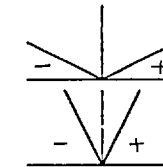
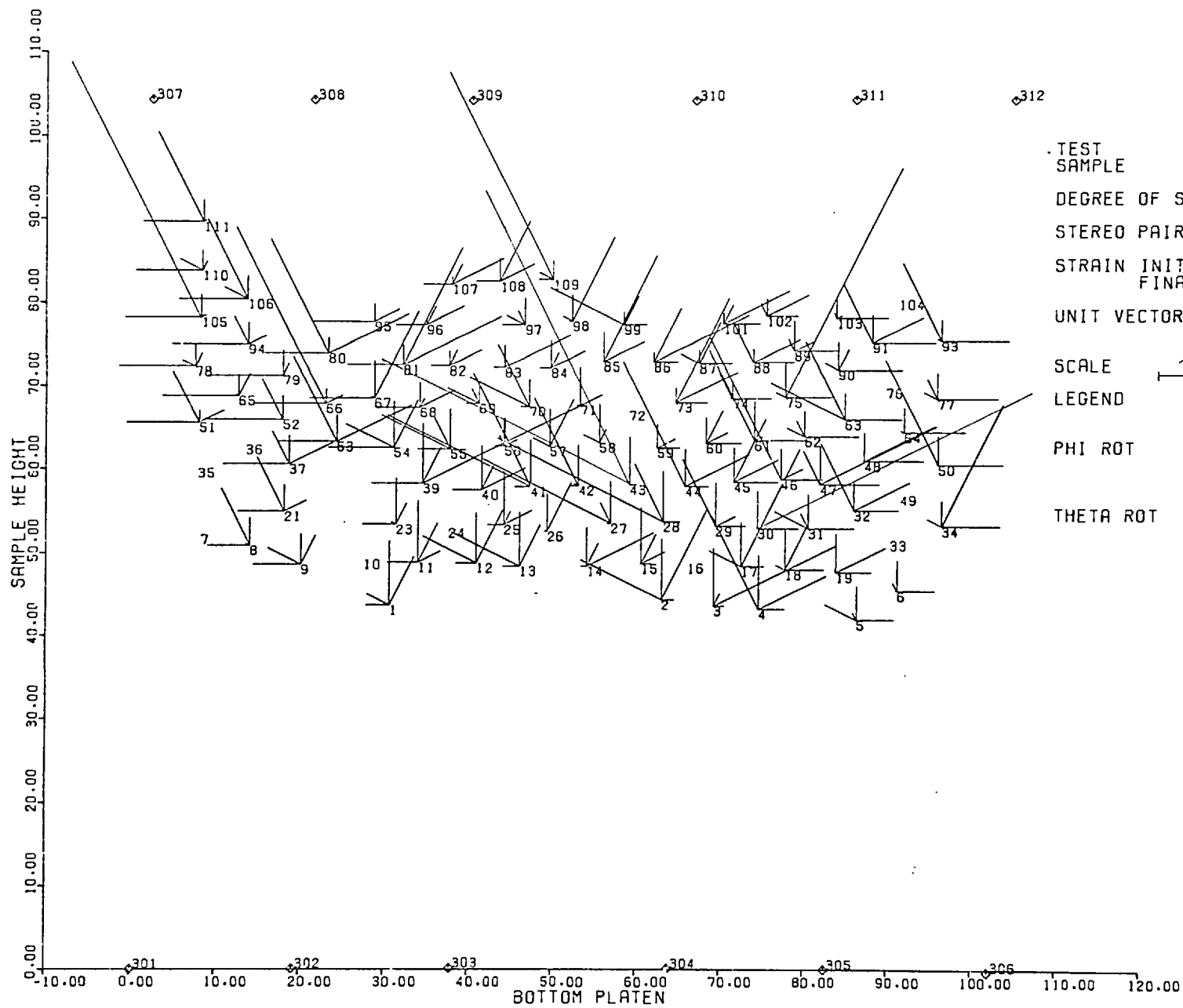
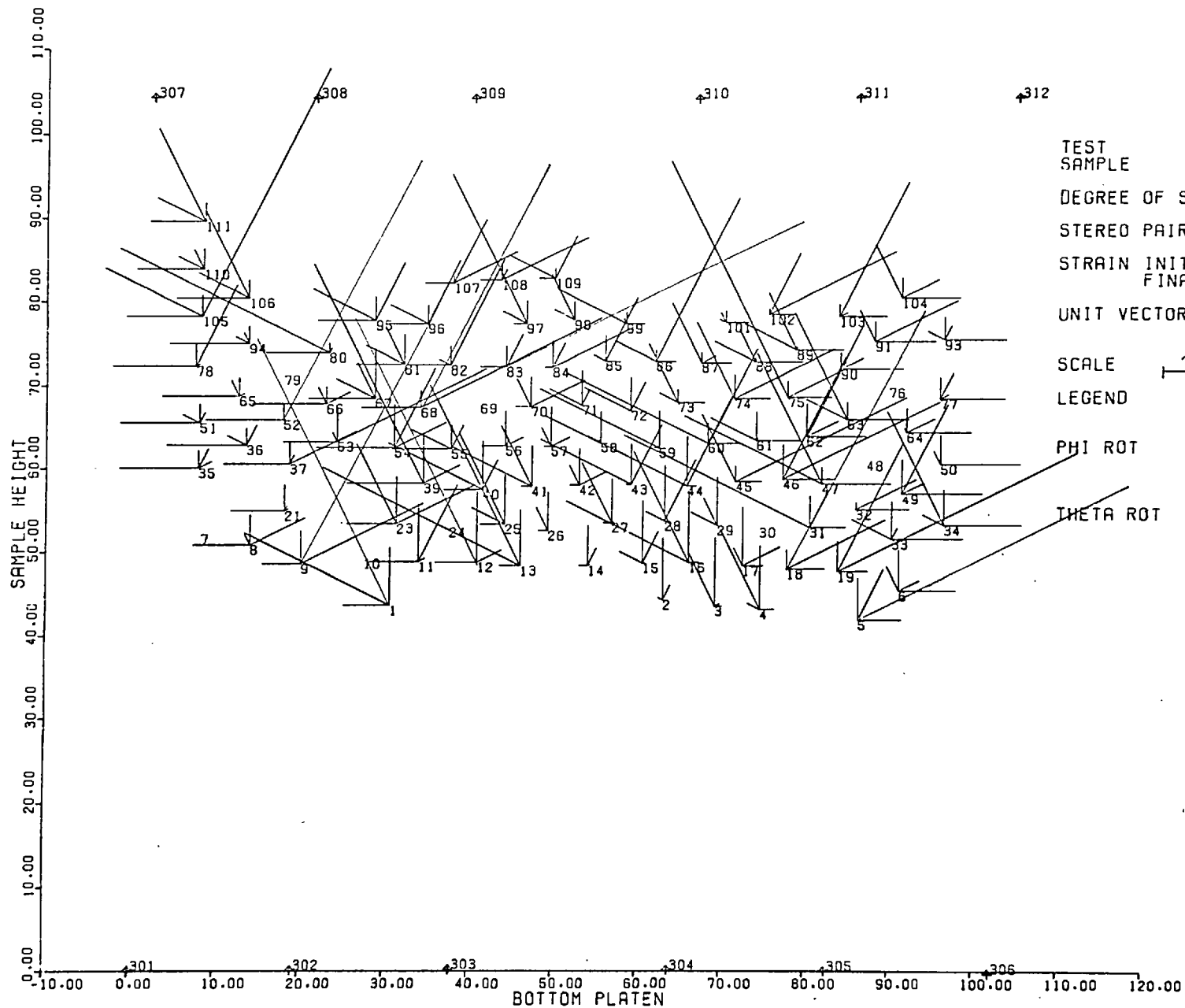


FIG 7.54 DISPLACEMENT - ROTATION FIELD OF MARKERS IN XY PLANE



TEST SAMPLE	2201/5 PLANE STRAIN (DRAINED) GLASS BALLS
DEGREE OF SAT.	FULLY SAT.
STEREO PAIR NO.	FIRST 5 FINAL 6
STRAIN INITIAL	8.197
STRAIN FINAL	10.370
UNIT VECTOR DISP.	HOR. X] 2mm VER. Y]
SCALE	ROT 10mm]] .2rad
LEGEND	
PHI ROT	
THETA ROT	

FIG 7.55 DISPLACEMENT - ROTATION FIELD OF MARKERS IN XY PLANE



TEST
SAMPLE

DEGREE OF SAT.

STEREO PAIR NO.

STRAIN INITIAL
FINAL

UNIT VECTOR DISP.

SCALE $\overline{10mm}$

LEGEND

PHI ROT

THETA ROT

2201/6

PLANE STRAIN (DRAINED)
GLASS BALLS

FULLY SAT.

FIRST 6
FINAL 7

10.370
13.913

HOR.X]
VER.Y]

$\overline{3mm}$

$\overline{.2rad}$

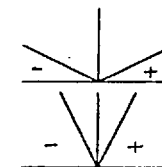


FIG 7.56 DISPLACEMENT - ROTATION FIELD OF MARKERS IN XY PLANE

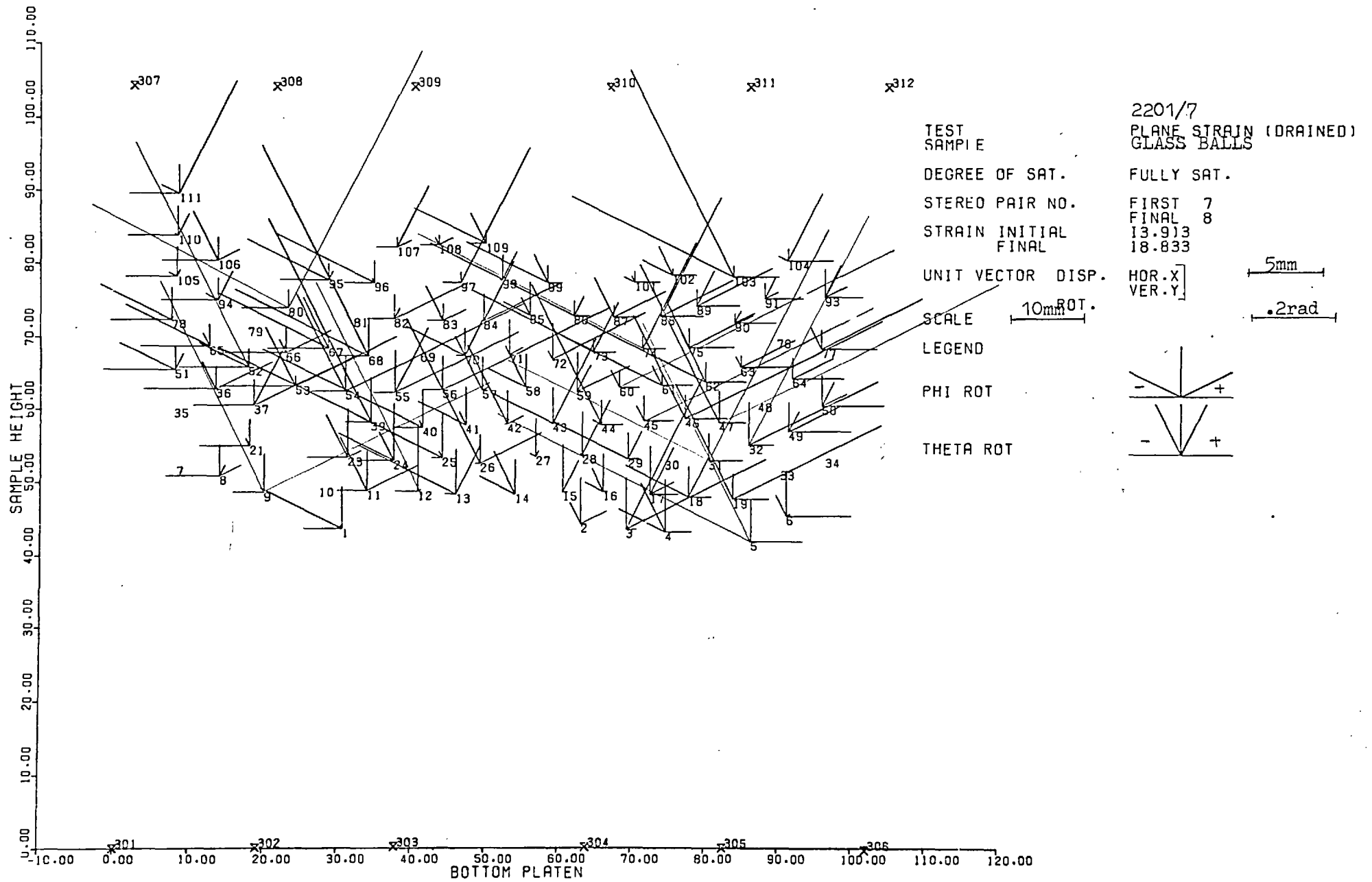


FIG 7.57 DISPLACEMENT - ROTATION FIELD OF MARKERS IN XY PLANE

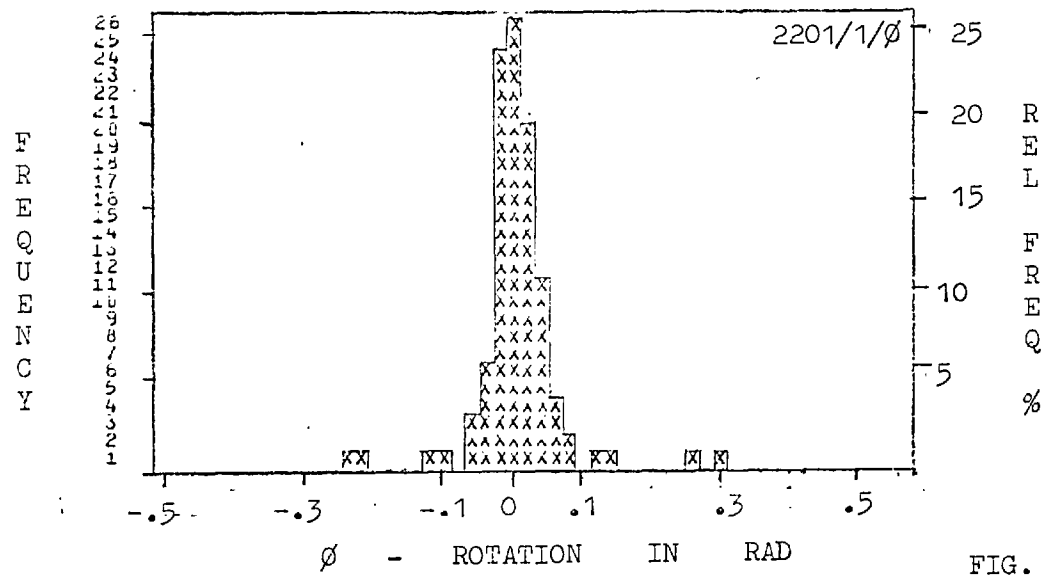


FIG. 7.58

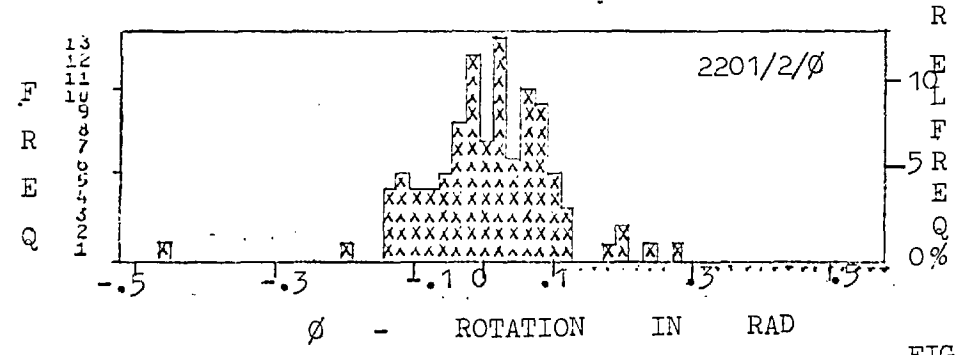
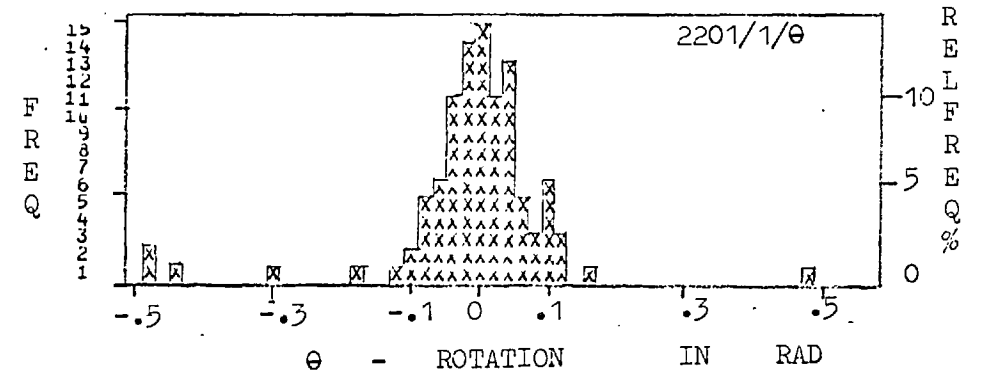


FIG. 7.59

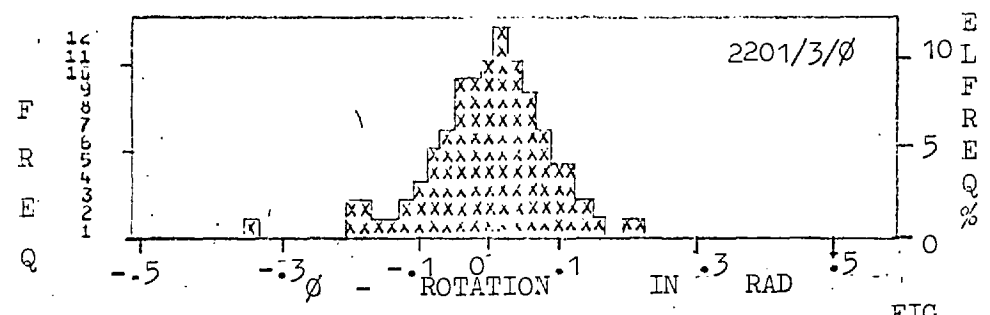
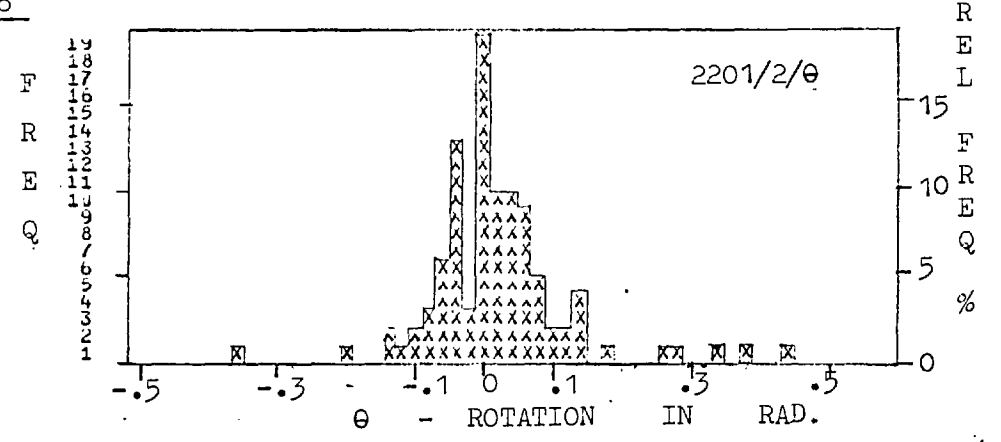
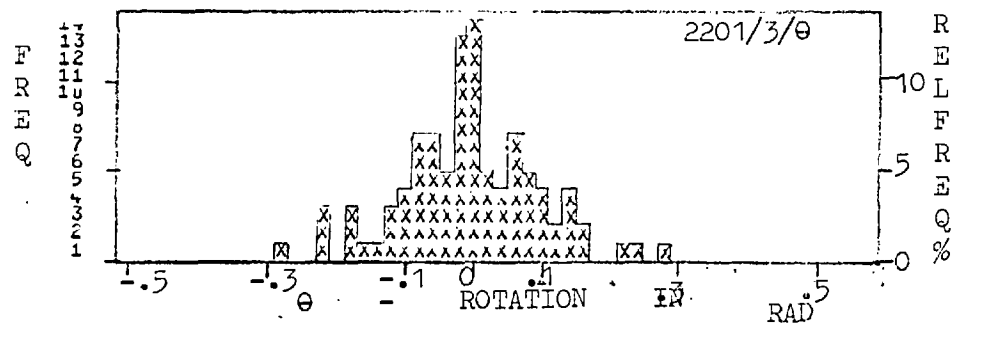


FIG. 7.60



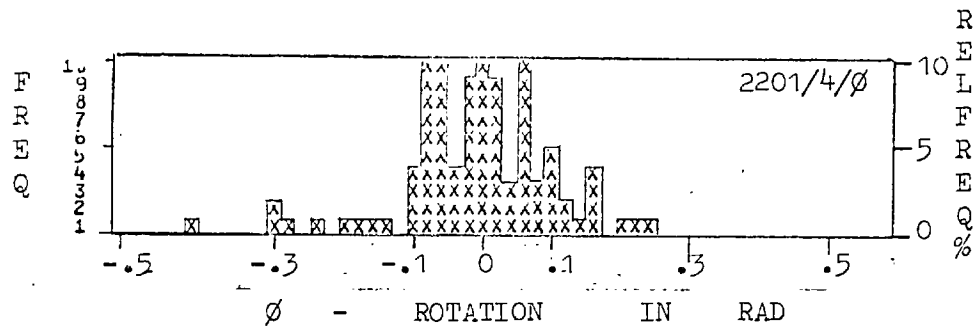


FIG. 7.61

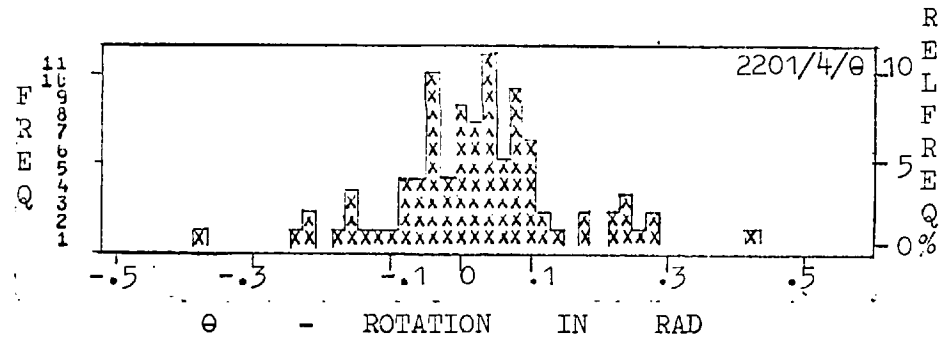


FIG. 7.62

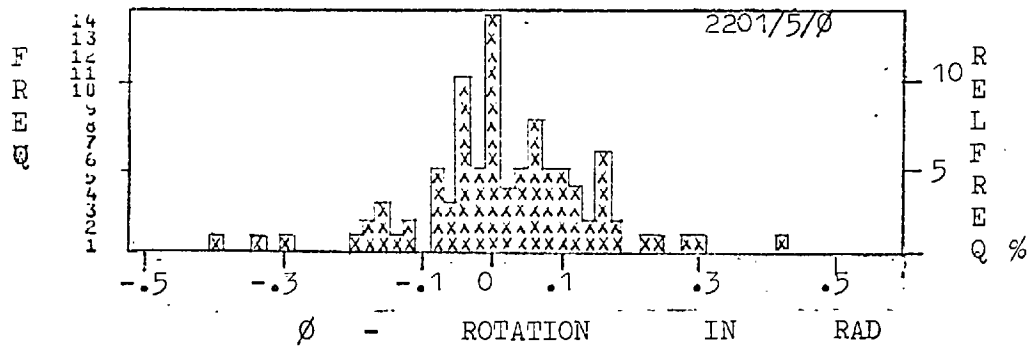


FIG. 7.63

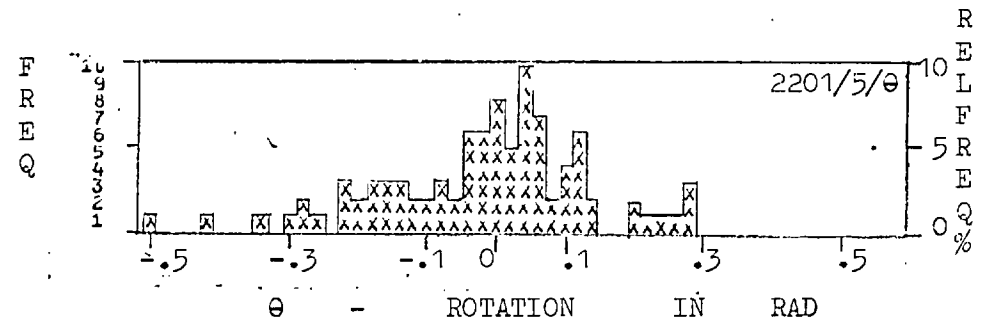
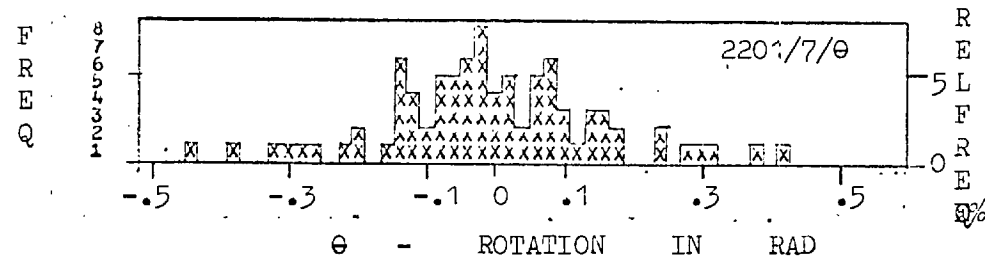
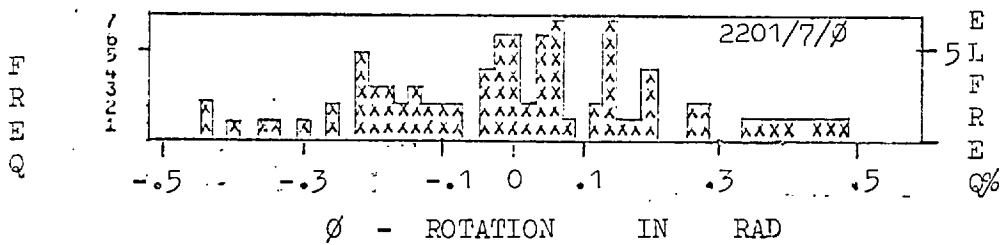
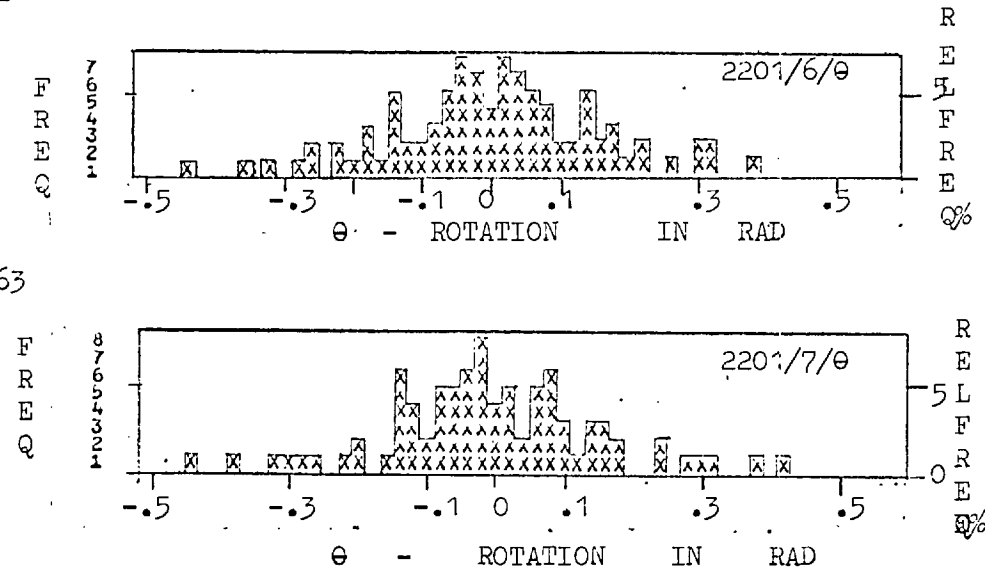
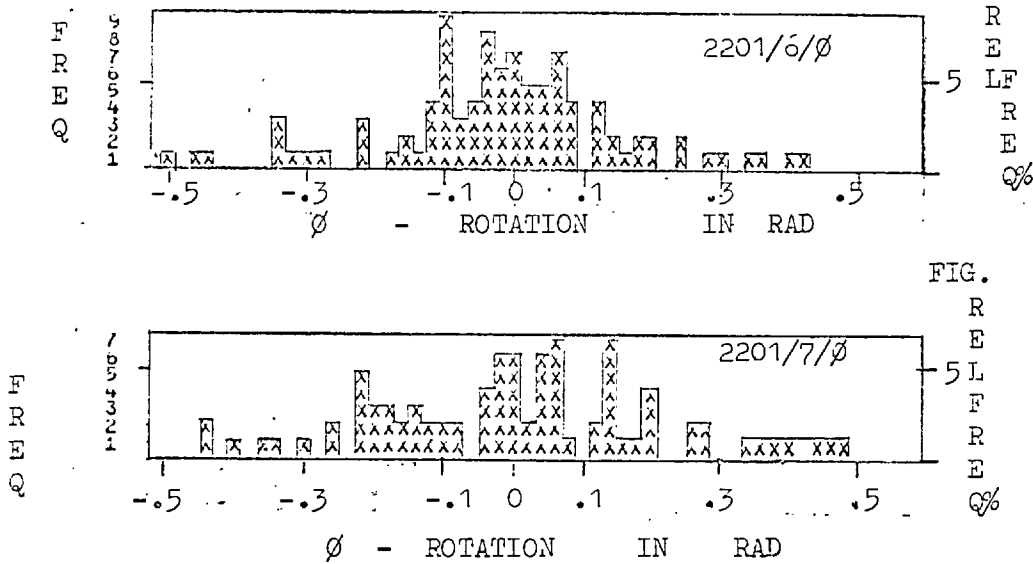
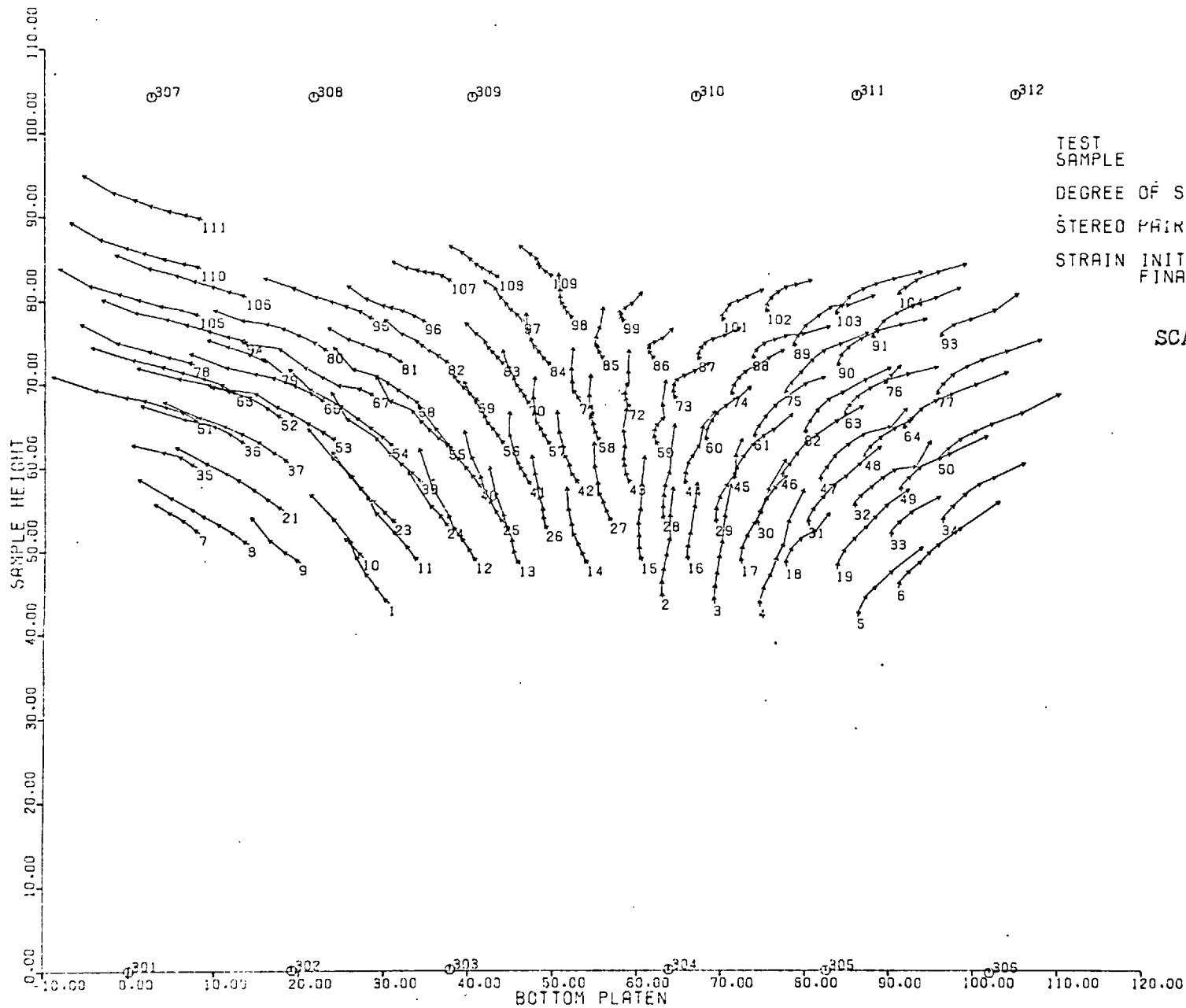


FIG. 7.64





TEST
SAMPLE

DEGREE OF SAT.

STEREO PAIR NO.

STRAIN INITIAL
FINAL

PLANE STRAIN (DRAINED)
GLASS BALLS

FULLY SAT.

FIRST 1

LAST 8

0.0

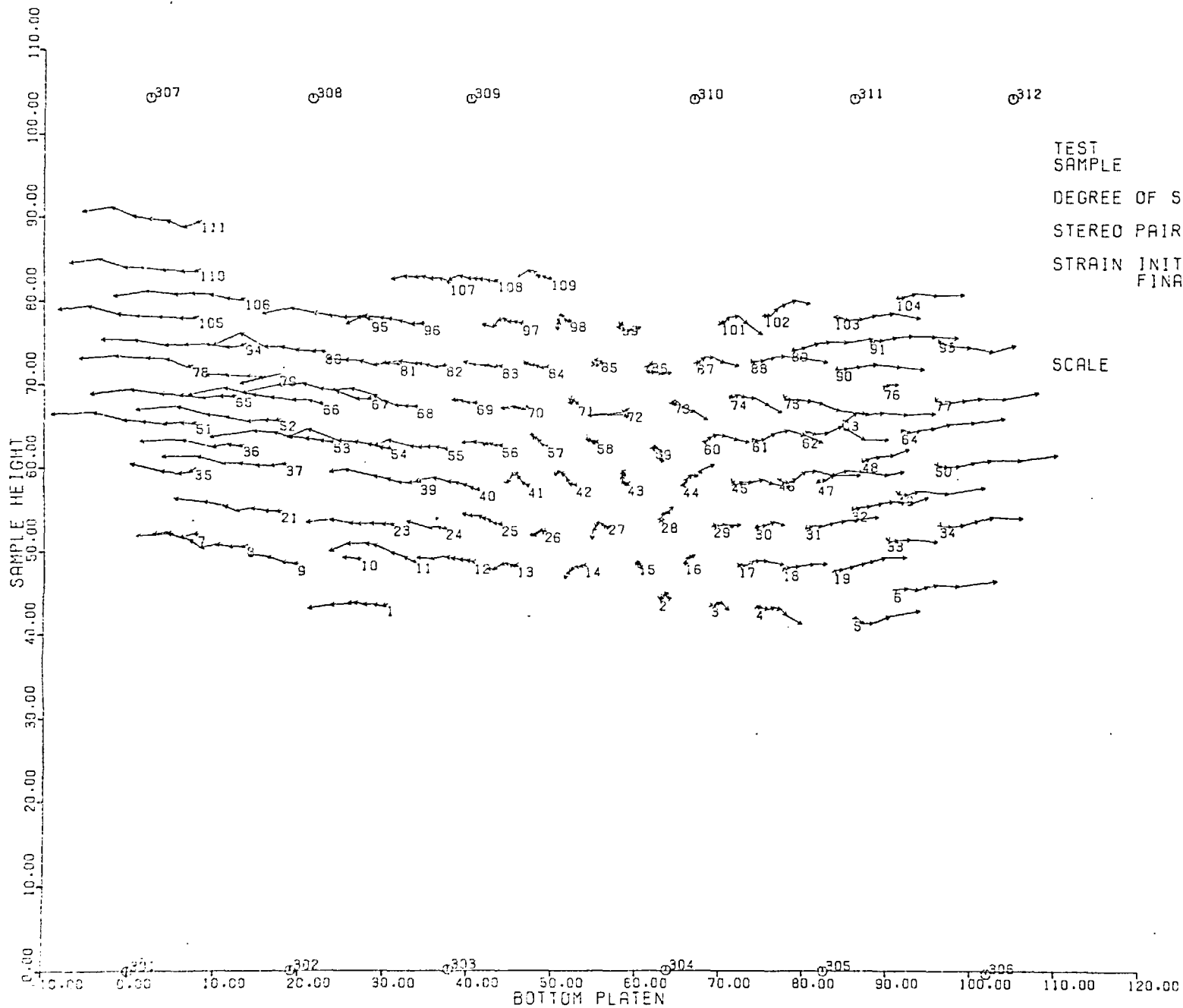
18.833

SCALE

10mm

FIG 7.65

TRACE OF DISPLACEMENTS OF MARKER CENTRES ON XY PLANE



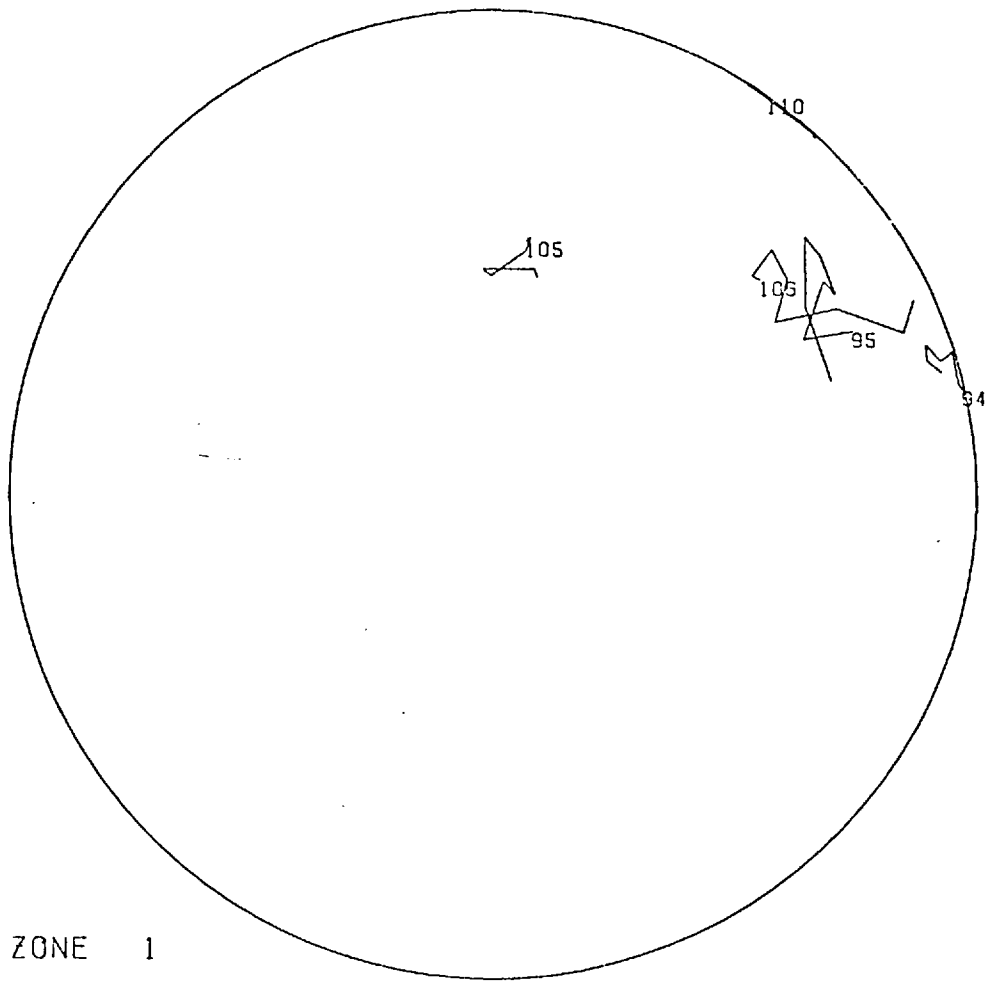
TEST SAMPLE	PLANE STRAIN (DRAINED)
DEGREE OF SAT.	GLASS BALLS
STEREO PAIR NO.	FULLY SAT.
STRAIN INITIAL	FIRST 1
FINAL	LAST 8
	0.C
	18.833

SCALE

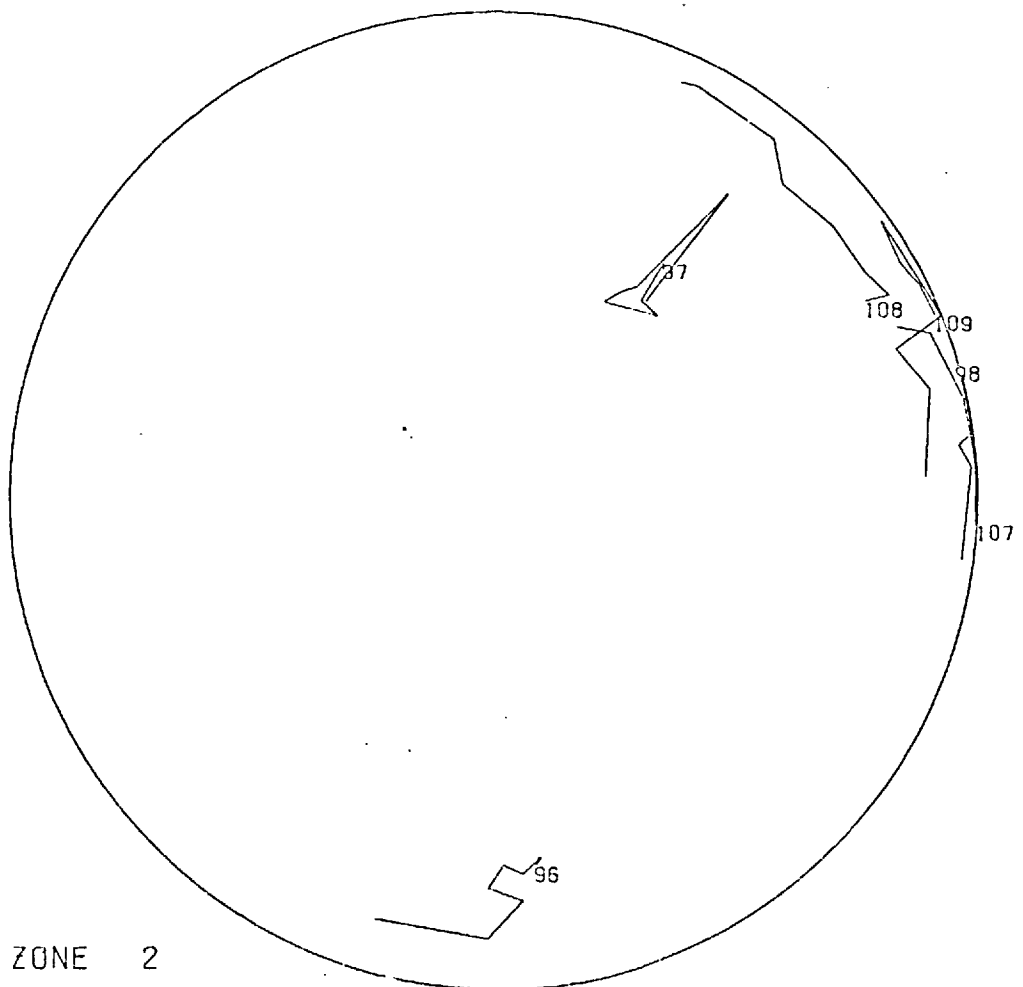
10mm

FIG 7.66

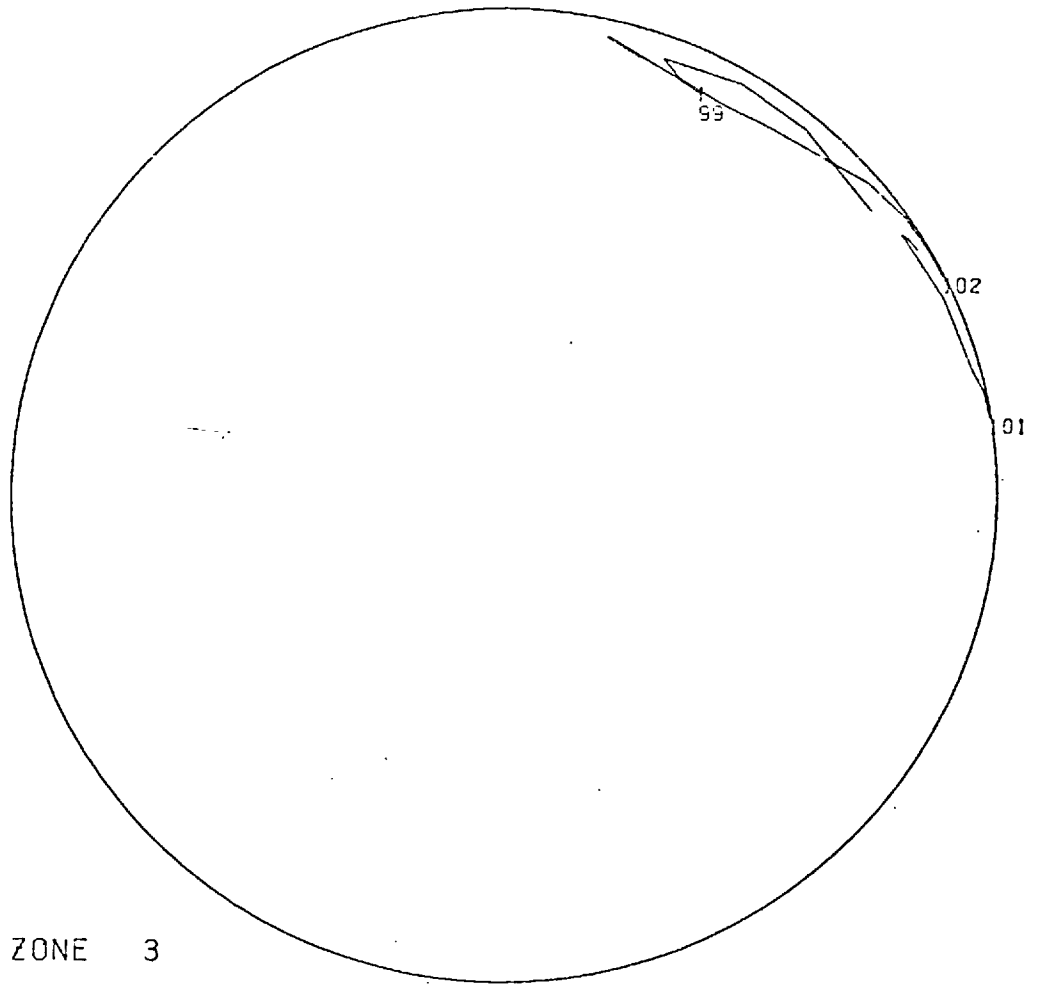
TRACE OF DISPLACEMENTS OF MARKER CENTRES ON XZ PLANE



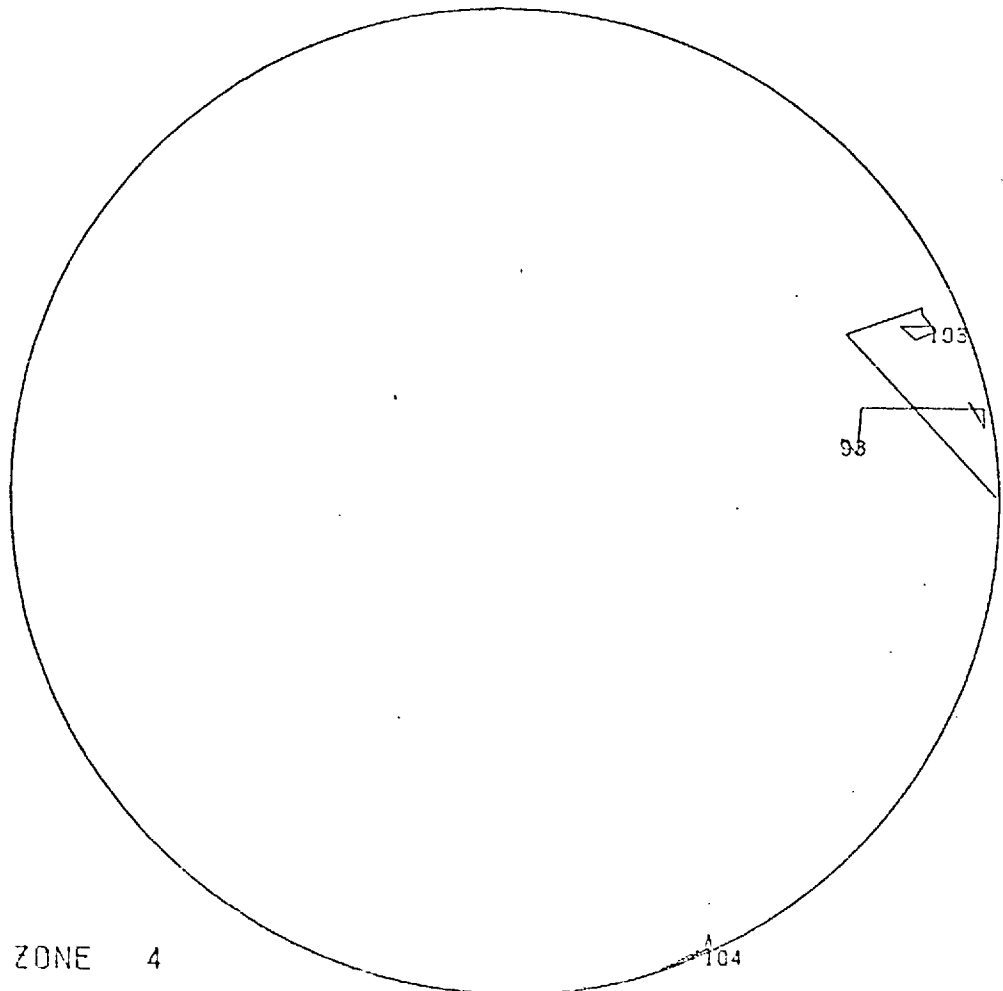
A) ZONE 1



B) ZONE 2

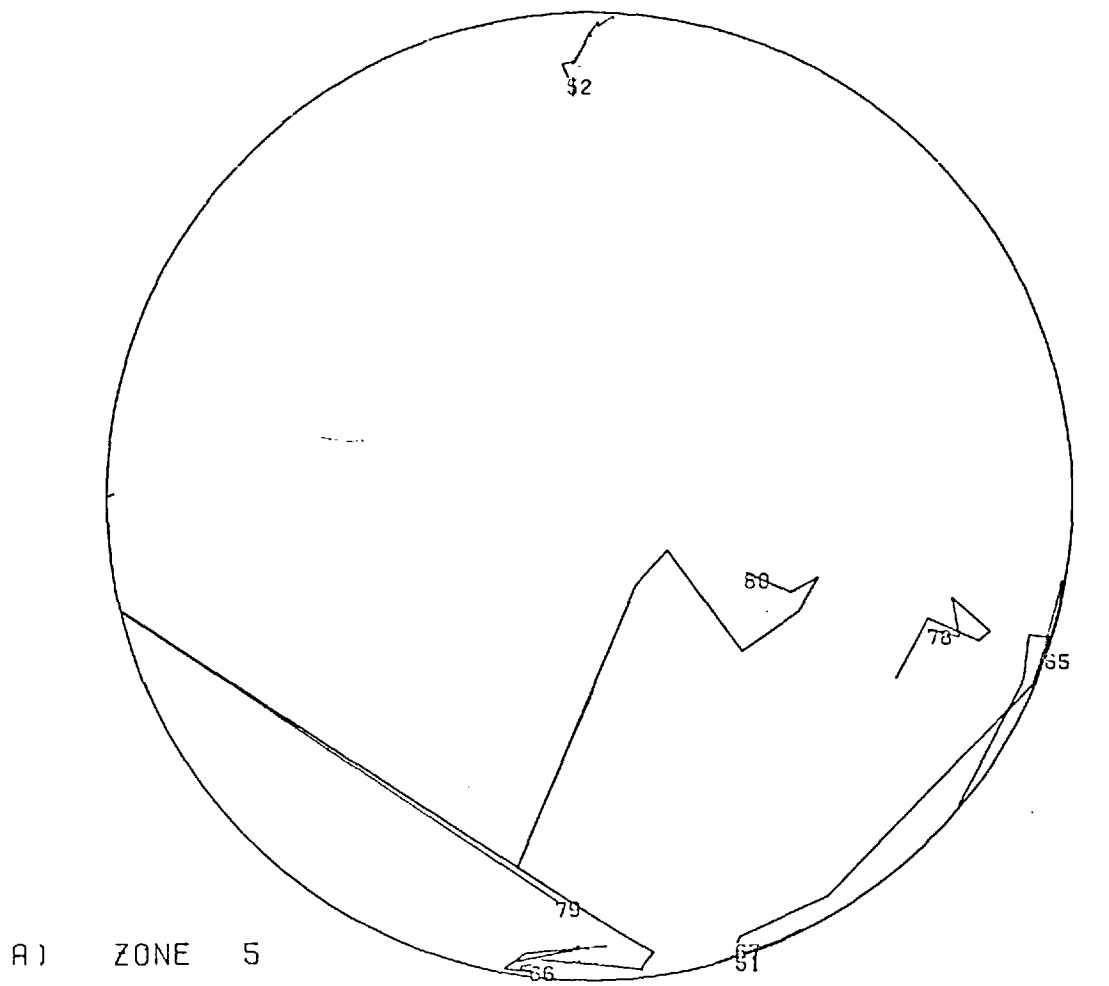


A) ZONE 3

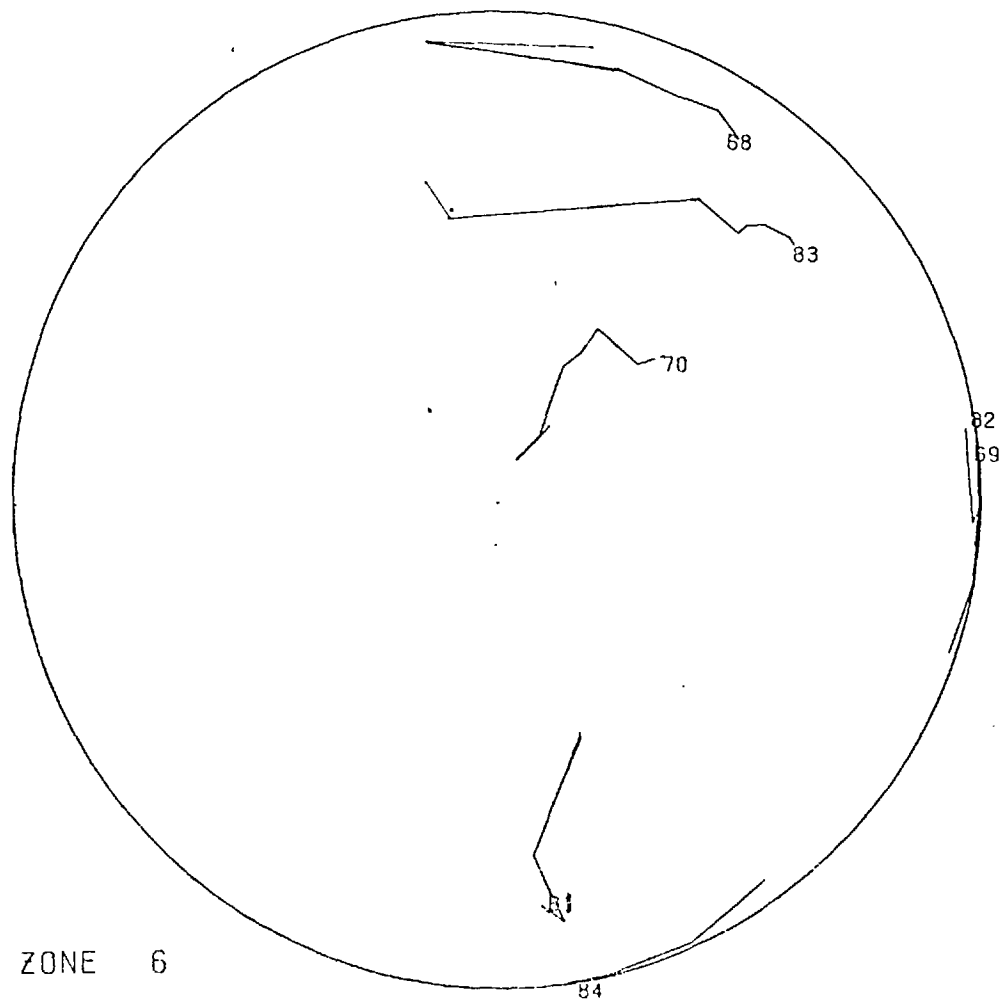


B) ZONE 4

FIG 7.68 TRACE OF PARTICLE ROTATION ON STERONEET



A) ZONE 5



B) ZONE 6

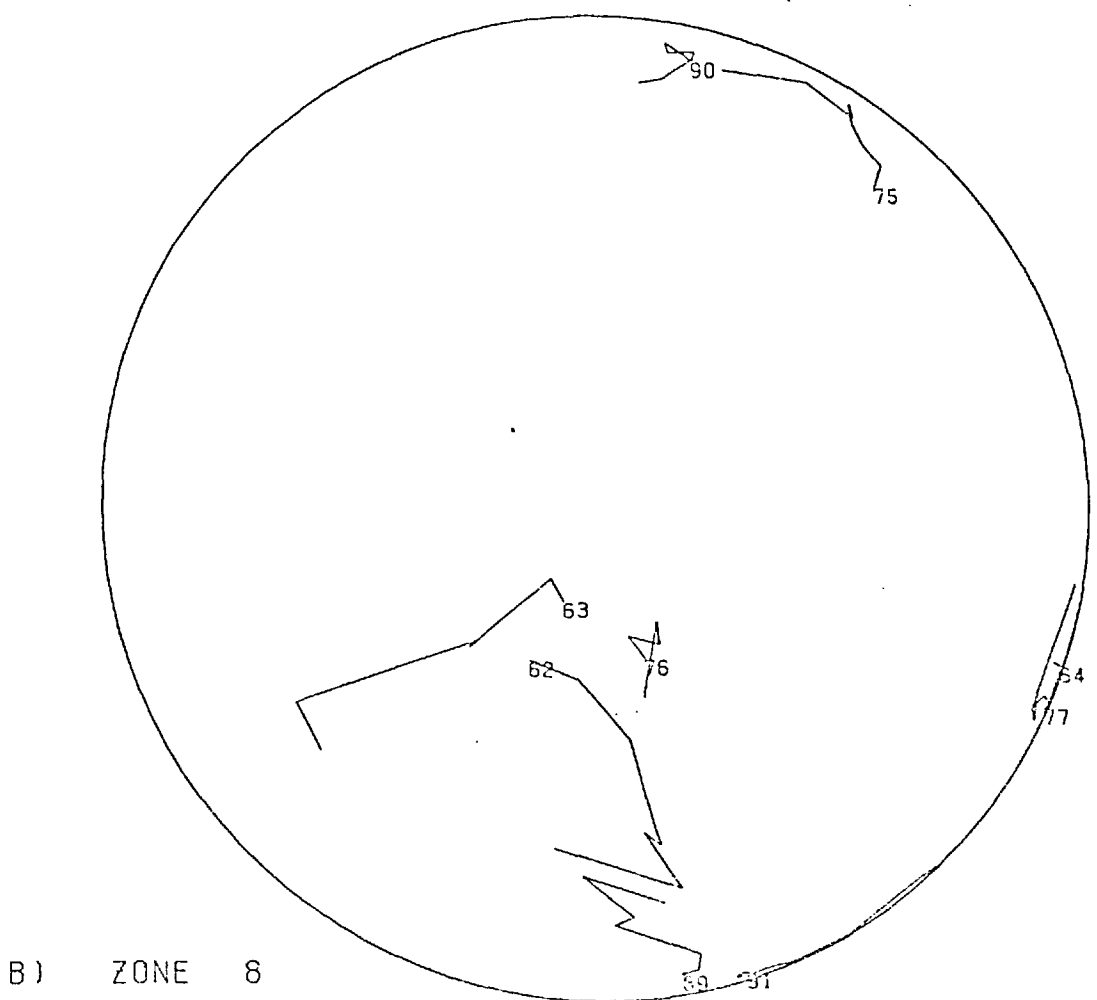
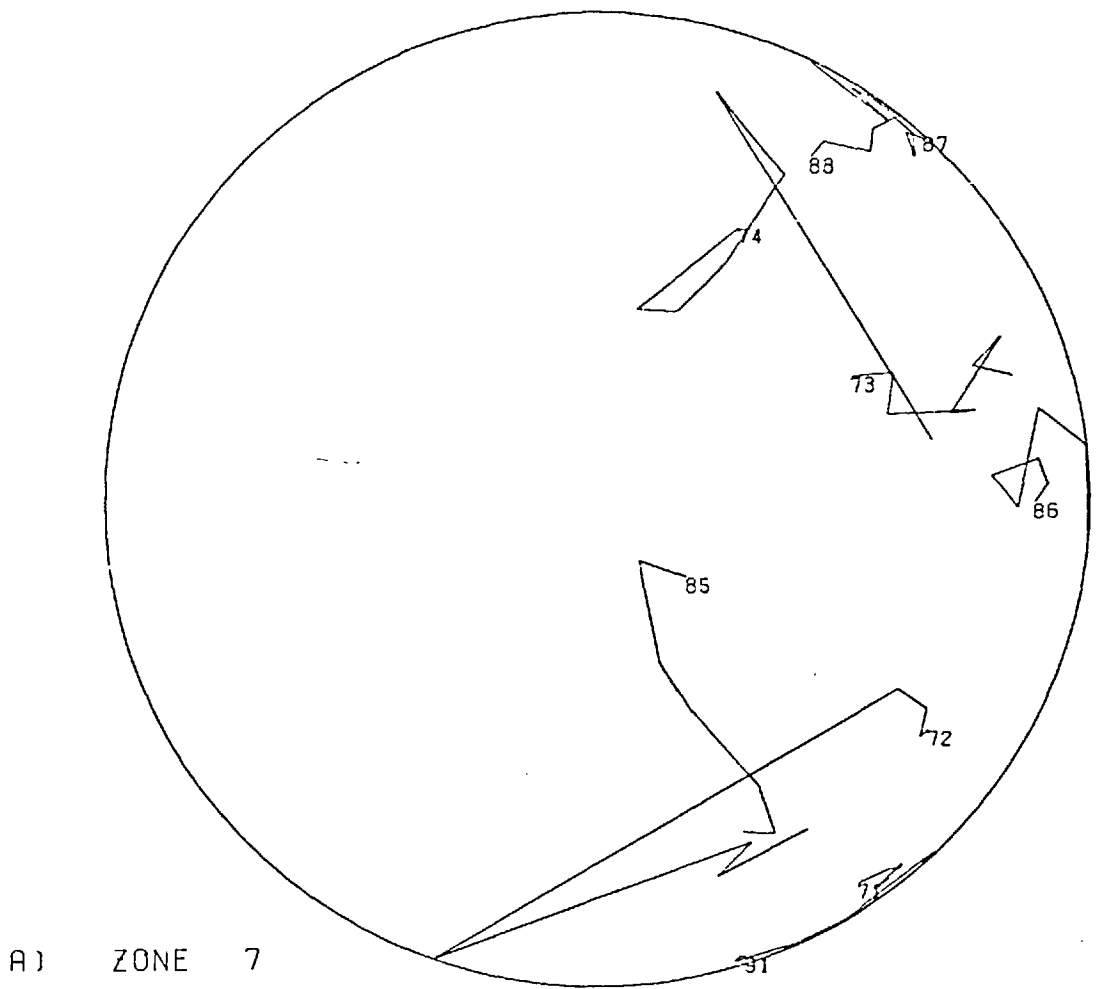


FIG 7.70 TRACE OF PARTICLE ROTATION ON STEREO NET TEST NO 2201

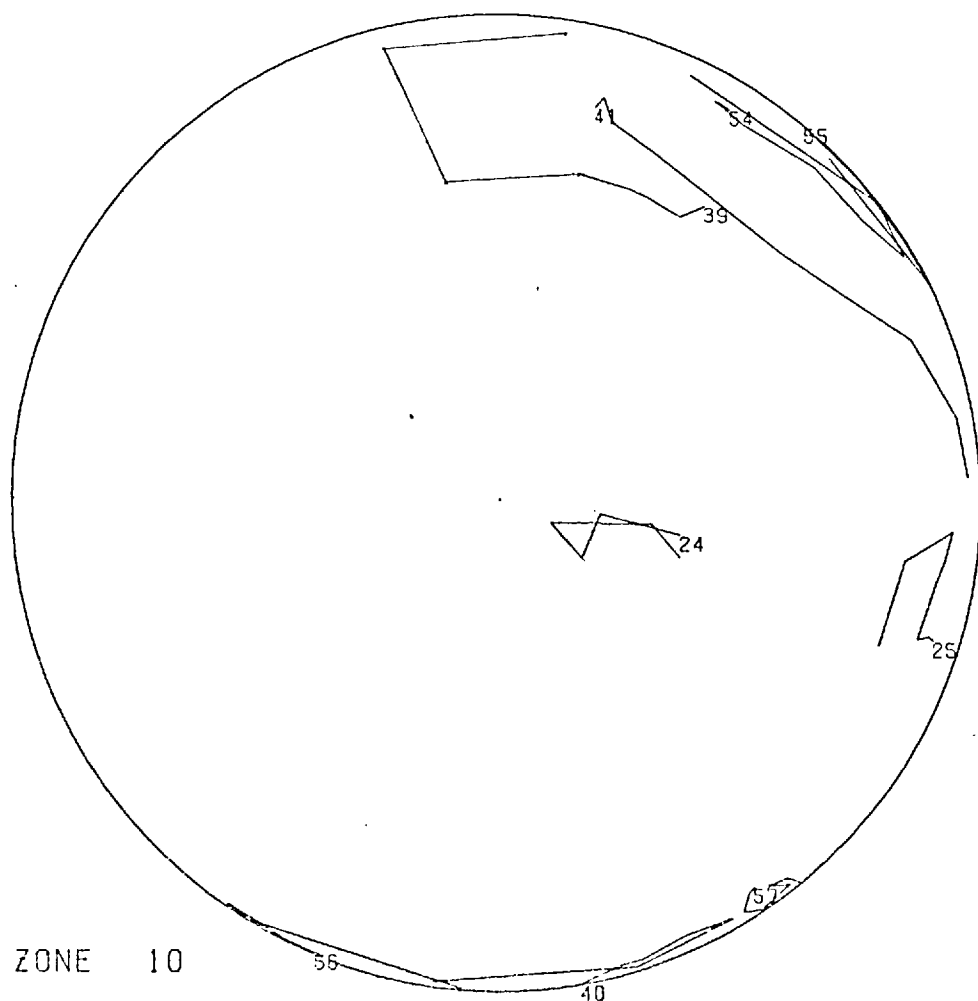
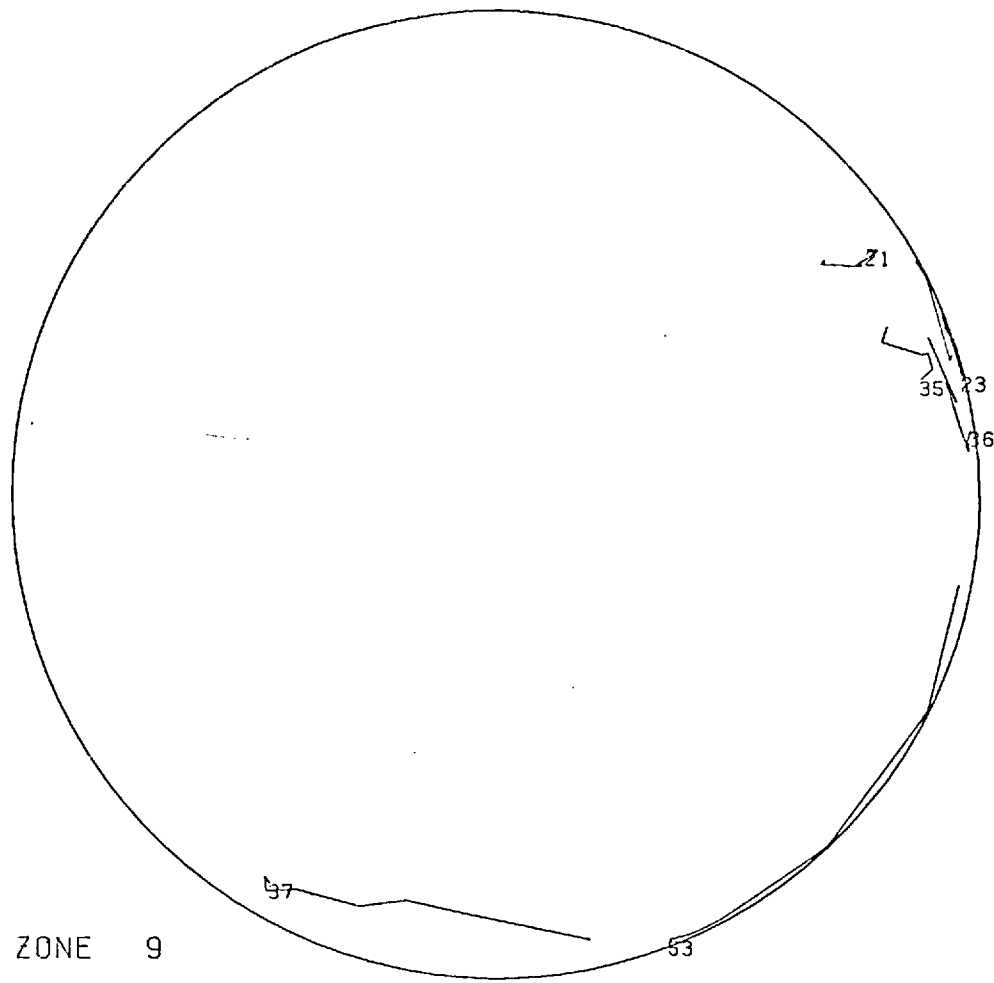
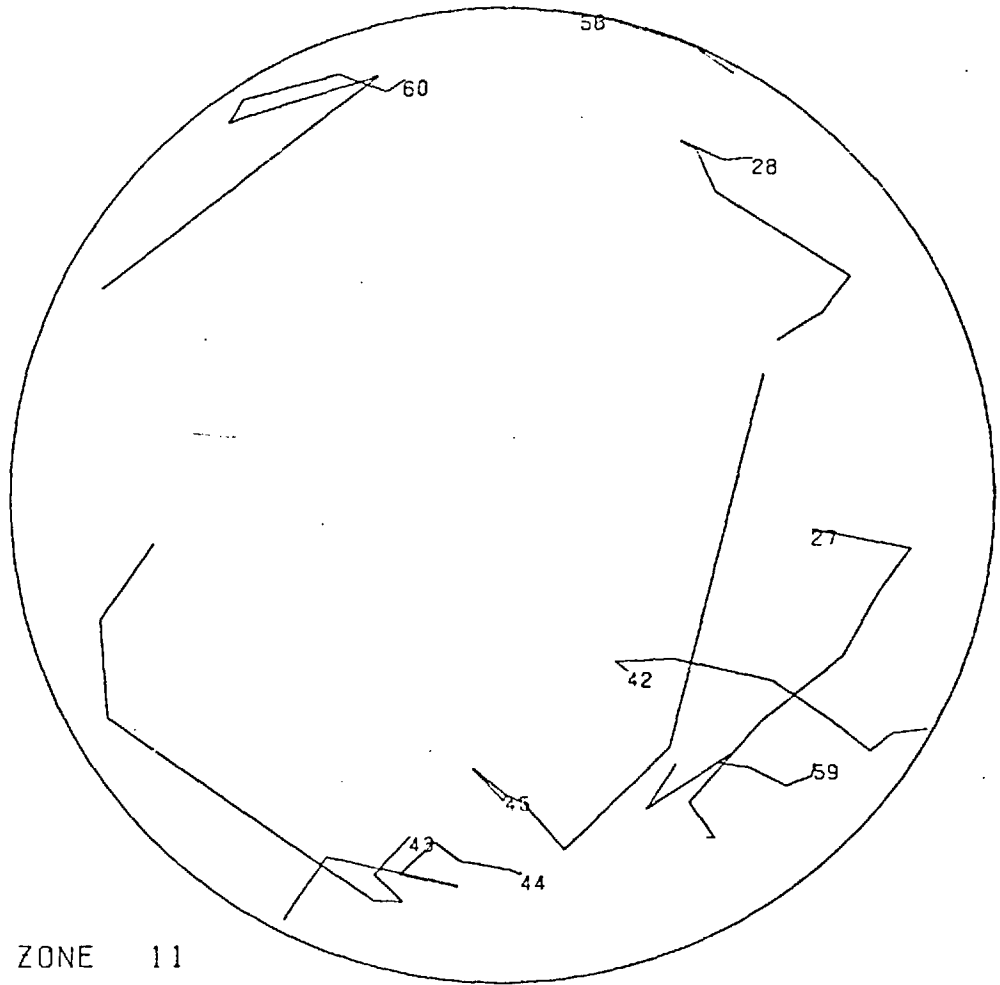
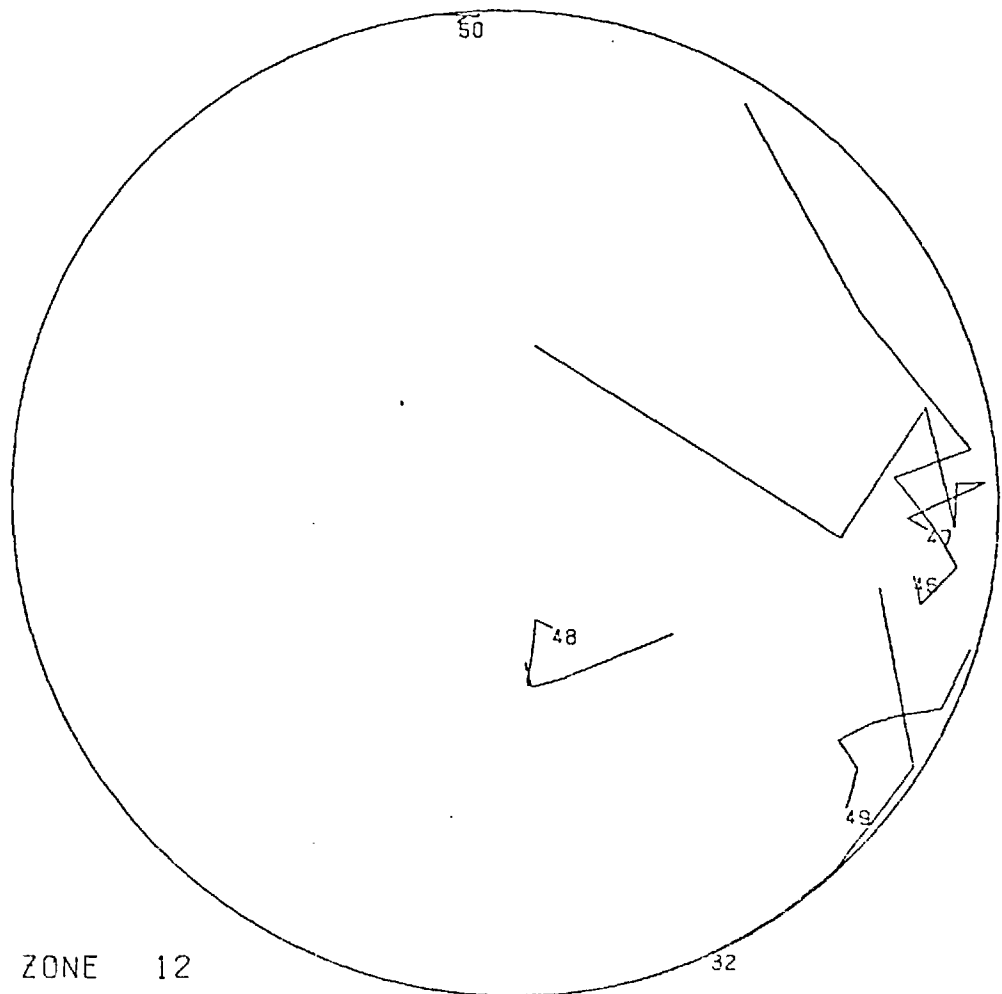


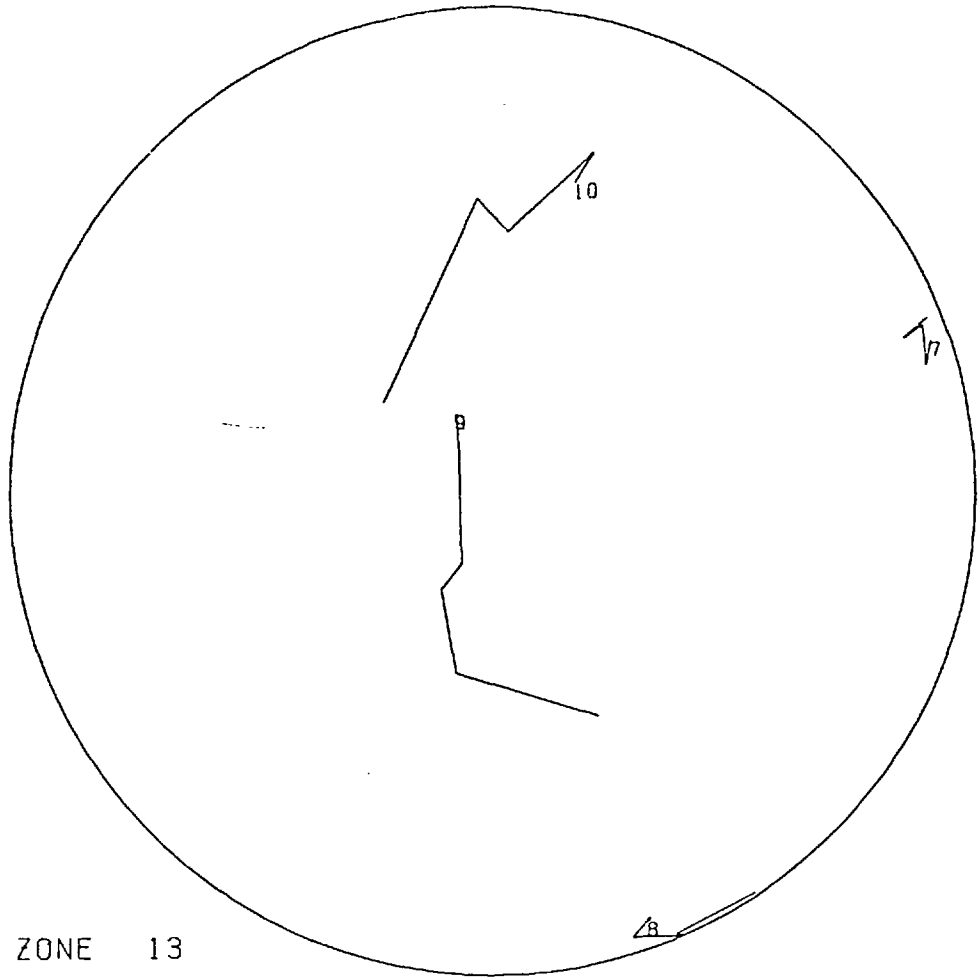
FIG 7.71 TRACE OF PARTICLE ROTATION ON STERONEP TEST NO 2201



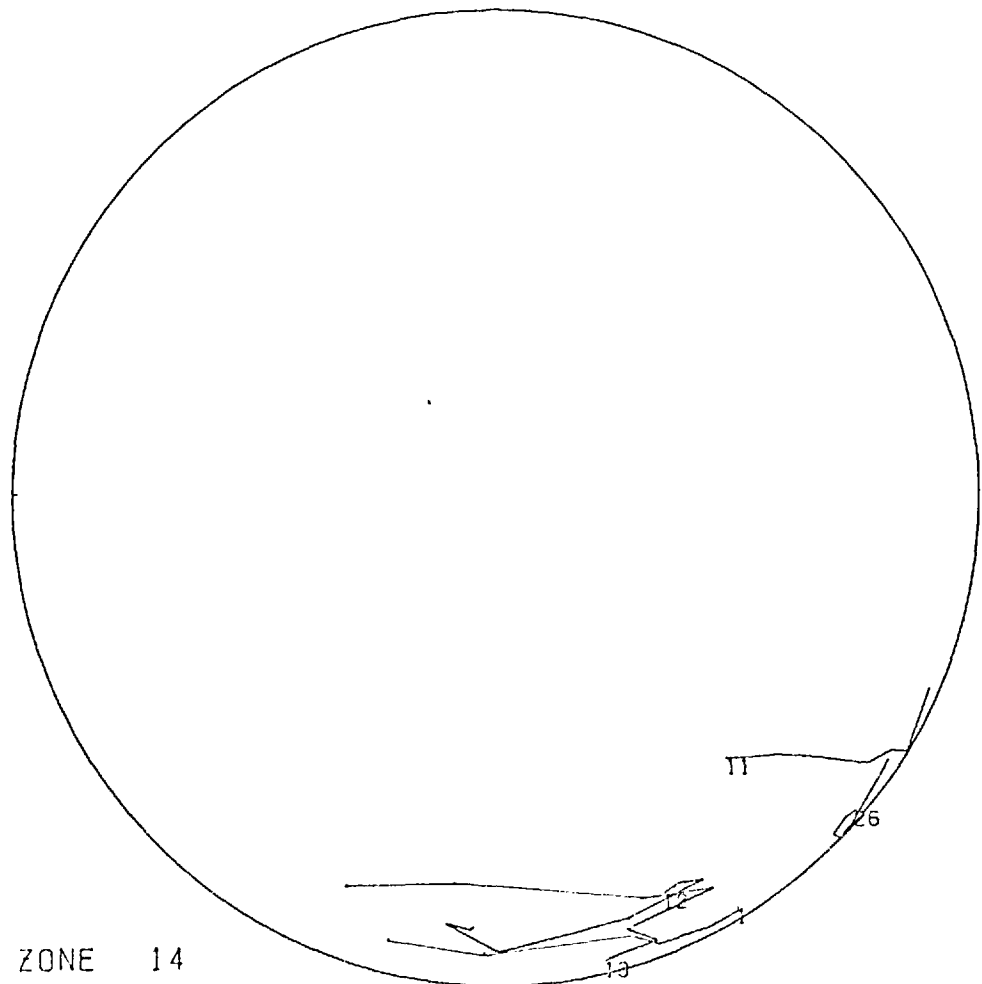
A) ZONE 11



B) ZONE 12

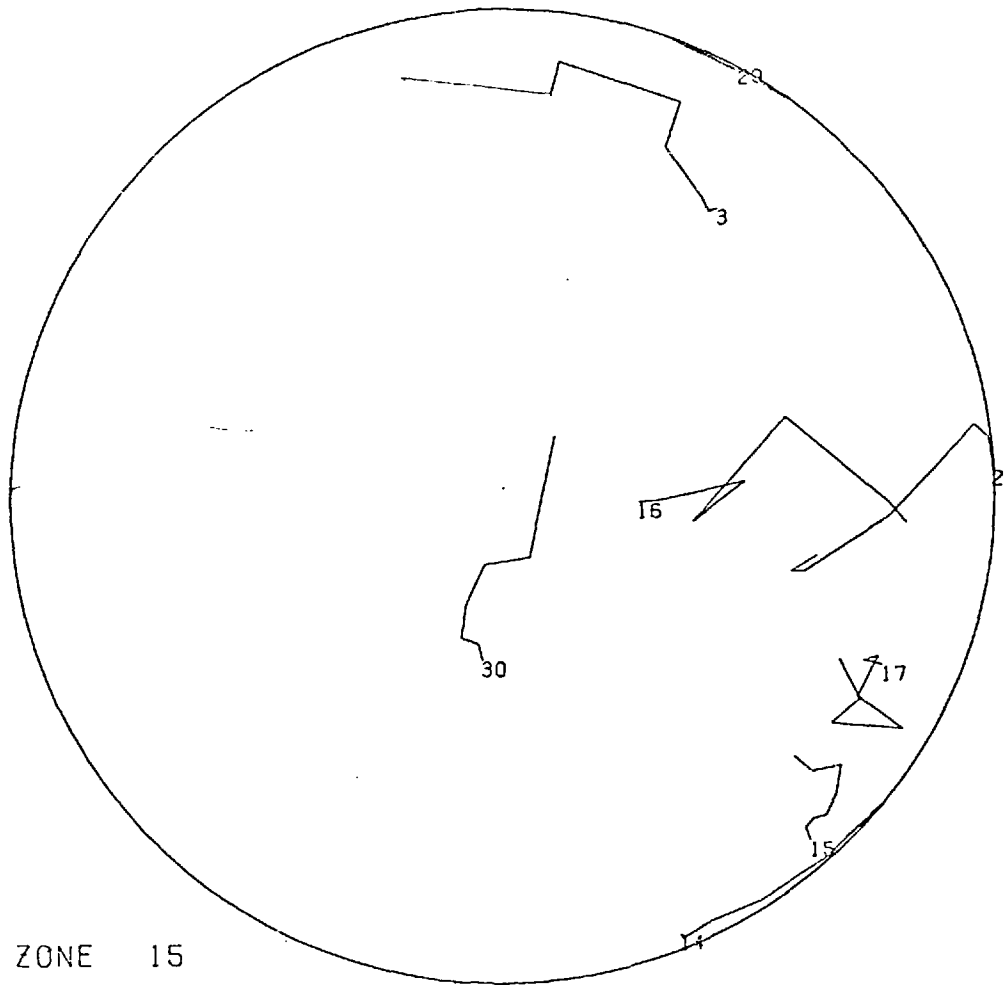


A) ZONE 13

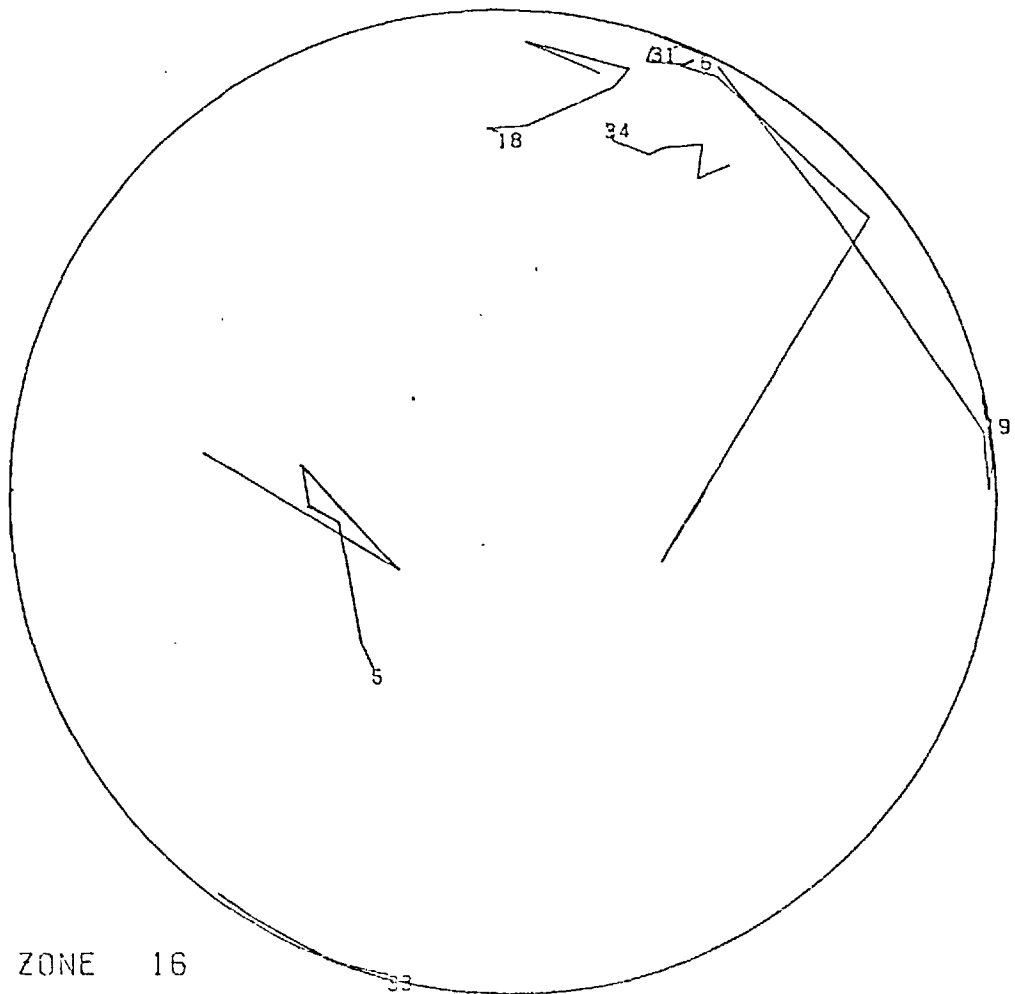


B) ZONE 14

FIG 7.73 TRACE OF PARTICLE ROTATION ON STEREO NET



A) ZONE 15



B) ZONE 16

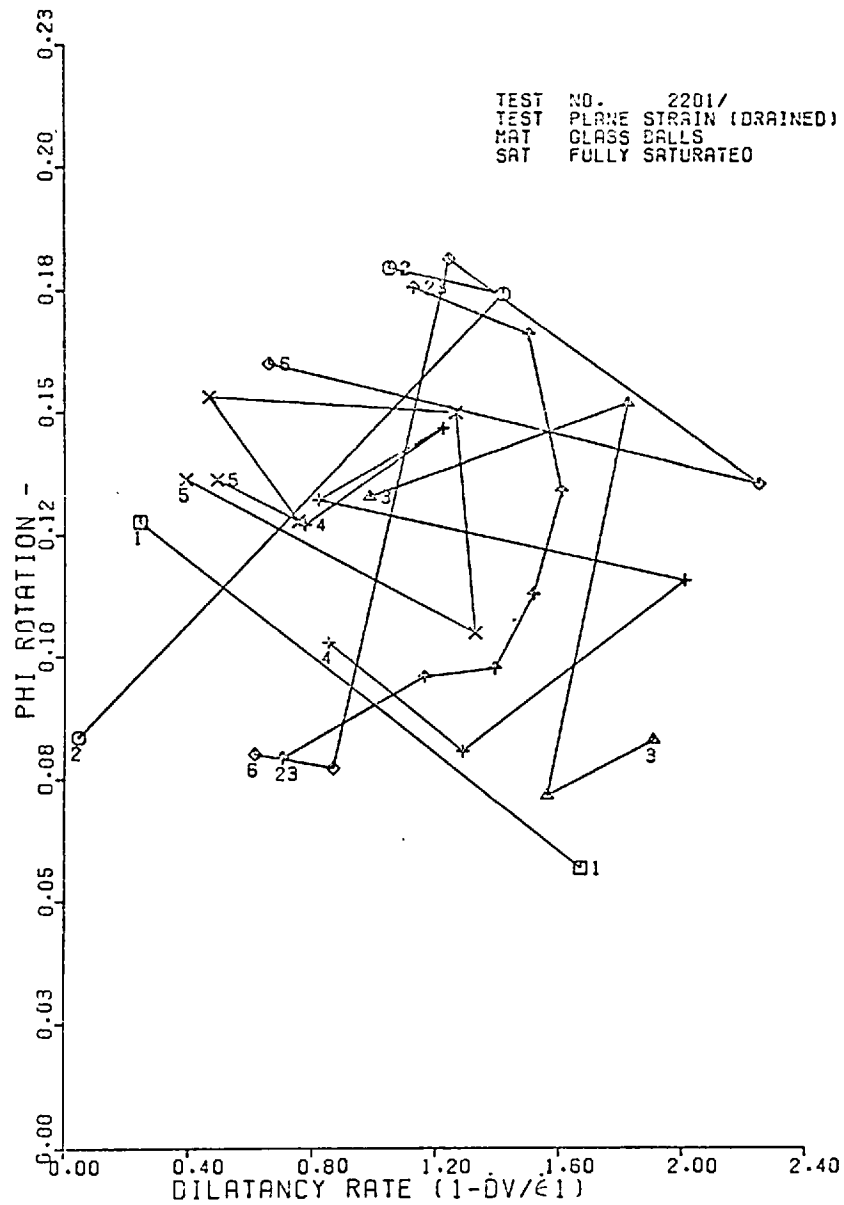


FIG.7.75-PHI ROTATION - DILATANCY PLOT

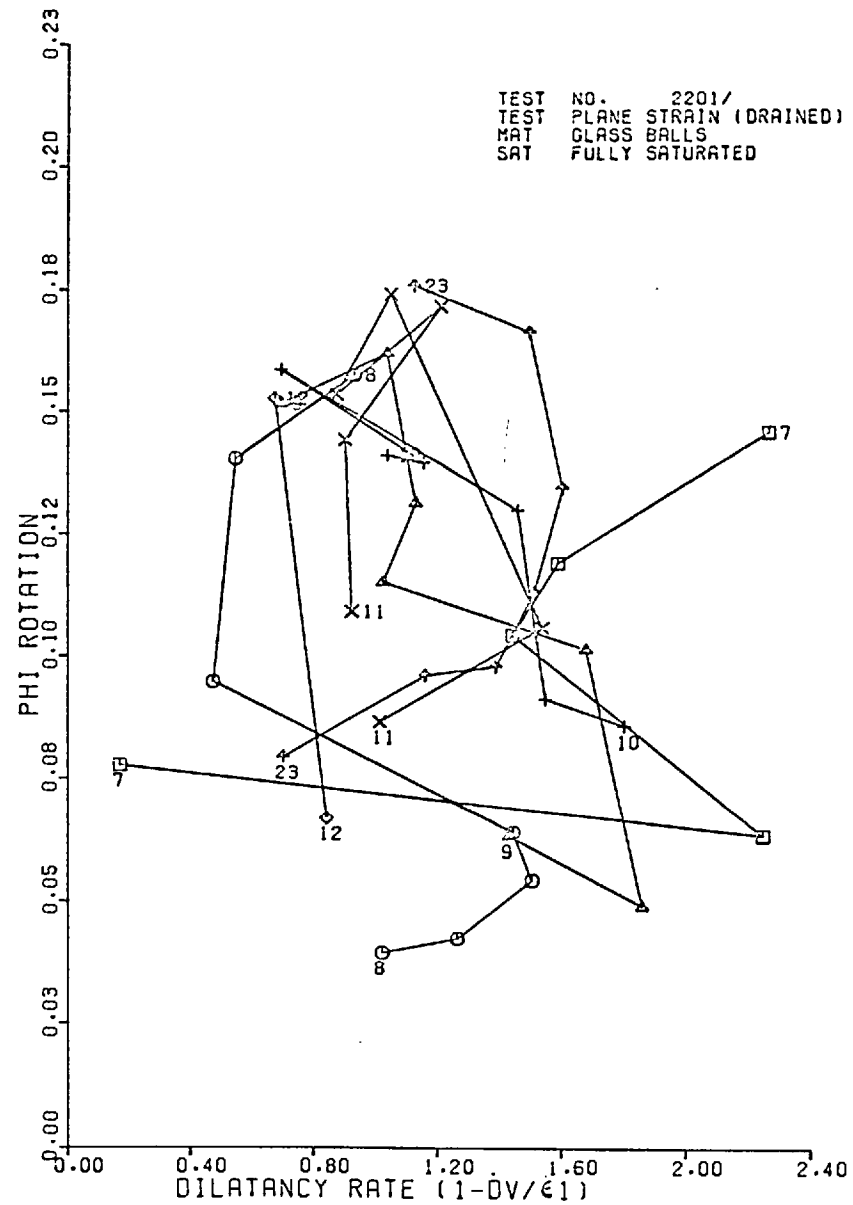


FIG.7.76-PHI ROTATION - DILATANCY PLOT

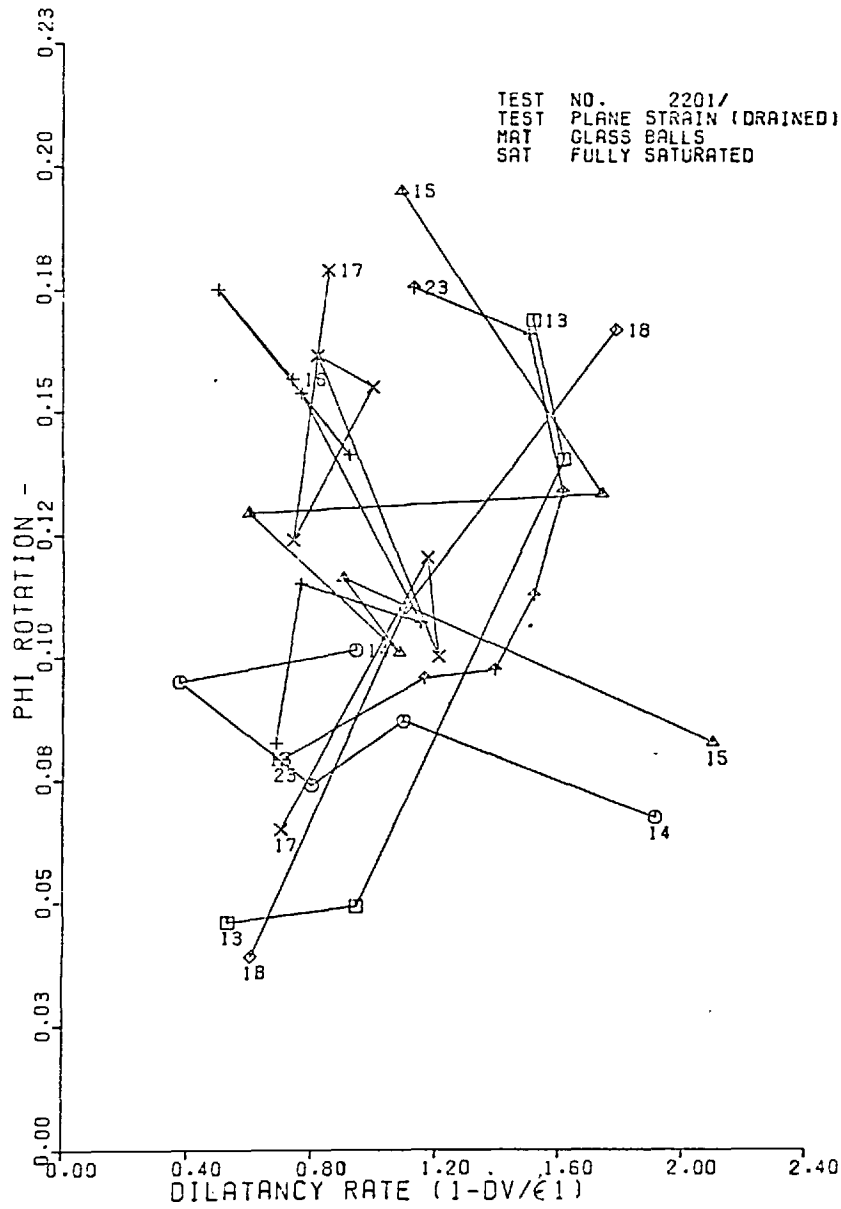


FIG.7.77-PHI ROTATION - DILATANCY PLOT

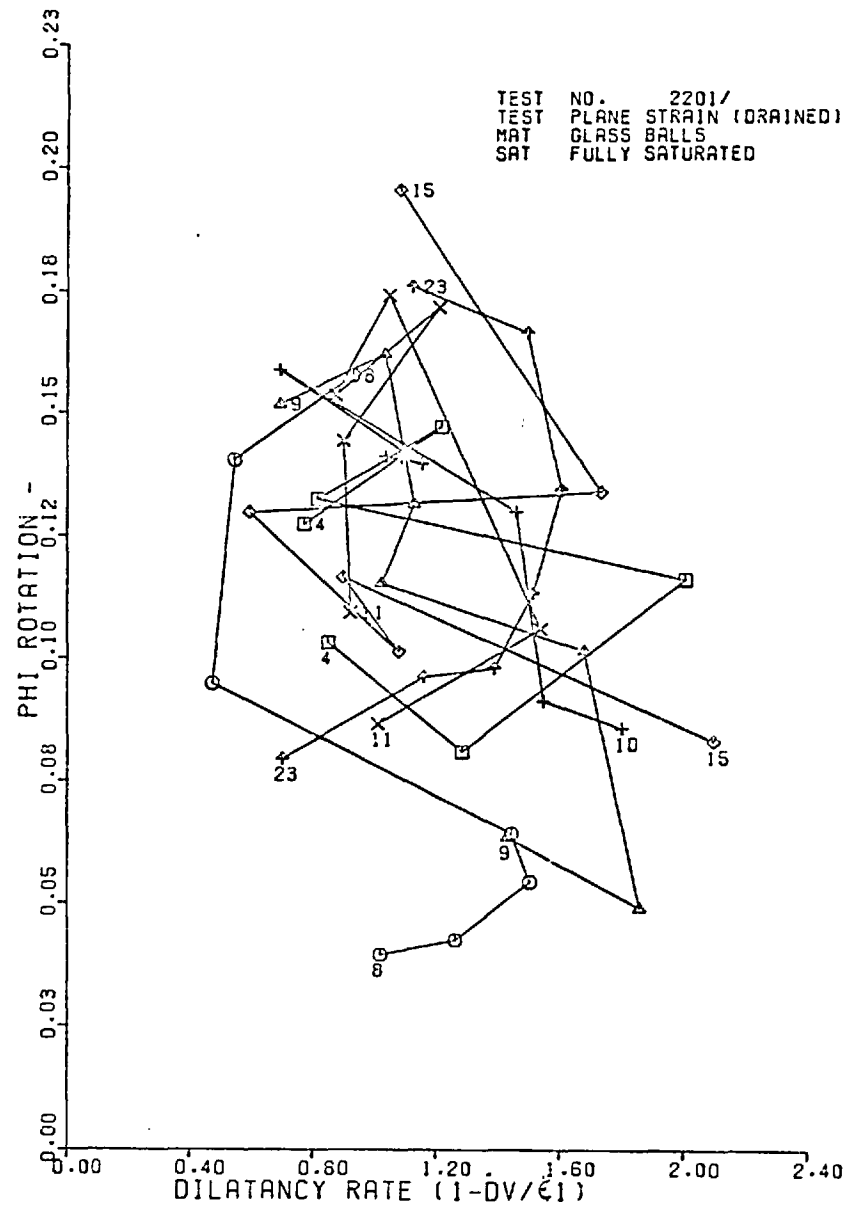


FIG.7.78-PHI ROTATION - DILATANCY PLOT

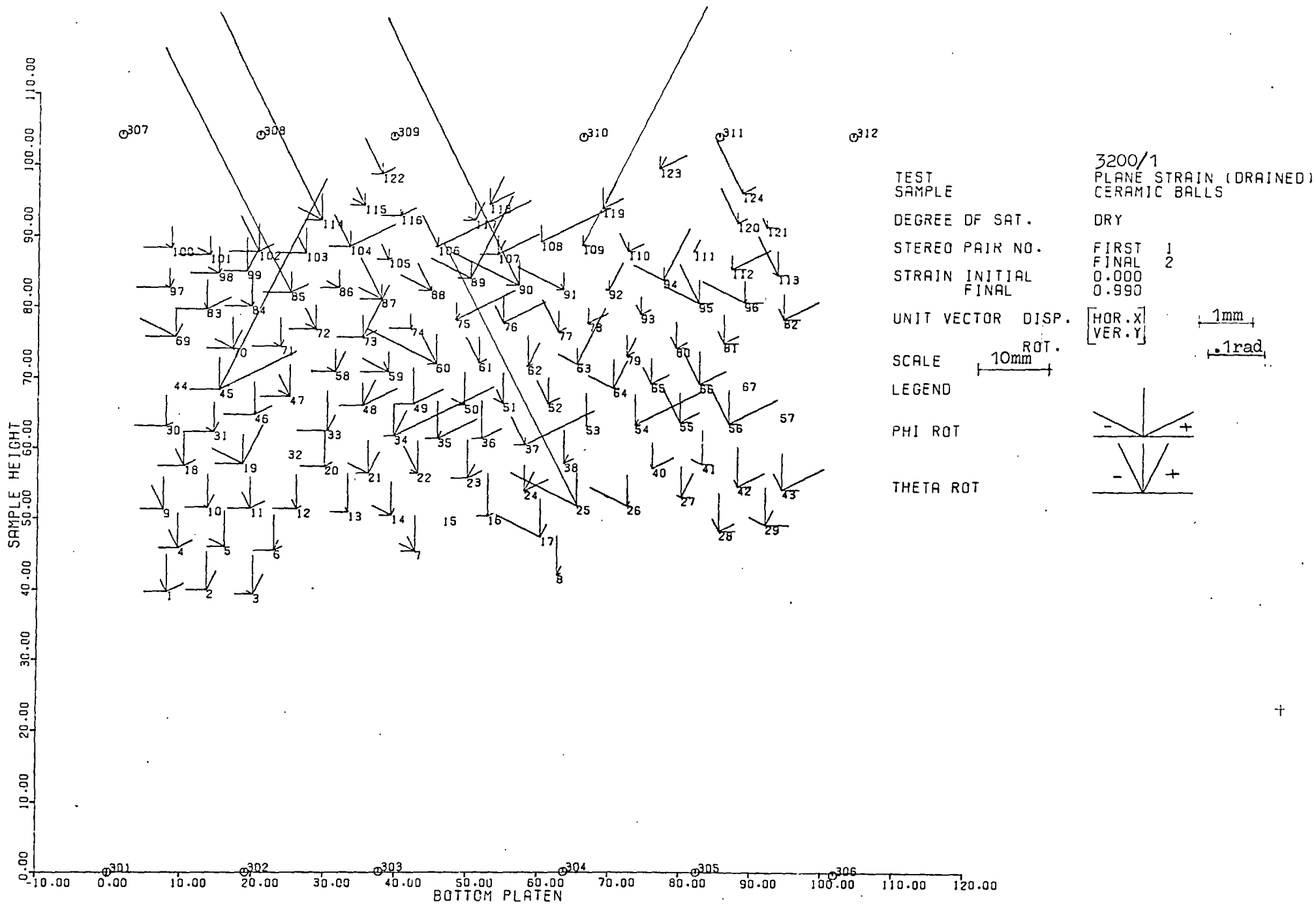
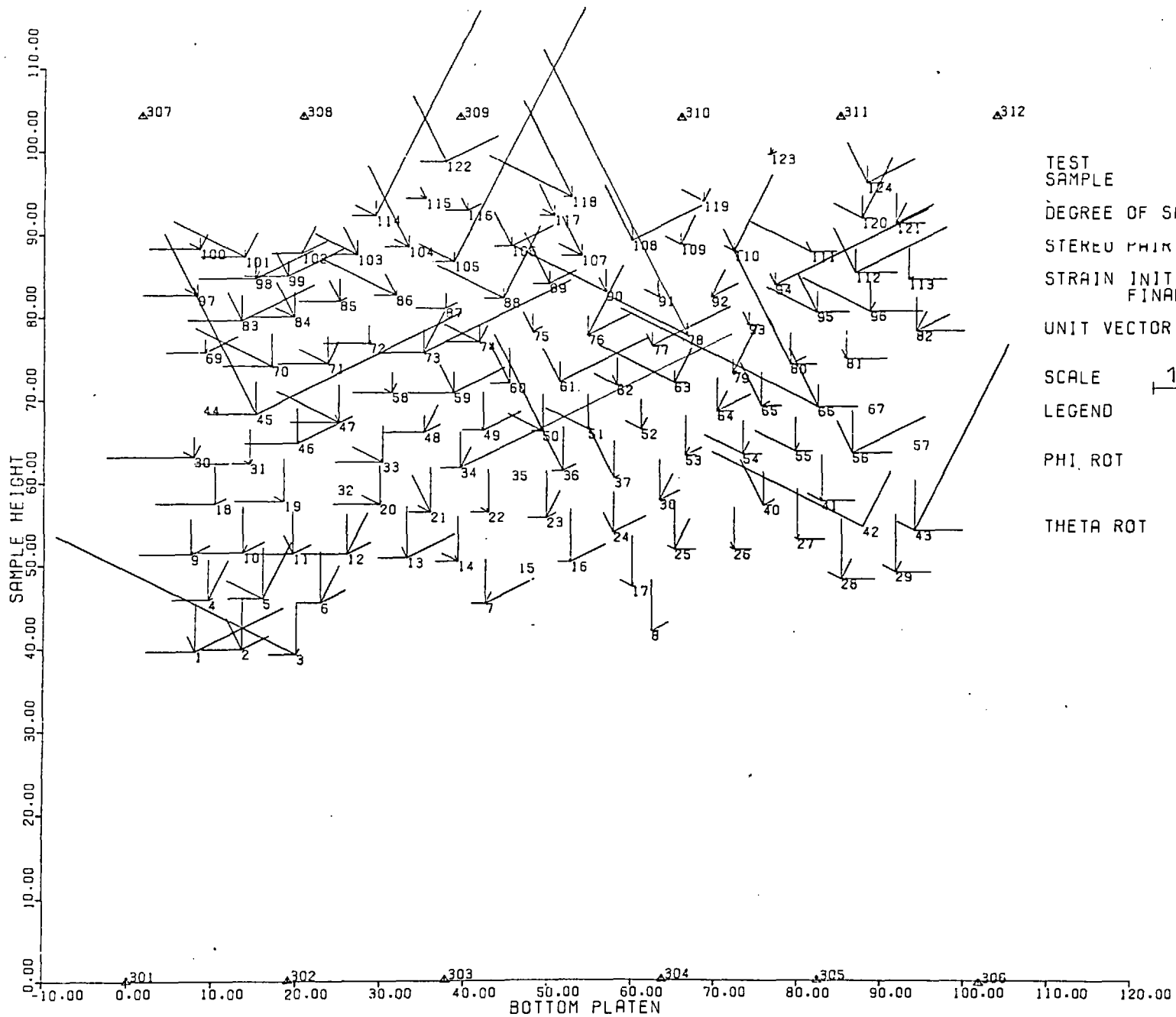


FIG 7.79 DISPLACEMENT - ROTATION FIELD OF MARKERS IN XY PLANE




3200/2
 PLANE STRAIN (DRAINED)
 CERAMIC BALLS

TEST SAMPLE
 DEGREE OF SAT. DRY
 STEREO PAIR NO. FIRST 2
 FINAL 3
 STRAIN INITIAL 0.990
 FINAL 3.211

UNIT VECTOR DISP. $\begin{bmatrix} \text{HOR. X} \\ \text{VER. Y} \end{bmatrix}$ $\begin{matrix} \text{2mm} \\ \text{.2rad} \end{matrix}$

SCALE $\begin{matrix} \text{ROT.} \\ \text{10mm} \end{matrix}$

LEGEND

PHI ROT 

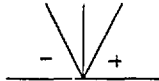
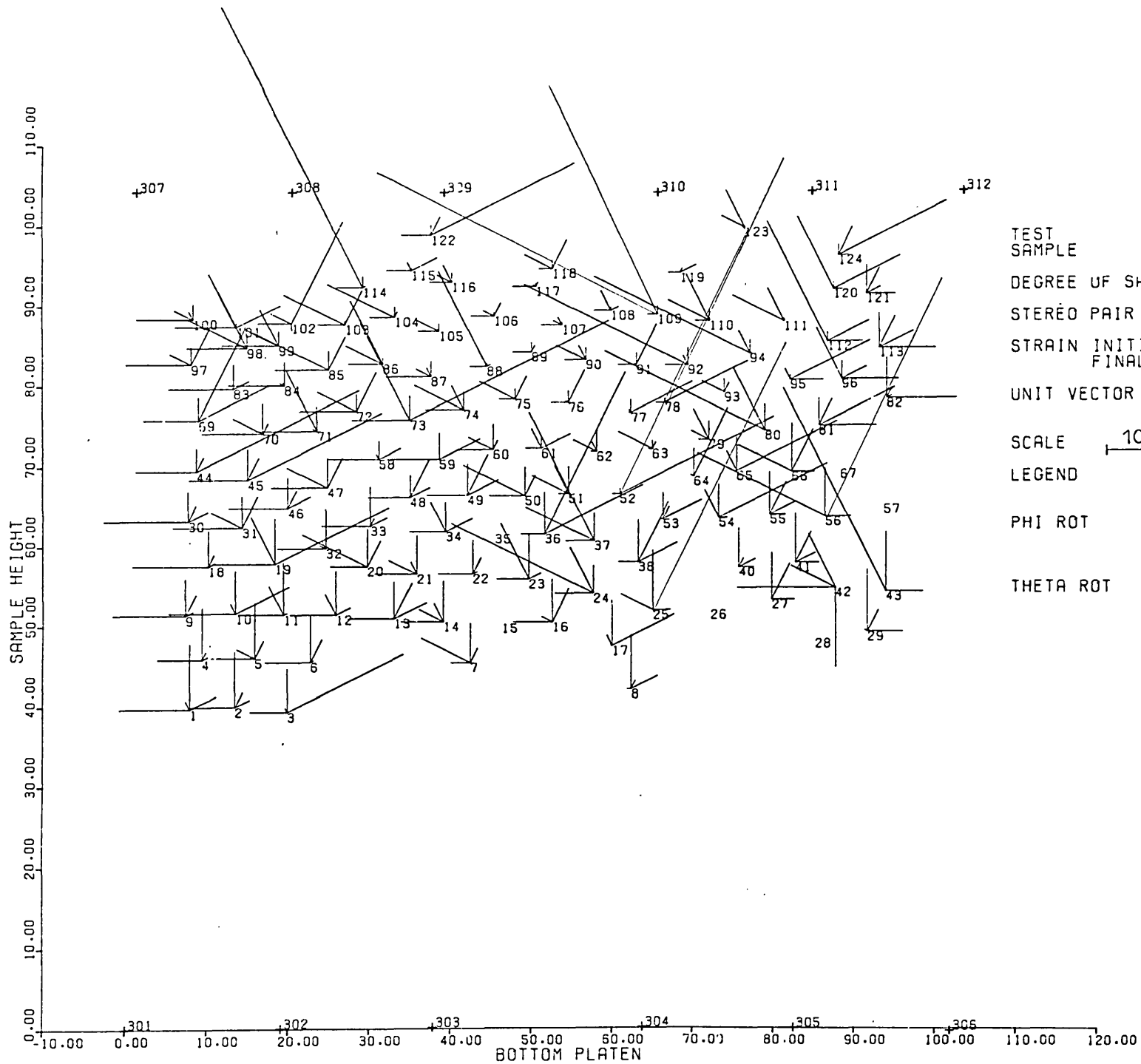
THETA ROT 

FIG 7.80 DISPLACEMENT - ROTATION FIELD OF MARKERS IN XY PLANE



TEST SAMPLE

3200/3
PLANE STRAIN (DRAINED)
CERAMIC BALLS

DEGREE OF SHI.

DRY

STEREO PAIR NO.

FIRST 3

FINAL 4

STRAIN INITIAL
FINAL

3.211

5.612

UNIT VECTOR DISP.

HOR. X
VER. Y

2mm

SCALE 10mm ROT.

.2rad

LEGEND

PHI ROT



THETA ROT

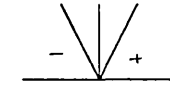
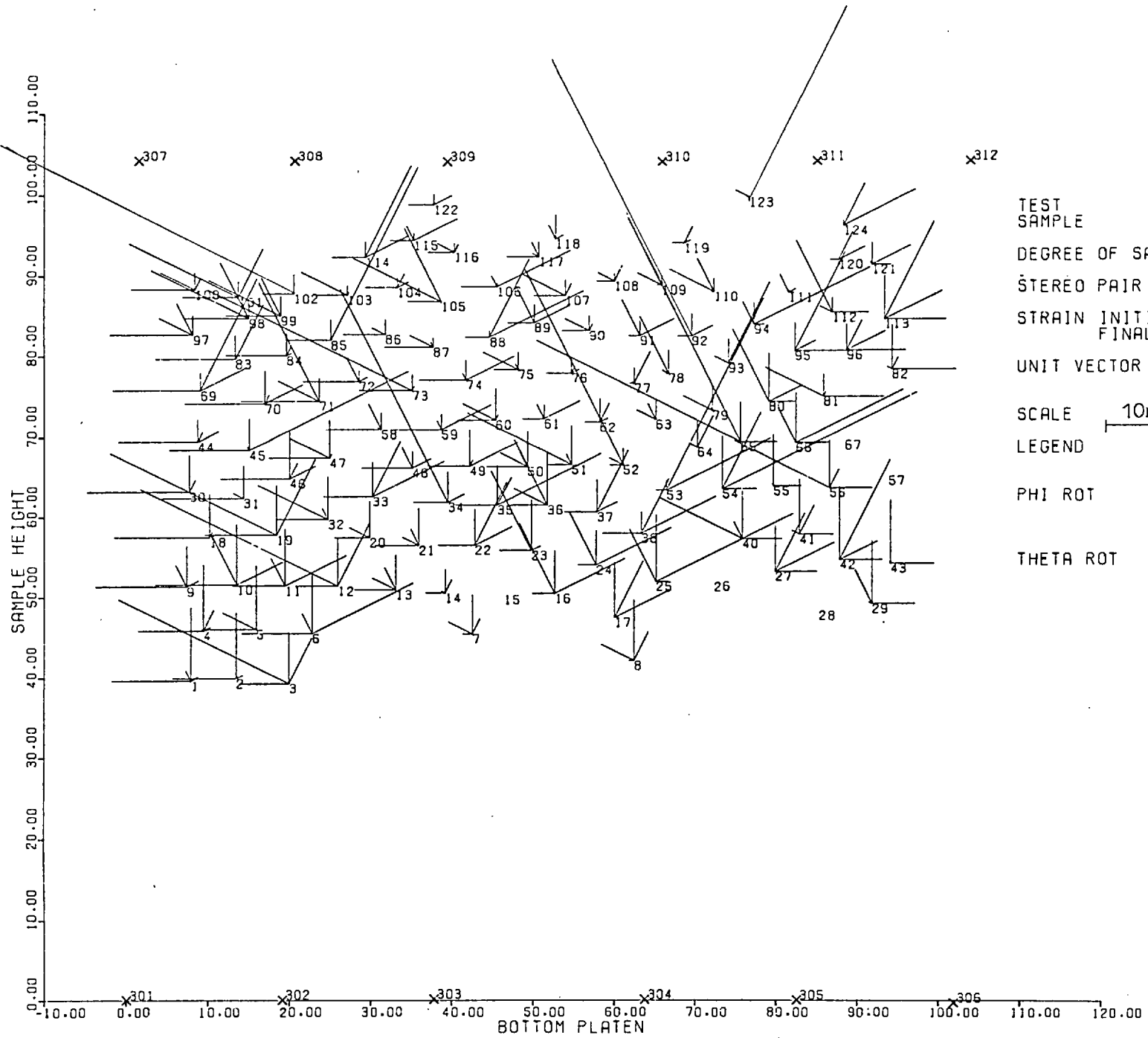


FIG 7.81 DISPLACEMENT - ROTATION FIELD OF MARKERS IN XY PLANE



3200/4
 TEST SAMPLE PLANE STRAIN (DRAINED)
 CERAMIC BALLS
 DEGREE OF SAT. DRY
 STEREO PAIR NO. FIRST 4
 FINAL 5
 STRAIN INITIAL 5.612
 FINAL 8.156
 UNIT VECTOR DISP. [HOR.X] 2mm
 [VER.Y] .2rad
 SCALE 10mm ROT.
 LEGEND
 PHI ROT
 THETA ROT

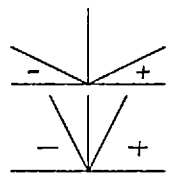
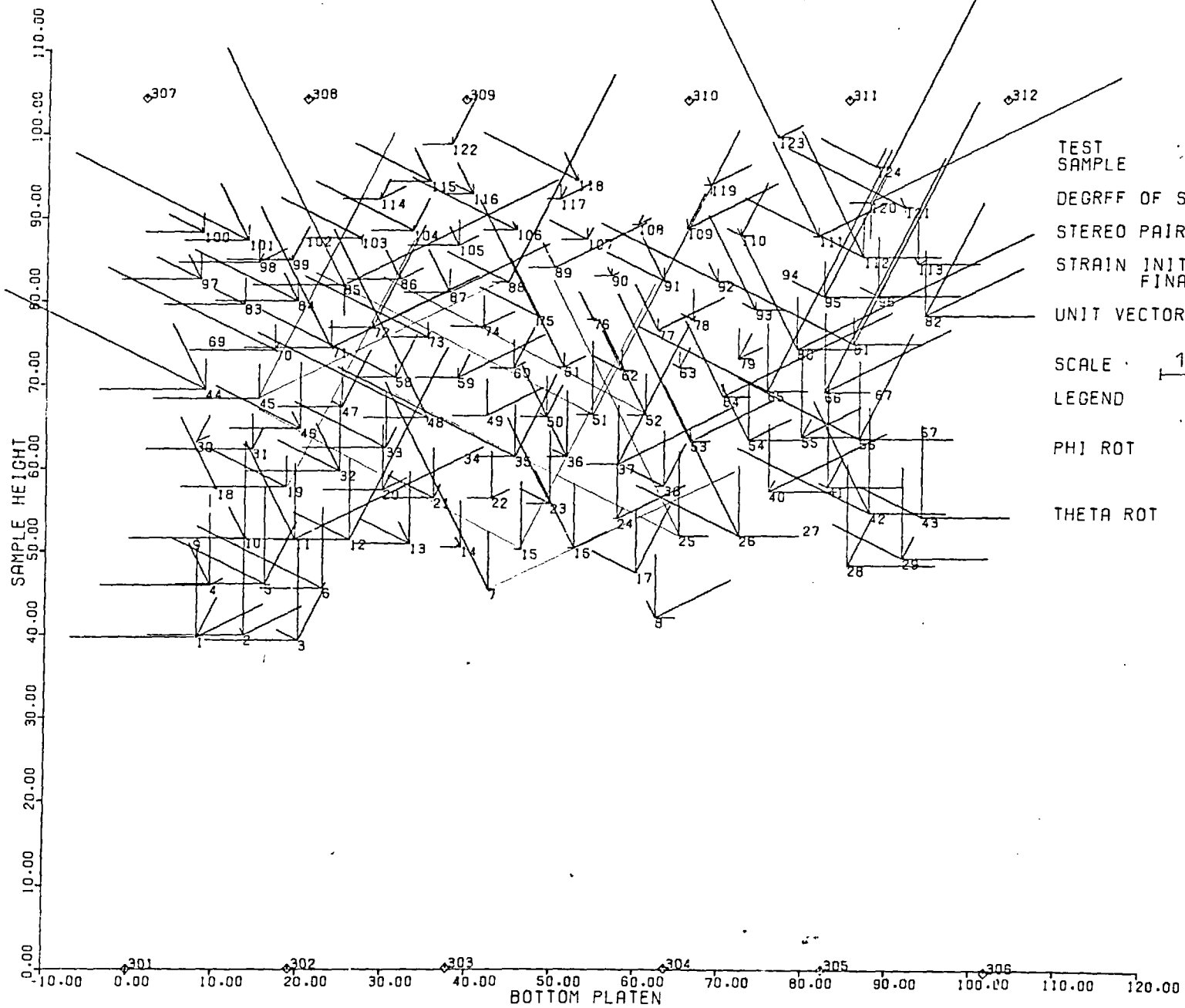
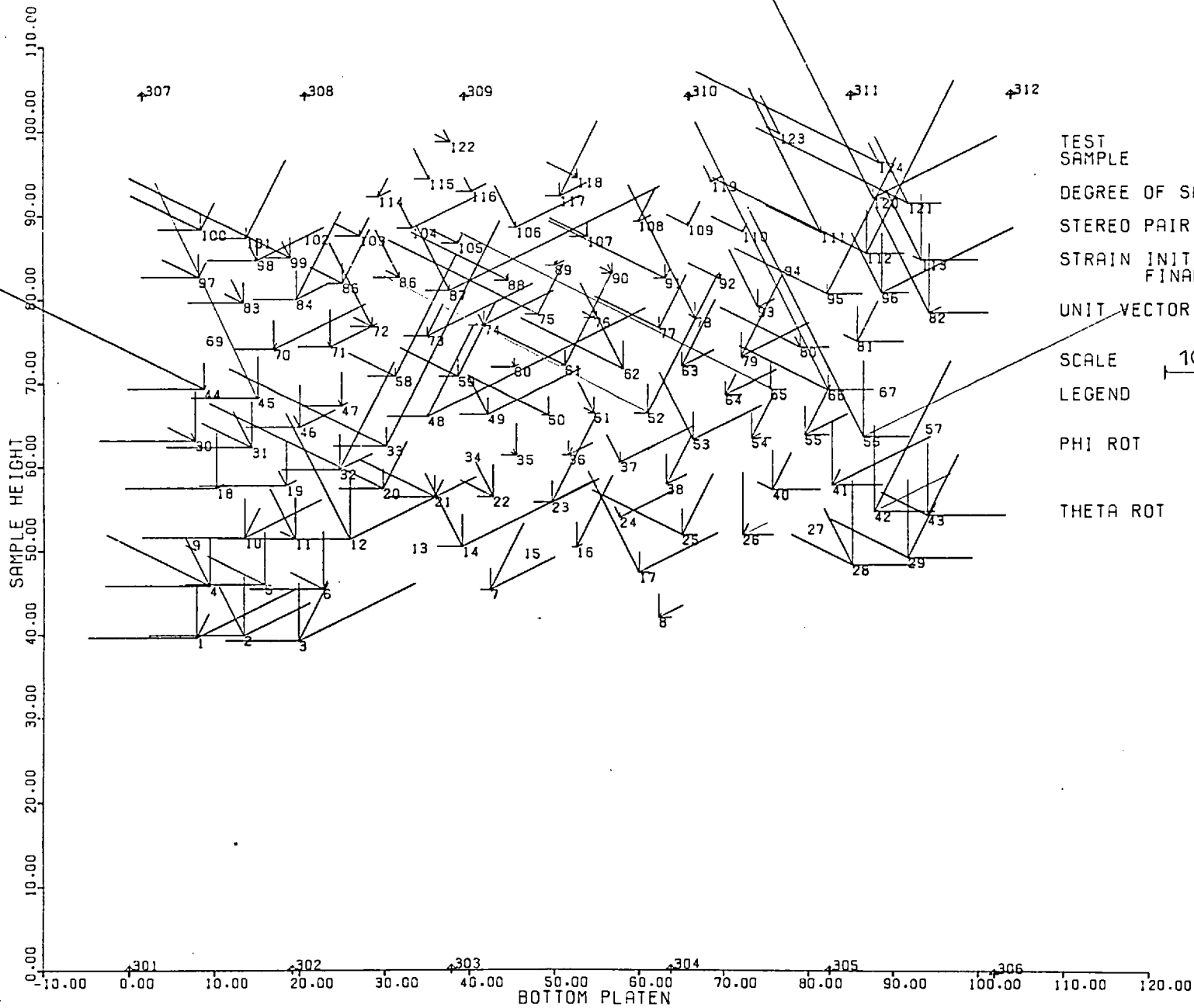


FIG 7.82 DISPLACEMENT - ROTATION FIELD OF MARKERS IN XY PLANE



TEST SAMPLE : 3200/5
 PLANE STRAIN (DRAINED)
 CERAMIC BALLS
 DEGREE OF SAT. : DRY
 STEREO PAIR NO. : FIRST 5
 FINAL 6
 STRAIN INITIAL : 8.156
 FINAL : 11.899
 UNIT VECTOR DISP. : $\begin{bmatrix} \text{HOR. X} \\ \text{VER. Y} \end{bmatrix}$ $\begin{matrix} \text{---} 2\text{mm} \text{---} \\ \text{---} .2\text{rad} \text{---} \end{matrix}$
 SCALE : $\begin{matrix} \text{---} 10\text{mm} \text{---} \\ \text{ROT.} \end{matrix}$
 LEGEND :
 PHI ROT :
 THETA ROT :

FIG 7.83 DISPLACEMENT - ROTATION FIELD OF MARKERS IN XY PLANE



TEST SAMPLE 3200/6
 PLANE STRAIN (DRAINED)
 CERAMIC BALLS
 DEGREE OF SAT. DRY
 STEREO PAIR NO. FIRST 6
 FINAL 7
 STRAIN INITIAL 11.899
 FINAL 15.704
 UNIT VECTOR DISP. [HOR. X] 3mm
 [VER. Y] .2rad
 ROT. 10mm
 SCALE 10mm
 LEGEND
 PHI ROT
 THETA ROT

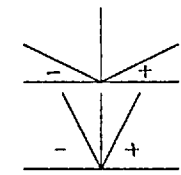


FIG 7.84 DISPLACEMENT - ROTATION FIELD OF MARKERS IN XY PLANE

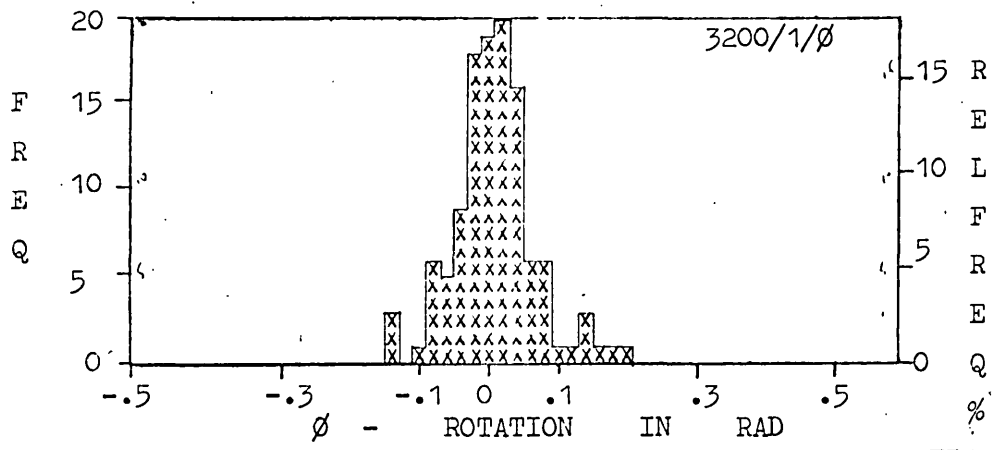


FIG. 7.85

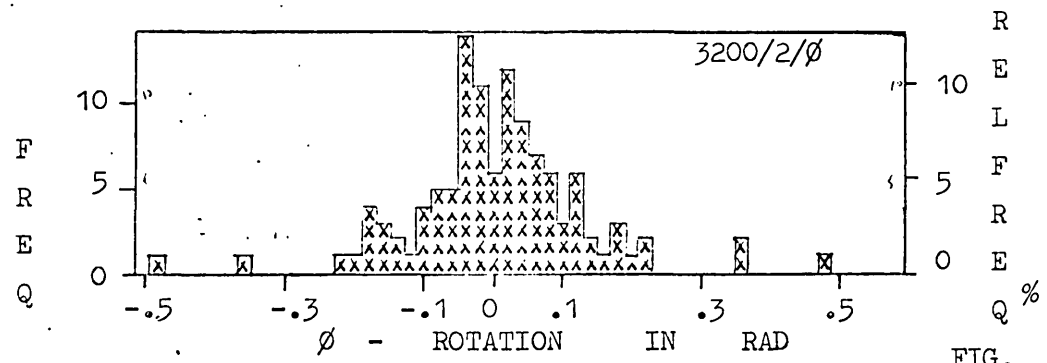
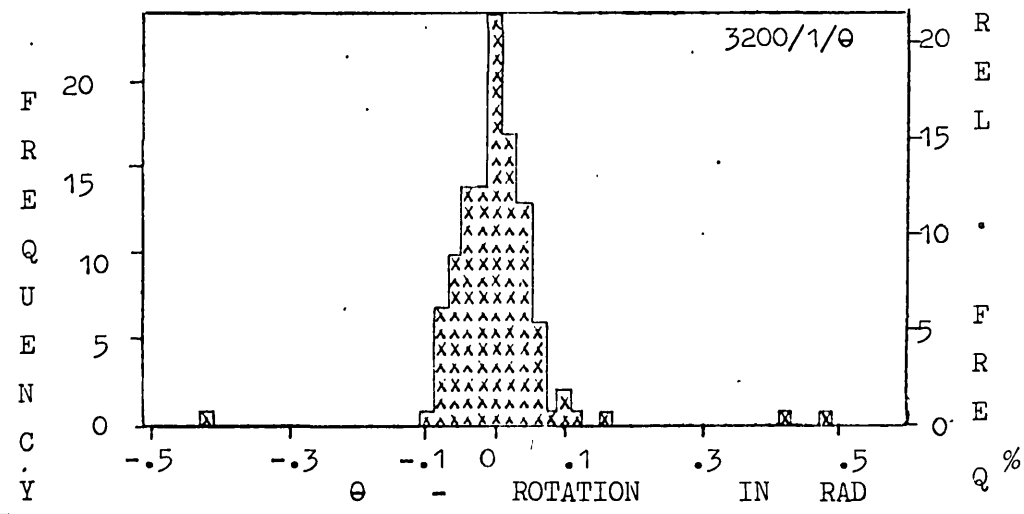


FIG. 7.86

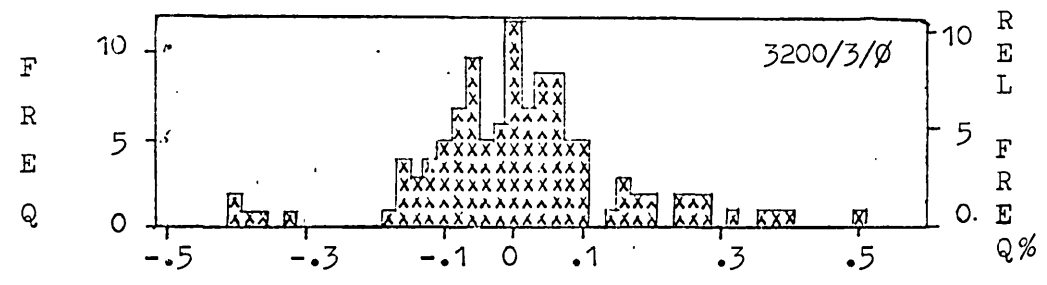
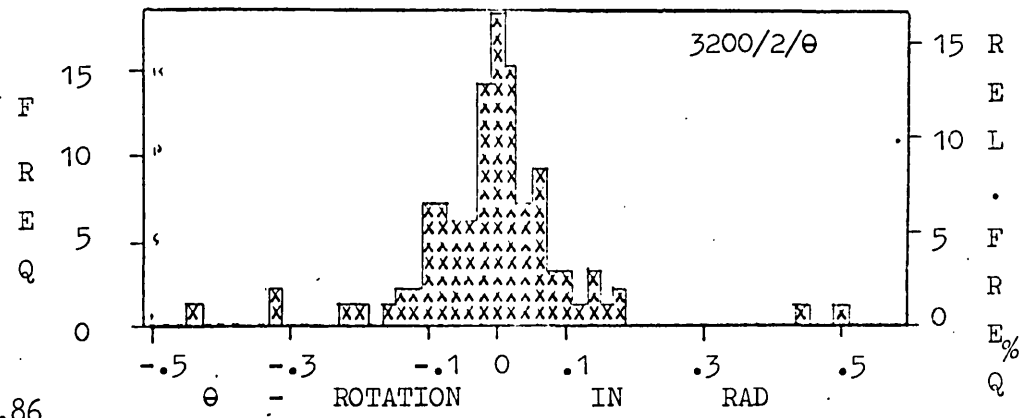
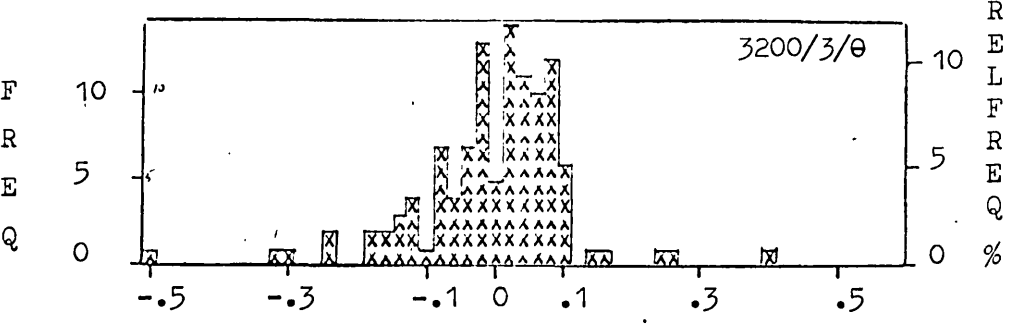


FIG. 7.87



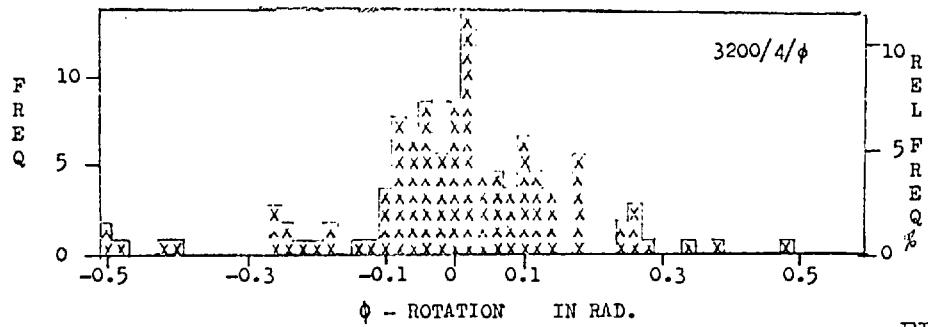


FIG. 7.88

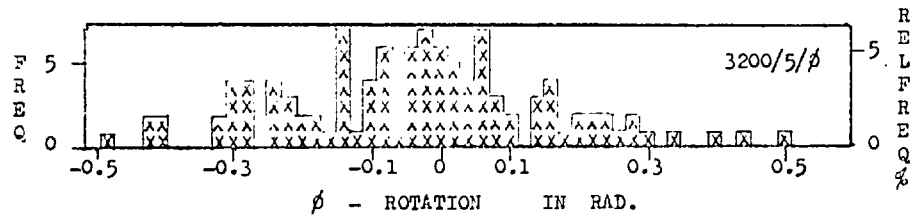
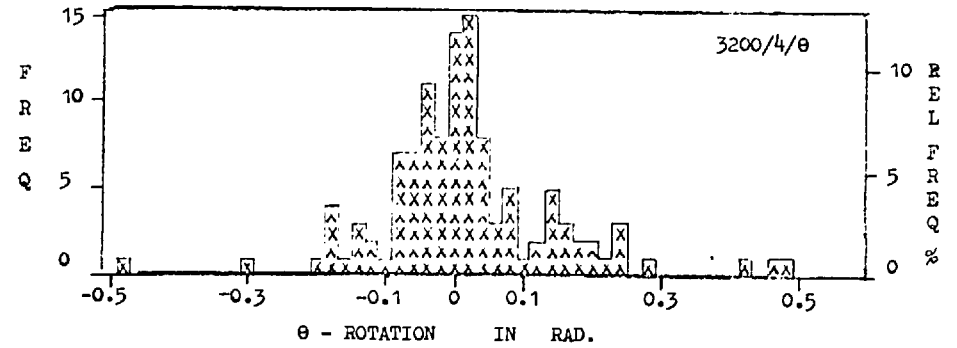


FIG. 7.89

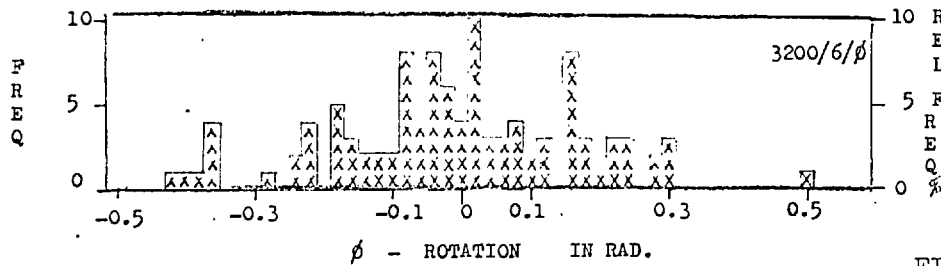
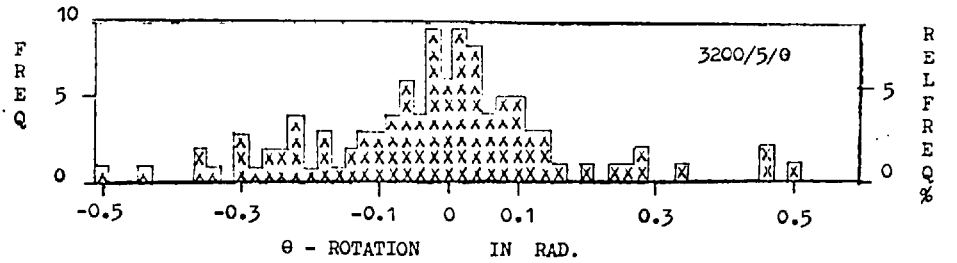
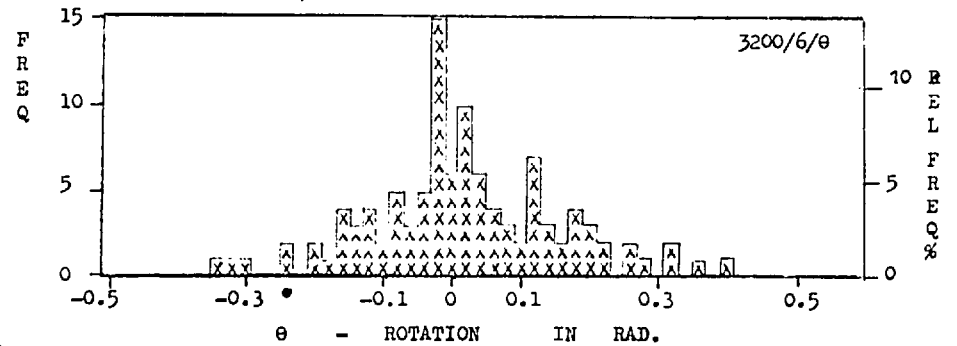
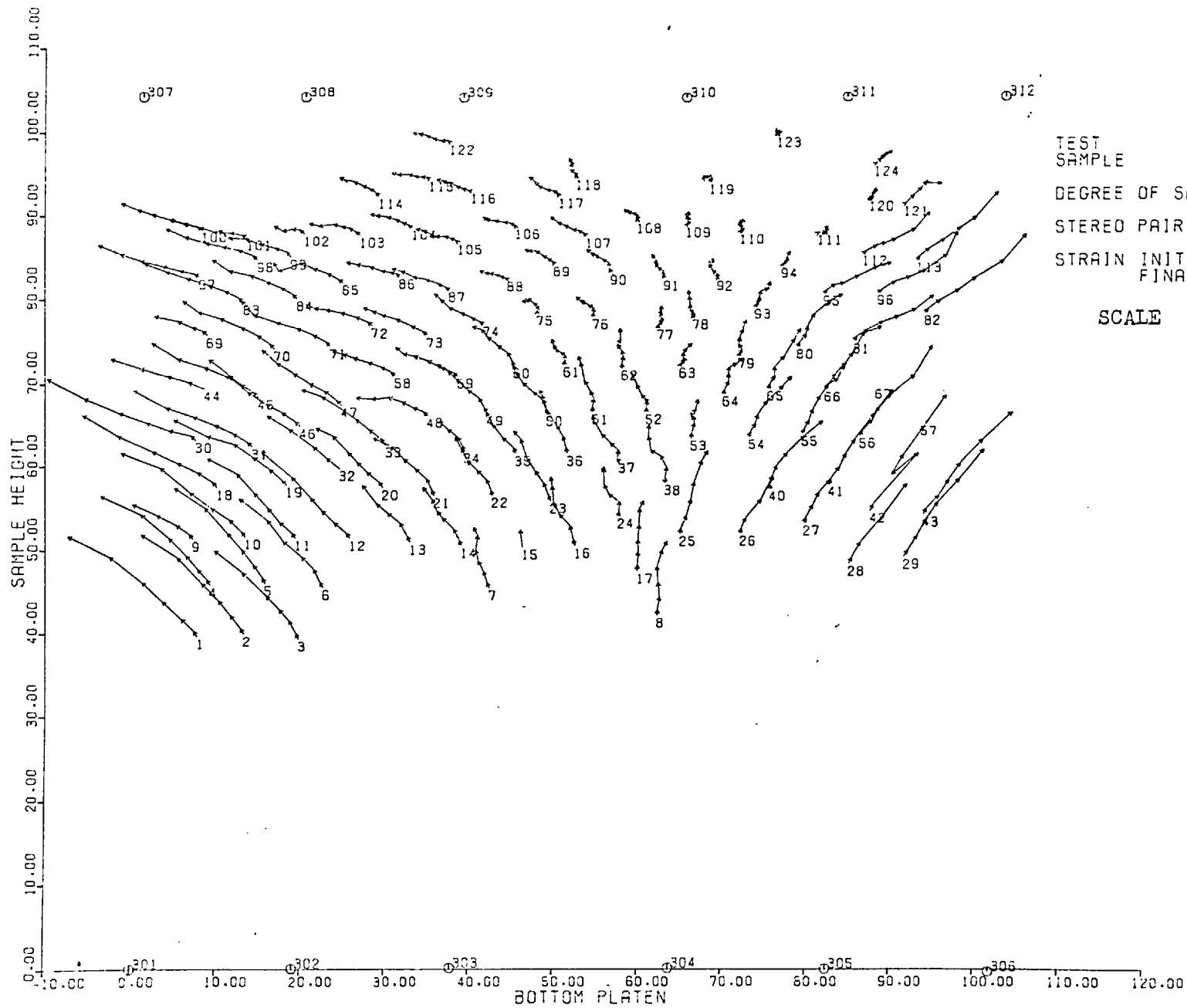


FIG. 7.90





TEST SAMPLE
 DEGREE OF SAT.
 STEREO PAIR NO.
 STRAIN INITIAL
 FINAL

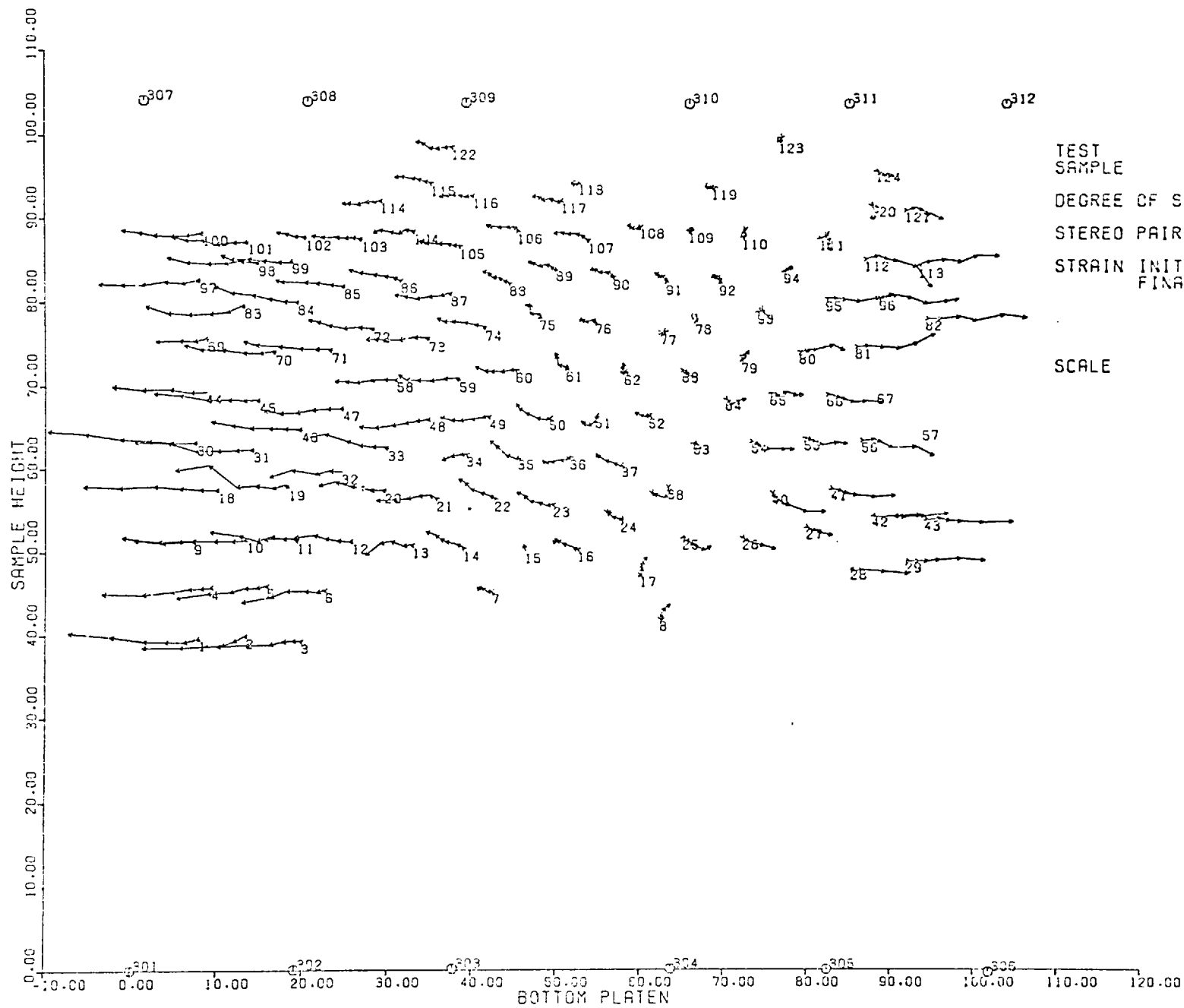
3200
 PLANE STRAIN (DRAINED)
 CERAMIC BALLS
 DRY
 FIRST 1
 LAST 7
 0.0
 15.704

SCALE

10mm

FIG 7.91

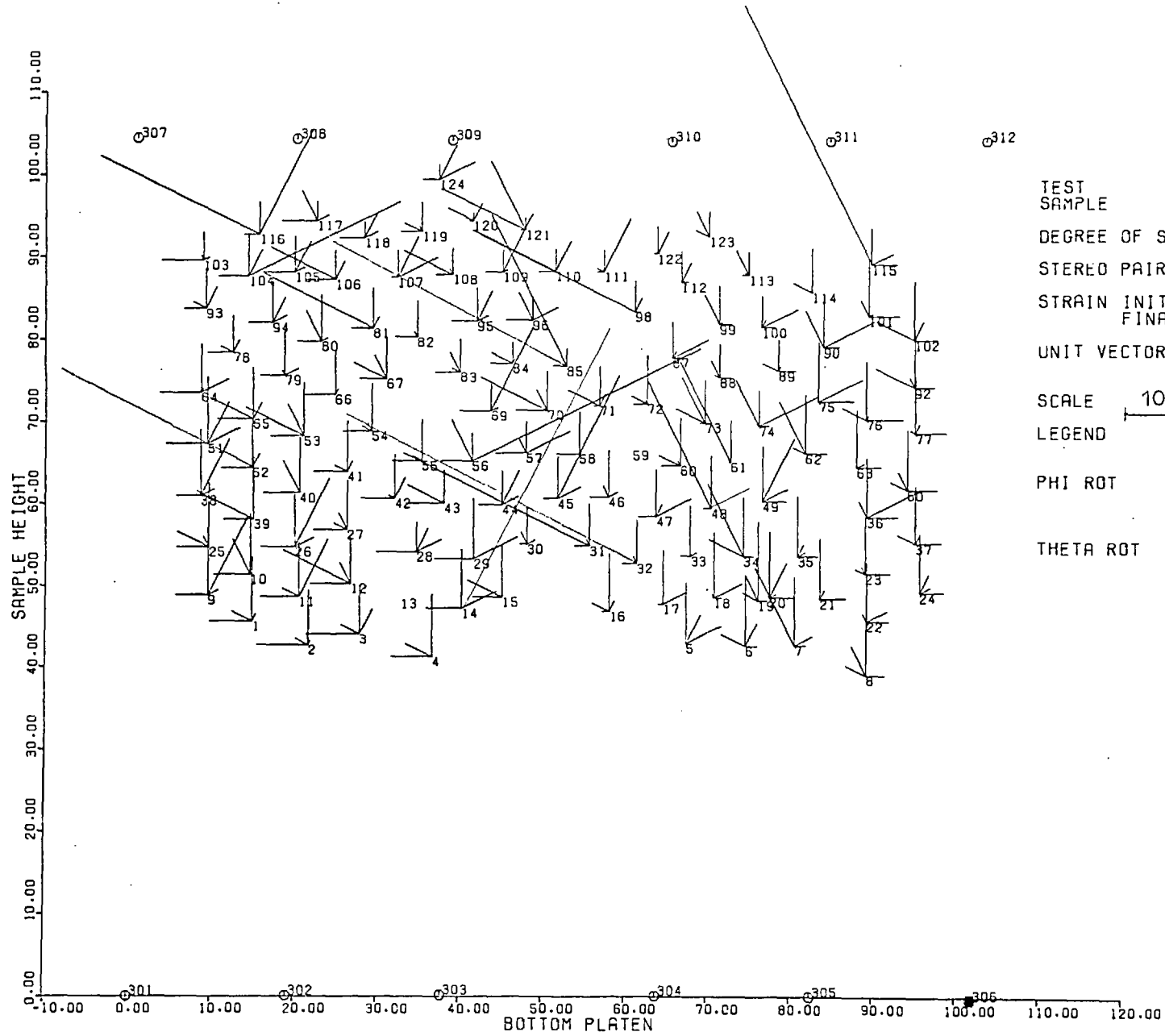
TRACE OF DISPLACEMENTS OF MARKER CENTRES ON XY PLANE



TEST SAMPLE 3200
 DEGREE OF SAT. PLANE STRAIN (DRAINED)
 STEREO PAIR NO. CERAMIC BALLS
 STRAIN INITIAL DRY
 STRAIN FINAL FIRST 1
 LAST 7
 0.0
 15.704
 SCALE 10mm

FIG 7.92

TRACE OF DISPLACEMENTS OF MARKER CENTRES ON XZ PLANE



TEST SAMPLE
 DEGREE OF SAT. FULLY SAT.
 STEREO PAIR NO. FIRST 1
 FINAL 2
 STRAIN INITIAL 0.0
 FINAL 1.546
 UNIT VECTOR DISP. ROT.
 SCALE 10mm
 LEGEND
 PHI ROT
 THETA ROT

3201/1

PLANE STRAIN (DRAINED)
 CERAMIC BALLS

FULLY SAT.

FIRST 1
 FINAL 2

0.0
 1.546

HOR. X
 VER. Y

1mm

.1rad

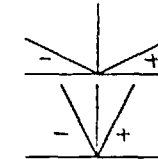
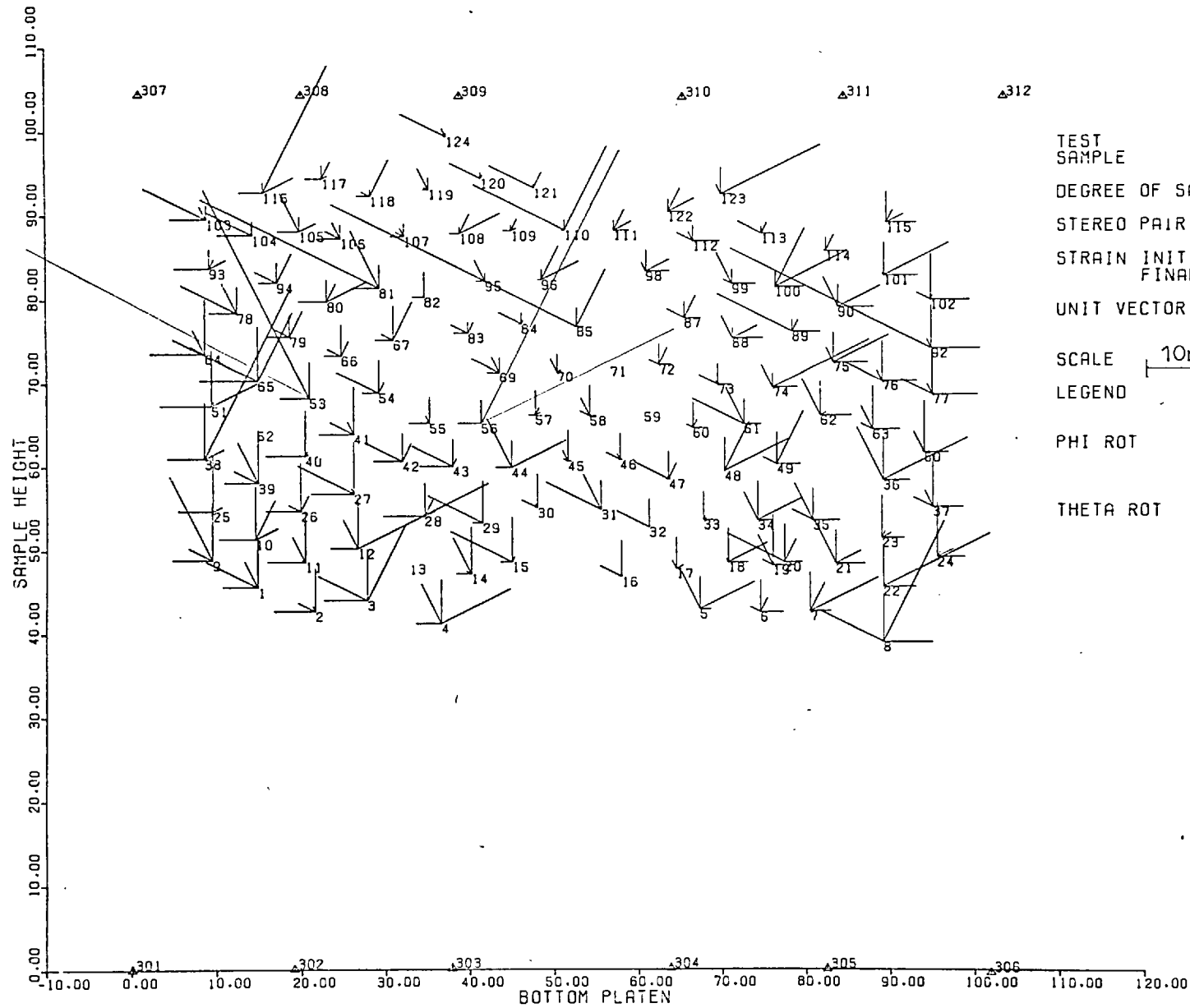


FIG 7.93 DISPLACEMENT - ROTATION FIELD OF MARKERS IN XY PLANE




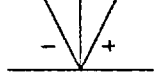
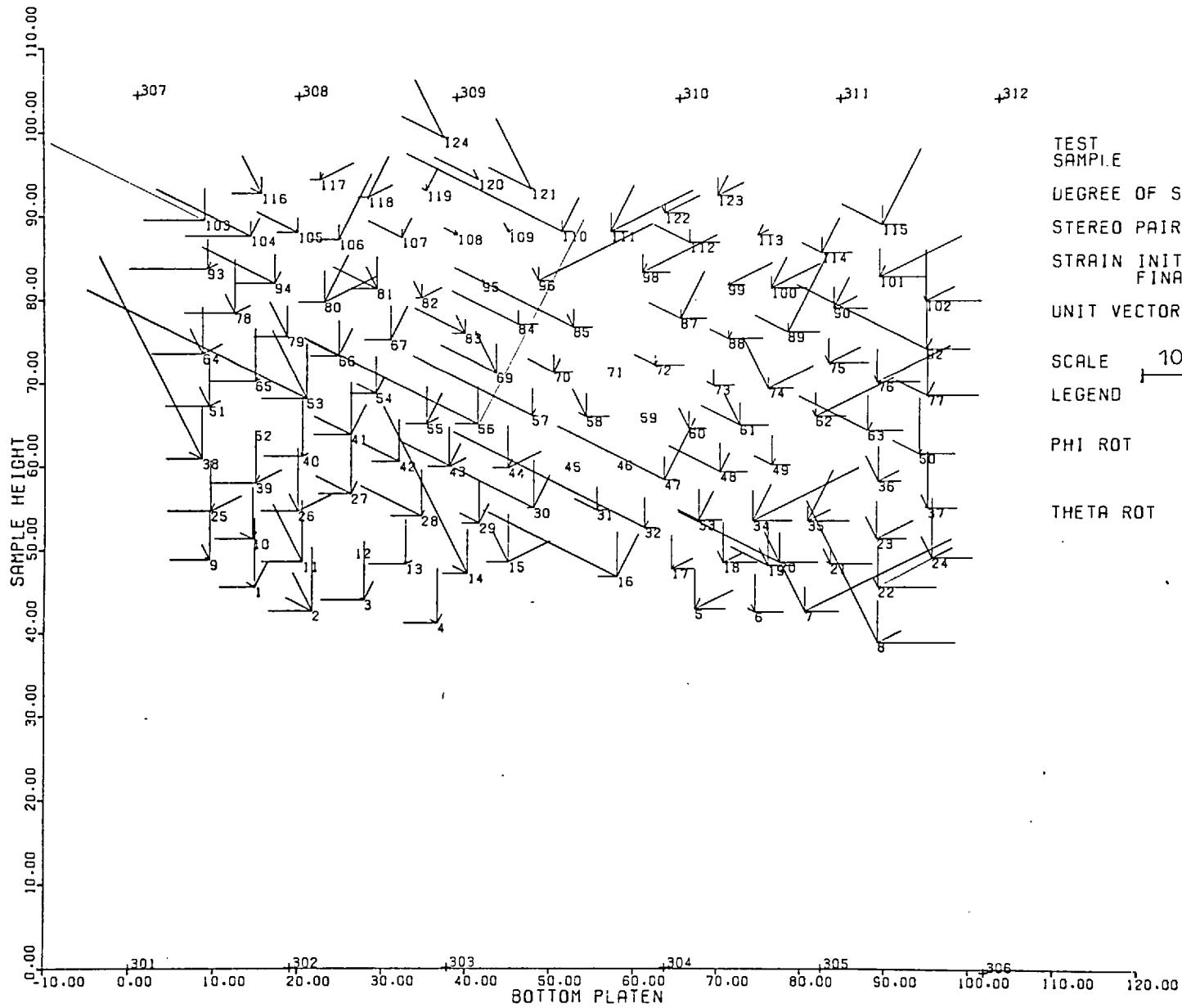
TEST SAMPLE 3201/2
 PLANE STRAIN (DRAINED)
 CERAMIC BALLS
 DEGREE OF SAT. FULLY SAT.
 STEREO PAIR NO. FIRST 2
 FINAL 3
 STRAIN INITIAL 1.546
 FINAL 3.876
 UNIT VECTOR DISP. ROT. HOR. X
VER. Y
 SCALE 10mm 2mm
 LEGEND .2rad
 PHI ROT 
 THETA ROT 

FIG 7.94 DISPLACEMENT - ROTATION FIELD OF MARKERS IN XY PLANE



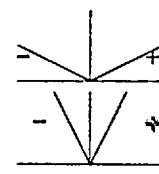
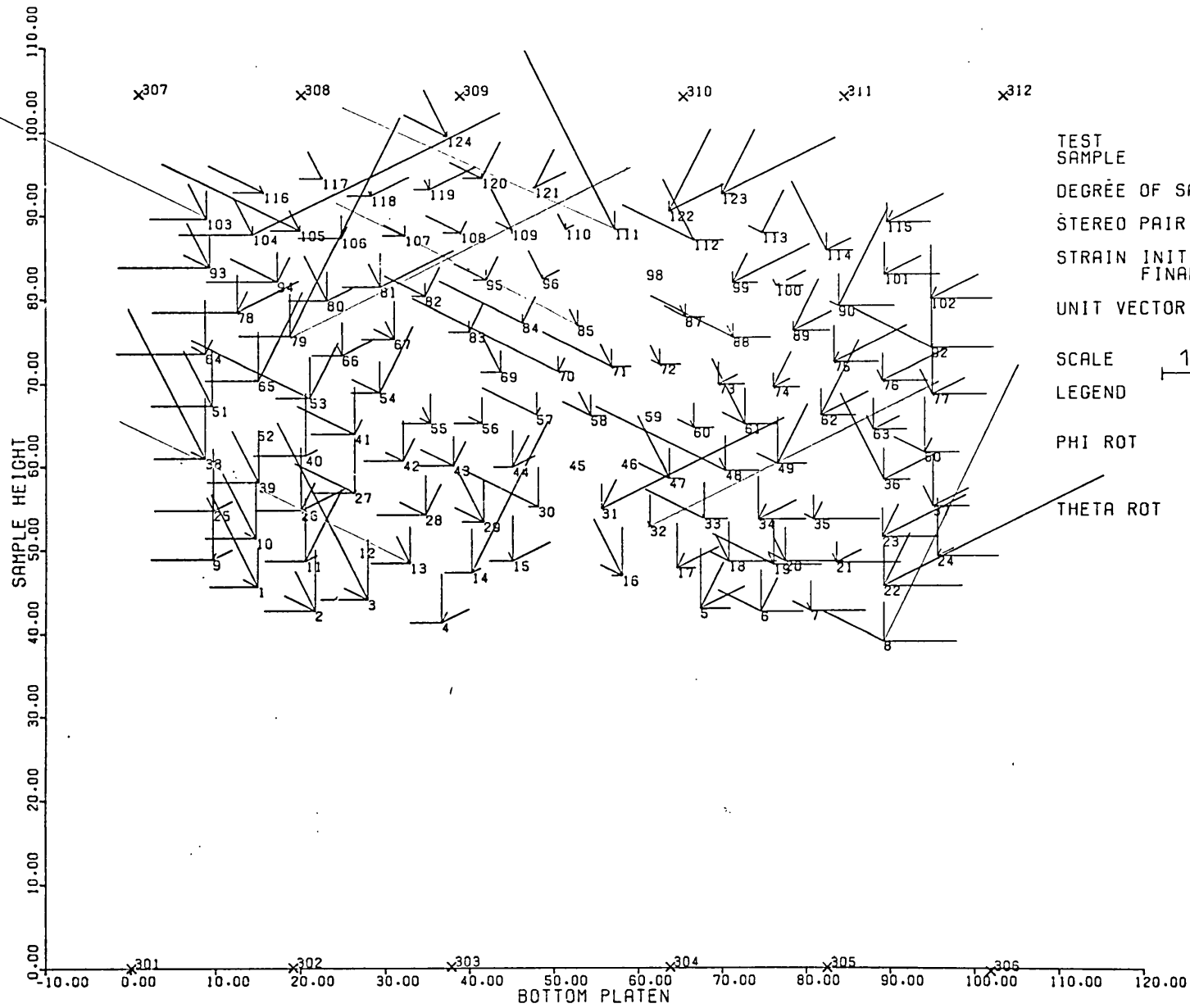
TEST SAMPLE 3201/3
 PLANE STRAIN (DRAINED)
 CERAMIC BALLS
 DEGREE OF SAT. FULLY SAT.
 STEREO PAIR NO. FIRST 3
 FINAL 4
 STRAIN INITIAL 3.876
 FINAL 6.263
 UNIT VECTOR DISP. [HOR.X VER.Y] 2mm
 SCALE 10mm ROT. .2rad
 LEGEND 
 PHI ROT
 THETA ROT

FIG 7.95 DISPLACEMENT - ROTATION FIELD OF MARKERS IN XY PLANE



TEST SAMPLE
 DEGRÉE OF SAT.
 STEREO PAIR NO.
 STRAIN INITIAL
 FINAL
 UNIT VECTOR DISP.
 ROT.
 SCALE 10mm
 LEGEND
 PHI ROT
 THETA ROT

3201/4
 PLANE STRAIN (DRAINED)
 CERAMIC BALLS

FULLY SAT.

FIRST 4
 FINAL 5
 6.263
 8.531

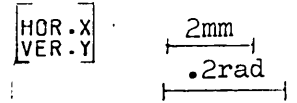
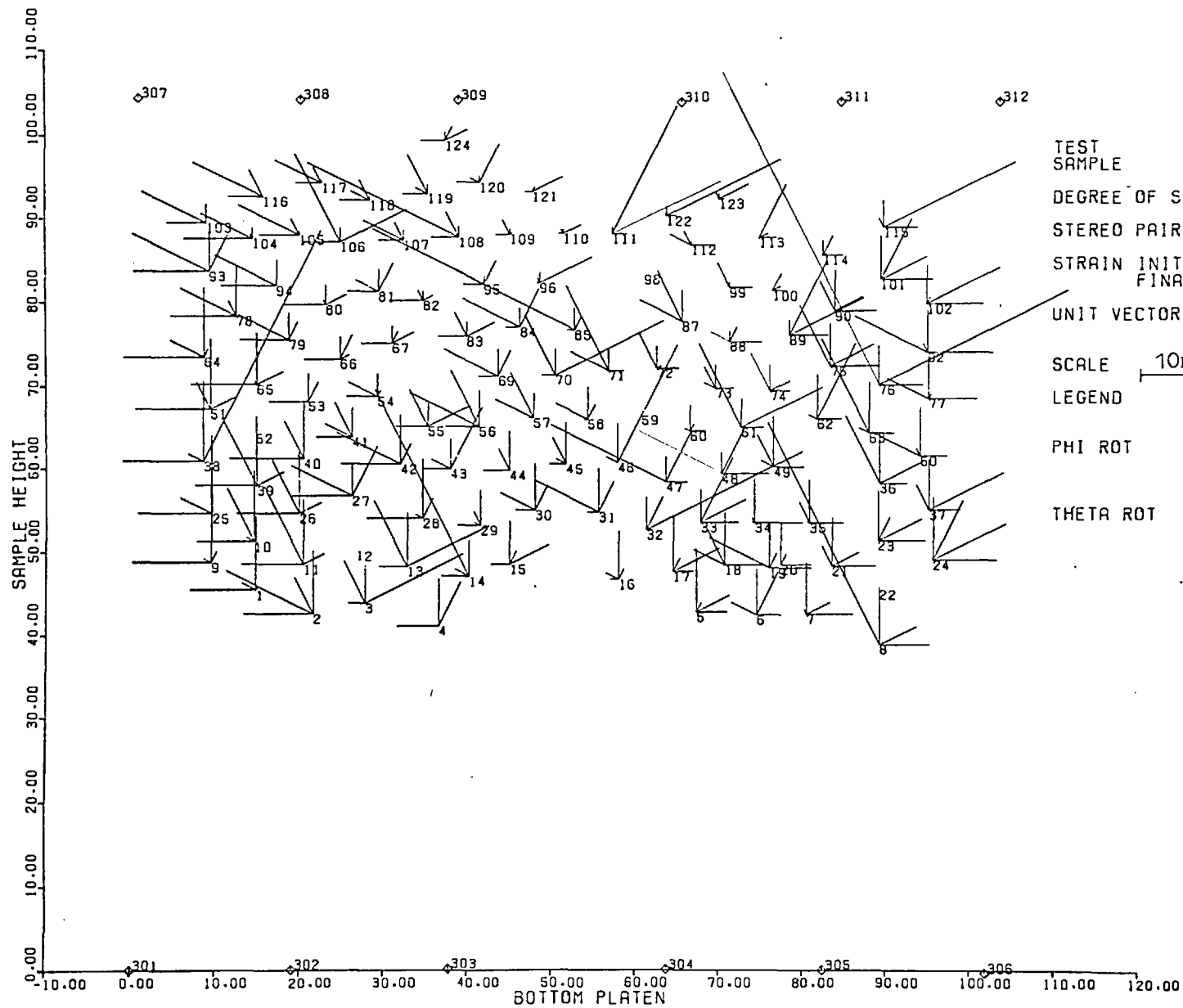


FIG 7.96 DISPLACEMENT - ROTATION FIELD OF MARKERS IN XY PLANE



TEST SAMPLE

DEGREE OF SAT.

STEREO PAIR NO.

STRAIN INITIAL
FINAL

UNIT VECTOR DISP.

SCALE 10mm

LEGEND

PHI ROT

THETA ROT

3201/5
PLANE STRAIN (DRAINED)
CERAMIC BALLS

FULLY SAT.

FIRST 5
FINAL 6
8.531
11.130

HOR. X
VER. Y

2mm
.2rad

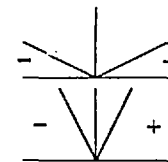
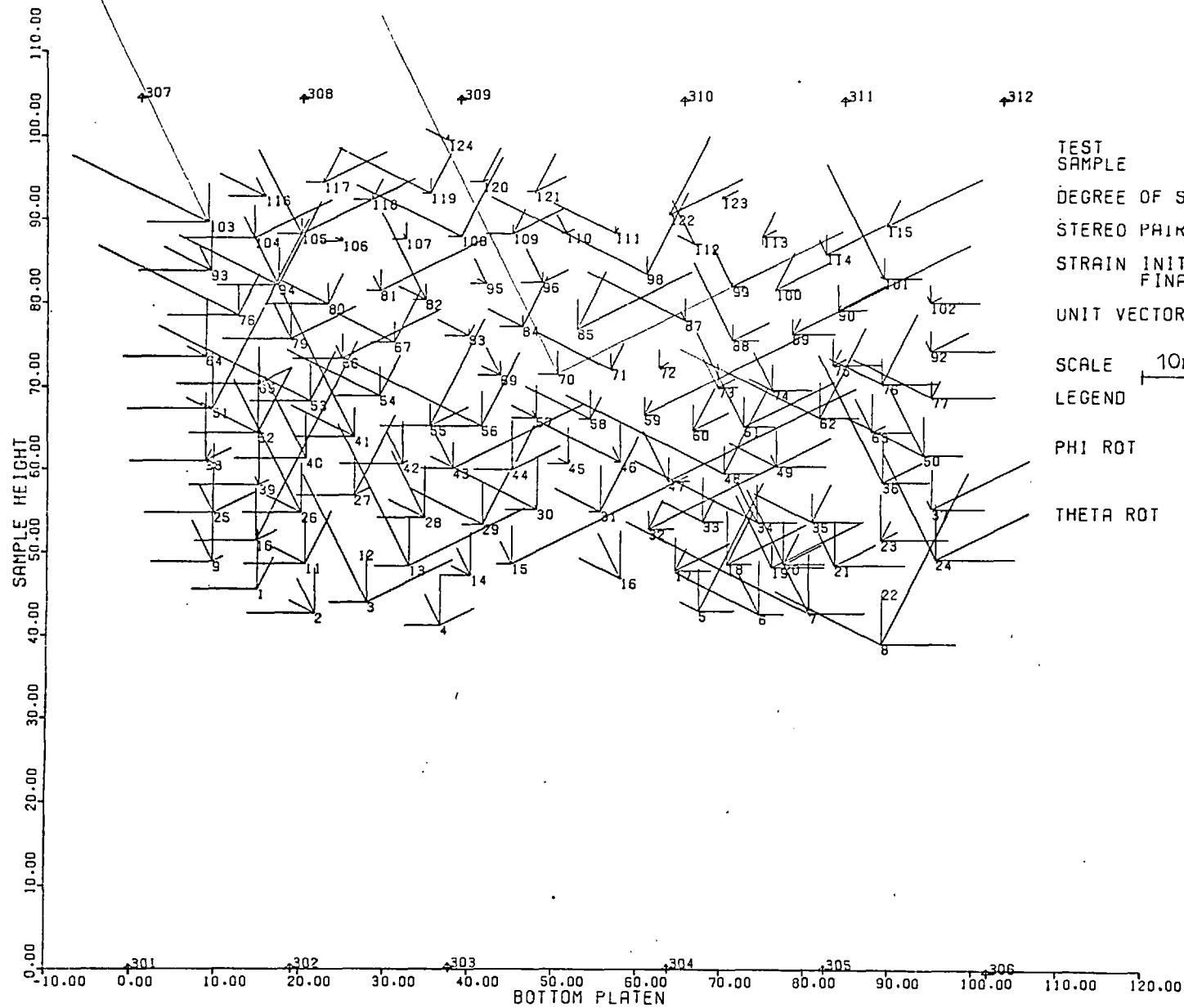


FIG 7.97 DISPLACEMENT - ROTATION FIELD OF MARKERS IN XY PLANE



TEST SAMPLE
 DEGREE OF SAT. FULLY SAT.
 STEREO PAIR NU. FIRST 6
 FINAL 7
 STRAIN INITIAL 11.130
 FINAL 15.102
 UNIT VECTOR DISP. ROT.

HOR-X
VER-Y

 SCALE 10mm
 LEGEND
 PHI ROT
 THETA ROT

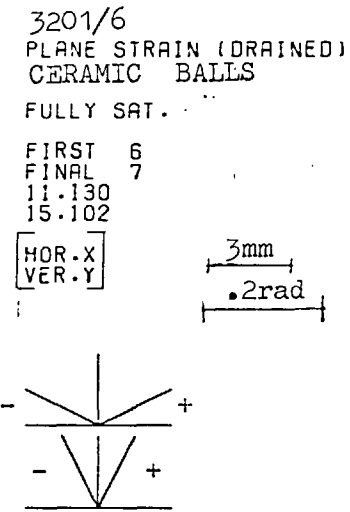
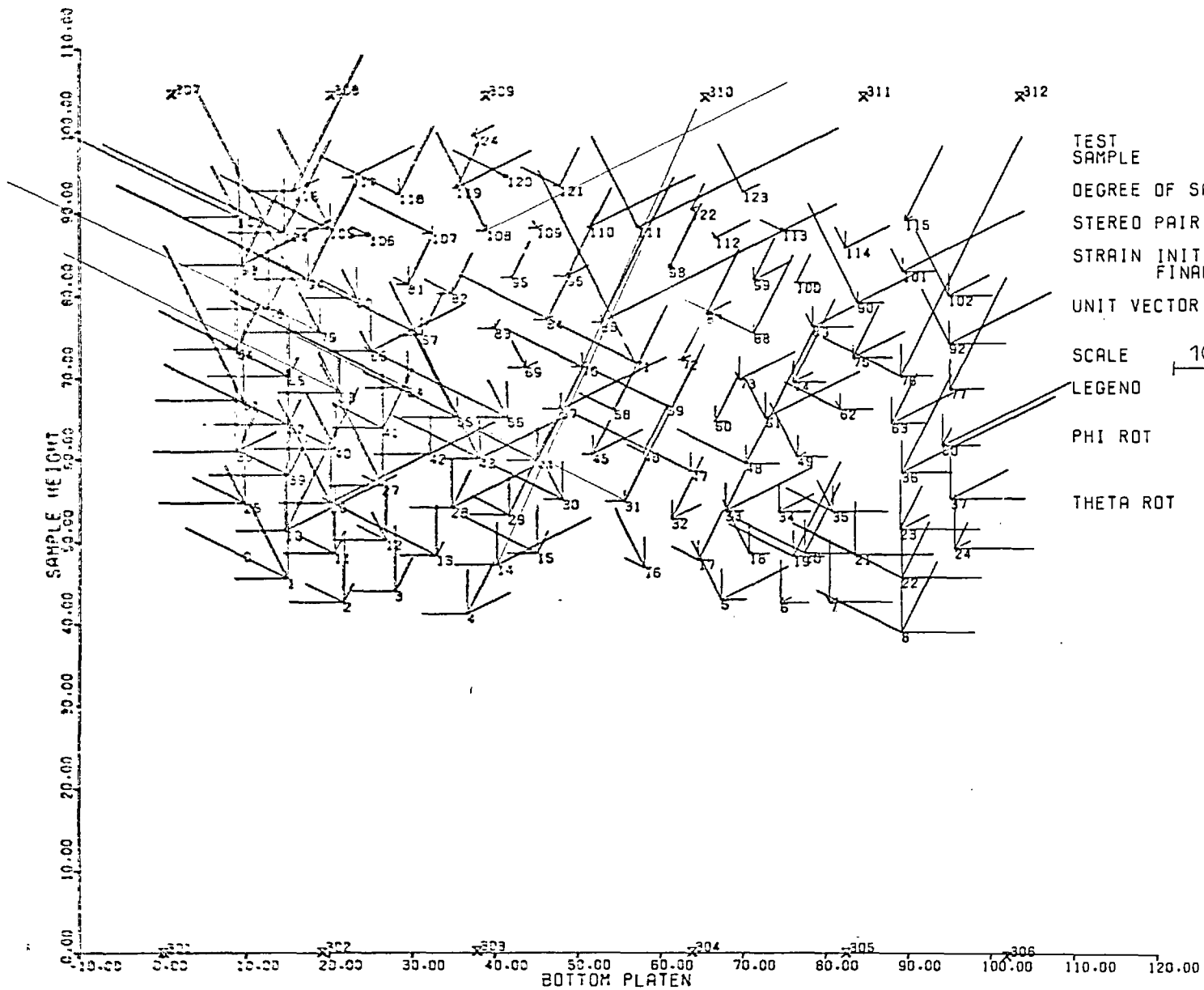


FIG 7.98 DISPLACEMENT - ROTATION FIELD OF MARKERS IN XY PLANE



TEST SAMPLE 3201/7
 DEGREE OF SAT. FULLY SAT.
 STEREO PAIR NO. FIRST 7
 STRAIN INITIAL FINAL 15.102 8
 20.193
 UNIT VECTOR DISP. ROT. 10mm
 SCALE 5mm .2rad
 LEGEND
 PHI ROT
 THETA ROT

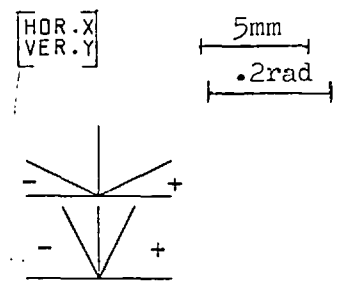


FIG 7.99 DISPLACEMENT - ROTATION FIELD OF MARKERS IN XY PLANE

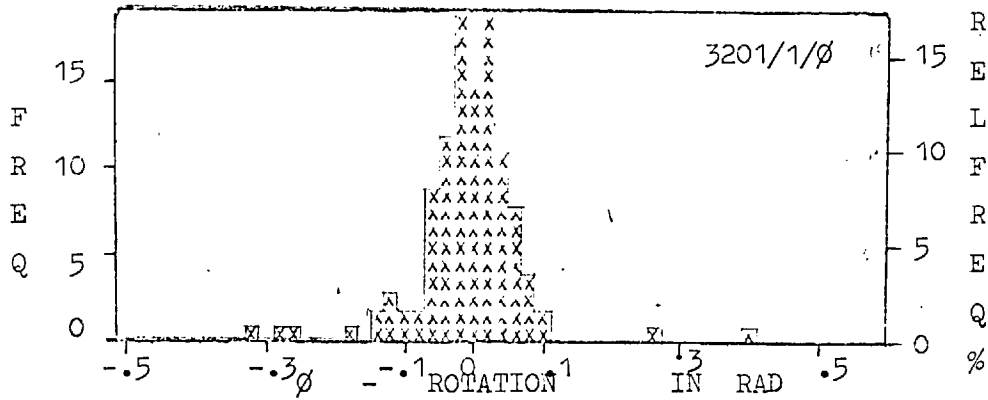


FIG. 7.100

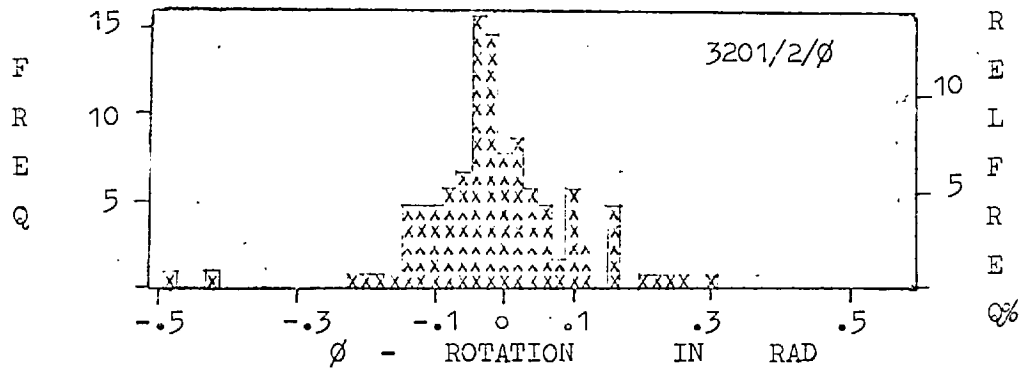
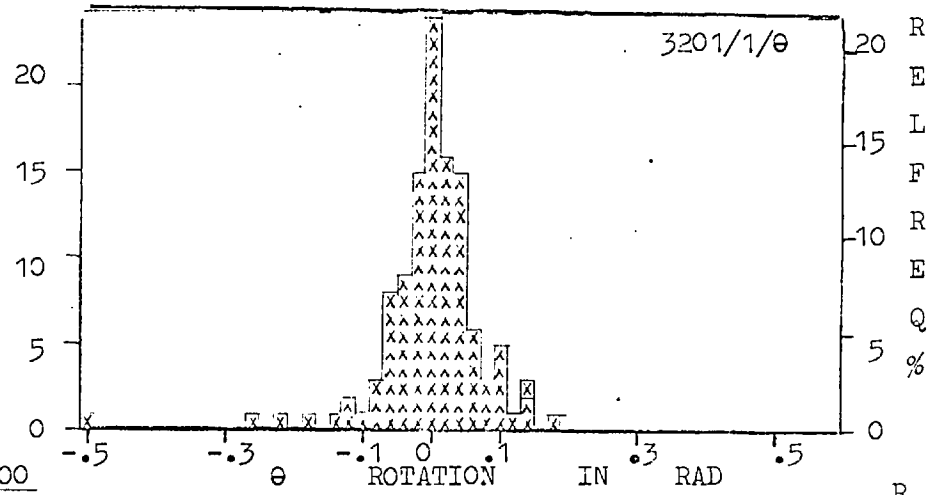


FIG. 7.101

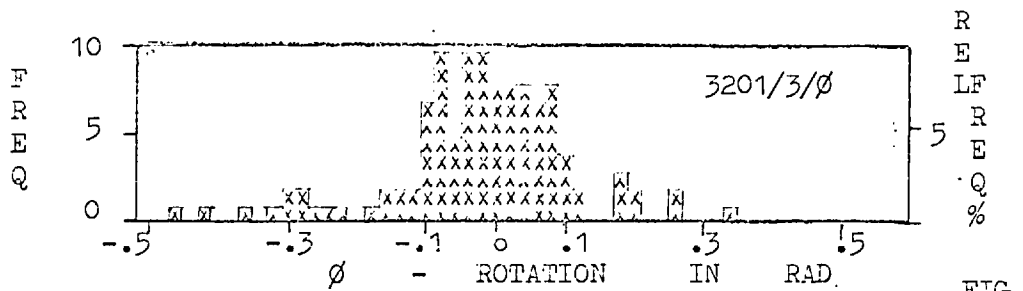
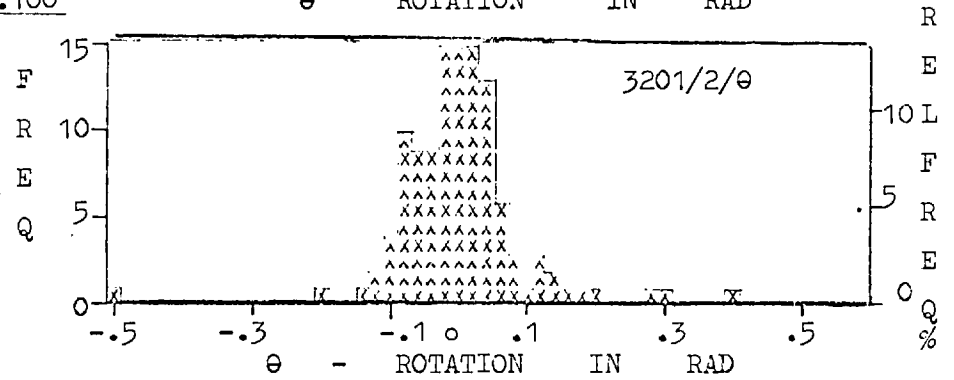
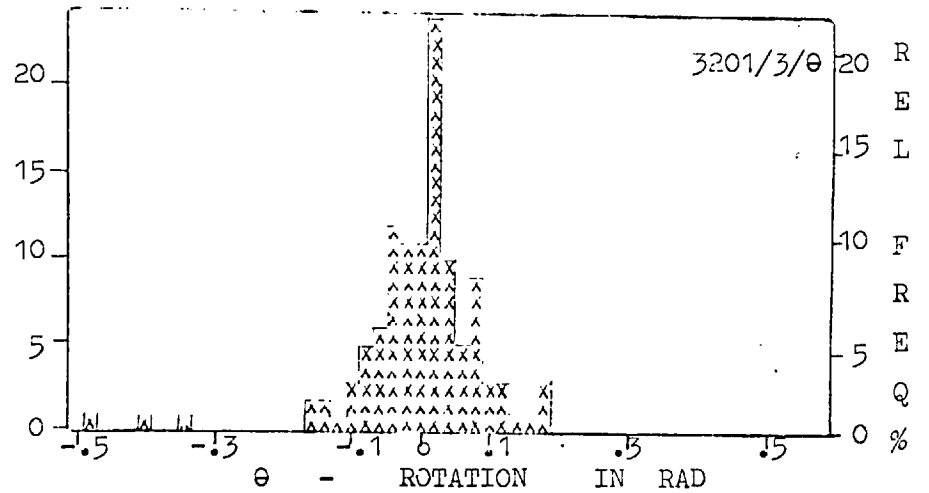


FIG. 7.102



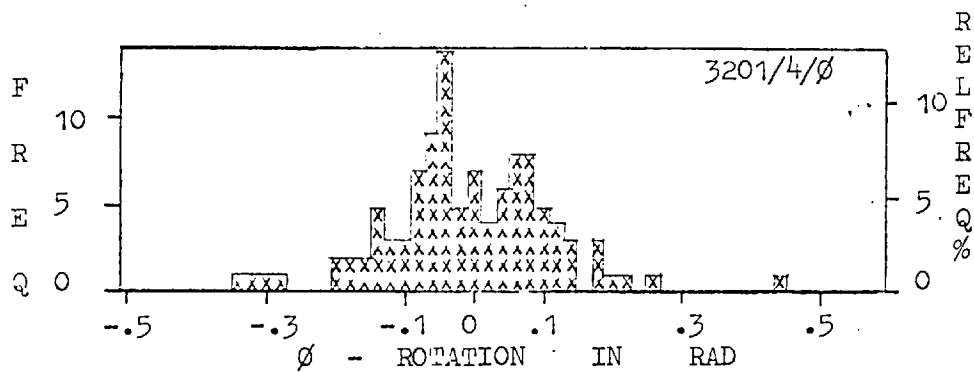


FIG. 7.103

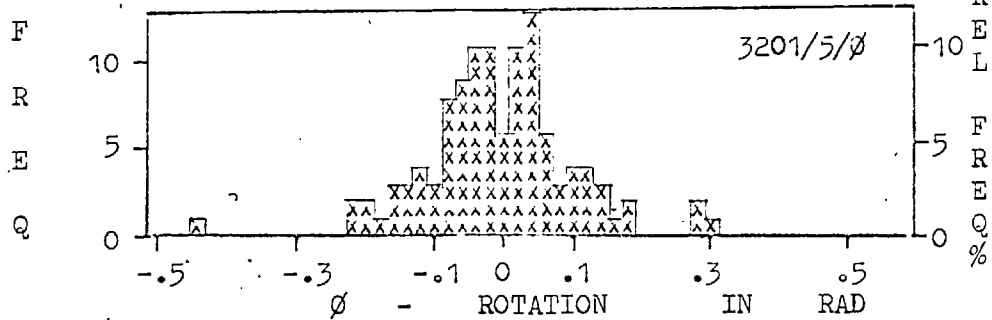
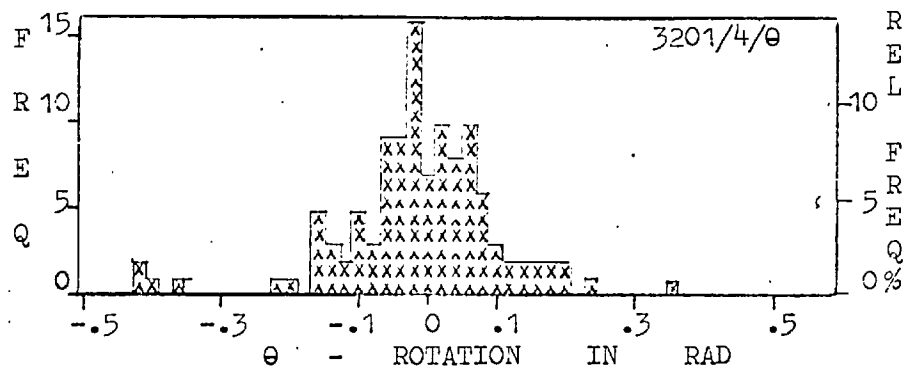


FIG. 7.104

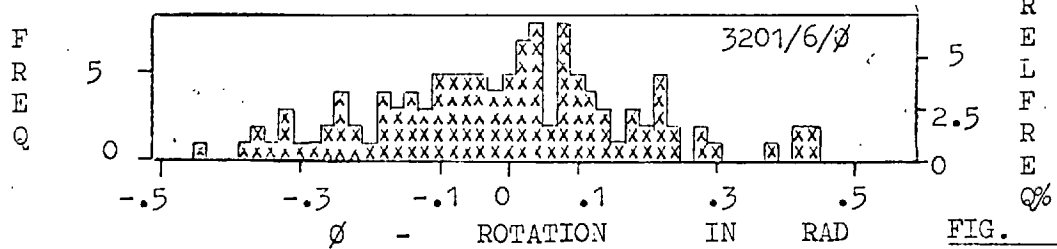
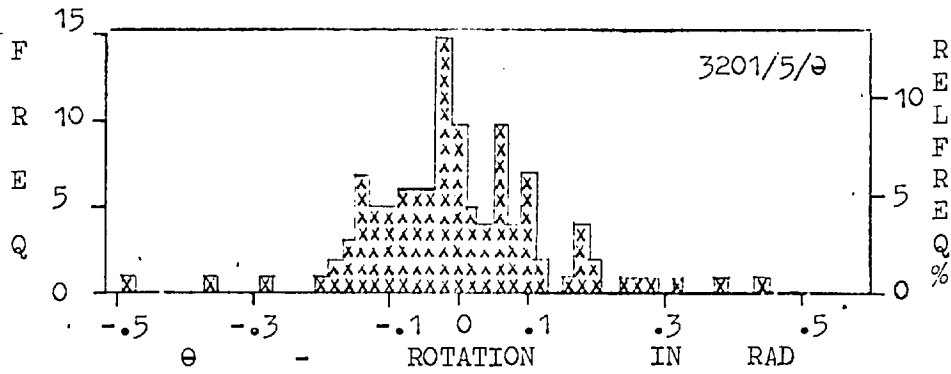


FIG. 7.105

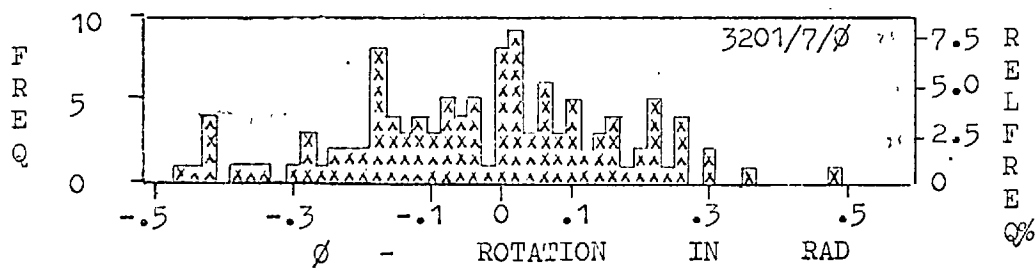
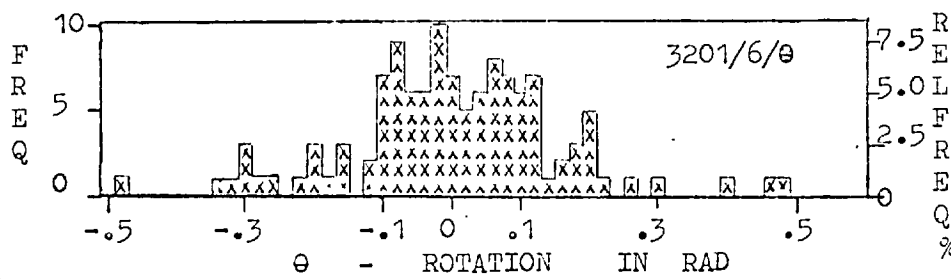
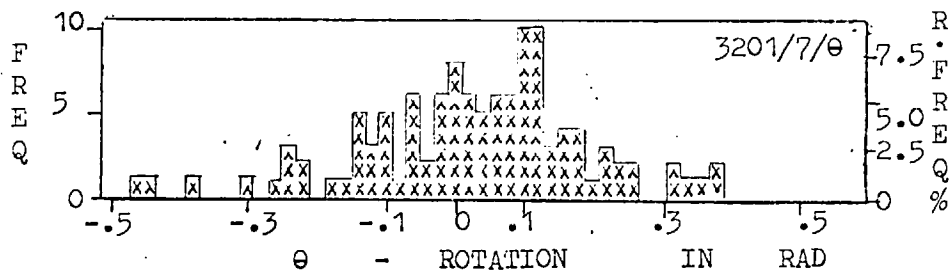
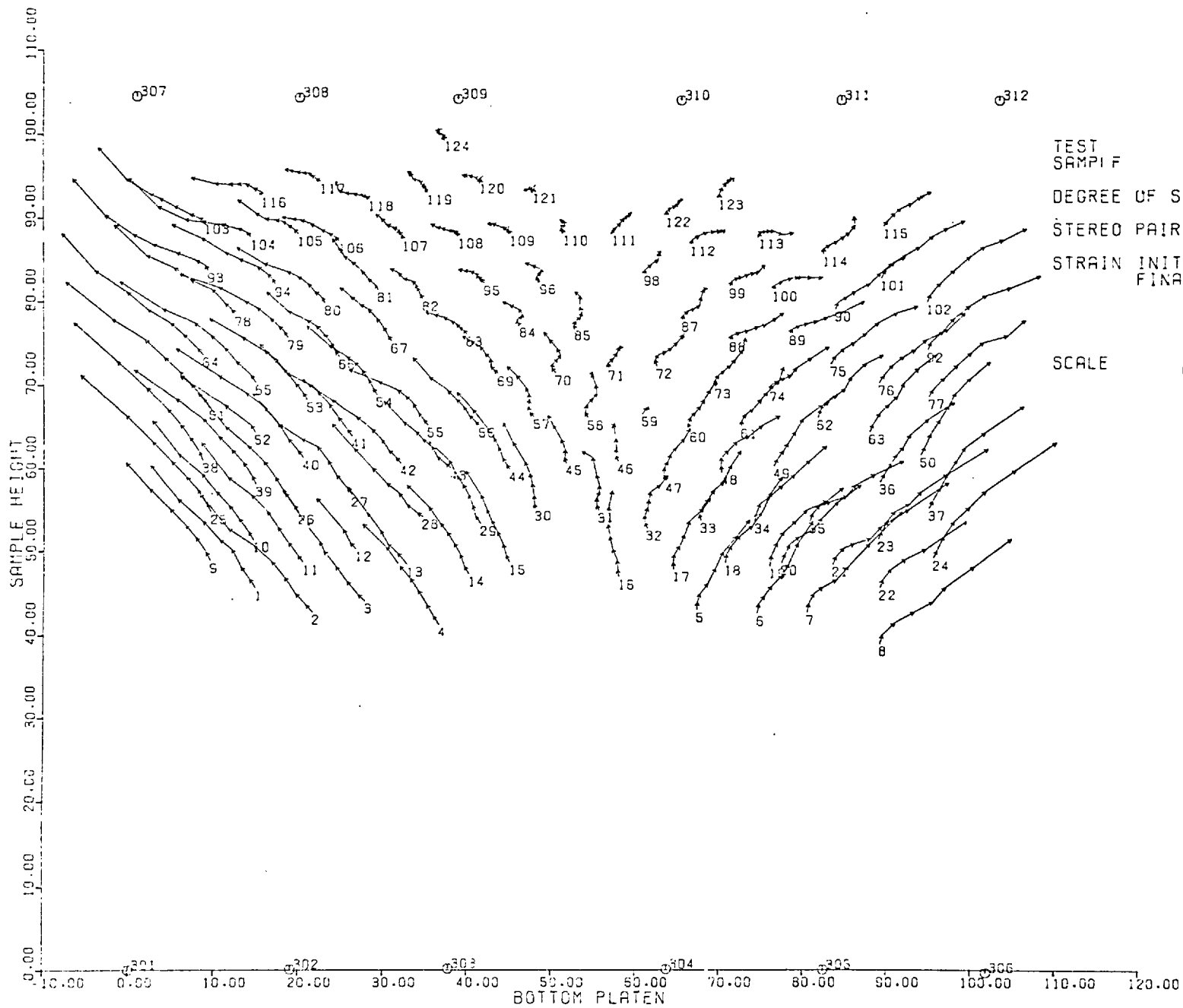


FIG. 7.106





TEST
SAMPLIF

DEGREE OF SAT.

STEREO PAIR NO.

STRAIN INITIAL
FINAL

3201
PLANE STRAIN (DRAINED)
CERAMIC BALLS

FULLY SAT.

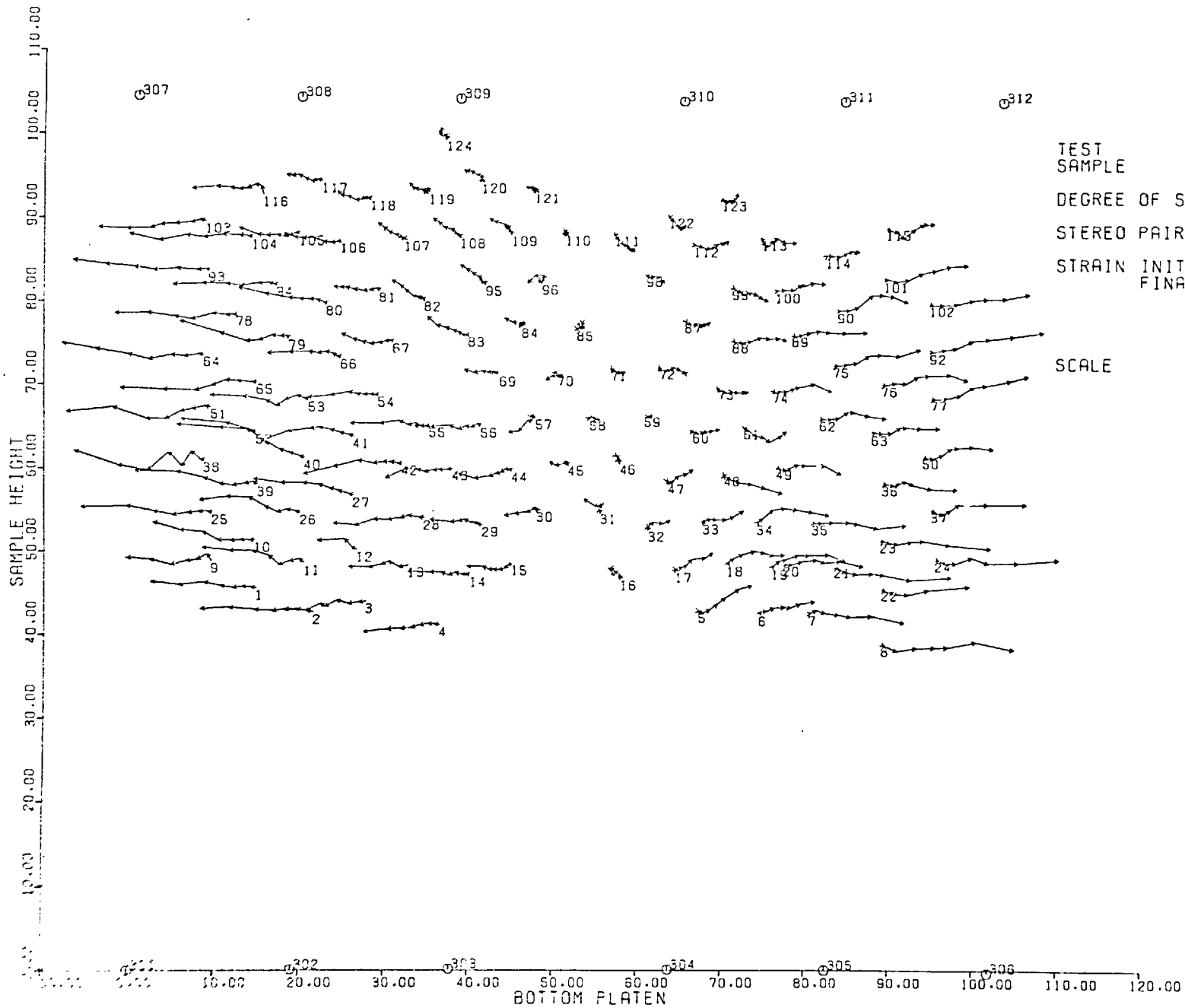
FIRST 1
LAST 8

0.0
20.193

SCALE 

FIG 7.107

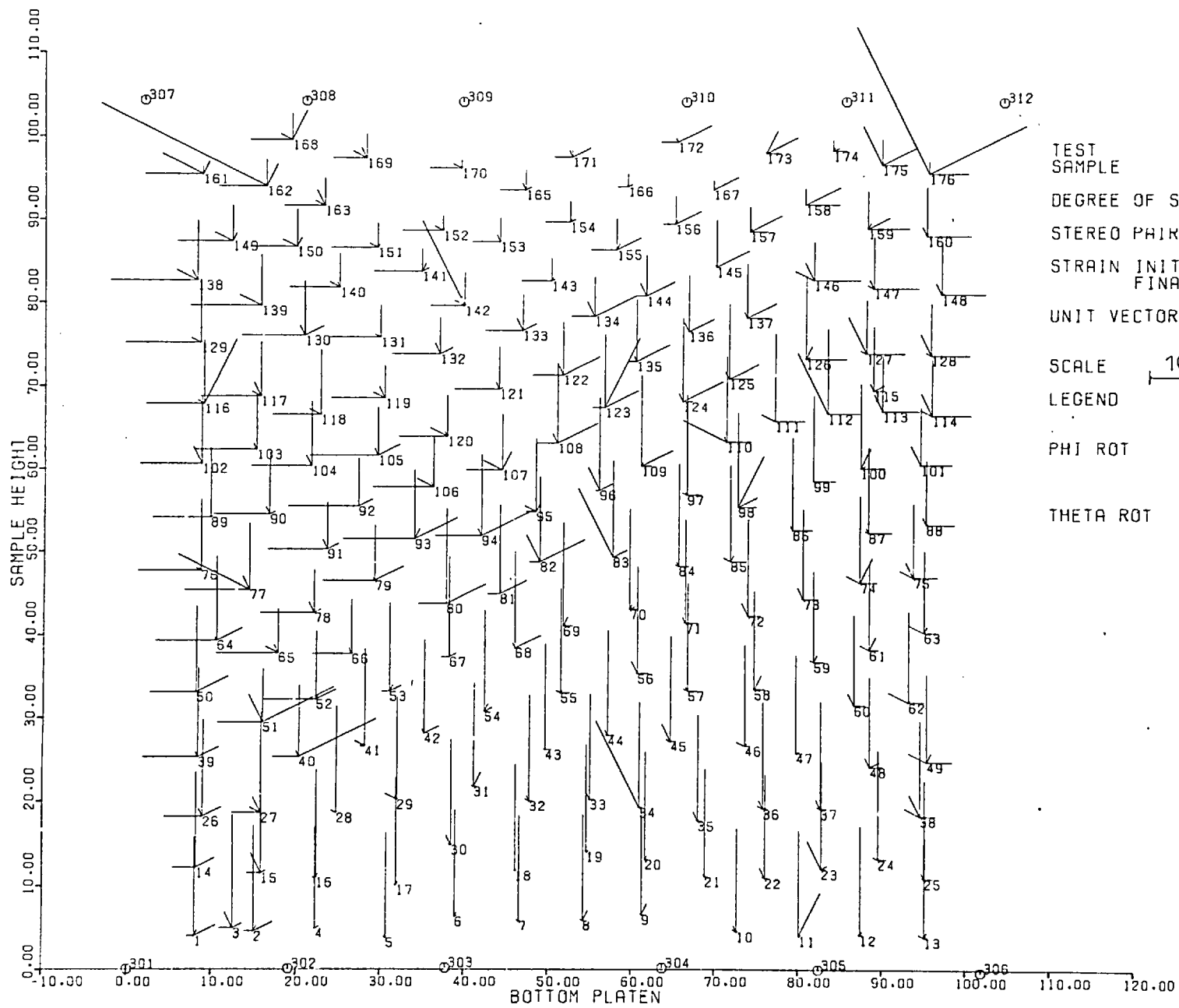
TRACE OF DISPLACEMENTS OF MARKER CENTRES. ON XY PLANE



TEST SAMPLE
 DEGREE OF SAT. FULLY SAT.
 STEREO PAIR NO. FIRST 1
 LAST 8
 STRAIN INITIAL 0.000
 FINAL 20.193

3201
 PLANE STRAIN (DRAINED)
 CERAMIC BALLS

SCALE 10mm



4200/1
 PLANE STRAIN (DRAINED)
 PTFE CHUNKS

TEST SAMPLE
 DEGREE OF SAT. DRY
 STEREO PAIR NO. FIRST 1
 FINAL 2
 STRAIN INITIAL 0.000
 FINAL 1.583

UNIT VECTOR DISP. HOR. X
VER. Y 1mm

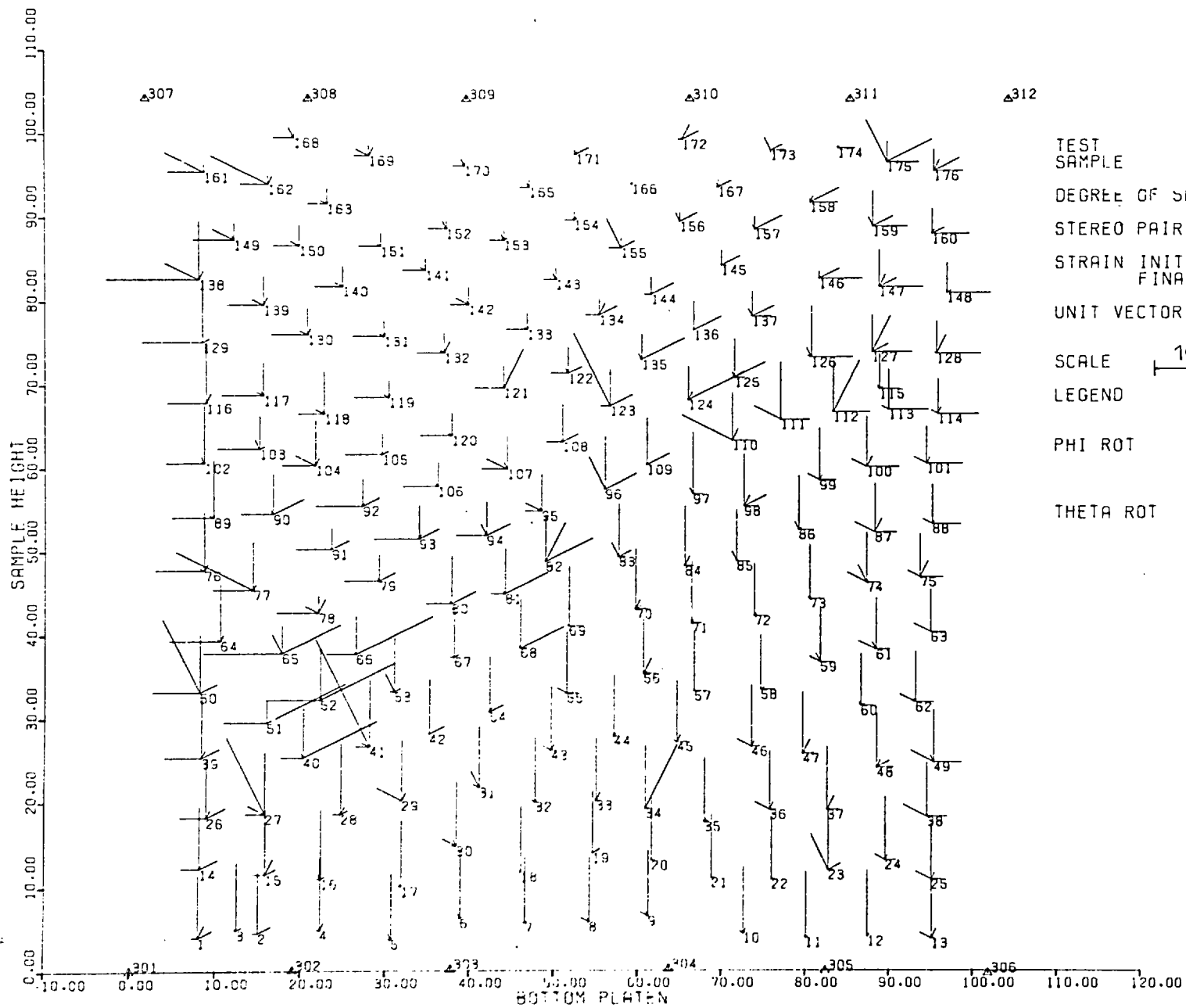
SCALE 10mm ROT. 1rad

LEGEND

PHI ROT - +

THETA ROT - +

FIG 7.109 DISPLACEMENT - ROTATION FIELD OF MARKERS IN XY PLANE



TEST
SAMPLE

DEGREE OF SAT.

STEREO PAIR NO.

STRAIN INITIAL
FINAL

UNIT VECTOR DISP.

SCALE $\overline{10mm}$ ROT.

LEGEND

PHI ROT

THETA ROT

4200/2

PLANE STRAIN (DRAINED)
PTFE CHUNKS

DRY

FIRST 2
FINAL 3

1.583
3.545

HOR. X
VER. Y

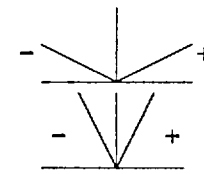
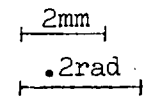
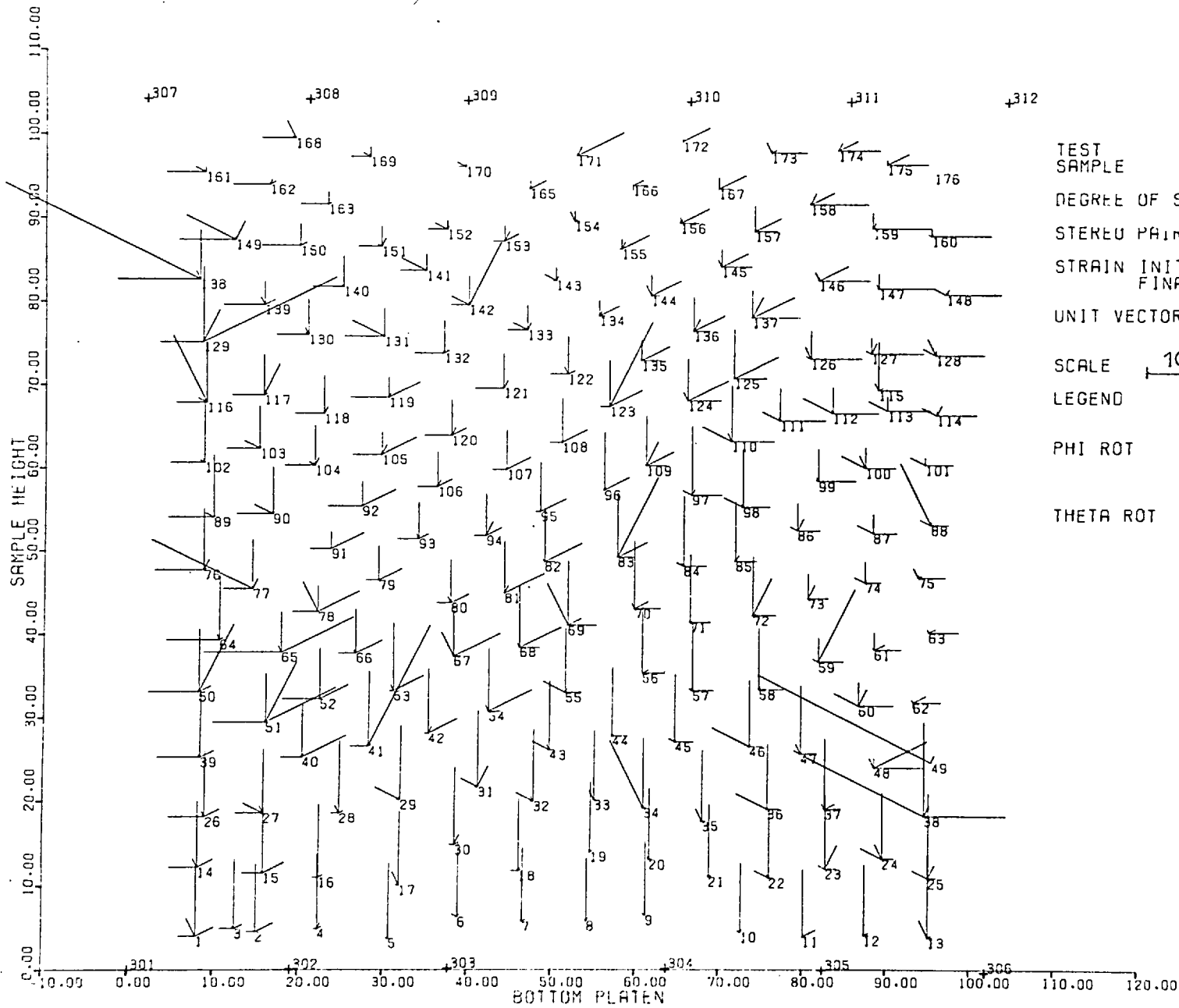


FIG 7.110 DISPLACEMENT - ROTATION FIELD OF MARKERS IN XY PLANE

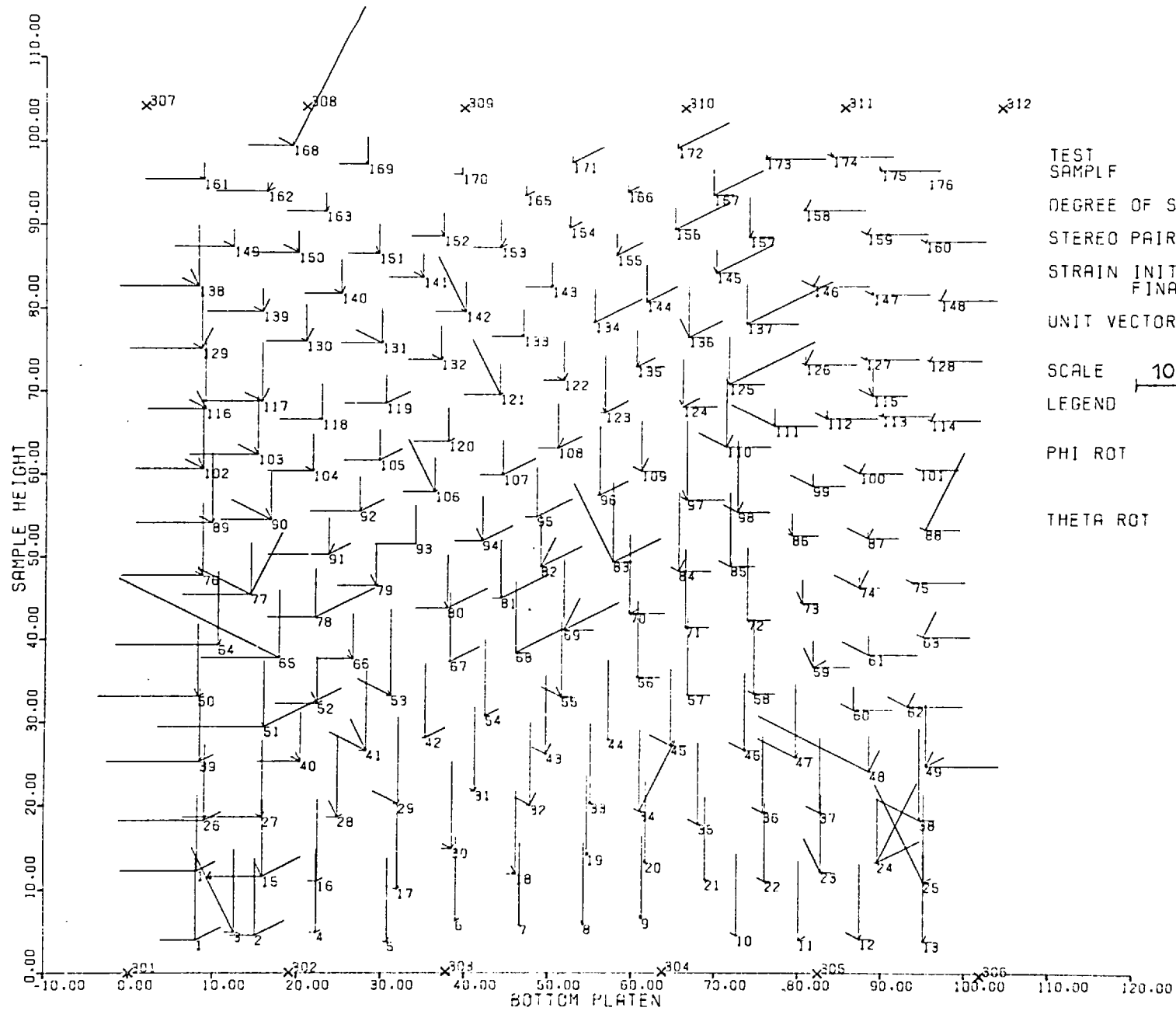


TEST SAMPLE 4200/3
 DEGREE OF SHI. PLANE STRAIN (DRAINED)
 STEREO PAIR NO. PTFE CHUNKS
 STRAIN INITIAL FIRST 3
 STRAIN FINAL FINAL 4
 UNIT VECTOR DISP.

HOR. X	2mm
VER. Y	.2rad

 SCALE 10mm ROT.
 LEGEND
 PHI ROT
 THETA ROT

FIG 7.111 DISPLACEMENT - ROTATION FIELD OF MARKERS IN XY PLANE



TEST
SAMPLF

DEGREE OF SAT.

STEREO PAIR NO.

STRAIN INITIAL
FINAL

UNIT VECTOR DISP.
ROT.

SCALE

LEGEND

PHI ROT

THETA ROT

4200/4

PLANE STRAIN (DRAINED)
PTFE CHUNKS

DRY

FIRST 4

FINAL 5

5.678

8.126

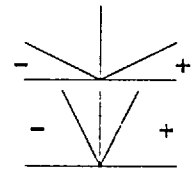
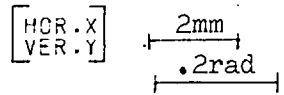
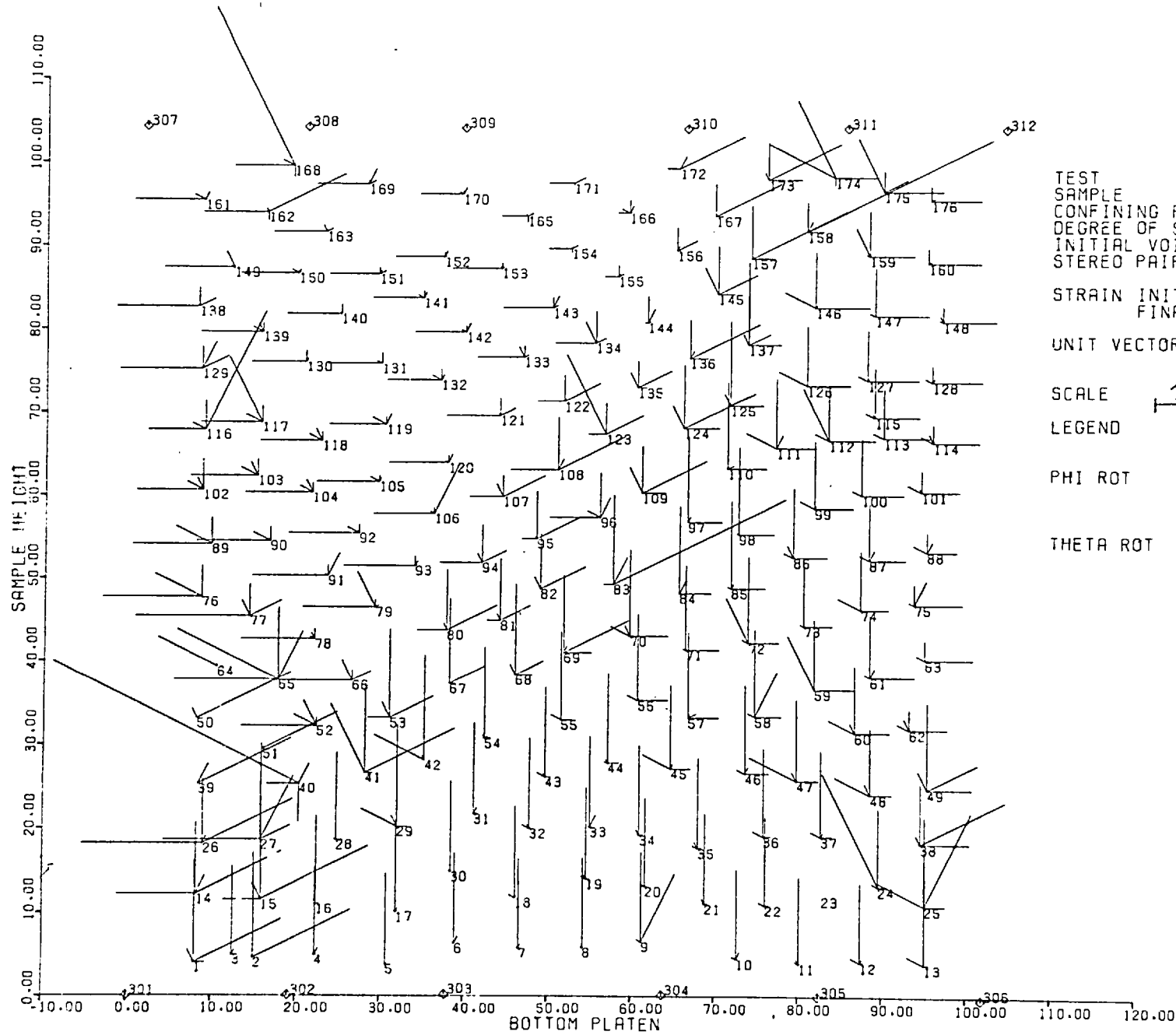
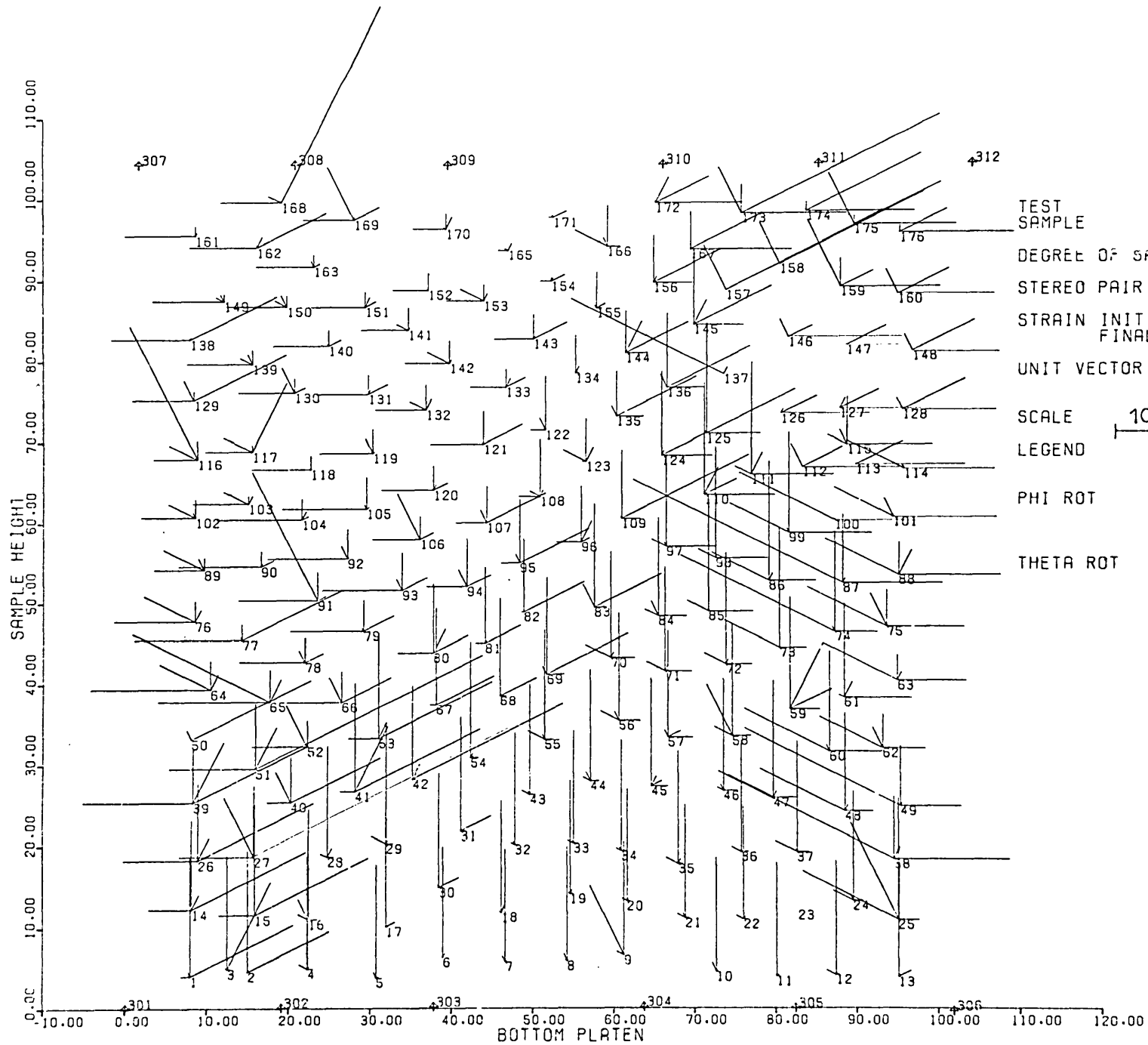


FIG 7.112 DISPLACEMENT - ROTATION FIELD OF MARKERS IN XY PLANE



TEST 4200/5
 SAMPLE PLANE STRAIN (DRAINED)
 CONFINING PRESSURE PTFE CHUNKS
 DEGREE OF SAT. DRY
 INITIAL VOID RATIO
 STEREO PAIR NO. FIRST 5
 FINAL 6
 STRAIN INITIAL 8.126
 FINAL 10.763
 UNIT VECTOR DISP. [HOR.X] 2mm
 ROT. [VER.Y] .2rad
 SCALE 10mm
 LEGEND
 PHI ROT - +
 THETA ROT - +

FIG 7.113 DISPLACEMENT - ROTATION FIELD OF MARKERS IN XY PLANE



TEST SAMPLE

DEGREE OF SAT. DRY

STEREO PAIR NO. FIRST 6 FINAL 7

STRAIN INITIAL 10.763 FINAL 15.884

UNIT VECTOR DISP. ROT.

SCALE 10mm

LEGEND

PHI ROT

THETA ROT

4200/6
PLANE STRAIN (DRAINED)
PTFE CHUNKS

DRY

FIRST 6
FINAL 7
STRAIN INITIAL 10.763
FINAL 15.884

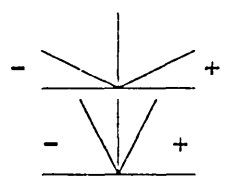
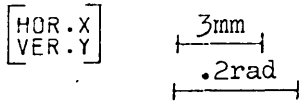
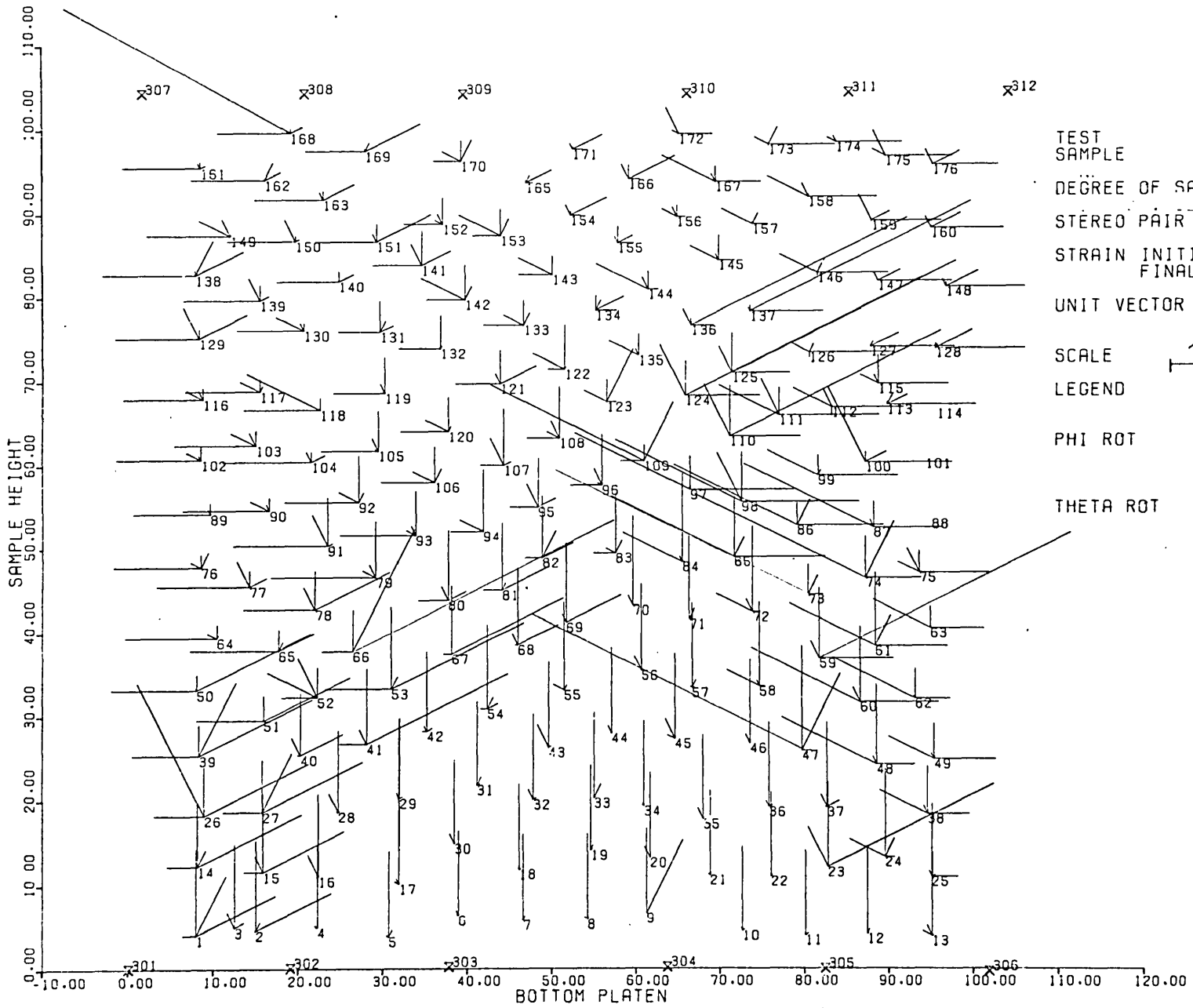


FIG 7.114 DISPLACEMENT - ROTATION FIELD OF MARKERS IN XY PLANE



TEST SAMPLE

DEGREE OF SAT.

STEREO PAIR NO.

STRAIN INITIAL
FINAL

UNIT VECTOR DISP.

SCALE

LEGEND

PHI ROT

THETA ROT

4200/7
PLANE STRAIN (DRAINED)
PIPE CHUNKS

DRY

FIRST 7
FINAL 8
15.884
20.832

HOR. X
VER. Y

ROT.
10mm

5mm
0.2rad

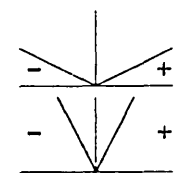


FIG 7.115 DISPLACEMENT - ROTATION FIELD OF MARKERS IN XY PLANE

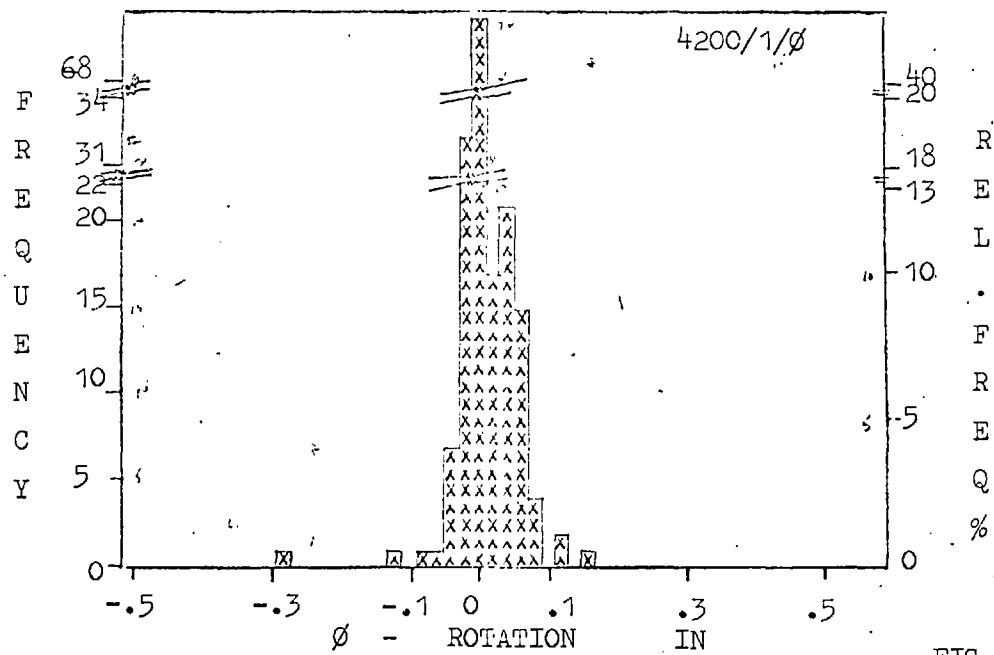


FIG. 7.116

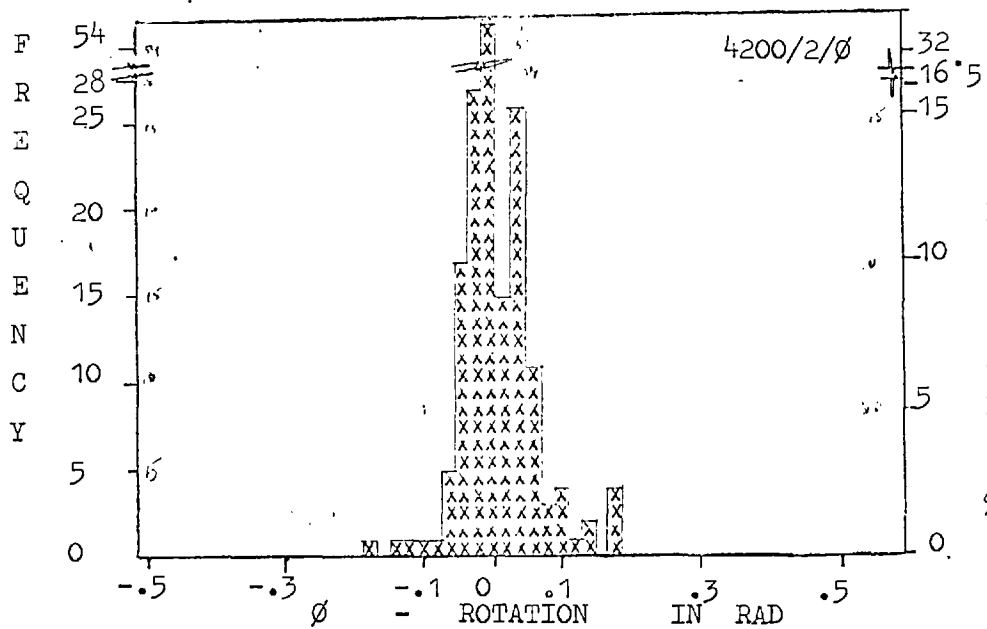
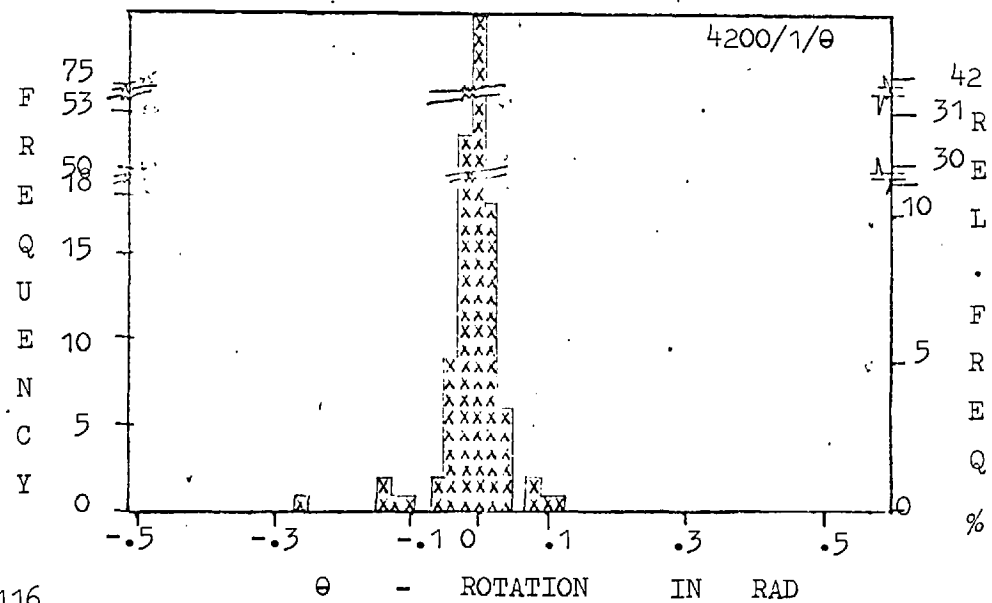
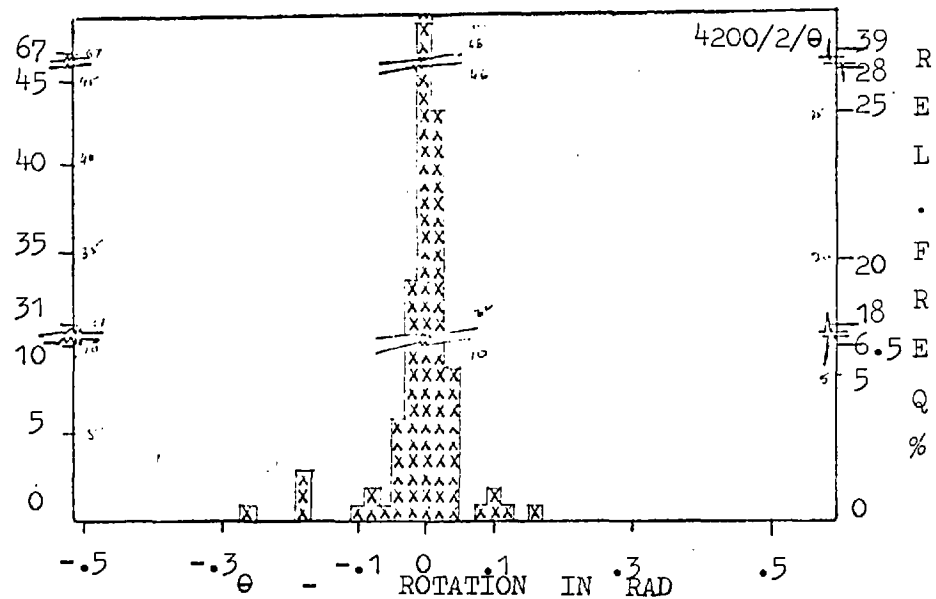


FIG. 7.117



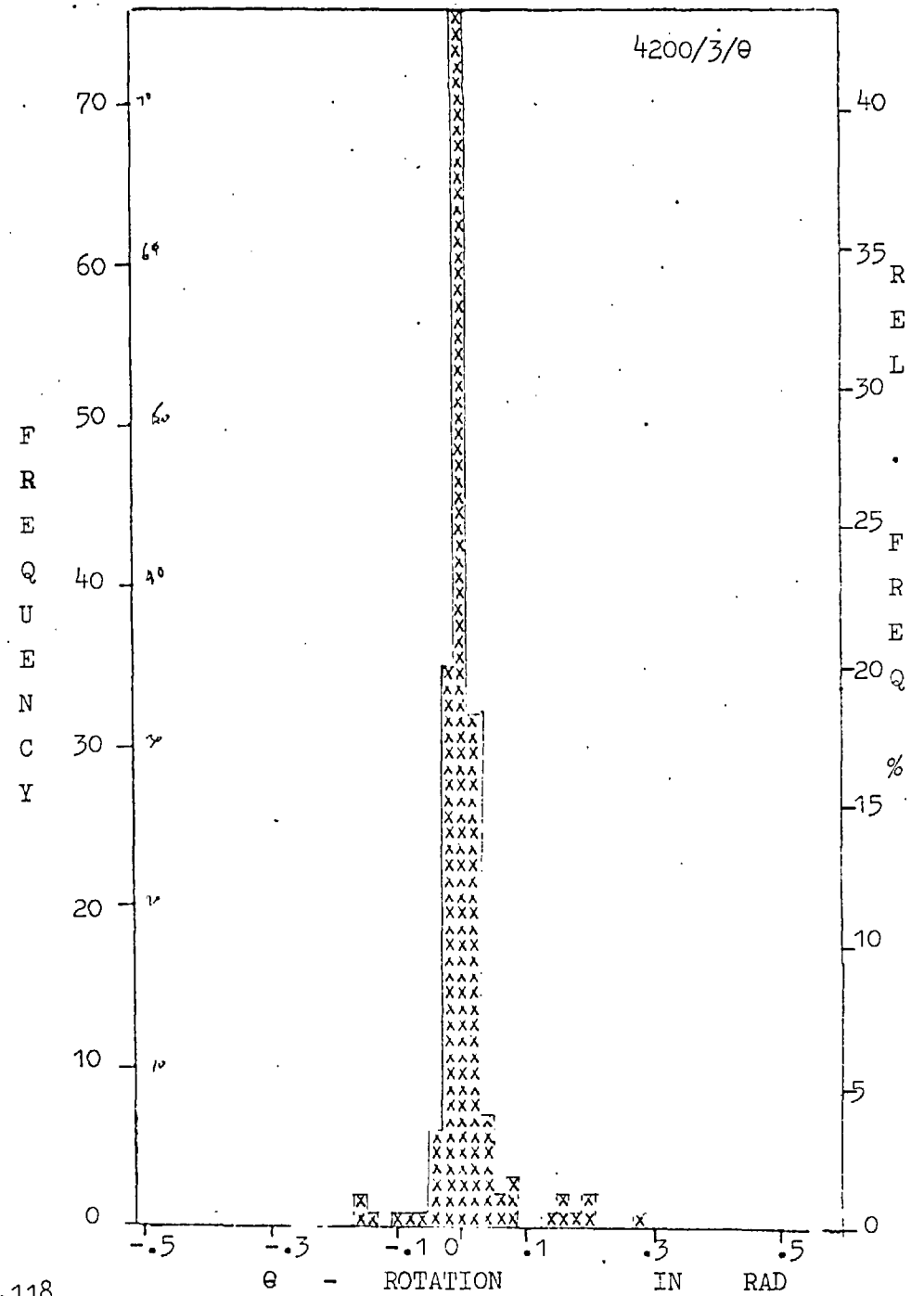
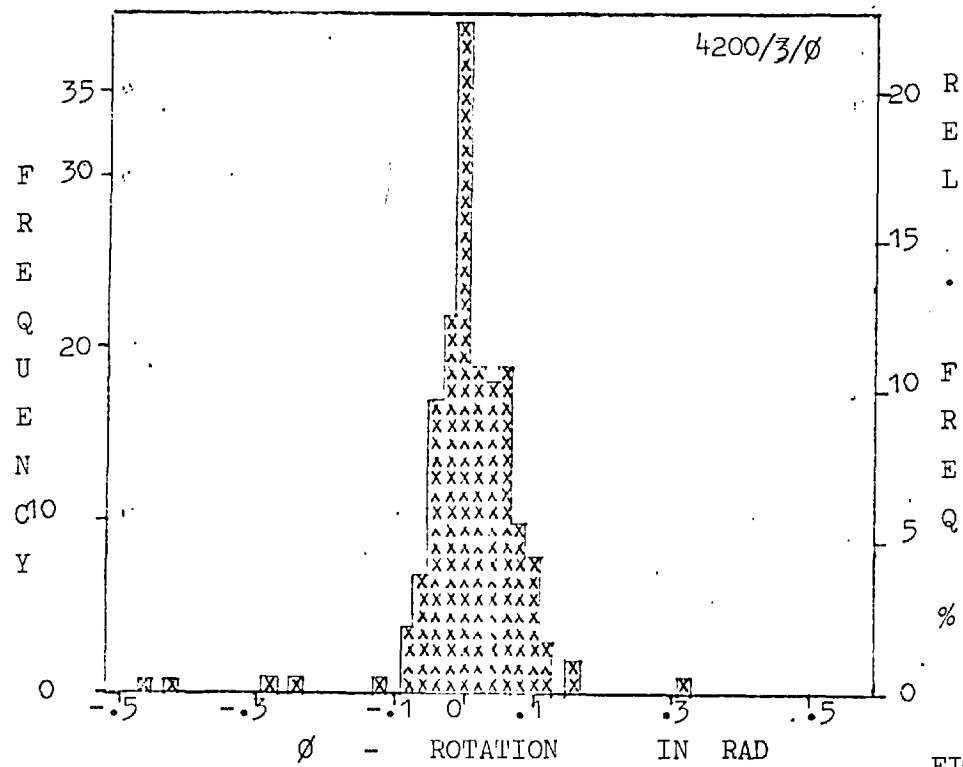


FIG. 7.118

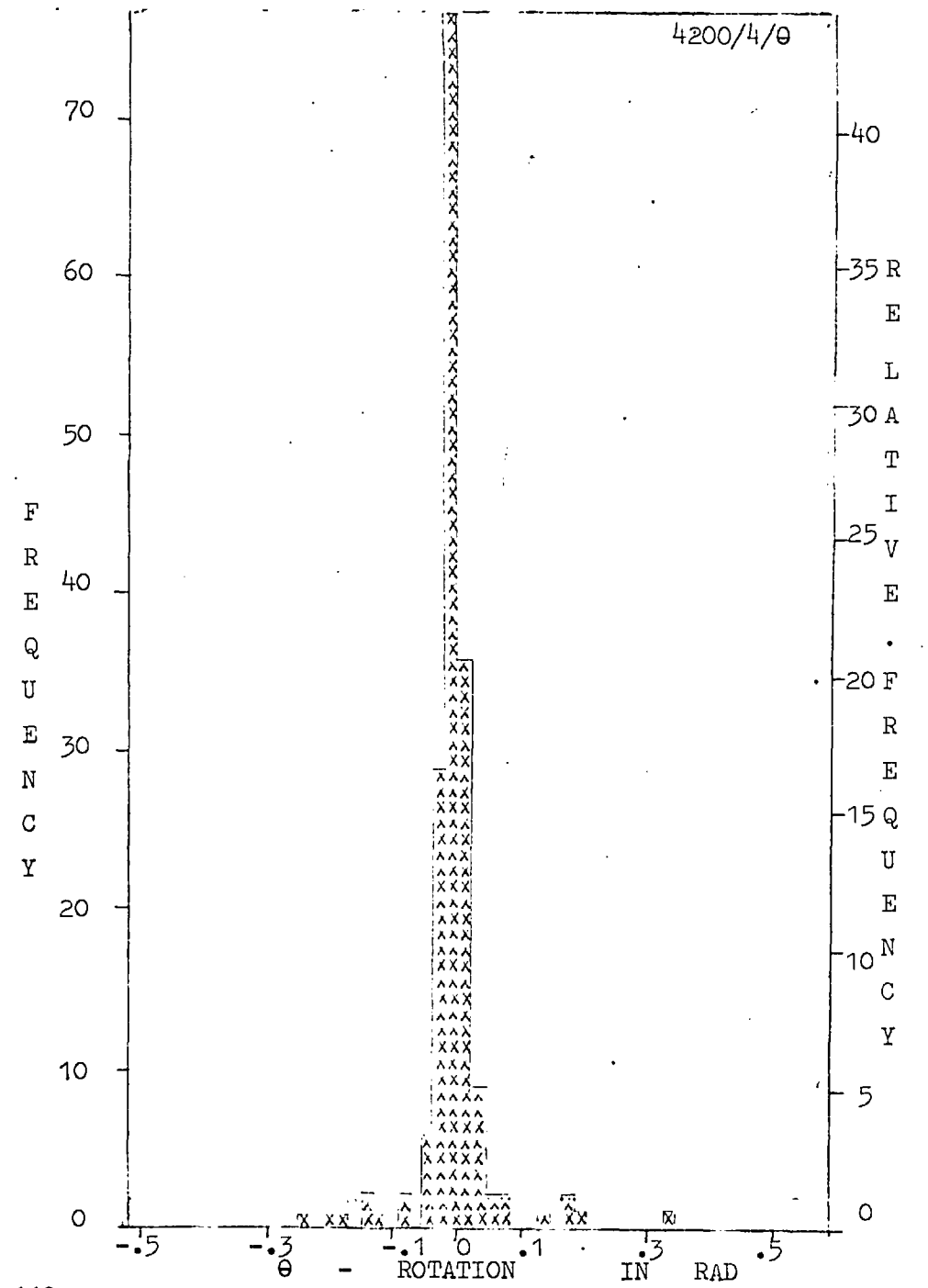
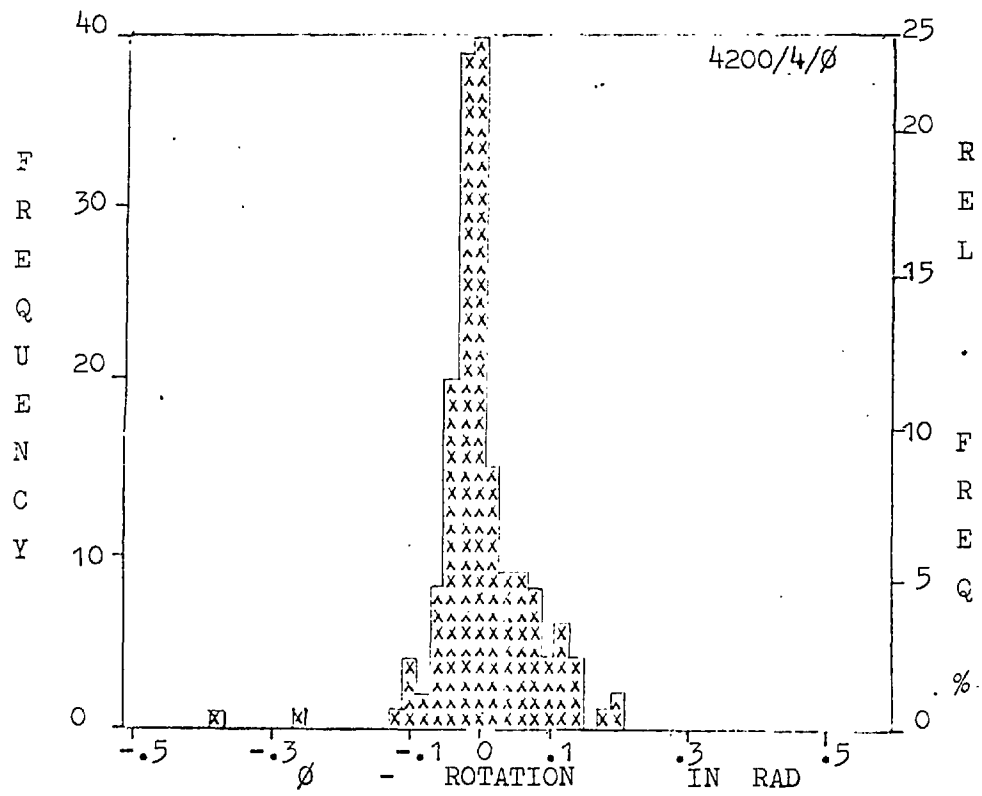


FIG. 7.119

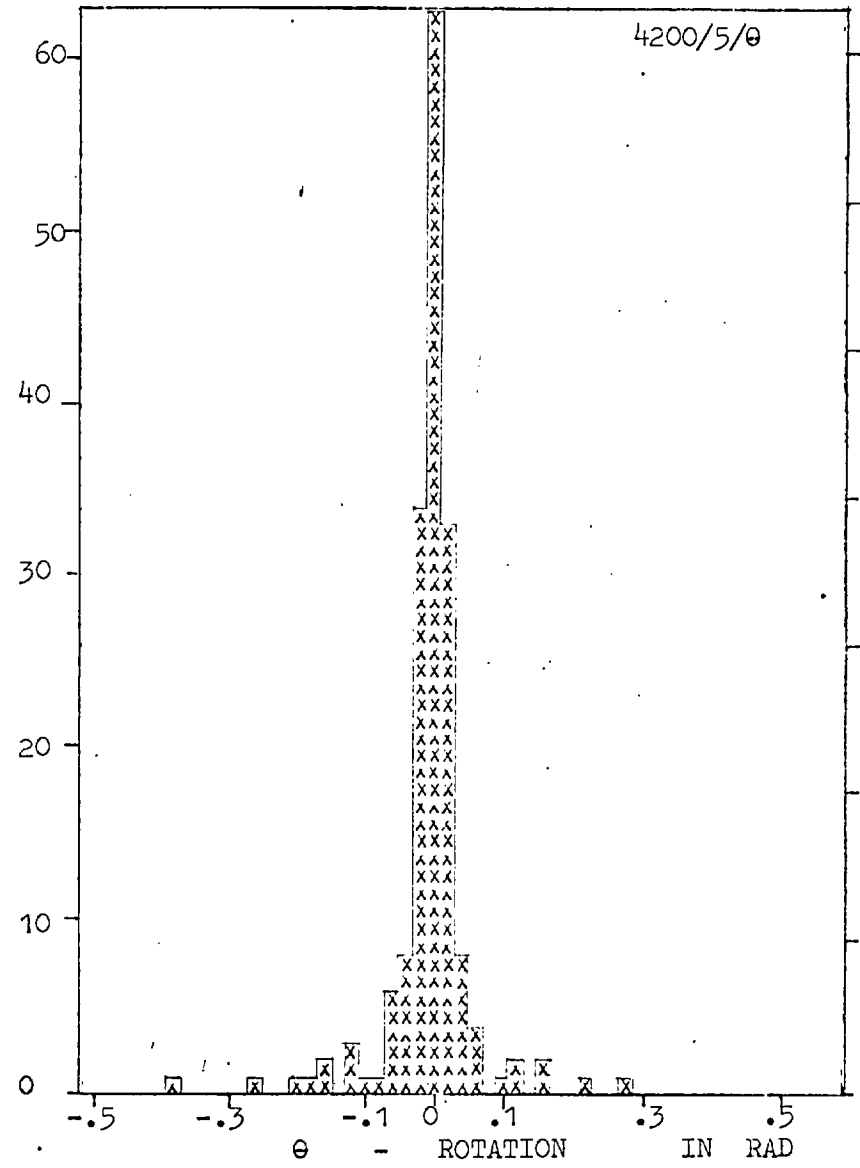
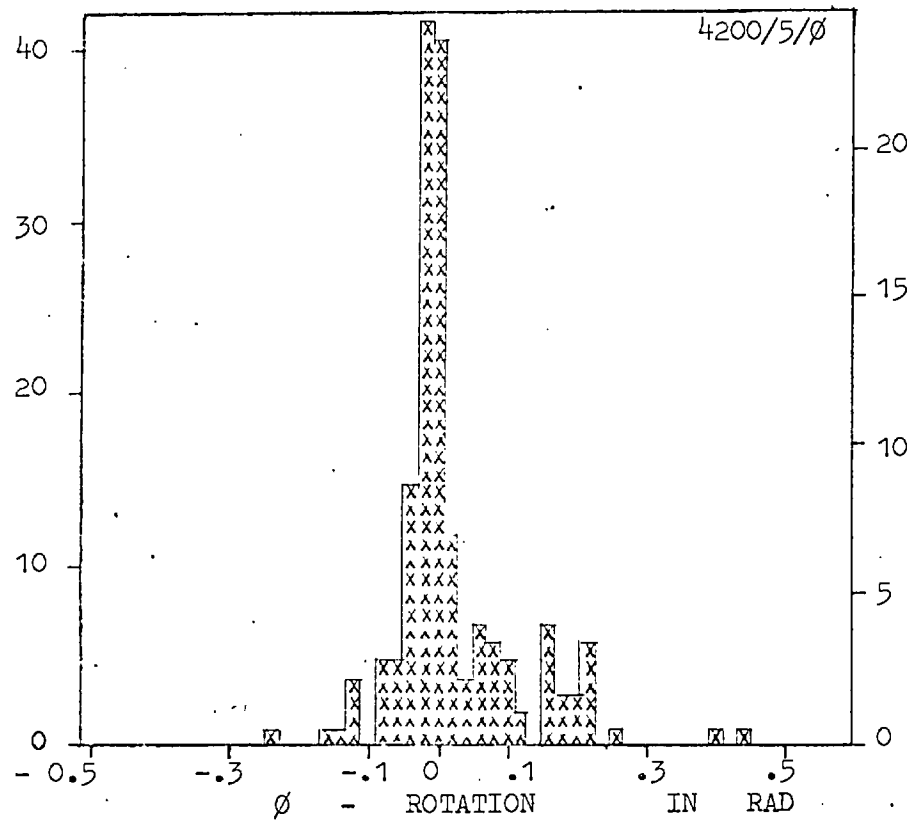


FIG. 7.120

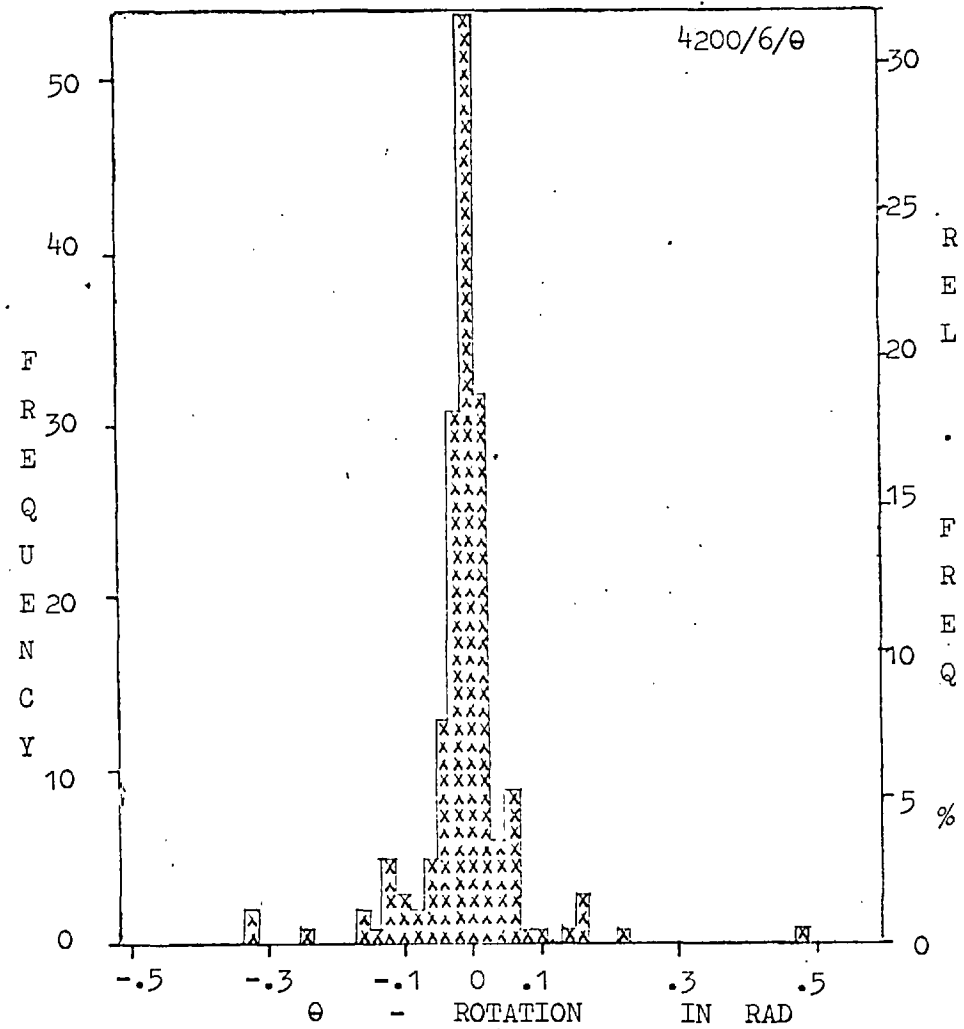
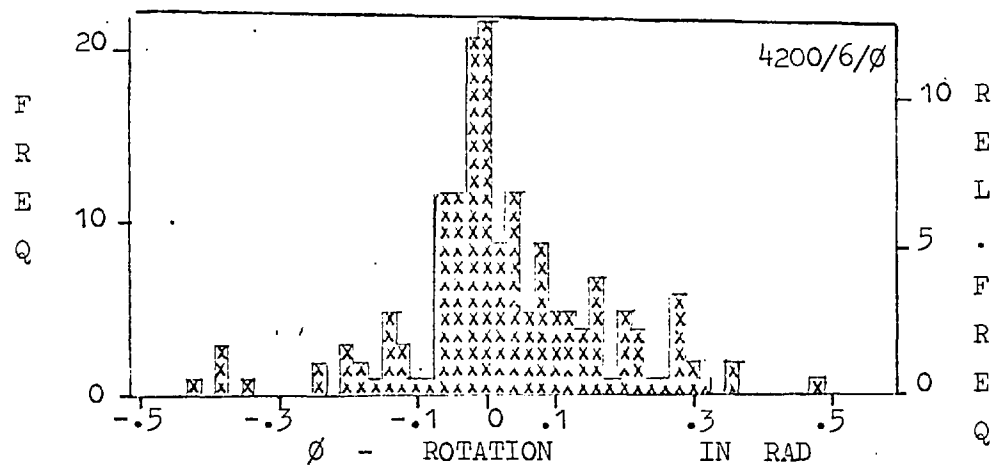


FIG. 7.121

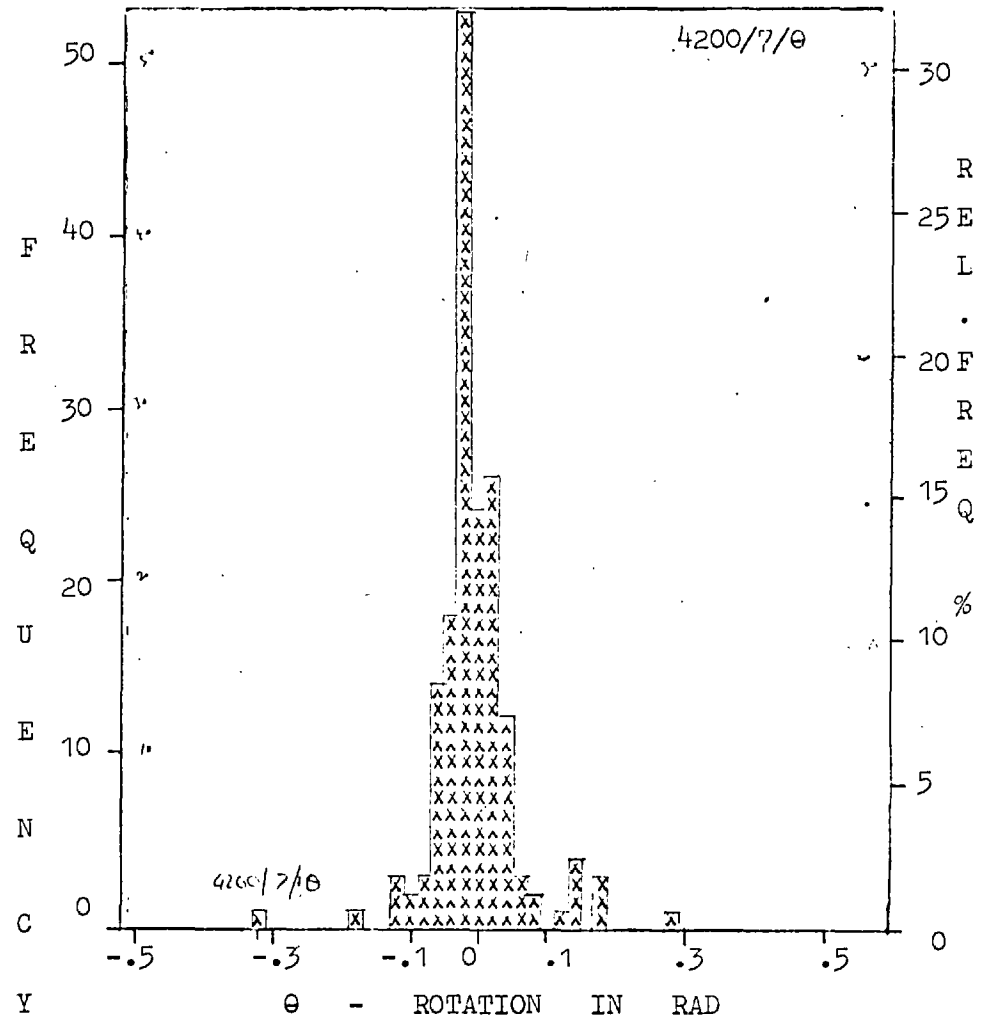
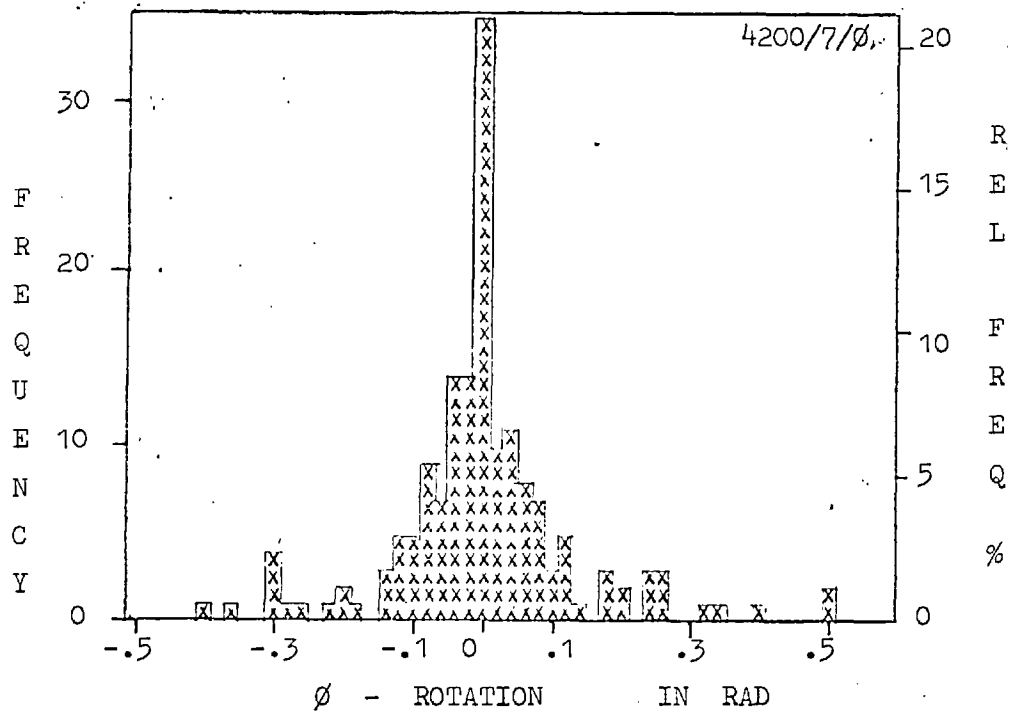
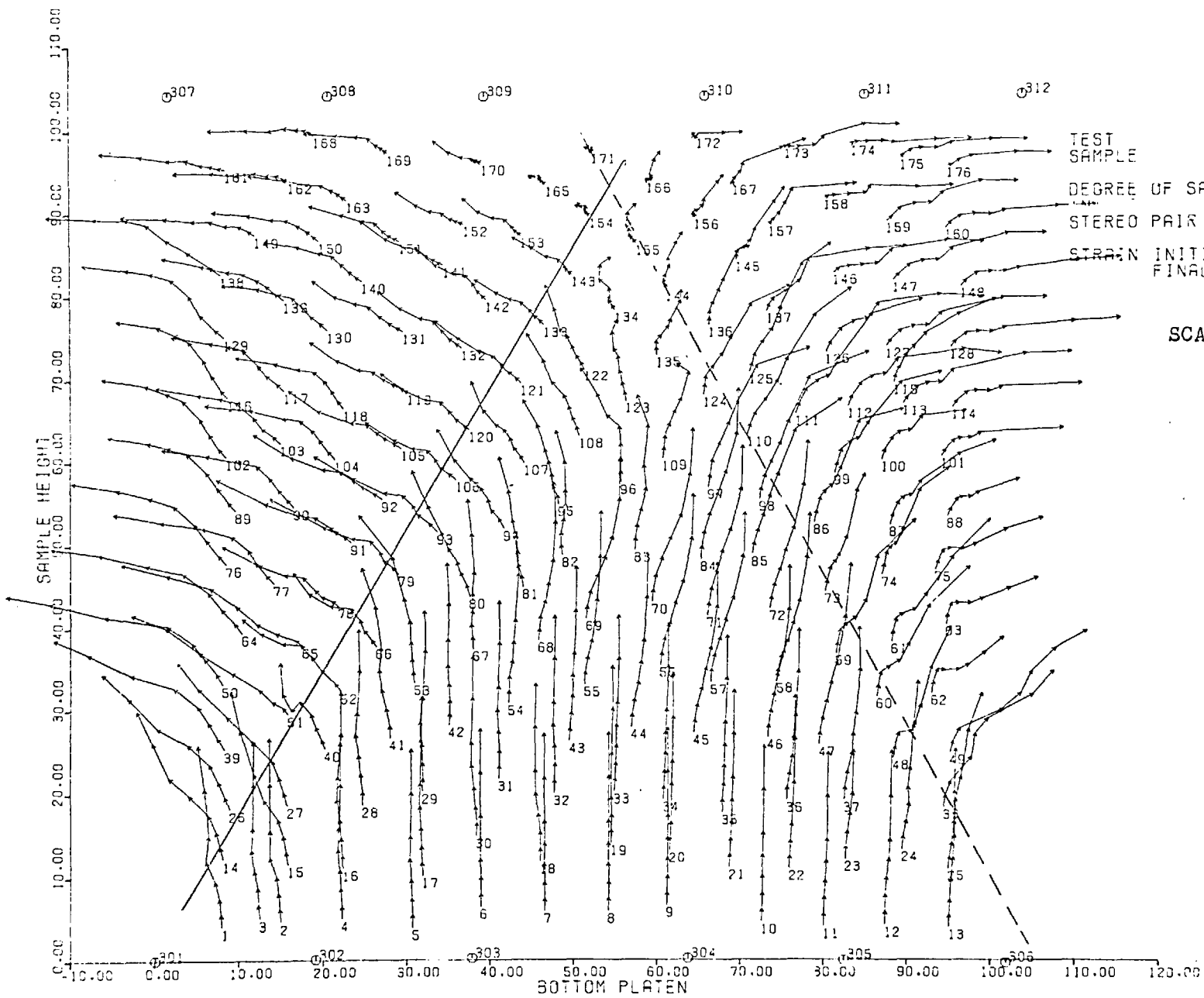


FIG. 7.122



TEST SAMPLE
 DEGREE OF SAT.
 STEREO PAIR NO.
 STRAIN INITIAL
 FINAL

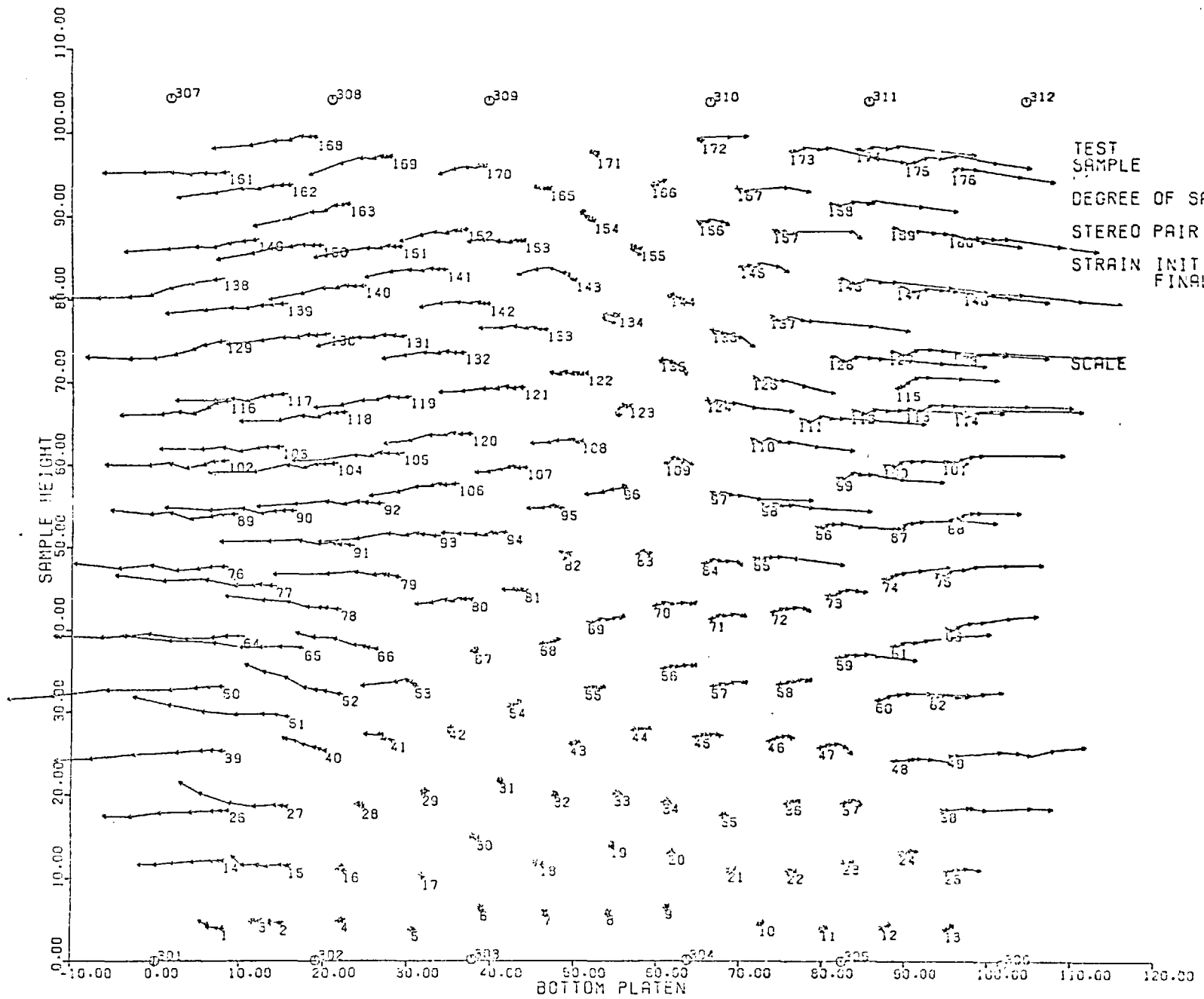
4201
 PLANE STRAIN (DRAINED)
 PTFE CHUNGS

DRY
 FIRST 1
 LAST 8
 0.0
 20.632

SCALE 10mm

FIG 7.123

TRACE OF DISPLACEMENTS OF MARKER CENTRES ON XY PLANE



TEST SAMPLE
 DEGREE OF SAT.
 STEREO PAIR NO.
 STRAIN INITIAL
 FINAL

4201
 PLANE STRAIN (DRAINED)
 PIPE CHUNKS
 DRY
 FIRST 1
 LAST 8
 0.0
 20.832

SCALE

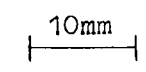
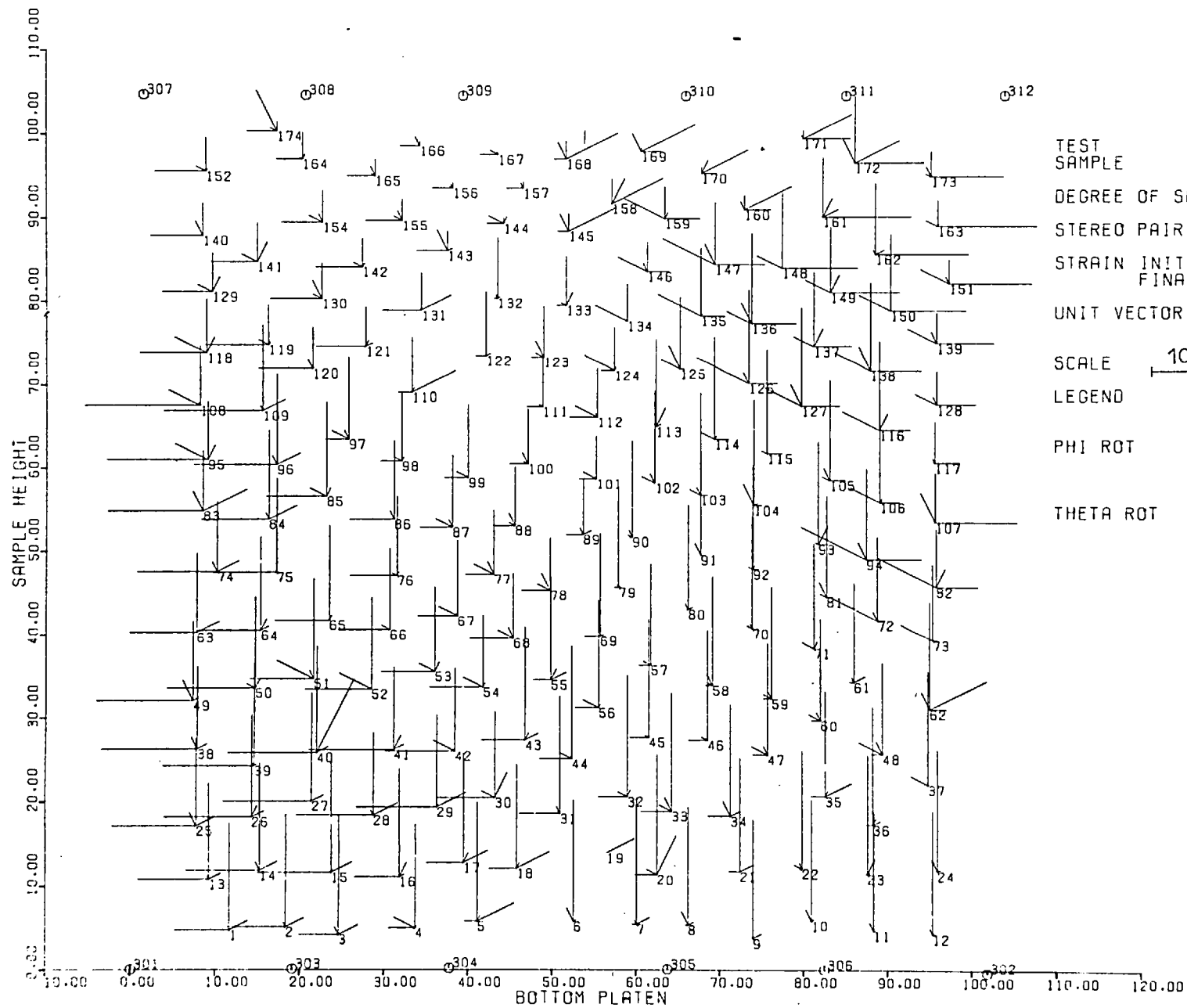


FIG 7.124 TRACE OF DISPLACEMENTS OF MARKER CENTRES ON XZ PLANE



TEST
SAMPLE

DEGREE OF SAT.

STEREO PAIR NO.

STRAIN INITIAL
FINAL

UNIT VECTOR DISP.

SCALE $\overbrace{10\text{mm}}^{\text{ROT.}}$

LEGEND

PHI ROT

THETA ROT

4201/1

PLANE STRAIN (DRAINED)
PTFE CHUNKS

FULLY SAT.

FIRST 1
FINAL 2

0.0
1.782

HOR. X
VER. Y

$\overbrace{1\text{mm}}$
 $\overbrace{.1\text{rad}}$

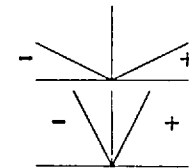
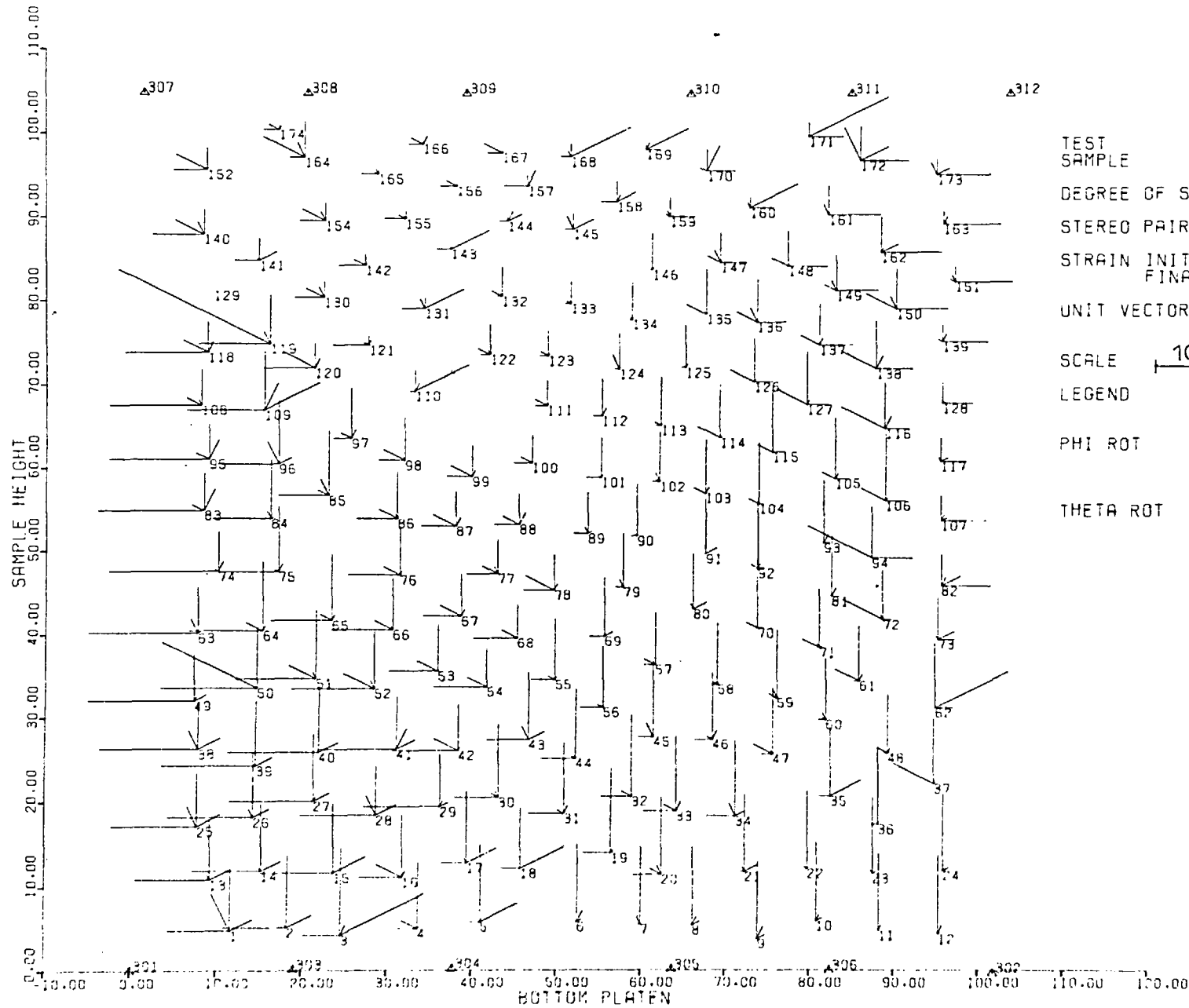


FIG 7.125 DISPLACEMENT - ROTATION FIELD OF MARKERS IN XY PLANE



TEST
SAMPLE

DEGREE OF SAT.

STEREO PAIR NO.

STRAIN INITIAL
FINAL

UNIT VECTOR DISP.

SCALE

LEGEND

PHI ROT

THETA ROT

4201/2

PLANE STRAIN (DRAINED)
PTFE CHUNKS

FULLY SAT.

FIRST 2
FINAL 3

1.782
4.037

HOR. X
VER. Y

2mm
2rad

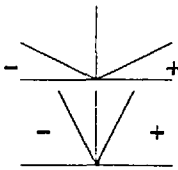
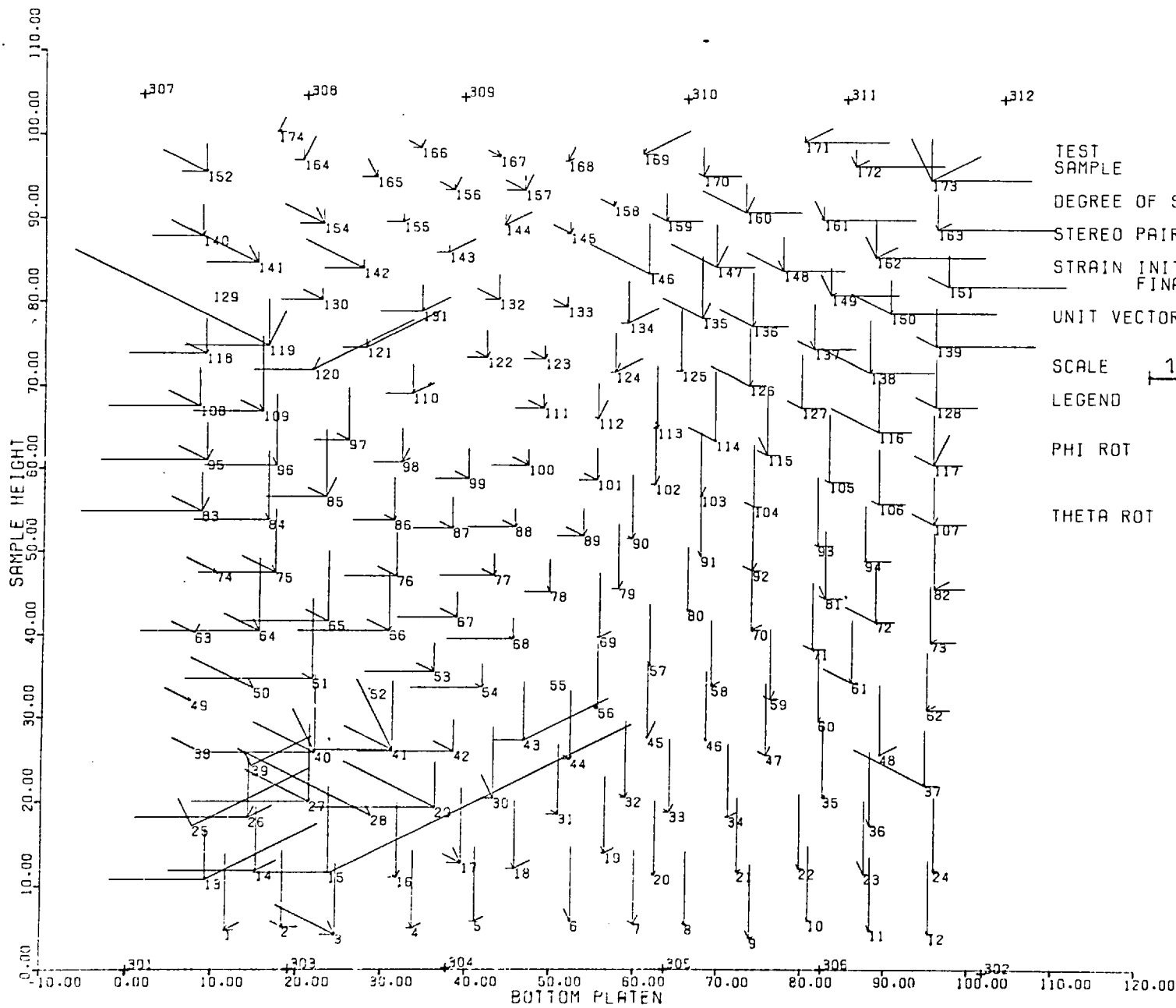


FIG 7.126 DISPLACEMENT - ROTATION FIELD OF MARKERS IN XY PLANE



TEST SAMPLE
 DEGREE OF SAT.
 STEREO PAIR NO.
 STRAIN INITIAL FINAL
 UNIT VECTOR DISP.
 SCALE 10mm
 LEGEND
 PHI ROT
 THETA ROT

4201/3
 PLANE STRAIN (DRAINED)
 PTFE CHUNKS
 FULLY SAT.
 FIRST 3
 FINAL 4
 4.037
 6.263

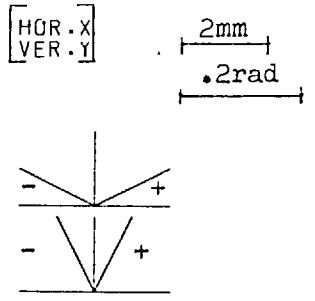


FIG 7.127 DISPLACEMENT - ROTATION FIELD OF MARKERS IN XY PLANE

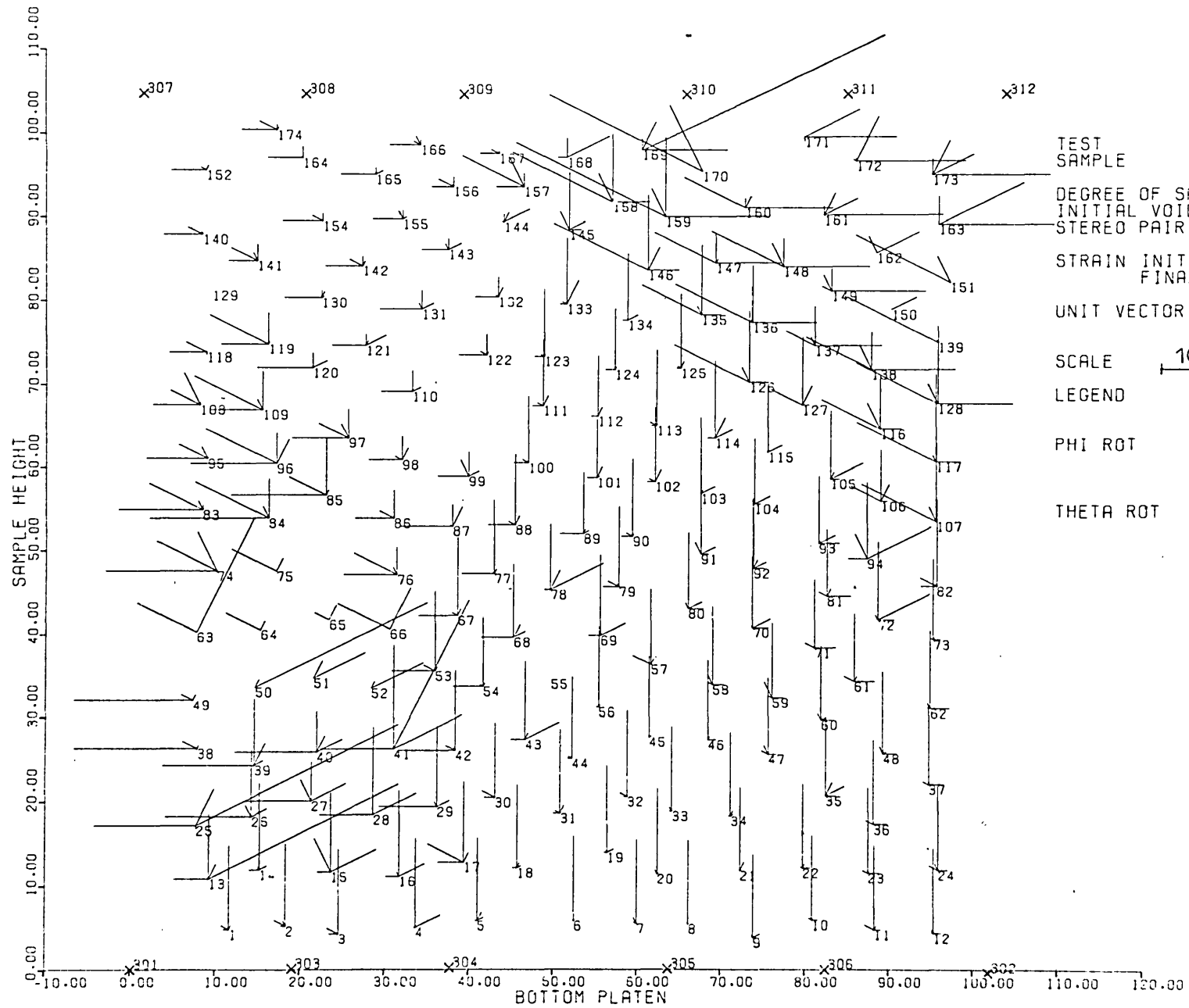
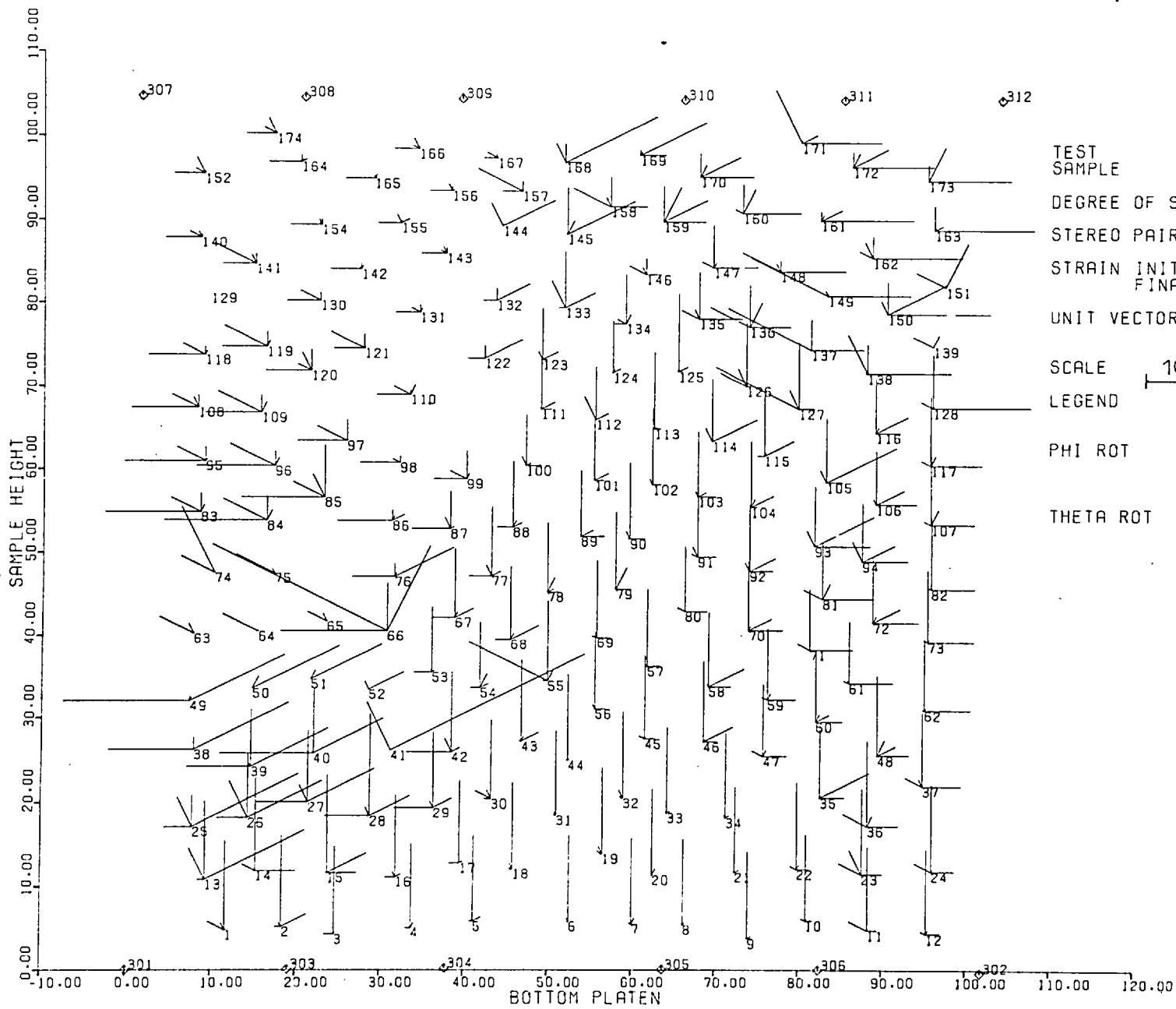


FIG 7.128 DISPLACEMENT - ROTATION FIELD OF MARKERS IN XY PLANE



TEST SAMPLE
 DEGREE OF SAT.
 STEREO PAIR NO.
 STRAIN INITIAL
 STRAIN FINAL
 UNIT VECTOR DISP.
 ROT.
 SCALE 10mm
 LEGEND
 PHI ROT
 THETA ROT

4201/5
 PLANE STRAIN (DRAINED)
 PTFE CHUNKS
 FULLY SAT.
 FIRST 5
 FINAL 6
 8.747
 11.328

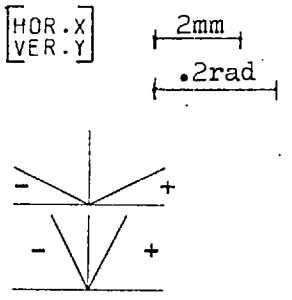
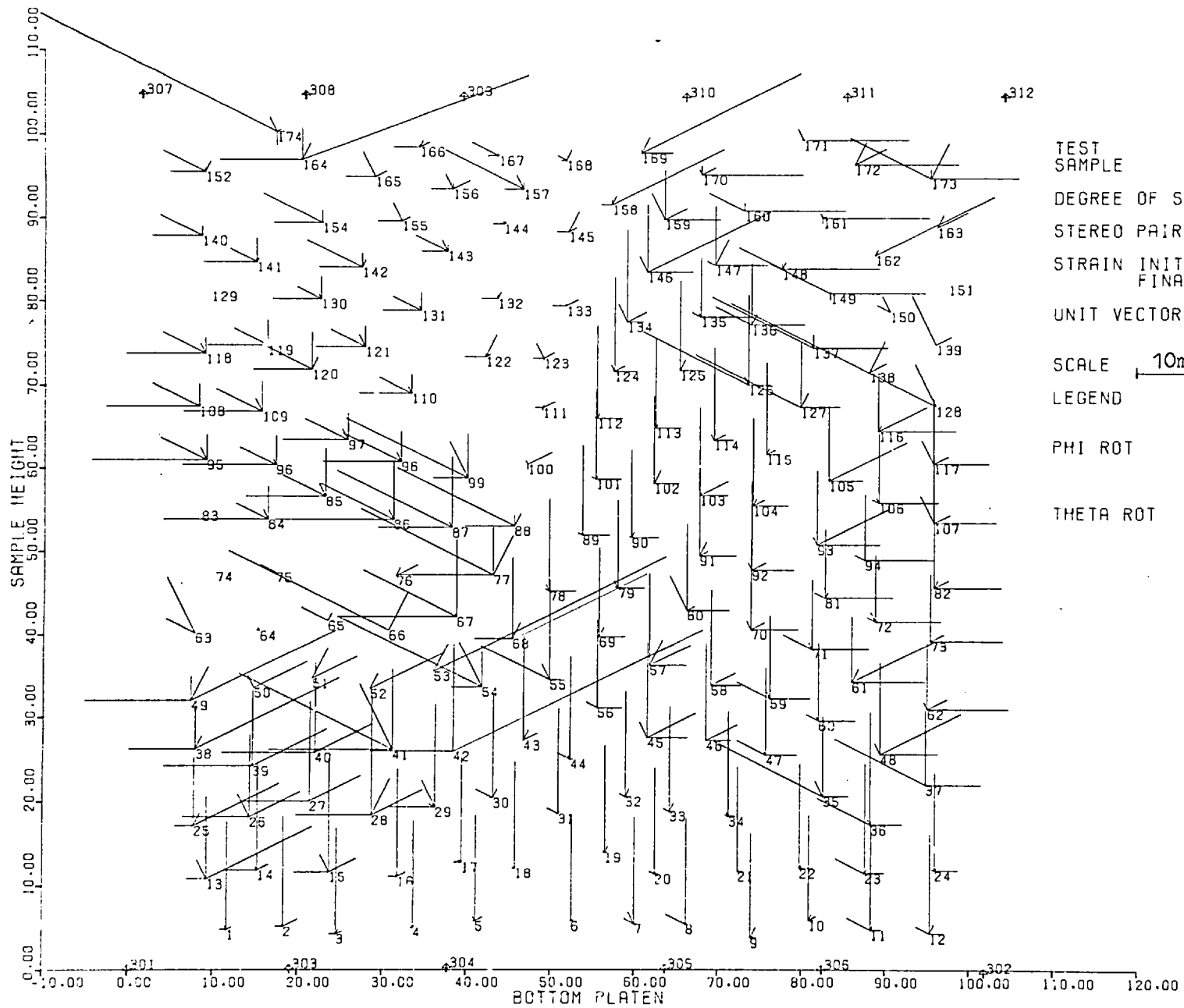


FIG 7.129 DISPLACEMENT - ROTATION FIELD OF MARKERS IN XY PLANE



TEST SAMPLE

DEGREE OF SAT.

STEREO PAIR NO.

STRAIN INITIAL
FINAL

UNIT VECTOR DISP.

SCALE 10mm ROT.

LEGEND

PHI ROT

THETA ROT

4201/6

PLANE STRAIN (DRAINED)

FULLY SAT.

FIRST 6
FINAL 7

11.328
16.019

HOR. X
VER. Y

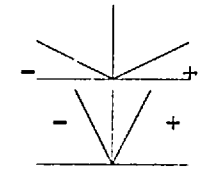
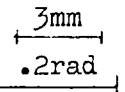
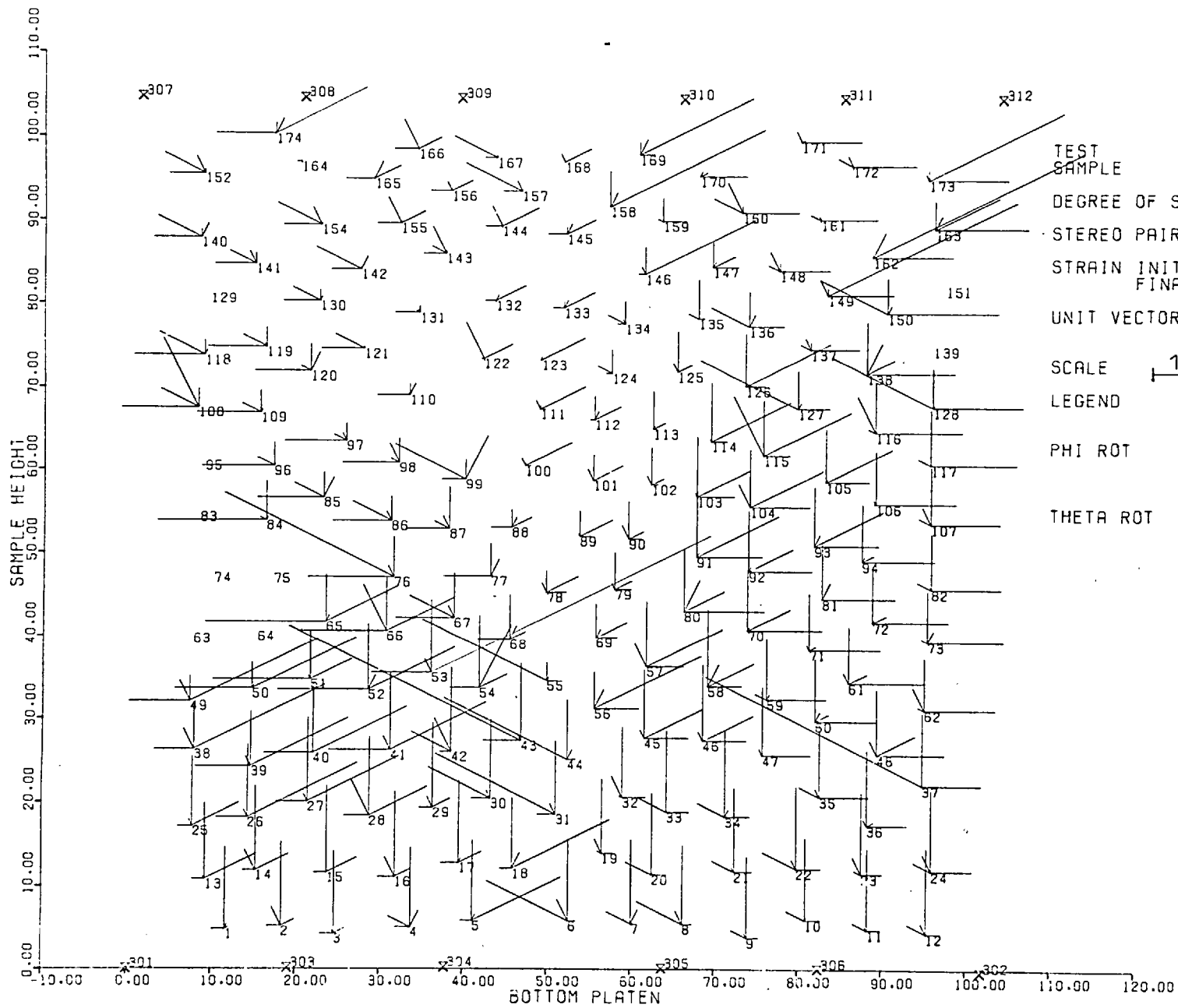


FIG 7.130 DISPLACEMENT - ROTATION FIELD OF MARKERS IN XY PLANE



TEST SAMPLE
 DEGREE OF SAT.
 STEREO PAIR NO.
 STRAIN INITIAL
 FINAL
 UNIT VECTOR DISP.
 SCALE 10mm
 LEGEND
 PHI ROT
 THETA ROT

4201/7
 PLANE STRAIN (DRAINED)
 PTFE CHUNKS
 FULLY SAT.
 FIRST 7
 FINAL 8
 16.019
 20.964

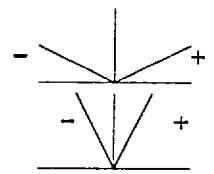
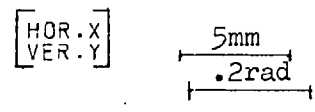


FIG 7.131 DISPLACEMENT - ROTATION FIELD OF MARKERS IN XY PLANE

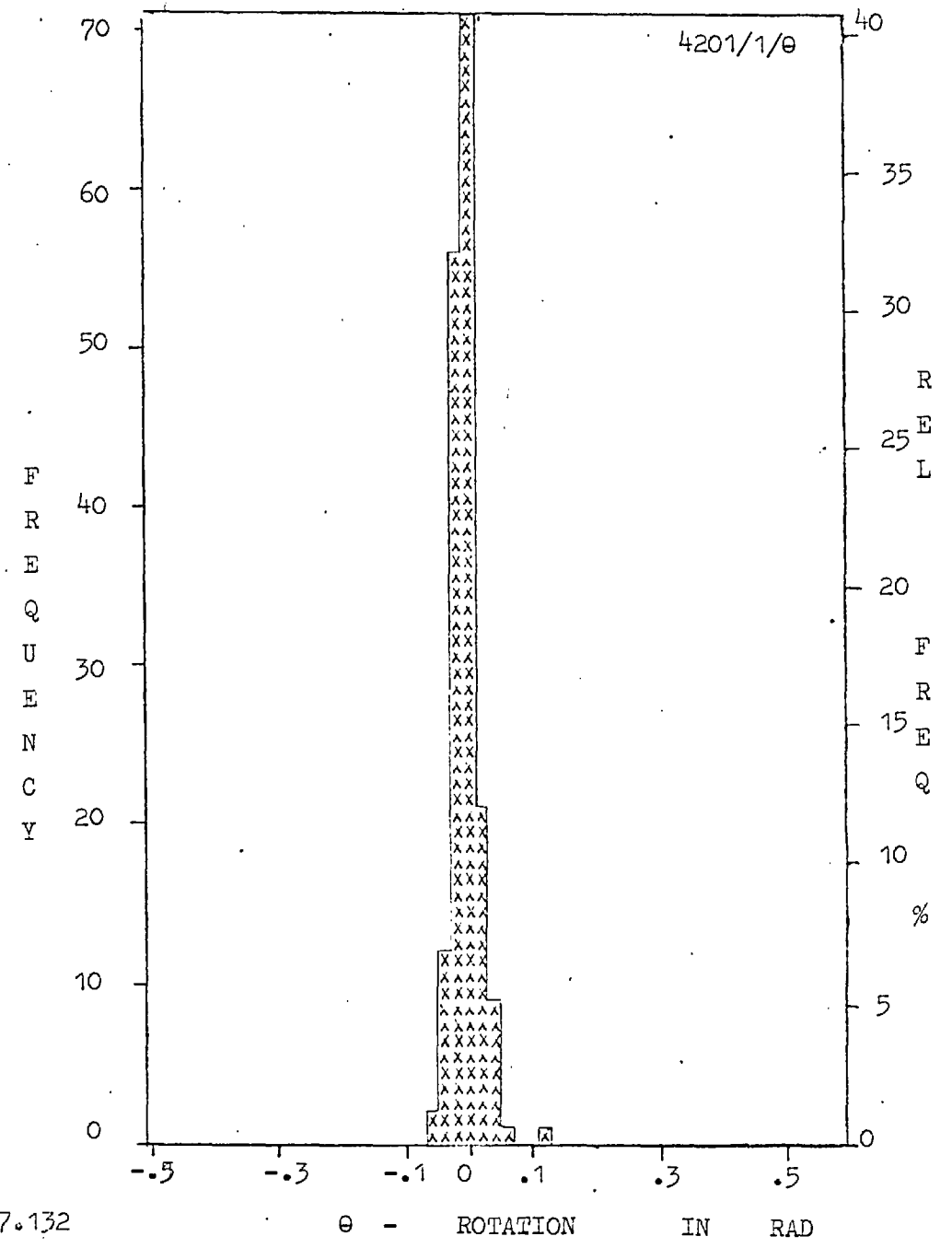
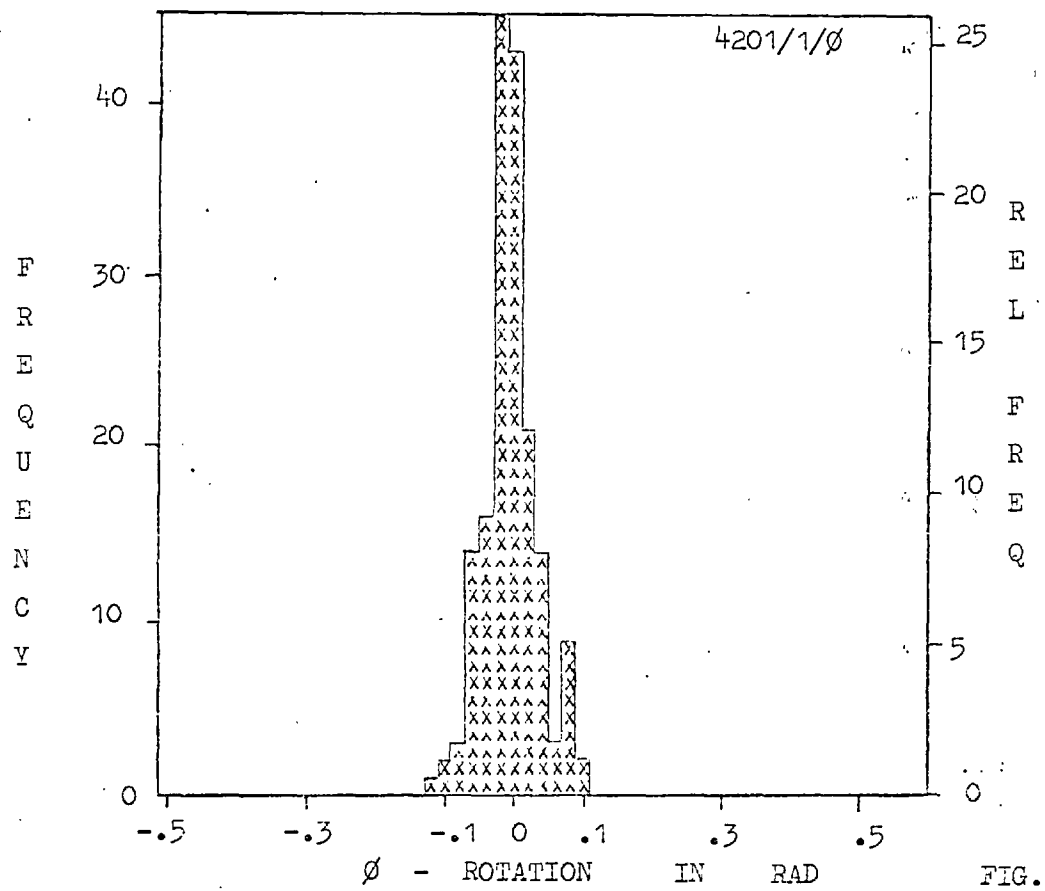


FIG. 7.132

4201/2/φ

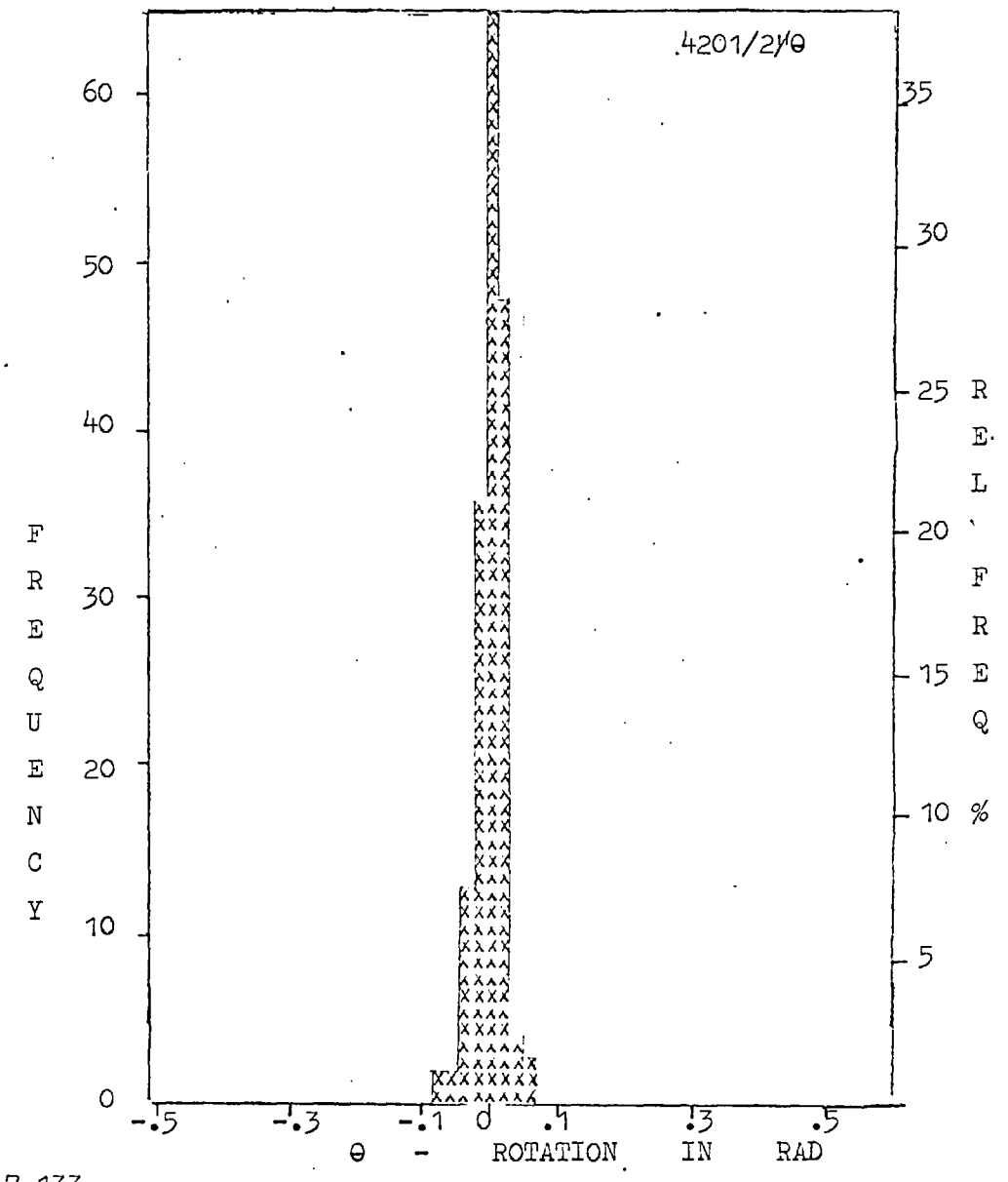
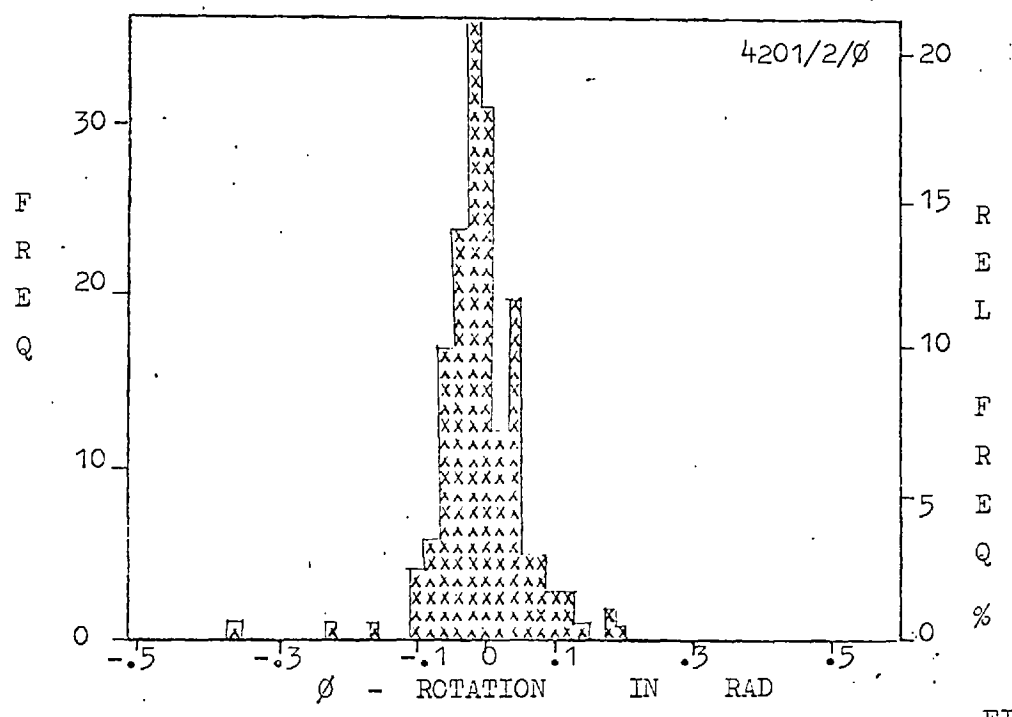


FIG. 7.133

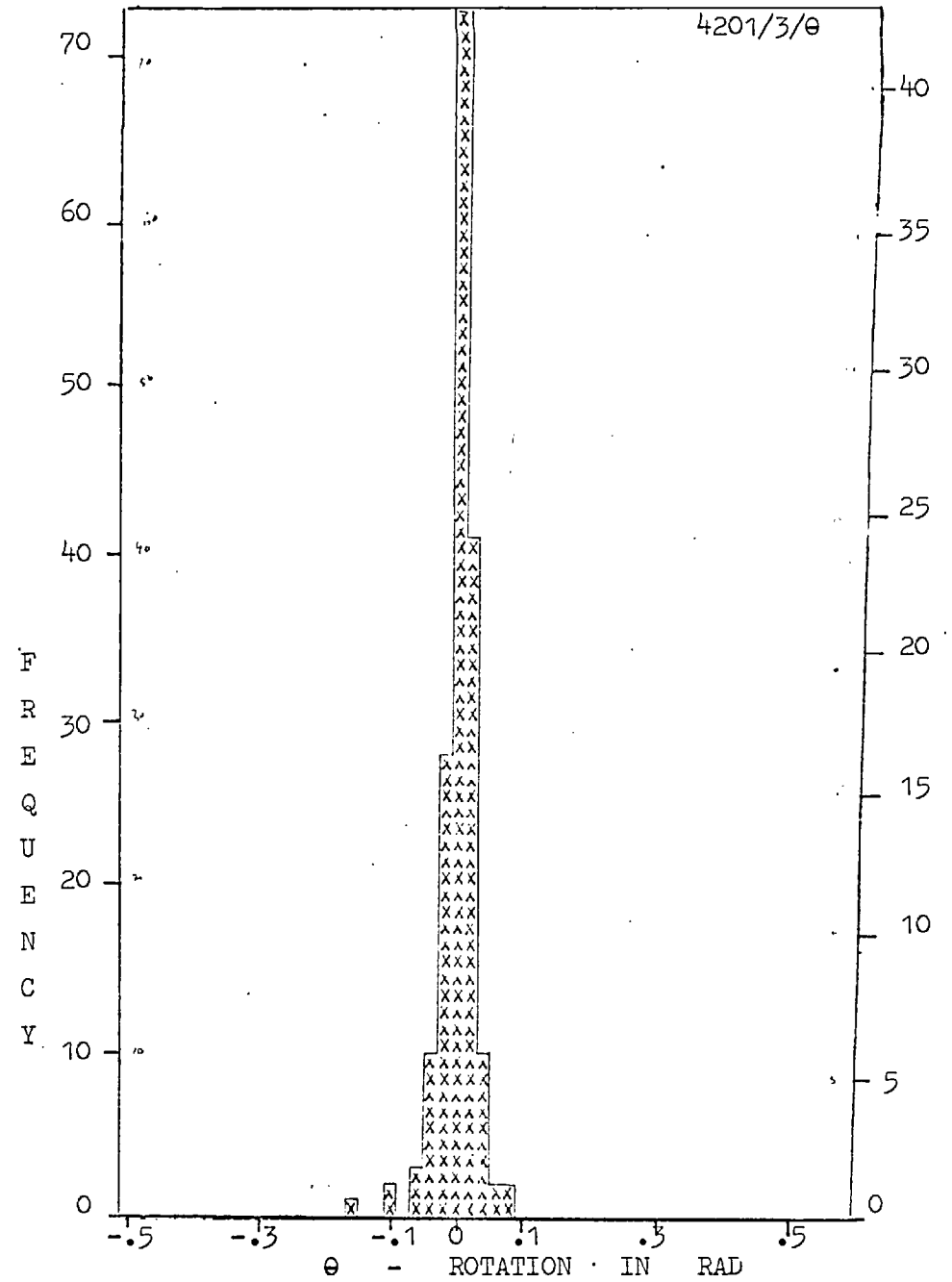
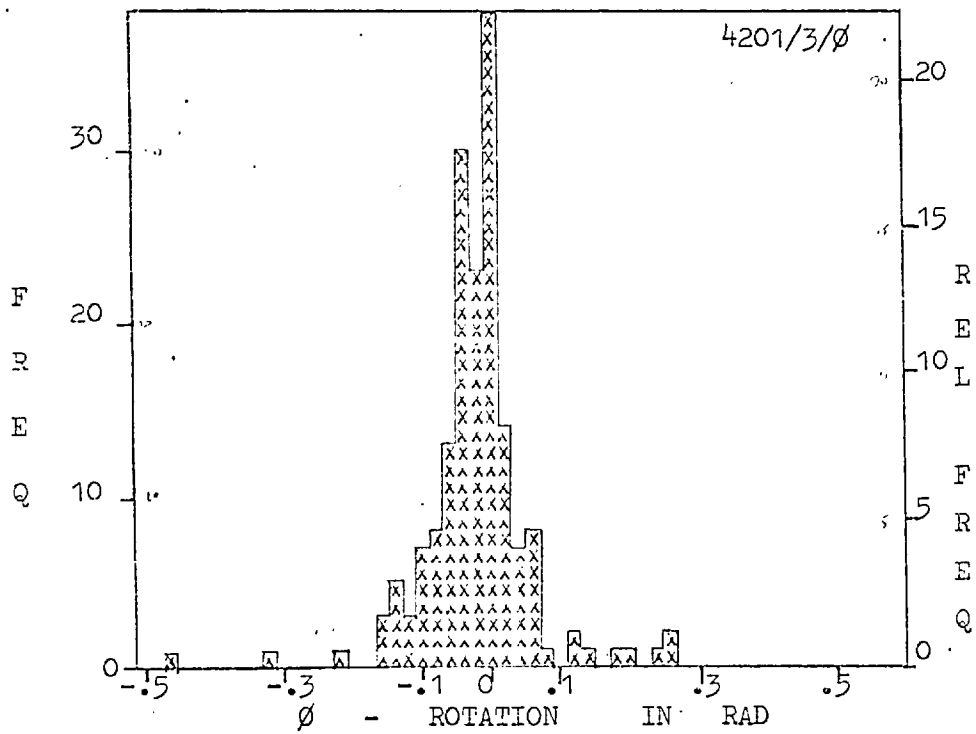


FIG. 7.134

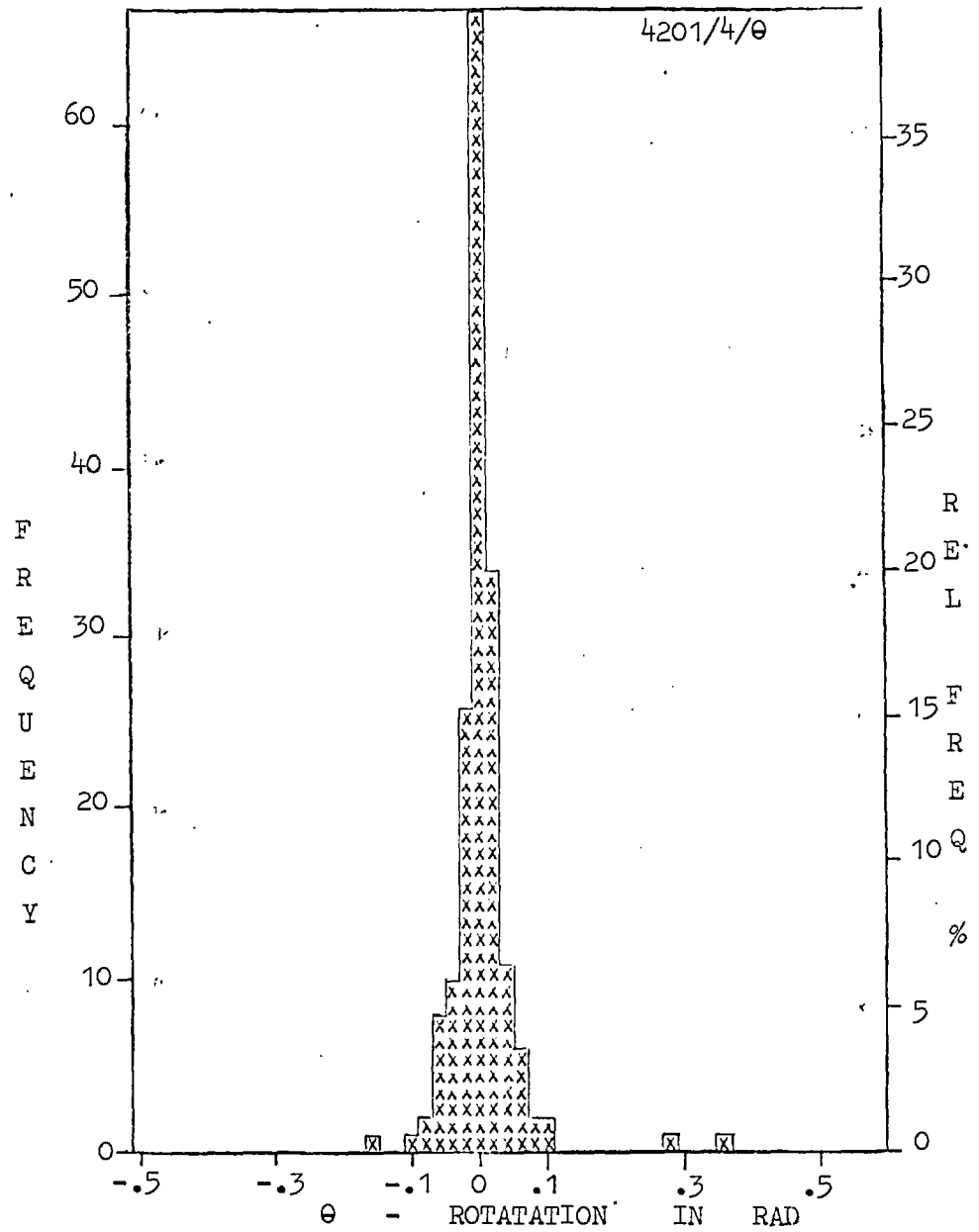
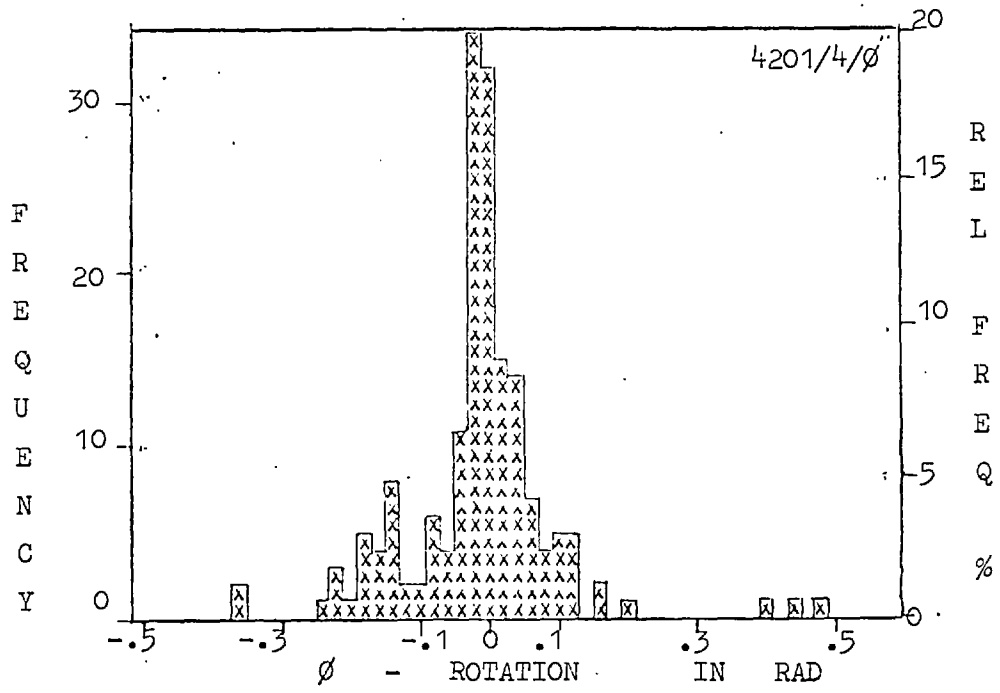


FIG. 7.135

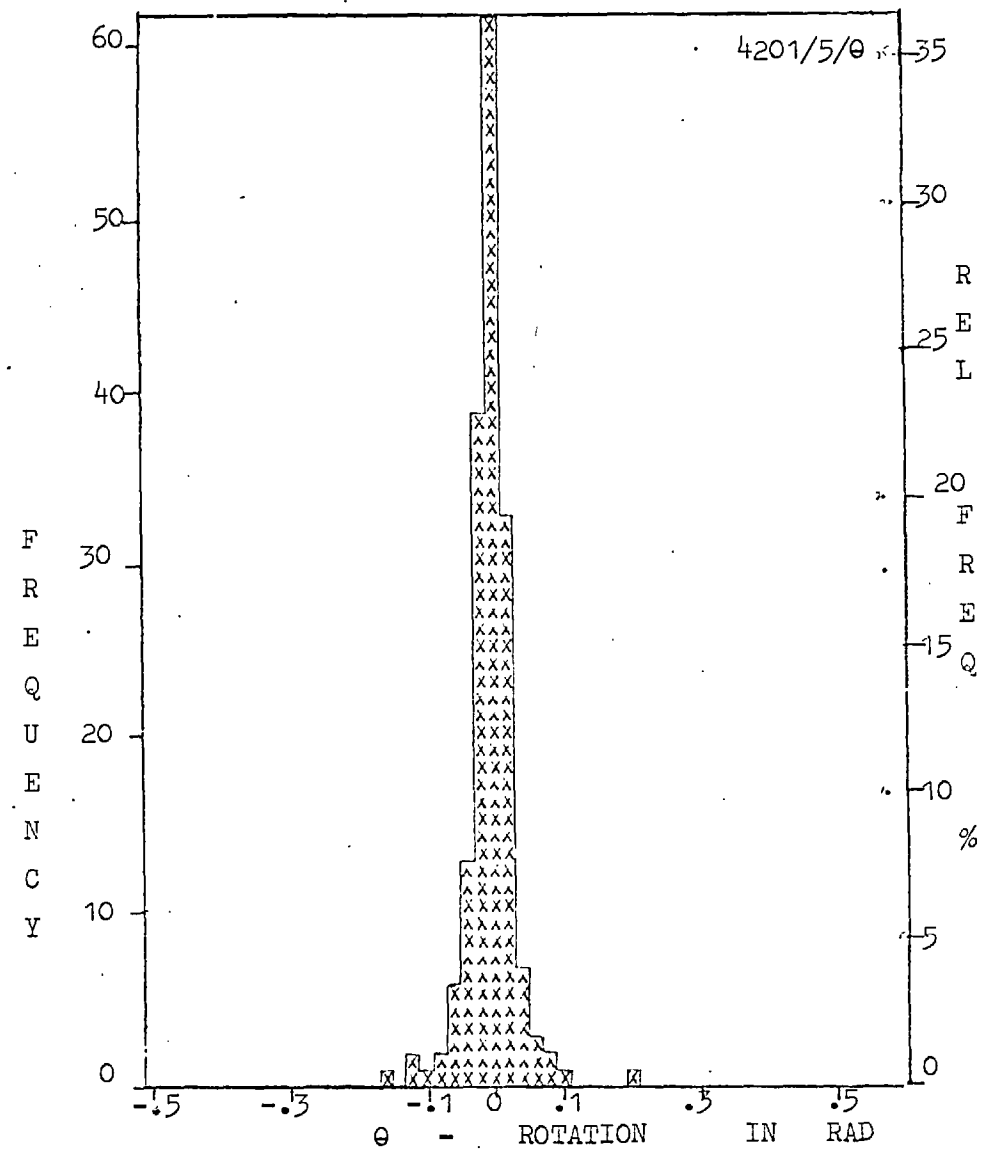
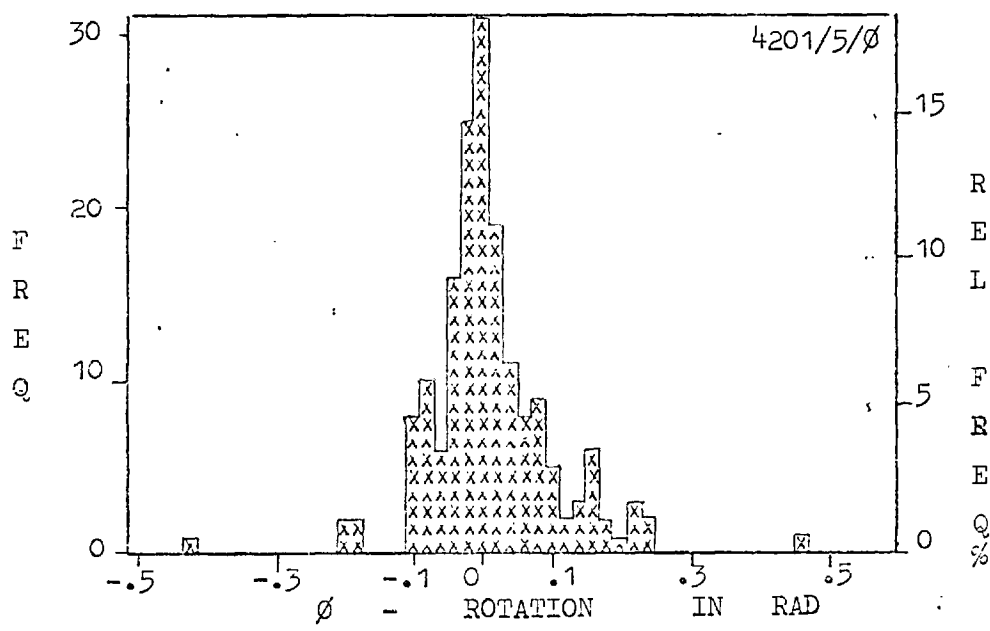


FIG. 7.136

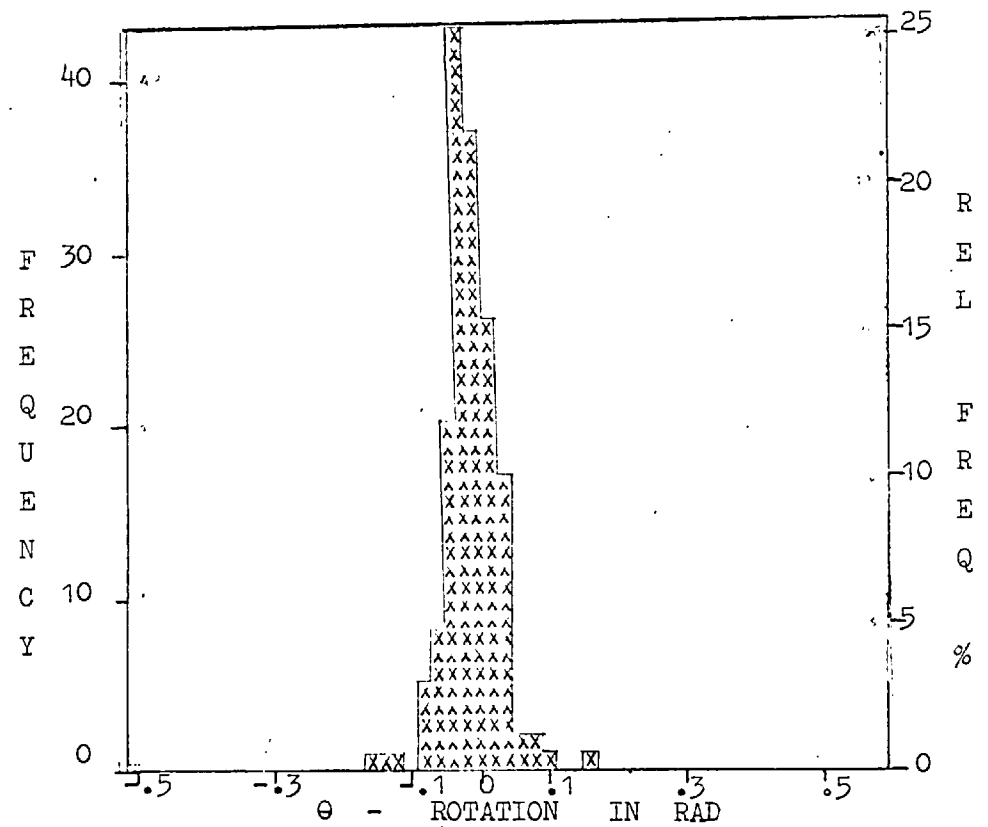
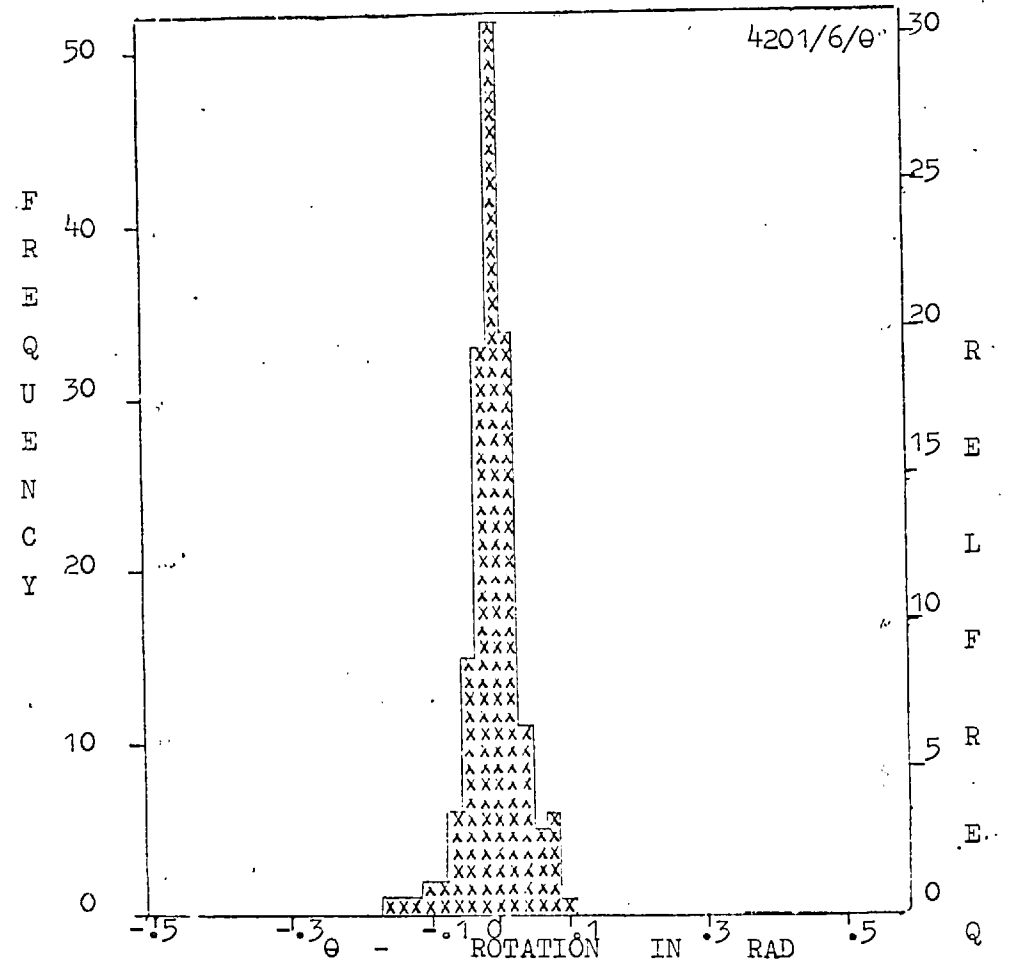
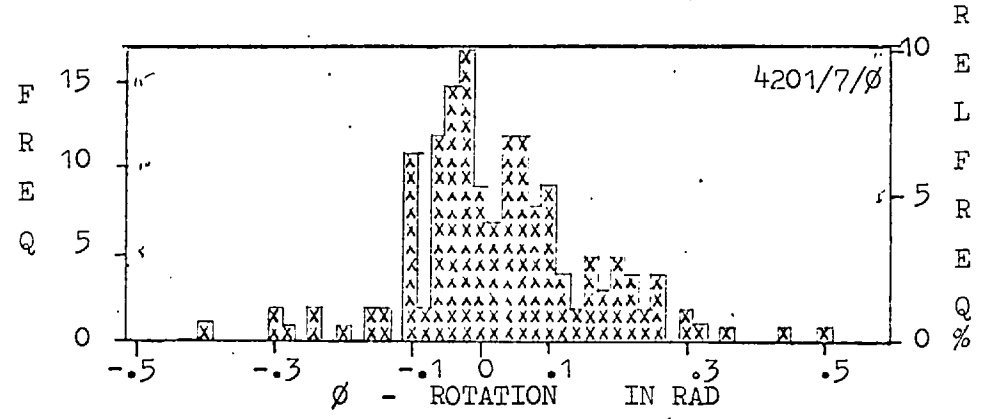
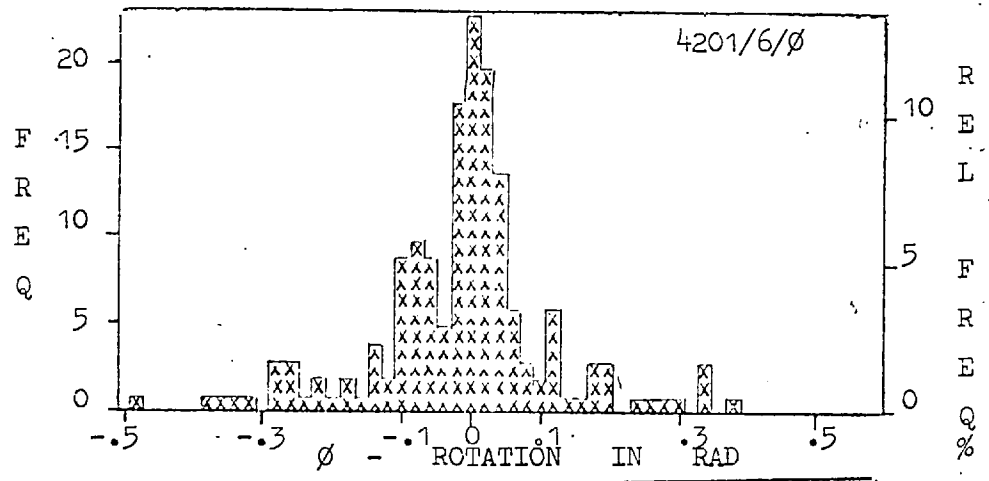
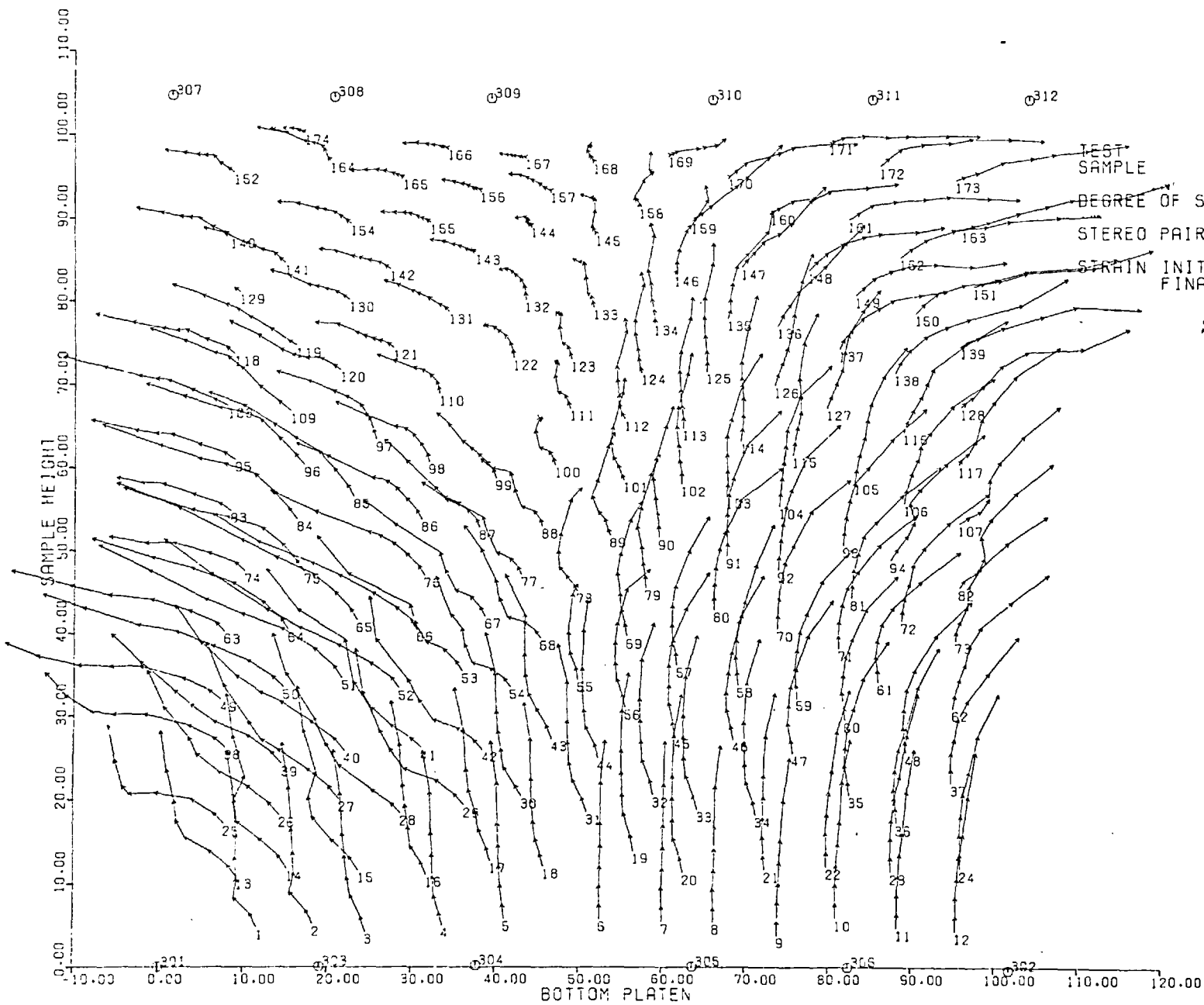


FIG. 7.137

FIG. 7.138

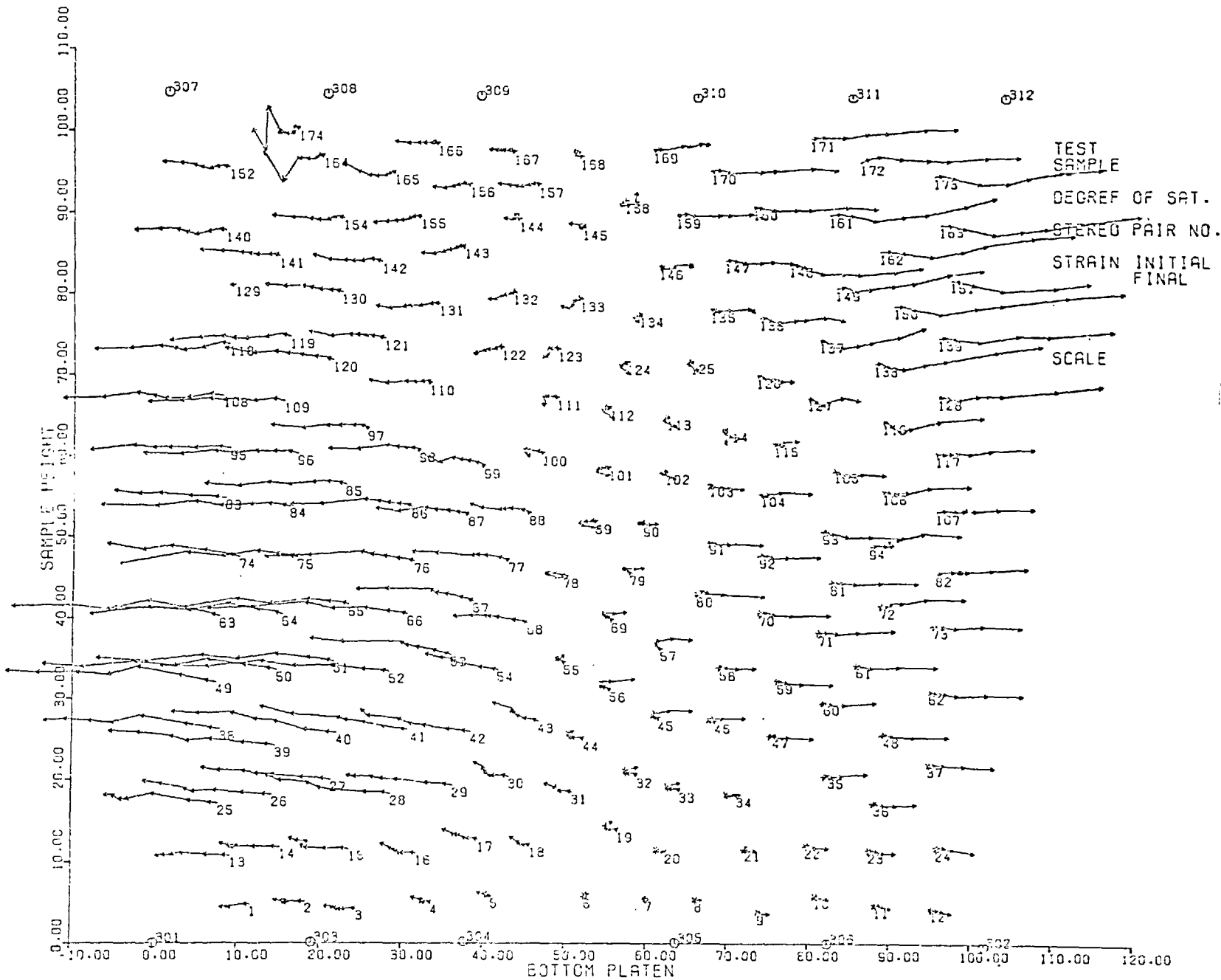


TEST SAMPLE
 DEGREE OF SAT.
 STEREO PAIR NO.
 STRAIN INITIAL
 FINAL

4201
 PLANE STRAIN (DRAINED)
 PIPE CHUNKS
 FULLY SAT.
 FIRST 1
 LAST 8
 0.0
 20.964

SCALE 10mm

FIG 7.139 TRACE OF DISPLACEMENTS OF MARKER CENTRES ON XY PLANE

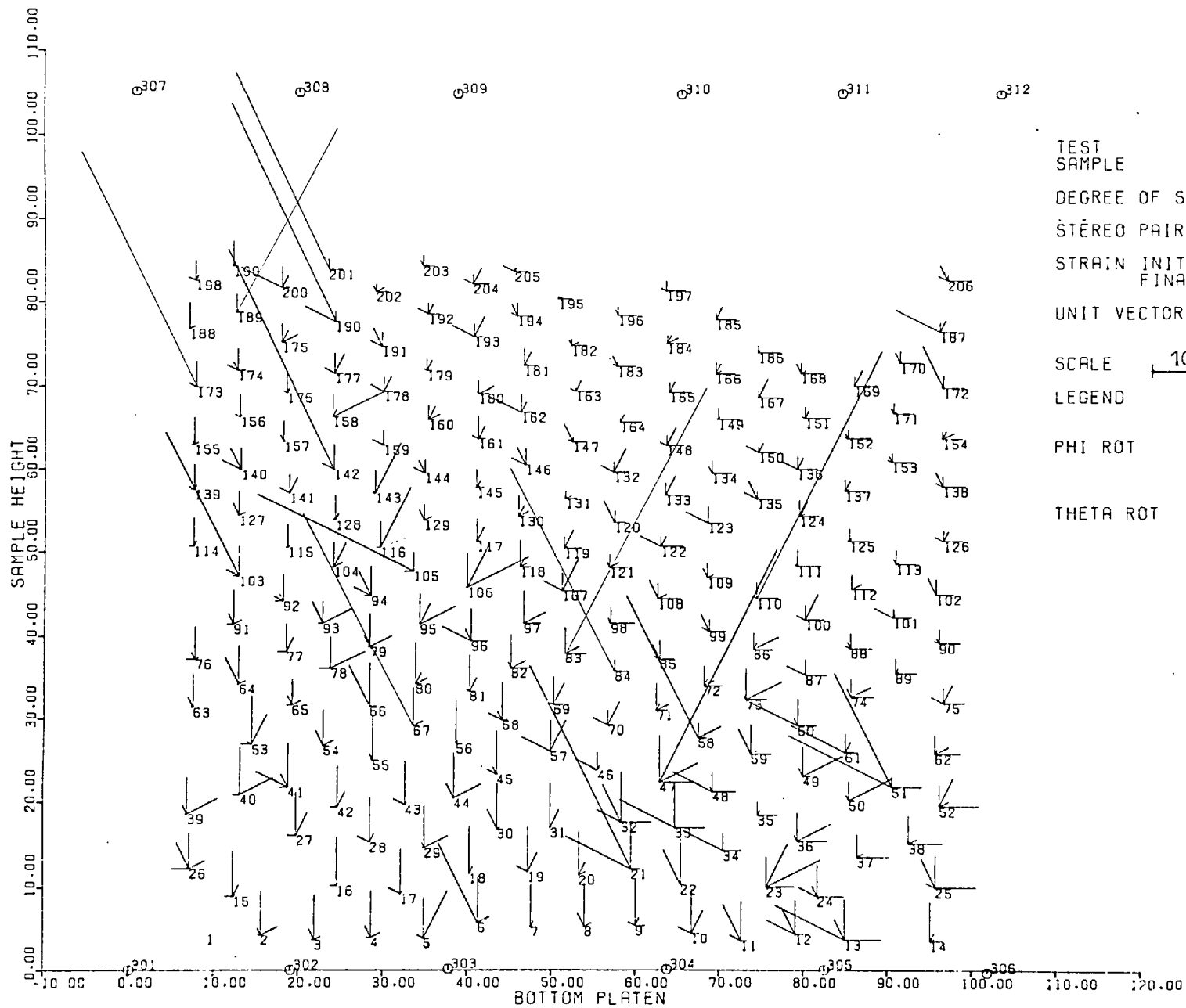


4201
 PLANE STRAIN (DRAINED)
 PTFE CHUNKS
 FULLY SAT.
 FIRST 1
 LAST 8
 0.0
 20.964

10mm

FIG 7.140

TRACE OF DISPLACEMENTS OF MARKER CENTRES ON XZ PLANE



TEST SAMPLE

DEGREE OF SAT.

STEREO PAIR NO.

STRAIN INITIAL
FINAL

UNIT VECTOR DISP.

SCALE $\overbrace{\hspace{1cm}}^{\text{ROT.}}$ 10mm

LEGEND

PHI ROT

THETA ROT

5150/1

PLANE STRAIN (DRAINED)
POLYPROPYLENE BALLS

DRY

FIRST 1
FINAL 2
O.C.
0.631

HOR. X
VER. Y

1mm

1rad

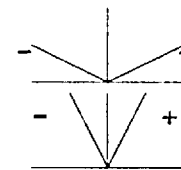
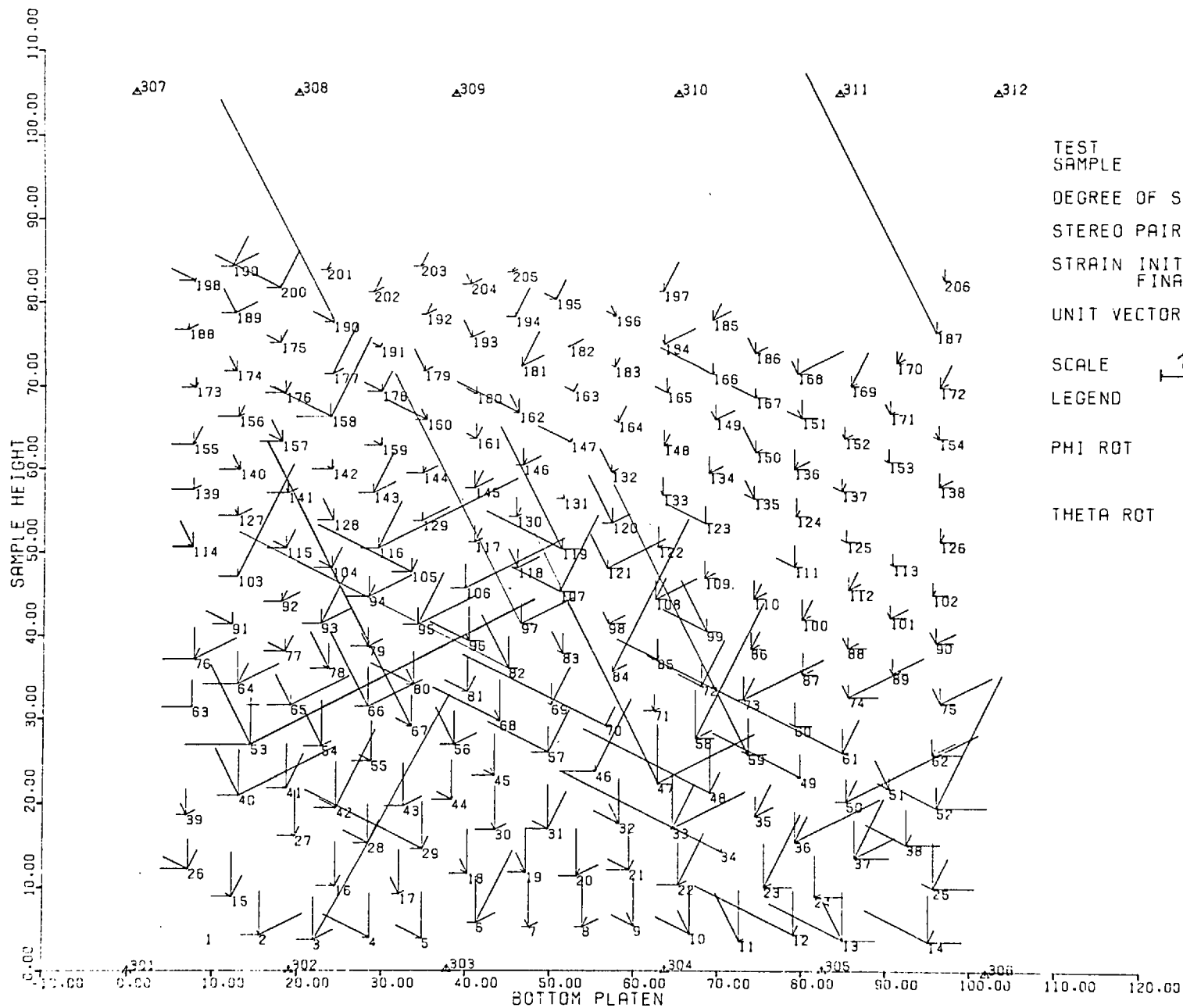


FIG 7.141 DISPLACEMENT - ROTATION FIELD OF MARKERS IN XY PLANE



TEST
SAMPLE

DEGREE OF SAT.

STEREO PAIR NO.

STRAIN INITIAL
FINAL

UNIT VECTOR DISP.

SCALE $\overbrace{10\text{mm}}^{\text{ROT.}}$

LEGEND

PHI ROT

THETA ROT

5150/2

PLANE STRAIN (DRAINED):
POLYPROPYLENE SPHERES

DRY

FIRST 2

FINAL 3

0.631

2.054

$\begin{bmatrix} \text{HOR. X} \\ \text{VER. Y} \end{bmatrix}$

$\overbrace{2\text{mm}}$
 $\overbrace{.2\text{rad}}$

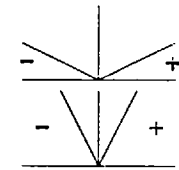
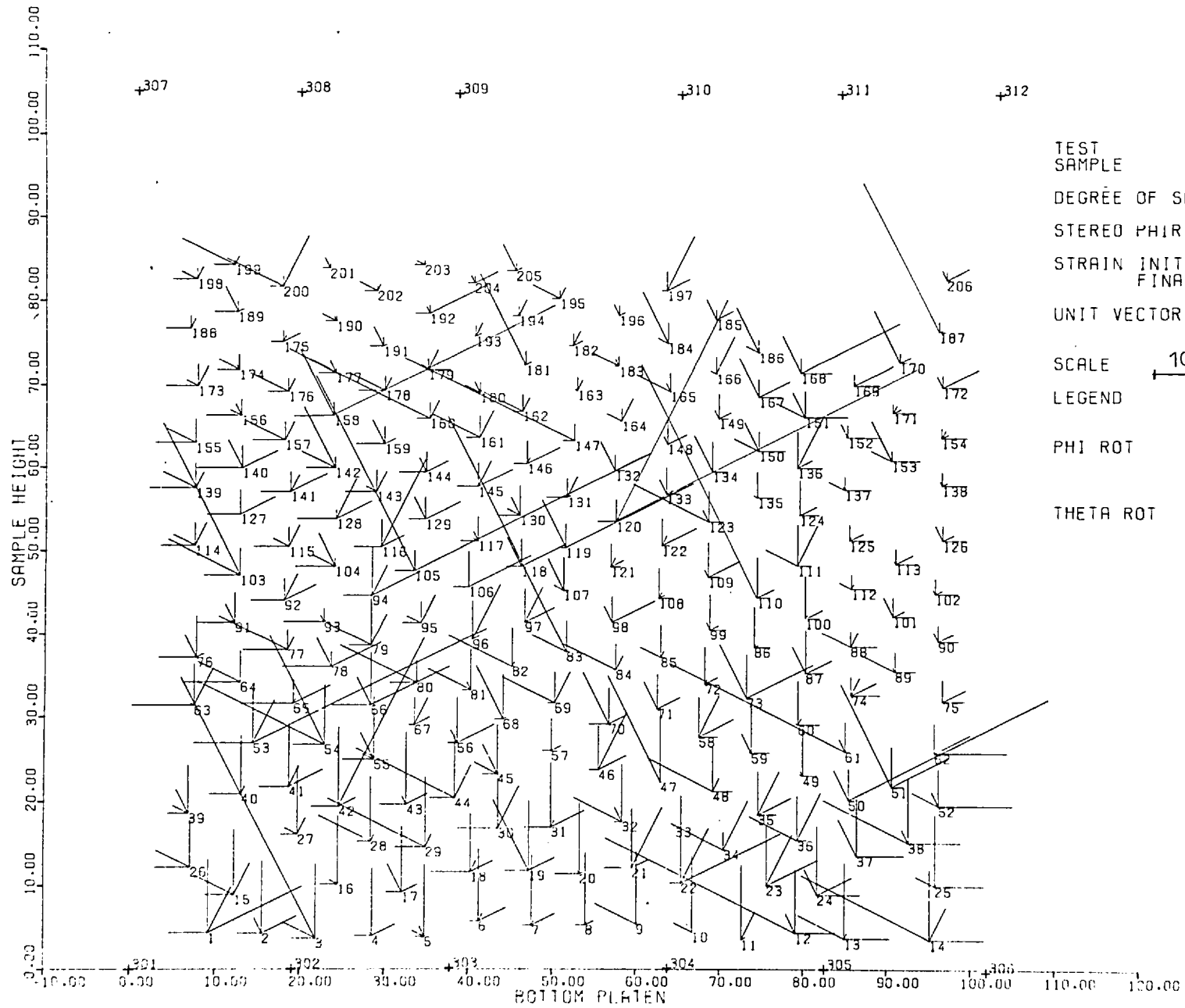


FIG 7.142 DISPLACEMENT - ROTATION FIELD OF MARKERS IN XY PLANE.



TEST SAMPLE 5150/3
 PLANE STRAIN (DRAINED)
 POLYPROPYLENE SPHERES

DEGREE OF SAT. DRY

STEREO PAIR NO. FIRST 3
 FINAL 4

STRAIN INITIAL 2.054
 FINAL 4.260

UNIT VECTOR DISP.

HOR. X
VER. Y

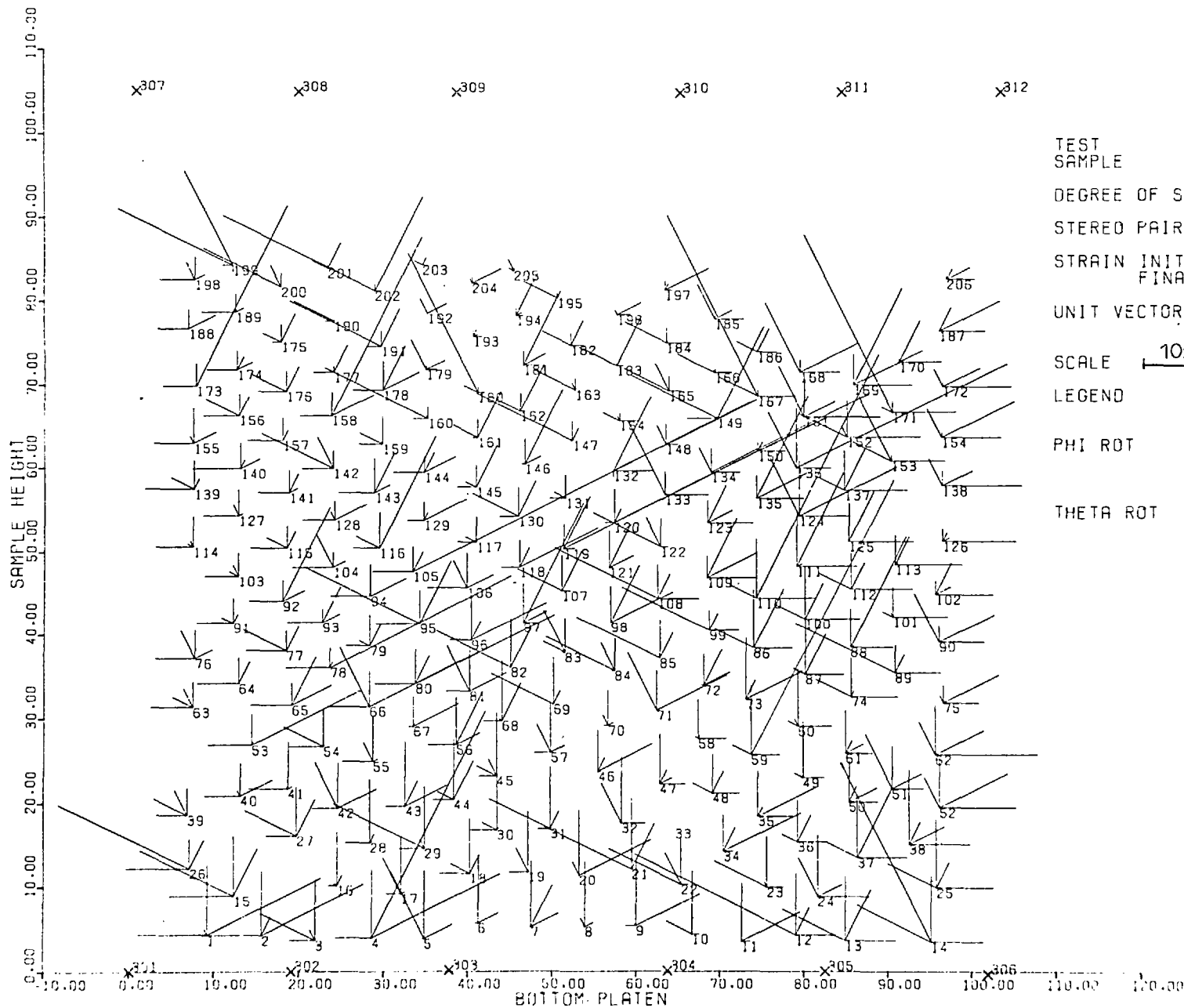
SCALE 10mm $\overline{\text{ROT.}}$ 2mm $\overline{.2\text{rad}}$

LEGEND

PHI ROT

THETA ROT

FIG 7.143 DISPLACEMENT - ROTATION FIELD OF MARKERS IN XY PLANE



5150/4
 TEST SAMPLE PLANE STRAIN (DRAINED)
 POLYPROPYLENE SPHERES
 DEGREE OF SAT. DRY
 STEREO PAIR NO. FIRST 4
 FINAL 5
 STRAIN INITIAL 4.260
 FINAL 6.181
 UNIT VECTOR DISP. [HOR.X] 2mm
 [VER.Y] .2rad
 SCALE 10mm ROT.
 LEGEND
 PHI ROT
 THETA ROT

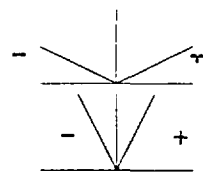
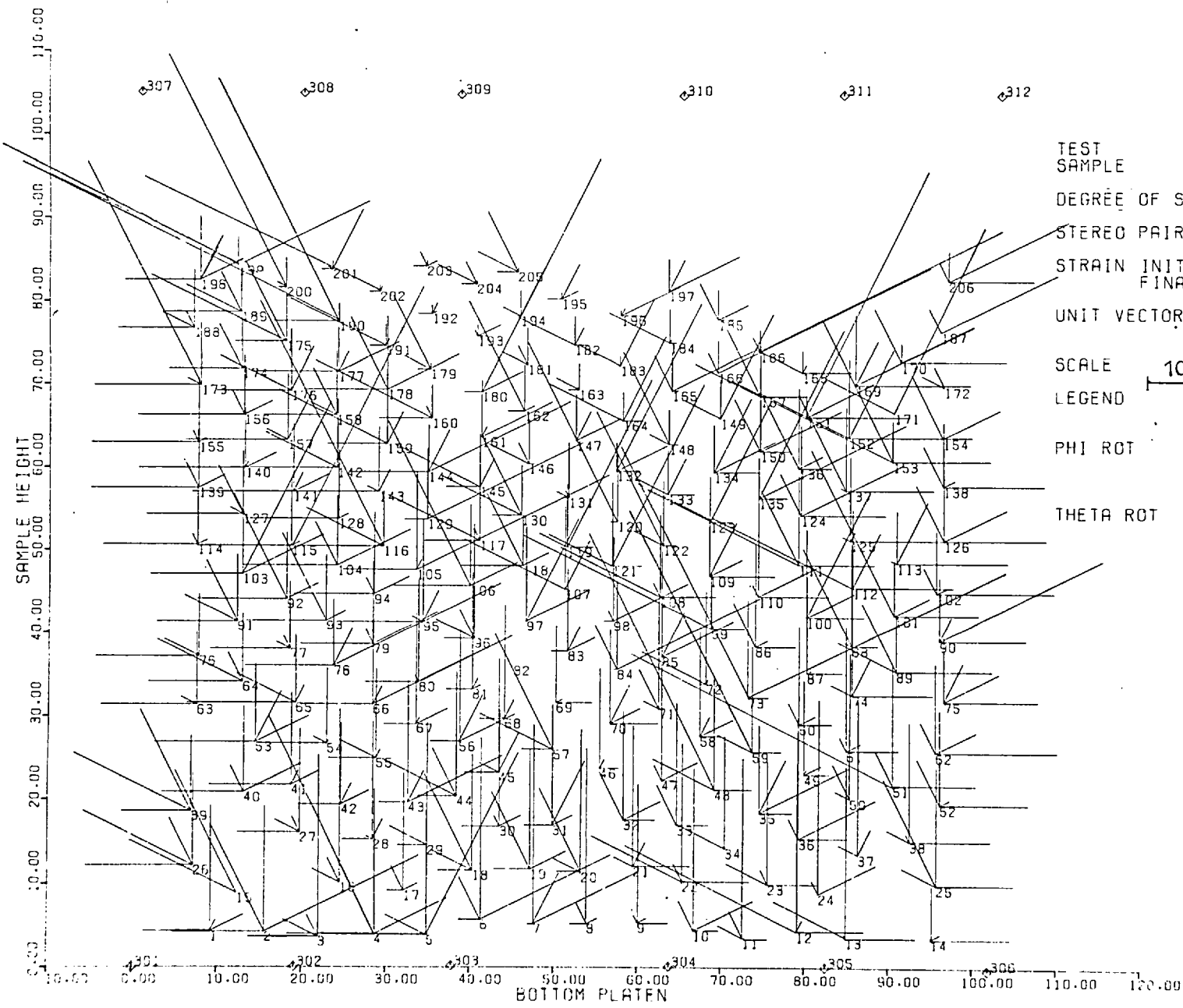


FIG 7.144 DISPLACEMENT - ROTATION FIELD OF MARKERS IN XY PLANE



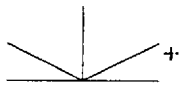
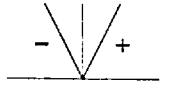
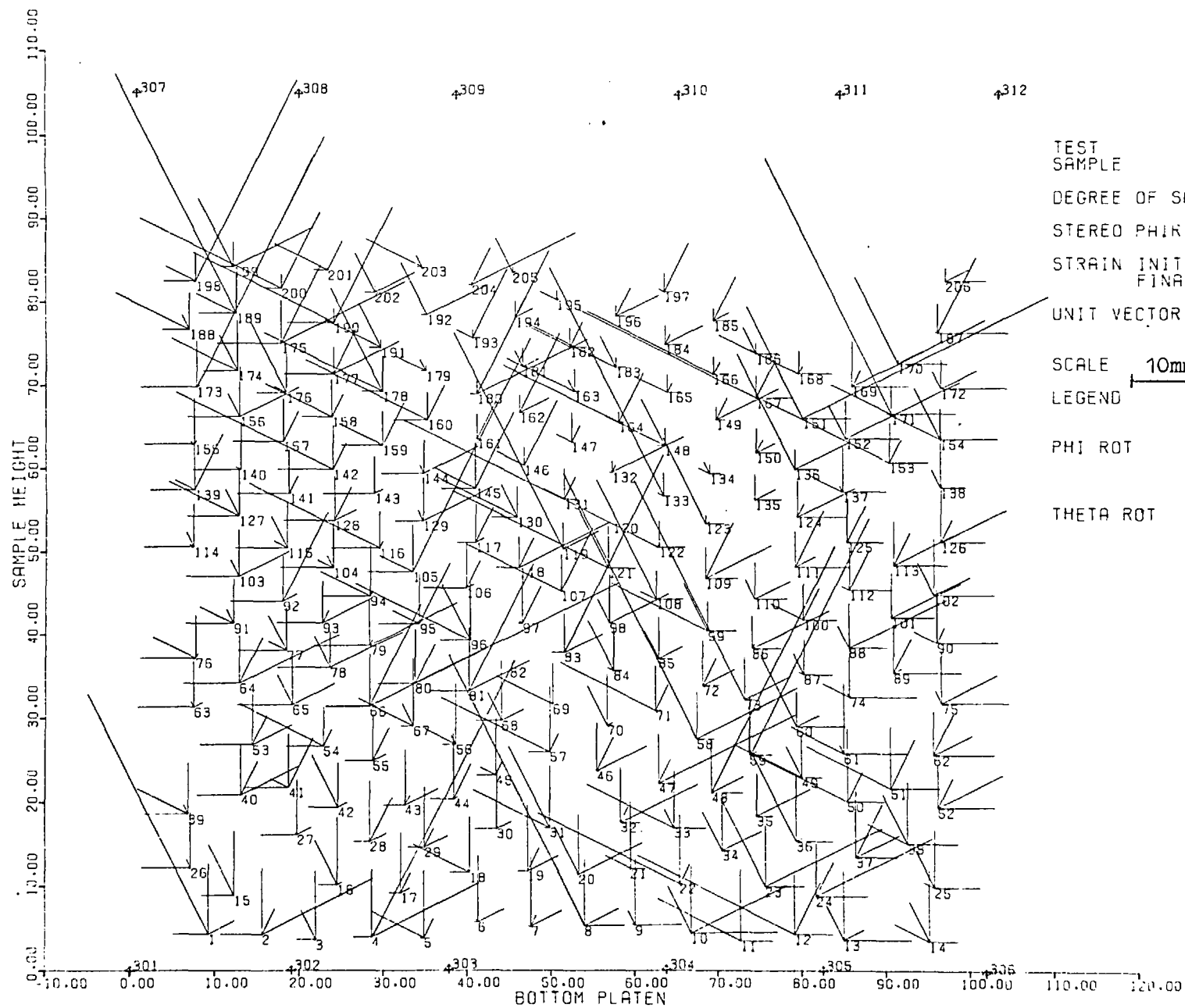
TEST SAMPLE 5150/5
 PLANE STRAIN (DRAINED)
 POLYPROPYLENE SPHERES
 DRY
 DEGREE OF SAT. FIRST 5
 STEREO PAIR NO. FINAL 6
 STRAIN INITIAL 6.181
 FINAL 9.974
 UNIT VECTOR DISP. [HOR.X] 2mm
 [VER.Y] 2rad
 ROT. 10mm
 SCALE 10mm
 LEGEND
 PHI ROT - 
 THETA ROT - 

FIG 7.145 DISPLACEMENT - ROTATION FIELD OF MARKERS IN XY PLANE



TEST
SAMPLE

DEGREE OF SAT.

STEREO PAIR NO.

STRAIN INITIAL
FINAL

UNIT VECTOR DISP.
ROT.

SCALE 10mm

LEGEND

PHI ROT

THETA ROT

5150/6

PLANE STRAIN (RANDOM)
POLYPROPYLENE SPHERES

DRY

FIRST 6
FINAL 7
9.974
12.989

[HOR. X
VER. Y]

3mm
•2rad

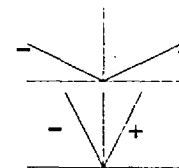
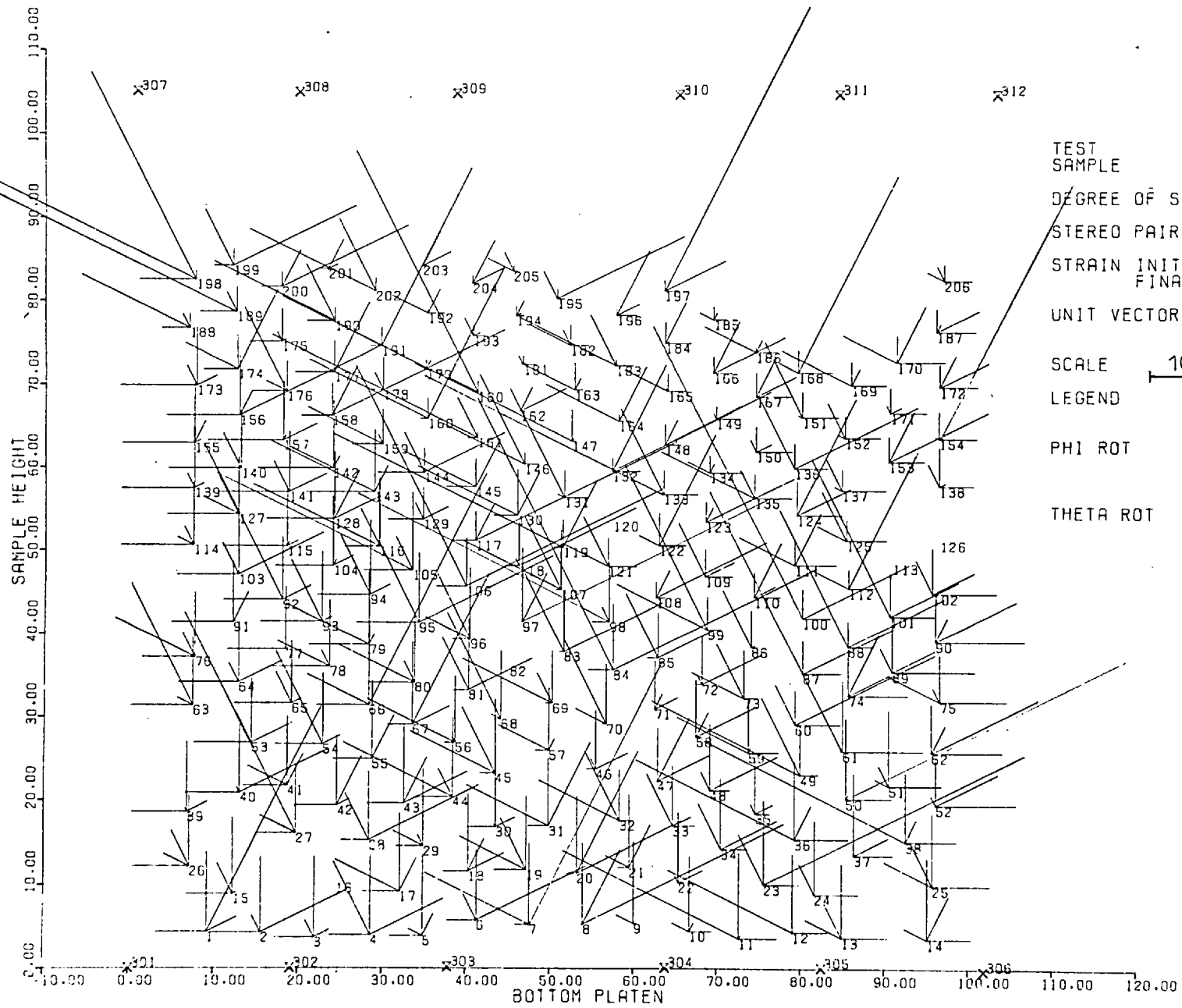


FIG 7.146 DISPLACEMENT - ROTATION FIELD OF MARKERS IN XY PLANE



TEST
SAMPLE

DEGREE OF SAT.

STEREO PAIR NO.

STRAIN INITIAL
FINAL

UNIT VECTOR DISP.

SCALE 10mm

LEGEND

PHI ROT

THETA ROT

5150/7

PLANE STRAIN (DRAINED)
POLYPROPYLENE SPHERES

DRY

FIRST 7

FINAL 8

12.989

17.742

HOR. X
VER. Y

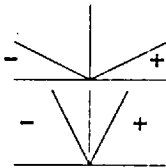
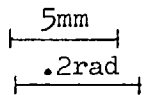


FIG 7.147 DISPLACEMENT - ROTATION FIELD OF MARKERS IN XY PLANE

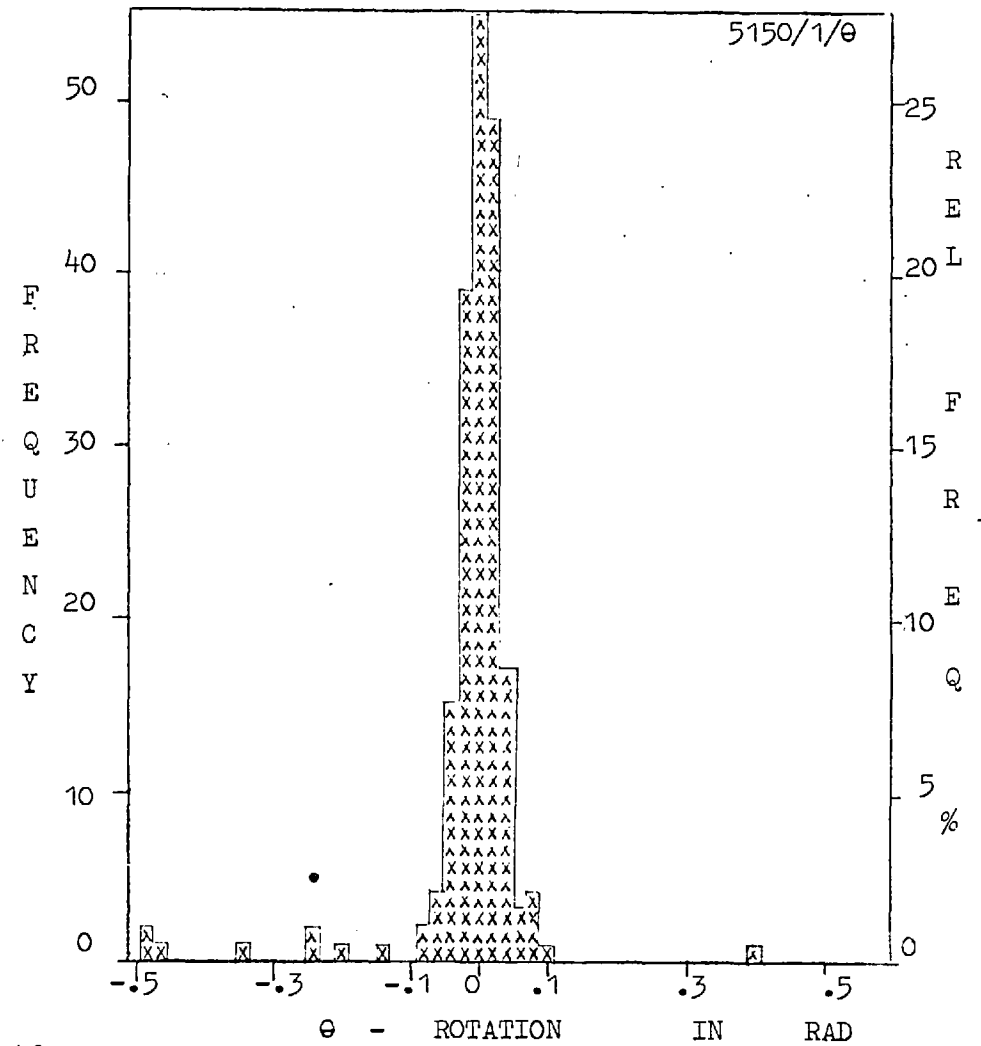
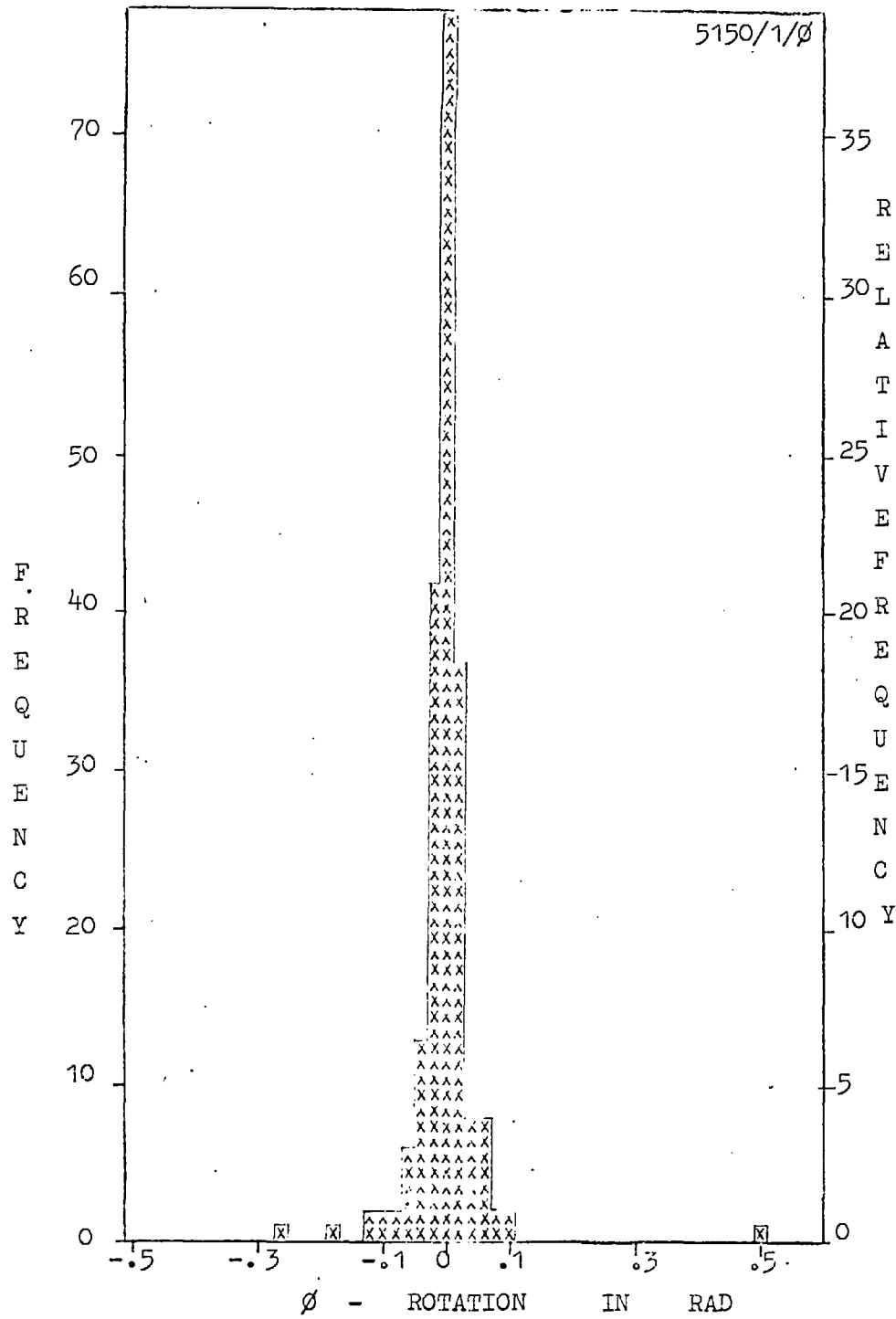


FIG. 7.148

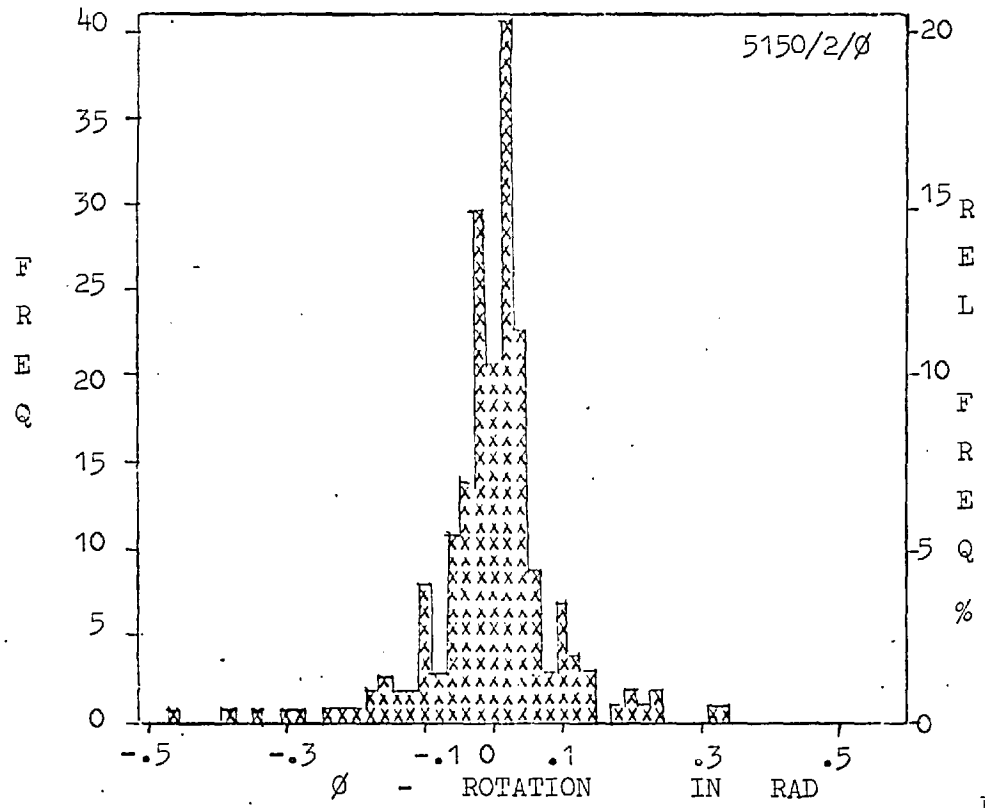


FIG. 7.149

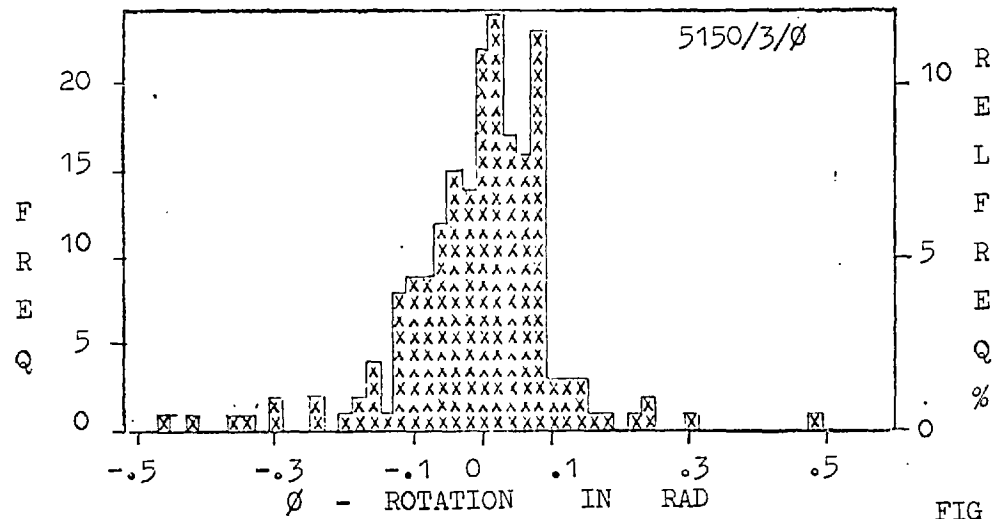
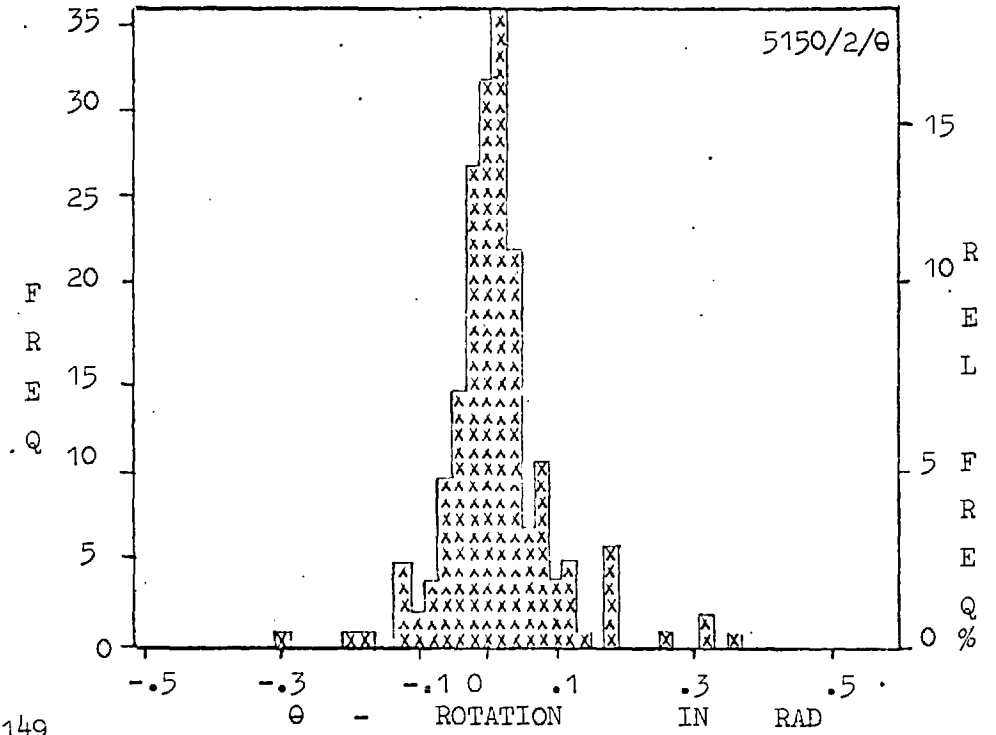
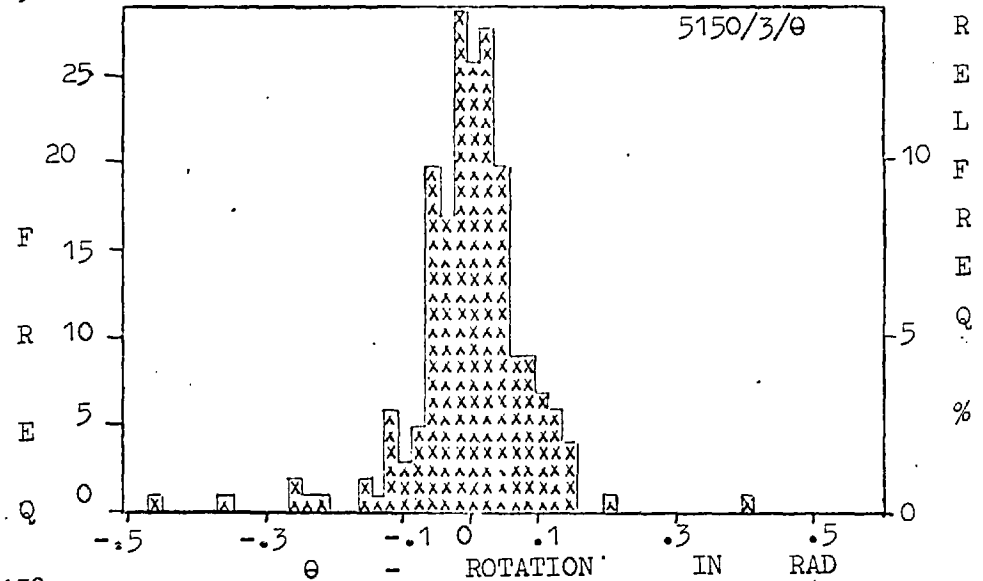


FIG 7.150



5150/4/θ

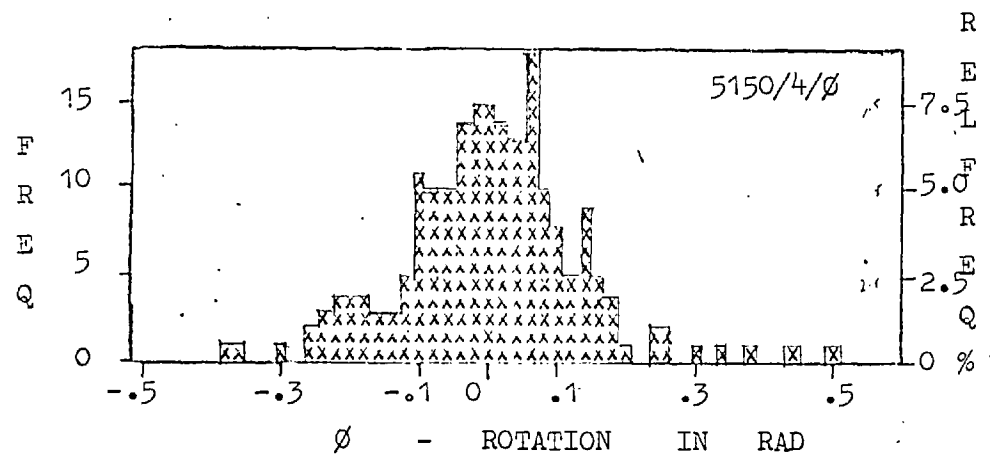


FIG. 7.151

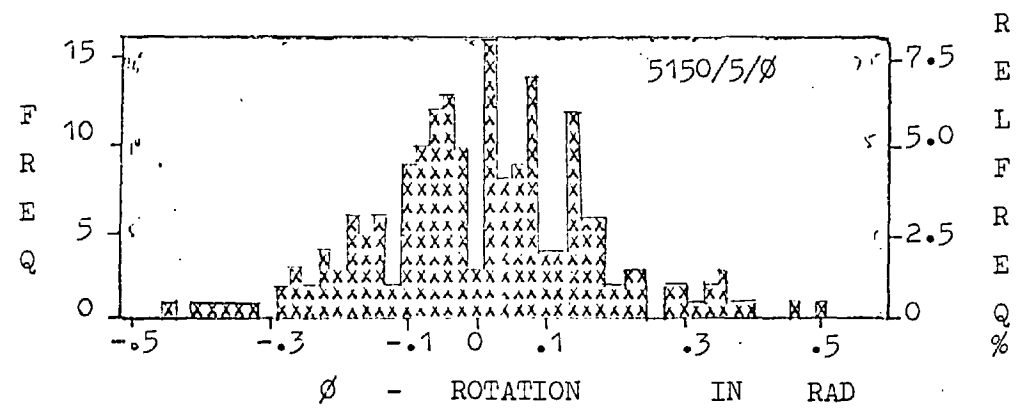
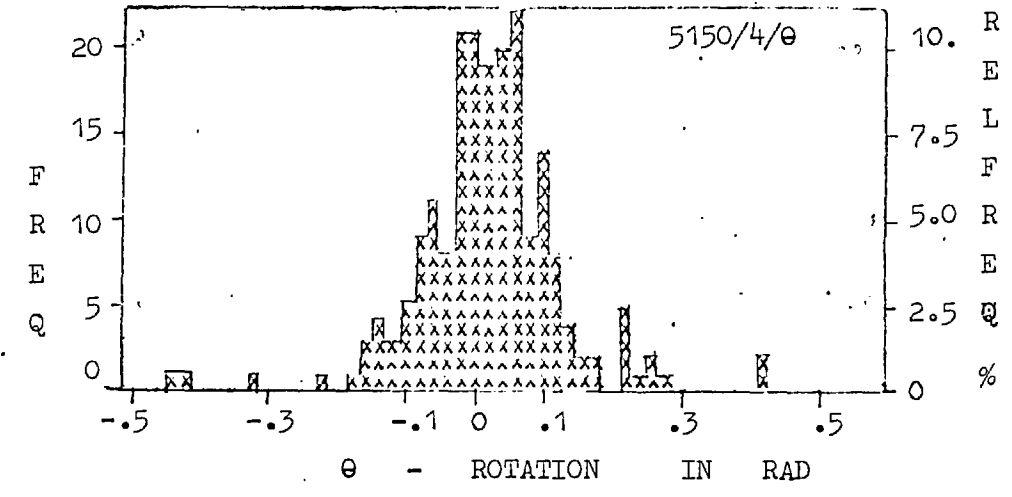
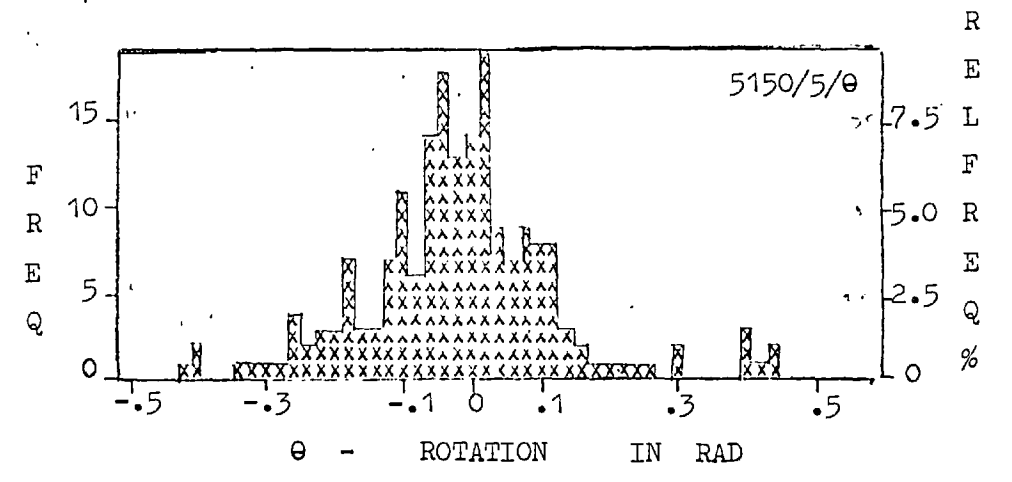


FIG. 7.152



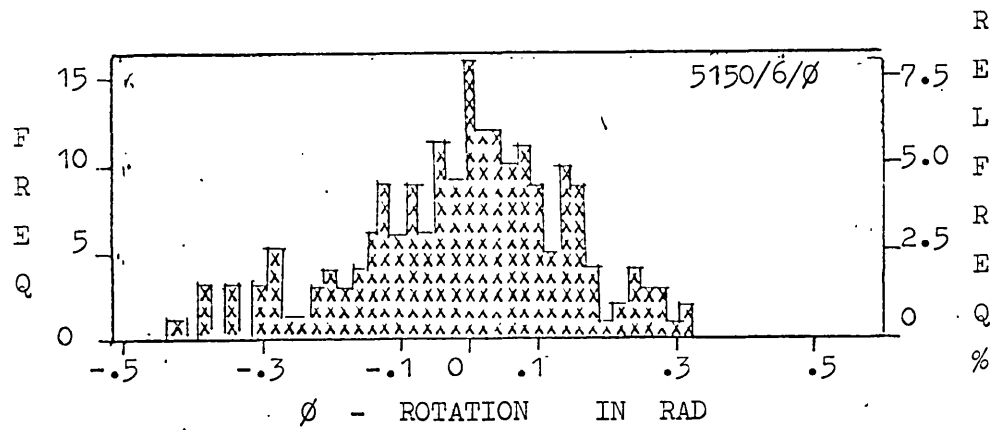


FIG. 7.153

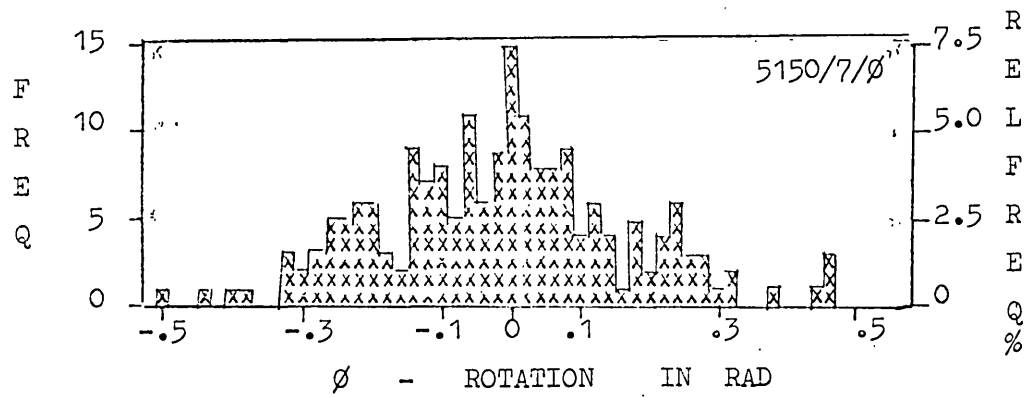
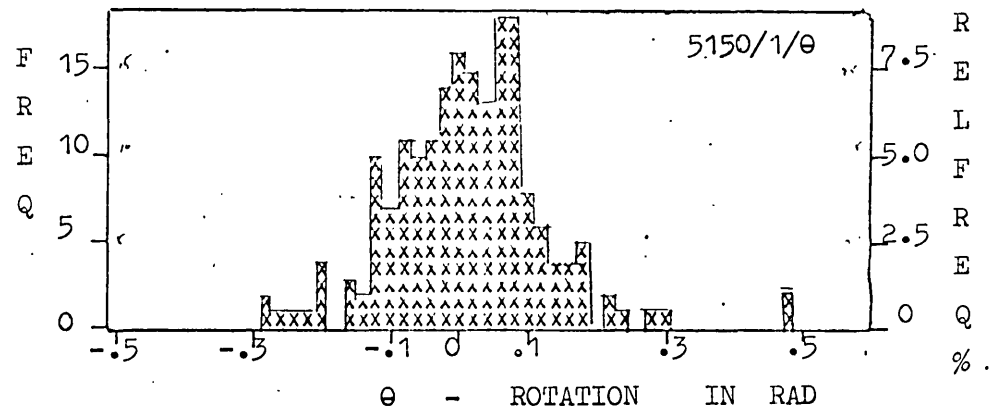
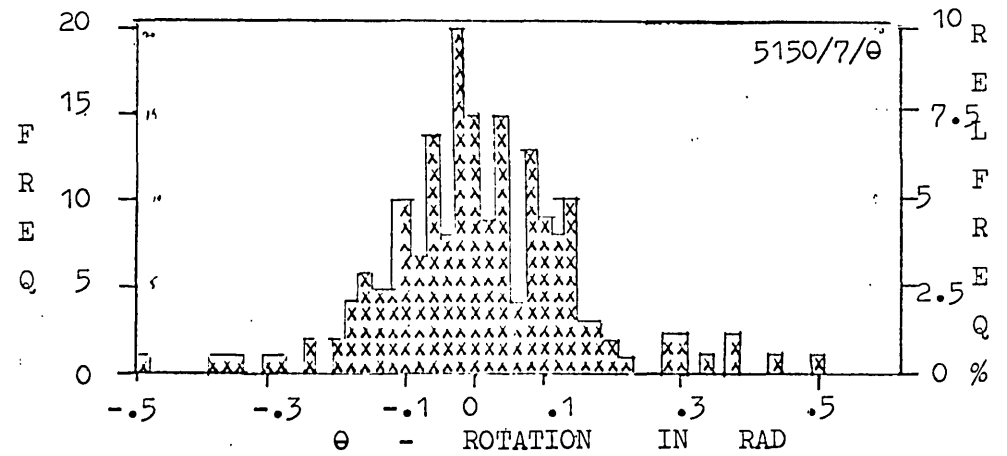
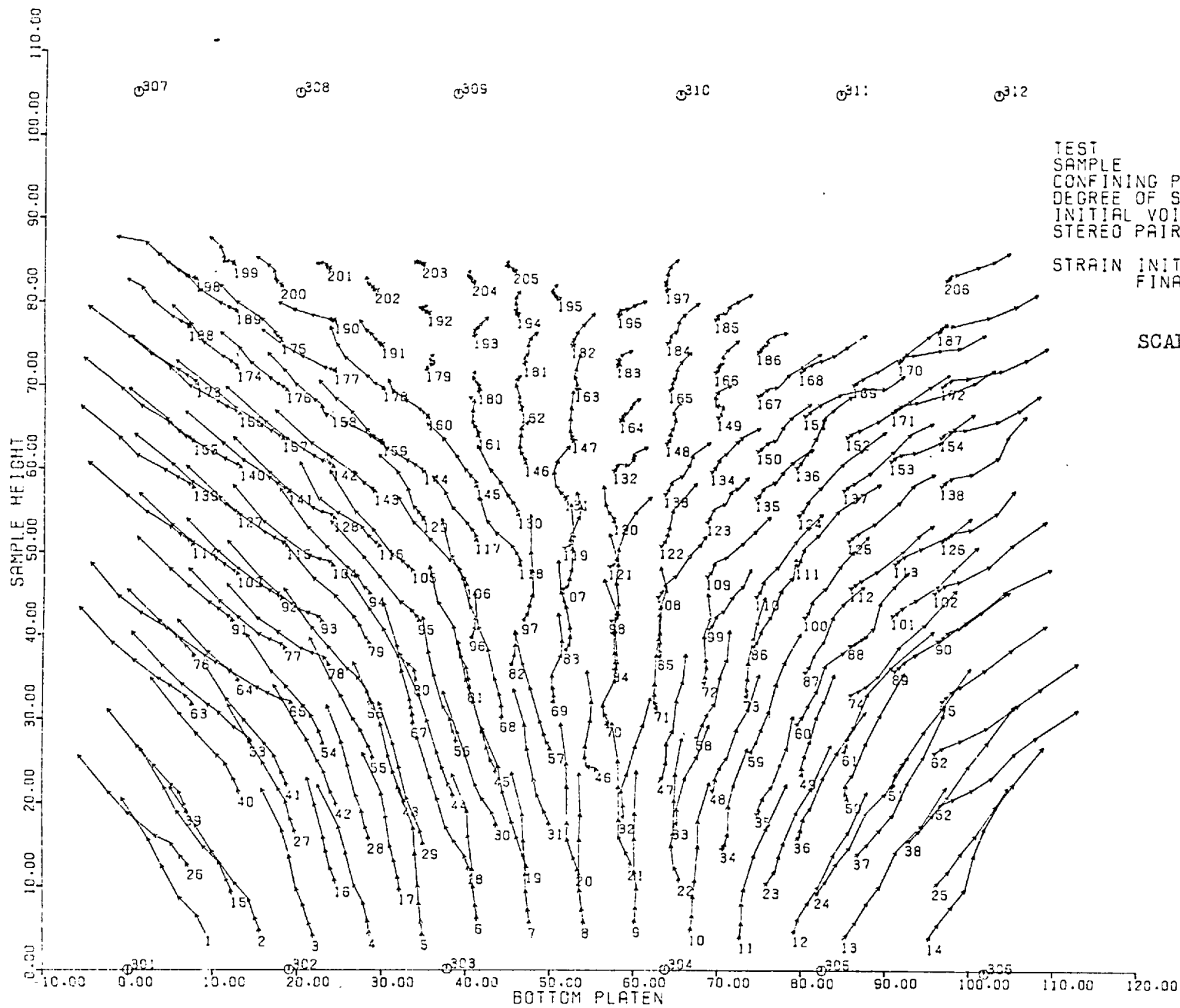


FIG. 7.154





TEST
 SAMPLE
 CONFINING PRESSURE
 DEGREE OF SAT.
 INITIAL VOID RATIO
 STEREO PAIR NO.

5150
 PLANE STRAIN (DRAINED)
 POLYPROPYLENE BALLS
 KP
 DRY
 FIRST 1
 LAST 8
 0.0
 17.742

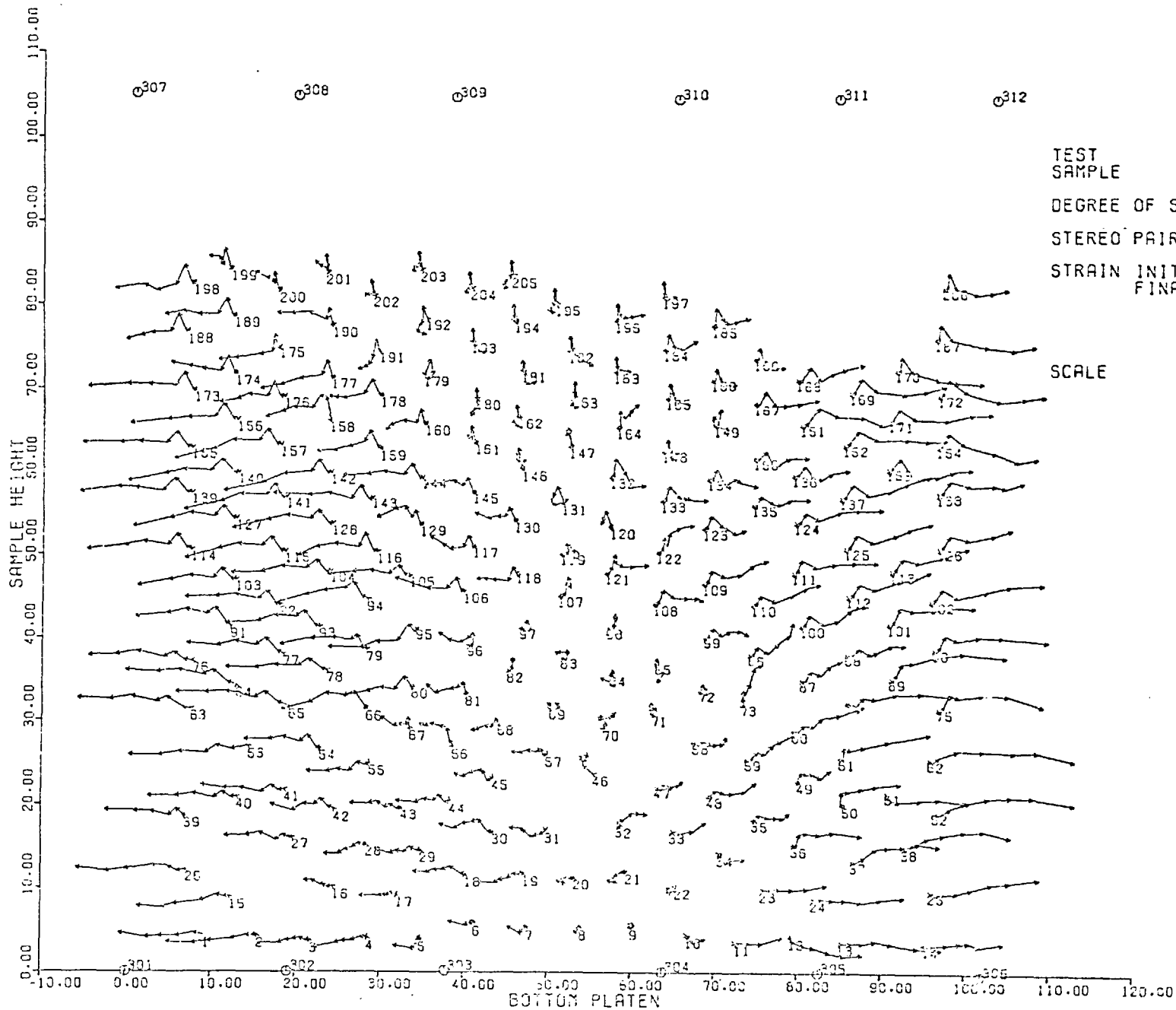
STRAIN INITIAL
 FINAL

SCALE

10mm

FIG 7.155

TRACE OF DISPLACEMENTS OF MARKER CENTRES ON XY PLANE



TEST
SAMPLE

DEGREE OF SAT.

STEREO PAIR NO.

STRAIN INITIAL
FINAL

5150
PLANE STRAIN (DRAINED)
POLYPROPYLENE BALLS

DRY

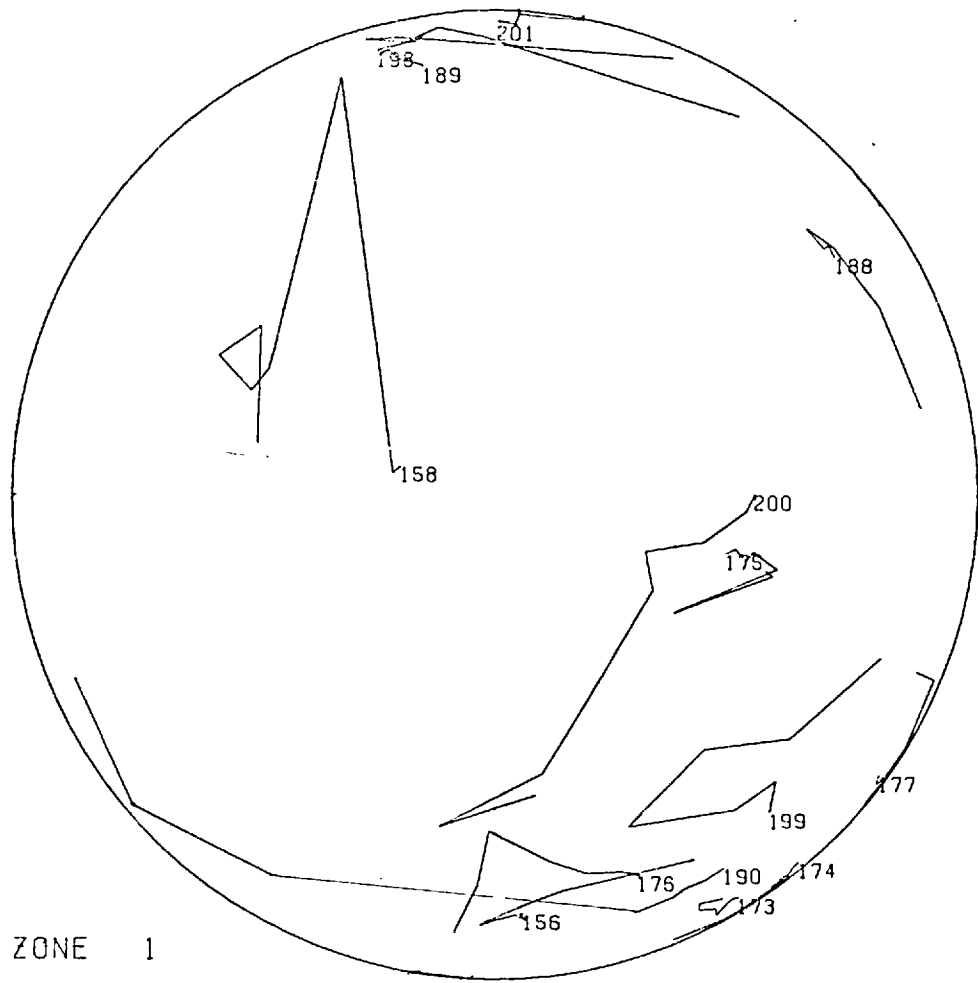
FIRST 1
LAST 8
0.0
17.742

SCALE

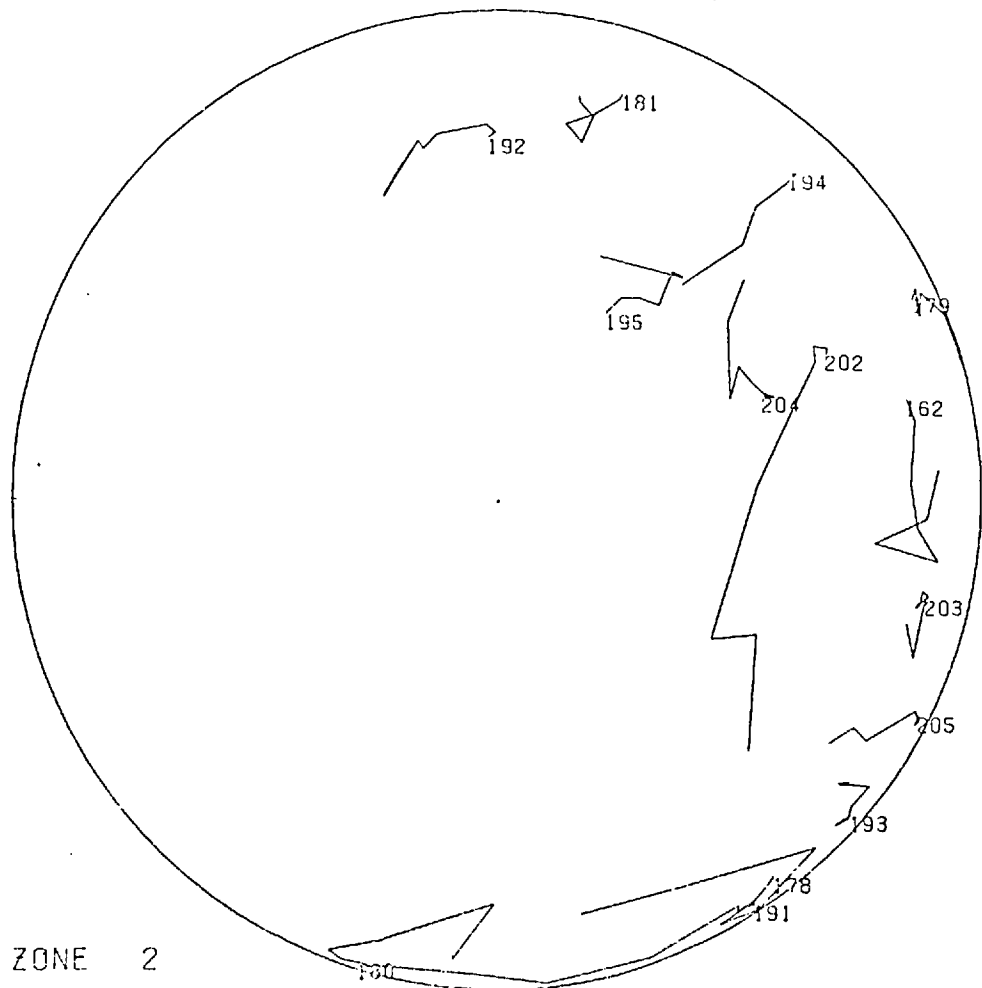
10mm

FIG 7.156

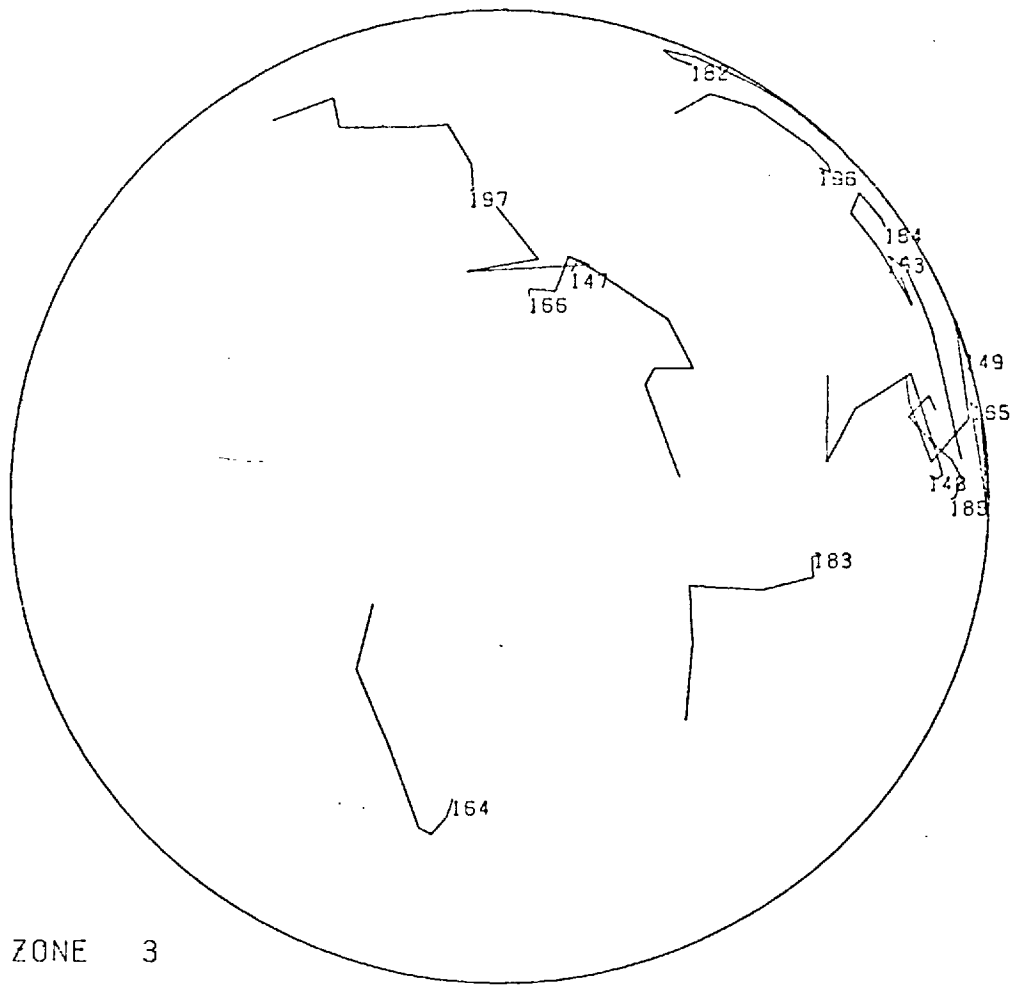
TRACE OF DISPLACEMENTS OF MARKER CENTRES ON XZ PLANE



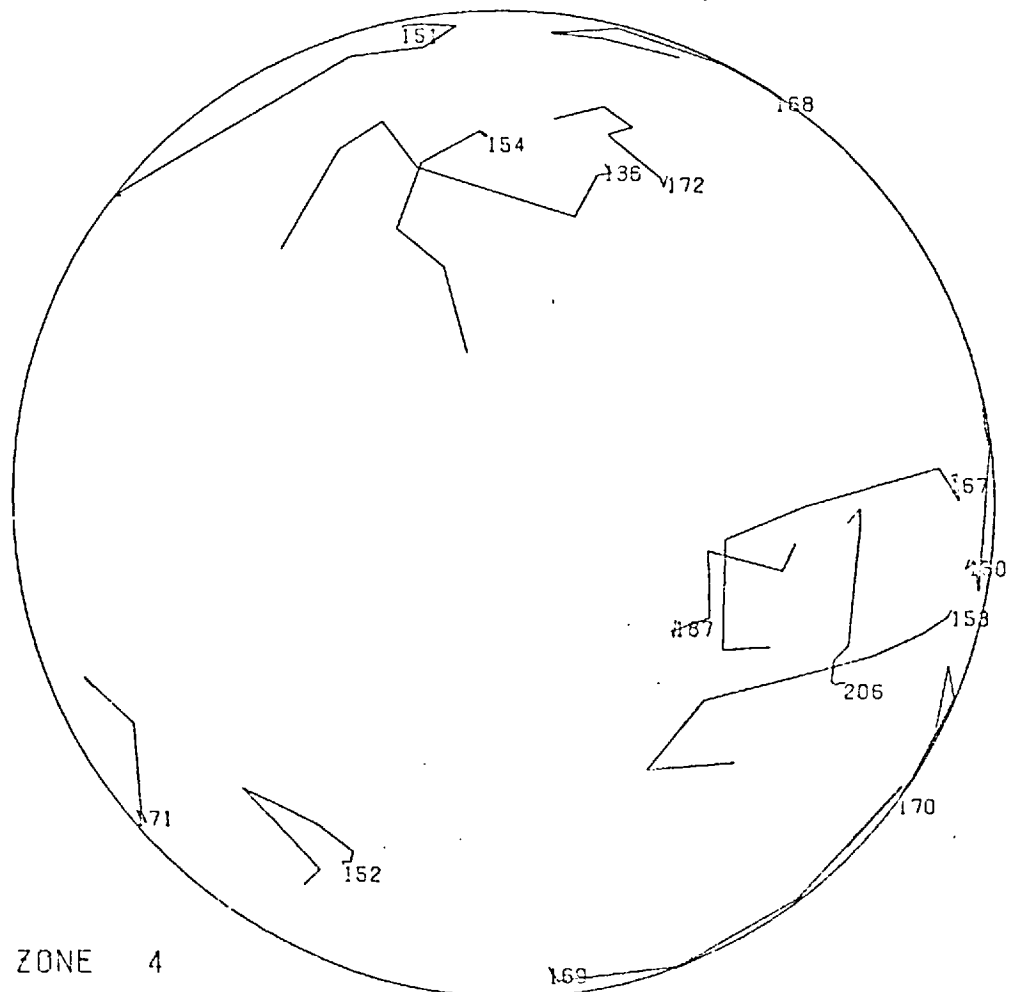
A) ZONE 1



B) ZONE 2

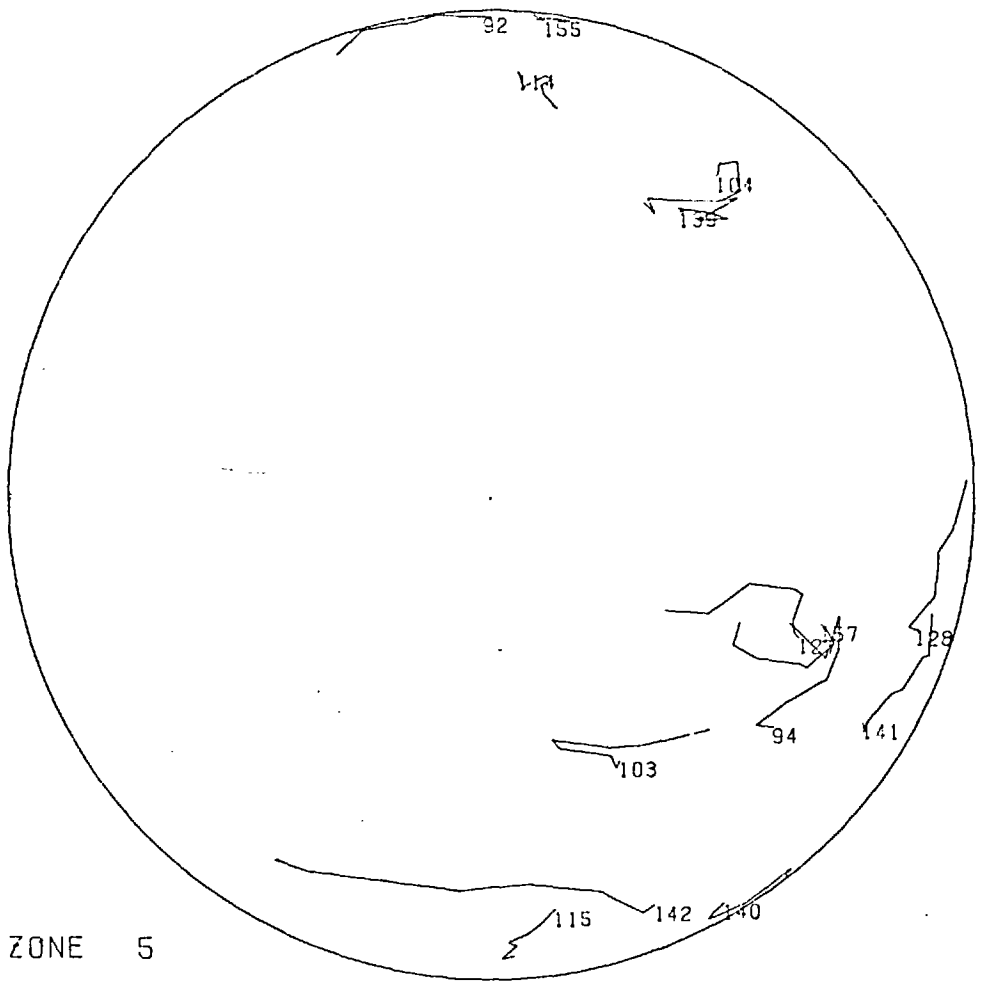


A) ZONE 3

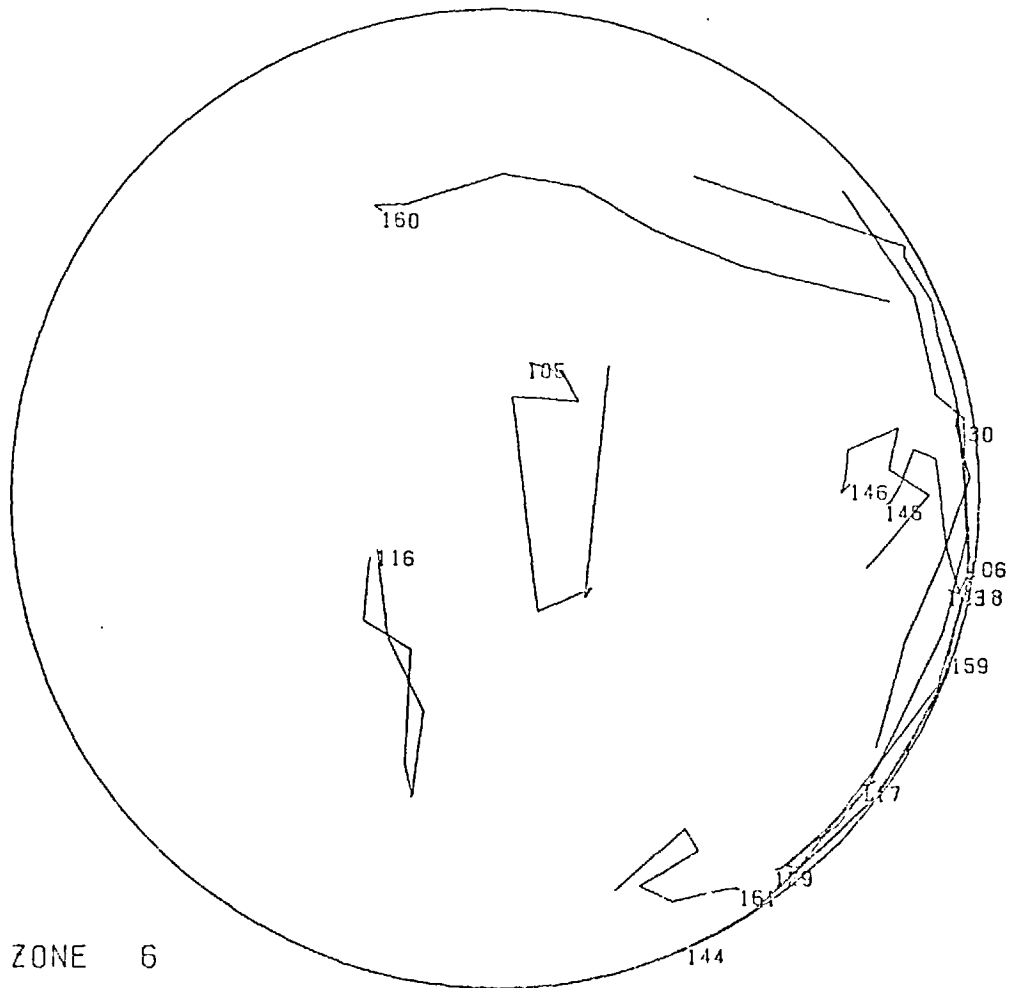


B) ZONE 4

FIG 7.158 TRACE OF PARTICLE ROTATION ON STERONEET



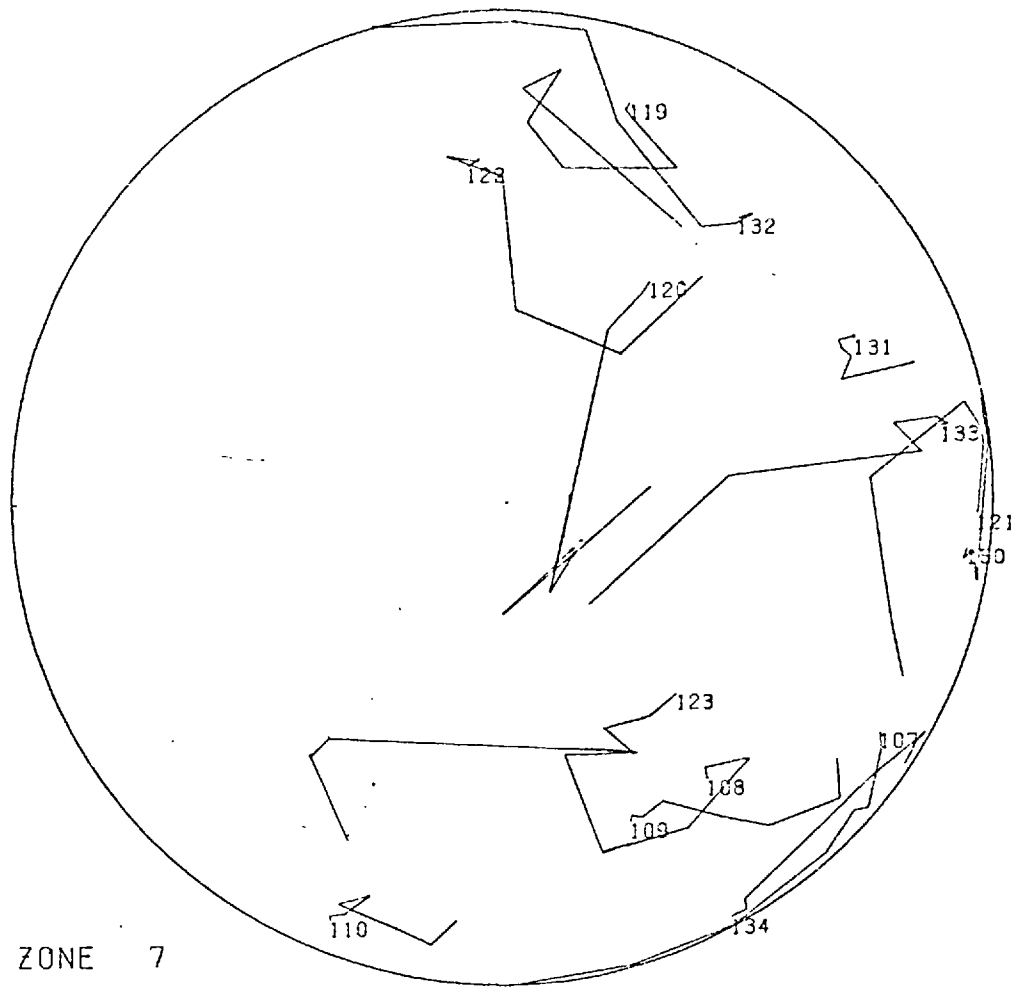
A) ZONE 5



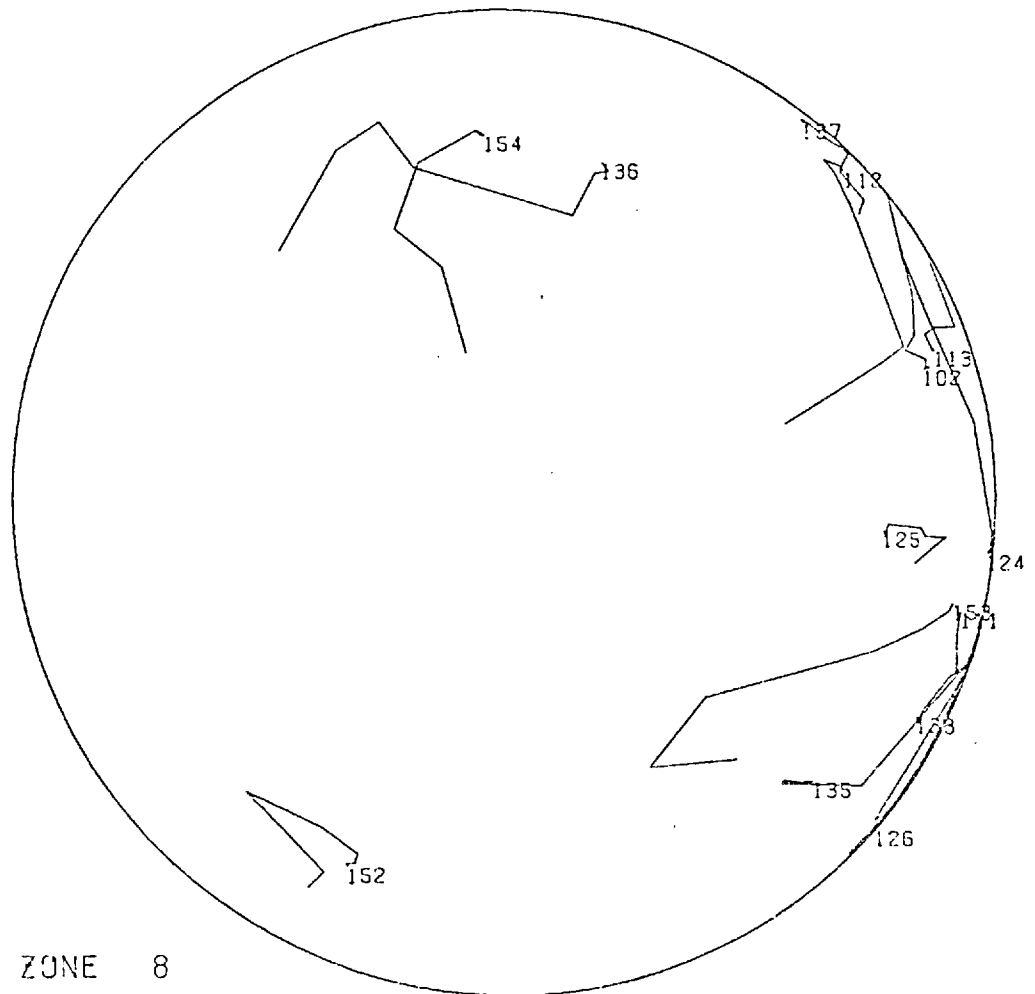
B) ZONE 6

FIG 7.159 TRACE OF PARTICLE ROTATION ON STERONEET

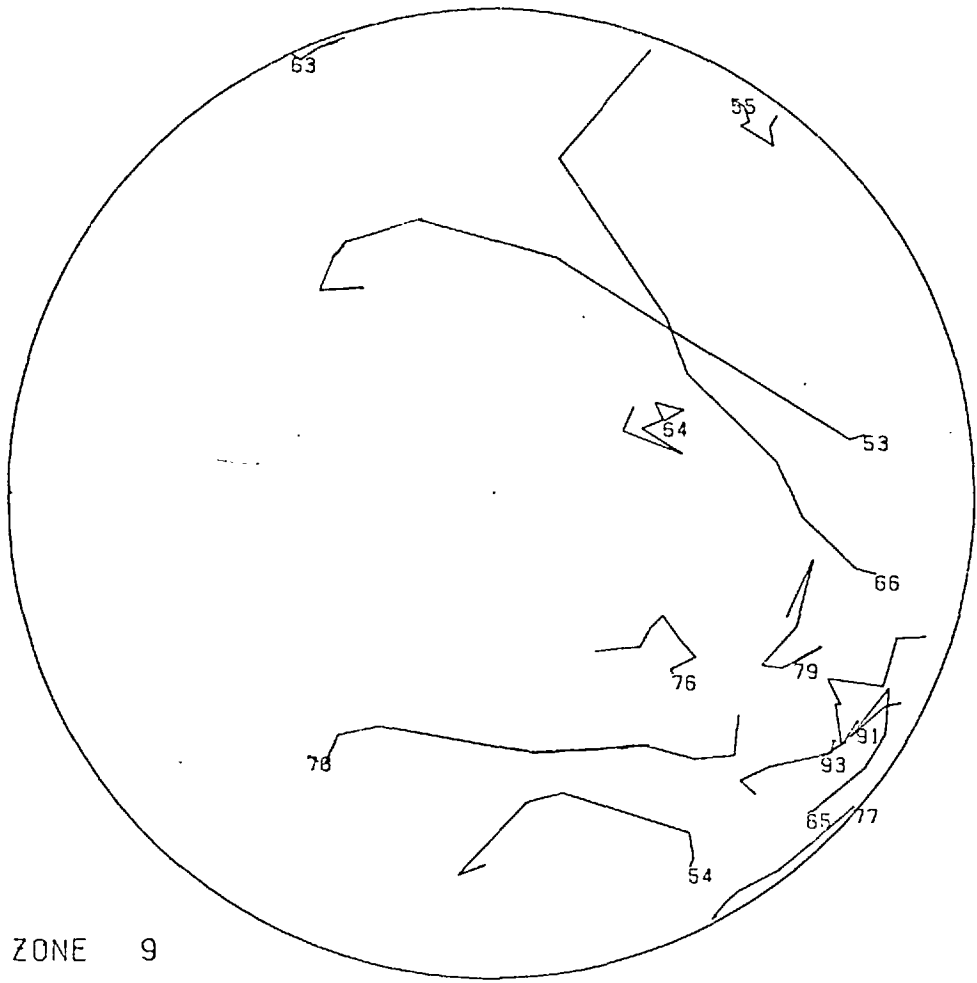
TEST NO 5150



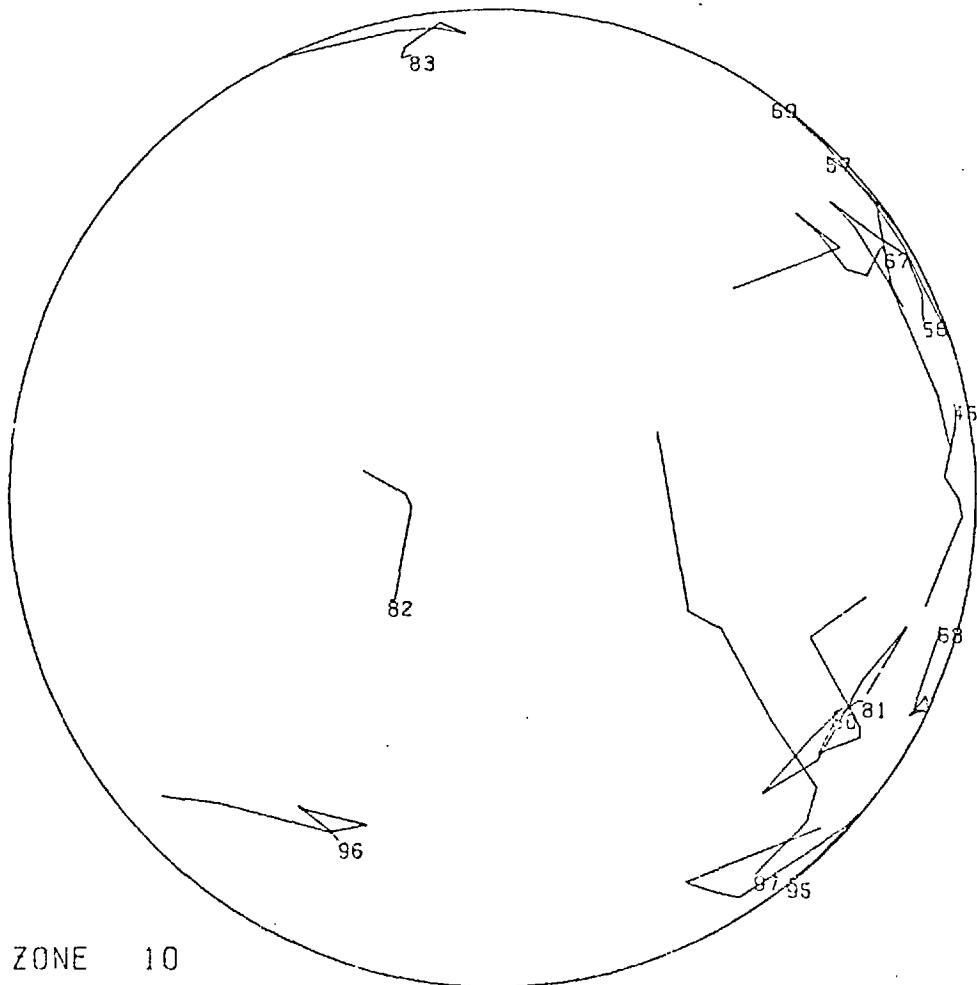
A) ZONE 7



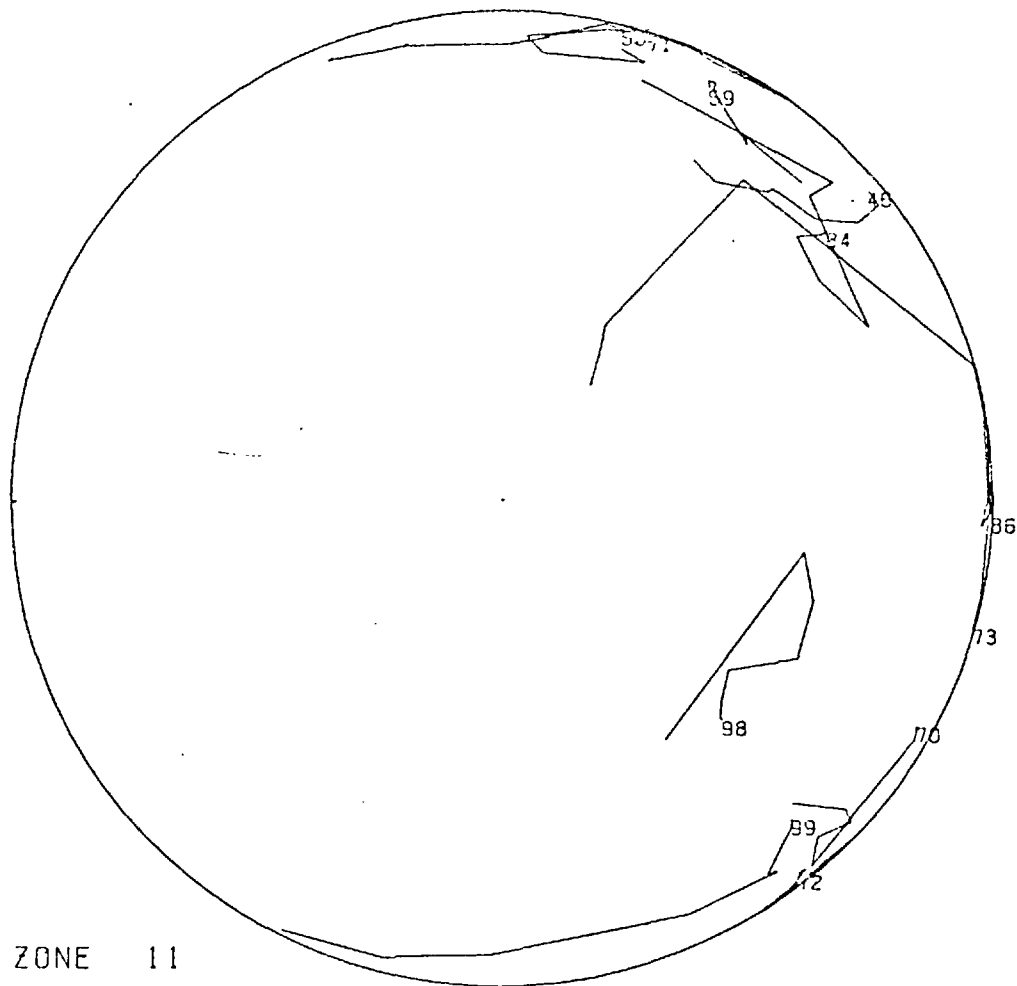
B) ZONE 8



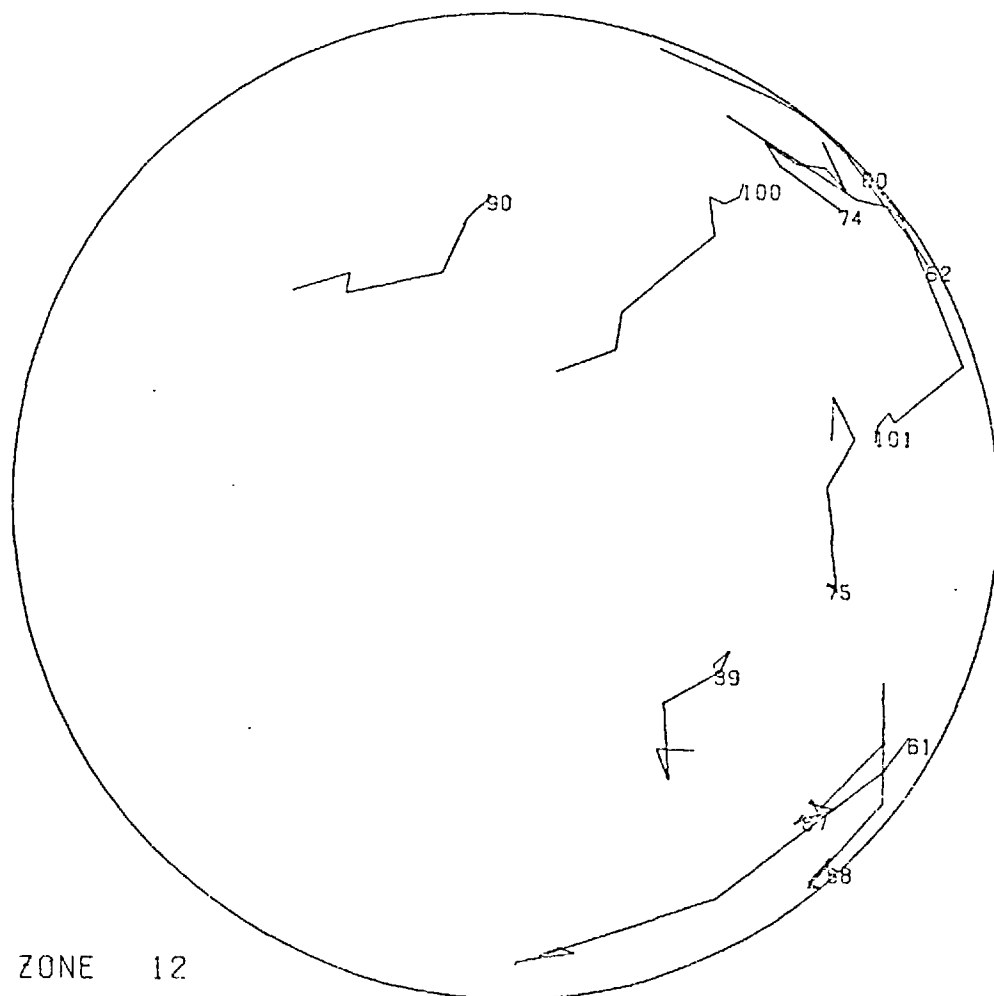
A) ZONE 9



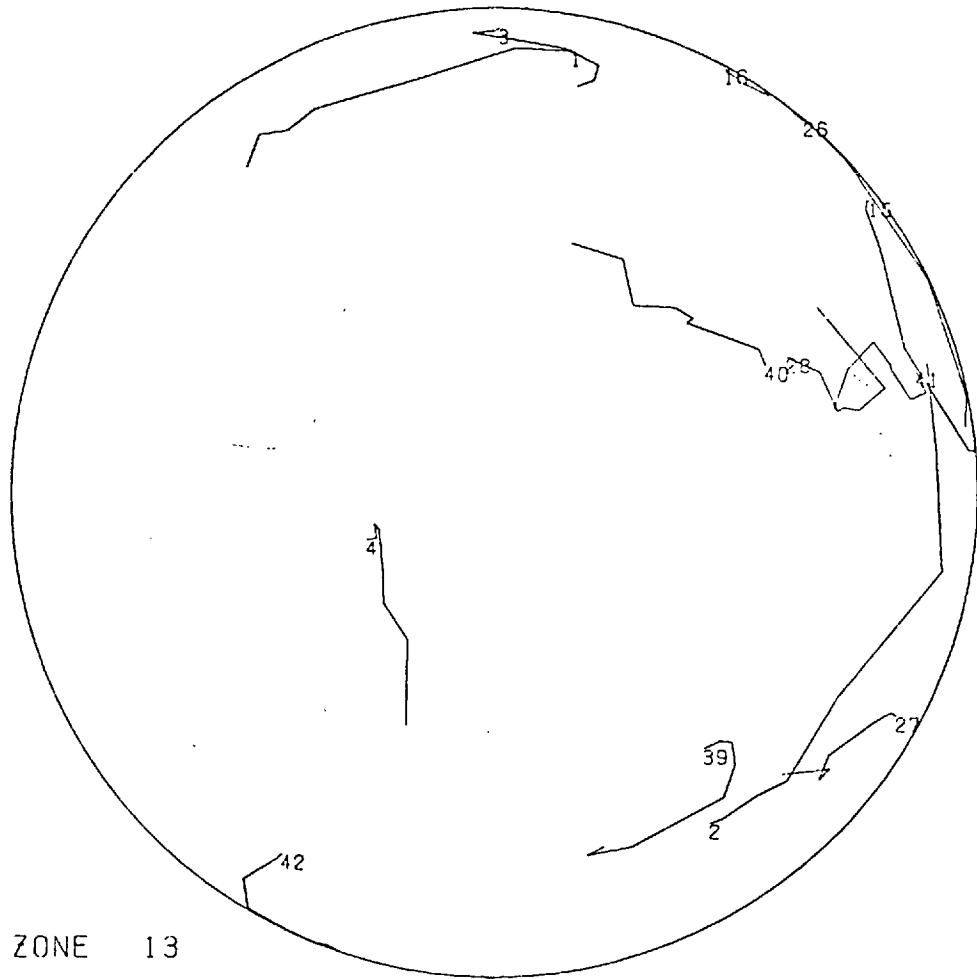
B) ZONE 10



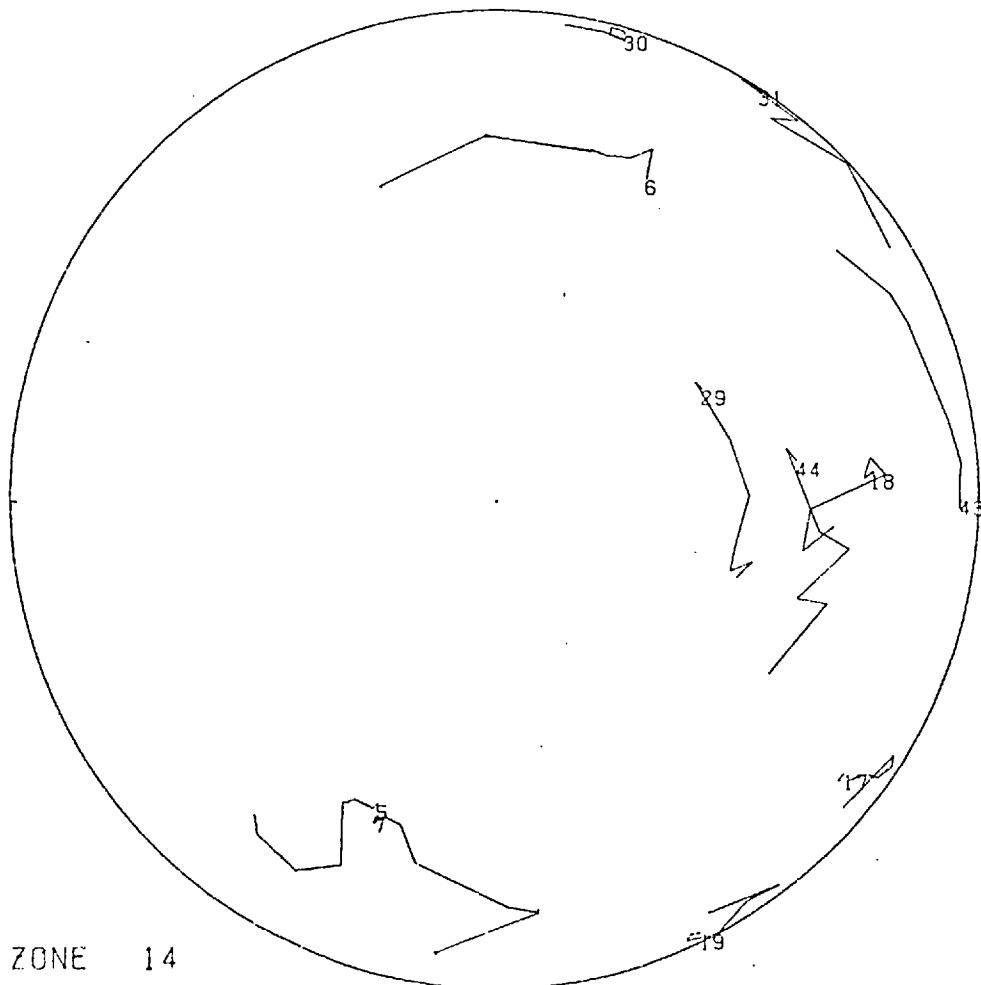
A) ZONE 11



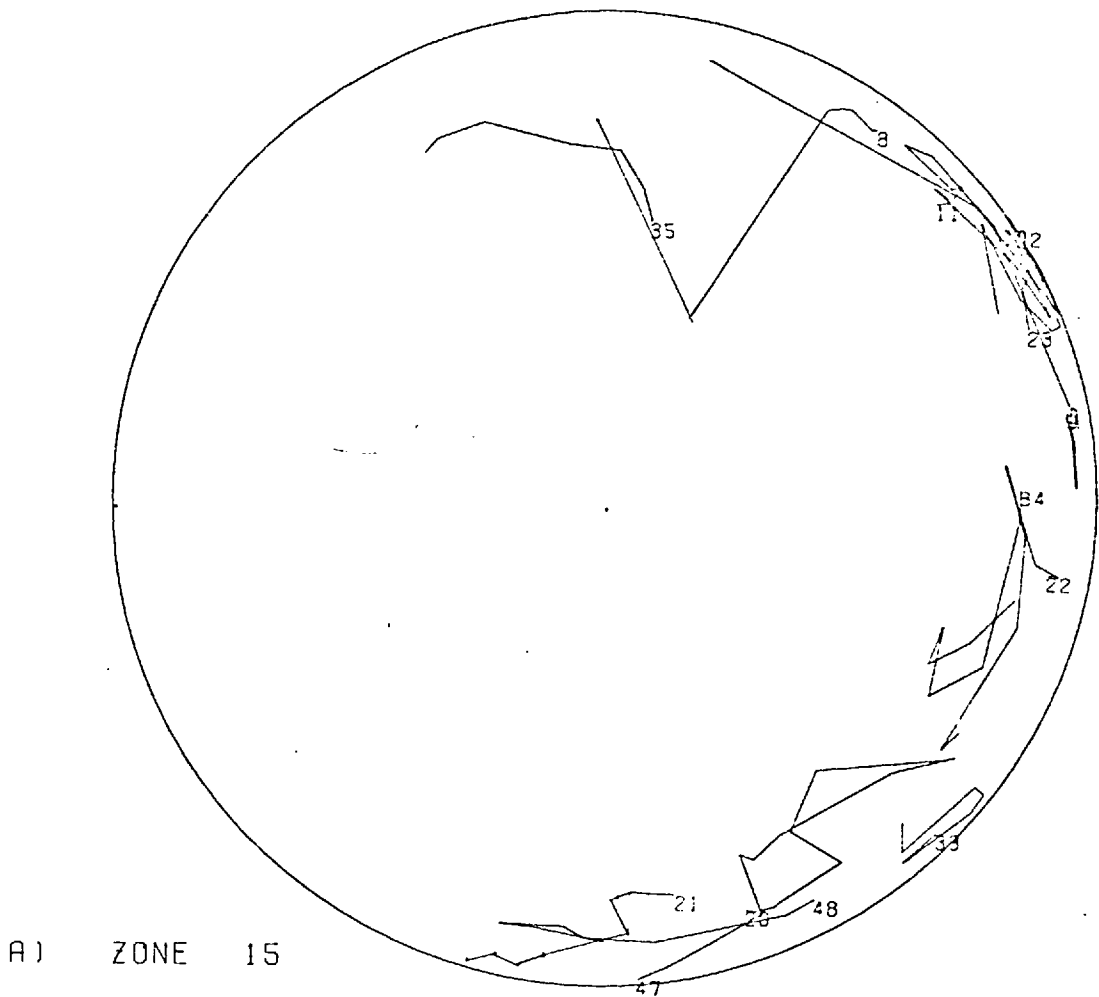
B) ZONE 12



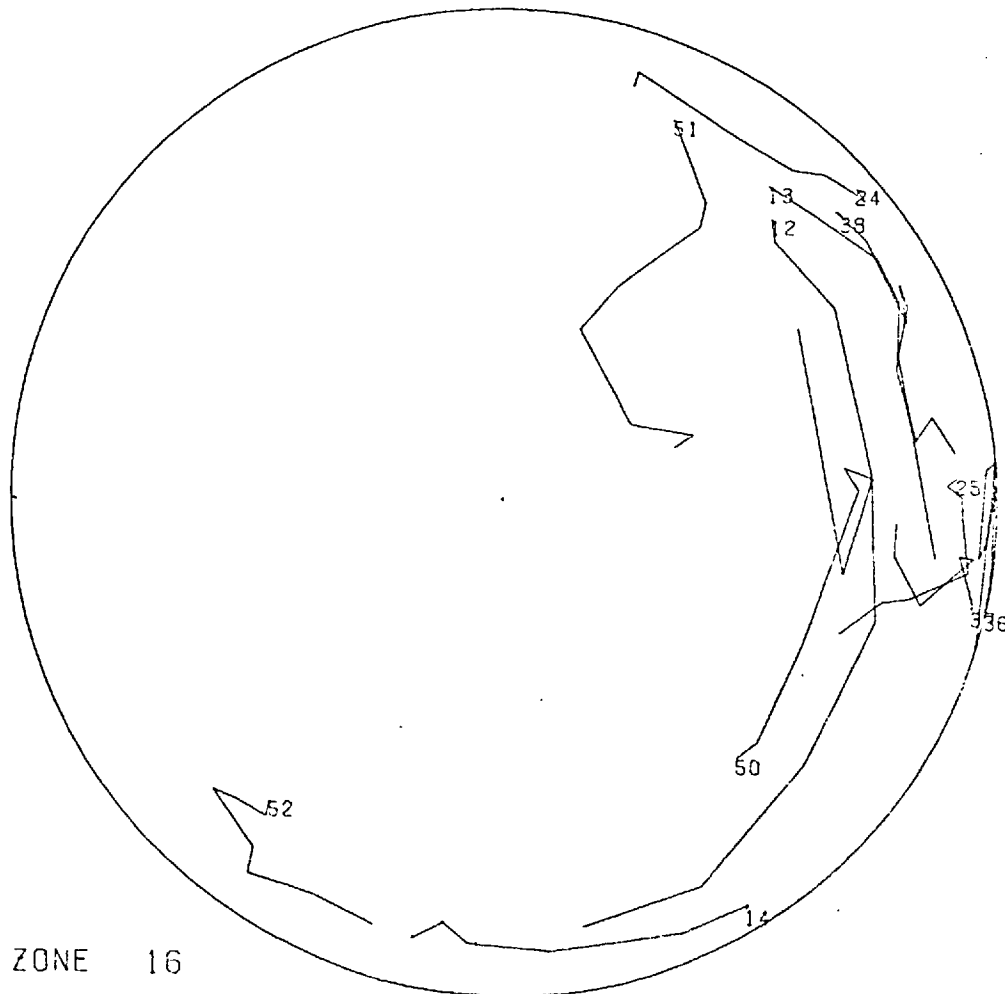
A) ZONE 13



B) ZONE 14



A) ZONE 15



B) ZONE 16

FIG 7.164 TRACE OF PARTICLE ROTATION ON STEREO NET

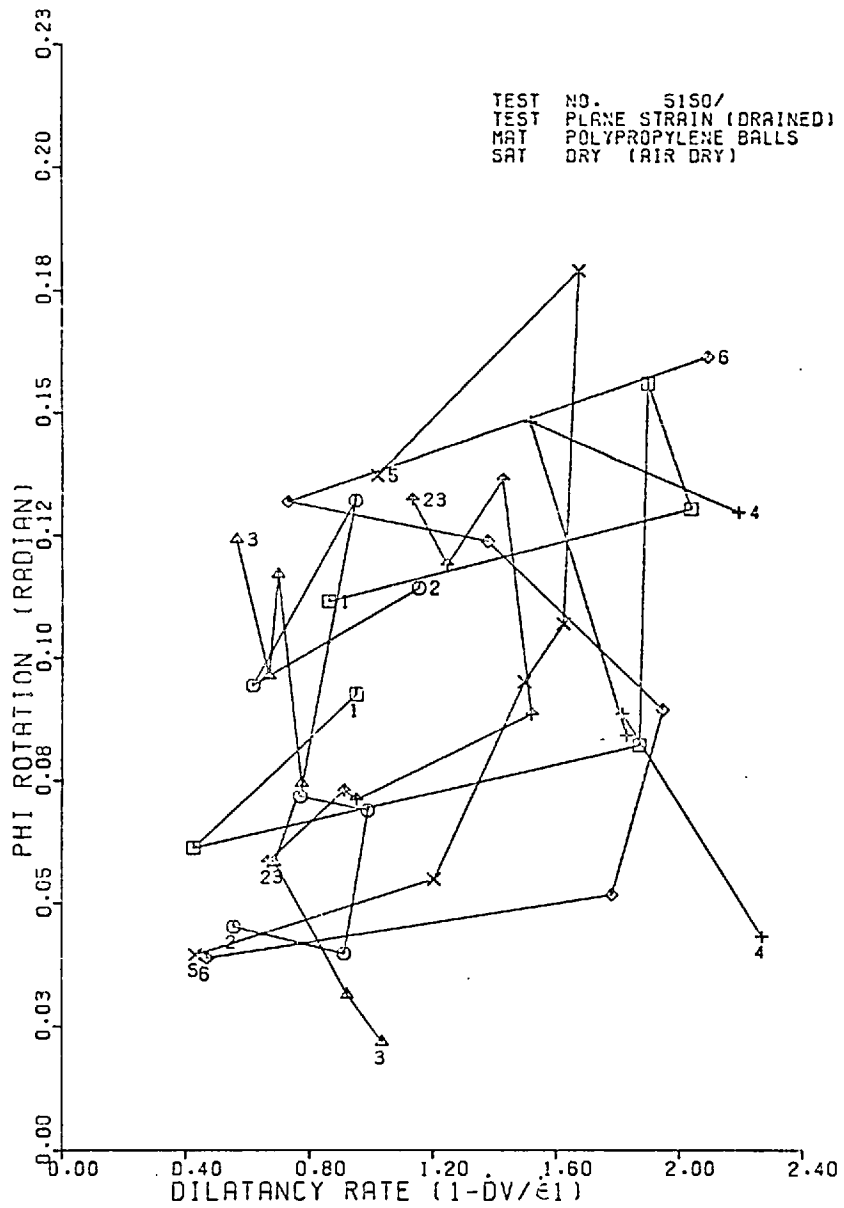


FIG. 7.165 PHI ROTATION - DILATANCY PLOT

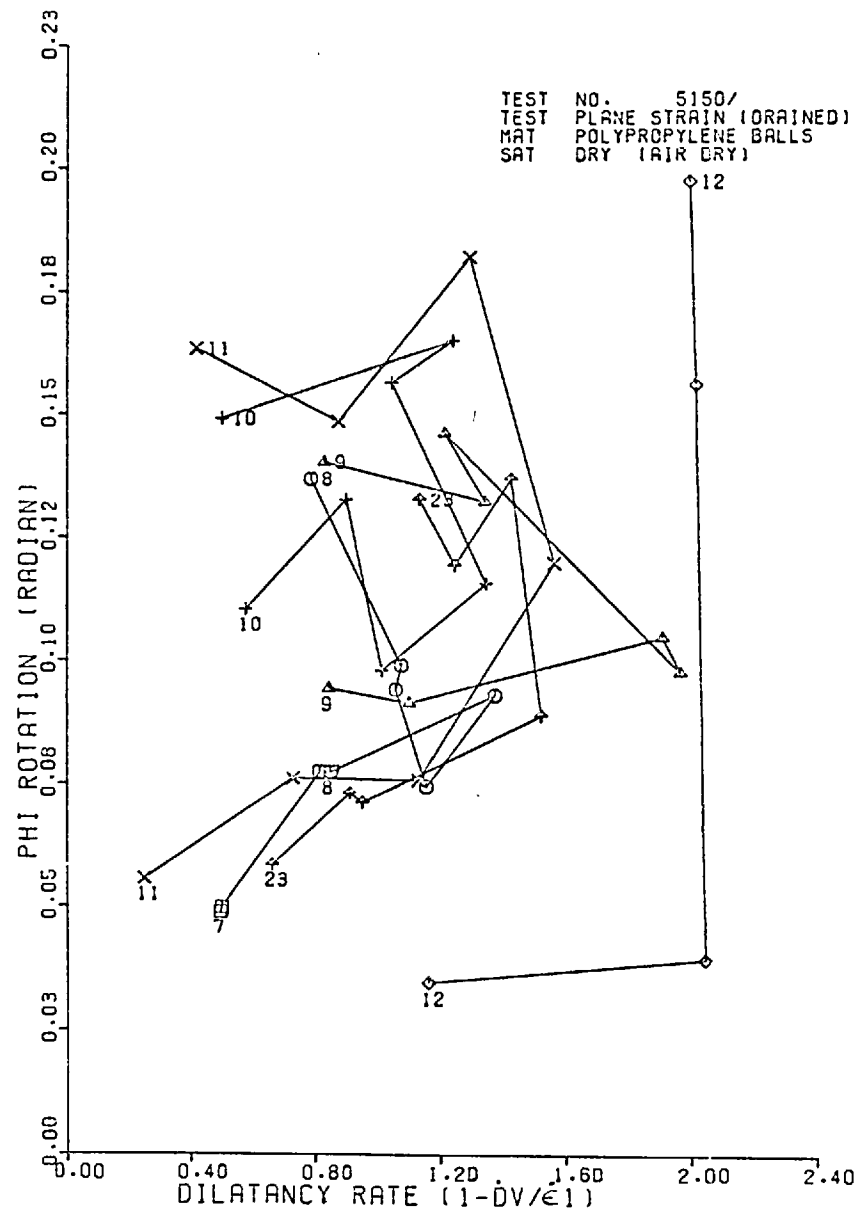


FIG. 7.166 PHI ROTATION - DILATANCY PLOT

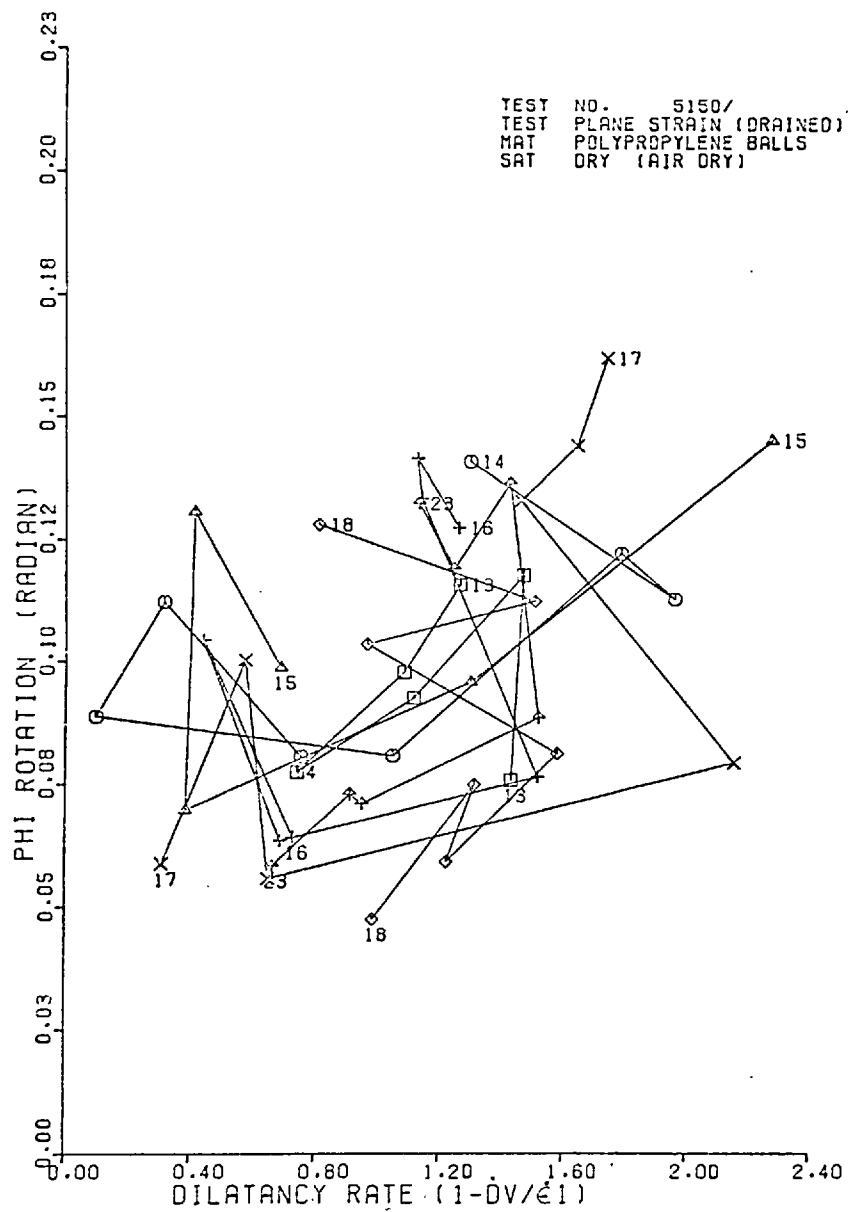


FIG. 7.167 PHI ROTATION - DILATANCY PLOT

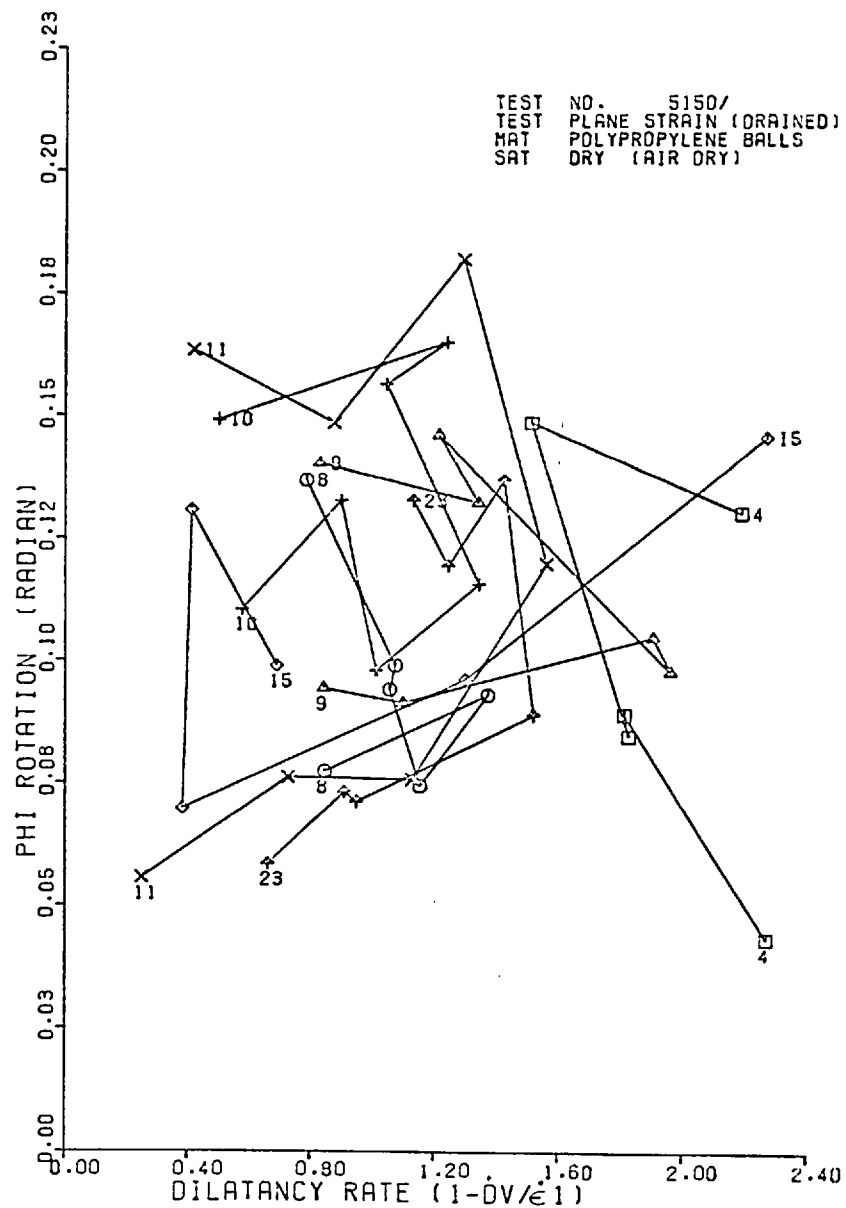
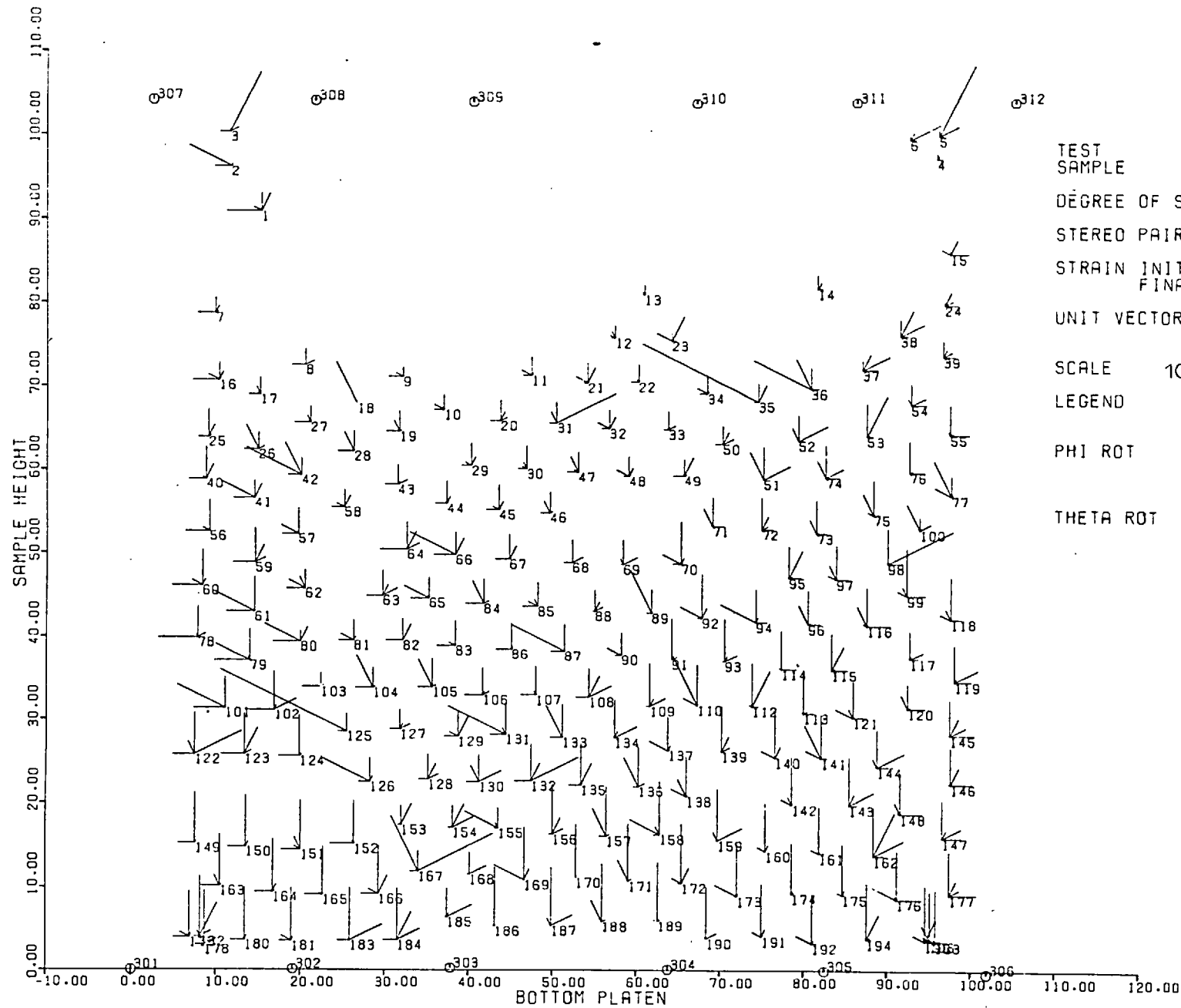


FIG. 7.168 - PHI ROTATION - DILATANCY PLOT



TEST
SAMPLE

DEGREE OF SAT.

STEREO PAIR NO.

STRAIN INITIAL
FINAL

UNIT VECTOR DISP.

SCALE 10mm

LEGEND

PHI ROT

THETA ROT

5201/1
PLANE STRAIN (DRAINED)
POLYPROPYLENE BALLS

FULLY SAT.

FIRST 1
FINAL 2

0.000
0.871

HOR.X 1mm
VER.Y .1rad

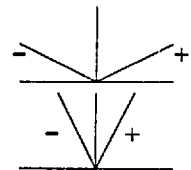
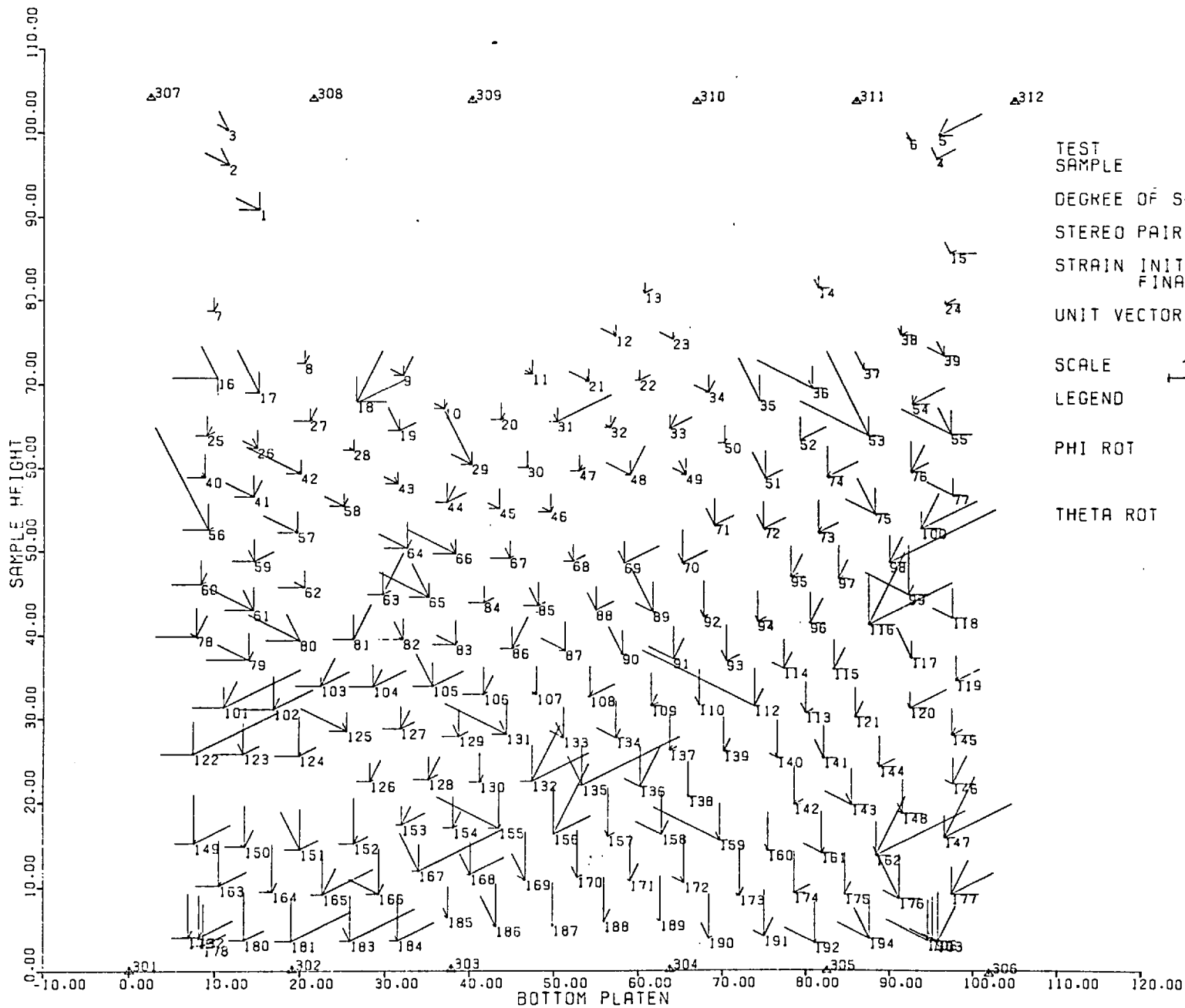


FIG 7.169 DISPLACEMENT - ROTATION FIELD OF MARKERS IN XY PLANE



TEST
SAMPLE

DEGREE OF SAT.

STEREO PAIR NO.

STRAIN INITIAL
FINAL

UNIT VECTOR DISP.

SCALE $\frac{10\text{mm}}{1}$

LEGEND

PHI ROT

THETA ROT

5201/2
PLANE STRAIN (DRAINED)
POLYPROPYLENE SPHERES

FULLY SAT.

FIRST 2
FINAL 3
0.871
2.019

HOR. X $\frac{2\text{mm}}{1}$
VER. Y $\frac{.2\text{rad}}{1}$

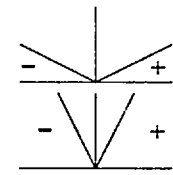
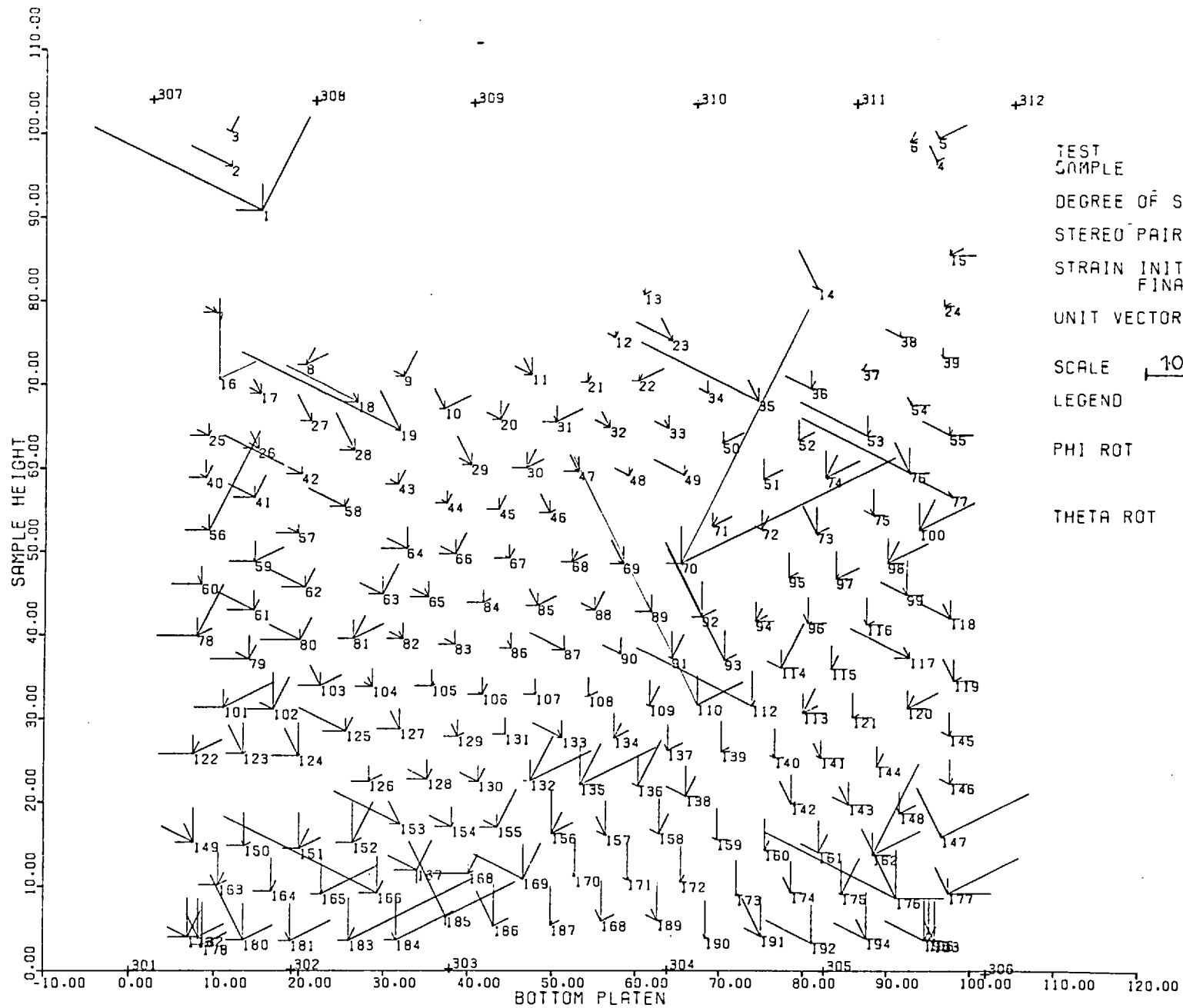


FIG 7.170 DISPLACEMENT - ROTATION FIELD OF MARKERS IN XY PLANE



TEST
SAMPLE

DEGREE OF SAT.

STEREO PAIR NO.

STRAIN INITIAL
FINAL

UNIT VECTOR DISP.

SCALE

LEGEND

PHI ROT

THETA ROT

5201/3
PLANE STRAIN (DRAINED)
POLYPROPYLENE SPHERES

FULLY SAT.

FIRST 3

FINAL 4

2.019

3.289

HOR. X
VER. Y

2mm

.2rad

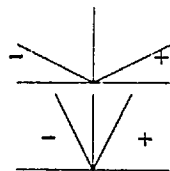
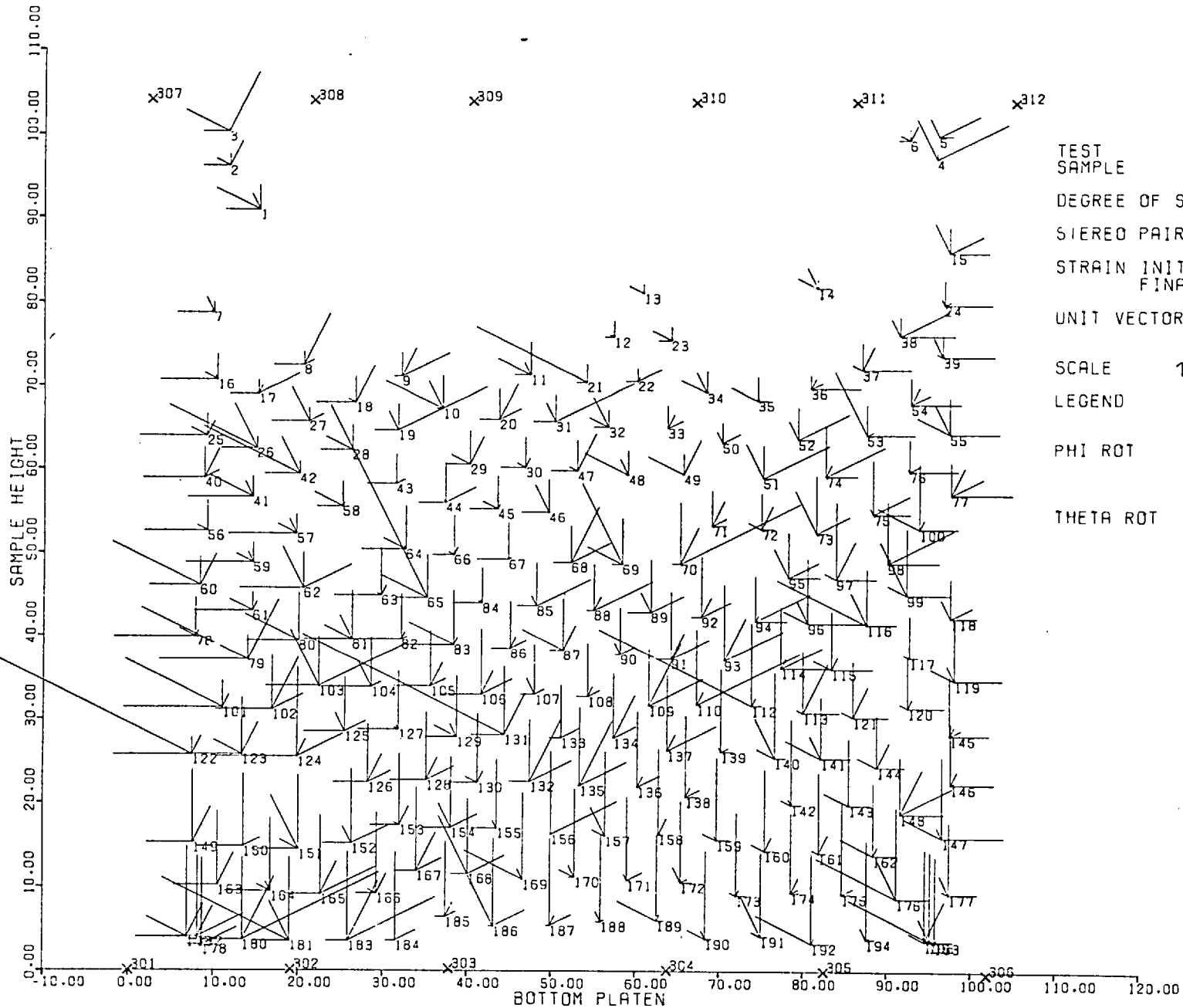


FIG 7.171 DISPLACEMENT - ROTATION FIELD OF MARKERS IN XY PLANE



TEST
SAMPLE

DEGREE OF SAT.

STEREO PAIR NO.

STRAIN INITIAL
FINAL

UNIT VECTOR DISP.

SCALE 10mm
ROT.

LEGEND

PHI ROT

THETA ROT

5201/4
PLANE STRAIN (DRAINED)
POLYPROPYLENE SPHERES

FULLY SAT.

FIRST 4
FINAL 5

3.289
5.924

HOR.X 2mm
VER.Y .2rad

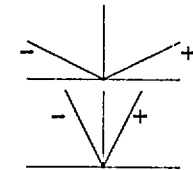
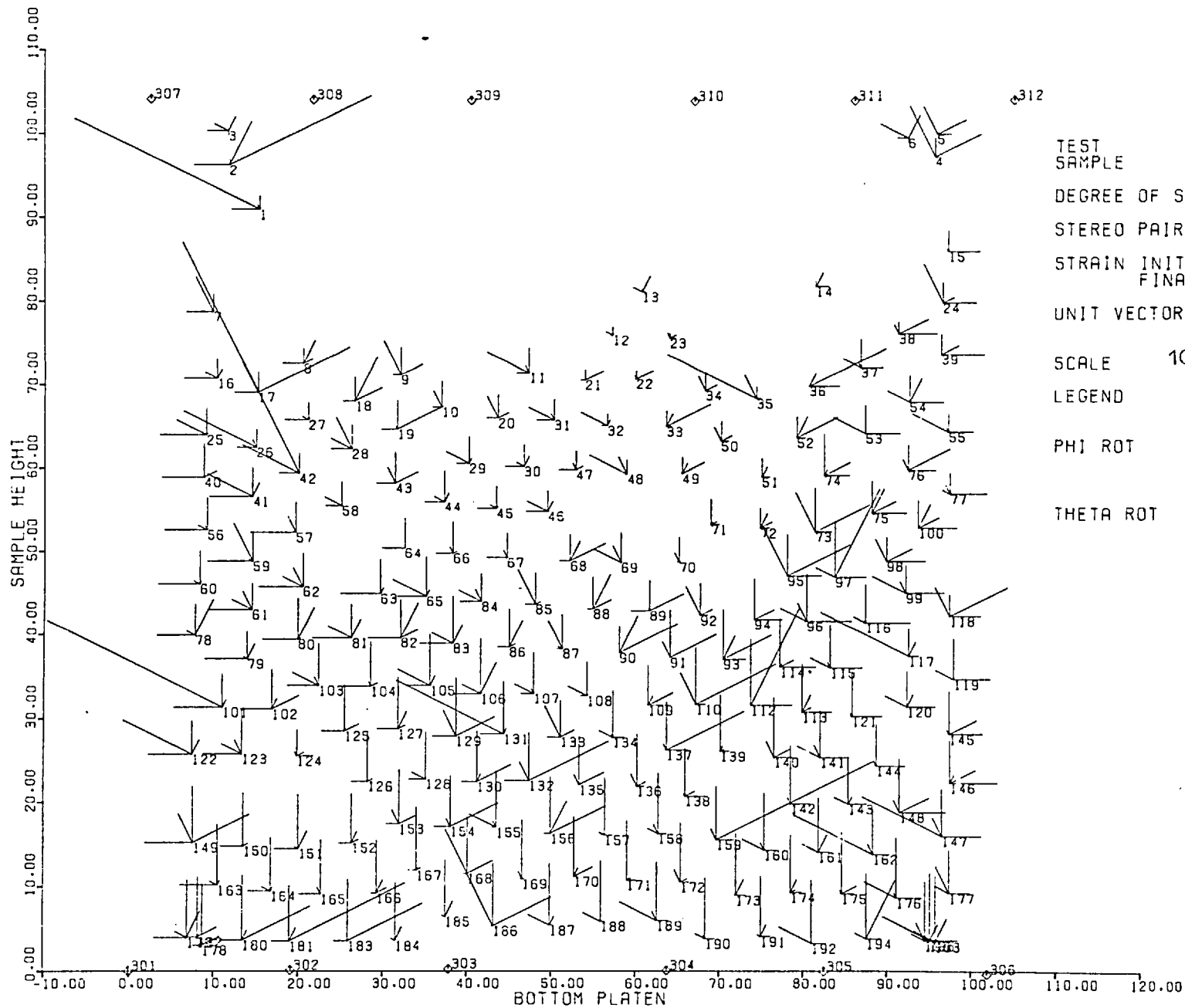


FIG 7.172 DISPLACEMENT - ROTATION FIELD OF MARKERS IN XY PLANE



TEST
SAMPLE

DEGREE OF SAT.

STEREO PAIR NO.

STRAIN INITIAL
FINAL

UNIT VECTOR DISP.

SCALE 10mm
LEGEND

PHI ROT

THETA ROT

5201/5

PLANE STRAIN (DRAINED)
POLYPROPYLENE SPHERES

FULLY SAT.

FIRST 5
FINAL 6

5.924
7.754

HOR.X 2mm
VER.Y .2rad

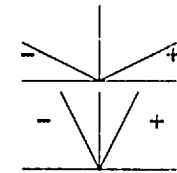
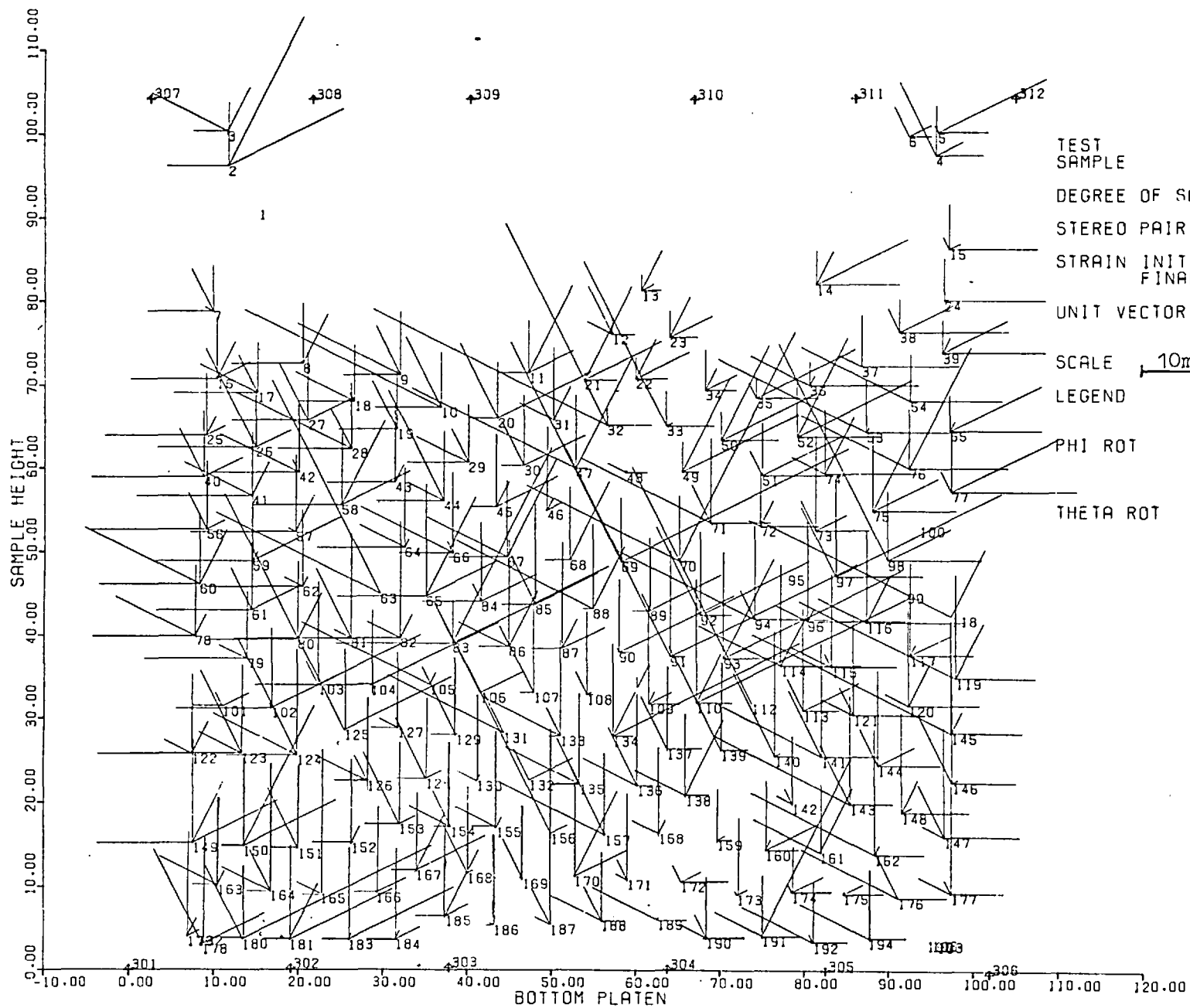


FIG 7.173 DISPLACEMENT - ROTATION FIELD OF MARKERS IN XY PLANE



TEST
SAMPLE

DEGREE OF SAT.

STEREO PAIR NO.

STRAIN INITIAL
FINAL

UNIT VECTOR DISP.

ROT.

SCALE

LEGEND

PHI ROT

THETA ROT

5201/6
PLANE STRAIN (DRAINED)
POLYPROPYLENE SPHERES

FULLY SAT.

FIRST 6
FINAL 7

7.754
13.800

HOR. X 3mm
VER. Y 2rad

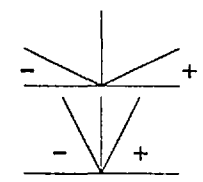


FIG 7.174 DISPLACEMENT - ROTATION FIELD OF MARKERS IN XY PLANE

5201/1/0

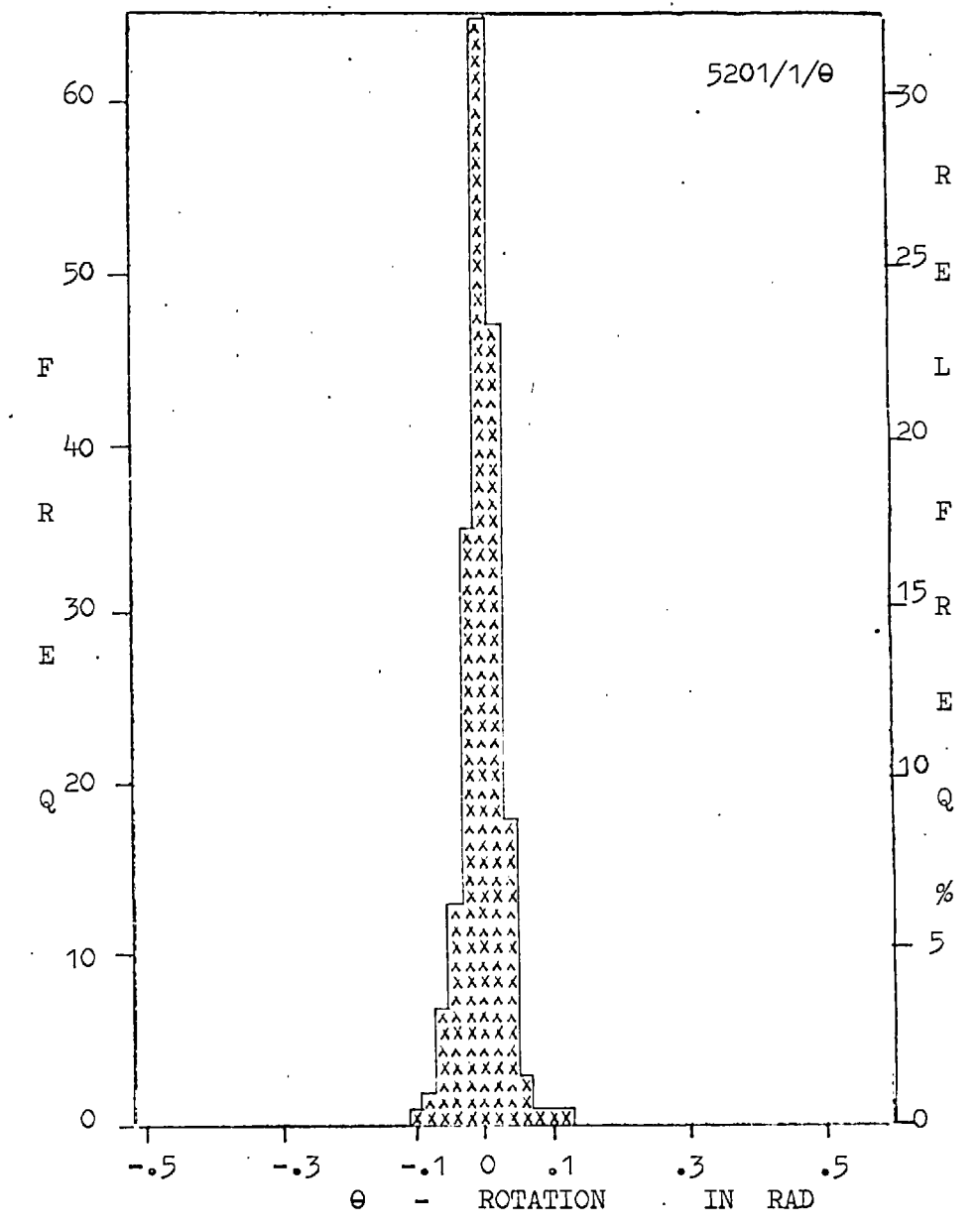
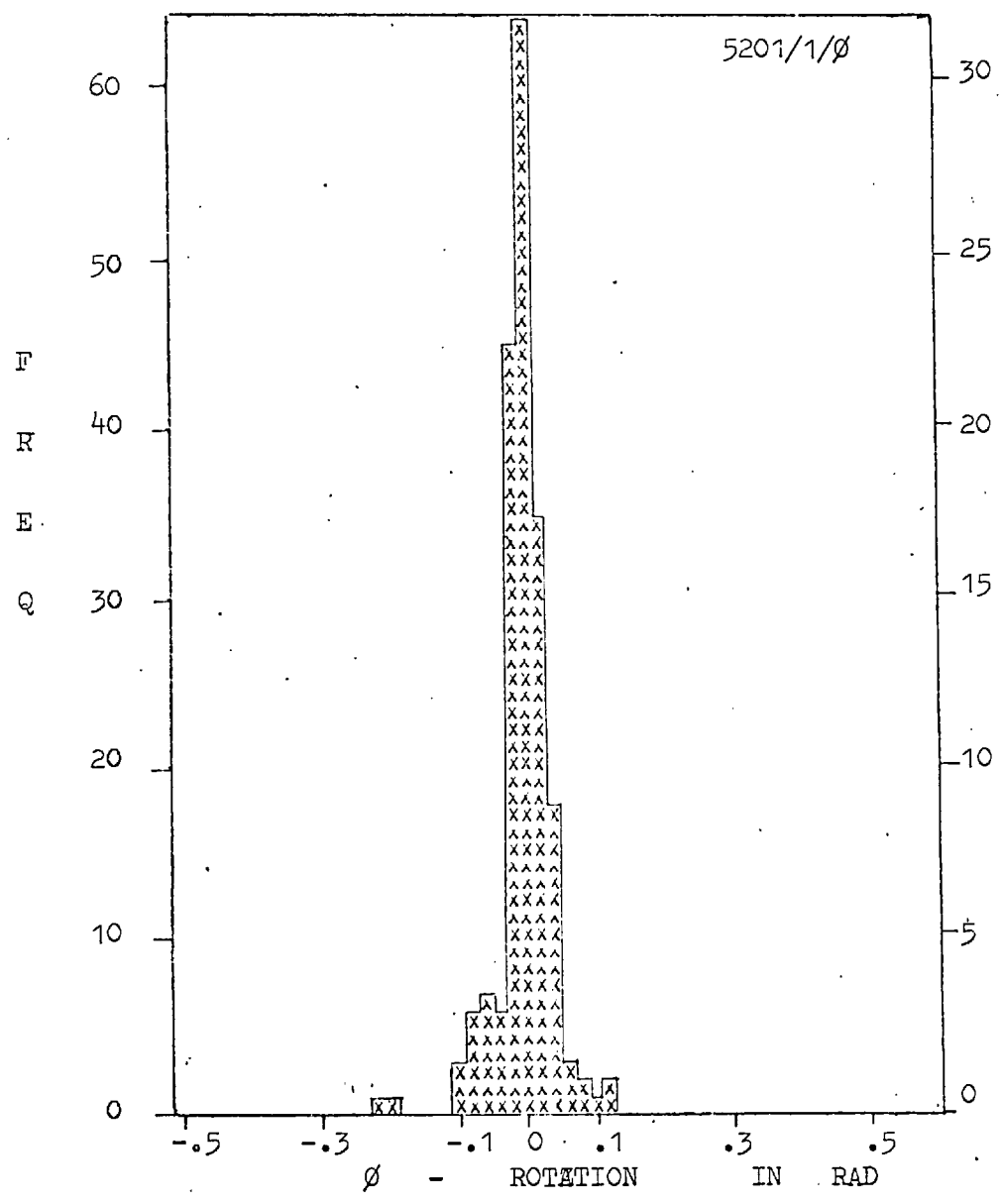


FIG. 7.175

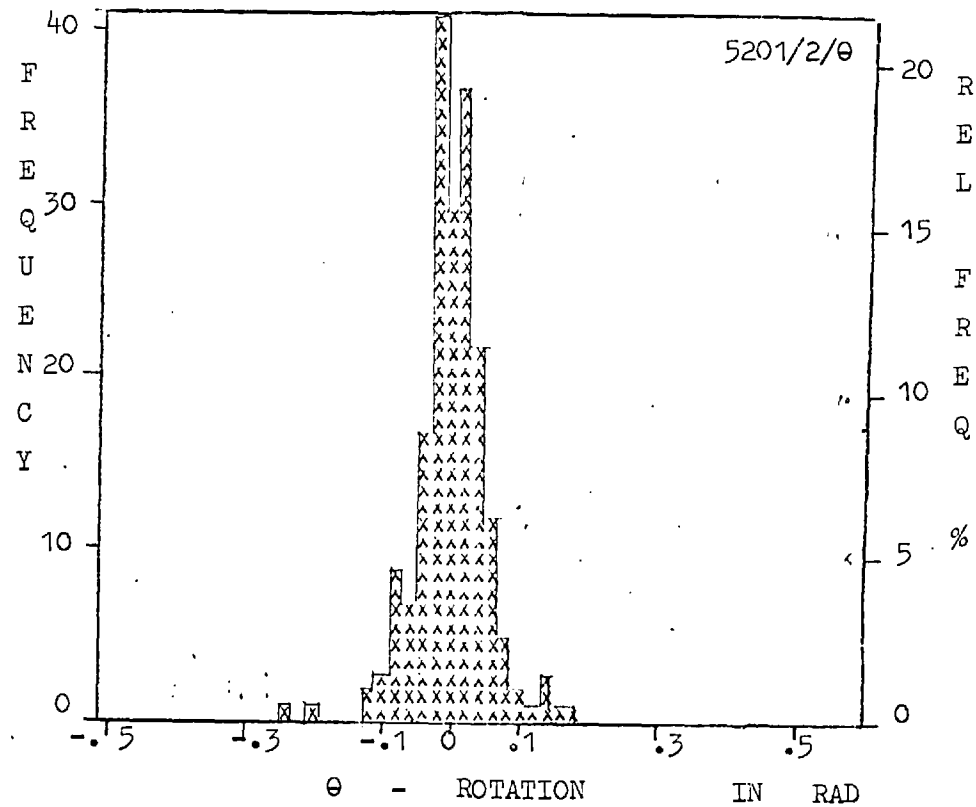
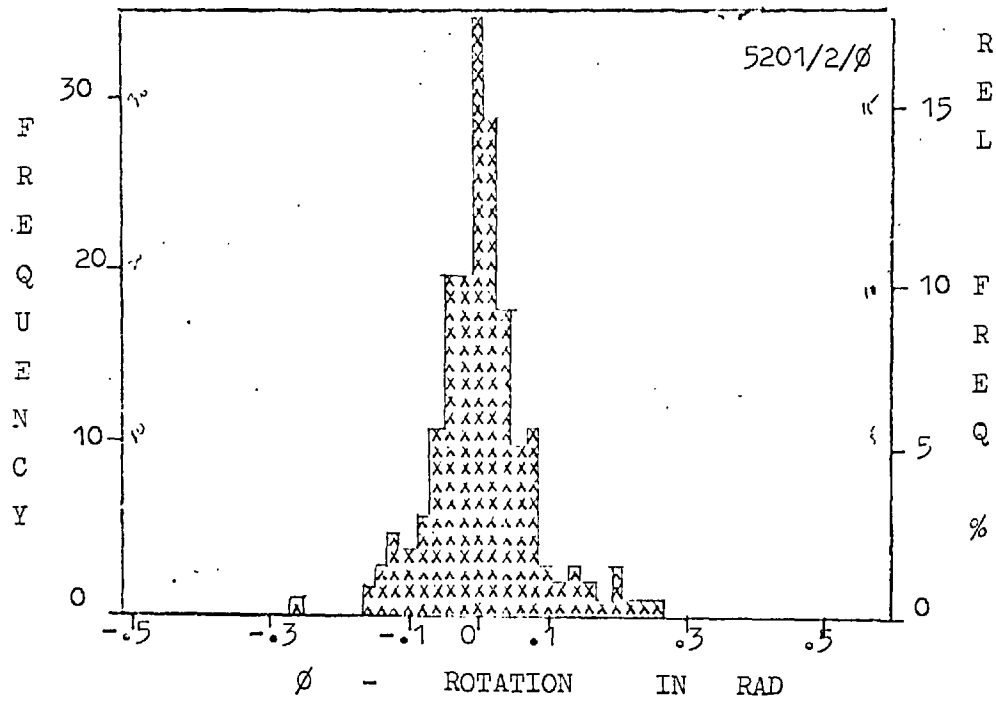


FIG. 7.176

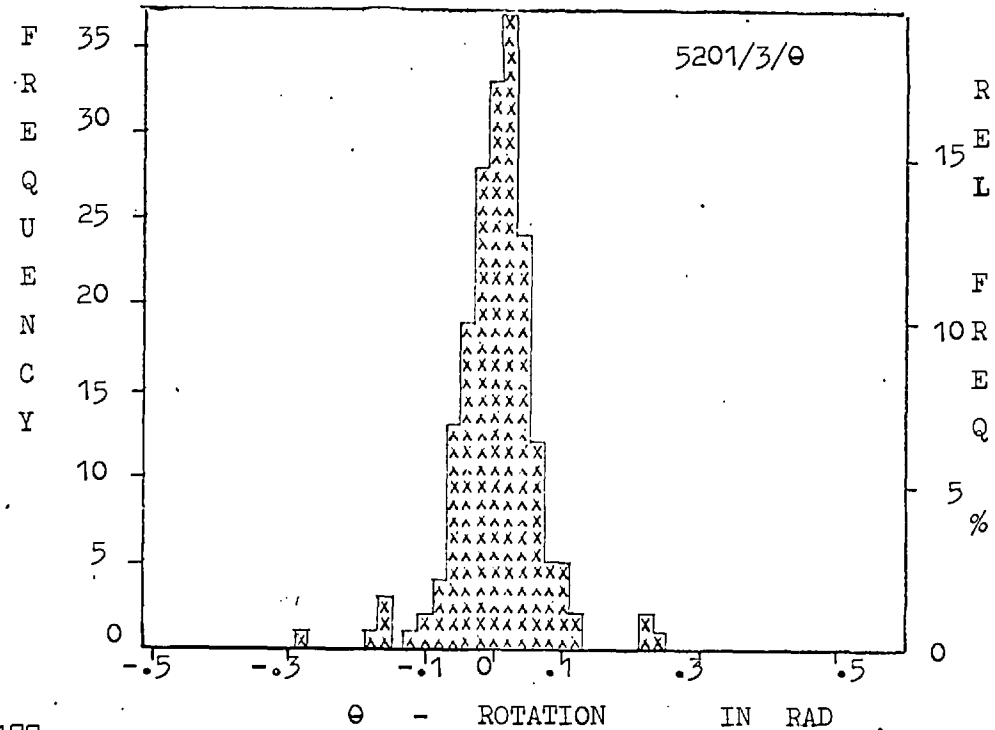
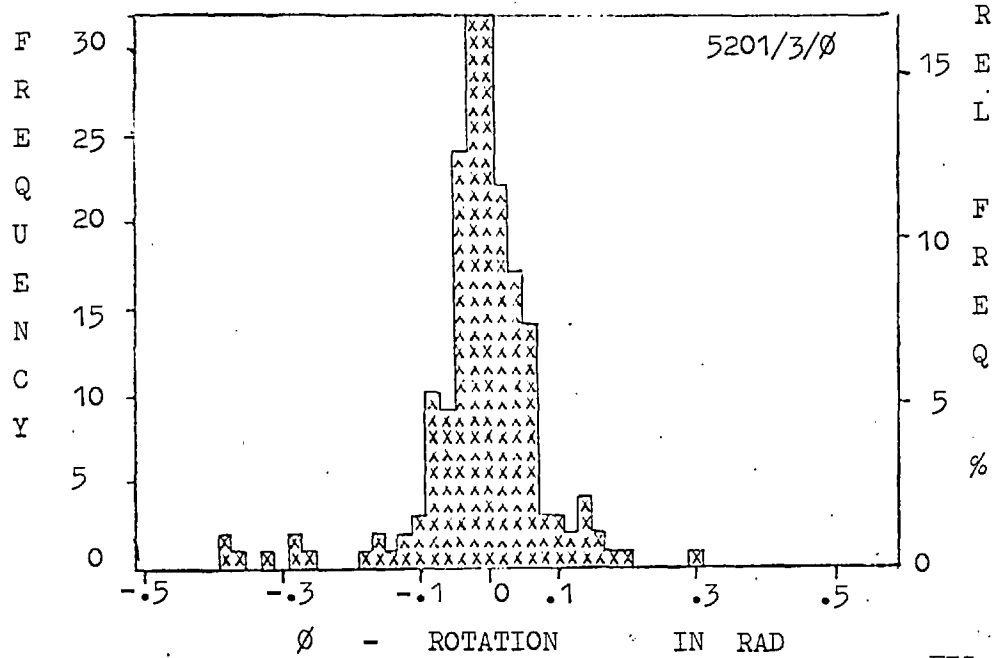


FIG. 7.177

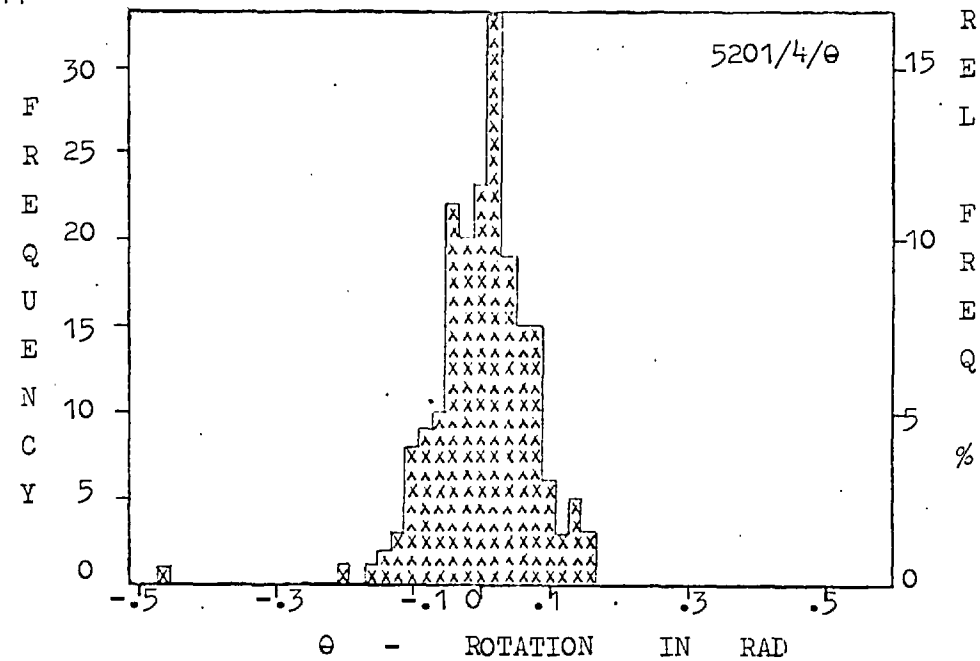
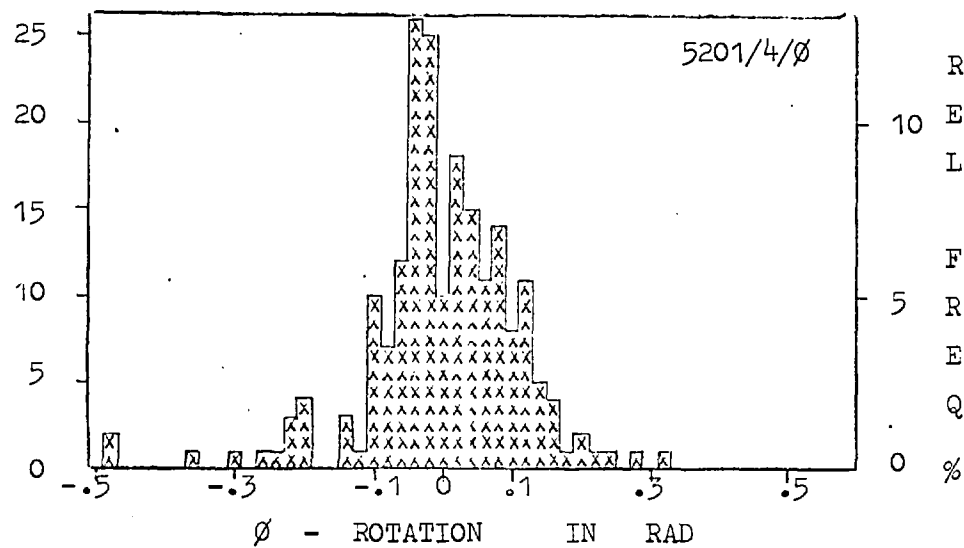


FIG. 7.178

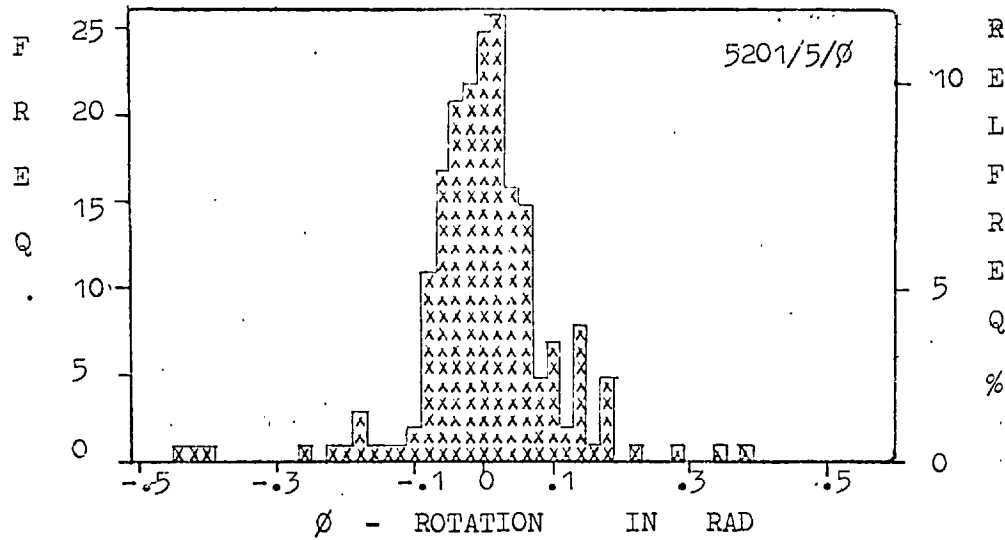


FIG. 7.179

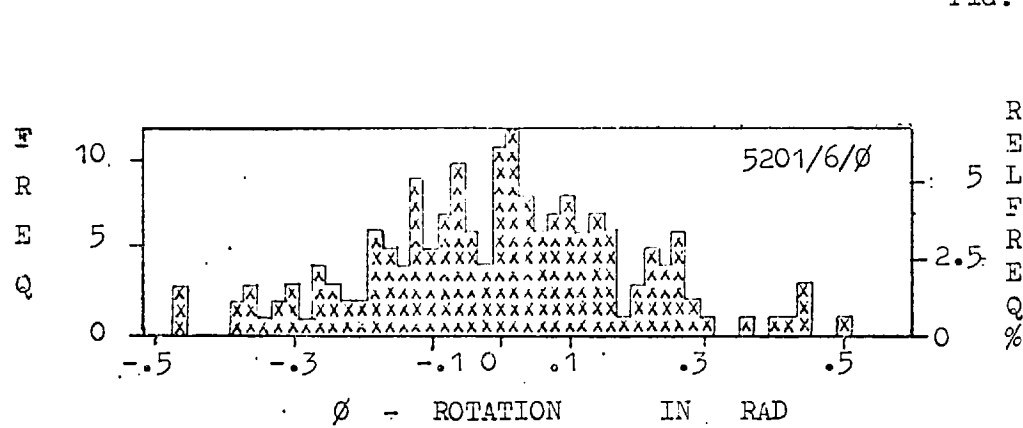
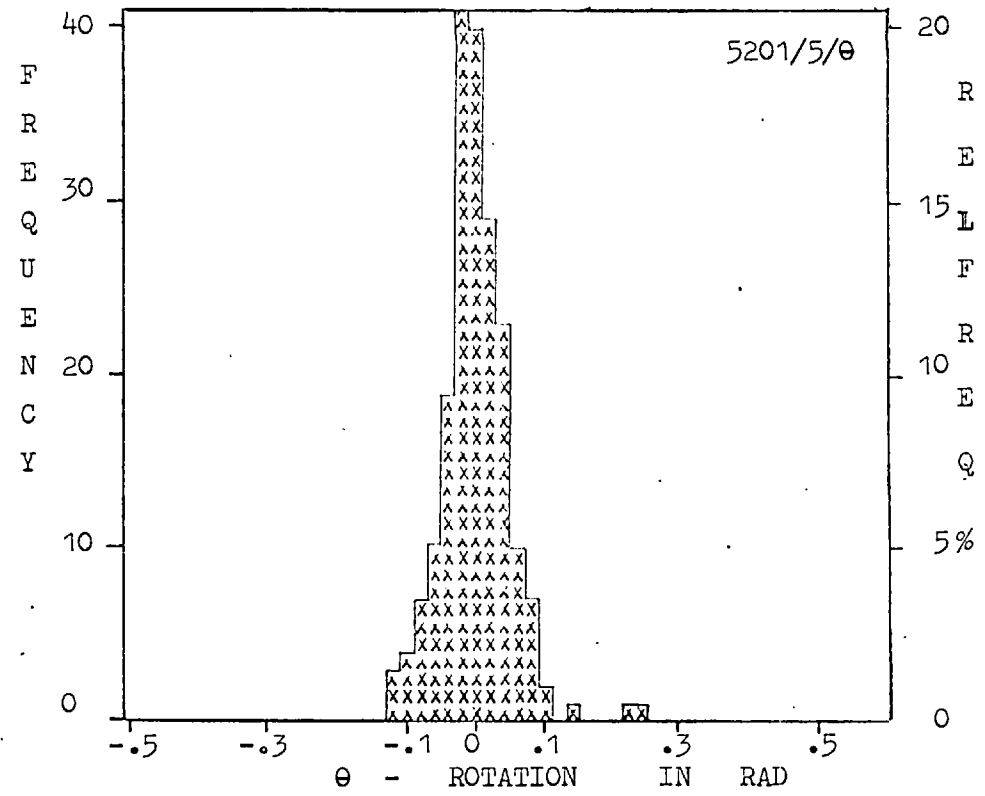
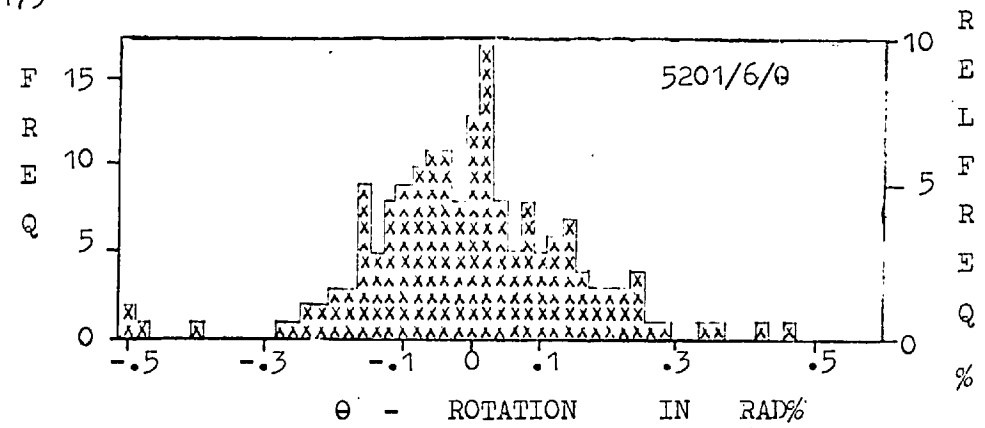
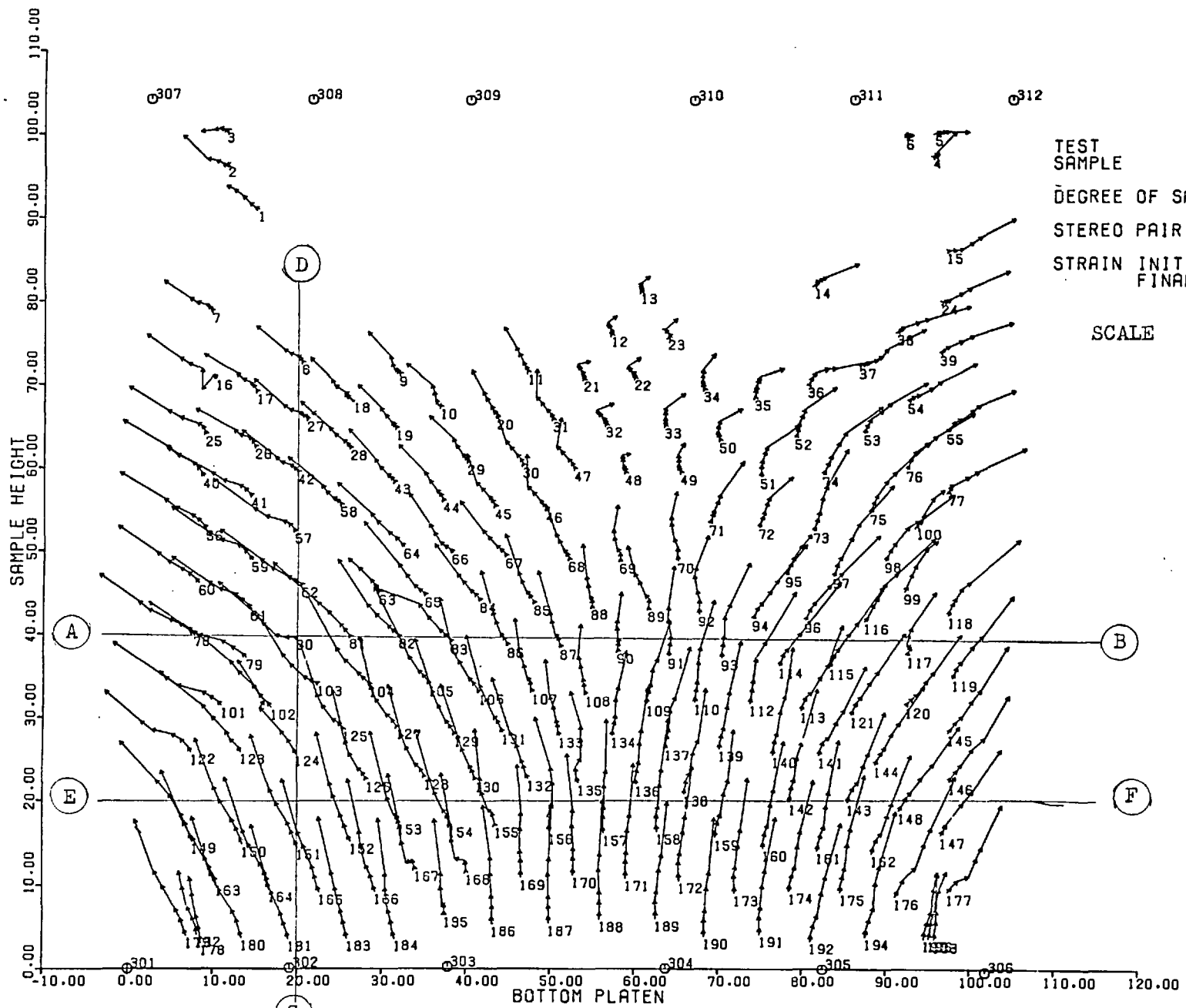


FIG. 7.180





TEST SAMPLE
 DEGREE OF SAT.
 STEREO PAIR NO.
 STRAIN INITIAL
 FINAL

5201
 PLANE STRAIN (DRAINED)
 POLYPROPYLENE BALLS
 FULLY SAT.
 FIRST 1
 LAST 7
 0.000
 13.800

SCALE

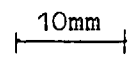
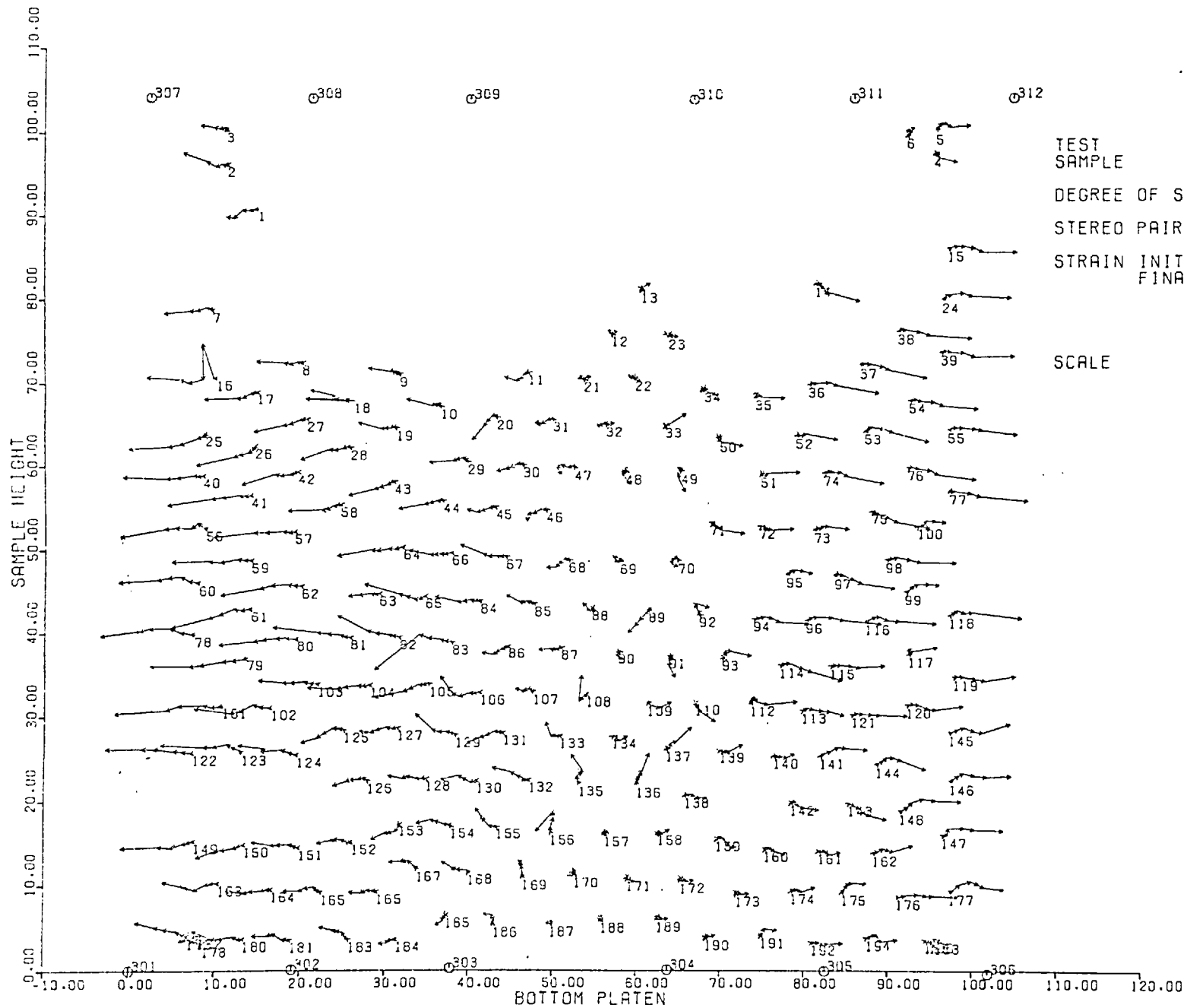


FIG 7.181

TRACE OF DISPLACEMENTS OF MARKER CENTRES ON XY PLANE



TEST
SAMPLE

DEGREE OF SAT.

STEREO PAIR NO.

STRAIN INITIAL
FINAL

SCALE

5201

PLANE STRAIN (DRAINED)
POLYPROPYLENE BALLS

FULLY SAT.

FIRST 1
LAST 7
0.0
13.8

10mm

FIG 7.182

TRACE OF DISPLACEMENTS OF MARKER CENTRES ON XZ PLANE

TEST NO 5201
DEF. INC. 5
POLYPROPYLENE

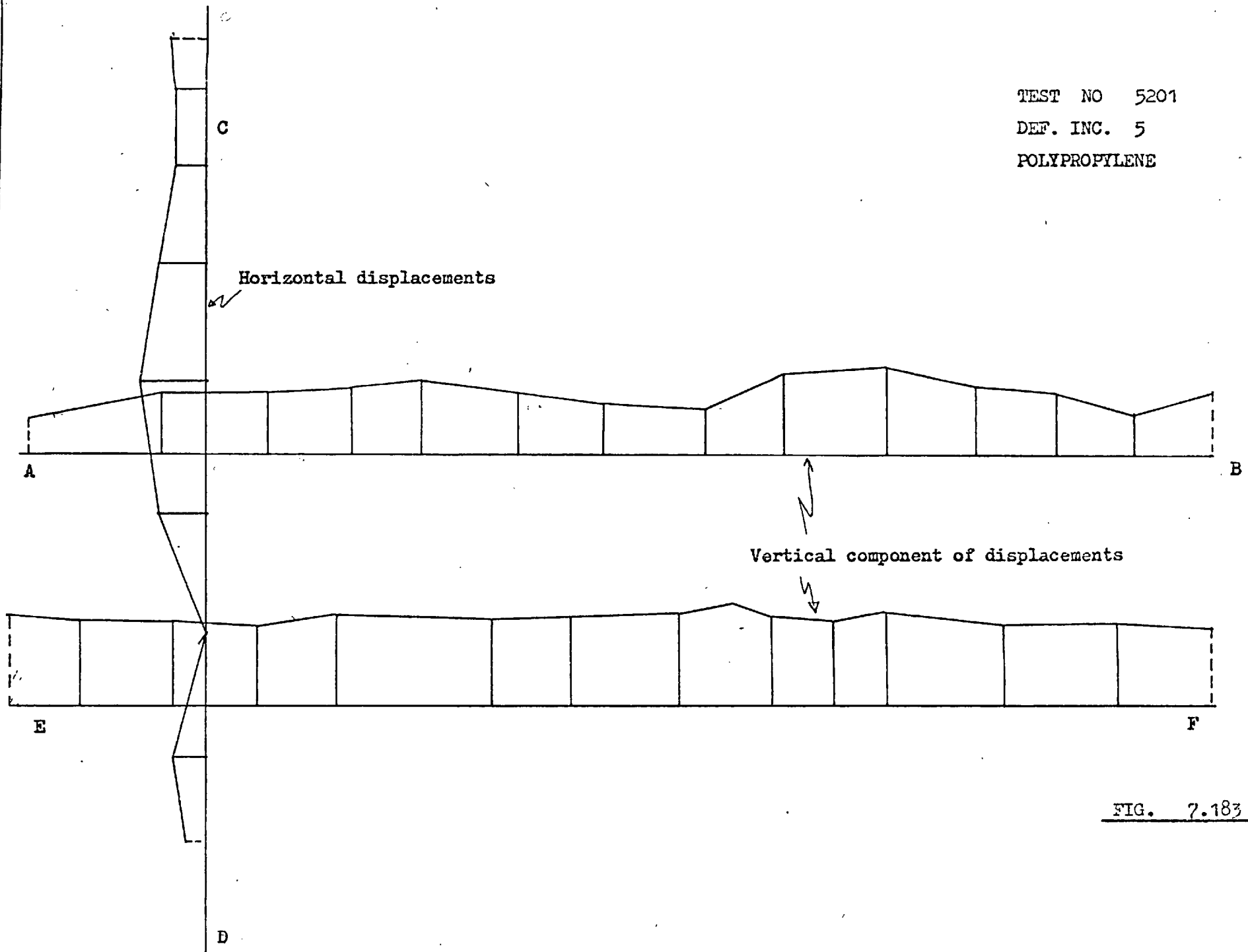


FIG. 7.183

0.69	-0.48	0.60
0.24	-0.68	1.09
0.43	0.41	1.92
0.63	-0.54	2.78
0.49	-0.87	2.43
-0.84	-0.85	0.40

0.65 0.65 SHEAR STRAIN 4200.3

0.16	-1.85	-2.22
-2.95	-8.04	6.72
-4.49	-1.56	1.74
-1.74	-2.61	-5.92
1.05	-0.28	1.81
-0.47	-1.68	-1.88

0.14 SHEAR STRAIN 4200.6

SAMPLE BOUNDARY

0.33	-0.91	-0.30
0.17	-0.74	-0.09
0.44	0.35	0.13
0.69	-0.03	-0.54
1.27	-0.20	0.11
0.09	-0.36	-0.08

0.28 0.28 SHEAR STRAIN 4200.2

SAMPLE BOUNDARY

-0.22	-1.63	1.33
-0.31	-1.30	0.77
-2.35	-0.19	1.54
-0.49	0.01	2.36
1.35	-0.03	1.33
-0.33	-1.23	-0.95

0.52 SHEAR STRAIN 4200.5

SAMPLE BOUNDARY

0.19	-0.51	0.16
-0.10	-0.55	0.24
0.28	0.11	0.35
0.18	-0.18	-0.03
0.27	-0.00	0.35
-0.00	-0.21	-0.03

0.25 0.25 SHEAR STRAIN 4200.1

SAMPLE BOUNDARY

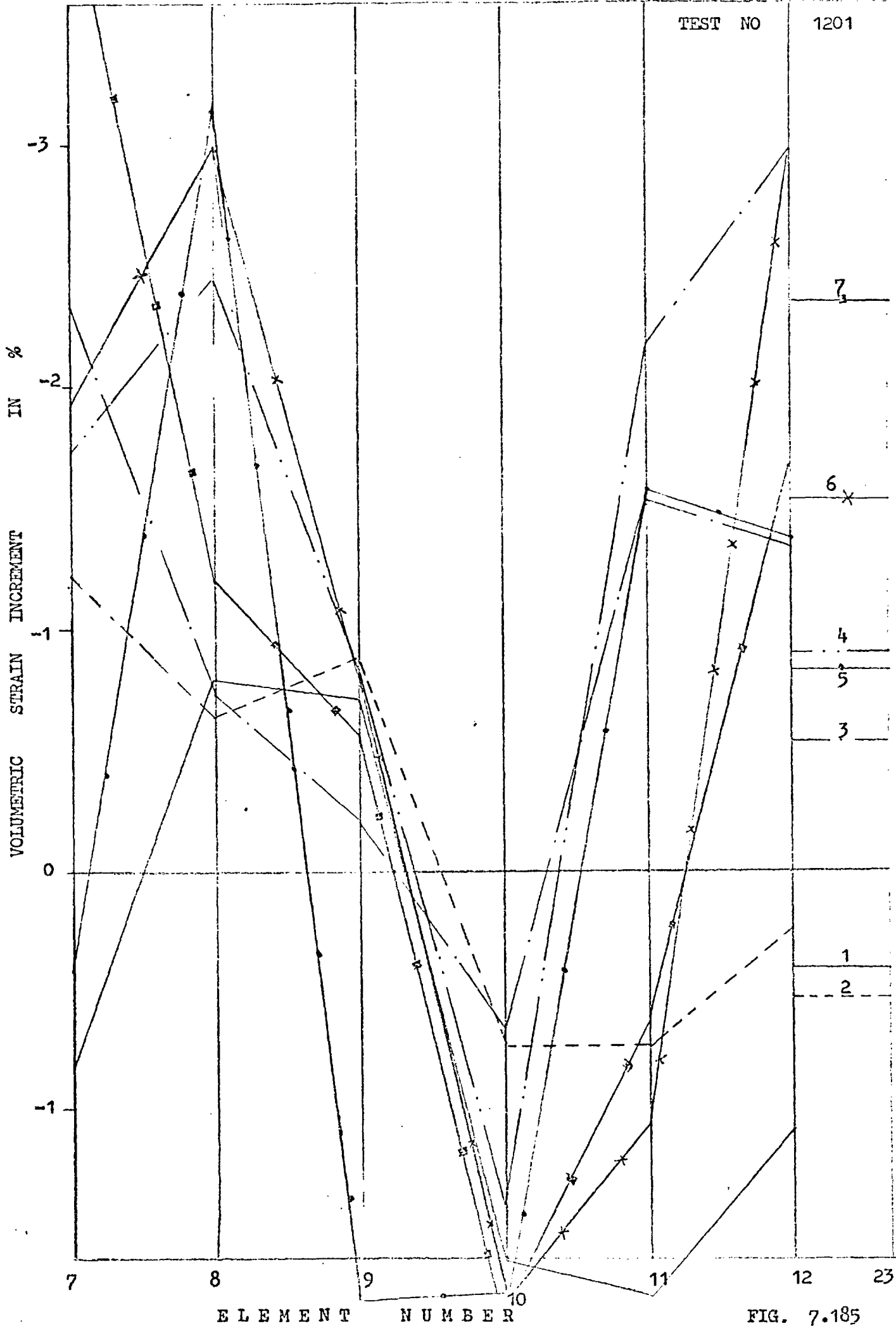
0.01	-0.60	1.59
0.71	-1.08	2.33
0.11	-0.10	3.20
0.64	-0.71	4.14
0.91	-0.66	3.21
-0.39	-1.06	-1.30

0.77 SHEAR STRAIN 4200.4

FIG. 7.184

TEST NO

1201



ELEMENT NUMBER

FIG. 7.185

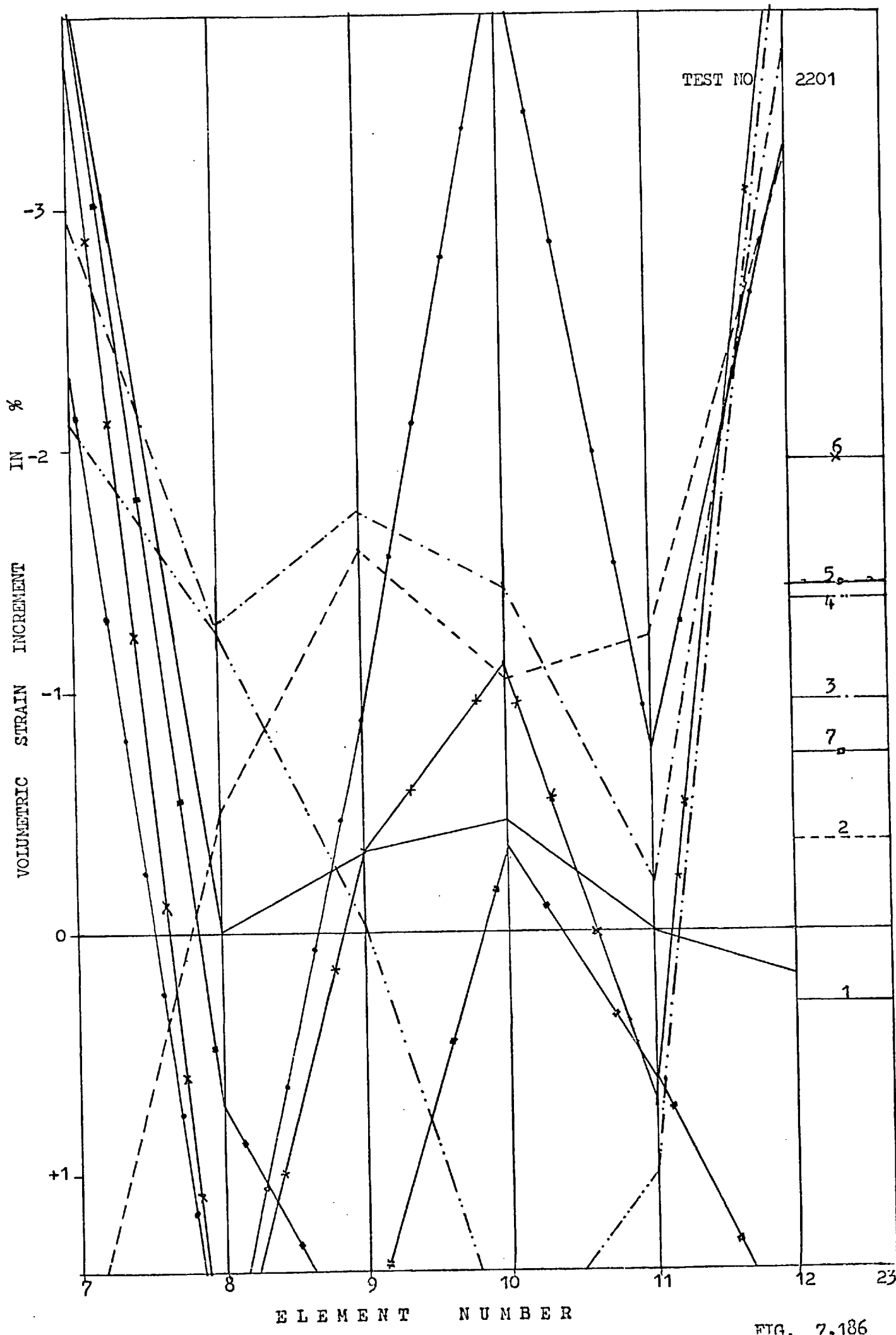


FIG. 7.186

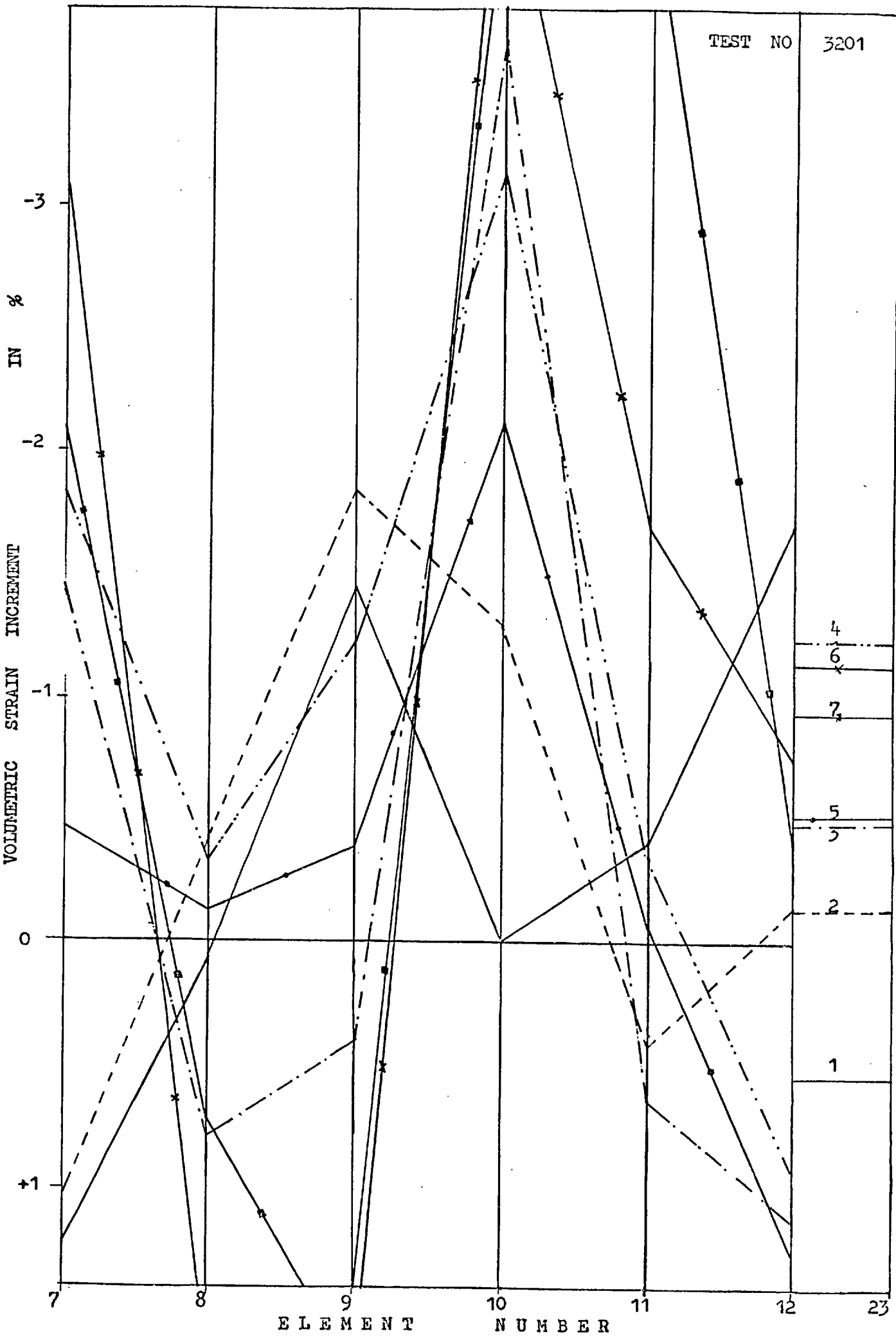
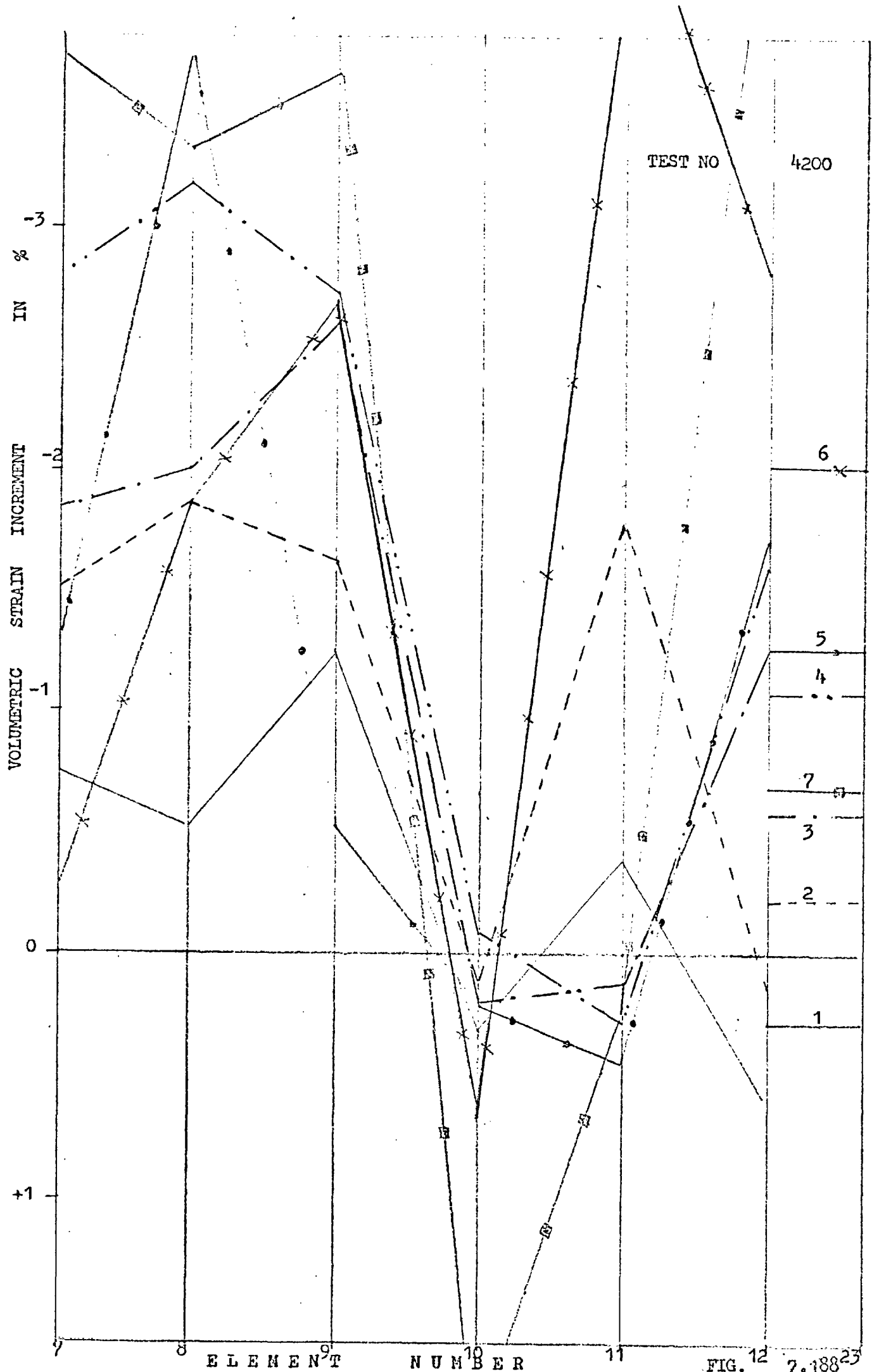


FIG. 7.187



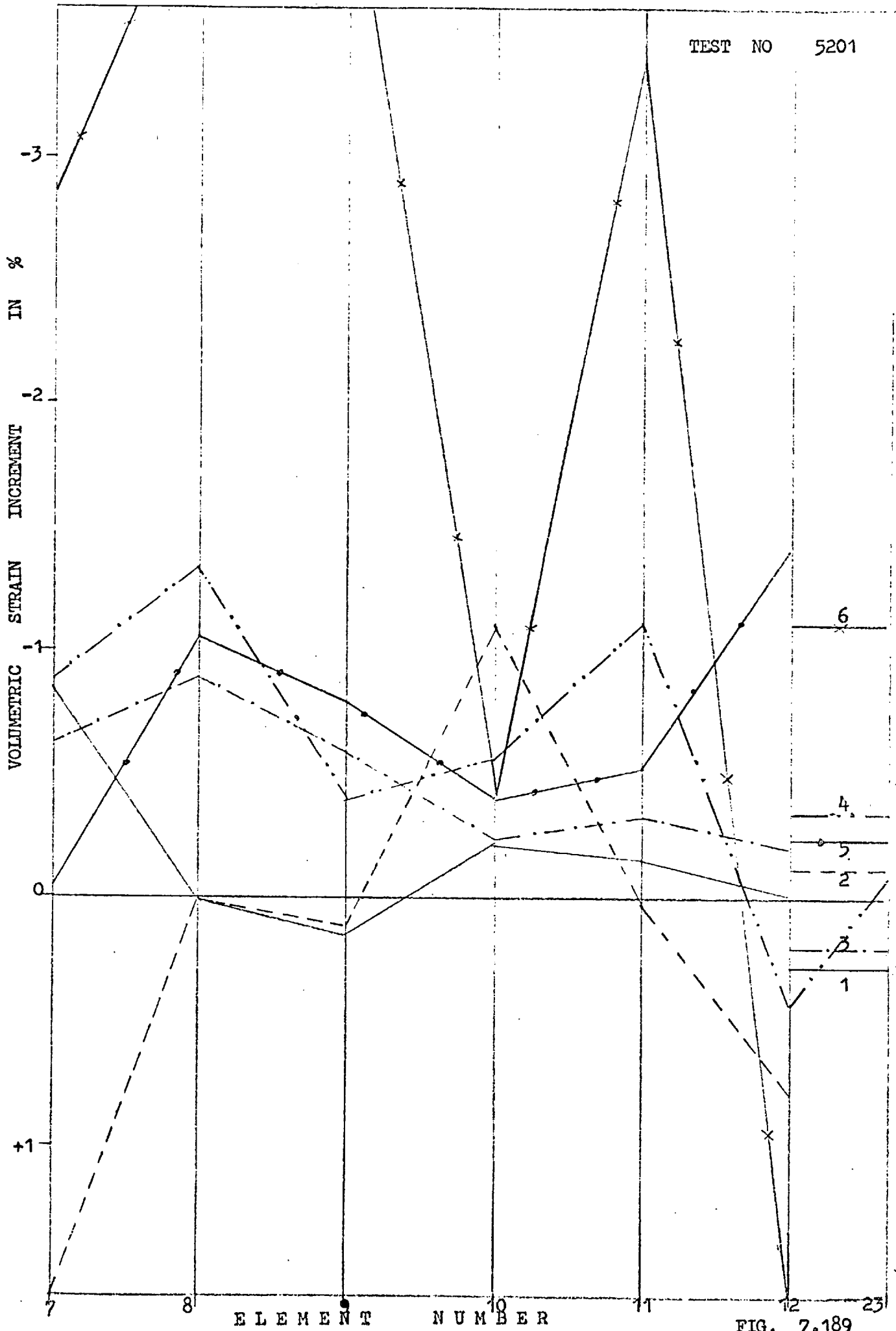


FIG. 7.189

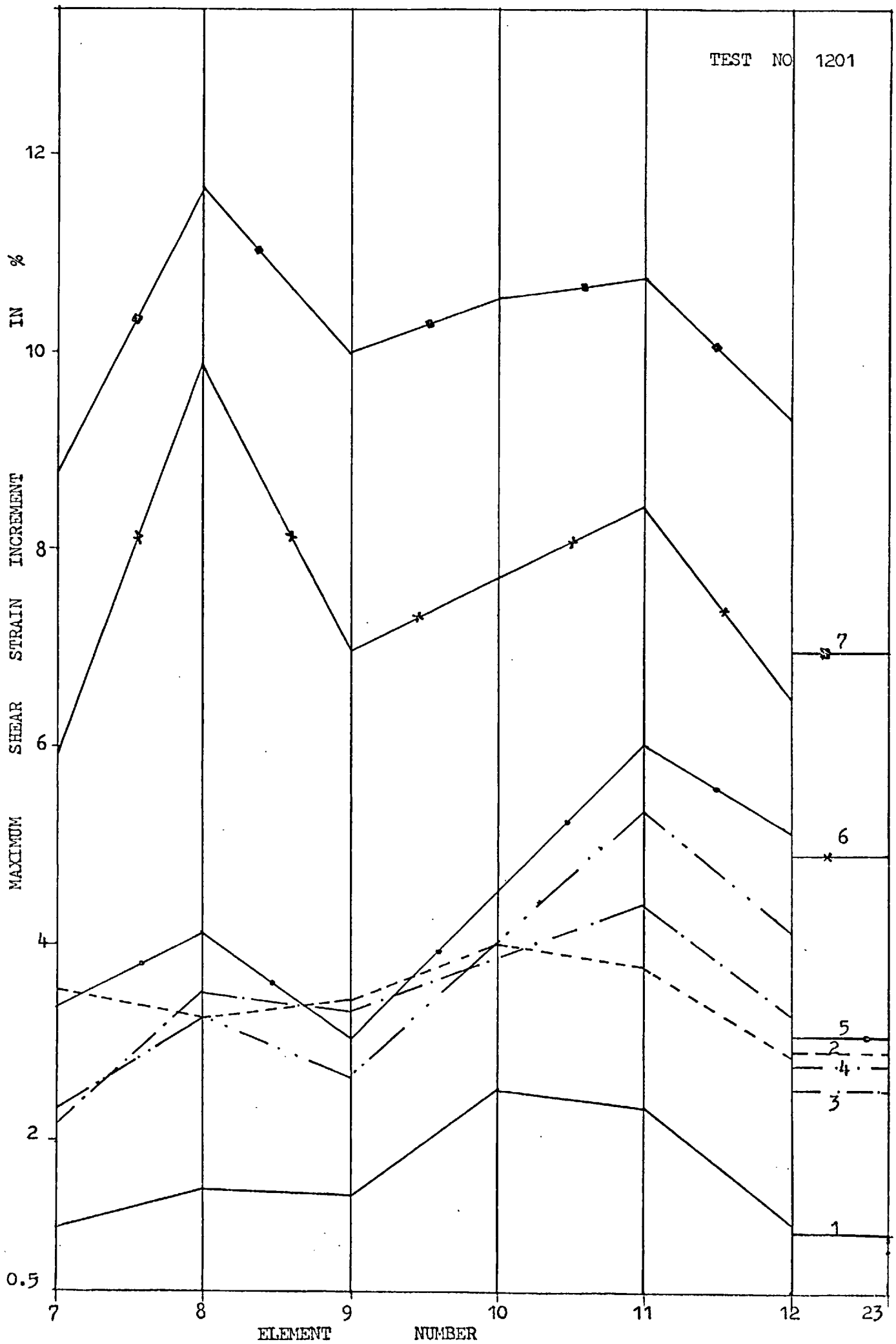


FIG. 7.190

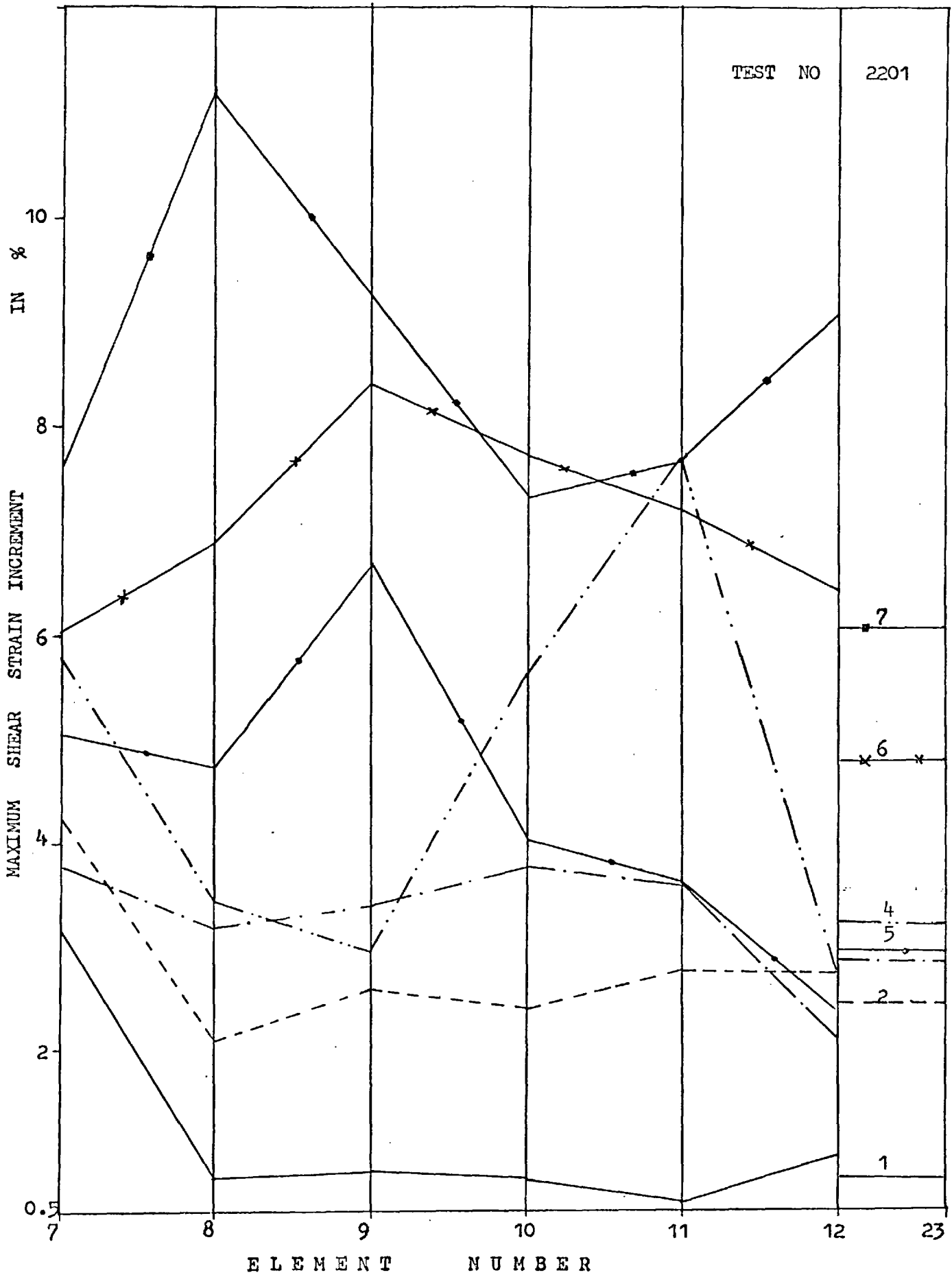
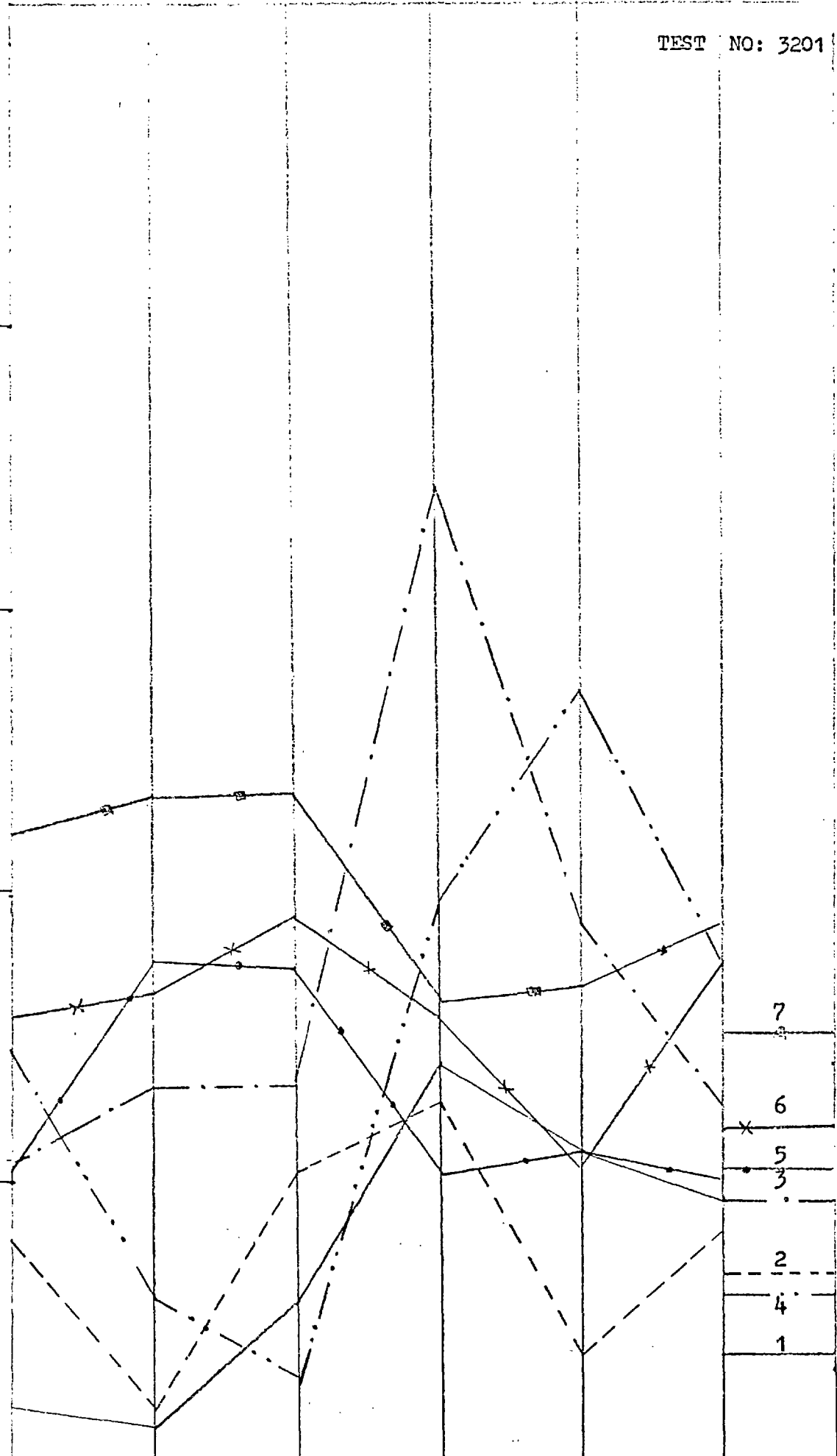


FIG. 7. 191

TEST NO: 3201

IN %
16
12
8
4
0

MAXIMUM SHEAR STRAIN INCREMENT



ELEMENT NUMBER

FIG. 7.192

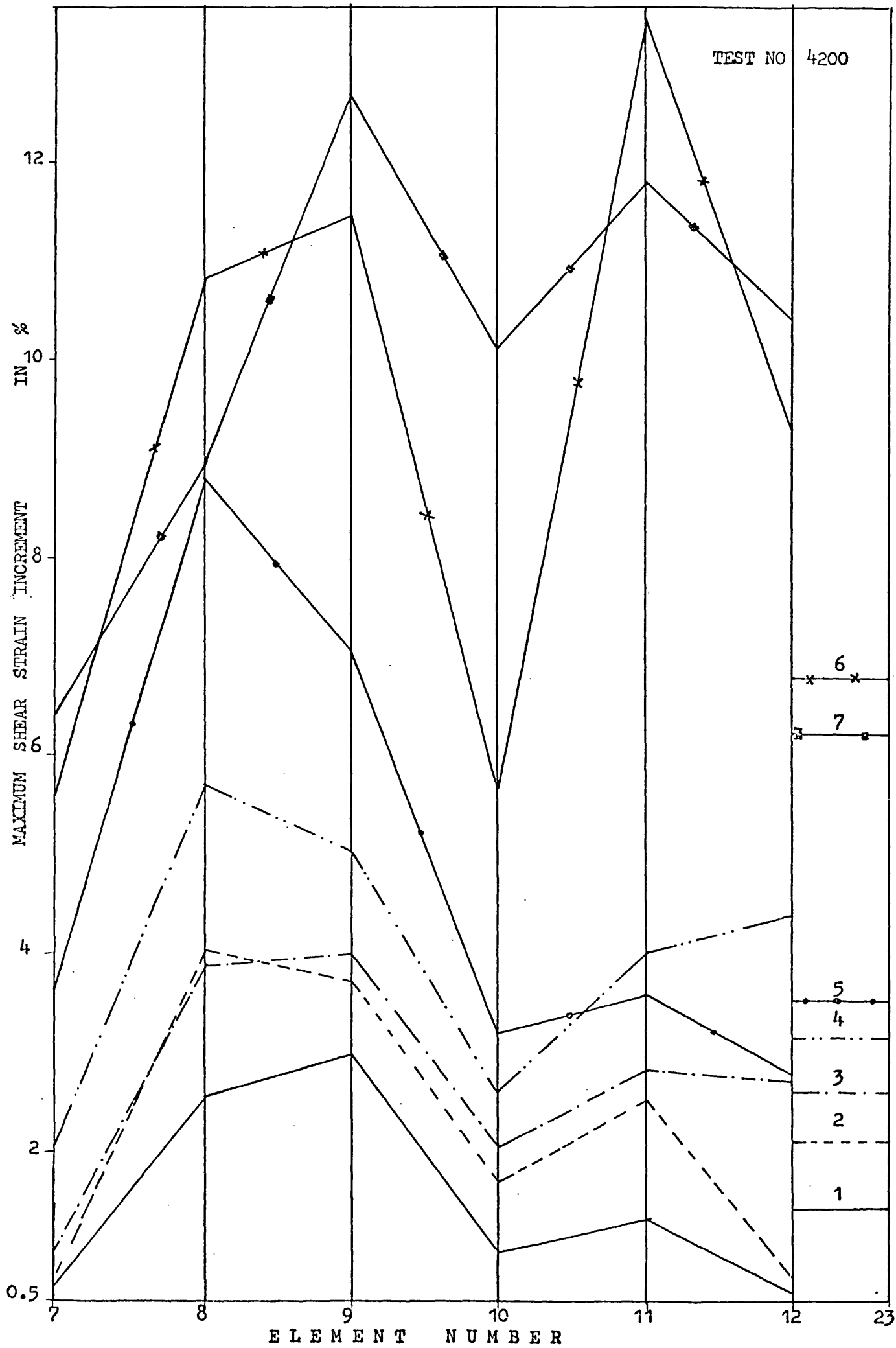


FIG. 7.193

TEST NO 5201

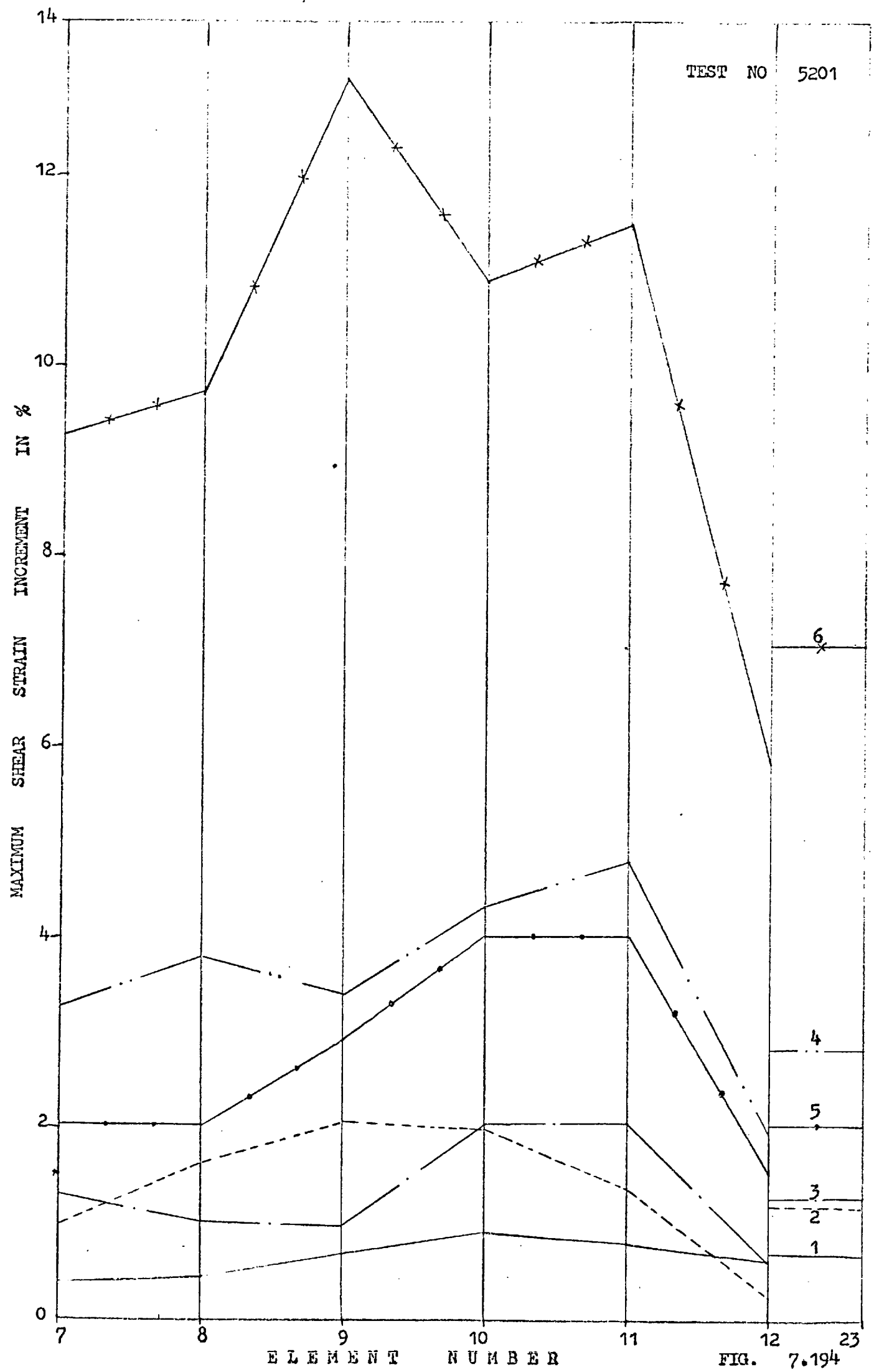


FIG. 7.194

Table 7.1 Statistical Analysis of Incremental Rotations (Relative) of Marker Particles in Dry Test Samples

S. No.	Material	Test No.	R O T	P A R	Deformation Increment						
					1	2	3	4	5	6	7
1	Gravel	1200	φ	N	72	72	70	70	71	69	
				x	-0.0022	-0.0008	-0.0074	0.0029	0.0218	0.0125	
				σ	0.0190	0.0462	0.0724	0.0915	0.1321	0.0963	
			θ	N	69	71	69	69	71	69	
				x	0.0159	-0.0037	-0.0026	0.0081	-0.0135	-0.0078	
				σ	0.0698	0.0687	0.0800	0.0907	0.1296	0.1301	
2	Glass	2200	φ	N	103	103	107	108	106	101	98
				x	-0.0012	0.0170	-0.0120	0.0094	0.0230	0.0214	0.0077
				σ	0.0618	0.1327	0.1122	0.1197	0.1601	0.2039	0.2026
			θ	N	101	103	107	102	101	103	102
				x	0.0012	-0.0068	0.0092	-0.0037	-0.0186	-0.0134	-0.0086
				σ	0.0802	0.0950	0.0970	0.1128	0.1210	0.1451	0.1518
3	Ceramic	3200	φ	N	117	114	116	118	108	107	
				x	0.0089	0.0052	0.0110	0.0020	-0.0330	-0.0090	
				σ	0.0594	0.1260	0.1509	0.1611	0.1936	0.1738	
			θ	N	114	114	111	115	106	108	
				x	0.0014	-0.0058	-0.0049	0.0162	-0.0219	0.0168	
				σ	0.0847	0.1122	0.1123	0.1323	0.1749	0.1405	
4	PTFE	4200	φ	N	175	175	174	174	173	170	165
				x	0.0077	0.0093	0.0084	0.0041	0.0206	0.0262	0.0026
				σ	0.0401	0.0509	0.0780	0.0667	0.0912	0.1421	0.1325
			θ	N	175	175	174	174	174	174	171
				x	-0.0074	-0.0014	0.0055	0.0023	-0.0049	-0.0053	-0.0063
				σ	0.0353	0.0423	0.0492	0.0539	0.0633	0.0735	0.0608
5	Polypropylene	5150	φ	N	205	202	201	202	197	201	191
				x	-0.0018	-0.0029	-0.0066	0.0024	0.0103	-0.0041	0.0073
				σ	0.0522	0.0983	0.1092	0.1302	0.1648	0.1513	0.1774
			θ	N	198	198	200	201	193	191	190
				x	-0.0086	0.0146	-0.0047	0.0209	-0.0159	0.0117	-0.0145
				σ	0.0800	0.0774	0.0859	0.1075	0.1451	0.1126	0.1034

Table 7.2 Statistical Analysis of Incremental Rotations (Relative) of Marker Particles in Saturated Test Samples.

S. No.	Material	Test No.	R O T	P A R	Deformation Increment						
					1	2	3	4	5	6	7
1	Gravel	1201	ϕ	N	70	71	68	65	69	67	62
				x	-.0083	.0039	0.0065	-.0028	0.0093	-.0900	0.0061
				σ	0.0682	0.0842	0.1199	0.100	0.1233	0.1115	0.1633
			θ	N	69	68	66	67	69	70	66
				x	-.0064	-.0127	0.0076	-.0245	.0148	0.1200	-.0064
				σ	0.1053	0.0800	0.1061	0.1163	0.0773	0.1088	0.1266
2	Glass	2201	ϕ	N	104	102	100	96	95	97	88
				x	0.0046	0.0037	0.0010	-.0108	0.0175	-.0167	0.0048
				σ	0.0622	0.0966	0.0880	0.1099	0.1262	0.1724	0.2011
			θ	N	102	99	98	93	94	92	87
				x	-.0078	0.0210	-.0065	0.0239	-.0170	0.0020	-.0064
				σ	0.1130	0.1057	0.0998	0.1225	0.1489	0.1540	0.1552
3	Ceramic	3201	ϕ	N	114	114	113	108	114	120	117
				x	-.0084	-.0126	-.0255	-.0087	-.0026	-.0073	-.0292
				σ	0.0824	0.1112	0.1320	0.1199	0.1325	0.1838	0.1886
			θ	N	117	116	115	114	114	119	116
				x	-.0024	0.0017	-.0026	-.0118	-.0084	0.0035	0.0307
				σ	0.0801	0.0966	0.0948	0.1194	.1061	0.1521	0.1589
4	PTFE	4201	ϕ	N	173	173	171	171	173	165	169
				x	-.0050	-.0071	-.0215	-.0130	0.0117	-.0127	0.0320
				σ	0.0390	0.0623	0.0799	0.1055	0.0924	0.1338	0.1337
			θ	N	173	173	172	172	173	170	165
				x	-.0044	-.0013	0.0	0.0038	-.0043	-.0024	-.0074
				σ	0.0223	0.0230	0.0281	0.0479	0.0365	0.0382	0.0392
5	Poly- propy- lene	5201	ϕ	N	194	192	193	200	199	182	
				x	-.0034	0.0064	-.0108	-.0005	0.0026	-.0015	
				σ	0.0401	0.0736	0.0878	0.1100	0.0999	0.1874	
			θ	N	194	195	193	199	198	179	
				x	0.0012	0.0010	0.0029	0.0040	-.0002	-.0068	
				σ	0.0208	0.0535	0.0601	0.0725	0.0495	0.1486	

Table 7.3 Statistical Analysis of Incremental Rotations (Absolute) of Marker Particles in Dry Test Samples

S. No.	Material	Test No.	R O T	P A R	Deformation Increment								
					1	2	3	4	5	6	7		
1	Gravel	1200	ϕ	N	72								
				x	0.0122	0.0314	0.0474	0.0623	0.0970	0.0764			
				σ	0.0147	0.0340	0.0552	0.0672	0.0923	0.0598			
			θ	N	69	71	69	69	71	69			
				x	0.0368	0.0419	0.0519	0.0557	0.0930	0.0815			
				σ	0.0614	0.0546	0.0609	0.0721	0.0913	0.1018			
2	Glass	2200	ϕ	N	103	103	107	108	106	101	98		
				x	0.0435	0.0897	0.0841	0.0846	0.1213	0.1666	0.1604		
				σ	0.0439	0.0992	0.0752	0.0852	0.1070	0.1195	0.1240		
			θ	N	101	103	107	102	101	103	102		
				x	0.0475	0.0674	0.0675	0.0821	0.0837	0.1101	0.1165		
				σ	0.0647	0.0703	0.0703	0.0774	0.0893	0.0954	0.0978		
2	Ceramic	3200	ϕ	N	117	114	116	118	108	107			
				x	0.0434	0.0884	0.1069	0.1129	0.1530	0.1350			
				σ	0.0415	0.0899	0.1071	0.1150	0.1232	0.1098			
			θ	N	114	114	111	115	106	108			
				x	0.0456	0.0700	0.0784	0.0892	0.1276	0.1065			
				σ	0.0714	0.0878	0.0805	0.0990	0.1217	0.0933			
4	PTFE	4200	ϕ	N	175	175	174	174	173	170	165		
				x	0.0243	0.0337	0.0472	0.0430	0.0571	0.1011	0.0850		
				σ	0.0336	0.0392	0.0626	0.0512	0.0741	0.1033	0.1016		
			θ	N	175	175	174	174	174	174	171		
				x	0.0186	0.0219	0.0244	0.0253	0.0323	0.0389	0.0395		
				σ	0.0309	0.0361	0.0430	0.0477	0.0546	0.0627	0.0466		
5	Poly- pro- pylene	5150	ϕ	N	205	202	201	202	197	201	191		
				x	0.0251	0.0629	0.0748	0.0968	0.1284	0.1171	0.1382		
				σ	0.0458	0.0756	0.0798	0.0871	0.1038	0.0951	0.1114		
			θ	N	198	198	200	201	193	191	190		
				x	0.0354	0.0505	0.0567	0.0766	0.1048	0.0844	0.1034		
				σ	0.0723	0.0604	0.0647	0.0783	0.1016	0.0755	0.0938		

Table 7.4 Statistical Analysis of Incremental Rotations (Absolute) of Particles in Saturated Test Samples

S. No.	Material	Test No.	R O T	P A R	Deformation Increment						
					1	2	3	4	5	6	7
1	Gravel	1201	φ	N	70	71	68	65	69	67	62
				x	0.0454	0.0563	0.0729	0.0668	0.0823	0.0812	0.1294
				σ	0.0515	0.0627	0.0954	0.0744	0.0922	0.0770	0.0999
			θ	N	69	68	66	67	69	70	66
				x	0.0638	0.0534	0.0694	0.0705	0.0623	0.0800	0.0924
				σ	0.0840	0.0610	0.0806	0.0957	0.0481	0.0748	0.0867
2	Glass	2201	φ	N	104	102	100	96	95	97	88
				x	0.0350	0.0704	0.0658	0.0800	0.0920	0.1260	0.1561
				σ	0.0517	0.0663	0.0585	0.0761	0.0882	0.1189	0.1268
			θ	N	102	99	98	93	94	92	87
				x	0.0643	0.0683	0.0747	0.0910	0.1115	0.1180	0.1172
				σ	0.0933	0.0834	0.0666	0.0855	0.1002	0.0989	0.1020
3	Ceramic	3201	φ	N	114	114	113	108	114	120	117
				x	0.0519	0.0808	0.0956	0.0920	0.0960	0.1450	0.1506
				σ	0.0645	0.0790	0.0942	0.0773	0.0914	0.1132	0.1172
			θ	N	117	116	115	114	114	119	116
				x	0.0492	0.0617	0.0617	0.0837	0.0790	0.1131	0.1262
				σ	0.0633	0.0743	0.0720	0.0860	0.0714	0.1078	0.1014
4	PTFE	4201	φ	N	173	173	171	171	173	165	160
				x	0.0290	0.0429	0.0524	0.0660	0.0611	0.0703	0.0850
				σ	0.2646	0.0458	0.0641	0.0832	0.0703	0.0995	0.0938
			θ	N	173	173	172	172	173	170	165
				x	0.0155	0.0163	0.0174	0.0250	0.0225	0.0259	0.0284
				σ	0.0167	0.0162	0.0220	0.0410	0.0290	0.0282	0.0280
5	Poly- pro- pylene	5201	φ	N	194	192	193	200	199	182	
				x	0.0251	0.0516	0.0553	0.0789	0.0657	0.1466	
				σ	0.0316	0.0530	0.0691	0.0767	0.0753	0.1167	
			θ	N	194	195	193	199	198	179	
				x	0.0208	0.0382	0.0410	0.0529	0.0352	0.1110	
				σ	0.0213	0.0376	0.0439	0.0497	0.0349	0.0991	

TABLE 7.5

ELEMENT NO.	HOR. DISP. (Incremental) (4200) DEFORMATION INCREMENT						
	1	2	3	4	5	6	7
1	-.79627	-.99927	-1.17673	-1.47136	-1.85773	-2.94164	-4.33736
2	-.48760	-.43479	-.28490	-.59780	-1.25760	-1.40360	-1.36800
3	-.04892	.03251	.53400	.63258	.13667	2.98300	1.72592
4	.56533	1.04973	1.61750	1.82938	1.45100	5.83911	4.25367
5	-.91358	-1.18242	-1.05900	-1.70367	-2.00592	-2.82717	-4.57267
6	-.68418	-.89275	-.65375	-.92217	-1.47933	-2.14267	-2.53875
7	.12060	.16791	.64910	.76110	.48370	1.55320	2.41810
8	.47503	.98331	1.14523	1.32631	1.27631	6.85138	5.07820
9	-.82464	-1.38236	-1.15900	-2.10073	-3.33100	-4.13182	-4.63264
10	-.04073	-.03013	.21673	.04155	.03000	-.14918	-.83818
11	.14433	.34042	.63167	.69617	.76842	1.04458	.48075
12	.22400	.47237	.80450	1.22675	1.18413	2.40400	3.43113
13	-.26600	-.45692	-.59600	-1.33167	-1.26517	-1.41425	-1.27933
14	.01473	-.04501	-.09567	-.14356	.06544	.12167	.02144
15	.04720	.10031	.08010	.06450	.10270	.17360	.01470
16	.12825	.31603	.97733	.45817	.53982	1.19518	.96133

TABLE 7.6

ELEMENT NO.	VER (TOT) DISP. (Incremental) (4200)						
	1	2	3	4	5	6	7
1	.49318	.57945	.48291	.73755	.08400	.42009	.41527
2	.31850	.30031	.40410	.59940	.11800	.67140	1.19390
3	.44442	.37383	.43283	.81592	1.02433	1.77883	.64858
4	.50089	.61901	.20413	.06713	.79889	.70667	.03267
5	.88917	1.26325	1.41508	1.59483	.51617	.73325	.97092
6	.84083	.84503	1.09350	1.14283	.63742	1.79917	2.62792
7	1.24550	1.29780	1.48090	1.79440	1.82920	3.75050	1.97350
8	1.11223	1.37933	.56054	.21515	1.44054	2.23308	.61310
9	.93364	1.19401	1.38236	1.73664	.90527	1.45582	1.75527
10	1.47745	1.64782	1.82445	2.16645	2.48745	4.47682	4.64173
11	1.55658	1.76933	2.00867	2.37692	2.66150	5.07733	4.92867
12	1.32063	1.51263	.43213	.41113	1.48100	3.65463	2.74862
13	1.43453	1.92703	2.03042	2.31453	2.29617	4.40900	4.18483
14	1.59644	1.96656	2.24611	2.56522	2.78589	5.32411	5.08478
15	1.60730	1.92231	2.13870	2.48610	2.72810	5.28210	5.11410
16	1.52758	1.80953	2.10300	2.25342	2.44891	4.81864	4.69142

TABLE

7.7

ELEMENT NO.	Z - COMP DISP. (Incremental) (4200)						
	1	2	3	4	5	6	7
1	-.02464	-.14433	-.02045	-.47418	.03336	-.49836	-.56536
2	.05770	-.08880	.32410	-.29020	.30420	-.14650	-.28790
3	.09025	-.26142	.39758	-.37275	.29600	-.41767	-.45817
4	.10722	-.40822	.43725	-.22575	.38278	-.86133	-.54600
5	-.06892	-.07575	-.17250	-.45392	.33100	-.38717	-.03967
6	-.00783	-.06575	.24967	-.35108	.07383	-.42200	-.14442
7	.04650	-.36790	.50590	-.41730	-.04590	-.56860	-.37920
8	.15223	-.33333	.62562	-.04492	.02069	-.25592	-.28180
9	.07664	.11191	-.01764	-.04018	.59527	-.04445	.40800
10	.13445	-.01936	.23582	-.25945	.32545	-.20191	.13991
11	.18475	-.14900	.39258	-.18075	.21433	-.12250	-.01242
12	.12513	-.13850	.47900	.05163	.19613	.11675	.03525
13	.02353	.09225	.01803	-.06750	.20408	-.02675	.35842
14	.07973	.01000	.09289	-.13222	.21244	-.09789	.09933
15	.05590	-.04400	.10290	-.09010	.06710	-.06700	.00480
16	.04653	.01425	.12483	.04967	-.04382	.05555	-.18050

TABLE 7.8

ELEMENT NO.	VER (UNI)DISP. (Incremental) (4200)						
	DEFORMATION INCREMENT						
	1	2	3	4	5	6	7
1	.22349	.27155	.28836	.32549	.33932	.67366	.66578
2	.25112	.30984	.33697	.38510	.40864	.81032	.79109
3	.25520	.31247	.33826	.38588	.40330	.74766	.66177
4	.22177	.26925	.28492	.32919	.36208	.67818	.65358
5	.61247	.75344	.80763	.91141	.96209	1.89412	1.89829
6	.65121	.80311	.87203	.99534	1.06786	2.09867	2.04530
7	.61007	.74333	.79565	.89564	.93893	1.77303	1.59684
8	.63465	.77692	.83111	.96113	1.05663	2.03015	1.94957
9	1.00196	1.24295	1.35202	1.55133	1.66564	3.27859	3.27484
10	1.05446	1.29822	1.40328	1.60004	1.70712	3.27079	3.08929
11	1.03546	1.27273	1.37233	1.55892	1.65568	3.15795	2.93834
12	1.01280	1.24889	1.35156	1.57544	1.73031	3.37488	3.24430
13	1.40017	1.73337	1.87967	2.15395	2.31543	4.49809	4.35120
14	1.43726	1.77784	1.92812	2.20522	2.36495	4.56903	4.37012
15	1.43087	1.76957	1.91993	2.19839	2.35966	4.56178	4.36516
16	1.41322	1.74894	1.89954	2.17538	2.34089	4.54026	4.37034

TABLE 7.9

ELEMENT NO.	VER (NCR) DISP. (Incremental) (4200)						
	1	2	3	4	5	6	7
1	.26970	.30783	.19455	.41156	-.25532	-.25357	-.25051
2	.06733	-.00954	.06713	.21430	-.29064	-.13892	.40281
3	.18921	.06135	.09457	.43004	.62104	1.03118	-.01319
4	.27912	.34975	-.08080	-.26206	.43681	.02849	-.62091
5	.27670	.50981	.60745	.68342	-.44592	-1.16087	-.92738
6	.18963	.04191	.22147	.14749	-.43045	-.29950	.58262
7	.63543	.55447	.68525	.89876	.68127	1.97747	.37666
8	.47753	.60245	-.27057	-.74597	.38391	.20292	-1.33647
9	-.06833	-.04895	.03034	.18530	-.76037	-1.82277	-1.51956
10	.42300	.34963	.42117	.56842	.78034	1.20603	1.55244
11	.52112	.49661	.63634	.81799	1.00582	1.91938	1.99033
12	.30733	.26373	-.91944	-1.16431	-.24931	.27975	-.49567
13	.09441	.19372	.15074	.16009	-.01926	-.08909	-.16637
14	.15918	.18872	.31800	.36000	.42094	.75509	.71466
15	.17643	.15273	.21877	.28771	.36844	.72032	.74894
16	.11436	.06064	.20346	.07803	.10802	.27838	.32108

TABLE 7.10

ELEMENT NO.	HORIZONTAL STRAIN (Incremental) (22)1 DEFORMATION INCREMENT						
	1	2	3	4	5	6	7
1	-.49700	-2.97600	-3.95900	-5.26800	-4.32500	-6.30000	-6.18500
2	-2.66700	.43500	-5.03400	-6.15200	-5.44400	-6.52900	-10.57300
3	-.96300	-3.45500	-4.61900	-4.06000	-5.58900	-7.03000	-8.44000
4	-1.07600	-3.45700	-4.29500	-2.74300	-7.15900	-8.67700	-7.67800
5	-.49900	-3.65900	-3.14500	-5.20200	-3.84300	-5.87300	-5.36400
6	-.58700	-3.35000	-3.55300	-7.28200	-1.82700	-6.42500	-7.23000
7	-2.86400	.56000	-5.07300	-6.32800	-5.56300	-6.72800	-10.33900
8	-.76600	-2.34600	-3.84300	-4.09100	-2.85400	-4.21500	-10.46100
9	-1.07500	-3.45200	-4.28800	-2.90100	-7.07300	-8.53800	-7.65600
10	-1.06000	-2.93000	-4.49300	-4.41400	-5.47200	-8.04500	-7.49900
11	-.62100	-3.36100	-3.64200	-7.16200	-1.87300	-6.55600	-7.34000
12	-.96800	-4.26500	-4.01500	-5.02200	-4.08700	-9.47100	-7.21200
13	-.77100	-2.35900	-3.82600	-4.07000	-2.78000	-4.17600	-10.79600
14	-.95900	-3.57100	-3.37000	-2.61800	-3.01800	-2.48300	-5.33100
15	-1.05900	-2.92300	-4.49000	-4.40700	-5.46700	-7.97200	-7.49000
16	-.92300	-2.80000	-3.85900	-5.18100	-3.65700	-5.57300	-6.38500
17	-.97900	-4.27700	-4.01800	-5.02200	-4.08500	-9.47300	-7.27400
18	-1.07700	-4.47100	-4.89000	-4.32600	-3.21000	-8.63700	-8.70800
23	-.70300	-2.72000	-3.44700	-3.99200	-3.80700	-5.93100	-6.43400

TABLE

7.11

ELEMENT NO.	VERTICAL STRAIN DEFORMATION INCREMENT					(Incremental)	(2201)
	1	2	3	4	5	6	7
1	5.20800	-1.93800	2.35900	1.90300	.28900	.98900	-1.76700
2	-.32800	2.45500	1.63000	2.35000	1.68400	4.49600	10.07200
3	.31300	1.79600	1.85400	2.59100	1.36900	3.80600	8.57200
4	1.26200	2.68200	2.13600	-5.34700	8.90100	7.02400	9.91700
5	1.27400	2.75400	2.46800	-4.14100	8.93300	7.80000	11.00000
6	.96700	3.87700	2.86000	3.16900	2.78300	.40800	-1.21100
7	-3.57500	5.57400	2.08800	4.19300	3.23900	2.84200	4.17800
8	.75000	1.85200	2.55100	2.82000	6.23100	8.22400	11.21500
9	.75000	1.85100	2.54700	2.82500	6.23400	8.20400	10.99900
10	.58600	1.88000	3.07000	6.46100	1.06000	6.91400	7.20500
11	.61200	2.15300	3.46100	8.16600	1.18300	7.29900	7.93200
12	1.15100	1.03000	.35600	.29300	.79300	2.57800	10.71400
13	1.46900	2.52800	-1.15500	-.25600	-.81100	2.11200	6.63700
14	.47700	3.25500	4.21900	7.51300	3.20700	7.56200	2.92600
15	.50100	3.24600	4.14800	7.43000	2.91500	7.30700	2.85700
16	1.35900	3.66900	3.35000	6.77000	3.97300	11.42100	8.81300
17	1.40400	3.64700	3.32300	6.14300	4.10400	12.84700	8.60800
18	1.79400	4.05700	1.64500	1.77000	.98900	4.74100	1.14700
23	1.00600	2.33600	2.47500	2.63000	2.36500	3.95000	5.71000

TABLE, 7.12

ELEMENT NO.	VOLUMETRIC STRAIN (Incremental) (2201) DEFORMATION INCREMENT						
	1	2	3	4	5	6	7
1	4.71100	-4.91400	-1.60000	-3.36500	-4.03600	-5.31100	-7.95200
2	-3.01400	2.89000	-3.40400	-3.80200	-3.76100	-2.03200	-.50100
3	-.65100	-1.65900	-2.76600	-1.46800	-4.21900	-3.22400	.13200
4	.18600	-.77400	-2.15900	-8.09100	1.74200	-1.65300	2.23900
5	.77500	-.90500	-.67800	-9.34300	5.09100	1.92700	5.63600
6	.38000	.52700	-.69200	-4.11300	.95600	-6.01700	-8.44100
7	-6.43900	6.13400	-2.98500	-2.13600	-2.32400	-3.88500	-6.16200
8	-.01600	-.49400	-1.29200	-1.27100	3.37700	4.00800	.75400
9	-.32500	-1.60100	-1.74100	-.07600	-.84000	-.33300	3.34400
10	-.47400	-1.05100	-1.42300	2.04700	-4.41200	-1.13100	-.29400
11	-.00900	-1.20800	-.18100	1.00400	-.69100	.74300	.59200
12	.18300	-3.23400	-3.65800	-4.72800	-3.29400	-6.89300	3.50300
13	.69800	.15800	-4.98100	-4.32600	-3.59100	-2.06500	-4.15900
14	-.48300	-.31600	.84800	4.89500	.19000	5.07900	-2.40400
15	-.55800	.32300	-.34100	3.02300	-2.55300	-.66500	-4.63400
16	.43700	.86900	-.50900	1.58900	.31600	5.84800	2.42800
17	.42500	-.63000	-.69500	1.12100	.01900	3.37400	1.33400
18	.71700	-.41400	-3.24500	-2.55600	-2.22100	-3.89600	-7.56100
23	.30300	-.38400	-.97200	-1.36200	-1.44200	-1.98100	-.72500

CHAPTER 8

THE SIGNIFICANCE OF OBSERVED DEFORMATION BEHAVIOUR WITH RESPECT TO CURRENT STRESS-STRAIN MODELS.

8.1 INTRODUCTION

In the last chapter, it was shown that the deformation response of a granular mass under an applied deformation or applied force system depends primarily on the fabric of the medium and thus, ultimately, on the shapes and sizes of the constituent particles and their position in the fabric. The complete kinematic of this deforming mass would then include the complex geometric description of the contacts between the contiguous particles at any instant of their deformation history. The distribution of contact points which is the inherent property of a granular mass, has to be known in order to be able to predict its behaviour under the action of forces. The situation is made more complex if the constituent particles deform and fracture. The serious drawback in dealing with a granular assembly based on particulate approach is our mathematical inadequacies to define its geometry efficiently with continuous concepts.

Perhaps due to this major limitation most of the strength-deformation theories, whether developed from continuum approach or from particulate approach, end up with a final form involving certain parameters, such as stress and strain, which are essentially valid for continuous bodies only. It has, therefore, become customary to give the relationship between the local deformation and internal forces. In these approaches, the local deformation is characterized by the strain tensor and the internal forces by the stress tensor. The strain components are related to the displacements while the stress components must satisfy the equations of motion. These

variables remain indeterminate until additional equations are established to relate these two tensors. Such equations are termed constitutive equations. They depend on the manner in which the material resists deformation. Since these equations are obtained to describe the behaviour of a material, not the behaviour of a body, they should involve variables which characterize the local state, for example an equation which related stress and strain at a point.

In order to evaluate the existing strength-deformation theories or to obtain a stress-strain relationship from the experimental data along the conventional lines, the discrete force distribution and the displacement of the particles observed have to be transformed into a stress and strain rate tensors.

Before the existing strength-deformation may be examined, it is convenient here to include a short comment on the relevance of the stress and strain concepts as applied to the particulate mass.

8.2 RELEVANCE OF STRESS AND STRAIN CONCEPTS IN PARTICULATE MECHANICS.

As mentioned earlier, stress and strain are the two basic concepts of continuum mechanics which are generally used in the formulation of stress-deformation relationship of granular soils.

Once the discrete data is suitably represented by continuous functions, then one can utilize powerful techniques which were originally developed for continuous medium. Perhaps this is one of the major temptation amongst the soil theoreticians to think in terms of continuum mechanics, although they are fully aware that in reality it is not the case. Stress and strain concepts, as applied to discrete medium, are misleading particularly when the

fundamental properties determining the behaviour of a granular assembly are investigated. Being the averages, they conceal the real physical quantities which are responsible for the mechanical behaviour of the granular assembly.

8.2.1 Average Stress

In a granular medium, the real stresses are only non-zero in the particles. These stresses should, therefore, be represented by some discontinuous function which jumps from a value of zero in the void space to a finite value in the particle. However, when the stress concept of continuum is applied the real stress is averaged over the region surrounding a given point so that the stress could be considered as a continuous function of position.

Unfortunately, there is not a single method of averaging the forces available which could be used without any reservations. In the absence of such a method, different methods of averaging the forces have been used. Sometimes the deformation mechanism, assumed or observed, affects the computed value of stresses. For instance based on the assumed deformation mechanism, that is, the granular mass deforms mainly due to sliding between rigid groups of constituent particles, Rowe (1971, p. 158) defined the effective principal stresses as follows:-

$$\sigma_1 = \sum_1^{n_{s1}} L_1 \quad \text{and} \quad \sigma_3 = \sum_1^{n_{s3}} L_3 \quad (8.1)$$

where L_1 and L_3 are the resultant forces acting on each group of particles and on the sliding contact representative of the group, and n_{s1} and n_{s3} are the sliding contacts per unit area in the major and minor principal stress directions.

The above relations were then used by him to obtain the following relationship between $K (= \tan^2 (45^\circ + \phi_f/2))$, dilatancy rate D and $\tan\alpha$:

$$\tan\alpha = D\sqrt{K} \quad (8.2)$$

$$\text{where } \tan\alpha = \bar{n}_{s1}/\bar{n}_{s3} \quad (8.3)$$

The validity of the above relationship will obviously depend on \bar{n}_{s1} and \bar{n}_{s3} and thus, in turn, on the basic assumption made in finding the average stresses.

On the other hand, tests carried out by Drescher and de Josselin de Jong (1972) and by Oda and Konishi (1974 a) on photo-elastic cylinders or discs show that all particle contacts participate in transferring the load irrespective of whether they are critically oriented or not, from the sliding point of view. The effective principal stress can be obtained by adding the component of contact forces acting in the direction of the stress on all the contacts per unit area.

$$\sigma_1 = \sum_1^{n_1} L_1 \quad \text{and} \quad \sigma_3 = \sum_1^{n_3} L_3 \quad (8.4)$$

where L_1 and L_3 are the contact forces acting in the direction of Principal stresses σ_1 and σ_3 respectively.

n_1 and n_3 are the numbers of contacts per unit area in the major and minor principal stress direction.

Drescher and the Josselin de Jong (1972) used an averaging procedure over a representative elementary area so as to obtain the average stress from the measured discrete contact forces. They used the method proposed

by Hill and Weber. It must be appreciated that there is a real problem of selecting the representative area particularly when the contact force distribution shows very wide variations in the neighbourhood of the point under consideration.

Although it is desirable to measure the contact forces acting on all the particle contacts and monitor them throughout the deformation of a test sample, it is practically impossible to measure them inside the test samples made from the real granular soils or from other materials such as the materials used in this investigation. No internal forces and their distribution can, therefore, be obtained. In these conditions, one is bound to make some suitable simplifying assumptions.

The following assumptions are, therefore, made here:

- 1) The stress distribution inside the test sample is uniform and is not affected by the local variations in the internal strains.
- 2) The direction and magnitude of the internal stresses can be determined from the measured external boundary stresses or forces.
- 3) The direction of principal stress axes does not change with deformation for the plane strain test conditions.

Similar assumptions have been made by other researchers when it was not possible to measure internal force distribution and thus the stress distribution inside a test sample, for example, see Arthur and Menzies (1972). In the present investigation the average stresses were obtained by averaging the boundary forces according to the method outlined in Chapter 6.

8.2.2 Average Strain Increment

In the last chapter two peculiarities of the granular mass were pointed out, namely the non-analytic character of the linear translation of individual particles and rotation of the constituent particles. The current stress-strain models of the particulate materials, rotation of individual particles is, as far as known to the writer, not considered. Consequently this discussion will be restricted to displacements and strains only.

Even if the effect of rotation on the deformation behaviour of granular assembly is ignored, the non-analytic character of the particle displacements inhibits the use of the concept of strain, in its true sense. However, the strain increments and the internal strain distribution of the granular test samples are obtained in order to compare the observed deformation behaviour with the existing theories. Nevertheless the need for the search of the new concepts and parameters for the correct modelling of deformation behaviour of granular materials must be emphasized.

Unfortunately, there is not a single method available which could be used to obtain average strain tensor from the discrete observations of the displacement of particles. Various researchers favour different methods. It is rather difficult to justify the use of one particular method. The method used for the calculation of strain increments is outlined in Appendix B.

8.3 NON-CO-AXIALITY OF PRINCIPAL STRESS AND PRINCIPAL STRAIN INCREMENT DIRECTIONS.

In most of the existing stress-strain models for cohesionless granular soils, the coincidence of these two axes is generally assumed, for example

by Rowe (1962), Horne (1965, 1969), Gudehus (1969, 1972) and by Schofield and Wroth (1968). This is one of the most controversial assumptions of geotechnical engineering. Although recently it has attracted the attention of many theoreticians and experimentalists, a clear picture is yet to emerge.

In the absence of a clear picture, it will be interesting to examine the observed behaviour of particulate materials. A brief discussion, based on the experimental observations of the present study as well as of other research workers, is, therefore, included here. Figures 8.1-8.3 show the plots of the angle ξ , which is the angle between the major principal strain direction and the horizontal axis, which in our case happens to coincide with σ_3 -direction, of various stages of deformation history of a typical test (Test no. 3201). Following conclusions may be drawn from the data presented here:

- a) Local variations:- The direction of the major principal strain increment of each of the elements of a test sample is not constant but varies randomly from one element to other for a given deformation increment. Further the direction of an element randomly changes during its deformation history. It can be suggested that the direction strain axes not necessarily coincides and the local variations in their directions are quite obvious.
- b) Global variations:- On an average the divergence between the direction of principal strain increment axes calculated from the geometry of the boundary of the test sample and the principal stress directions is found to vary within a few degrees. It may, therefore, be said that these two sets of axes are practically coincident when the global behaviour of the test sample is examined.

It may, however, be noted that the above conclusions are based on the assumptions of the principal stress direction which are given in the previous sub-section. It should also be mentioned that every effort was made to prepare the test samples with isotropic packing of the particles as was possible so as to minimise the possibility of the presence of inherent anisotropy in the initial particle packing. The observed variation in the values of ξ may, therefore, be attributed to the characteristic of the granular test sample. In fact the local variations i.e., in the values of ξ was observed in all the tests carried out for the present study.

Oda and Konishi (1974, a) have presented the experimental evidence obtained from their 2-D simple shear test on photo-elastic discs, see Figure 8.4. This Figure shows that the principal stress and principal strain increment axes do not coincide with each other, at least up to the peak. Incidentally, they did not make any assumption regarding the disposition of the principal stress axes because they were able to measure the contact forces and their distribution inside the test sample.

Arthur and Menzies (1972) have also presented the deformation data which clearly corroborates the above conclusions. The example of an axial strain increment map and the example of a map of the angles between axes of stress and strain increment for the cubical triaxial cell presented by them are reproduced in Figures 8.5(a) and 8.6(a) respectively. With the help of the data presented in these maps, histograms have been plotted, see Figures 8.5(b) and 8.6(b). Study of these figures reveal that although on an average the principal strain increment direction is coincident with the corresponding principal stress direction, local variations in the magnitude of strain increments and in the angles between axes of stress and strain

presented in their Table 1 supports the above contention of local random behaviour of test sample at all stages of its deformation history.

Mandl and Fernandez Luque (1972), Spencer (1964, 1971), Spencer and Kingston (1973), de Josselin de Jong (1958, 1959) have shown mathematically that the principal stress and principal strain rate axes need not necessarily coincide. Their observation is valid only for the shear deformation conditions when the sample is plastically flowing (i.e. under fully developed flow conditions in the deforming granular media). Drescher and de Josselin de Jong (1972) have presented experimental results which support the contention put forward by de Josselin de Jong (1958, 1959) that the two axes rotate within the limits

$$-\phi'/2 < \xi' < \phi'/2$$

where ϕ' is the angle of internal friction, ξ' is the angle between the directions of the principal stress axes and of the principal strain rate axes.

The observed data of the present test series and the published evidence cited above indicate the possibility of non-coincidence of the two axes probably at every stage of deformation. The non-co-axiality of axes must therefore, be taken into account in the formulation of correct and realistic stress-strain relationship for particulate materials. As mentioned earlier in this section, the co-axiality of the principal axes of strain rates and stress is generally assumed in the present stress strain theories. Even some of the originators of existing theories were fully aware of this situation, still they ignored it. It can only suggest the mathematical difficulties involved, for correctly modelling the behaviour. If, however, a complete and more

general theory of stress-strain behaviour of granular material is desired, then a suitable method must be found to overcome this mathematical obstacle.

8.4 EVALUATION OF CURRENT STRESS-STRAIN MODELS WITH PARTICULAR REFERENCES TO THE STRESS-DILATANCY MODEL.

Current stress-strain models for cohesionless granular soils and for other similar materials can broadly be classified under two main headings, namely:-
a) theories based on continuum mechanics, and b) theories based on particulate mechanics.

In the past number of stress-strain models for cohesionless granular materials, which are based on continuum approach, have been proposed, for example by Roscoe et al (1958), Gudehus (1972). Major contribution in this field is made by the Cambridge Soil Mechanics Research Group. They developed two separate soil models, namely- Cam clay and Granta gravel, for use under different situations, for details see Schofield and Wroth (1968). The model for medium dense and dense cohesionless soils, which is relevant to the present series of tests, is the Granta - gravel model. This model is based on the assumption that no strain is allowed prior to the peak stress ratio, i.e. the material behaves as a rigid - plastic material. Reference to stress strain curves, Figures 6.4-6.13, show that strain does occur before the sample reaches its peak strength. This model does not give correctly the pre-peak behaviour of the medium dense to dense granular samples. In fact it is relevant only to the large strains which occur when the material is very nearly close to the normal consolidation conditions or has experienced a peak stress-ratio. Skinner (1975) has shown that neither the Granta gravel model nor the cam-clay model can be applied to granular materials.

Particulate approach was long recognized as the correct approach for the study of granular material. However, very little progress has been made so far. Nevertheless Rowe (1962) has made a notable contribution in this field. Although his theory has been criticized from various angles, no better theory is yet available as far as the writer is aware. In the past few years, attempts have been made for the development of new theories. Most of these theories stem from the same basic assumptions on which the Rowe's stress-dilatancy is based. Consequently the final form of their relationship is not very different than that of the S-D theory. It is worth noting that some investigators have themselves suggested that rolling of particles is likely to be one of the mechanism of deformation. Still they did not include its effect in their final formulation of their theories. It is, therefore, sufficient if we verify the stress-dilatancy theory with the observed data.

Stress dilatancy plots of all the elements and for all the stages of deformation for two typical tests namely glass (wet), test no. 2201 and PTFE, test no. 4200, are presented in Figures 8.6-8.13. These plots also show the theoretical R-D relations obtained by assuming $\phi_f = \phi_\mu$ and $\phi_f = \phi_{cv}$ in the Rowe's stress-dilatancy relationship:

$$R = \tan^2(45^\circ + \phi_f/2) \cdot D$$

where

R is the principal effective stress ratio

D is the dilatancy rate

ϕ_f is the modified mean angle of interparticle friction.

In the absence of any theoretical relationship between ϕ_μ and ϕ_{cv} for the plane strain tests,

Horne's $\phi_{\mu} - \phi_{cv}$ plot was used to find the value of ϕ_{cv} for the experimentally determined value of ϕ_{μ} of these materials. It is worth mentioning that during certain stages of deformation some elements showed either very large (positive) values or very low (negative) values of dilatancy factor. In order to keep the plots of reasonable size, only those values of (R, D) have been plotted which are within the range of the plots. However, reference can be made to Table B.2, which gives the value of D as well as the element number and the stage of deformation for which the point has not been plotted in Figures 8.7-8.1.14.

A close examination of these figures will show that the stress-dilatancy relation is in general not satisfied locally. One of the reasons for this is that the dilatancy rate 'D' is too sensitive when the value of the major principal strain increment $\dot{\epsilon}_1$ is very small. Further these plots suggest that the R-D values, particularly of dilatancy rate of an element varies randomly with increase in axial deformation although the global dilatancy rate, curve 23, shows a general trend of increase in its value up to certain stages of deformation and then it decreases as the deformation continues. From these figures, it can further be inferred that the stress dilatancy relation does not correctly model the global behaviour of the Sample because the observed global R-D curve, curve 23 in Figures 8.6-8.13 does not lie close to the theoretical line ($\phi_f = \phi_{cv}$). In spite of this, the empirical formulation namely $R = K.D$ where $K = \tan^2(45 + \phi_f/2)$ in which ϕ_f is obtained from the observed R-D plots by using curvefitting method, give satisfactory results and its use, specially in the absence of any better method, is recommended. Nonetheless the need for further work cannot be over-emphasized.

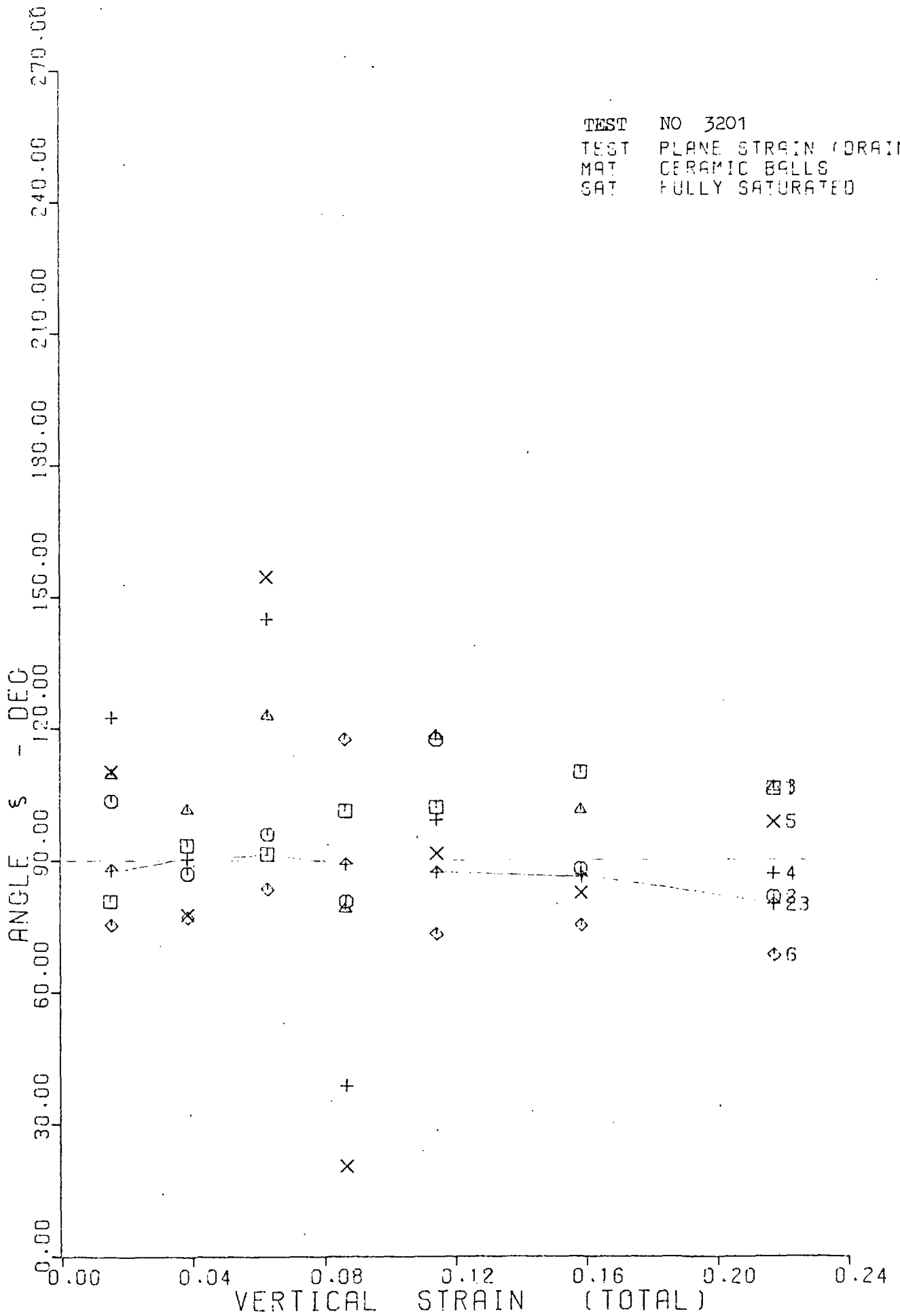


FIG 8.1 DEFORMATION - ANGLE S.

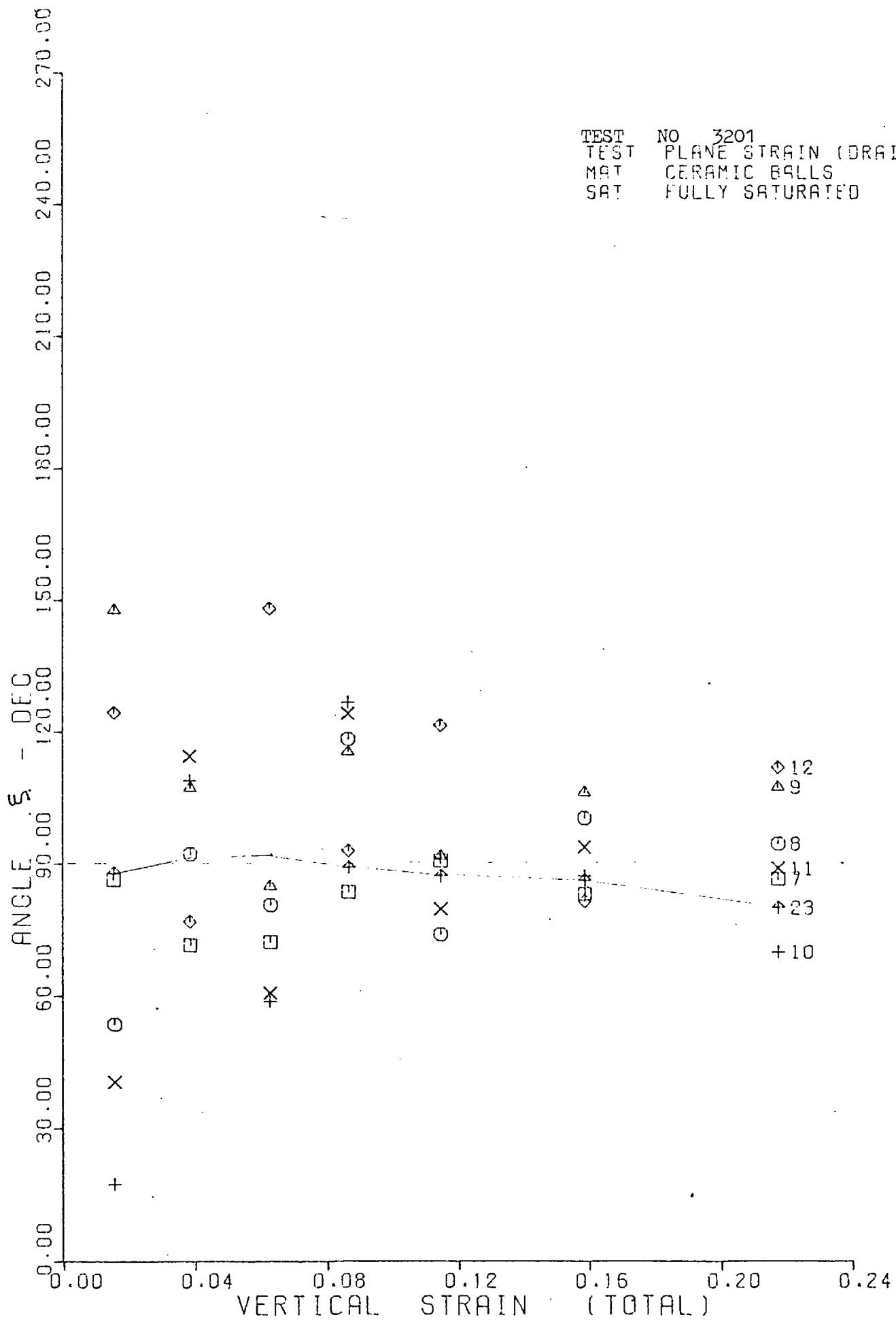


FIG 8.2 DEFORMATION - ANGLE 5

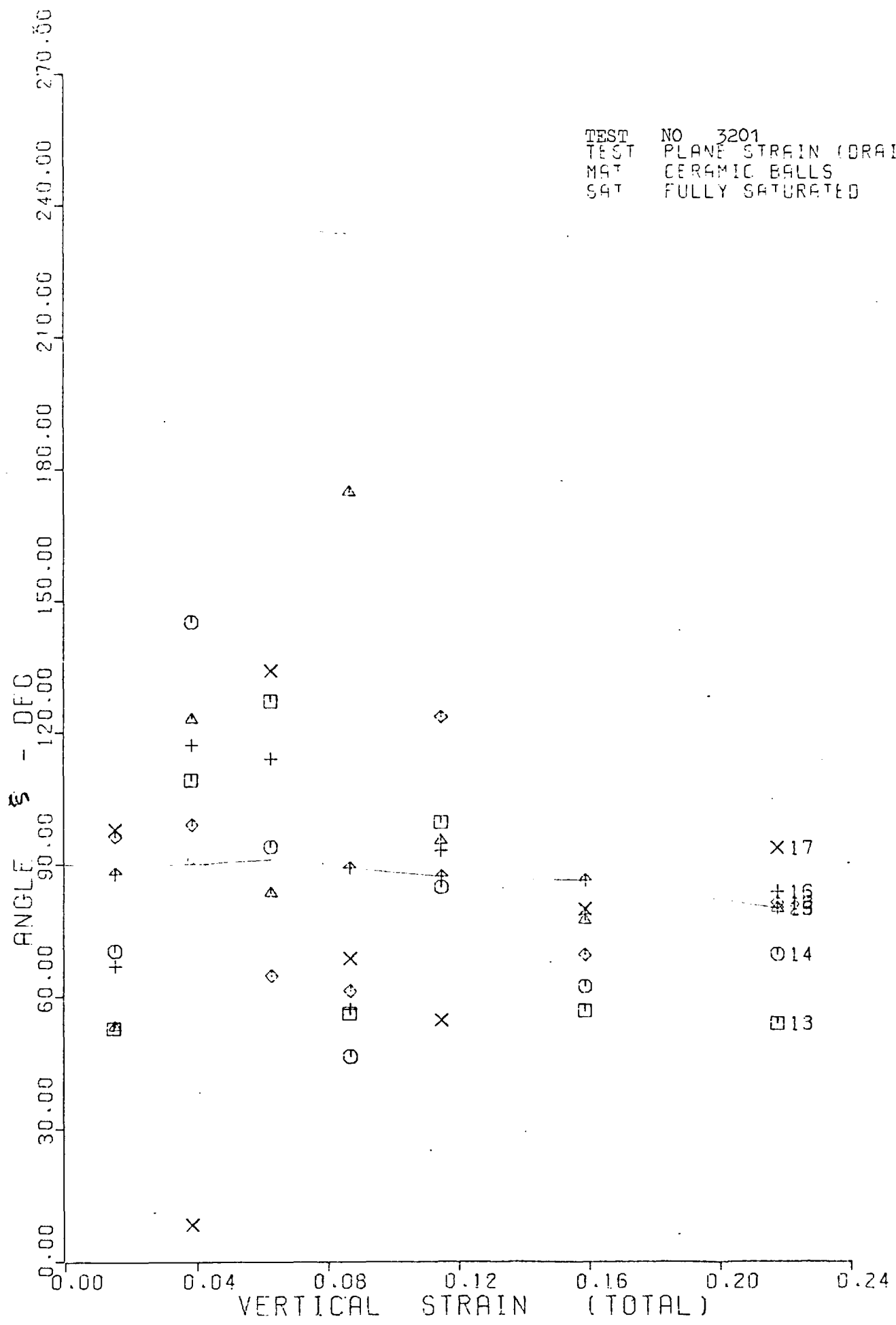
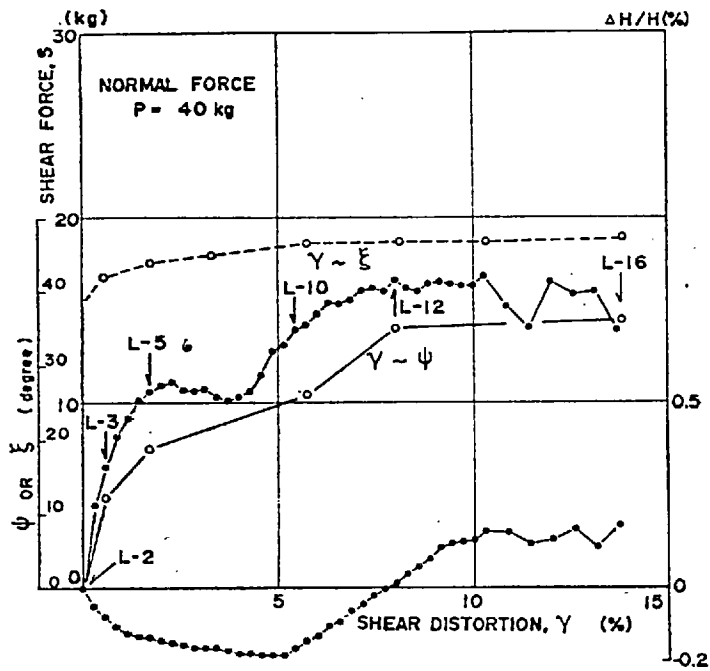
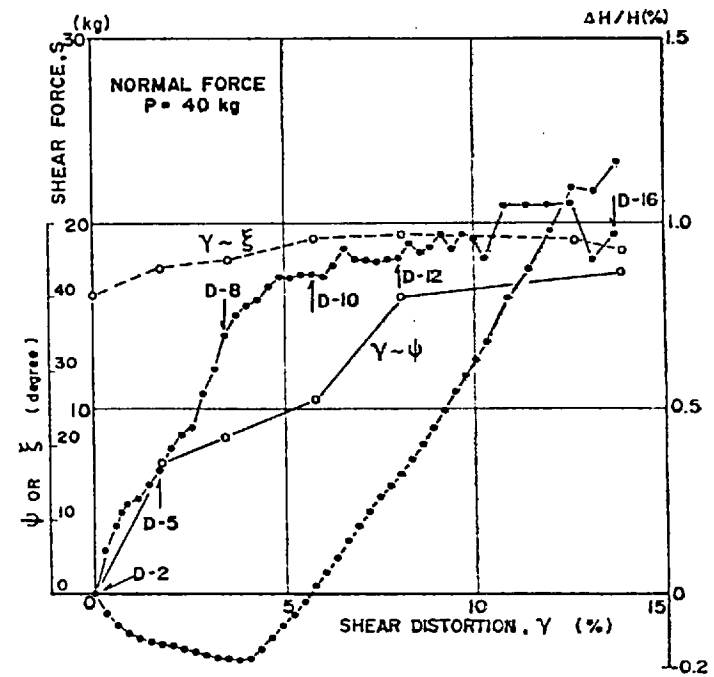


FIG 8.3 DEFORMATION - ANGLE ξ



a) Relations between shear force (S), shear distortion (γ), rate of thickness change ($\Delta H/H$), inclination angle of maximum principal stress axis (ψ) and inclination angle of maximum principal strain increment axis (ξ) for experimental series of dense model



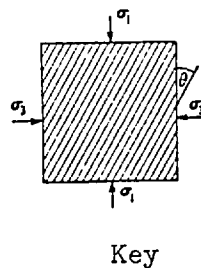
b) Similar diagram to Fig. (a) for experimental series of loose model.

(After Oda & Konishi, 1974b)

FIG. 8.4

(a)

5.42	4.48	2.90	4.34	4.34	4.04	5.05
4.71	5.05	3.93	4.04	3.19	2.63	
4.69	5.26	5.84	4.00	3.62	3.60	3.95
4.48	4.26	3.59	4.48	4.48	5.28	
3.99	3.97	3.81	3.44	2.60	3.63	3.53
4.68	3.67	4.05	3.18	3.97	2.03	
4.28	5.02	3.28	4.01	3.92	2.11	2.34
4.59	4.51	3.59	3.71	3.11	4.41	
4.73	5.58	4.60	4.07	4.41	4.77	4.59
5.72	5.92	4.19	6.09	5.29	3.51	
6.84	3.53	5.24	4.63	4.07	3.51	4.02
4.53	2.63	4.62	2.58	2.11	4.28	
4.19	3.77	3.76	5.22	5.25	4.81	3.58



Average axial strain = 4.16 Standard deviation = 0.92
 * Sample boundary *

a) Map of axial strain (After Aurther & Menzies, 1972) *

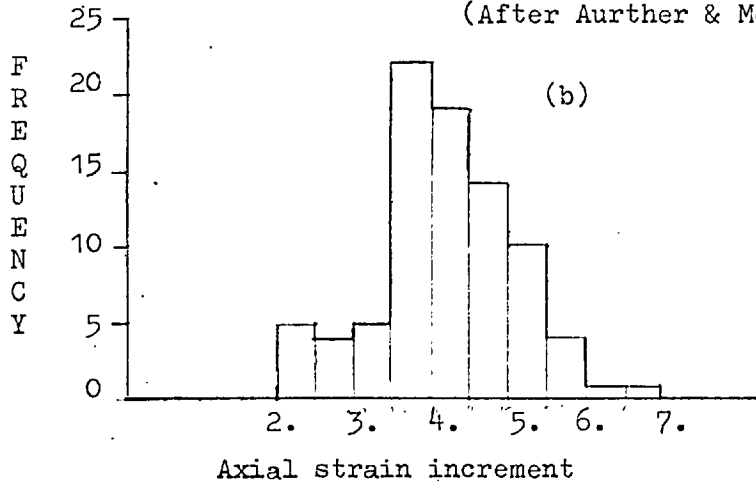


FIG. 8.5

(a)

-2.1	-1.6	2.4	-4.0	-1.0	6.8	1.3
-0.9	-1.9	4.6	1.7	-3.2	-2.2	
-5.9	4.3	1.2	-7.8	-1.1	-7.9	8.5
-4.6	0.7	-2.0	-4.8	-1.6	-1.0	
-1.1	-0.1	-1.4	4.1	-12.5	4.8	-4.7
1.1	-1.4	-2.0	-1.9	2.5	-1.8	
2.4	-1.0	-1.1	-2.0	2.6	-6.8	-14.0
0.4	-3.9	-2.5	-0.5	0.2	3.3	
3.6	-0.6	-2.2	-3.1	0.4	3.8	-2.6
1.8	-4.2	4.5	-0.1	1.2	1.7	
-1.3	-6.8	-3.7	9.6	-3.2	-0.7	0.2
-6.5	-12.0	-4.2	-0.8	-2.3	7.0	
-10.3	-1.6	-4.5	-1.4	-0.1	6.9	-2.3

Average angle = -1.05° Standard deviation = 4.30°
 * Sample boundary *

a) Map of the angles between axes of stress and strain increment.

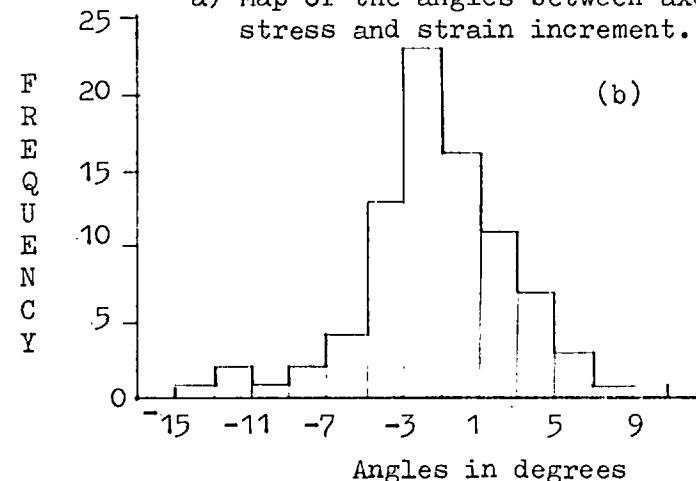


FIG. 8.6

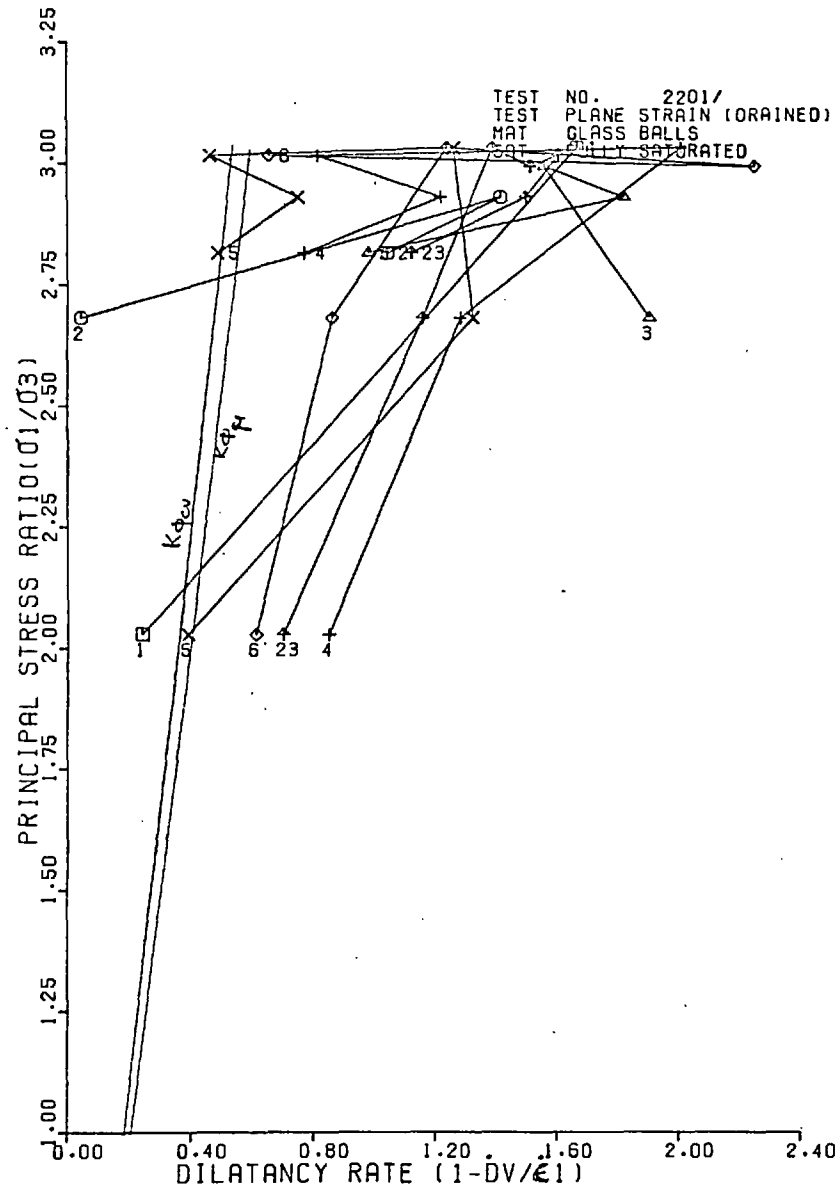


FIG 8.7 STRESS - DILATANCY PLOTS(MAJOR)

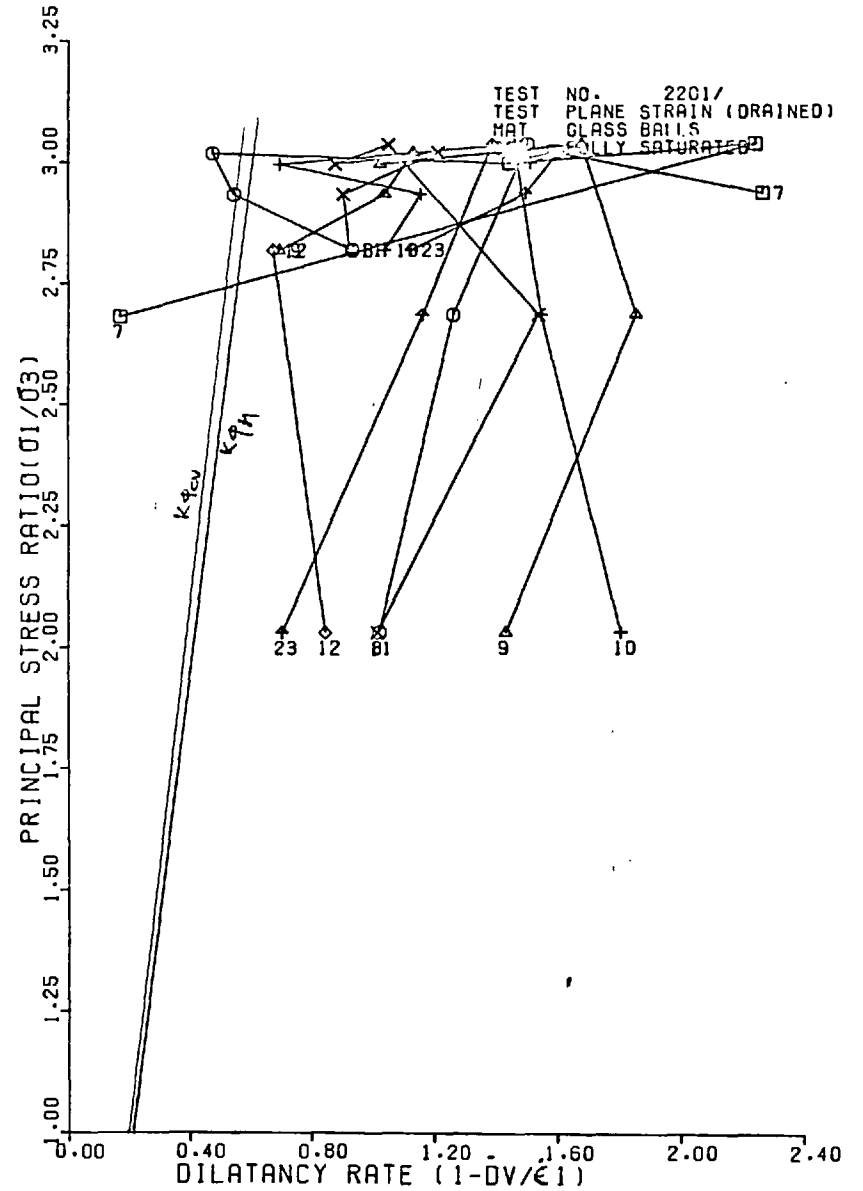


FIG 8.8 STRESS - DILATANCY PLOTS(MAJOR)

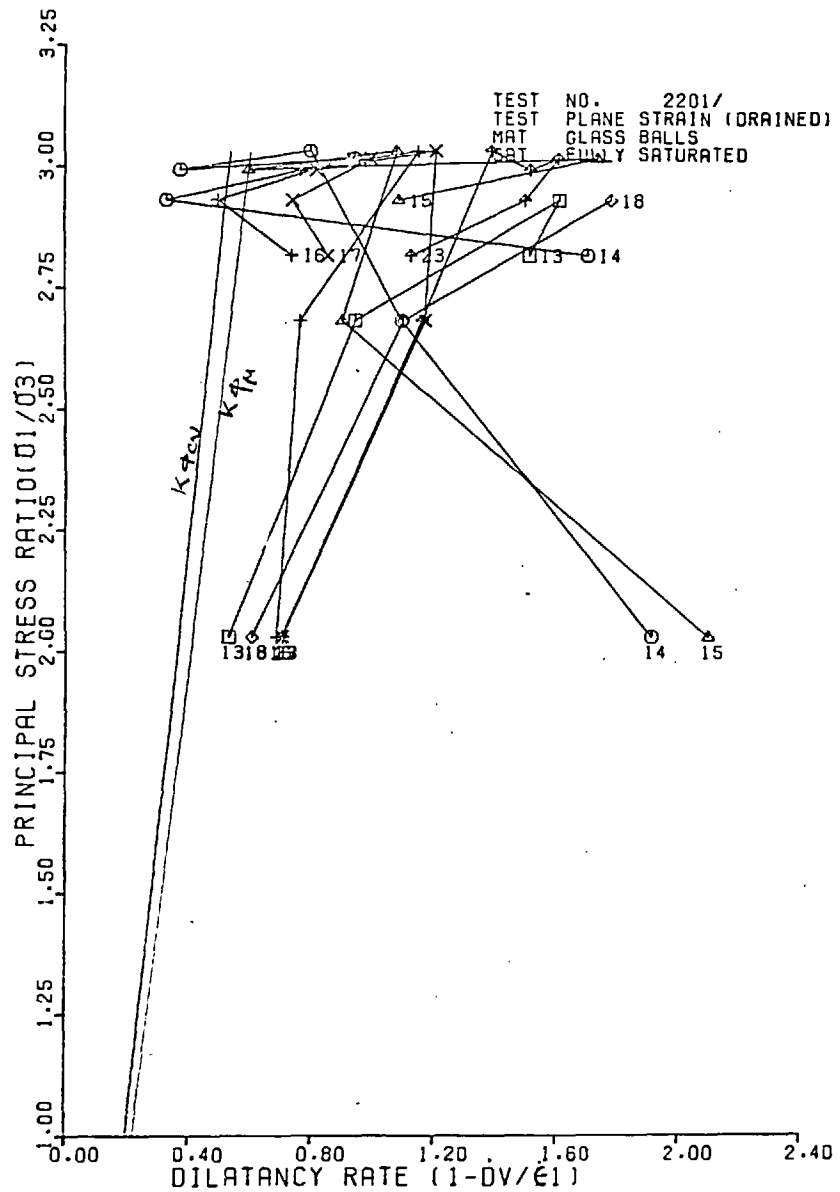


FIG 8.9 STRESS - DILATANCY PLOTS(MAJOR)

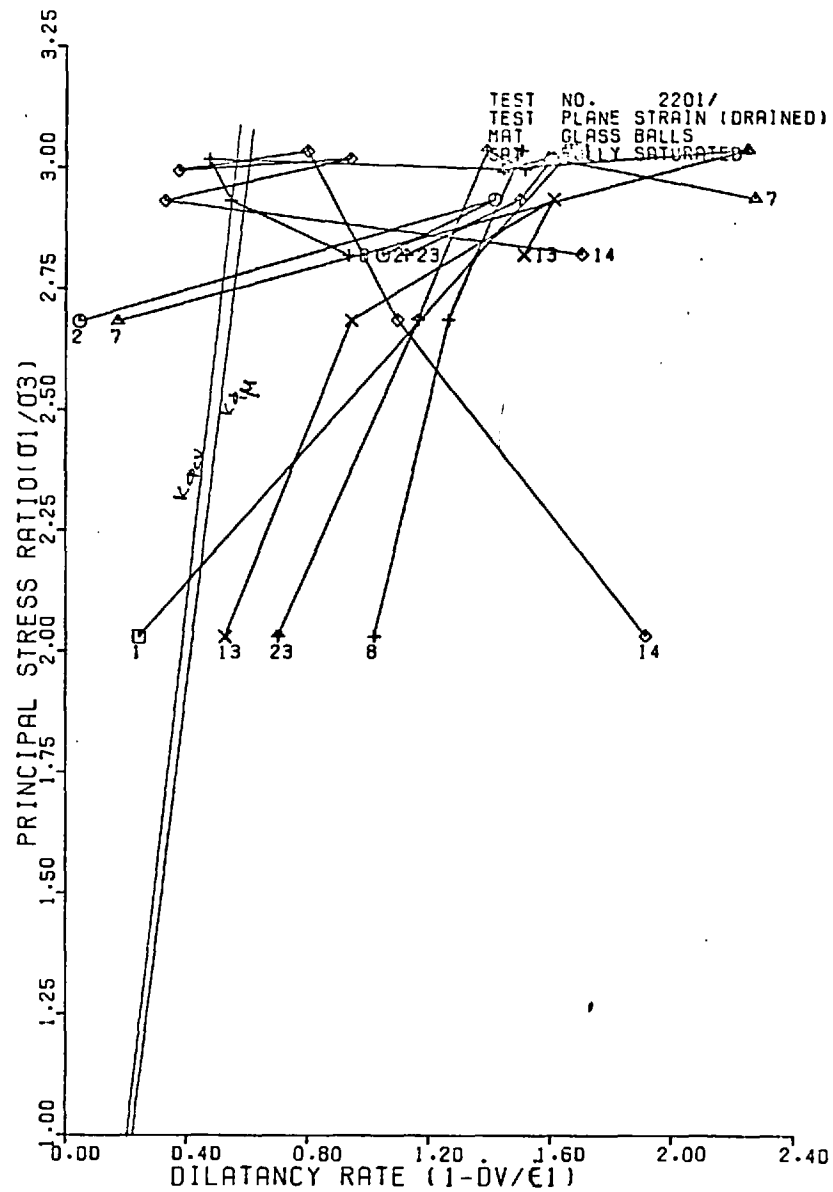


FIG 8.10 STRESS - DILATANCY PLOTS(MAJOR)

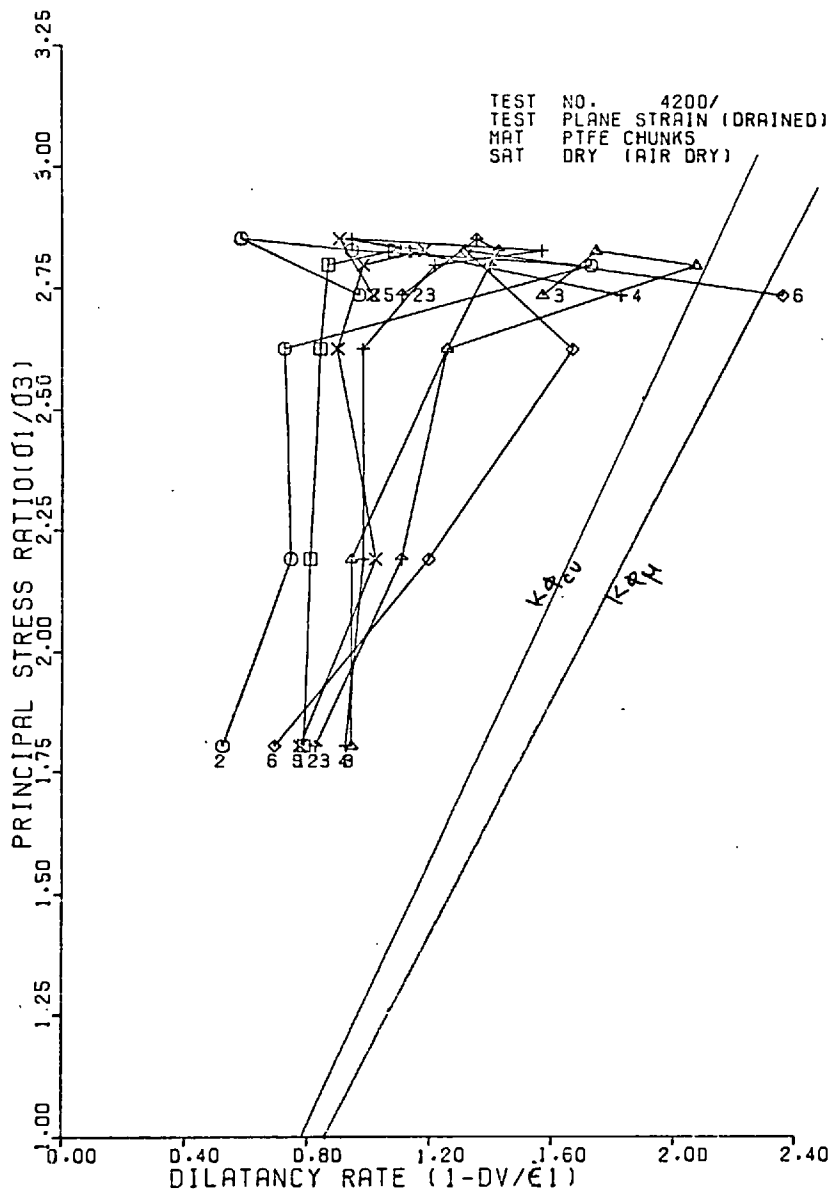


FIG 8.11-STRESS - DILATANCY PLOTS(MAJOR)

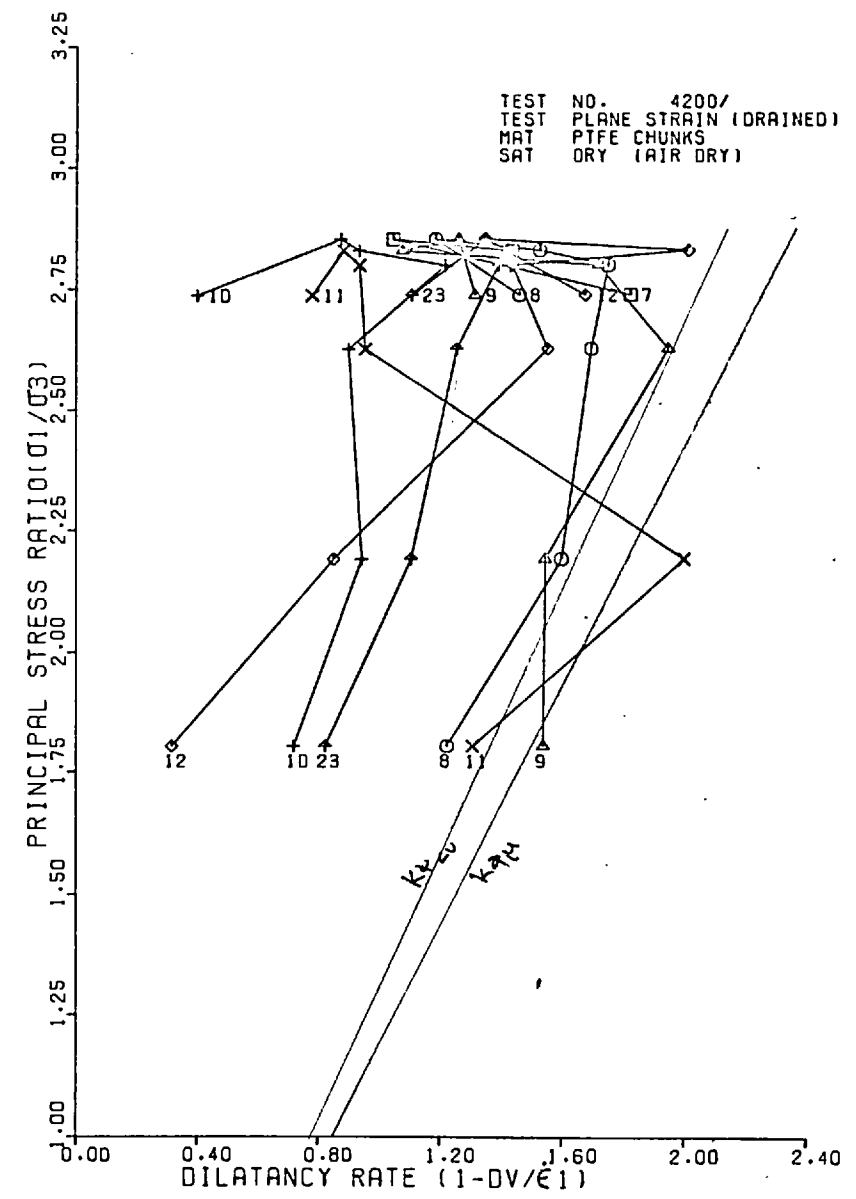


FIG 8.12-STRESS - DILATANCY PLOTS(MAJOR)

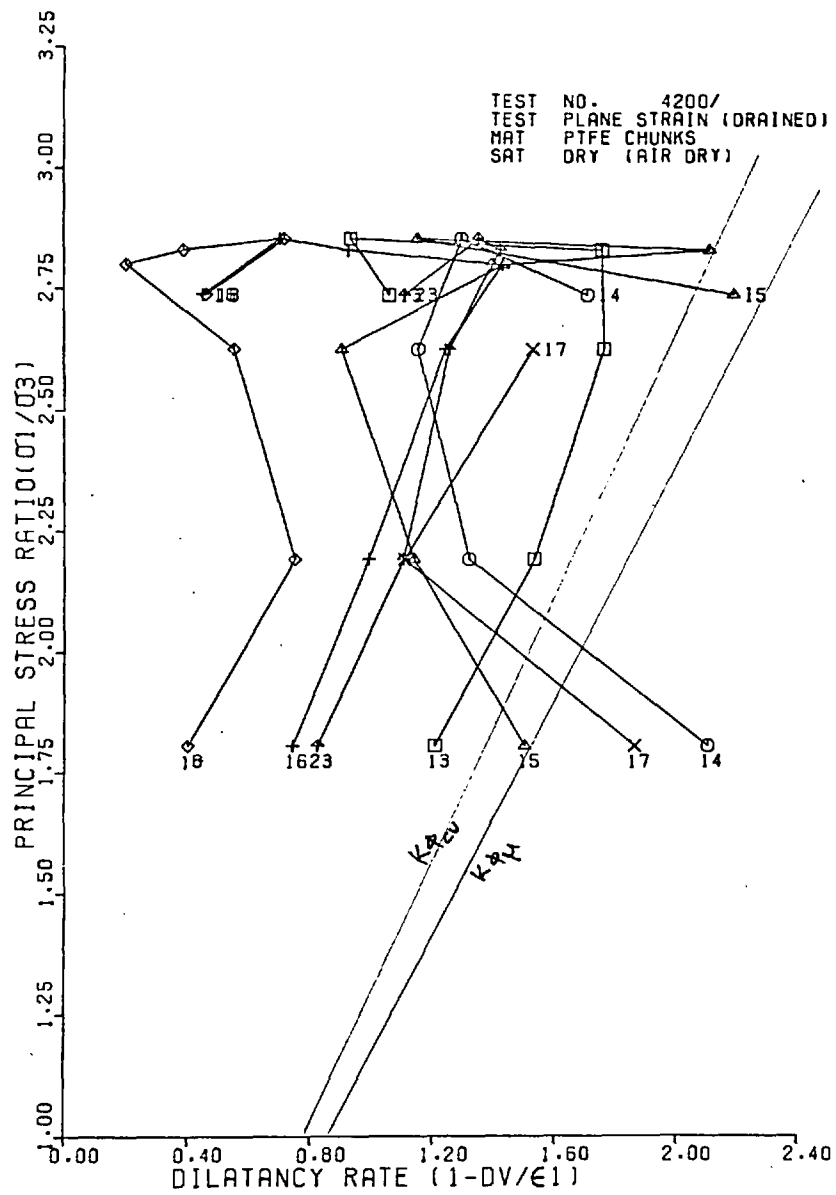


FIG 8.13-STRESS - DILATANCY PLOTS(MAJOR)

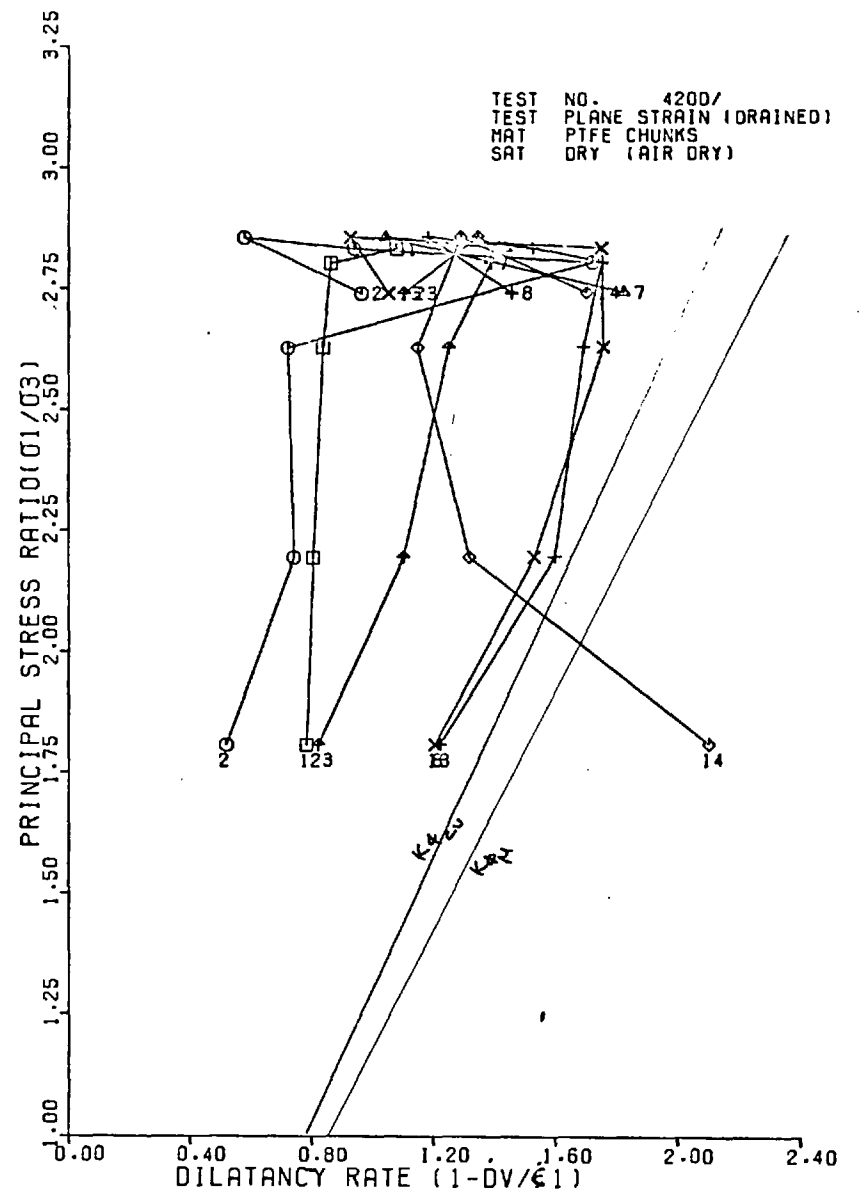


FIG 8.14-STRESS - DILATANCY PLOTS(MAJOR)

CHAPTER 9

CONCLUSIONS AND RECOMMENDATIONS FOR FURTHER WORK

9.1 SUMMARY AND CONCLUSIONS

In this investigation the main emphasis was placed on the microscopic study (far above the atomic level) rather than on the macroscopic study of deformation behaviour of granular soils. However, the observations at macroscopic level, that is, at the external boundaries of the test samples were taken in a usual way as are done in conventional soil tests. Additional efforts were made in the development of new techniques and apparatus for this investigation.

In the existing particulate theories, it is generally assumed that the interparticle friction plays a major role. Despite of the important role which is assumed to be played by interparticle friction, no systematic study of interparticle friction of soil forming minerals has been made. The published data of some materials are often the centre of controversy. In order to avoid any controversy about the use of particular value of ϕ_{μ} , actual interparticle friction tests were performed on the four out of the five test materials used in this study. It was found that if the surface topography of the particles were kept under strictly controlled conditions, reproducible values of friction with acceptable scatter could be obtained. Throughout the test programme every effort was made to keep practically similar surface topographical conditions i.e. surface roughness and surface cleanliness of the test particles. Experimental observation clearly showed that the glass under wet condition possesses very high coefficient of friction i.e. between 0.7-0.9 provided its surface was initially very

carefully and meticulously cleaned and subsequently the cleanliness was maintained throughout the test.

It was found that the coefficient of surface friction is not a constant property of a material but it changes with normal load. Brittle, hard materials, particularly glass, showed increase in friction with increase in normal force. Whilst in the case of visco-elastic polymeric materials namely PTFE and polypropylene friction decreases with increase in normal load.

The study of surface frictional properties of test materials has clearly shown particularly in the case of glass that it is not correct to compare the coefficient of friction of a material tested by different researchers even by the same investigator unless the materials are exactly similar in all respect and tested under exactly similar conditions.

X-ray photogrammetry was used for tracing the movements of the representative particles which were approximately located in a vertical plane which was parallel and midway between the two σ_2 -platens. The configuration of X-ray set-up used was such that the advantage of readily available general program of data reduction could not be taken. A special computer program was developed and used for solving numerically the photogrammetric problem. The accuracy obtained from the X-ray photogrammetric observations was very satisfactory. However, there is a need for further research if the level of the desired accuracy is to be increased further.

Test samples, prepared from the five selected materials, were tested under plane strain compression test conditions and were fully drained during the tests. Further test samples were tested under two extreme conditions of saturation namely dry and saturated (with deaired distilled

water. The stress-strain curves obtained from the measurement of boundary-forces and -deformations, Fig. 6.4-6.13 appear continuous and reasonably smooth. Any unsmoothness of these curves can be attributed to the use of large deformation increments between the successive radiography, at rather large intervals. Since the packing conditions and shape of the particles, excepting of PTFE samples, were similar, the stress-strain curves show approximate similarity. From these curves it appears that the surface frictional properties of the constituent particles do not significantly influence their macroscopic behaviour.

The deformation data of the representative particles, also called markers, obtained from X-ray photogrammetric observations formed the basis of the particulate study of this investigation. From the study of the original data as well as processed according to the scheme mentioned in Chapter 7, the following main conclusions can be made:-

1. The movement of individual particles appear to be continuous but erratic in nature. Therefore these linear movements can not be modelled by a continuous analytic function.
2. Almost every particle in the sample is likely to experience rotation during the deformation history of the test sample. It can, therefore, be said that rotation of the constituent particles of a test sample is the peculiarity of the cohesionless granular mass. Further the rotation of the particles occur randomly.
3. Non-uniformity of displacements is not eliminated even by taking the average displacements or rotations over a number of particles in a pre-selected region called element.

4. Large rotations of rotund particles in isolation were observed specially during early stages of deformation and these rotations were not necessarily in the strain plane (Fig. 7.4). The occurrence of these rotations suggests that the presence of roller particles is highly probable. From these observations supported by the displacement-rotation plots it can be inferred that the mechanism of deformation particularly of test samples prepared from rotund particles, cannot primarily be of sliding. Also rolling mechanism alone cannot exist at least under the test conditions used in this study.
5. Components of strain were calculated, of course based on the concept of continuum mechanics, and also the dilatancy factor D . The strain distribution inside the test sample was found to be non-uniform. Consequently the dilatancy factor showed the variation. During the deformation history, the magnitude as well as the direction of principal strain increments were generally observed to vary randomly. These variations result in very large values of D , even when the element is not showing large dilatancy.
6. If the magnitude and direction of principal stresses is assumed to be fixed by the external force measurements and if it is assumed that principal stress direction does not change and is independent of the local variations in the strain increment, principal stress direction and principal strain increment directions are non-co-axial.
7. Behavioural trend, particularly of incremental volumetric strains and incremental maximum shear strain, indicated the mechanics of deformation and the significance of particle shape, surface hardness and of the granular fabric.

8. The experimental evidence obtained from this investigation has clearly shown that the fabric of the test sample plays a major role and it is supplemented by other mechanical properties, particularly the compliance, of the constituent particles. From the study of experimental data it appears that surface friction of particles does not significantly affect the deformation mechanism of the test samples. With the help of column-like structures, whose presence was suggested by the behavioural trend of volumetric strains increment and max. shear increment plots and also by the published data on the 2-dimensional tests, and with the help of the mechanical properties particularly compliance and surface hardness, it is possible to explain satisfactorily the reason of obtaining same angle of internal friction of two different materials having different coefficients of surface friction, but both initially packed under similar conditions and also tested similar conditions.
9. As mentioned earlier, non-uniformity in the internal strain increment distribution resulted in the non-uniformity of dilatancy rate distribution inside the test sample. The stress-dilatancy plots, which were obtained from the force-displacement measurements made on the boundaries of the test samples, show that there is a little correlation between the observed stress-dilatancy relation and the theoretical relation either based on the measured value of ϕ_{μ} or based on the value of ϕ_{cv} obtained from the Horne's theoretical relation.

9.2 RECOMMENDATIONS FOR FURTHER WORK

In this investigation the mechanism of deformation put forward is tentative but may form as a basis for discussion and further work. This certainly does not amount to model (picture) the mechanics of deformation of granular mass under any given deformation condition. The proposed

mechanism deals only with plane deformation with the given constraints, and it has yet to be shown that proposed mechanism can model the deformation mechanism for all the test conditions relevant to plane strain tests condition and then only whether they can model the full three dimensional deformation situations. In addition to the experimental verification of the proposed mechanism of deformation, concerted are needed for finding some main parameters which could be used in characterising or averaging the discrete behaviour of the particulate materials and for finding a method of relating microscopic behaviour with macroscopic behaviour. This will, of course, require theoretical investigation.

APPENDIX A

ERROR ANALYSIS

A.1 GENERAL

In real situations no measurement, with whatever care and sophistication it is made, is always loaded with errors and therefore, no absolute value for such a measurement, in a mathematical sense, may be given. These errors may be classified into two main categories:-

a) instrumental errors due to the precision with which the instruments could be read, and b) observational errors which propagate due to the errors made in taking or recording the observations. The computed results based on these measurements, are affected from yet another source of errors. This is due to the fact that certain simplifying assumptions have to be made for the mathematical formulation of the real conditions. All of these errors can also be classified under two general headings: random errors and systematic errors.

Since every measurement and the results based on such measurements are burdened with errors arising from various sources both known and unknown, it is essential to know the accuracy of observations or of a parameter calculated from such measurements, and to know how adversely it affects the interpretation of the results. In this study the experimental investigations, for the convenience of this discussion, can be divided into two distinct stages: a) friction tests of various materials and b) experimental study of deformation behaviour of test samples made from these materials. The errors involved in these two stages of the investigations will now be discussed.

A.2 FRICTION TESTS

The fundamental quantities involved in the measurement of coefficient of friction are vertical force W , frictional resistance F and contact angle between the two sliding surfaces ' θ '. The relationship between these quantities has been given in equation 3.16 and is reproduced below

$$\mu = \tan \phi_{\mu} = F \cos \theta / (2W) \quad (\text{A.1})$$

The contribution made by various sources of errors can be written as:

$$\frac{d\mu}{\mu} = \frac{dF}{F} - \frac{dW}{W} - \tan \theta \cdot d\theta \quad (\text{A.1})$$

where prefix d to the quantities μ , θ , F and W denotes the change in their values.

By using the theory of errors, the above relationship can be written in terms of standard errors as follows:-

$$\sigma_{\mu} = \sqrt{\left(\frac{\sigma_F}{F}\right)^2 + \left(\frac{\sigma_W}{W}\right)^2 + \left(\tan \theta \cdot \sigma_{\theta}\right)^2} \quad (\text{A.3})$$

It must be noted that the measurement of W was affected by the friction at the universal joint whereas that of F , particularly at low loads, was influenced by the change in the temperature inside the enclosure where the friction apparatus was placed during the test. The variation in contact angle occurs if the particles in a given geometric configuration are different in shapes than assumed in the mathematical formulation. In the present investigation the particles

used were approximately spherical except those of polypropylene, which were spherical for all practical purposes. For these particles it is obvious to expect certain variation in contact angle θ when tested under the configuration shown in Figure 3.4. The contribution made by these sources of errors are given in Table A.1 for the extreme range of loading conditions investigated in this study. Reference to this table shows the maximum absolute errors in the friction measurements are less than 6% for very low friction materials tested under very low loads and are about 1% for high frictional materials tested under a load of 4.0N. These figures suggest that the errors are not significant. The effect of other sources of errors, for example possible modification or change in the surface conditions during the tests, cannot be separated and is, therefore, assumed to be random in nature. The combined effect of all the errors due to various sources can be represented in the form of a RMSE (Root Mean Square Error) provided that these errors can be considered as random errors. The RSME for various friction tests are given in Table 3.1 to 3.3.

A.3 ERROR PROPAGATION IN PLANE STRAIN TESTS AND IN X-RAY PHOTO-PROGRAMMETRIC OBSERVATIONS

a) Errors in Plane Strain Test

The results of plane strain tests are affected by various sources of errors including sample size, platen friction, and confining effect of membrane. Various methods have been proposed by different researchers for estimating the contribution made by these factors including the three major factors given above. It is rather difficult to say with total confidence about the correctness or otherwise of these estimates,

particularly when the stress distribution on the sample-platen interface is not known. Instead of applying corrections to the measured values of stresses and deformations, steps should be taken to minimise the effect of various sources of errors. In the plane strain compression tests of this investigation, every practical step was taken, see Chapter 2. It may, therefore, be expected that the effect from these sources of error will be small.

Experimental evidence produced by this study supports the above statement. For example, deformation behaviour at particle level has clearly shown that the plastic stripped rubber membrane did give better results than those obtained by using sandwiched rubber membrane sheets as recommended by Green (1969). Further, since all the tests reported here were performed under more or less similar test conditions, the error propagating in plane strain tests on various test samples and test materials will be of the same order of magnitude. These errors will not affect significantly the comparative study of the test samples of various materials tested under given conditions, see Chapter 2.

b) Error Propagation in Deformation Studies at Microscopic Level

The basic tool used for the measurement of deformation of the granular fabric at particle level was X-ray photogrammetry. The sources of errors, which are inherent in the photogrammetric configuration used, will evidently influence the data for the deformation study at microscopic level.

In the X-ray photogrammetry, as used here, a radiograph is considered as a central projection of the object on a flat surface (idealised film plane). This basic assumption, however, is an approx-

imation and as a consequence, the differences between results of application of the mathematical model and the physical reality are found.

Some of the examples illustrating the difference between the mathematical formulation and the situation in reality are given below:-

i) The radiograph is assumed to be a central projection of the radiographed object. It is, therefore, assumed that somewhere in or near the X-ray head or target there exists a projection centre, photographically speaking. In other words the X-rays are being emitted from a mathematical point source. In reality no such point exists, instead the bundle of X-rays are emanating from focus of finite size. Consequently penumbra is formed around the boundaries of the image of an object, which is one of the sources of errors.

ii) There does not even exist a mathematical plane of projection as the emulsion has a certain thickness and the situation is made further complex when the X-ray films, as used in this study, have double layers of emulsion coated on either side of the base for practical reasons. The image points would appear to be, consequently, located at different depths depending, amongst various factors, upon the intensity of radiation and the film developing process used.

iii) The film base is assumed to be a perfect plane and to be dimensionally stable. In reality, especially when using X-ray films loaded in conventional film-cassettes, appreciable film distortion may be found. Further the storing conditions and processing technique used for exposed radiographs, the shrinkage of film emulsion may occur, which may be different in different parts of the negative.

The correspondence between reality and the mathematical model adopted can, therefore, be very approximate. The degree of difference between these two depends on the data acquisition configuration and method of data reduction employed, and also on the operator's performance who is actually reading the stereo-radiographs.

Since there are so many factors, both known and unknown, which can affect the photogrammetric results, the services of an experienced stereo-comparator operator were utilized for reading the radiographs of all tests whose results are presented here. This, in fact, resulted in obtaining the image coordinates of all the object points with higher accuracy. This would be obvious when the results of error analysis will be presented later in this section (and see Table A.2). Further, it will be seen that the accuracy of observations is approximately constant. The variations may be attributed to the material used rather than to the operator's observational errors.

One of the basic requirements of using the variation - of - coordinates method is that the observations must be free from any systematic errors and have been adjusted for such errors, if any. One of the advantages of using the analytical approach is that effect of these systematic errors can easily be incorporated in the system provided that suitable mathematical models are available for each of the systematic errors expected to be present. In contrast to the conventional photogrammetry where these models for image refinements (models for corrections of lens distortions and film deformations) are available, no such models, to the best of writer's knowledge, are yet available particularly for the X-ray photogrammetric data acquisition used here.

Although it was realised that there is a need for further work for formulating suitable mathematical models for such systematic errors, which is itself a research topic on its own, no effort was made in this direction, because of the scope of the present study. Instead it was assumed that all the errors were random.

c) Accuracy of Image Coordinates

As explained in Section 5.105, the observation equations and normal equations can be written in matrix notation as:-

$$\begin{bmatrix} B \end{bmatrix} \begin{bmatrix} O \end{bmatrix} = \begin{bmatrix} \ell \end{bmatrix} + \begin{bmatrix} v \end{bmatrix} \quad (\text{A.4})$$

and

$$\begin{bmatrix} B \end{bmatrix}^T \begin{bmatrix} B \end{bmatrix} \begin{bmatrix} O \end{bmatrix} = \begin{bmatrix} B \end{bmatrix}^T \begin{bmatrix} \ell \end{bmatrix} \quad (\text{A.5})$$

where $\begin{bmatrix} B \end{bmatrix}$ is coefficient matrix of the observation equations of the order $(m \times n)$

$\begin{bmatrix} O \end{bmatrix}$ is the orientation parameter matrix of the order $(n \times 1)$

$\begin{bmatrix} \ell \end{bmatrix}$ is observation matrix of the order $(m \times 1)$

$\begin{bmatrix} v \end{bmatrix}$ is residual matrix of order $(m \times 1)$

n is number of unknown orientation parameters

m is number of observations.

Once the orientation parameters are known, these can be substituted in the original set of observation equations (A.4) and consequently the least squares residuals, $\begin{bmatrix} v \end{bmatrix}$, which in turn can be used to compute the standard deviation of an observation of unit weight σ_o . Gauss

formula for σ_o was used, which can easily be derived to be

$$\sigma_o^2 = \frac{[v]^T [v]}{m - n} \quad (\text{A.6})$$

For all the stereo-radiographs of a given test, the values of σ_o were calculated. The mean value of σ_o for all the stereo-pairs of the same test was obtained. Calculations were repeated for all the tests of this investigation. The mean standard errors of unit weight for all the tests are tabulated in Table A.2.

Since standard error of unit weight can be regarded as a basic expression for the accuracy of image coordinates with which they were read, the computational results of σ_o are very satisfactory. It should be noted that the radiographs were obtained under conditions which cannot be termed as ideal or even close to those which exist in the conventional aerial photogrammetry.

d) Accuracy of Object Coordinates

It is well known that the inverse of the coefficient-matrix of the normal equations, equations A.5, pre-multiplied by σ_o^2 , is the variance - covariance matrix of the unknowns, a relationship which is generally expressed in the matrix form

$$\sigma_{xx} = \sigma_o^2 \left([B]^T [B] \right)^{-1} \quad (\text{A.7})$$

The typical diagonal term of the matrix on the right hand side of equation (A.7) gives the mean-square-error or 'variance' of the unknown.

Utilizing these equations root-mean-square-error (RMSE) for the calculated object coordinates were obtained for all the stereo-radiographs of a test. These calculations were repeated for all the tests. The average RMS errors for all the tests are summarised in Table A.2. From this table it can be seen that the accuracy of calculation of X and Y coordinates of the object points is the same as that of the image coordinates. However, the accuracy of calculation of Z is not as good as that of X and Y. It is not surprising to obtain a lower accuracy in Z. One of the basic reasons of this is the accuracy of reading the object coordinates of control points. It may be recalled that the machine used for measuring the Z coordinates of these points was a universal milling machine and its precision of observations was definitely crude and poor in comparison with the stereo-comparator, which was used for measuring the X and Y coordinates. In addition to this major source of error, other factors, which might have affected its accuracy, may possibly be bulging of the σ_2 -platens under pressure. Further, it can be speculated that the calculated accuracy are also affected by the presence of systematic errors which were disregarded in the mathematical formulation of the photogrammetric problem.

Despite these large errors in estimation of Z coordinates of the tips of the marker wires, the interpretation of the basic data generated from the photogrammetric observations is not significantly affected. It is mainly due to our major interest in tracing the movement of particles in the XY plane, which is normal to the σ_2 -direction. However, the information of movement in the other planes is used here but the results are conditional by the outlined inaccuracies.

e) Accuracy of the Measurement of Orientation of a marker Particle
in Object Space

In order to define the orientation of a marker particle completely in object space, the spatial coordinates of the centre of the marker wire and the angular orientation of the longitudinal centre line of the marker wire (cylindrical in shape) were calculated from the readings of the four X-ray images of corners of the wire.

It can be easily shown with the help of theory of errors, that the accuracy of the measurement of the centre of the wire and its angular orientation can be given by the following relationship:-

(i) RMSE of linear coordinates, for example for X coordinates of:

(a) centre of the end of the marker wire, herein called tip

$$\sigma_{xt} = \sigma_x / \sqrt{2} \quad , \text{ and} \quad (\text{A.8})$$

(b) centre of the marker wire

$$\sigma_{xc} = \sigma_x / 2 \quad (\text{A.9})$$

where σ_x is the RMSE of measured X-coordinates

(ii) RMSE of angular orientation say in XY plane

$$\sigma_\phi^2 = (\cos \phi / r)^2 (2\sigma_{xt})^2 + (\sin \phi / r)^2 (2\sigma_{yt})^2 \quad (\text{A.10})$$

where σ_ϕ is the RMSE of angular orientation ϕ ,

σ_{xt} & σ_{yt} are the RMSE's of the coordinates of the tip of

marker wires and are assumed to be the same for both the tips.

ϕ is the most probable angular orientation of the marker wire in the XY plane

r is the length of projection of the marker wire.

If the values of σ_{xt} from equation (A.8) are substituted in Eqn. (A.10) and it is assumed that the RMSE's of X and Y coordinates are equal, the maximum RMSE of angular measurement can be shown to be

$$\sigma_{\phi} = \sigma_x / r \quad (\text{A.11})$$

For typical values of $\sigma_x = \sigma_y = 0.04$ mm and $r = 5.0$ mm, the values of various RMS errors work out to be

(i) RMSE's of linear coordinates:

$$\sigma_{xt} = 0.028 \text{ mm}$$

$$\sigma_{ct} = 0.020 \text{ mm}$$

(ii) RMSE of angular orientations

$$\sigma_{\phi} = 0.008 \text{ radian.}$$

The RMSE's of incremental displacements and angular rotations, which are calculated by subtracting their initial values before the application of deformation from their respective final quantities at the end of the deformation, will be $\sqrt{2}$ times of their relevant values. For example these values for the typical case considered above will be 0.040, 0.028 mm and 0.011 rad. respectively.

Table A.1 Maximum Absolute Error in the Values of the Coefficient of Friction (Equation A.2)

Most probable value of μ	Vertical Load W (N)	dW (N)	$\frac{dW}{W}$ (%)	Frictional resistance F (N)	dF (N)	$\frac{dF}{F}$ %	Contact Angle ϕ (rad)	d ϕ (rad)	tan ϕ d ϕ (%)	$\frac{d\mu}{\mu}$ %
0.05	0.4	0.002	0.5	0.0462	0.002	4.3	0.524	0.01	0.577	5.4
	4.0	0.002	0.05	0.462	0.002	0.43	0.524	0.01	0.577	1.45
0.8	0.4	0.002	0.5	0.739	.004	0.55	0.524	0.01	0.577	1.63
	4.0	0.002	0.05	7.39	0.025	0.35	0.524	0.01	0.577	1.00

Table A.2 Mean RMS Errors of Data Reduction

Test No.	Test Specimen		Standard Error of Unit Weight (μm)	Mean RMSE of Coordinates (μm)		
	Material	Sat.		X	Y	Z
1200	Gravel	Dry	41	36	41	137
1201	Gravel	Sat	45	36	40	130
2200	Glass	Dry	42	36	39	128
2201	Glass	Sat	49	42	48	143
3200	Ceramic	Dry	42	38	40	112
3201	Ceramic	Sat	43	33	40	121
4200	PTFE	Dry	33	31	32	132
4201	PTFE	Sat	36	35	33	140
5150	Poly-propylene	Dry	34	30	30	135
5201	Poly-propylene	Sat	35	30	32	137

APPENDIX B

COMPUTATION OF STRAINS AND DILATANCYa. ZONALISATION

For the computation of strains and dilatancy rates, the area of the XY-plane covered by the marker particles is divided into 16 approximately equal sub-areas or zones, see Fig. B.1 (a). For each of these zones, the spatial coordinates, herein called nodal coordinates, are calculated by taking the mean of the respective coordinates of the centre of the marker particles located inside the sub-area or zone. The node, which is defined by the nodal coordinates, is then assumed to represent the deformation characteristics of the group of particles in a given area. The components of linear displacements at a given node can easily be calculated by subtracting the respective coordinates of the node before and after the given deformation increment.

Although the zones are approximately of equal size and rectangular in shape, the configuration of the layout of the nodes is not regular, which, in fact, depends upon the number of marker particles present in a given zone and their disposition in that zone. For such irregular arrangement of nodes, calculation of strains on the basis of "triangular elements" obviates the necessity of having the nodes arranged in a regular array and also reduces errors due to significant geometry changes:

Although the necessary data and computer facilities are available for the calculation of strains in three dimensions, only the strains pertaining to the two dimensional marker plane are calculated for three main reasons. Firstly, it is true that replacing a body deforming in all the three

directions by a body which is restricted to deform in only two-dimensions brings in the element of over-simplification and so does the application of theory using infinitesimal strains .

Secondly, the experimental evidence, presented in Chapter 7 in the form of flow diagrams of the marker particles, for instance see Figure 7.18 suggests that only a small no. of particles show movement in the Z-direction. Further these diagrams show that these movements occur both in the positive and in the negative Z-directions. The effect of these movements becomes smaller on the average displacement behaviour of a group of particles as the number of particles in the group is increased. With large numbers of particles in a group, the average displacement behaviour becomes two-dimensional.

Thirdly, mathematics and consequently numerical computations are much simpler for two-dimensional strain analysis than those for three-dimensional deformation problems.

The schematic arrangement of the triangular elements is shown in Figure B.1 (b). Figure B.2 shows the typical triangular element considered, with nodes i, j, k numbered in anti-clockwise order.

The displacements of a node have two components in X- and Y- directions respectively. Writing in matrix notation:-

$$\{\delta_i\} = \begin{Bmatrix} u_i \\ v_i \end{Bmatrix} \quad (B.1)$$

Consequently the element displacements can be represented by six components and are given below as a vector

$$\{\delta\}^e = \begin{Bmatrix} \delta_i \\ \delta_j \\ \delta_k \end{Bmatrix} \quad (\text{B.2})$$

If it is assumed that a uniform strain is taken to be caused by a linear displacement field, the displacements u and v are given by two linear polynomials

$$\begin{aligned} u &= a_1 + a_2x + a_3y \\ v &= a_4 + a_5x + a_6y \end{aligned} \quad (\text{B.3})$$

The six constants 'a' can be determined if the measured dimensions of the triangle and the measured displacements of the corners i , j , k are substituted in equations (B.3).

The strain at any point within the element can be defined by its three components

$$[\epsilon] = \begin{Bmatrix} \epsilon_x \\ \epsilon_y \\ \gamma_{xy} \end{Bmatrix} = \begin{Bmatrix} -\frac{\delta u}{\delta x} \\ -\frac{\delta u}{\delta y} \\ -\left(\frac{\delta u}{\delta y} + \frac{\delta v}{\delta x}\right) \end{Bmatrix} \quad (\text{B.4})$$

where compressive strains are positive.

The relationship between strain and displacements can be written as

$$[\epsilon] = [B] \{\delta\}^e \quad (B.5)$$

for the triangular element the $[B]$ matrix can be written as

$$[B] = \frac{1}{2\Delta} \begin{bmatrix} b_i & 0 & b_j & 0 & b_k & 0 \\ 0 & c_i & 0 & c_j & 0 & c_k \\ c_i & b_i & c_j & b_j & c_k & b_k \end{bmatrix} \quad (B.6)$$

in which $b_i = y_j - y_k$ (B.7)

$$c_i = x_k - x_j$$

with the other coefficients obtained by a cyclic permutation of subscripts in the order i, j, k and where

$$2\Delta = \det \begin{vmatrix} 1 & x_i & y_i \\ 1 & x_j & y_j \\ 1 & x_k & y_k \end{vmatrix} = 2 \text{ (area of triangle } i, j, k) \quad (B.8)$$

Using the above equations, a computer program can be written for calculating the basic strain increments.

Once the basic strain increments ϵ_x , ϵ_y and ϵ_{xy} ($= \frac{\gamma_{xy}}{2}$) have been calculated, the magnitude of the principal strain increments and

their directions can be determined either by constructing the Mohr's circle of strain increment (Fig. B.3 (b)) or by using the following equations

$$\begin{matrix} \dot{\epsilon}_1 \\ \dot{\epsilon}_3 \end{matrix} = \frac{1}{2} \left((\dot{\epsilon}_x + \dot{\epsilon}_y) \pm \sqrt{(\dot{\epsilon}_x - \dot{\epsilon}_y)^2 + 4\dot{\epsilon}_{xy}^2} \right) \quad (\text{B.9})$$

$$\xi = \frac{1}{2} \tan^{-1} \frac{2\dot{\epsilon}_{xy}}{\dot{\epsilon}_x - \dot{\epsilon}_y} \quad (\text{B.10})$$

where ξ is the inclination of the principal compressive strain increment direction to the x-axis and is taken positive in the anti-clockwise direction as shown in Figure B.3 (a).

In addition to the above deformation parameters, the following are also calculated

i) Volumetric strain increment, $\dot{\epsilon}_v$

$$\dot{\epsilon}_v = \dot{\epsilon}_1 + \dot{\epsilon}_3 \quad (\text{B.11})$$

ii) Maximum shear strain rate, $(\dot{\epsilon}_{xy})_{\max}$

$$(\dot{\epsilon}_{xy})_{\max} = \frac{1}{2}(\dot{\epsilon}_1 - \dot{\epsilon}_3) \quad (\text{B.12})$$

iii) Angle of dilation, ν , see Figure B.4 (b)

$$\sin \nu = -\dot{\epsilon}_v / (\dot{\epsilon}_1 - \dot{\epsilon}_3) \quad (\text{B.13})$$

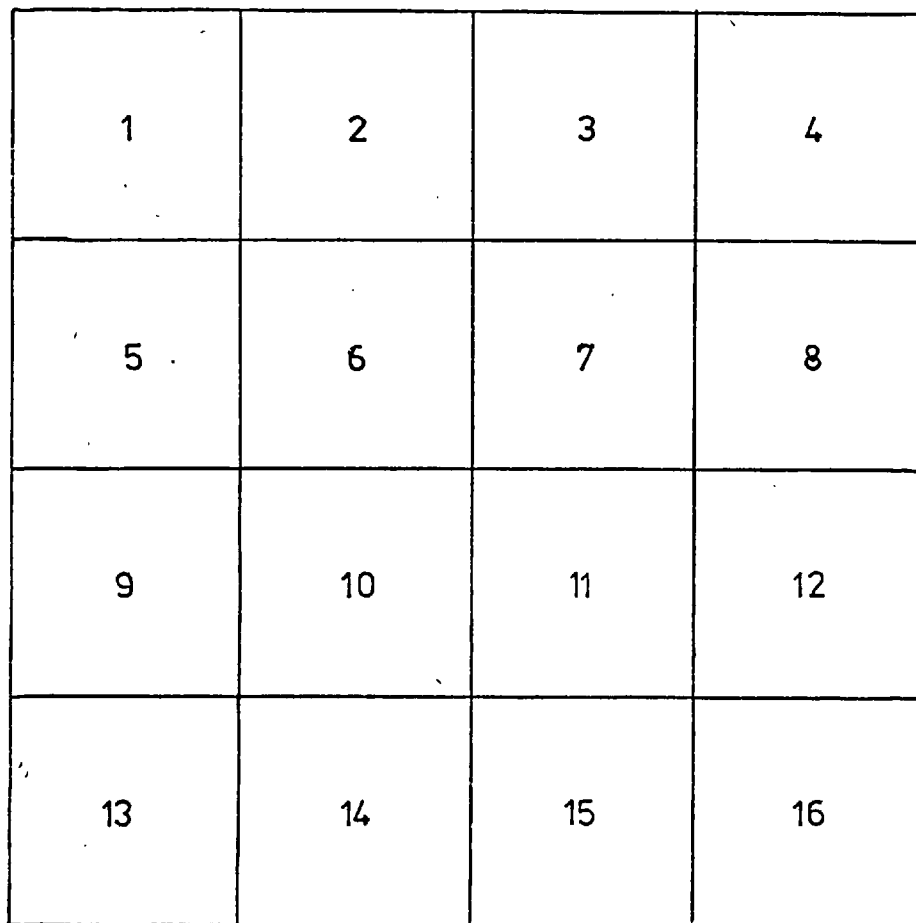
iv) Zero extension angles α and β

$$\alpha = \xi + (45^\circ - \frac{\nu}{2})$$

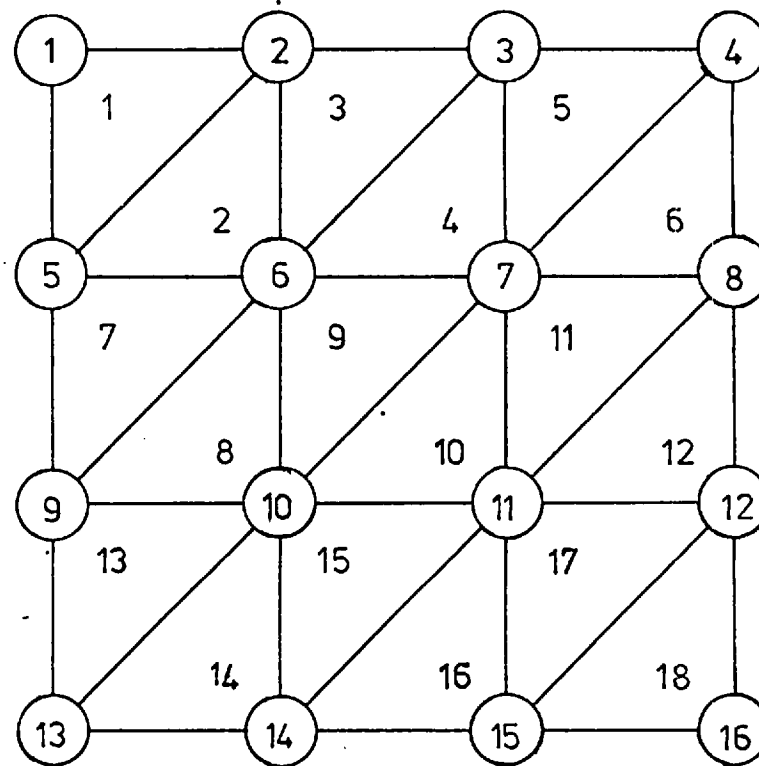
$$\beta = \xi - (45^\circ - \frac{\nu}{2})$$

(B.14)

A computer program has been developed by the writer for calculating all the deformation parameters mentioned above. Also a separate program was written for determining the nodal coordinates of the triangular elements and for obtaining the average rotations of the marker particles enclosed in the combined area represented by the three nodes of a triangular element. A computer printout of the calculated values of all the deformation parameters for two typical elements is reproduced in Table B.1.



a) ZONES



b) ELEMENTS

FIG. B.1 Zonalisation of the strain plane

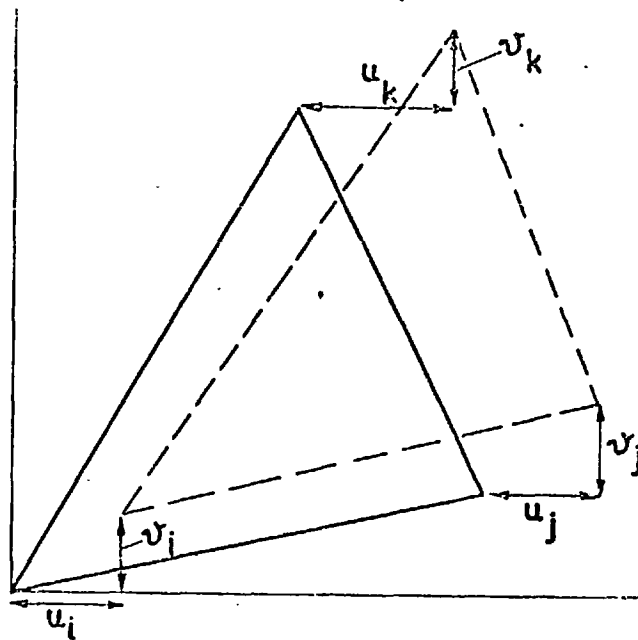
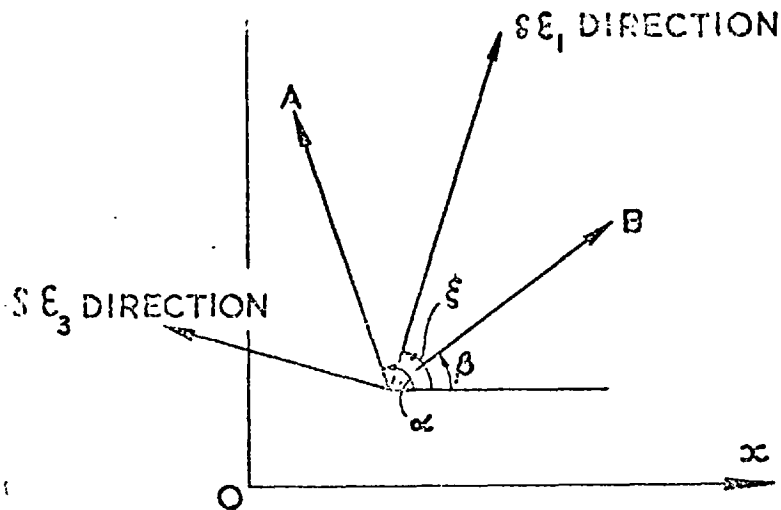
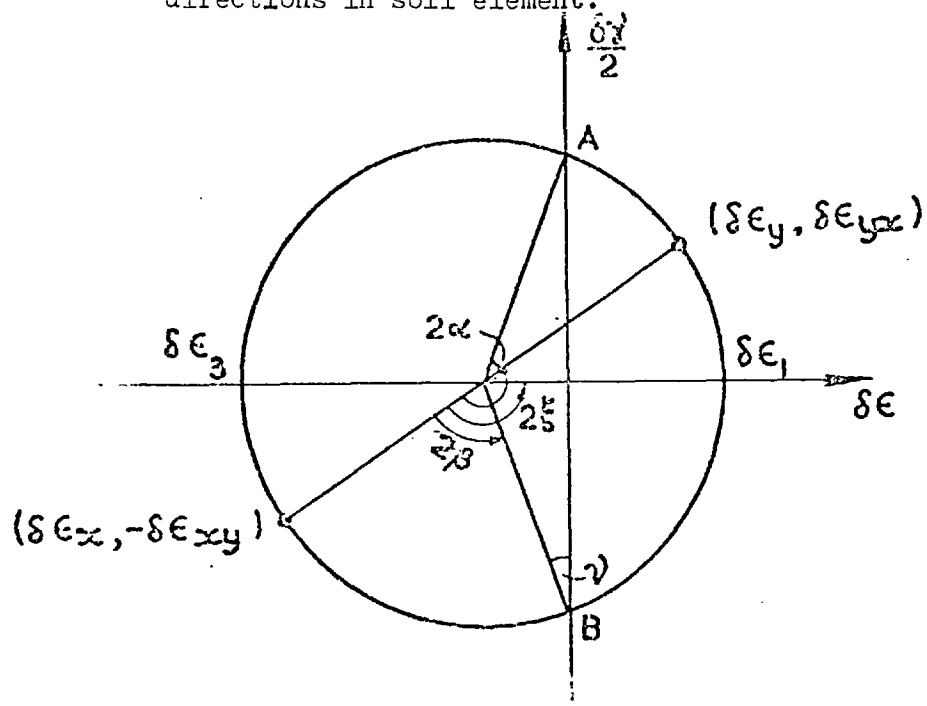


Fig. B.2 Initial and final configuration of a triangular element



a) Principal compressive strain increment and Zero extension directions in soil element.



b) The associated Mohr's circle of strain increment

REFERENCES

- ACKERMANN, F. (1964). Precision of strip triangulation theory and statistical tests. *Photogrammetria*, 19, No. 7, 393.
- AMONTONS, M. (1699). De la resistance causee dans les machines. *Histoire de l'Academie Royale des Sciences, Anne MDCXCIX*, Amsterdam, 1734, 259-282.
- ANDRAWES, K.Z. and BUTTERFIELD, R. (1973). The measurement of planar displacements of sand granis. *Tech. notes, Géotechnique*, 23, 571-576.
- ARCHARD, J.E. (1957). Elastic deformation and the laws of friction. *Proc. Roy. Soc.*, A243, 190-205.
- ARTHUR, J.R.F. (1962). Strains and lateral force in sand. Ph.D. Thesis, University of Cambridge.
- ARTHUR, J.R.F. (1971). New techniques to measure new parameters. *Proc. Roscoe Mem. Symp.*, Cambridge, 340-346.
- ARTHUR, J.R.F. and DUNSTAN, T. (1969). Radiography measurements of particle packing. *Nature, Lond.*, 223, 464-468.
- ARTHUR, J.R.F. & MENZIES, B.K. (1972). Inherent anisotropy in a sand. *Géotechnique* 20, 115-128.
- ASHKENAZI, V. (1970). Adjustment of control networks for precise engineering surveys. *Chartered Surveyor*, 102, No. 7, 314-320.
- BARDEN, L. (1969). A quantitative treatment of the deformation behaviour of granular material in terms of basic particulate mechanics. *Proc. Southampton, 1969. Civil Engs. Materials Conf.*, Wiley Interscience, Part 2, 599-612.
- BARTON, R.R. (1972). A study of interparticle friction of sand with respect to mass strength. M.Sc. Thesis, Manchester University.

- BISHOP, A.W. (1954). Correspondence on "Shear characteristics of a saturated silt, measured in triaxial compression" by A.D.M. Penman, Géotechnique 4, 43-45.
- BISHOP, A.W. and GREEN, G.E. (1965). The influence of end restraint on the compressive strength of a cohesionless soil. Géotechnique, 15, 243-66.
- BISHOP, A.W. and HENKEL, D.J. (1962). The measurement of soil properties in the triaxial test. London: Edward Arnolds Ltd.
- BOROWICKA, H. (1973). Rearrangement of grains by shear tests with sand, Proc. 8th Int. Conf. Soil Mech. Found. Engng., Moscow, 1.1, 71-77.
- BOWDEN, F.P. (1967). The area of contact between rough surfaces and flats. Discussion, J. Lub. Tech. Trans ASME, F89, 87-91.
- BOWDEN, F.P. & BROOKES, C.A. (1966). Frictional anisotropy in non metallic crystals Proc. Roy. Soc., A295, 244-258.
- BOWDEN, F.P., BROOKES, C.A. and HANWELL, A.E. (1964). Anisotropy of friction in crystals. Nature, London, 203, 27-30.
- BOWDEN, F.P. & HANWELL, A.E. (1966). The friction of clean crystal surfaces. Proc. Roy. Soc., A295, 233-243.
- BOWDEN, F.P., MOORE, A.J.W. & TABOR, D. (1943). The ploughing and adhesion of sliding metals. J. appl. Phys., 14, 80-91.
- BOWDEN, F.P. & TABOR, D. (1954). Friction and lubrication of solids, Part I. Oxford: Clarendon Press.
- BOWDEN, F.P. & TABOR, D. (1964). Friction and lubrication of solids, Part II. Oxford: Clarendon Press.
- BOWDEN, F.P. & TABOR, D. (1966). Friction, lubrication and wear: a survey of work during the last decade. Brit. J. appl. Phys., 17, 1521-1544.
- BOWDEN, F.P. and TABOR, D. (1967). Friction and lubrication, London: Methuen.

- BRACE, W.F. (1963). Behaviour of quartz during indentation. *J. Geology*, 71, No. 5, 581-595.
- BRITISH STANDARD INSTITUTION (1955). Glossary of term used in Radiology. British standard 2597: 1955. London: British Standard Institution.
- BUTTERFIELD, R. and ANDRAWES, K.Z. (1971). The visualization of planar displacement fields. *Proc. Roscoe. Mem. Symp. Cambridge*, 467-475.
- BUTTERFIELD, R., HARKNESS, R.M. & ANDRAWES, K.Z. (1970). A stereo-photogrammetric method for measuring displacement fields. *Géotechnique*, 20, 308-314.
- BYERLEE, J.D. (1967). Theory of friction based on brittle fracture. *J. appl. Phys.* 38, 2928.
- BYERLEE, J.D. (1970). The mechanics of stick-slip. *Tectonophysics*, 9, 475-486.
- CAQUOT, A. (1934). Equilibre des massifs à frottement interne stabilité des terres pulvérulentes ou cohérentes. Paris: Gauthier-Villars.
- COLBACK, P.S.B. & WIID, B.L. (1965). The influence of moisture content on the compressive strength of rock. *Proc. Rock. Mech. Symp. at Univ. of Toronto, Pub. Mines Branch, Dept. of Mines & Tech. Surv., Ottawa, Canada*.
- COWIN, S.C. (1974). A theory for flow of granular materials. *Powder Tech.* 9, 61-69.
- DANTU, P. (1957). Contribution a l'étude mécanique et géométrique des milieux pulvérulents. *Proc. 4th Int. Conf. Soil Mech. Found. Engng., London*, 1, 144-148.
- DAVIS, H.E. and WOODWARD, R.J. (1949). Some laboratory studies of factors pertaining to the bearing capacity of soils. *Proc. H.R.B.*, 29, 467-476.

- de JOSSELIN de JONG G. (1958). The undefiniteness in kinematics for friction materials. Proc. Conf., Brussels on earth pressure problems, 1, 55-70.
- de JOSSELIN de JONG, G. (1959). Static and kinematics in the failable zone of a granular material. Ph.D. Thesis, University of Delft.
- de JOSSELIN de JONG, G. (1964). Lower bound collapse theorem and lack of normality of strain rate to yield surface for soils. Proc. IUTAM Symp. On Rheology & Soil Mechanics, Grenoble, 69-78.
- de JOSSELIN de JONG, G. (1967). Session 3- Shear Strength of Soil other than clay. "Free discussion" Proc. Oslo Conf. on Soil. Mech. Found. Engng., Oslo, 2, 199-200.
- de JOSSELIN de JONG, G. (1971). The double sliding, free rotating model for granular assemblies. Tech. note. Géotechnique. 21, 155-163.
- DERESIEWICZ, H. (1958). Mechanics of granular matter. Advance in App. Mechanics, 5, Academic Press, New York, 233-306.
- DRESCHER, A. & de JOSSELIN de JONG, G. (1972). Photoelastic verification of a mechanical model for the flow of a granular material. J. Mech. Phys. Solids, 20, 337-351.
- DUFFY, J. and MINDLIN, R.D. (1957). Stress-strain relations and vibrations of a granular medium. J. appl. Mech., 79, 585-593.
- EDEN, J.A. (1962). The conditions necessary for plotting stereo models in which the set principal distance is not the same as that of the taking camera. Photogramm. Engng., 28, no. 1, 73-81.
- EL-RUWAYIH, A.A. (1975). "Stress-strain characteristics of rockfill, and of clays under high pore water tension". Ph.D. thesis, London University.
- ESTEN, R.D., et. al (1966). Automation of Stereo compilation, Chapter 15, Manual of Photogrammetry, volume I, Falls Church: American Society of Photogrammetry.

- FAIG, W. (1974). Personal communication.
- FRYDMAN, S. (1972). An inquiry into the stress strain behaviour of particulate media. Ph.D. Thesis, Technion, Israel Inst. of Techn.
- GERBER, E. (1929). "Untersuchungen ueber die Drückverteilung im Oertlich Belasteten Sand". Dissertation, Technische Hochschule, Zürich.
- GIBSON, R.E. and MORGENSTERN, N.R. (1963). Stress-dilatancy, earth-pressures, and slopes. Discussion, Proc. Am. Soc. civ. Engrs., 89, SM6, 127-129.
- GREEN, A.E. (1969). Strength and compressibility of granular materials under generalized strain conditions. Ph.D. Thesis, University of London.
- GREENWOOD, J.A. (1967). The area of contact between rough surfaces and flats. J. Lub. Tech. , Trans. ASME, F89, 81-87.
- GREENWOOD, J.A. and TRIPP, J.H. (1967). The elastic contact of rough spheres. J. Appl. Mech., 34, 153.
- GREENWOOD, J.A. & WILLIAMSON, J.B.P. (1966). Contact of nominally flat surfaces. Proc. Roy. Soc., A295, 300-319.
- GUDEHUS, G. (1969,a). Granular media as Rate-independent simple materials: Constitutive relations. Powder Tech., 3, 344-351.
- GUDEHUS, G. (1969, b). Rheological & statistical models for dry granular materials. Proc. colloquium über "Stoffverhalten Körniger Medien", Karlsruhe, 41-61.
- GUDEHUS, G. (1972). Elastic-Plastic Constitutive equations for dry sand. Arch. Mech. Stosow. 24 (1972) No. 3, pp. 395-402.
- HABIB, P. (1964). The role of friction in granular media by Haythronthwaite. Discussion. Proc. IUTAM Symp. on Rheology and Soil Mechanics. Grenoble. 163.

- HAFIZ, M.A.A. (1950). Strength characteristics of sands and gravels in direct shear. Ph.D. Thesis, London University.
- HALLERT, B. (1970). X-ray Photogrammetry. Basic Geometry and Quality, Amsterdam: Elsevier.
- HAMBLY, E.C. & ROSCOE, K.H. (1969). Observations and predictions of stresses and strains during plane strain of 'wet' clays. Proc. 7th Int. Cong. Soil Mech. Found. Engng, Mexico, 1, 173-181.
- HASHIN, Z. (1965). Elasticity of random media. Trans. Soc. Rheol. 9, No. 1, 381-406.
- HAYTHRONTHWAITE, R.M., (1964). The role of friction in granular media. Proc. IUTAM Symp. Rheology & Soil Mechanics. Grenoble, 160-162.
- HOBBS, D.W. (1970). The behaviour of broken rock under triaxial compression. Int. J. Rock Mech. & Min. Sci., 7, 125-148.
- HOLLAND, L. (1964). The properties of glass surfaces. London: Chapman & Hall.
- HOLUBEC, I. (1966). The yielding of cohesionless soils. Ph.D. Thesis. University of Waterloo.
- HORN, H.M. & DEERE, D.U. (1962). Frictional characteristics of minerals. Géotechnique, 12, 319-335.
- HORNE, M.R. (1965). The behaviour of an assembly of rotund cohesionless particles; Part I & II. Proc. Roy. Soc., A286, 62-97.
- HORNE, M.R. (1969). The behaviour of an assembly of rotund cohesionless particles. Part III. Proc. Roy. Soc., A310, 21-34.
- JAEGER, J.C. (1959). The frictional properties of joints in rock. Geofis. pura appl., 43, 148-158.
- JAEGER, J.C. (1971). Friction of rocks and stability of rock slopes. Eleventh Rankine Lecture. Geotechnique, 21, 97-134.

- JAMES, R.G. (1973). Determination of strains in soils by radiography. Report No.: CUED/C-Soils/LNI (a) (1973). Engng. Dept., Cambridge University.
- JOHNSON, K.L. (1955). Surface interaction between elastically loaded bodies under tangential forces. Proc. Roy. Soc., A230, 531-548.
- KARARA, H.M. (1971). New trends in close-range photogrammetry. Proc. Symp. Close-range photogrammetry. Am. Soc. Photogrammetry, Falls Church, 231-238.
- KINGSTON, M.R. & SPENCER, A.J.M., (1970). General yield conditions in plane deformation of granular media. J. Mech. Phys. Solids. 18, 233-243.
- KO, H.Y. & SCOTT, R.F. (1967). A new soil testing apparatus. Géotechnique, 17, 40-57.
- KODAK Ltd. (1965). Industrial Radiography. London: Kodak Ltd.
- LAFEBER, D. (1966). Soil structural concepts. Engug. Geology, 1, 261-290.
- LEE, I.K. and INGLES, O.G. (1968). Ch. 4: Strength and deformation of soil & Rocks in Soil Mechanics - Selected Topics. (LEE, I.K. ed.). London: Butterworths, pp. 195-294.
- LEONARDO DA VINCE, (1452-1519). Note books, translated into English by Edward MacCurdy: Jonathan Cape, London, 1938.
- LEUSSINK, H. & BRAUNS, J. (1969). on Regular sphere packings as models for cohesionless soils. Contributions & discussion on mech. properties of rockfill & gravel materials. Proc. speciality Session No. 13, 7th Int. Conf. Soil Mech. Found. Engng., 111-113.
- LEUSSINK, H. and WITTKE, W. (1963). Difference in triaxial and plane strain shear strength. Proc. Symp. "Lab. shear testing of soils", ASTM STP No. 361, 77-89.

- LOGANI, K.L. (1973). Dilatancy model for the failure of rocks. Ph.D. Thesis, Iowa State University.
- MANDL, G. & FERNANDEZ LUQUE, R. (1970). Fully developed plastic shear flow of granular materials. *Geotechnique*, 20, 277-307.
- MARACHI, N.D., CHAN, C.K., SEED, H.B. & DUNCAN, J.M. (1969). Strength and deformation characteristics of rockfill materials. Report No. TE-69-5 to State of California, Department of Water Resources, Dept. of Civil Eng., University of California, Berkeley.
- MARSAL, R. (1973). Ch. 4: Mechanical properties of rockfill. Embankment dam Engineering, Casagrande volume. (Hirschfeld, R.C. & Poulos, H.G., ed.). New York: John Wiley.
- MATSUOKA, H. (1974, a). A microscopic study on shear mechanism of granular materials. *Soils & Found.*, 14, No. 1, 29-43.
- MATSUOKA, H. (1974, b). Stress-strain relationships of sands based on the mobilised plane. *Soils & Foundation*, 14, No. 2, 47-62.
- MATSUOKA, H. (1974, c). Dilatancy characteristics of soil. *Soils & Found.* 14, No. 3, 13-24.
- McFARLANE, J.C. & TABOR, D. (1950). Relation between friction & adhesion. *Proc. Roy. Soc.* A262, 244-253.
- MILES, M.J. (1968). The theory of the analytical solution of the stereogram. *Photogramm. Rec.*, 6, No. 32, 196-201.
- MINDLIN, R.D. (1954). Mechanics of granular media. *Proc. 2nd U.S. Nat. Congr. Appl. Mech.*, 13-20.
- MINDLIN, R.D. & DERESIEWICZ, H. (1953). Elastic spheres in contact under varying oblique forces. *J. appl. Mech.* 20, 327-344.
- MOGAMI, T. (1965). A statistical theory of mechanics of granular materials. *J. Faculty of Engng., University of Tokyo*, (B), 28, No. 2, 65-79.

- MOGAMI, T. (1966, a). Angle of internal friction of granular material and a simple transient phenomenon. *Trans. Jap. Soc. Civ. Engr.*, No. 128, 63-67.
- MOGAMI, T. (1966, b). On the deformation of granular materials. *Trans. Jap. Soc. Civ. Engr.*, No. 129, 39-44.
- MOGAMI, T. (1967). Mechanics of granular materials composed of particles of various size. *Trans. Jap. Soc. Civ. Engrs.* No. 137, 43-47.
- MOGAMI, T. (1968). On the critical state line proposed by Roscoe et al. *Soils & Found.*, 4, No. 4, 1-9.
- MOGAMI, T. (1969, a). Mechanics of granular material as a particulated mass. *Proc. 7th Int. Conf. Soil Mech. Found. Engng.*, Mexico, 1, 281-285.
- MOGAMI, T. (1969, b). Panel discussions - Session 1 - Shear Strength of Soils. *Proc. 7th Int. Conf. Soil Mech. Found. Engng.*, Mexico, 3, 169-171.
- MOGAMI, T. and IMAI, G. (1967). On the failure of the granular material. *Soil & Found.*, 7, No. 3, 1-19.
- MOGAMI, T. and IMAI, G. (1969). Influence of grain to grain friction on shear phenomena of granular material. *Soils & Found.*, 9, No. 3, 1-15.
- MOGAMI, T. & YOSHIKOSHI, H. (1968). On the angle of internal friction of coarse material. *Acta Technica Acad. Scientiarum Hungaricae*, 63, 193-197.
- MOGAMI, T. & YOSHIKOSHI, H. (1971). On the influence of particle breakage & particle shape on shearing resistance of coarse granular materials. *Asian Reg. Conf. Soil Mech. Found. Engng.*, Bangkok, 1, 141-146.
- MORGENSTERN, N.R. and TCHALENKO, J.S. (1967). Microscopic structure in kaolin subjected to direct shear. *Géotechnique*, 17, No. 4, 309-328.

- MUNRO, J. & JOWITT, P.W. (1974). Information theory and granular material. Res. Report. SAM 74/1, Systems & Mech., Dept. Civil Eng., Imperial College, London.
- MURAYAMA, S. (1964). A theoretical consideration on a behaviour of sand. Proc. IUTAM Symp. "On Rheology and Soil Mechanics", Grenoble, 146-157.
- MURAYAMA, S. and MATSUOKA, H. (1973). A microscopic study on shearing mechanism of soils. Proc. 8th Int. Conf. Soil Mech. Found. Engng., Moscow, 1.2, 293-298.
- MURAYAMA, S. & YAGI, N. (1965). Written contribution to session 2. Soil Properties - Shear strength and consolidation. Proc. 6th Int. Conf. Soil Mech. Found. Engng., Montreal, 3, 343-346.
- MURRELL, S.A.F. (1965). The effect of triaxial stress systems on the strength of rocks at atmospheric temperatures. Geophys. J., 10, 231-281.
- ODA, M. (1972, a). Initial fabrics and their relations to mechanical properties of granular material. Soils & Found. 12, No. 1, 17-36.
- ODA, M. (1972, b). The mechanism of fabric changes during compressional deformation of sand. Soils & Found., 12, No. 2, 1.
- ODA, M. (1972, c). Deformation mechanism of sand in triaxial compression tests. Soils & Found. 12, No. 4, 45-63.
- ODA, M. (1974). A mechanical and statistical model of granular material. Soils & Found., 14, No. 1, 13-27.
- ODA, M. (1975). On stress-dilatancy relation of sand in simple shear test. Soils and Found., 15, No. 2, 17-30.
- ODA, M., KOBAYASHI, H., YAMAZAKI, Y & ONODERA, T. (1972). A new technique for determination of void ratio and its variation within deformed granular material. Report, Dept. Found. Eng., Faculty Sc. & Eng., Saitama University, 3, 39.

- ODA, M. & KONISHI, J. (1974a). Microscopic deformation mechanism of granular material. *Soils & Foundation*, 14, No. 4, 25-38.
- ODA, M. & KONISHI, J. (1974b). Rotation of principal stresses in granular material during simple shear. *Soils & Found.*, 14, No. 4, 39-54.
- PARKIN, A.K. (1965). On the strength of packed spheres. *J. Aust. Math. Soc.*, 4, pt. 4, 443.
- PATTON, F.D. (1966). Multiple modes of shear failure in rock. *Proc. 1st Cong. Int. Soc. Rock Mech.*, 1, 509-513.
- PROCTER, D.C. (1974). An upper bound value for ϕ_f in the stress-dilatancy equation. *Géotechnique*, 24, 269-288.
- PROCTER, D.C. & BARTON, R.R. (1974). Measurements of the angle of inter-particle friction. *Géotechnique*, 24, 581-604.
- PUTNER, T. (1959). Methods of cleaning glass by vapor degreasing and ultrasonically agitated solvents. *Brit. J. Appl. Phys.*, 10, 332.
- READES, D.W. (1972). Stress-strain characteristics of a sand under three-dimensional loading. Ph.D. Thesis, London University.
- REYNOLDS, O. (1885). On the dilatancy of media composed of rigid particles in contact with experimental illustration. *Phil. Mag. (5 series)* 20, 469-481.
- REYNOLDS, O. (1886). Experiments showing dilatancy, a property of granular material, possibly connected with gravitation. *Proc. Royal Institution of Great Britain*, Feb. 12, 1886.
- ROSCOE, K.H. (1970). The influence of strains in Soil Mechanics. Tenth Rankine Lecture. *Géotechnique*, 20, No. 2, 129-170.
- ROSCOE, K.H., ARTHUR, J.R.F. and JAMES, R.G. (1963). The determination of strains in soils by an X-ray method. *Civil Engng. Publ. Wks. Rev.*, 58, No. 684, pp. 873-876 and No. 685, pp. 1009-1012.
- ROSCOE, K.H., BASSETT, R.H. & COLE, E.R. (1967). Principal axes observed during simple shear of a sand. *Proc. Geot. Conf., Oslo*, 1, 231-237.

- ROSCOE, K.H. & SCHOFIELD, A.N. (1964). Stress-dilatancy, earth pressures and slopes. Discussion, Proc. Am. Soc. civ. Engrs., 90, SM1, 136-150.
- ROSCOE, K.H., SCHOFIELD, A.N. and THURAI RAJAH. A. (1963). An evaluation of test data for selecting a yield criterion for soils. Proc. Symp. Lab. Shear testing of soils, Ottawa, ASTM STP, No. 361, 111-128.
- ROSCOE, K.H., SCHOFIELD, A.N. & WROTH, C.P. (1958). On the yielding of soils. Géotechnique, 8, 22-52.
- ROWE, P.W. (1962). The stress-dilatancy relation for static equilibrium of an assembly of particles in contact. Proc. Roy. Soc., A269, 500-527.
- ROWE, P.W. (1963). Stress-dilatancy, earth pressures, and slopes. Proc. Am. Soc. Civ. Engrs., 89, SM3, 37.
- ROWE, P.W. (1964). Stress-dilatancy, earth pressure and slopes. Reply to discussion. Proc. Am. Soc. civ. Engrs., 90, SM4, 145-180
- ROWE, P.W. (1969). The relation between the shear strength of sands in triaxial compression, plane strain and direct shear. Géotech. 19, 75-86.
- ROWE, P.W. (1971). Theoretical meaning and observed values of deformation parameters for soil. Proc. Roscoe Mem. Symp., Cambridge, 143-194.
- ROWE, P.W. (1973). The mechanism of fabric changes during compressional deformation of sand. Discussion. Soils and Found., 13, No. 2, 94.
- ROWE, P.W. & BARDEN, L. (1964). Importance of free ends in triaxial testing. Proc. Am. Soc. Civ. Engrs., 90, SM1, 1-27.
- ROWE, P.W., BARDEN, L. and LEE, I.K. (1964). Energy components during the triaxial cell and direct shear tests. Geotéchnique, 14, 247-261.
- RUBENSTEIN, C. (1956). A general theory of the surface friction of solids. Proc. Phys. Soc., B69, 921.
- RUIZ, M.D., CAMARGO, F.P., MIDEA, N.F. & NIEBLE, C.M. (1968). Some consideration regarding the shear strength of rock masses. Proc. 2nd Int. Symp. Rock Mech., Madrid, 159-169.

- SCHMID, H.H. (1953). An analytical treatment of the orientation of a photogrammetric camera. Ballistic Res. Lab. Rep. No. 880.
- SCHMID, H.H. (1971). On the influence of systematic errors in the least squares treatment of Photogrammetric data. Proc. Symp. - Aerial triangulation. University College, London, 35-65.
- SCHOFIELD, A. & WROTH, P. (1968). Critical State Soil Mechanics. New York: McGraw Hill.
- SCHUT, G.H. (1958-59). Construction of orthogonal matrices and their application in analytical photogrammetry. *Photogrammetria*, 15, No. 4, 149-162.
- SCOTT, R.F. (1963). Principles of Soil Mechanics. Reading, Addison-Wesley Pub. Co.
- SCOTT, R.F. (1964). Stress-dilatancy, earth pressures and slopes. Discussion, Proc. Am. Soc. civ. Engrs., 90, SMI, 133-135.
- SHARMA, S.K. (1973). The simultaneous adjustment of photogrammetric and field survey observations. M. Phil. Thesis, University of Nottingham.
- SHARMA, Y.K. (1972). Mechanics of particulate media. M.Sc. Thesis. University of London.
- SHOOTER, K.V. & TABOR, D. (1952). The frictional properties of plastics. Proc. Phys. Soc., B65, 661-671.
- SKEMPTON, A.W. (1960). Effective stress in soils, concrete and rocks. Conf. on Pore Pressure and Suction in Soils. London, Butterworths.
- SKINNER, A.E. (1969). A note on the influence of interparticle friction on the shearing strength of a random assembly of spherical particles. Tech. note. *Géotechnique*, 19, 150-157.
- SKINNER, A.E. (1975). The effect of high pore water pressures on the mechanical behaviour of sediments. Ph.D. Thesis, University of London.

- SKINNER, A.E. (1976). Personal Communication.
- SPENCER, A.J.M. (1964). A theory of the kinematics of ideal soils under plane strain condition. *J. Mech. Phys. Solids*, 2, 337-351.
- SPENCER, A.J.M. (1971). Fully developed plastic shear flow of granular materials. Discussion. *Géotechnique*, 21, 190-192.
- SPENCER, A.J.M. and KINGSTON, M.R. (1973). Plane mechanics and kinematics of compressible ideal materials. *Rheologica Acta*. 12, 194.
- TASSIOS, T.P. & SOTIROPOULOS, B.P. (1973). Strength & deformability of sands under various conditions. *Proc. 8th Int. Conf. Soil Mech. Found. Engng.*, Moscow, 1.2, 411-417.
- TAYLOR, D.W. (1948). Fundamentals of soil mechanics. New York: John Wiley.
- TERZAGHI, K. (1920, a). New facts about surface-friction. *Phys. Rev.*, No. 5. XVI, No. 1, 54-61.
- TERZAGHI, K. (1920, b). Old earth-pressure theories & new test results. *Engng. News Rec.*, 85, 632-637.
- TERZAGHI, K. (1925). Erdbaumechanik auf bodenphysikalischer Grundlage. Leipzig: Deuticke.
- TEWINKEL, G.C. (1975). Discussion on aerial triangulation in the U.S.A. *Photogramm. Rec.*, 8, No. 45, 260.
- TEWINKEL, G.C. et al (1966). Ch. 2: Basic mathematics of photogrammetry. Manual of Photogrammetry, volume I. Fall Church: Am. Soc. Photogramm.
- THOMPSON, E.H. (1958-59). An exact linear solution of the problem of absolute orientation. *Photogrammetria*, 15, No. 4, 163-179.
- THOMPSON, E.H. (1959). A method for construction of orthogonal matrices. *Photogramm. Rec.*, 3, No. 13, 55.
- THOMPSON, E.H. (1962). The theory of the method of least squares. *Photogramm. Rec.* 4, No. 19, 54.

- THOMPSON, M.M. (Ed.) (1966). Manual of Photogrammetry. Volume I & II.
Falls Church: American Society of Photogrammetry.
- THURSTON, C.W. & DERESIEWICZ, H. (1959). Analysis of a compression test of a model of a granular medium. *J. appl. Mech.*, 81, 251-258.
- TOMBS, S.G. (1969). Strength and deformation characteristics of rockfill. Ph.D. Thesis, London University.
- TONG, P.Y.L. (1970). Plane strain deformation of sands. Ph.D. Thesis, University of Manchester.
- TROLLOPE, D.H. (1971). The collapse of clastic aggregates. *Proc. 1st Aus.-New Zealand Geomechanics Conf., Melbourne*, 1, 204.
- VERMAN, L.C. & BANERJEE, S. (1946). Effect of container walls on packing density of particles. *Nature, Lond.*, 157, 584-585.
- WITKE, W. (1963). Vienna method of shear testing. Discussion. *Proc. Symp. on Laboratory Shear Testing of Soils. Ottawa. ASTM STP.* No. 361, 314.
- WROTH, C.P. (1971). Discussion on Session 1. "The meaning and measurement of basic soil parameters (1)." *Proc. Roscoe Mem. Symp., Cambridge*, 122-124.
- WROTH, C.P. and SIMPSON, B. (1971). Discussion on Session 2. "The meaning and measurement of basic soil parameters (2)." *Proc. Roscoe Mem. Symp., Cambridge*, 258.